



Université
de Toulouse

THÈSE

En vue de l'obtention du
DOCTORAT DE L'UNIVERSITÉ DE TOULOUSE

Délivré par :

Institut National Polytechnique de Toulouse (INP Toulouse)

Discipline ou spécialité :

Génie des Procédés et de l'Environnement

Présentée et soutenue par :

Elham Farouk MOHAMED

le : 20 Mai 2011

Titre :

Removal of organic compounds
from water by adsorption and photocatalytic oxidation

Ecole doctorale :

Mécanique, Energétique, Génie civil et Procédés (MEGeP)

Unité de recherche :

Laboratoire de Génie Chimique (LGC), Toulouse

Directeur(s) de Thèse :

Henri DELMAS

Rapporteurs :

M. Iordan NIKOV

M. Stephan BROSILLON

Autre(s) membre(s) du jury

Mme. Marie-Hélène MANERO

Présidente du Jury

Mme. Caroline ANDRIANTSIFERANA

Examinatrice

Mme. Florence BENOIT-MARQUIE

Examinatrice

Mme. Sabine SOCHARD

Examinatrice

M. Cedric VALLET

Examinateur

Scientific production

Publications in International Conferences as Poster:

1. **E.F. MOHAMED**, C. ANDRIANTSIFERANA, H. DELMAS, A. M. WILHELM. *Élimination des Composés Phénoliques par Charbons Actifs Issus de Boues. X^{èmes} Journées Cathala-Letort de prospective scientifique et technique, SFGP, Octobre 2008 "Le Génie des Procédés au service de l'Environnement - Enjeux et défis.*
2. **E.F. MOHAMED**, C. ANDRIANTSIFERANA, H. DELMAS, A. M. WILHELM. Competitive Adsorption of Phenolic Compounds from Aqueous Solution using Sludge Based Activated Carbon. *the International Green Process Engineering Congress and the European Process Intensification Conference, 14-17 June 2009, Venice, Italy.*
3. **E.F. MOHAMED**, C. ANDRIANTSIFERANA, H. DELMAS, A. M. WILHELM. Photocatalytic Regeneration of Activated Carbon Saturated with Phenol using Novel Kind of Combined TiO₂-AC Tissue. *International Journée Européenne de la photocatalyse, JEP), 21 et 22 Septembre 2009, Cité Mondiale, Bordeaux (France).*
4. **E.F. Mohamed**, C. Andriantsiferana, H. Delmas. Influence of Temperature, pH and Inorganic Salt on the Removal of Phenols from Aqueous solution and Industrial Effluent onto Commercial Activated Carbon S23. *International IWA: « Sustainable Solution for Small Water and Wastewater Treatment Systems (S2Small 2010) 19-22 April 2010, Girona, Catalonia (Spain).*

Publications in International Conferences as Oral Presentation:

1. **E.F. MOHAMED**, C. ANDRIANTSIFERANA, H. DELMAS. Towards a New Sustainable Sequential Process for Wastewater Treatment using Sludge Based Activated Carbon. *3rd International Conference of Environmental Research Division,*

Under The Theme of Environmental Science & Technology, NRC, Cairo, Egypt 2008, April 1-3, 2008.

2. **E.F. MOHAMED**, C. ANDRIANTSIFERANA, H. DELMAS, Photocatalytic oxidation of phenol under UV irradiation on a combined TiO₂-AC Tissue. International “Ozone and UV: Leading-edge science and technologies” 23-27 May 2011, Paris, France.

Scientific papers :

1. C. J. LEBIGUE, C. ANDRIANTSIFERANA, N. KROU , C. AYRAL , **E.F. MOHAMED**, A.M. WILHELM ,H. DELMAS , L. LE COQ , C. GERENTE ,K. M. SMITH , S. PULLKET , G FOWLER , N.J.D. GRAHAM (2010). Application of sludge-based carbonaceous materials in a hybrid water treatment process based on adsorption and catalytic wet air oxidation. Journal of Environmental Management .**91**: 2432 – 2439.
2. **E.F. MOHAMED**, C. ANDRIANTSIFERANA, A.M. WILHELM , H. DELMAS (2011). Competitive adsorption of phenolic compounds from aqueous solution using sludge based activated carbon. Environmental Technology. Pages 1–12.

Acknowledgement

This thesis is the result of many a long hour involving arduous research and the culmination of a process that included the constant assistance, support & guidance afforded to me by my professors whom I am deeply indebted. This achievement been accomplished, in no small measure, due to their sheer professionalism and dedication which they demonstrated time after time. It is to them that I owe my heartfelt thanks and the overwhelming sense of satisfaction that I feel at this stage.

First of all, I would like to express my deepest appreciation to my supervisor, Prof. Henri DELMAS, for his guidance, encouragement, tremendous support and advice throughout my work. His effort, time and patience in proofreading and giving useful comments and suggestions on my manuscript and research presentations were invaluable. He has also encouraged and challenged me in ways that enhanced my professional growth.

Special thanks to Dr. Caroline ANDERIANSEFERANA, co-director of thesis, who greatly enriched my knowledge & constantly inspired me and who, in my pursuit of this thesis, had to sacrifice many of her precious hours. She has been able to skillfully manage this research without forgetting the ever essential human relationships. From deep inside thank you and your family for their opportune support and help.

I would like to acknowledge Prof. Iordan NIKOV and Prof. Stephan BROSILLION for accepting to be the Reporters of my thesis and Prof. Marie H el ene MANERO, Dr. Florence BENOIT-MARQUIE, Dr. Sabine SOCHARD and Dr. Cedric VALLET to be a part of the jury member. I'm grateful for their valuable suggestions on the thesis work.

I also would like to express my gratitude towards all the staff members of LGC for their invaluable help. Special thanks to Jean-Louis NADALIN, Lahcen FARHI, Alec MAUNOURY, Christine REY ROUCH, Marie-Line PERN and Lucien POLLINI for their great help.

I would also like to thank all the people in the LGC who have provided me help and friendship over the past four years. my special thanks to my colleagues and friends, Harold , Cinthia, Mary, Isa , Cathy, Benjamin, Nicola , Marianne, Raluca, Ali, Joaquim and Rana for their moral supports during the completion of this research work and who have contributed to make my stay very pleasant.

I am the most grateful to my husband Gamal AWAD who overflows me with love and inspiration day by day; I share this accomplishment with you. Thank you for your encouragement, for believing in my capabilities, moral supports in all the good and hard times and patience in the last years. I would like to thank my children (Amr and Reem) from the bottom of my heart for their love.

To Zinab and Farouk, my beloved parents, I dedicate this work in their loving memory and honour. Daddy, although you are not here in flesh anymore, you continuously inspire me in everything I do. You honed me into the person that I am right now. Mom, thank you so much for being my first teacher. Dad, thank you for teaching me how to be a strong person unconsciously by making me get back up whenever I stumble. Daddy and Mommy, thank you for being the best parents I ever had, for the unconditional love that you gave me, and for instilling me the confidence that I am capable of doing anything I put my mind to.

Special thanks to all my family members especially my sweet sister Eman , my brothers Ahmed and Ehab , for their continuous faith and support. I would like to thank my country Egypt for funding my research for four years.

Finally, always thank God for giving me so much blessings, and I ask that I will be able to use such gifts to help those in need.

ELHAM

Abstract

In order to explore a new sequential process for water treatment its two steps, adsorption on activated carbon and in situ photocatalytic oxidative regeneration, were investigated successively.

Several commercial activated carbons (AC) and sewage sludge based activated carbons (SBAC) were tested with several phenols and one dye as pollutants. Despite low BET surface SBAC exhibits convenient adsorption properties.

Photocatalysis on TiO_2 was carried out with several materials to achieve activated carbon adsorption-regeneration process: a multilayer tissue with fixed granular AC and TiO_2 on a sheet, a composite with TiO_2 , CVD deposited on AC, and AC- TiO_2 powder mixture for comparison. Promising results were obtained especially with TiO_2 deposited on AC proving the vicinity of adsorption and photocatalytic sites to be beneficial.

Keywords: water treatment; sludge; activated carbons; multicomponent adsorption; phenols; tartrazine azo dye; TiO_2 ; regeneration; H_2O_2 ; photocatalysis; advanced oxidation

Résumé

Les effluents industriels sont constitués de molécules de natures très diverses, plus ou moins réfractaires aux classiques traitements biologiques. Les normes de rejets évoluant régulièrement vers des contraintes de plus en plus sévères, il semble aujourd'hui nécessaire de proposer des solutions complémentaires pour atteindre de hauts rendements d'épuration. Le premier procédé mis en œuvre dans ce travail est l'adsorption sur charbon actif. Le caractère novateur de cette technique se situe dans l'utilisation de charbons actifs fabriqués à partir de boues de stations d'épuration d'eaux usées. La seconde méthode est un procédé hybride innovant combinant adsorption et photocatalyse avec TiO_2 . Les eaux industrielles ciblées sont les effluents colorés, représentés par la tartrazine, et les effluents phénolés représentés par le phénol, l'acide *p*-hydroxybenzoïque, le *p*-chlorophénol et le *p*-nitrophénol. Pour traiter par adsorption les eaux chargées en phénols, plusieurs charbons actifs commerciaux et six charbons de boues ont été utilisés. Il ressort de cette première étude que, malgré leurs faibles surfaces spécifiques, certains charbons de boues présentent des performances très satisfaisantes. Le procédé séquentiel combinant adsorption et photocatalyse a été réalisé avec plusieurs matériaux: un tissu Ahlstrom contenant du charbon et du TiO_2 , un charbon actif avec dépôt de TiO_2 par MOCVD puis un mélange de charbon actif et TiO_2 en poudre. Des résultats prometteurs ont été obtenus pour dégrader la tartrazine, en particulier avec le TiO_2 déposé sur charbon actif montrant que la proximité de sites d'adsorption et photocatalytique améliore les performances de l'oxydation.

Mots-Clés: adsorption, charbon actif, colorant, phénol, photocatalyse, TiO_2 , traitement de l'eau, valorisation de boue de station d'épuration

Contents

General introduction	1
Work Accomplished	4
CHAPTER I:LITERATURE REVIEW	
A. Adsorption	6
1. Fundamentals of the adsorption	6
1.1. General definition of adsorption.....	6
1.1.1. Physical Adsorptions.....	6
1.1.2. Chemical Adsorptions.....	6
1.2 Adsorption Mechanisms	6
1.3. Physical properties of the adsorbent.....	7
1.3.1. Adsorbent porous.....	7
1.3.2. Adsorbent specific surface area.....	8
2. Activated carbon	9
2.1. Preparation of activated carbon.....	9
2.1.1 Physical activation.....	9
a. Carbonisation	9
b. Activation.....	9
2.1.2. Chemical activation.....	10
2.2. Preparation of activated carbon from sewage raw materials.....	11
2.3. Chemical structure of the activated carbon.....	11
2.3.1. The textural properties.....	11
2.3.2. Surface functional groups.....	12
2.4. Adsorption of phenolic compounds by activated carbon.....	14
2.4.1 Adsorption interactions of phenolic compounds.....	14
a. π - π dispersion interactions.....	14
b. Solvent effect.....	14
c. Electron donor-acceptor complexes.....	15
d. Phenomenon of the oligomerization (irreversible adsorption).....	15
2.4.2. Factors affecting the adsorbent/adsorbate interactions.....	16
2.4.2.1. Influence of nature of the adsorbate.....	16
a. Effect of electron donor/acceptor substituent groups.....	16
b. The molecular size.....	17
c. Solubility.....	18
d. Hydrophobicity.....	18
2.4.2.2. Influence of solution conditions	18
a. Solution pH.....	18
b. Temperature.....	19

c. Addition of inorganic salts.....	20
2.4.3. Competitive adsorption.....	21
3. Adsorption Isotherm.....	21
3.1. Modelling Techniques.....	22
3.1.1. Single component adsorption isotherms models.....	23
a. Langmuir Model (Type I).....	23
b. Freundlich Model (Type II).....	24
3.1.2. Multi-component system models.....	25
a. Multi-component Langmuir model.....	25
b. Multi-component Langmuir-Freundlich model.....	26
B. Advanced oxidation process, AOP.....	28
1. Introduction.....	28
2. Homogeneous photo-oxidation	30
3. Heterogeneous photocatalysis.....	31
3.1. Semiconductor system.....	32
3.2 Titanium Dioxide (TiO ₂) Photocatalyst.....	33
3.2.1. Mechanism of UV/TiO ₂ photocatalysis.....	35
3.2.2. Factors affecting TiO ₂ Photocatalyst.....	38
a. pH.....	38
b. Substrate concentration.....	40
c. Light intensity.....	40
d. Temperature.....	42
e. Photocatalyst dosage.....	42
f. Effect of electron acceptors.....	43
3.2.3. TiO ₂ support.....	44
4. Photocatalytic treatment of organic compounds.....	48
4.1. Phenols.....	49
4.1.1. Intermediates of phenol photodegradation.....	50
4.2. Dyes.....	53
5. Kinetic models for photocatalysis process	55
5.1. Langmuir-Hinshelwood kinetic model.....	55
5.2. First-order kinetic model.....	56
CHAPTER II: MATERIALS AND METHODS	
1. The model molecules, materials and oxidizing agents.....	57
1.1. Phenol and three substituted phenols.....	57
1.2. Tartrazine.....	59
1.3. The activated carbons.....	59

1.3.1. Commercial activated carbon F22 and S23.....	60
1.3.2. Sewage sludge based activated carbons.....	60
1.4. The Ahlstrom tissues.....	61
a. Materials used for tissue production.....	61
b. Types of media used.....	62
1.5. Activated carbon coated by TiO ₂	65
2. Analytical techniques.....	65
2.1. Analytical methods for liquid solutions.....	65
2.1.1. High Performance Liquid Phase Chromatography or HPLC.....	65
2.1.2. Global Measures of the organic pollutants.....	69
a. Chemical Oxygen Demand: COD	69
b. Colorimetric method for the measurement of COD (Method Hach 8000).....	70
c. COD: Operating protocol	70
d. Standard method for the measure of TOC.....	71
2.2. Characterisation methods of the activated carbons.....	72
2.2.1. Textural properties.....	72
2.2.1.1. Gas porosimeter.....	72
2.2.1.2. The helium pycnometer.....	74
2.2.2. Structural properties.....	75
a. Elemental analysis CHNSO.....	75
b. Ash content.....	77
c. Metal content by ICP-AES.....	77
d. The thermogravimetric analysis (TGA).....	78
2.2.3. Chemical surface properties.....	78
a. Boehm titration.....	78
b. pH at the point of zero charge.....	79
c. SEM/EDX	79
3. The experimental studies.....	80
3.1. Device for isotherm: the multifunction thermostatic bath.....	80
3.1.1. Operating protocol	80
3.1.2. Adsorption equilibrium studies.....	81
a. Monocomponent isotherms.....	81
b. Multicomponent isotherms.....	81
3.2. Study the effects of various parameters on the adsorption.....	81
a. Influence of pH on phenols adsorption.....	81
b. Influence of salt addition on phenols adsorption.....	82
c. Influence of temperature on phenols adsorption.....	82
3.3. The photocatalytic “channel” reactor.....	82
3.4. Glass photocatalytic reactor.....	86

3.5. Fixed bed photocatalytic reactor.....	89
3.6. Radiometer.....	91
CHAPTER III: ADSORPTION OF PHENOLS ONTO DIFFERENT ACTIVATED CARBONS	
1. Introduction.....	92
2. The adsorbents : commercial activated carbons and sewage based activated carbons.....	92
2.1. Textural properties: Specific surface area and pore volume.....	92
2.2. Chemical analysis of the activated carbons.....	94
2.2.1. Elemental analysis and ash content.....	94
2.2.2. CHNSO analysis.....	95
2.3. Chemical analysis of the surface.....	95
2.3.1. pH.....	95
2.3.2. Boehm titration: surface functions.....	96
2.3.3. Thermogravimetric analysis (TGA).....	97
3. Preliminary study: Effect of different experimental factors on phenols adsorption onto activated carbon	100
3.1. Effect of solution pH	100
3.2. Effect of an inorganic salt: NaCl	102
3.3. Effect of temperature.....	104
4. Adsorption performance of activated carbons of various origins.....	105
4.1 Single component system.....	105
4.1.1 Screening of different activated carbons: phenol as reference model.....	105
4.1.2. Model application for phenol adsorption.....	106
4.1.3. Adsorption of different substituted phenols onto S23, F22 and SA_DRAW.....	107
a-Single solute solution Isotherm.....	107
b- Langmuir and Freundlich models.....	110
4.2. Competitive adsorption of P, PHBA, PCP and PNP.....	111
5.Conclusion.....	115
CHAPTE IV:PHOTOCATALYTIC OXIDATION	
A- Oxidation using tissue.....	116
1. Introduction.....	116
2. Characterization of materials.....	117
2.1. Surface area and porosity.....	117
2.2. Electron microscopic analysis.....	118

2.3. Energy dispersive X-ray microanalyses (EDX).....	119
2.4. Thermogravimetric analysis of the original activated carbon	121
3. Adsorption isotherms.....	122
3.1. Comparison of the adsorption isotherms of different adsorbents.....	122
3.2. Comparison of the Langmuir and Freundlich models parameters	123
4. Kinetics of adsorption and photocatalytic oxidation of phenol onto AC media....	125
4.1. Direct photolysis of phenol onto AC media.....	126
4.1.1. Control test	126
4.1.2. Quantity of adsorbed phenol during successive cycles	130
4.2. Evolution of physical properties of AC media.....	131
4.2.1. BET surface area and pore size distribution.....	131
4.2.2. Thermogravimetric Analysis	132
5. Kinetics of adsorption and photocatalytic oxidation of phenol onto AC / TiO₂ tissue.....	133
5.1. Adsorption step of phenol onto tissue.....	133
5.1.1. Kinetic adsorption cycles of phenol onto tissue.....	133
5.1.2. The adsorbed phenol quantity during the adsorption cycles.....	137
5.2. Photodegradation step of phenol onto tissue.....	141
5.2.1. Kinetics of photodegradation cycles of phenol onto tissue.....	142
5.2.2. Regeneration efficiency	146
5.2.3. Kinetic model for photodegradation of phenol	148
5.2.4. Chemical Oxygen Demand	152
5.3. Physical properties of activated carbon in the tissue	155
5.3.1. BET surface area and pore-size distribution.....	155
5.3.2. Thermogravimetric analysis	157
6. Effect of H₂O₂ addition on the photocatalytic degradation of phenol.....	159
6.1. The operating conditions: quantity of H ₂ O ₂	159
6.2. Control test.....	160
6.3. Kinetics of adsorption and photocatalytic oxidation of phenol onto tissue with H ₂ O ₂ addition	161
6.3.1. Evolution of adsorption step	161
6.3.2. Photodegradation step.....	162
a. Kinetic of photodegradation cycles of phenol	162
b. Model application for photodegradation of phenol in the presence of H ₂ O ₂	165
6.3.3. Synergetic effect of H ₂ O ₂ addition to TiO ₂ in the tissue.....	167

6.3.4. Regeneration efficiency of tissue in presence of H ₂ O ₂	168
6.3.5. Photo-mineralization of phenol in the presence of H ₂ O ₂	169
6.4. Evolution of physical properties of activated carbon in the tissue	173
6.4.1. BET surface area and pore-size	173
6.4.2. Thermogravimetric analysis	173
7. Photocatalytic oxidation of phenol using fixed bed continuous reactor	175
B. Photocatalytic degradation of Tartrazine using immobilized TiO₂ on activated carbon S23.....	180
1. Photocatalysis using TiO₂ deposited on activated carbon: AC/TiO₂.....	181
1.1. Materials	181
1.2. Characterization of AC / TiO ₂ sample.....	181
1.2.1. Electron microscopic analysis	182
1.2.2. Energy dispersive X-ray microanalyses (EDX).....	182
1.2.3. Physical properties.....	185
1.2.4. Thermal gravimetric analysis.....	186
1.3. Adsorption isotherms.....	186
1.4. Photolysis and photocatalysis of Tartrazine	188
1.4.1. Adsorption / photocatalytic oxidation cycles.....	191
2. Photocatalytic oxidation of Tartrazine	195
2.1. Kinetic of Tartrazine photodegradation cycles	195
2.2. Regeneration efficiency.....	198
2.3. Photocatalytic mineralization of Tartrazine.....	198
2.4. Physical properties of activated carbon after the oxidation cycles of Tartrazine	201
2.4.1. BET surface area and pore-size distribution.....	201
2.4.2. Thermogravimetric analysis.....	202
3. Conclusions.....	204
CHAPTER V: CONCLUSIONS AND FUTURE WORK.....	205
REFERENCES	208
ANNEXES	

List of figures

		Page
Fig.I-1:	Schema of the mechanism of molecule adsorption using microporous adsorbent (Tchobanoglous <i>et al.</i> , 2003).....	7
Fig.I-2:	Schematic representation of different types of pores.....	8
Fig.I-3:	Schematic representation of external and internal adsorbent surface....	8
Fig.I-4:	Schema of the process of activated carbon manufacturing.....	10
Fig.I-5:	Arrangement of carbon atoms in graphite crystal (a); microstructure of the activated carbon (b).....	12
Fig.I-6:	Surface functional groups of the activated carbon.....	13
Fig.I-7:	Molecules studied by Gokturk and Kaluc (2008).....	17
Fig.I-8:	Classification of adsorption isotherms.....	22
Fig.I-9:	Suitability of water treatment technologies according to the Chemical Oxygen Demand, COD (Andreozzi <i>et al.</i> , 1999).....	29
Fig.I10:	Main advanced oxidation processes (AOP).....	29
Fig.I-11:	Configuration of the electronic bands of conductor, semi-conductor and insulator materials.....	33
Fig. I-12:	Crystallographic forms of TiO ₂ : (a): anatase; (b): rutile; (c): brookite...	35
Fig.I-13:	Formation of hydroxyl radicals and superoxide ions on the TiO ₂ surface (Huchon, 2002).....	36
Fig.I-14:	Influence of the mass of catalyst on the reaction rate, <i>r</i>	43
Fig.I-15:	Role of AC in the enhanced activity of TiO ₂ (Liu <i>et al.</i> , 2007).....	46
Fig.I-16:	A possible reaction mechanism of phenol oxidation in the presence of illuminated TiO ₂	52
Fig. I-17:	Reaction pathway for the wet oxidation of phenol with AC in presence of hydrogen peroxide.....	52
Fig. I-18:	Scheme route for phenol oxidation by Fenton's reagent.....	53
Fig.II-1:	Schematic representation of media AC.....	62
Fig.II-2:	Schematic representation of media AC / TiO ₂ , composition and photo.....	63
Fig.II-3:	Schematic representation of media TiO ₂ , composition and photo.....	64
Fig.II-4:	Schematic diagram of the principal technique of HPLC.....	66
Fig.II-5:	Thermostatic oven DRB 200 and spectrophotometer DR/2500.....	71
Fig. II-6:	The different techniques of analysis for solid characterization.....	72
Fig.II.7:	Simplified functional diagram of helium pycnometer.....	74
Fig.II-8:	Schema of the elemental analyser for CHNS analyses.....	76
Fig.II-9:	Schematic representation of the classification of Boehm titration.....	78
Fig.II-10:	Static multifunction thermostatic bath used for the adsorption isotherm.....	80
Fig. II -11:	Schematic representation and photography of the channel reactor.....	82
Fig.II-12:	Schematic and photography of the thermostated cylindrical reactor.....	86
Fig.II-13:	Photography of the fixed bed photocatalytic reactor.....	89
Fig. III-1:	Thermogravimetric analysis of the two commercial activated carbons..	98
Fig. III-2:	Thermogravimetric analysis of the sludge based activated carbons.....	99
Fig. III-3:	Effect of pH on the adsorption of P (a) and PHBA (b) onto AC S23 at	

	25°C.....	101
Fig.III-4:	Effect of NaCl addition on the adsorption of P (a) and PHBA (b) onto AC S23 at 25°C (pH = 6.3 for P and 3.5 for PHBA).....	103
Fig. III-5:	Effect of different temperatures on the adsorption of P (a) and PHBA (b) onto AC S23 (pH = 6.3 for P and 3.5 for PHBA).....	104
Fig. III-6:	Adsorption isotherms of phenol onto different activated carbon materials at 25 °C (experimental data : symbols, Langmuir model: lines and Freundlich model: dotted lines).....	105
Fig.III-7:	Adsorption isotherms at 25°C of single component of phenol, PHBA, <i>p</i> -nitrophenol and <i>p</i> -chlorophenol onto activated carbons (a) SA_DRAW, (b) S23 and (c) F22.	108
Fig. III-8:	Comparison of experimental data of adsorption isotherms with the calculated data by Langmuir- Freundlich model for equimolar mixture of phenol, PHBA, <i>p</i> -nitrophenol and <i>p</i> -chlorophenol onto SA_DRAW (a), S23 (b) and F22 (c) at 25 °C.....	114
Fig. IV-1:	SEM image of the original granular AC (x350, left and x 3000, right)..	118
Fig. IV-2:	SEM image of AC in TiO ₂ / AC tissue (x350, left and x 3000, right)...	118
Fig. IV-3:	SEM image of the surface of TiO ₂ media (x 1000, right) (Thevenet <i>et al.</i> , 2005).....	119
Fig IV-4:	Cross sectional SEM of the original granular AC (a) and AC in the TiO ₂ /AC tissue (b; Region I & Region II) in which two different regions are pointed out.....	120
Fig. IV-5:	EDX diagrams of the original granular AC (a) and AC in the TiO ₂ /AC tissue in two different regions (b; Region I & Region II).....	120
Fig. IV- 6:	Thermogravimetric analysis of the original granular AC.....	121
Fig. IV-7:	Adsorption isotherms of phenol onto original granular AC, AC media, TiO ₂ / AC tissue and TiO ₂ media at 25 °C.....	122
Fig. IV-8:	Schematic representation of one cycle of the sequential process.....	125
Fig. IV-9:	Adsorption /UV irradiation cycles of phenol (C ₀ = 0.88 g/L) onto activated carbon media at 25 °C.....	127
Fig. IV-10:	Adsorption cycles of phenol (C ₀ = 0.88 g/L) onto activated carbon media at 25°C.....	128
Fig. IV-11:	Evolution of phenol concentration under UV irradiation during 4 cycles of photo-oxidation onto AC media at 25 °C (C ₀ = 0.88 g/L)....	128
Fig. IV-12:	Photolysis of phenol without activated carbon at 25 °C.....	128
Fig. IV-13:	Comparison of the quantity of adsorbed phenol during the cycles of adsorption (■) for AC media (□ : sum of the adsorbed quantities of phenol from cycle 1 to cycle 4, ▨ q _{isotherm}).....	130
Fig. IV-14:	Comparison of thermogravimetric analysis of AC media; used AC after phenol adsorption and UV irradiation and non used AC.....	132
Fig. IV-15:	Adsorption and photocatalytic oxidation cycles of phenol (C ₀ = 0.88 g/L) onto TiO ₂ /AC tissue at 25 °C.....	134
Fig.IV-17:	Kinetic of the phenol adsorption cycles onto TiO ₂ /AC tissue after the	

	regeneration using two different initial phenol concentrations, 0.88 g/L (a) and 0.45 g/L (b).....	134
Fig.IV-18:	Comparison of the quantity of adsorbed phenol during the cycles of adsorption (■) onto tissue (□: sum of the adsorbed quantities of phenol, ▨ q_{isotherm} , ▩ $q_{\text{estimated}}$ estimated quantity of phenol) for initial phenol concentrations of 0.88 g/L (a) and 0.45 g/L (b).....	136
Fig.IV-19:	Kinetic of the phenol oxidation cycles onto TiO ₂ /AC tissue using two different initial phenol concentrations; 0.88 g/L (a) and 0.45 g/L (b)...	138
Fig.IV-20:	Comparison of the phenol degradation kinetic for the two different initial phenol concentrations during the first cycle of the photocatalytic oxidation.....	144
Fig. IV-21:	Effect of the initial phenol concentration on the regeneration efficiency during photocatalytic degradation runs onto tissue.....	145
Fig.IV-22:	Comparison between the experimental (symbols) and theoretical (lines) data during the photocatalytic degradation cycles of phenol onto tissue [T: 25 °C, C ₀ ; 0.45 g/L (a) and 0.88 g/L (b)]. The lines represent the values calculated from the kinetic model of pseudo first order.....	147
Fig.IV-23:	Comparison of apparent rate constant (K _{ap}) between two different initial phenol concentrations during the photocatalytic oxidation runs onto tissue.....	150
Fig. IV-24:	Kinetics of the photocatalytic disappearance of COD during phenol removal (C ₀ = 0.88 g/L).....	151
Fig. IV-25:	Evolution of COD initial and final during 4 photocatalytic oxidation cycles of tissue as compared to the COD final of phenol (C ₀ = 0.88 g/L).....	153
Fig.IV-26:	Comparison between the COD experimental (symbols) and theoretical (lines) data during the photocatalytic degradation cycles of phenol onto tissue within 120 min (T: 25 °C, C _i ; 0.88 g/L). The lines represent the values calculated from the kinetic model of pseudo first order.....	155
Fig.IV-27:	Comparison of thermogravimetric analysis of the activated carbon in Ahlstrom tissue; used AC (at the end of consecutive oxidation runs without cleaning, rinsed with H ₂ O, and cleaning with acetonitrile/US) and non used AC using two initial phenol concentrations; 0.88 (a) and 0.45 g/L (b).....	158
Fig.IV-28:	Kinetic of phenol removal by UV/H ₂ O ₂ and TiO ₂ media at 25 °C (C _{i phenol} = 0.88 g/L, V _{H₂O₂} = 50 ml).....	160
Fig.IV-29:	Kinetics of phenol adsorption cycles onto tissue at 25 °C.	162
Fig.IV-30:	Comparison of the quantity of adsorbed phenol (■) during the cycles of adsorption onto tissue (□: sum of the adsorbed quantities of phenol from cycle 1 to cycle 6, ▩: sum of the adsorbed quantities of phenol without H ₂ O ₂ , ▨ : q_{isotherm}).	162
Fig. IV-31:	Kinetics of phenol photocatalytic degradation cycles onto tissue in the	

	presence of H ₂ O ₂ at 25 °C.	164
Fig.IV-32:	Comparison between the experimental (symbols) and theoretical (lines) data during the photocatalytic degradation cycles of phenol onto tissue in the presence of H ₂ O ₂ (T: 25 °C, C ₀ ; 0.88 g/L).	166
Fig. IV-33:	Comparison between the regeneration efficiency of tissue (AC/TiO ₂) during the photocatalytic degradation runs in the presence and absence of H ₂ O ₂	168
Fig. IV-34:	Total Organic Carbon (TOC) removal from the solution during 5 cycles of photocatalytic degradation of phenol by tissue (TiO ₂ /AC) in the presence of H ₂ O ₂	169
Fig. IV-35:	Comparison between TOC _{initial} , at the beginning of oxidation (t = 0) and TOC _{final} , at the end of the oxidation process and the TOC calculated from oxalic (TOC _{f,oxalic}) and phenol concentration at the end of reaction (TOC _{f,phenol}) during 5 photocatalytic oxidation cycles by TiO ₂ in tissue in the presence of H ₂ O ₂	171
Fig.IV-36:	Comparison between TOC values of the experimental (symbols) and theoretical (lines) data during the photocatalytic degradation cycles of phenol onto tissue within 360 min in the presence of H ₂ O ₂ (T: 25 °C, C ₀ ; 0.88 g/L).....	172
Fig. IV-37:	Comparison of thermogravimetric analysis of the activated carbon in tissue; used AC (at the end of 5 consecutive cycles in the presence of H ₂ O ₂) and virgin AC.....	174
Fig.IV-38:	Kinetic adsorption of phenol (C _i = 0.2 g/l) onto TiO ₂ /AC tissue (12.7 g) at 25 °C.	176
Fig.IV-39:	Continuous photocatalytic oxidation of phenol in fixed bed type reactor (TiO ₂ /AC tissue) at 25°C (C _i =0.0179 g/L, flow rate= 2 ml/min) mass of tissue = 12.7 g).....	176
Fig.IV-40 :	Comparison between the experimental (symbols) and theoretical (lines) data of phenol photodegradation using TiO ₂ /AC tissue in fixed bed reactor (T: 25 °C, C _i ; 0.0179 g/L).....	178
Fig. IV-41:	SEM image of AC (a) and AC/TiO ₂ (b).....	182
Fig.IV-42:	Cross sectional SEM of AC (a) and AC/TiO ₂ (b I & b II) sample in which two different regions are pointed out.....	183
Fig.IV-43:	EDX diagrams of AC (a) and AC/TiO ₂ composite (b I & b II), obtained in two different regions: region I (b I) and region II (b II).....	184
Fig.IV-44:	Thermal gravimetric analysis of the original AC S23 and AC/ TiO ₂ composite.....	186
Fig.IV-45:	Isotherms of Tartrazine adsorption onto suspension mixture of AC - TiO ₂ and onto TiO ₂ deposited onto AC at 25 °C.....	187
Fig.IV-46:	Direct photolysis of Tartrazine using UV irradiation at 25 °C (photon flux; 47.5 W/m ² , Treated volume = 1L).....	189
Fig.IV-47:	Kinetics of Tartrazine adsorption in the dark onto TiO ₂ catalyst at 25 °C.	190
Fig.IV-48:	Kinetic of Tartrazine photodegradation by TiO ₂ catalyst under UV irradiation at 25 °C (photon flux; 47.5 W/m ²).....	190
Fig.IV-49:	Kinetic of Tartrazine adsorption cycles onto AC-S23 + TiO ₂ mixture at 25 °C.....	192
Fig.IV-50:	Kinetic of Tartrazine adsorption cycles onto AC /TiO ₂ composite at 25 °C.....	192

Fig.IV-51:	Comparison of the kinetics of the first adsorption cycle of Tartrazine. Comparison of a mixture AC-S23 +TiO ₂ and AC/TiO ₂ composite (CVD).....	193
Fig.IV-52:	Comparison of the quantity of adsorbed Tartrazine during the cycles of adsorption for AC / TiO ₂ composite (□), a mixture of AC +TiO ₂ (■) and the estimated adsorbed quantity for AC/TiO ₂ composite; assuming that only the adsorption process occurs (▣) at 25°C.....	193
Fig. IV-53:	Kinetics of Tartrazine photocatalytic degradation cycles using solid mixture of AC and TiO ₂ (photon flux: 47.5 W/m ²).....	197
Fig.IV-54:	Kinetics of Tartrazine photocatalytic degradation cycles using AC/ TiO ₂ composite (photon flux: 47.5 W/m ²).....	197
Fig. IV-55:	Comparison of the regeneration efficiency of suspension mixture of AC - TiO ₂ and AC/TiO ₂ composite.....	198
Fig.IV-56:	Total Organic Carbon (TOC) remaining in the solution during 5 cycles of photocatalytic degradation of Tartrazine by the suspension mixture of TiO ₂ and AC.....	199
Fig.IV-57:	Total Organic Carbon (TOC) remaining in the solution during 4 cycles of photocatalytic degradation of Tartrazine by AC/ TiO ₂ composite.....	200
Fig. IV-58:	Comparison between final TOC removal by the suspension mixture of AC - TiO ₂ and that by the AC/ TiO ₂ composite during 4 photocatalytic oxidation cycles of Tartrazine.....	200
Fig.IV-59:	Comparison between TGA of virgin AC/TiO ₂ and used AC/TiO ₂ samples (a) and used AC S23-TiO ₂ mixture (b).	203

List of tables

	Page
Table I-1 : IUPAC classification of pore sizes.....	7
Table I-2: Some examples of monocomponent isotherms models.....	25
Table I-3 List of homogeneous AOPs	31
Table I-4: Band gap energy and wavelength sensitivity of semiconductors (Stumm, 1992).....	32
Table I-5: Mechanism steps of photochemical oxidation reaction on the TiO ₂ surface.....	37
Table I-6: Photocatalytic degradation of different organic compounds by heterogeneous photocatalysis (Gaya <i>et al.</i> , 2008).....	49
Table II-1: The physico-chemical properties of phenols studied.....	58
Table II-2: The physico-chemical properties of tartrazine	59
Table II-3: Main characteristics of commercial activated carbons studied.....	60
Table II-4: Activated carbons resulting from the pyrolysis of municipal stations of sewage sludges.....	61
Table II-5: Composition of the activated carbon media.....	63
Table II-6: Composition of the media AC / TiO ₂	64
Table II-7: Composition of the media TiO ₂	64
Table II-8: Methods of separation by HPLC for the pollutants during the adsorption process.....	68
Table II-9: Methods of separation by HPLC for the pollutants during the oxidation process.....	68
Table II-10: Main elements of the channel reactor.....	83
Table II-11: Operating conditions of adsorption/photocatalysis cycles with the channel reactor	85
Table II-12: Operating conditions of adsorption/photocatalysis cycles into glass photocatalytic reactor.....	88
Table II-13: The experimental conditions of adsorption / photocatalysis runs into fixed bed photocatalytic reactor.....	90
Table III-1: Comparison between the textural physical properties of two commercial and six sludge based activated carbons	93
Table III.2: Metal composition analysis of the activated carbons estimated by ICP-AES.....	94
Table III-3: Elemental analysis of the activated carbons.....	95
Table III-4: Values of pH _{PZC} and pH of contact for the activated carbons.....	96
Table III-5: Results of Boehm titration.....	97
Table III-6: Parameters of Langmuir and Freundlich models for the adsorption of phenol on the all studied activated carbons at 25 °C.....	106

Table III-7:	Favorable or unfavorable effects of molecules characteristics in single solute adsorption.....	109
Table III-8:	Parameters of Langmuir and Freundlich models for the adsorption of single solute of P, PCP, PNP and PHBA on three types of activated carbons at 25 °C	111
Table IV-1:	Apparent surface area and pore volume distribution of AC powder and TiO ₂ media.....	118
Table IV-2:	EDX elemental composition of the original granular AC and AC in TiO ₂ /AC tissue, in two different regions as indicated in Fig. IV-4...	119
Table IV-3:	Parameter constants of Langmuir and Freundlich models for phenol adsorption.....	125
Table IV-4:	Physical properties of AC media (before and after adsorption/UV cycles).....	131
Fig. IV-5:	Adsorption and photocatalytic oxidation cycles of phenol (C ₀ = 0.45 g/L) onto TiO ₂ /AC tissue at 25 °C.....	135
Table IV-6:	Evolution of the phenol adsorption percentages (based on the decrease in concentration) during the adsorption cycles using two phenol concentrations onto TiO ₂ / AC tissue.....	149
Table IV-7:	Pseudo first-order apparent constants (K_{ap}) and correlation coefficients (R^2) corresponding to different initial phenol concentrations (0.45 g/L and 0.88 g/L, before dark adsorption) during the consecutive photocatalytic oxidation runs.....	154
Table IV-8:	Pseudo first-order apparent constants (K_{ap}) and correlation coefficients (R^2) detected in COD removal during the consecutive photocatalytic oxidation runs; C _{i phenol} (0.88 g/L).....	156
Table IV-8:	Comparison of physical properties of used (5 cycles) and virgin AC in the tissue with two initial phenol concentrations; 0.88 and 0.45 g/L.....	156
Table IV-9:	Pseudo first-order apparent constants (K_{ap}) and correlation coefficients (R^2) during the consecutive phenol photocatalytic oxidation runs in the presence of H ₂ O ₂	165
Table IV-10:	Apparent first order rate constants detected in the photodegradation of phenol by UV irradiation of tissue (TiO ₂ /AC) and Synergetic factor (S) in the presence and in the absence of H ₂ O ₂	167
Table IV-11:	Pseudo first-order apparent constants (K_{ap}) and correlation coefficients (R^2) for TOC removal during the consecutive phenol photocatalytic oxidation runs in the presence of H ₂ O ₂	172
Table IV-12:	Comparison of physical properties of used AC in the tissue after the 5 adsorption-regeneration cycles with and without H ₂ O ₂ addition and virgin AC.....	173
Table IV-13:	The values of the apparent rate constant (k_{ap}) and correlation coefficient (R^2) of the first order model for phenol photocatalytic oxidation onto tissue in fixed bed reactor	178
Table IV-14:	EDX elemental composition of AC and TiO ₂ /AC composite, in two different regions as indicated in Fig .IV-42.....	183
Table IV-15:	Main characteristics of studied samples	185

Table IV-16:	Experimental conditions of Tartrazine adsorption.....	187
Table IV-17:	Parameter constants of Langmuir and Freundlich models for Tartrazine	188
Table IV-18:	Comparison of the of Tartrazine adsorbed quantity during the cycles of adsorption for AC / TiO ₂ composite, a mixture of AC +TiO ₂ and the estimated adsorbed quantity for AC/TiO ₂ composite	194
Table IV-19:	Physical properties of AC in both studied systems; AC/ TiO ₂ composite and suspension mixture of TiO ₂ and AC as compared to the virgin.....	201

Abbreviations

AC	Activated carbon
AOP	Advanced oxidation
BET	Brunauer, Emmet and Teller
B.J.H.	Barrett, Joyner and Halenda
C_e	Concentration at equilibrium (g.L^{-1})
C_i	Initial liquid-phase concentration of solute
C'	Adsorption constant of gaz used (-).
C_DMAD	Carbonised Dewatered Mesophilic Anaerobically Digested sludge
C_DRAW	Carbonised Dewatered Raw sludge
CHNSO	Carbon, Hydrogen, Nitrogen, Sulfur, Oxygen,
CO2A_DSBS	CO ₂ Activated Dewatered Secondary Biological Sludge
COD_{eq}	Chemical Oxygen Demand at equilibrium (mg.L^{-1})
d	diameter of pores
EDX	Energy Dispersive X-ray analysis
HPLC	High Performance Liquid Phase Chromatography
ICL	Imperial College of London
IUPAC	International Union Pure Applied Chemistry
k_{ap}	Constant of first order model
K_f	Freundlich constant ($\text{L.mg}^{-1}.\text{g}^{-1}$)
K_L	Langmuir constant (L.g^{-1})
M_{O_2}	Molecular mass of oxygen (g.mol^{-1})
$M_{C_aH_bN_cO_dCl_e}$	Molecular mass of compound $C_aH_bN_cO_dCl_e$ (g.mol^{-1})
m_{solid}	Mass of solid sample
n	Freundlich constant
N_A	Avogadro number (mol^{-1})
p	Adsorption equilibrium pressure (Pa)
p_0	Vapour pressure of adsorbat at adsorption temperature (Pa)

pH_{pzc}	pH at the point of zero charge
q_e	Adsorbed quantity at equilibrium
q_{max}	Maximum adsorbed quantity
R²	Coefficient constant
S_{BET}	Specific surface of solid
SEM	Scanning Electron Microscopy
TGA	Thermogravimetric analysis
TOC	Total organic carbon
UV	Ultra-Violet
V	Volume
V_m	Volume of the gaz necessary to form a complete monolayer on the surface (m ³)
V_{mol}	Molecular volume of gaz (m ³ .mol ⁻¹)
PAHB	P-hydroxybenzoic Acid
PCP	p-chlorophenol
PCM	Physico-Chemical Mixture
PNP	p-nitrophenol
ph	Phenol
SA_DMAD	Steam Activated Dewatered Mesophilic Anaerobically Digested sludge
SA_DRAW	Steam Activated Dewatered Raw sludge
SBAC	Sewage Sludge based activated carbon
log K_{ow}	the octanol-water partition coefficient

General Introduction

Sustainable water supply is an increasing demand in today's world. In addition to water amounts needed for agriculture, water quality is fundamental for human life and the whole earth ecology. Among the wide variety of problems concerning water the reduction of pollution is a major issue. Water treatments are most often based on biological processes which are now conveniently installed in all the developed countries. The main remaining problem concerns non biodegradable compounds most often coming from industrial or agricultural activities. Besides very harmful dissolved heavy metal, most of these pollutants are organics, and may be very dangerous for human health.

Other processes should then been implemented, before or after biological treatments, depending on the toxicity for the microorganisms achieving biological treatments, and concentrations of the non biodegradable pollutants.

Adsorption on activated carbon for achieving high water purification is very widely used, and most often as a post treatment as its cost would be excessive for concentrated pollution (Dabrowski *et al.*, 2005; Fierro *et al.*, 2008; Pan *et al.*, 2008; Ahmed *et al.*, 2010). Indeed while adsorption on activated carbon is a very efficient technique to reduce organic pollution of water, convenient and cheap regeneration of the adsorbent is the main issue concerning adsorption economy. For most applications regeneration is achieved in few special plants at high temperature (>900°C) where about 15% of the initial activated carbon is lost. In the case of industrial wastewaters, due to possible hazardous products, this technique is not allowed and the saturated activated carbon becomes itself a waste, leading to restricted use of this adsorption technique to very low pollutant concentration.

Besides adsorption many recent developments concern chemical oxidative treatments, from the simple hydrothermal treatment needing high temperature and pressure, wet air oxidation (WAO), or its catalytic version (CWAO) at milder conditions, to much more efficient oxidations performed at room temperature and often called "Advanced Oxidation Processes" (AOP). These AOP generally use stronger oxidant than oxygen, like ozone and specially OH radicals, generated either by UV, photocatalysis, Fenton reagent, or electrochemistry at a convenient potential (Vora *et al.*, 2009; Ahmed *et al.*, 2011).

The team “Multiphase Reactions and Reactors”, at “Laboratoire de Génie Chimique” Toulouse, has been engaged for many years on these topics starting with oxidation by ozone and pressurized air then by Fenton and photo Fenton processes and by electrochemistry. Recently a sequential process coupling adsorption and oxidation (AD-OX process) was proposed (Krou, 2010): Pollutants are adsorbed in the first step providing purified water, then the batch oxidative step achieves simultaneously “in situ” the degradation of the adsorbed pollutants and the regeneration of the adsorbent. The oxidative step is catalyzed by the activated carbon playing successively the role of adsorbent and of catalyst of its own regeneration under moderate pressure and temperature. Despite its very attractive concept this process suffers two major drawbacks : i) corrosion due to Cl^- ions often present in wastewater is extremely severe at 150°C , ii) activated carbon cannot be conveniently regenerated when phenolic compounds are concerned due to oxidative coupling (or oligomerization) occurring in presence of dissolved oxygen, especially at the temperature requested by oxidation. These oligomerized phenolic compounds are chemisorbed and then very difficult to degrade, leading to pore clogging and dramatic reduction of activated carbon surface area.

Clearly better results were found with Fenton and even better with photo Fenton oxidative regeneration (Muranaka *et al.*, 2010). Nevertheless Fenton process needs addition of iron ions as catalyst, which is undesired in the treated water, and hydrogen peroxide which is consumed being a significant cost in this process.

Another oxidative technique able to perform activated carbon regeneration at low temperature and low operation and investment cost could be photocatalysis with TiO_2 as both catalyst and UV lamps are not expensive. Nevertheless the dramatic development of investigations on photocatalytic processes is probably partly due to its intrinsic sustainability when prospecting solar energy as the only consumption, if the photocatalyst is conveniently maintained (Zhanga *et al.*, 2011).

The aim of this work is to start to investigate the extension of the AD-OX process to photocatalysis expecting to maintain the high separation quality of adsorption on activated carbon and to improve the regeneration when using photocatalysis instead of pressurised air. It should be recalled that in AD-OX concept, contrary to AOP, the water treatment is not achieved by oxidation but by adsorption, the oxidative step being needed only for pollutant degradation and subsequent activated carbon regeneration.

Then this work will be divided into two main parts:

- Adsorption on activated carbons, including two commercial activated carbons and also new activated carbonaceous materials prepared from sewage sludge. As wastewater is most often composed of a mixture of pollutants we have also investigated model mixtures of phenolic compounds. In addition a more complex pollutant, tartrazine has also been investigated.
- Photocatalytic regeneration of activated carbon, using several photocatalytic media, available commercially or prepared at LGC. Due to their different shape (sheets or powders) they have to be operated in different types of reactors. The efficiency of this oxidative step is investigated within two aspects: i) pollutant and COD degradation during photocatalysis, and moreover ii) re-adsorption on the regenerated activated carbon. These two steps will be carried out several times during successive Adsorption-Oxidation cycles.

An important analytical work is required both for liquid and especially solid evolution during the two steps and the recycles. A special chapter has been dedicated to these analyses and to experimental methods.

The manuscript is then divided into four parts:

-Literature review

-Materials and methods

-Adsorption

-Photocatalysis

NB. This work being part of three research projects it has been constrained on several aspects: choice of activated carbons (ANR-PRECODD-PHARE), of sludge based activated carbons (EU Project REMOVALS-STREP-6th FP), of dye pollutant (tartrazine) (CTP - Région Midi Pyrénées).

Work Accomplished

The work done in this study has been presented in **five chapters** as discussed in the following text. The study begins with the literature review in **chapter I**. Literature of various types of toxic pollutants present in water; phenols, dyes, adsorption process, different adsorbents, activated carbon, advanced oxidation, photocatalytic degradation, mechanism of photosensitization of TiO₂ under UV have been summarized in this chapter.

In **chapter II** experimental procedures, description of reactors, instruments used and analytical techniques are discussed in details.

Chapter III, Adsorption of phenols onto different activated carbons, it includes study and compare two groups of different ACs; the first group was six sewage sludge based activated carbons (SBACs) produced from different sludge raw materials. The second group was two commercial activated carbons (PICA S23 and F22). Firstly, the physical and chemical properties of two groups of ACs were fully studied in order to understand the different between all the ACs studied. Secondly, scanning of the adsorption performance of all this ACs was investigated by using phenol compound as reference model. Thirdly among the six sewage sludge based ACs, we select that of the highest phenol adsorption capacity for the next study. In this part, we compare the performance of these SBACs with the two commercial ACs in both the single- and multi-component adsorption using phenol (P), p-chlorophenol (PCP); p-nitrophenol (PNP) and p-hydroxy benzoic acid (PHBA) as pollutants. The application of different isotherm models like Langmuir and Freundlich have been also investigated. The effect of different experimental parameters on the adsorption process such as effect of solution pH; effect of the presence of inorganic salt NaCl and effect of temperature have been also studied.

In **Chapter IV, Photocatalytic oxidation**, it includes two parts, in **Part A**, phenol degradation of two initial concentrations has been carried out in the presence of UV using different Ahlstrom Medias (tissues) in a “channel” type photo reactor. The kinetic degradation of phenol concentration with the time was investigated. Furthermore, the effect of this oxidation process on activated carbon regeneration and the effect addition of electron acceptors such as H₂O₂ were also studied. The degradation was studied by monitoring the change in substrate concentration employing HPLC analysis. The mineralisation of phenol was also determined by TOC and COD analysis. To study the effect of this type of oxidation on the AC properties, TGA and BET analyses were studied at the end of cycles and compared with the virgin one.

In **Part B**, the degradation of tartrazine as an alimentary dye was investigated using another coupled material of AC/TiO₂ prepared by Chemical Vapour Deposition (CVD) technique. As we studied with the AC/TiO₂ tissue, in this part, the performance of the AC/TiO₂ composite was investigated by following the decrease in tartrazine concentration with the time during all the adsorption and oxidation runs. The regeneration efficacy of the AC/TiO₂ composite was also studied. The TOC was also evaluated during the oxidation cycles. TGA and BET analysis were studied after the cycles and compared with the virgin one. Similar studies using a suspension mixture of commercial TiO₂ PC500 and AC S23 powders were compared to those found with the AC/TiO₂ composite.

In **chapter V**, the conclusions of the entire work are drawn.

CHAPTER I
LITERATURE REVIEW

A. Adsorption

1. Fundamentals of the adsorption

1.1. General definition of adsorption

Adsorption is a process in which a substance (adsorbate), in gas or liquid phase, accumulates on a solid surface. It is based on the capability of porous materials with large surfaces to selectively retain compounds on the surface of the solid (adsorbent). There are two types of adsorption; physical and chemical adsorptions.

1.1.1. Physical Adsorption

Physical adsorption is achieved by Van der Waals forces, dipole interactions, and hydrogen binding. There is no electron exchange between adsorbent and adsorbate. Because there is no activation energy required for physical adsorption, the time needed to reach equilibrium is very short. Physical adsorption is a non-specific and a reversible process.

1.1.2. Chemical Adsorption

Chemical adsorption results from the chemical link between adsorbent and adsorbate molecule, therefore it is specific as well as irreversible and chemical as well as electronic properties of adsorbent are changed. Binding between adsorbent and adsorbate by covalent bond is called weak chemical adsorption, and that by ionic bonds is called strong chemical adsorption.

1.2 Adsorption Mechanisms

The adsorption process of the adsorbate molecules from the bulk liquid phase into the adsorbent surface is presumed to involve the following stages (Fig.I-1):

1. Mass transfer of the adsorbate molecules across the external boundary layer towards the solid particle.
2. Adsorbate molecules transport from the particle surface into the active sites by diffusion within the pore-filled liquid and migrate along the solid surface of the pore.
3. Solute molecules adsorption on the active sites on the interior surfaces of the pores.
4. Once the molecule adsorbed, it may migrate on the pore surface through surface diffusion.

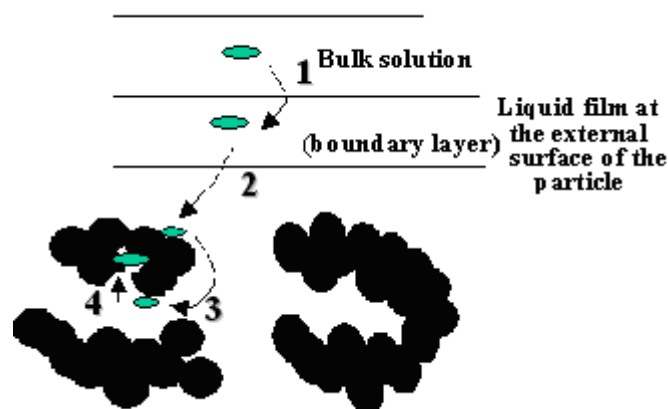


Fig.I-1. Schema of the mechanism of molecule adsorption using microporous adsorbent (Tchobanoglous *et al.*, 2003).

1.3. Physical properties of the adsorbent

The most important property of adsorbent, which determines its usage, is the pore structure and the specific surface area.

1.3.1. Adsorbent pores

The total number of pores, their shape and size determine the adsorption capacity and even the dynamic adsorption rate of the adsorbent. The range of pore sizes which is defined according to the International Union of Pure and Applied Chemistry (IUPAC) is summarized in Table I-1 (Rodriguez-Reinoso and Linares-Solano, 1989). A schematic representation of the porous structure of adsorbent is shown in Figure I-2.

Table I-1
IUPAC classification of pore sizes

Pores	Pore width (W ;nm)
Ultramicropores	$W < 0.7\text{nm}$
Supermicropores	$0.7 < W < 2\text{nm}$
Micropores	$W < 0.2$
Mesopores	2-50
Macropores	$W > 50$

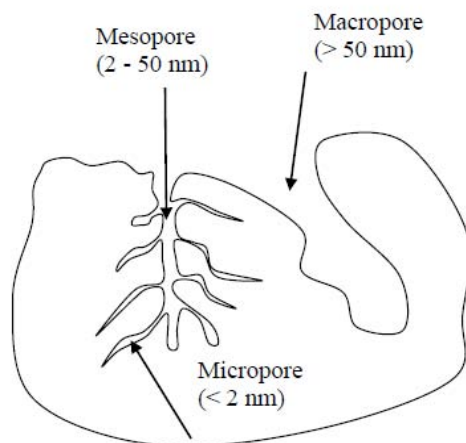


Fig.I-2. Schematic representation of different types of pores.

1.3.2. Adsorbent specific surface area

The specific surface area is another important property that determines adsorbent usage and its capacity. The total surface area of activated carbon, ranging from 500 to 2000 $\text{m}^2 \cdot \text{g}^{-1}$, quantifies adsorption sites for molecules to attach (Suhas and Carrot, 2007). The micropores usually provide the largest proportion of the internal surface of the activated carbon and contribute to most of the total pore volume. Mesopores, macropores and the nonporous surface of sample represent the external surface (Fig.I-3). Despite most of the adsorption takes place in the micropores, the meso- and macropores play also an important role in any adsorption process because they serve as passage for the adsorbate to reach micropores. Moreover, the multilayer adsorption only takes place in meso- and macropores.

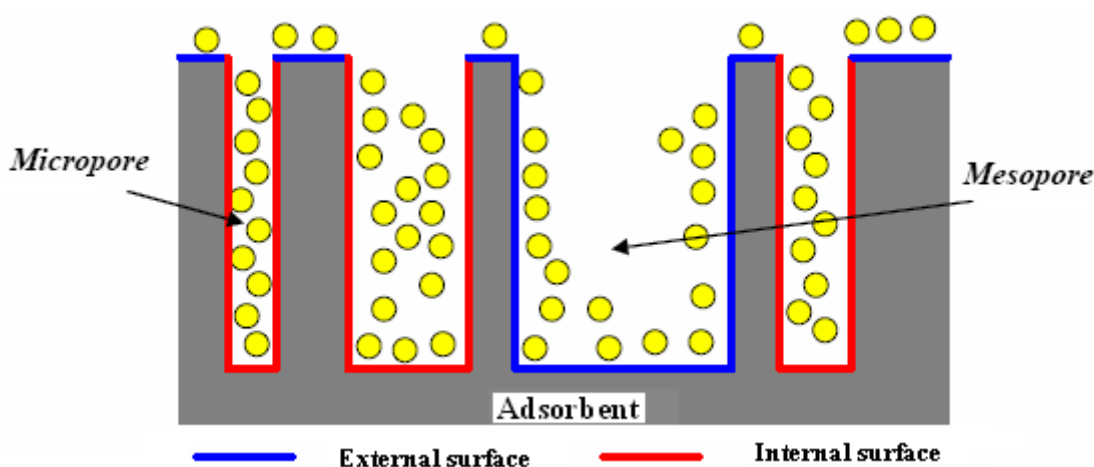


Fig.I-3. Schematic representation of external and internal adsorbent surface.

2. Activated carbon

The main adsorbent used in industry is the activated carbon. Activated carbon (AC) is a solid, porous, black carbonaceous material. As early as 1500 B.C., charcoal and carbonized wood have been used in drinking water filtration, as a medical adsorbent, and purifying agent in India and Egypt. Activated carbons can be produced from any carbonaceous solid precursor, synthetic or natural. It can be prepared from a large number of sources such as coconut shells, peat, black ash, charcoal, lignite, bituminous coal, and petroleum coke. Any carbon source can be converted into activated carbon via a number of methods. Different physical forms of activated carbon are produced depending on their application among these forms, the two most common forms are granular (GAC) forms to be used in adsorption columns and powder (PAC) forms for use in batch adsorption followed by filtration (Allen and Koumanova, 2005; Dabrowski *et al.*, 2005). Powdered activated carbon (PAC) was first produced commercially in Europe in the early 19th century. Activated carbon has high internal surface area and pore volume which make it very convenient to be used as adsorbent, catalyst, or catalyst supports in gas and liquid phase processes for purification and chemical recovery (Radovic, 2001).

2.1. Preparation of activated carbon

There are basically two methods for manufacturing activated carbons, i.e. physical and chemical activation (Fig.I-4).

2.1.1 Physical activation

It consists of two steps: carbonization and activation.

a. Carbonisation

Carbonization is an inert thermal process to convert the carbonaceous precursor into solid char and leaving other liquids and gaseous as by- products (Chattopadhyaya *et al.*, 2006). This takes place in the absence of air and at temperatures of 600 to 800 °C.

b. Activation

Activation is a sequence process to enhance the char porosity and to clean out the tar-clogging pores; thus increasing the total surface area of the produced activated carbon (Turmuzi *et al.*, 2004). The precursor and preparation methods (activation) not only determine its porosity but also the chemical nature of its surface, which consequently establishes its adsorptive and catalytic characteristics (Khalil *et al.*, 2001). Activation can be done either physically, chemically or by combination of both, known as physiochemical method. Physical

activation is the gasification of the resulting char with activating agent such as CO₂, steam or air at a high temperature (800-1000 °C) (Rio *et al.*, 2005b); the char develops a porous structure. The most widely used activating gas is steam because for a given temperature, the activated carbon produced with steam has larger adsorptive capacity and wider pore size distribution than that produced with CO₂.

2.1.2. Chemical activation

The two steps (carbonisation and activation) are carried out simultaneously in one step. The raw material is impregnated with certain chemical agent such as phosphoric acid (Haimour and Emeish, 2006), sulphuric acid (Martin *et al.*, 2003), potassium hydroxide (Fierro *et al.*, 2006) or zinc chloride (Tay *et al.*, 2001) in an inert atmosphere. The impregnated product is heated either at moderate or high temperatures (500-800 °C) under a flow of steam and the final temperature is kept for a short period of time under the steam flow then washed to remove the activating agent. Chemical activation is usually carried out if the raw material is wood or peat.

The yield of the chemical activation process is relatively large, i.e., it may exceed that of the physical activation method by up to 30 % wt. Other possible advantages of chemical activation are: (a) simplicity, no need of previous carbonisation of raw material; (b) lower temperatures of activation; and (c) good development of the porous structure (Dabrowski *et al.*, 2005). Additionally, some authors have studied the combination of these two methods (Hu *et al.*, 2001; Guo and Lua, 2000) to obtain activated carbon with specific surface properties.

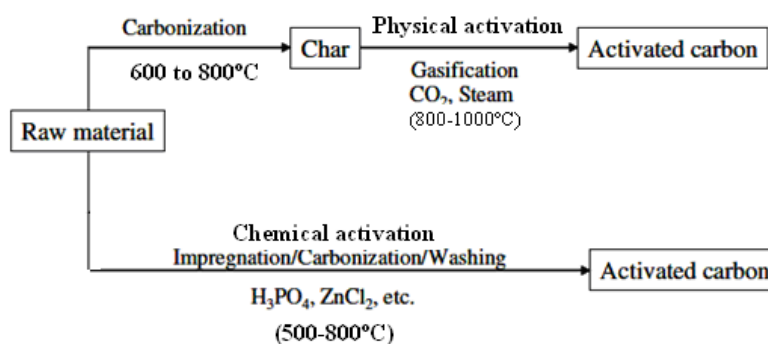


Fig.I-4. Schema of the process of activated carbon manufacturing.

2.2. Preparation of activated carbon from sewage raw materials

Searching for low cost activated carbons has been started a few decades ago as an alternative for expensive coal-based activated carbon. Biomass mainly derived from industrial and agricultural solid waste is a preferable option for activated carbon precursors (Malik, 2003; Ozacar and Sengil, 2003; Reddy and Kotaiah, 2006). Biomass materials are cheaper, renewable and abundantly available. Numerous successful attempts have been made to develop activated carbons from various range of agricultural solid waste such as bamboo, rice husk, rubber-wood sawdust, oil palm shell and coir pith (Namasivayam and Sangeetha, 2005; Kumar *et al.*, 2006; Adinata *et al.*, 2007; Hameed *et al.*, 2007).

Despite the prolific use of the ACs, it continues to be an expensive treatment process for large-scale application. Therefore, many efforts have been made to produce activated carbons from a range of residues, such as waste newspaper (Okada *et al.*, 2003), agricultural by-products (Rao *et al.*, 2006; Singh *et al.*, 2008) and sewage sludge (Rio *et al.*, 2005b; Wang *et al.*, 2008).

The use of waste, including those as difficult to manage as sewage sludge and used tyres, for the production of adsorbents makes waste economically valuable. Sewage sludge is being generated in an ever increasing amount due to the rapid urbanization and higher effluent criteria implemented in recent decades. Without proper treatment and disposal, it will cause a secondary pollution problem in the environment. Sewage sludge is carbonaceous in nature and rich in organic materials. Hence, it has the potential to be converted into some kinds of activated carbon if pyrolyzed under controlled conditions or with some chemical treatment (Calvo *et al.*, 2001; Otero *et al.*, 2003a, b; Rozada *et al.*, 2003 & 2005). This conversion could offer the combined benefits of reducing the volume of sludge and producing a valuable adsorbent with lower cost than commercial activated carbons. Several investigations have shown the feasibility of the conversion (Rio *et al.*, 2005a,b & 2006; Gutiérrez-Segura *et al.*, 2009; Liu C *et al.*, 2010). In our work, we will check some carbonaceous adsorbents prepared from municipal sludge.

2.3. Chemical structure of the activated carbon

2.3.1. The textural properties

During the carbonisation of the raw material in the preparation of activated carbon, the free elementary carbon atoms self assemble to form elementary graphite crystallites which

comprise 3 to 4 parallel hexagonal carbon ring layers (Fig.I-5a). The major structure of AC is composed of microcrystalline (amorphous) graphitic-like sheets, called “basal planes”, which are randomly cross-linked and surrounded by a number of unpaired electrons. These particular architectural features make AC enormously porous and useful for applications in catalysis and adsorption with a wide range of molecules (Fig.I-5b).

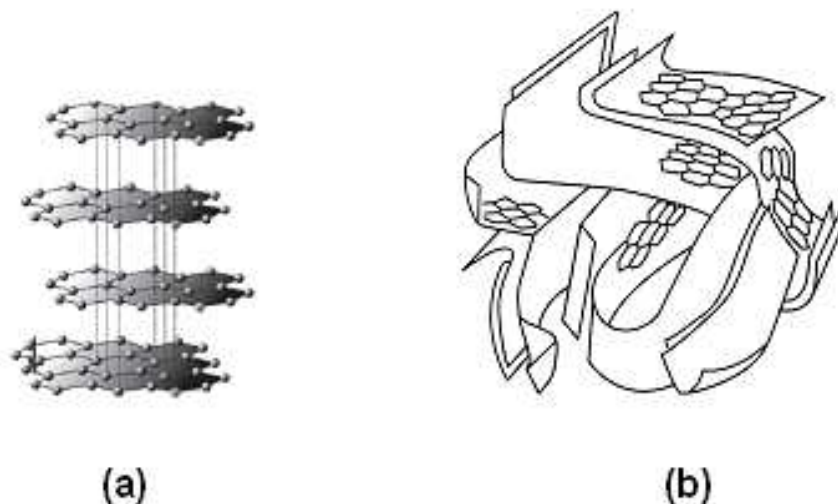


Fig.I-5. Arrangement of carbon atoms in graphite crystal (a); microstructure of the activated carbon (b).

2.3.2. Surface functional groups

The adsorption capacity of an AC is determined not only by the textural properties but also by the chemical nature of its surface (Bansal *et al.*, 1988). The surface of activated carbons is heterogeneous; it consists of faces of graphite sheets and edges of such layers. The edge sites are much more reactive than the atoms in the interior of the graphite sheets; chemisorbed foreign heteroatom, mainly containing nitrogen, hydrogen, halogen and particularly oxygen, are predominantly located on the edges (El-Sayed and Bandosz, 2004). Oxygen in the surface oxides is bound in the form of various functional groups. The surface chemical functional groups mainly derive from activation process, precursor, heat treatment and post chemical treatment. The surface functional groups can be classified into two major groups; acidic groups consisting mainly carboxylic, lactones and phenols, and basic groups such as pyrone, chromene, ethers and carbonyls (Boehm, 1994; Yang, 2003; Shen *et al.*, 2008) (Fig.I-6).

In the case of adsorption from liquid phase, the type of surface functional groups influences the process to a large extent changing the character of interactions between the solute molecules and carbon surface (Moreno-Castilla, 2004; Derylo-Marczewska *et al.*, 2008). Thus, the acidic or basic complexes formed on adsorbent surface determine the charge, the hydrophobicity, and the electronic density of the graphite layers, explaining the adsorbent activity differences towards various substances.

An increase of adsorption is observed with the decrease of concentration of acidic surface groups (Radovic *et al.*, 2001; Moreno-Castilla, 2004). The increase of acidic surface function groups reinforces the hydrophilic nature of carbonic and thus decreases its affinity to non polar organic compounds and conversely increases the adsorption capacity for polar molecules (Kim and Park, 2007; Leuch and Bandosz, 2007; Huang *et al.*, 2008). On the other hand, basic function groups lead essentially to hydrophobic carbons and display a strong affinity for organic molecules which have a limited solubility in water, like phenols (Stoekli and Hugi-Cleary, 2001).

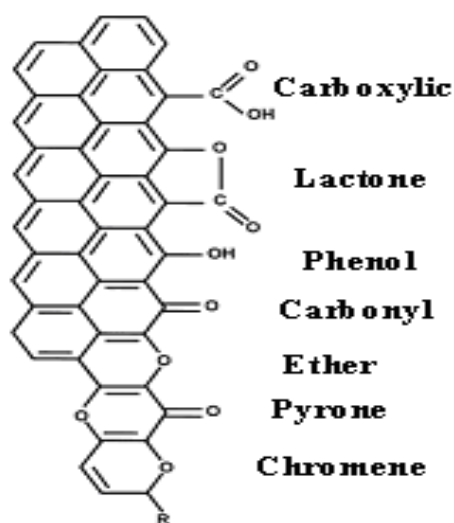


Fig.I-6. Surface functional groups of the activated carbon.

Moreover, the surface charge of carbon depends on the solution pH and its point of zero charge (pH_{PZC}); the pH value at which the surface charge is zero. For typical amphoteric carbons, the carbon surface is positively charged at $\text{pH} < \text{pH}_{\text{PZC}}$ and negatively charged at $\text{pH} > \text{pH}_{\text{PZC}}$. A negative charge will result from the dissociation of surface oxygen complexes

of acid character such as carboxylic and phenolic groups. The positive surface charge may be due to surface oxygen complexes of basic character like pyrones or chromenes, or due to the existence of electron-rich regions within the graphene layers acting as Lewis basic centers, which accept protons from the aqueous solution (Moreno-Castilla, 2004).

2.4. Adsorption of phenolic compounds by activated carbon

Phenols are persistent pollutants involving great damage to environment (Vázquez *et al.*, 2007). They have been designated as priority pollutants by the US Environmental Protection Agency (Rao and Viraraghavan, 2002). Activated carbon adsorption has proved to be the most effective treatment for phenolic compounds.

2.4.1 Adsorption interactions of phenolic compounds

Three important mechanisms have been proposed to interpret the adsorption behaviours of phenols on the activated carbon in previous studies, namely: the π - π dispersion interactions, the electron donor-acceptor complex and the solvent effects (Moreno-Castilla, 2004), beside the phenomenon of oligomerization.

a. π - π dispersion interactions

Different mechanisms were proposed to explain adsorption of aromatic compounds on activated carbon. The most widely accepted adsorption mechanism which was proposed by several authors is based on π - π dispersion interactions between the aromatic ring electrons in the compound and those on the activated carbon basal plane (Coughlin and Ezra, 1968; Radovic *et al.*, 2001; Rivera-Utrilla and Sanchez-Polo, 2002). Surface functional groups play an important role in determining the interactions between the organics and the activated carbon at the interface. The presence of basic groups causes an increase in the π -electron density in the graphene layers and thus an increase in the carbon adsorption potential, while the acidic groups decrease the basicity of activated carbons by attracting and thus localizing π -electrons in the graphene layers (Moreno-Castilla, 2004; Derylo-Marczewska *et al.*, 2008). Other authors (Fierro *et al.*, 2008; Yang *et al.*, 2008) reported that the molecule uptake was found to depend not only on the microporous volume, but also on the total number of basic and carbonyl groups, and on the ratio of acid to basic groups.

b. Solvent effect

The solvent effects should be taken into consideration in adsorption studies. Water molecules can be adsorbed on the surface oxygen groups by hydrogen bonding, which is unfavorable for the adsorption of phenols as some activated sites are occupied. Assuming that water molecules, adsorbed on oxygen groups, become secondary adsorption centres retaining other water molecules by means of H-bonds. The adsorbed water molecules block the entry of organic molecules to significant parts of the surface (Franz *et al.*, 2000; Pan *et al.*, 2008).

c. Electron donor-acceptor complexes

The electron donor–acceptor complex mechanism assumes that the aromatic rings of the adsorbate act as the electron acceptors and the basic sites on the carbon surface serve as the donors (Mattson *et al.*, 1969); where activated carbon acts as an electron donor, and the solute benzene ring has an electron withdrawing character. Nevertheless recently, some studies presented contradictory results (Jung *et al.*, 2001; Haydara *et al.*, 2003), in which the adsorption capacities of phenols could not be explained by the amounts of the basic sites. According to the thermodynamic analysis, the adsorption nature is primarily physical, then enhances with the increase of substitution degree, the more favourable adsorption of the substituted phenols should not be attributed to this mechanism.

d. Phenomenon of the oligomerization (irreversible adsorption)

The impact of surface properties of activated carbons on oligomerization of phenolic compounds was studied by Vidic *et al.* (1997). After studying the effects of acidic and basic surface functional groups, metals and metal oxide complexes, they concluded that oxygen-containing basic surface functional groups are primarily responsible for the catalytic properties of activated carbon in oligomerization. Moreover, the relative molecular size of the adsorbate to the pore size of the adsorbent is assumed to play a major role in the process of oligomerization on the surface of the activated carbon.

The oligomerization of phenolic compounds on the activated carbon surface has been confirmed by many researchers (Grant and King, 1990; Vidic *et al.*, 1993; Nakhla *et al.*, 1994; Tessmer *et al.*, 1997). Phenolic radicals are formed from phenol by the loss of a proton, form stable molecular products by coupling as dimers. Dimers may couple with another phenolate radical to give a trimer and so forth (Cooney and Xi, 1994). These oligomerized phenols are essentially irreversibly bound to carbon surface (Vidic *et al.*, 1997). As a

consequence, the regeneration of activated carbon after oligomerization of phenolic compounds is very difficult.

2.4.2. Factors affecting the adsorbent/adsorbate interactions

It has been established that the adsorption capacity of activated carbon (AC) for the liquid adsorption of phenolic compounds depends on a number of factors, not only the nature of the adsorbent (its pore structure, functional groups, ash content) but also the nature of the adsorbate; its pKa, functional groups present, polarity, aqueous solubility, molecular size and weight (Terzyk 2004; Zhang *et al.*, 2006a). Furthermore, the operation conditions such as solution pH, ionic strength and temperature are also involved in the adsorption, which might have implications on the adsorbent/adsorbate interactions (Canizares *et al.*, 2006; Vasiljevic *et al.*, 2006; Al-Degs *et al.*, 2008).

2.4.2.1. Influence of nature of the adsorbate

The adsorption performance of ACs for some phenols including 2,4-dichlorophenol (Wang *et al.*, 2007a,b), pentachlorophenol (Diaz-Flores *et al.*, 2006), 4-nitrophenol (Tang *et al.*, 2007) and chlorophenols have been reported in previous studies. It is generally assumed that the substituent groups are not directly involved in the interactions with the carbon surface (Dabrowski *et al.*, 2005), but they would change the molecular properties which in turn affect the adsorption process.

a. Effect of electron donor/acceptor substituent groups

The π - π interactions derive from the interactions between the π -electrons in the aromatic rings of the phenols and those in the graphene layers, which might comprise charge-transfer, dispersive force and polar electrostatic components. The introduction of substituent groups would alter the π - π interactions between phenols and the activated carbon. It is proposed that electron withdrawing groups enhance the π - π interactions by reducing the electron density of π -electrons, diminishing the repulsive electrostatic interactions between the aromatic rings. As both nitro (-NO₂) and chloro (-Cl) groups are electron-withdrawing groups, the π - π interactions are enhanced when increasing the number of these groups. The nitro group has stronger electron-withdrawing ability than the chloro group; hence the π - π interactions are stronger for nitrophenols than for chlorophenols. Some authors (Wang *et al.*,

2007a,b; Liu Q-S *et al.*, 2010) considered that this effect plays an important role in the adsorption of phenols on ACs.

Jung *et al.* (2001) studied the adsorption behaviour of phenol and chlorophenols on the activated carbon and found that the adsorption order was: phenol < 2-chlorophenol < 4-chlorophenol < 2,4-dichlorophenol < 2, 4, 6-trichlorophenol < pentachlorophenol, where the chloro- group is an electron-withdrawing group and therefore, the electron density in aromatic ring decreases as the number of chloro groups increases.

b. Molecular size

The molecular size also has some implications on the adsorption. The molecules with a suitable size would be adsorbed more favourably since they have more contact sites with the carbon surface. On the contrary, if the molecular size is relatively large, it will have difficulties in moving within pores with size not large enough, according to the so called steric effects. The steric effects are possibly caused by the following reasons: some extremely low size pores might be inaccessible for big molecules; the interior part of the pores might not be reached due to the blockage of the adsorbed molecules; the molecules could not be so compact in pores due to the introduction of the substituent groups. The adsorption kinetics and isotherm are affected notably at the molecular dimension of di-nitrophenol (DNP) and 4-nitrophenol (4-NP) (Pelekani and Snoeyink, 2000; Liu Q-S *et al.*, 2010). For example, Gokturk and Kaluc (2008) found that the safranin-O has a lower adsorption capacity than phenol; this can be explained by high molecular size of safranin-O (Fig.I-7)

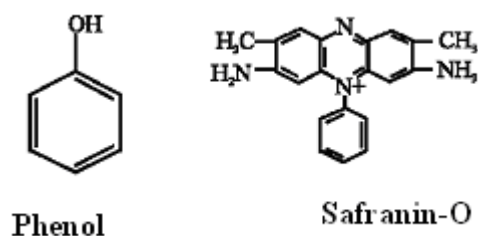


Fig.I-7. Molecules studied by Gokturk and Kaluc (2008).

Additionally, Liu C *et al.* (2010) cited that by comparison the adsorption of phenol with that of the different substituted phenols at low concentration range, it was found that their adsorption capacities follow the order of TCP > DNP ≈ DCP > 4-NP > 4-CP > 2-CP >

phenol, this result implies that only a small part of the micropores is filled in phenol adsorption, as phenol has smaller molecular size than the substituted phenols, and the micropore filling phenomenon is more evident for the substituted phenols.

Moreover, Attia *et al.* (2003) reported that the adsorption order; *p*-nitrophenol > methylene blue > rhodamine is proposed to be due to carbon porosity, related to the increased molecular dimensions of the solutes.

c. Solubility

Both, solubility and chemical structure of organics are factors of major importance in adsorption. On one hand, it is evident that the more the solubility in water the lower the adsorption capacity of a given compound. The dissolution of adsorbate usually relates to its polarity; the more polar adsorbate has higher solubility in a polar solution. The adsorption capacities are known to depend on the solubility of the phenols compounds in water. Moreno-Castilla *et al.* (1995b) reported that the adsorption capacity increases with decreasing water solubility of the phenolic compounds. Deryło-Marczewska *et al.* (2004) cited that nitrobenzene is adsorbed very strongly, 4-nitrophenol, 4-chlorophenol adsorb weaker and phenol adsorption is the weakest, the solubility is the important factor determining the adsorption equilibria. In addition, the higher solubility of phenol compared with *p*-nitrophenol (phenol is 5-fold more soluble than PNP) decreases its adsorbability to the carbon surface (Kumar *et al.*, 2007).

d. Hydrophobicity

The hydrophobic interactions are believed to make contributions to the adsorption of phenols (Moreno-Castilla, 2004). In aqueous solution, the adsorbate with higher hydrophobicity has stronger tendency to be adsorbed and retain on the carbon surface or in the pores. Hydrophobic compounds tend to be pushed to the adsorbent surface and hence they are more adsorbed than hydrophilic compounds.

2.4.2.2. Influence of solution conditions

a. Solution pH

Change of pH value in adsorption system could lead to the transformation of chemical characteristics on the surface of activated carbon and the form of the adsorbate, thus it plays an important role in the adsorption performance. Acidic or alkali species may change the surface chemistry of the adsorbent by reacting with the surface groups. These effects may lead

to significant alterations in the adsorption equilibrium depending on the pH (Garcia-Araya *et al.*, 2003). The functional groups exhibit pH-dependent interactions with water, which result in the transformation of the active sites (Contescu *et al.*, 1998; Radovic, 1999). The removal of acidic/basic species may thus give rise to a concomitant shift in pH of both the medium and the surface. The adsorbate is mainly in protonated form at $\text{pH} < \text{pKa}$ and in deprotonated form at $\text{pH} > \text{pKa}$. These effects may lead to significant alterations in the adsorption equilibrium depending on the pH (Laszlo *et al.*, 2007). According to previous reports (Hameed and Rahman, 2008; Li *et al.*, 2009) pKa values of phenol and PHBA at 30 °C are 9.89 and 4.8, respectively. When pH of solution goes beyond the pKa of phenols, phenols chiefly exist as negative phenolate ions whereas surface functional groups may be either neutral or negatively charged. Reduction in adsorption at high pH is possibly due to the increased solubility of phenol, the abundance of OH ions thereby increasing hindrance to diffusion of phenol ions and also increasing electrostatic repulsion between the negatively charged surface sites of the sorbent and phenolic ions. The ionic fraction of phenolate ion, ϕ_{ions} can be calculated from the Eq. (I-1) (Banat *et al.*, 2000):

$$\phi_{\text{ions}} = \frac{1}{1 + 10^{\text{pKa} - \text{pH}}} \quad (\text{I-1})$$

The ϕ_{ions} increases as the pH value increased. Thus, phenols being weak acid (pKa = 9.89 and 7.8 for phenol and 2,4-dichlorophenol, respectively) will be adsorbed to a lesser extent at higher pH values due to the repulsive force prevailing at higher pH (Khalid *et al.*, 2000).

Similarly, Singh *et al.* (2008) observed that the removal of phenol and 2,4-dichlorophenol decreases when increasing pH and the maximum adsorption was observed at the acidic pH for both phenols. Higher adsorption of phenols at lower pH has also been reported by others (Garcia-Araya *et al.*, 2003; Beker *et al.*, 2010). Therefore, we consider that phenols effectively adsorbed onto adsorbent are molecules not phenolate anions. Thus, the molecular interactions including hydrogen bonding, hydrophobic interaction and Van der Waals forces are the possible factors for the adsorption of phenols. Moreover, Amin (2009) reported that as the pH of the system increases, the number of negatively charged sites increases which do not favour the adsorption of direct blue-dye anions due to the electrostatic repulsion.

b. Temperature

It is known that ACs have strongly heterogeneous surfaces. The heterogeneity of the AC surface comes from two sources, namely geometrical and chemical. The geometrical heterogeneity (porosity) is the result of differences in the size and shape of pores. Chemical heterogeneity is associated with different functional groups at a surface, and with various surface contaminants. Both the chemical and geometrical heterogeneities contribute to the unique adsorption properties of ACs. The effect of carbon surface chemical composition on the adsorption of phenol decreases with rising temperature and geometrical heterogeneity determines adsorption of phenol at higher temperatures (Pan *et al.*, 2008). However, at ambient temperature, the influence of surface functionalities is significant. Additionally, the adsorption of water by ACs together with the change in the energy of phenol–water interactions with temperature greatly changes the mechanism of phenol adsorption.

The solvent effects are closely related to temperature, since temperature influences not only the adsorption of water but also the hydration degree of the phenolic molecules (Dabrowski *et al.*, 2005). This negative effect of temperature on the adsorption of phenol is expected for physical adsorption that is exothermic in nature in most cases (Catena and Bright, 1989; Halhouli *et al.*, 1997; Canizares *et al.*, 2006).

c. Addition of inorganic salts

The effect of three inorganic salts, KCl, KI and NaCl on the adsorption of phenol by commercial types of activated carbons was examined by several authors (Halhouli *et al.*, 1995). They found that the presence of such salts had only a very minor effect on phenol adsorbability. Kamble *et al.* (2007) clearly indicates that the salts have a substantially detrimental effect on the adsorption capacity in the presence of these ions which might also block the active sites of the adsorbent surface thus deactivating the adsorbent towards the organic molecules.

On the other hand, Tang *et al.* (2007) reported that the equilibrium adsorption amount of PNP increases with increasing sodium chloride. The proposed mechanisms of the enhanced adsorption involve interactions between water-ion and adsorbate-ion in this system. Sodium chloride dissociates into Na^+ and Cl^- in aqueous solution. There is a strong electrostatic field around the anions and cations, thus, an oriented array of water molecules is formed around these ions. The existence of ions enhances the combining powers between water–water

molecules and strengthens the hydrophobicity of the adsorbate in the opposite direction (Arafat *et al.*, 1999) which is beneficial for adsorption. Thus there is no general agreement on salt effects.

2.4.3. Competitive adsorption

The treatment of drinking water and wastewater by activated carbon sometimes involves a multitude of adsorbates competing for adsorption sites on the carbon surface. Thus, a thorough understanding of the competitive effect of various organic compounds on carbon adsorption is very important. Such competitive systems, especially those containing a large number of solutes, are very complex. Many factors influence adsorption equilibria as the structural and energetic heterogeneity of an adsorbent and the differences in physicochemical properties of adsorbates which makes it a very difficult problem (Lu and Sorial, 2007).

Natural Organic Matter (NOM) competes via two major mechanisms, direct site competition and pore blockage (Li *et al.*, 2003). Small, strongly adsorbing molecules of NOM with size comparable to that of the target compound are mainly responsible for direct site competition, thereby reducing the adsorption capacity for the target compound (Liding *et al.*, 2008).

Chern and Chien (2003) reported that in single system, AC has a higher affinity to p-nitrophenol (PNP) than to benzoic acid (BA) while in the competitive adsorption it was observed that the existence of PNP has a marked effect on decreasing BA adsorption, while the existence of BA has a less remarkable effect on decreasing PNP adsorption.

Moreover, Lu and Sorial (2004) reported that 2-methylphenol has more affinity than phenol on the binary solute systems on one granular activated carbon, and cited also that the possibility for the compound to get oligomerized becomes less as compared to the single solute system because of the competitive effect that would lead to less available sites.

3. Adsorption Isotherm

Adsorption isotherm expresses the quantity of material adsorbed per unit mass of adsorbent as a function of the equilibrium concentration of the adsorbate. The necessary data are derived from experiments where a specified mass of adsorbent is equilibrated with a known volume at a specific concentration of a chemical and the resultant equilibrium concentration is measured in solution by the mass balance equation:

$$q_e = \frac{(C_o - C_e) \times V}{m} \quad (\text{I-2})$$

Where C_o is initial liquid-phase concentration of solute, m is the mass of adsorbent and V is the isotherm solution volume.

At a given temperature, the relationship between the equilibrium concentration of adsorbate in the solution and the amount of adsorbate on adsorbent is called the adsorption isotherm. Adsorption isotherms are commonly categorized into five types which are shown in Figure I-8 (Sun and Meunier, 2003).

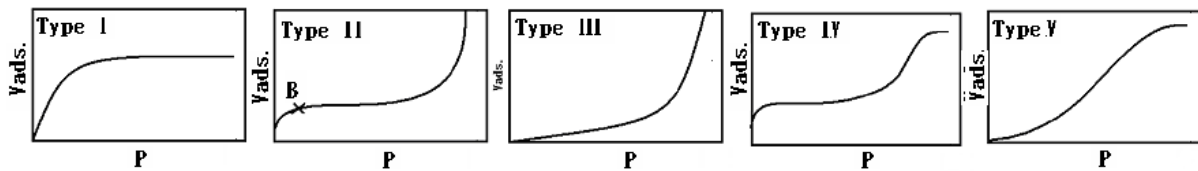


Fig.I-8. Classification of adsorption isotherms.

- (1) **Type I Isotherm:** These isotherms are used to characterize the sorption caused by predominantly microporous structure. This is also called the Langmuir isotherm and is used to describe monolayer adsorption.
- (2) **Type II isotherm:** These isotherms are used to describe multilayer physical adsorption on macroporous structure and are also called sigmoid isotherm. Point B expresses the formation of a monolayer adsorption and multilayer coverage starts right after the point B. Solids with mixed micro- and meso-porosity show Type II isotherms.
- (3) **Type III and Type IV:** These isotherms are found with microporous or mesoporous adsorbents and are convex at the high relative concentration. These are favoured by weak interactions between adsorbate-adsorbent systems and strong interaction between the adsorbate molecules lead to multilayer formation.
- (4) **Type V isotherm:** These isotherms are commonly shown for mesoporous materials. After the formation of monolayer, the multilayer coverage starts. The total pore volume governs the upper limit of adsorption.

3.1. Modelling Techniques

A number of models have been developed to represent the actual sorption/desorption processes of organic pollutants with various solid phases (Thibaud-Erkey *et al.*, 1996; Huang and Weber, 1997; Huang *et al.*, 1997; Aboul-Kassim, 1998). Some models have a theoretical basis; however, they may have only limited experimental utility because the assumptions involved in the development of the relationship apply only to a limited number of sorption processes. Other models are more empirical in their derivation, but tend to be more generally applicable. In the latter case, the theoretical basis is uncertain.

3.1.1. Single component adsorption isotherms models

Langmuir and Freundlich equations are the most commonly used for modelling single solute adsorption isotherms.

a. Langmuir Model (Type I)

The Langmuir adsorption model describes the equilibrium between aqueous and solid phase systems as a reversible chemical equilibrium between species (Langmuir, 1918; Stumm and Morgan, 1981; Buffle and Stumm, 1994). There are three main assumptions in Langmuir adsorption equation: (a) the adsorption energy is the same at all sites, (b) adsorption is on localized sites with no interaction between adsorbed molecules, and (c) the maximum adsorption possible is a complete monolayer. The adsorbent surface (solid phase) is made up of fixed individual sites where molecules of adsorbate (organic pollutant) may be chemically bound. This can be expressed mathematically by denoting an unoccupied surface site as $(-S)$ and the adsorbate in solution as species (A) , with concentration (C) , and considering the reaction between the two to form occupied sites $(-SA)$:



For the Langmuir adsorption isotherm, it is assumed that this reaction (Eq. I-3) has a fixed free energy of adsorption not dependent on the extent of adsorption and not affected by interaction among sites. In addition, each site is assumed to be capable of binding at most one molecule of adsorbate. If q_{max} is the maximum number of moles of a pollutant adsorbed per mass adsorbent when the surface sites are saturated with an adsorbate (full monolayer), and q_e is the number of moles of adsorbate per mass adsorbent at equilibrium, then according to the law of mass action Eq. (I-4) follows:

$$k = \frac{[-SA]}{[-S][A]} = \left[\frac{q_e}{(q_{max} - q_e) \cdot C_e} \right] \quad (I-4)$$

Where:

k is equilibrium constant, and C_e is the equilibrium concentration in solution. The rearrangement of Eq. (I-5) leads to the well known Langmuir equation:

$$q_e = \frac{q_{max} k C_e}{(1 + k C_e)} \quad (I-5)$$

For determination the constants in the Langmuir model, two versions of linearization can be used. Version 1 is represented by plotting C_e versus C_e/q_e , according to Eq. (I-6) used at high concentration. Version 2 is represented by plotting $1/C_e$ versus $1/q_e$, according to Eq. (I-7) used at low concentration.

$$\frac{C_e}{q_e} = \frac{C_e}{q_{max}} + \frac{1}{k q_{max}} \quad (I-6)$$

$$\frac{1}{q_e} = \frac{1}{q_{max}} + \frac{1}{q_{max} k C_e} \quad (I-7)$$

b. Freundlich Model (Type II)

The Langmuir model involves an assumption that the energy of adsorption is the same for all surface sites and not dependent on degree of coverage. Since in reality the energy of adsorption may vary because real surfaces are heterogeneous, the Freundlich adsorption model (Freundlich, 1926) attempts to account for this:

$$q = k_f \cdot C_e^n \quad (I-8)$$

Where C_e is the equilibrium concentration in solution, k_f is an equilibrium constant indicative of sorption strength and n = the degree of non-linearity (most often $n < 1$).

A linear form of Eq. (I-8) can be used as shown in Eq. (I-9):

$$\log q = \log k_f + n \cdot \log C_e \quad (I-9)$$

If $\log q$ is plotted as a function of $\log C$, a straight line should be obtained with an intercept on the ordinate of $\log k$ and slope n .

In addition to these two major models there is a wide range of available theoretical models and empirical fitting functions used to evaluate the monocomponent isotherms, table I-2 represent some examples of these models.

Table I-2
Some examples of monocomponent isotherms models

Model	Equation	Description
Langmuir-Freundlich	$q = q_{\max} \cdot \frac{(K \cdot C)^{\gamma}}{[1 + (K \cdot C)^{\gamma}]}$	Empirical model (monolayer adsorption on heterogeneous surface)
Jovanovic	$q = q_{\max} \cdot (1 - e^{-K \cdot C})$	Monolayer adsorption on homogeneous surface with the possibility of mechanical contacts between adsorbed and desorbed molecules.
Jovanovic-Freundlich	$q = q_{\max} \cdot (1 - e^{-(K \cdot C)^{\gamma}})$	Semi-empirical model adsorption on heterogeneous surface, derived from Jovanovic's model.
Brunauer-Emmett-Teller (BET)	$q = \frac{q_{\max} \cdot K_1 \cdot C}{(1 - K_2 \cdot C) \cdot (1 + (K_1 - K_2) \cdot C)}$	Describe the multi-layer adsorption (the adsorption of molecules to the surface of particles forms a new surface layer to which additional molecules can adsorb)
Toth	$q = q_{\max} \cdot \frac{K \cdot C}{[1 + (K \cdot C)^{\gamma}]^{1/\gamma}}$	Empirical model adsorption on heterogeneous surface

3.1.2. Multi-component system models

Multicomponent pollutants systems consist of more than one pollutant. The multicomponent adsorption involves competition among pollutants to occupy the limited adsorbent surface available and the interactions between different adsorbates. A number of models have been developed to predict multicomponent adsorption equilibrium using data from single component system adsorption isotherms.

a. Multi-component Langmuir model

The Langmuir model for competitive adsorption can be used as a common model for predicting adsorption equilibrium in multicomponent systems. This was first developed by Butler and Ockrent (1930) and is based on the same assumptions as the Langmuir model for single adsorbates.

It assumes that q_{\max} for all species are equal. This is expressed by Eq. (I-10):

$$q_{e,i} = \frac{q_{\max} \cdot k_i \cdot C_{e,i}}{1 + \sum_m k_m \cdot C_{e,m}} \quad (\text{I-10})$$

Where $q_{e,i}$ is the amount of component i adsorbed per unit weight of adsorbent, $C_{e,i}$ the equilibrium concentration of the component i and $C_{e,m}$ the equilibrium concentration of the other component m , q_{\max} , and k parameters obtained from Langmuir model for each species. Because of its mathematical simplicity, the multicomponent Langmuir adsorption model is widely used.

b. Multi-component Langmuir-Freundlich model

Because of the limited success of the generalized Langmuir model in predicting mixture equilibria, several authors have modified the equations by the introduction of a power law expression of Freundlich form. The resulting expression for the multicomponent Langmuir-Freundlich adsorption model is: (I-11).

$$q_{e,i} = \frac{q_{\max} \cdot (k_i \cdot C_{e,i})^{n,i}}{1 + \sum_m (k_m \cdot C_{e,m})^{n,m}} \quad (\text{I-11})$$

Where, n parameters obtained from Freundlich model for each single component.

The simple formula makes this method very attractive. Although not thermodynamically consistent, this expression (Eq. I-11) has been shown to provide a reasonably good empirical correlation of multicomponent equilibrium data (Dabrowski *et al.*, 2005).

The values of the Optimized Extend Langmuir-Freundlich model parameters were obtained from non linear regression. Optimization is made by using the generalized reduced gradient method (Solver Microsoft Excel) to minimize the residual sum of squares (RSS) as shown in equation (I-12):

$$RSS = \sum_{i=1}^m (q_{exp,i} - q_{t,i})^2 \quad (\text{I-12})$$

Where $q_{\text{exp},i}$ are the elements of the vector $q_{\text{exp},i}$ containing the given experimental adsorbed phase concentrations, m is data points and $q_{t,i}$ are the corresponding theoretical values.

Based on the objective function values (F_{OBJ}), relative average deviation (RAD) and a correlation coefficient (R^2) between the measured and the model-predicted values, statistical analysis was carried through to evaluate the models behaviour. The objective function (F_{OBJ}) and the relative average deviation (RAD) were calculated with the equations:

$$F_{OBJ} = \sum_{i=1}^m \left(\frac{q_{\text{exp } i} - q_{t i}}{q_{\text{exp } i}} \right)^2 \quad (\text{I-13})$$

$$RAD = \frac{100}{N} \sum_{i=1}^m \left(\frac{q_{\text{exp } i} - q_{t i}}{q_{\text{exp } i}} \right)^2 \quad (\text{I-14})$$

Where $q_{\text{exp}, i}$, and $q_{t,i}$ are the experimental and calculated values for each data point, respectively, and m is the number of experimental data.

B. Advanced oxidation process, AOP

1. Introduction

Advanced Oxidation Processes (AOPs) were defined by Glaze *et al.* (1987) as near ambient temperature and pressure water treatment processes which involve the generation of highly reactive radicals (specially hydroxyl radicals) in sufficient quantity to effect water purification (Blanco and Malato, 2001; Maldonado *et al.*, 2007). Advanced oxidation processes have proved to be one of the most effective treatments for wastewater that are difficult to be treated biologically. These are successfully used to decompose many toxic and bio-resistant organic pollutants in aqueous solution to acceptable levels, without producing additional hazardous by-products or sludge which requires further handling. These processes are based on the generation of the strongly oxidizing hydroxyl radicals ($\cdot\text{OH}$), which oxidize a broad range of organic pollutants that could be present in water and wastewaters (Akbal and Onar, 2003; Han *et al.*, 2004; Qamar *et al.*, 2006). Hydroxyl radicals are also characterized by a little selectivity of attack, attractive feature for an oxidant to be used in waste water treatment. Many different organic compounds are susceptible to be removed or degraded by means of hydroxyl radicals. Once hydroxyl radicals are generated, they can virtually oxidize and mineralize almost every organic molecule, yielding CO_2 and inorganic ions.

Practical application of AOP depends on the polluting load of wastes, normally expressed as COD (chemical oxygen demand) (Fig.I-9). Only wastes with relatively small COD contents ($\leq 5 \text{ g.L}^{-1}$) can be suitably treated by means of these processes (Andreozzi *et al.*, 1999) since higher COD contents would require the consumption of too large amounts of expensive reactants. In those cases, it would be more convenient to use wet oxidation or incineration: waste water with COD higher than 20 g.L^{-1} may undergo autothermic wet oxidation (Mantzavinos *et al.*, 1997; Luck, 1999).

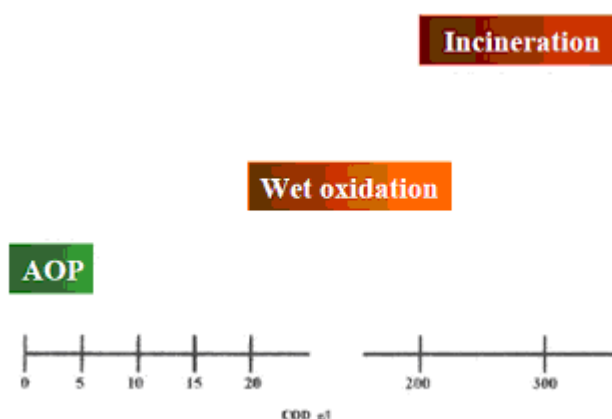


Fig.I-9. Suitability of water treatment technologies according to the Chemical Oxygen Demand, COD (Andreozzi *et al.*, 1999).

Different combinations of homogenous and heterogeneous methods which involve the generation of free radicals are, (i) photochemical irradiation with ultraviolet light (coupled with powerful oxidizing agents like ozone, hydrogen peroxide and /or a semiconductor), (ii) Fenton and Photo-Fenton catalytic processes (iii) Electron Beam Irradiation technique and (iv) Sonolysis (Fig.I-10). Most of these processes use UV range for degradation. The UV spectrum is arbitrarily divided into three bands: UV-A (315 to 400 nm), UV-B (280 to 315nm) and UV-C (100 to 280 nm). UV-A and UV-C are generally used in environmental applications. UV-A radiations are referred to as long wavelength radiations or black light and UV-C are referred to as short wave radiations.

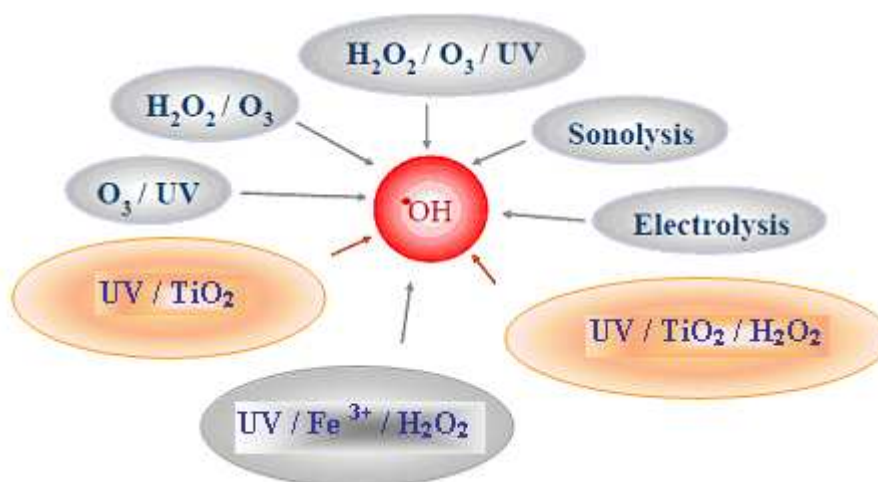


Fig.I-10. Main advanced oxidation processes (AOP).

Advanced oxidation processes based UV can be broadly classified into the following groups:

1. Homogeneous photo-oxidation.
2. Heterogeneous photo-oxidation: photocatalysis.

2. Homogeneous photo-oxidation

Homogeneous photo-oxidation refers to photo-reactions in a gas or liquid phase system, without any solid addition. The applications of homogeneous photodegradation to treat contaminated water, involves the use of an oxidant to generate radicals, which attack the organic pollutants to initiate oxidation. Several photochemical systems may be used in a homogeneous solution, such as:

1. Hydrogen peroxide (UV /H₂O₂)
2. Ozone (UV /O₃)
3. Hydrogen peroxide and Ozone (UV /O₃/H₂O₂): An increase in the rate of oxidative degradation has been observed in the combined UV/H₂O₂ process with O₃ (Sunder and Hempel, 1997; Safarzadeh-Amiri, 2001).
4. Photo-Fenton system (Fe³⁺ /H₂O₂): Fenton reaction was discovered by Fenton (1894) who reported that by using hydrogen peroxide and an iron salt as catalyst, several organic molecules could be oxidized.

Many of the AOP's listed in Table I-3 utilize hydrogen peroxide as oxidizing agent. The oxidising strength of hydrogen peroxide alone is relatively weak, but the addition of UV light enhances the rate and strength of oxidation through production of increased amounts of hydroxyl radicals. Hydrogen peroxide may also be used to enhance other AOPs if added in low concentrations, as the molecule easily splits into two hydroxyl radicals.

Table I-3
List of homogeneous AOPs

Method	Key reaction	Drawbacks
UV /H ₂ O ₂	$\text{H}_2\text{O}_2 + h\nu \longrightarrow 2\text{HO}^\bullet$	1) Absorb $\lambda < 300$ nm, a lesser component in solar radiation. 2) pH dependence. 3) Continuous supply of feed chemicals are required.
UV /O ₃	$\text{O}_3 + \text{H}_2\text{O} + h\nu \longrightarrow \text{O}_2 + \text{H}_2\text{O}_2$ $\text{O}_3 + \text{H}_2\text{O}_2 \longrightarrow \text{HO}^\bullet + \text{HO}_2^\bullet + \text{O}_2$	1) Absorb $\lambda < 300$ nm, a lesser component in solar radiation. 2) pH dependence 3) Continuous supply of feed chemicals are required. 4) Process is expensive
UV /O ₃ /H ₂ O ₂	$\text{O}_3 + \text{H}_2\text{O}_2 \longrightarrow \text{HO}^\bullet + \text{HO}_2^\bullet + \text{O}_2$	1) Absorb $\lambda < 300$ nm, a lesser component in solar radiation. 2) Applicable over a wider pH range.
Fe ³⁺ /H ₂ O ₂ (Photo Fenton)	$\text{H}_2\text{O}_2 + \text{Fe}^{2+} \longrightarrow \text{Fe}^{3+} + \text{OH}^\bullet + \text{OH}^-$ $\text{Fe}^{3+} + \text{H}_2\text{O} + h\nu \longrightarrow \text{Fe}^{2+} + \text{OH}^\bullet + \text{H}^+$	1) Sludge disposal problem formed during the process. 2) Continuous supply of feed chemicals are required. 3) Process is expensive

3. Heterogeneous photocatalysis

In recent two decades, (heterogeneous) photocatalysis has emerged as an efficient technology to purify air and water (Pera-Titus *et al.*, 2004; Mahmoodi *et al.*, 2006; Vohra *et al.*, 2006; Fujishima *et al.*, 2007; Wang X *et al.*, 2009). Heterogeneous photocatalysis means that the reactants and the photocatalyst are present in two or more phases. The basis of photocatalysis is the photoexcitation of a semiconductor solid as a result of the absorption of radiation, often but not exclusively in the near ultraviolet spectrum. Under near UV irradiation, a suitable semiconductor material may be excited by high energy photons

producing conduction band electrons and valence band holes. These charge carriers are able to induce reduction or oxidation, respectively, and react with both water and organic compounds. The holes are extremely oxidants and should thus be able to oxidize almost all chemicals, as well as water, resulting in the formation of hydroxyl radicals (Herrmann, 1999; Malato *et al.*, 2002; Detlef, 2004; Herrmann *et al.*, 2007; Mills and McFarlane, 2007; Allen *et al.*, 2008; Gaya and Abdullah, 2008).

3.1. Semiconductor system

The Semiconductors are substances with electronic structure characterized by a filled valence band and an empty conduction band. The energy difference between the conduction band and the valence band is called band gap energy. If an incident photon with energy equal or larger than the band gap energy reaches the semiconductor surface, an electron is promoted from the valence band to the conduction band leaving a hole behind it (Fox and Dulay, 1993; Hoffmann *et al.*, 1995; Serpone, 1995). Figure I-11 shows that the band gap energy is the main factor that defines the kind of substances; conductor, semi-conductor or insulator. The surface containing electrons and holes generates $\cdot\text{OH}$ radicals and other radicals formed by the oxidation of oxygen, water, or hydroxide ions. Direct oxidation of the pollutant may be possible by photo induced holes. Several UV/semiconductor systems have been used for the photocatalytic degradation of organic pollutants. Most of these semiconductor particles have photocatalytic properties (Bessa *et al.*, 2001; Salem, 2003; Byrappa *et al.*, 2006; Colon *et al.*, 2007) such as the metal oxides, TiO_2 , WO_3 , ZnO , and Fe_2O_3 . Table I-4 summarizes the most common semiconductors employed as photocatalysts, their band gap energies (E_{bg}) and respective wavelength sensitivity. Among the semiconductors reported in Table I-4, TiO_2 generally exhibits the highest photocatalytic activity in a wider range of environmental applications.

Table I-4
Band gap energy and wavelength sensitivity of semiconductors (Stumm, 1992)

Semiconductor	E_{bg} (eV)	λ (nm)
Fe_2O_3	2.3	539
TiO_2 (rutile)	3.0	413
TiO_2 (anatase)	3.2	388
WO_3	2.8	443
ZnO	3.2	388

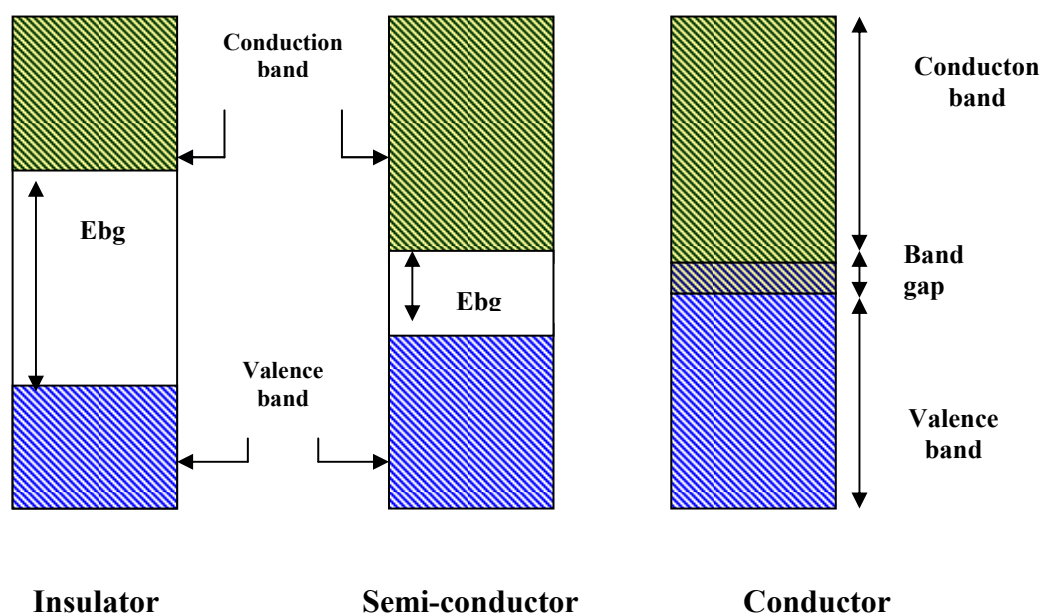


Fig.I-11. Configuration of the electronic bands of conductor, semi-conductor and insulator materials.

3.2. Titanium Dioxide (TiO₂) Photocatalyst

TiO₂ is an opaque white pigment. This has been widely used to make products as diverse as paper, plastics, lipstick, toothpaste, and pharmaceutical tablets (Frazer, 2001). Moreover, TiO₂ nanoparticles of 10-50 nm can be used in various applications, such as self-cleaning window glass, air and water purification systems.

According to IUPAC (International Union of Pure and Applied Chemistry), photocatalysis is defined as a catalytic reaction involving light absorption by a catalyst or by a substrate (Verhoeven, 1996). In 1972, Fujishima and Honda discovered the photocatalytic splitting of water on TiO₂ electrodes. Since then, intensive research efforts in understanding the fundamental processes and in enhancing the photocatalytic efficiency of TiO₂ have been displayed. In recent years, environmental cleanup applications have been one of the most active areas in heterogeneous photocatalysis. This is inspired by the potential application of TiO₂-based photocatalysts for the total destruction of organic compounds in polluted air and wastewaters without consumption of any chemical product (Fujishima *et al.*, 2000; Tryk *et al.*, 2000).

TiO₂ is the most extensively studied material for photocatalysts because of its strong oxidizing power, low toxicity, and long-term photostability (Li *et al.*, 2006; Zheng *et al.*, 2010). TiO₂ exists mainly in three polymorphs in nature, anatase (tetragonal, space group I41/amd), rutile (tetragonal, space group P42/mnm), and brookite (orthorhombic, space group Pbca) (Bakardjieva *et al.*, 2006). Among these crystal structures, rutile and anatase are commonly used in photocatalysis, whereas brookite is not photoactive. Generally, anatase phase is considered to have higher photoactivity than other phases (Wang *et al.*, 2007a).

The lattice structure of rutile and anatase can be described in terms of chains of TiO₆ octahedra as illustrated in Figure I-12. Rutile and anatase have similar crystal structures that are both tetragonal. The two crystal structures differ by the distortion of each octahedron and by the assembly pattern of the octahedral chains. Each Ti⁴⁺ ion is surrounded by an octahedron of six O₂⁻ ions. The octahedron in rutile is not regular, showing a slight orthorhombic distortion. The octahedron in anatase is significantly distorted so that its symmetry is lower than orthorhombic (Diebold, 2003). The difference in lattice structure of anatase and rutile causes different density and electronic band structure leading to different band gap. Therefore, the absorption thresholds correspond to 388 and 413 nm wavelength for the anatase and rutile phases, respectively.

The photocatalytic activity of two forms of TiO₂, anatase and rutile, are significantly different due to the band gap of anatase is 3.2–3.3 eV, slightly wider than that of rutile (3.0–3.1 eV), the conduction band edge of anatase being about 0.2 eV higher than that of rutile (Kawahara *et al.*, 2002).

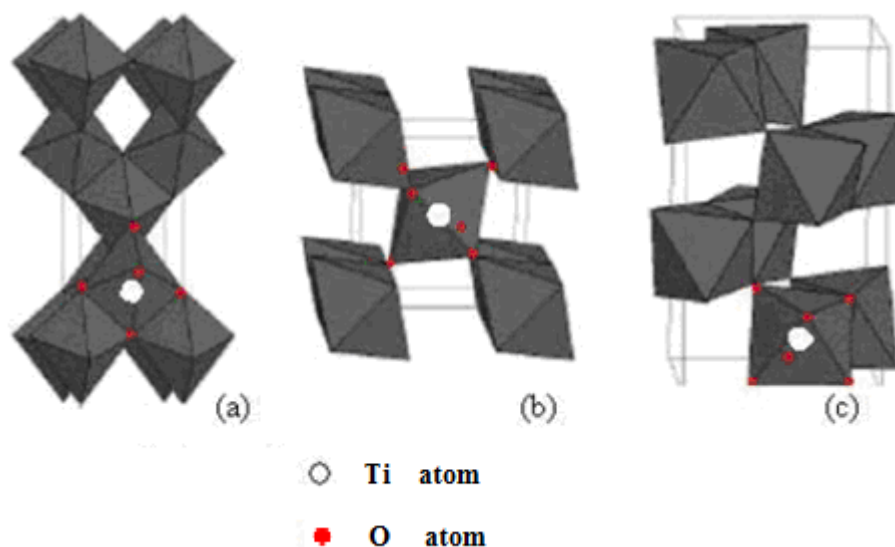


Fig. I-12. Crystallographic forms of TiO_2 : (a): anatase; (b): rutile; (c): brookite.

3.2.1. Mechanism of UV/ TiO_2 photocatalysis

As for classical heterogeneous catalysis, the overall process can be decomposed into five independent steps (Herrmann, 1999) :

1. Transfer of the reactants from the fluid phase to the surface
2. Adsorption on the TiO_2 surface
3. Reaction of the adsorbed molecules
4. Desorption of the reaction products
5. Transfer of the products from the interface region to the solution

The mass transfer steps (1) and (5) depend on reactant/product concentration as well as photocatalyst loading and particle size. Steps (2), (3), and (4) depend on the chemical compatibility of reactant and product molecules with the active sites. One of these steps will control the overall reaction rate. It is essential to understand which is controlling so that the photocatalyst or operating conditions can be varied to obtain optimum performance.

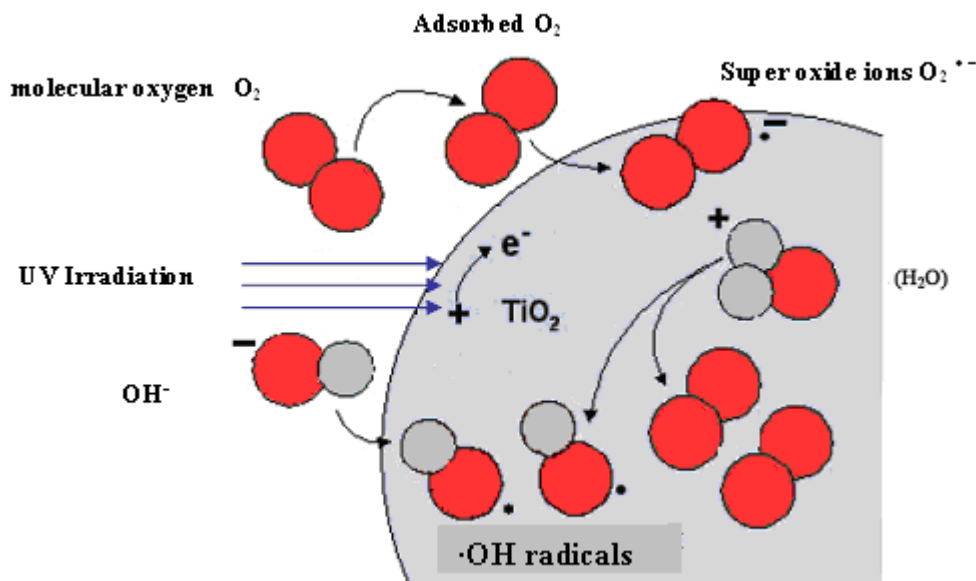
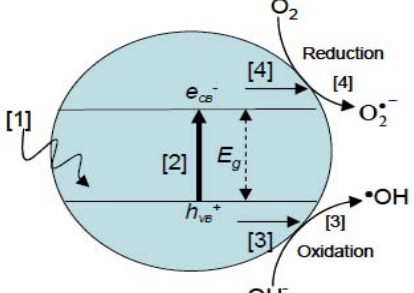


Fig.I-13. Formation of hydroxyl radicals and superoxide ions on the TiO_2 surface (Huchon, 2002).

The photocatalytic reaction occurs in the step (3); upon absorption of a photon, TiO_2 acts as photocatalyst forming a hole and an electron which produce reactive radicals (mainly $\cdot\text{OH}$ radicals). The hole reacts with water to generate the hydroxyl radical and the electron can reduce molecular oxygen, hydrogen peroxide or some other oxidizing agent in the solution or over the TiO_2 surface. This creates the reactive radicals responsible for the removal of hazardous components and may totally mineralize them (Table I-5 and Figure I-13).

Several steps are involved in photochemical mechanisms in solid TiO_2 . These steps are described in details by Hoffmann *et al.* (1995), de Lasa *et al.* (2005), Tompkins *et al.* (2005) and Naeem and Feng (2009). Firstly, the light energy ($h\nu$), greater than the band gap energy (E_g), strikes the surface of the catalyst and excites an electron from the valence band to the conduction band. A valence-band hole, $\text{VB } h^+$, is created, which migrates to the surface and initiates a reduction reaction. The valence-band hole and conduction-band electron can recombine in the bulk material and on the surface

Table I-5Mechanism steps of photochemical oxidation reaction on the TiO₂ surface.

<p>Schematic mechanism</p>	
<p>(a) Charge-carrier generation $\text{TiO}_2 + h\nu \rightarrow \text{TiO}_2 (h^+ + e^-)$</p>	<p>[1] Incident light energy photon ($h\nu$) greater than band gap energy, E_g (3.2 eV for TiO₂),</p> <p>[2] It excites electron from valence band to conduction band leaving a hole in the conduction band.</p>
<p>(b) Charge-carrier trapping Production of hydroxyl radicals</p> $H_2O_{ads} \rightarrow OH_{ads}^- + H_{ads}^+ \quad (\text{oxidative reaction})$ $h_{VB}^+ + OH^- \rightarrow \bullet OH$ <p>Production of super-oxide</p> $e_{CB}^- + O_2 \rightarrow O_2^{\bullet -} \quad (\text{reductive reaction})$	<p>[3] valence-band hole that successfully migrates to surface initiates oxidation reaction (Hoffmann <i>et al.</i>, 1995; Villarreal <i>et al.</i>, 2004).</p> <p>[4] conduction-band electron that successfully migrates to surface Initiating reduction reaction (Garcia and Takashima, 2003; Carp <i>et al.</i>, 2004; Lifongo <i>et al.</i>, 2004).</p>
<p>(c) Charge-carrier recombination $e^- + h^+ \rightarrow \text{TiO}_2 + \text{heat}$</p>	<p>The recombination of e^--h^+ pairs is reported as the main factor for limiting the oxidation rate of organic substrates.</p>
<p>(d) Photocatalytic degradation Pollutant + $OH\cdot \rightarrow POH\cdot$</p> $POH\cdot + (O_2, H_2O_2, OH\cdot) \rightarrow nCO_2 + mH_2O$	<p>Hydroxyl radicals and superoxide ions produced from steps [3] and [4] can attack any organic compound and can lead to chemical reactions (Redox) (Hoffmann <i>et al.</i> 1995; Doll and Frimmel, 2004).</p>

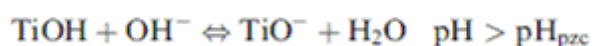
3.2.2. Factors affecting TiO₂ Photocatalyst

As previously discussed, there are several steps required for carrying out the process of photocatalytic oxidation. Any of those steps have the potential to limit the rate of pollutant degradation. The following factors can play an important role in enhancing or decreasing the photocatalytic process.

a. pH

The solution pH is an important variable in aqueous phase photocatalytic reactions. The pH of a solution influences adsorption and dissociation of substrate, catalyst surface charge, oxidation potential of the valence band and other physicochemical properties of the system (Shankar *et al.* 2004a,b). In accordance with Nerst's law, varying the solution pH would shift the energy of the valence and conduction band edges, by 0.059 per pH unit (at ambient temperature) (Moser *et al.*, 1991; Hoffmann *et al.*, 1995). This results in the valence band electron becoming more effective and the conduction band holes less effective at higher pH.

Additionally, the amphoteric behaviour of semiconductor titanium dioxide and the change of the surface charge properties of TiO₂ with the changes of pH values (Piscopo *et al.*, 2001; Rivera-Utrilla *et al.* 2001; Marci *et al.*, 2003) around its point of zero charge are given according to the following reactions:



For the TiO₂-P25, the pH_{zpc} is ranging from 5.8 and 6.8. In reality, the interpretation of pH effects on the efficiency of molecules photodegradation process is a very difficult task because three possible reaction mechanisms can contribute to the degradation, namely, hydroxyl radical attack, direct oxidation by the positive hole and direct reduction by the electron in the conducting band. It appears that the effect of pH on the degradation of the pollutants is variable and controversial since the positive holes are considered as the major oxidation species at low pH whereas hydroxyl radicals are considered as the predominant species at neutral or high pH levels (Augugliaro *et al.*, 2002; Lachheb *et al.*, 2002).

The pH affects significantly not only TiO₂ activity, but also changes pollutant structure (Piscopo *et al.*, 2001). For example, phenol has a pK_a of 9.95 and can be charged positively or negatively under the pH range studied; i.e., the interaction and affinity between both TiO₂ and phenol will be varied with the solution pH. So, the pH of the aqueous solution is a key factor for photocatalytic reaction and can affect the adsorption of pollutants on the photocatalyst surface, an important step for the photo-oxidation to take place (Naeem and Feng, 2009). The degradation rate of phenol decreased with the increase in pH (Silva and Faria, 2009). The highest degradation efficiency occurred at pH 5 as observed in the literature (Akbal and Onar, 2003). In aqueous media, phenol has a pK_a of 9.9 (at 25 °C); at pH < pK_a, it is in molecular form (C₆H₅OH) and at pH > pK_a the molecule undergoes deprotonation becoming negatively charged (C₆H₅O⁻, phenolate species). Similarly, Piscopo *et al.* (2001) reported that the effect of pH on the degradation rate of PHBA is not only dependent on the TiO₂ charge surface but also on the formation of hydroxyl free radicals. The PHBA is in the dissociated state at pH higher than pH = 4.48.

Moreover, low degradation rate at higher pH is attributed to the fact that when the concentration of OH⁻ ion is higher in the solution, it prevents the penetration of UV light to reach the catalyst surface (Qamar *et al.*, 2006). Furthermore, high pH favours the formation of carbonate ions which are effective scavengers of OH⁻ ions and can reduce the degradation rate (Akbal and Onar, 2003).

A pH dependence of the photocatalytic reactions has been reported for several organic compounds. For the photocatalytic degradation of Orange G, Hung *et al.* (2001) found that the degradation rate at pH 3 was twice higher than that at pH 7. Guettai and Amar (2005a) also reported that, when pH < 6 a strong adsorption of Methyl Orange on the TiO₂ particles is observed as a result of the electrostatic attraction of the positively charged TiO₂ with the dye and lead to high degradation rate. Several authors reported that the increase of pH improved the removal efficiency of humic acid and phenol in aquatic solutions (Iliev *et al.*, 2002; Yang and Lee, 2006). Similarly, Rahmani *et al.* (2008) found that phenol degradation efficiency is affected by pH, the results show that the degradation yields after 9 hr with pH= 3, 7 and 11 have been 59 %, 52 % and 83 %, respectively. Additionally, Mahalakshmi *et al.* (2009) claimed that the rate of photocatalytic degradation of aqueous propoxur solution increases when varying pH from 4 to 10.

b. Substrate concentration

Due to the fact that as the concentration of model pollutant increases, more molecules get adsorbed on the photocatalyst surface, the substrate concentration can influence the extent of adsorption and rate of reaction at the surface of the photocatalyst. It will be an important parameter for optimization between high degradation rate and efficiency (Pecchi *et al.*, 2001). Mahalakshmi *et al.* (2009) found the optimum propoxur concentration (200 mg. L⁻¹). Above this concentration, the rate decreases due to insufficient quantity of [•]OH radicals, as the formation of [•]OH radicals is a constant for a given amount of the catalyst.

Sauer *et al.* (2002) found that the degradation and mineralization efficiency of an anionic azo dye of reactive class may decrease with increasing substrate concentration. Other study (Qamar *et al.*, 2005a) noted that the degradation rate of dye increased with the increase in substrate concentration from 0.125 to 0.75 mM. A further increase in substrate concentration from 0.75 to 1 mM led to a decreased photocatalyst degradation. This may due to the fact that as the initial concentration of the dye increased, the colour of the irradiating mixture became more and more deep, which prevents the penetration of light to the surface of the photocatalyst (Wang *et al.*, 2007a). Similar observations were also reported for other pollutants (Wang K-H *et al.*, 2009). From Silva *et al.* (2007), the time needed to achieve nearly complete TPh (total phenols) removal of synthetic solution containing 13 organic compounds typically found in olive mill wastewaters by 0.75 g TiO₂/L catalyst loading expectedly increases with increasing initial concentration: 15 min at 163 mg/L and rises to 60 min at 650 mg/L.

Similarly, many authors (Zhu *et al.*, 2000; Epling and Lin, 2002; Konstantinou and Albanis, 2004) reported that the photo generation of holes or [•]OH radicals on the catalyst surface is reduced since the active sites are covered by dye ions. Another possible cause is the UV screening effect at a high dye concentration since a significant amount of UV may be absorbed by the dye molecules rather than the TiO₂ particles and then reduces the efficiency of the catalytic reaction.

c. Light intensity

Apparently, light irradiation plays a significantly important role in all of the photocatalytic reactions and determines the number of created e⁻-h⁺ pairs. Accordingly, increasing the incident photon rate would result in an increase in the photocatalytic reaction

rate. For a simple set of reactions including only charge-carrier generation, recombination, reduction and oxidation, it is easily derived that at low light intensity and correspondingly low carrier concentrations, the rate of oxidation of a particular compound is proportional to light intensity. This phenomenon indicates that high photon flux increases the probability of collision between photons and activated sites on the catalyst surface and enhances the rate of photocatalytic reaction.

The rate of photon absorption, and hence the initial reaction rate, follows a power law dependency on the incident UV light intensity. However, the limited surface area of catalyst particles and the diffusion rate of species involved in the reaction will reduce the efficiency of photons in inducing the oxidation reaction. It is well-documented in the literature that for heterogeneous photocatalysis, the dependence of the kinetic constant on the radiation intensity has been reported to follow a nonlinear relationship of the form:

$$r_{initial} \propto I^p \begin{cases} \text{weak light intensity: } (p = 1) \\ \text{medium light intensity: } (0.5 \leq p \leq 1) \\ \text{strong light intensity: } (p = 0.5) \end{cases}$$

Where I is the UV light intensity and p is the power-law dependency (Turchi and Ollis, 1990; Hermann, 1999; Zang and Farnood, 2005; Coleman *et al.*, 2005).

Several studies (Gogate and Pandit, 2004; Silva *et al.*, 2007) reported that the reason for the square root relationship has been explained by bulk recombination of e^- - h^+ pairs within the catalyst particles. Furthermore, at sufficient high light intensity levels, the collision between photons and the activated sites approaches its limit, and further increase in the light intensity will have no effect on the reaction rate.

Mahalakshmi *et al.* (2009) reported that the rate of degradation of propoxur increases with the increase in light intensity. When the intensity of incident light increases, the probability of excitation of electrons also increases and hence increases the degradation rate (Mehrotra *et al.*, 2003). Ling *et al.* (2004) studied the effect of incident light on the photodegradation of MB; it was found that the residence time of 15.2 min was required for 50 % photodegradation of 40 ml/L MB using 1.5 mWcm^{-2} light intensity, whereas 11 min was needed by using 5 mWcm^{-2} of light intensity. Chiou *et al.* (2008a) found an acceptably good

linear correlation exists between the apparent first- order rate constant of phenol photodegradation by TiO₂ and light intensity under the UV light intensity ranges of 20–400 W.

d. Temperature

Due to the photonic activation process, temperature has nearly no effects in the range ($20\text{ }^{\circ}\text{C} \leq T \leq 80\text{ }^{\circ}\text{C}$). At very low temperatures below $0\text{ }^{\circ}\text{C}$ or at very high temperature above $80\text{ }^{\circ}\text{C}$, the photocatalytic activity decreases. Thus, a photocatalytic experimental setup does not require severe temperature control. Accordingly, no significant effect of temperature increased from $30\text{ }^{\circ}\text{C}$ to $50\text{ }^{\circ}\text{C}$ was observed either for photodegradation of MB (Ling *et al.*, 2004) or of humic acid in the temperature range of $10\text{--}68\text{ }^{\circ}\text{C}$ (Palmer *et al.*, 2002).

Nevertheless, several works discussed on the secondary temperature effects. A slight benefit by using higher temperature for photocatalytic reactions was demonstrated by Trillas *et al.* (1995) and Chen and Ray (1998). It would be due to faster diffusion of $\cdot\text{OH}$ from the surface of the TiO₂ to the pollutant at higher temperature. However, a negative effect of temperature on the concentration of dissolved oxygen in the solution may be expected. Dissolved oxygen levels below a certain point may allow for electron-hole recombination at the surface of the TiO₂. Electron-hole recombination is dominant unless there is an electron acceptor such as oxygen available to absorb the excited electron. More importantly, a temperature increase will induce species desorption from the TiO₂ surface, decreasing the rate of reaction at low species concentrations (Chin *et al.*, 2006).

e. Photocatalyst dosage

It is well documented that the initial rates of reaction are directly proportional to the mass (m) of catalyst (Prakash *et al.*, 2002; Rabindranathan *et al.*, 2003; Lathasree *et al.*, 2004; Shankar *et al.*, 2004a). However, above a certain value of m , the reaction rate levels off and becomes independent of mass (Fig.I-14).

The increase in the efficiency seems to be due to the increase in the total surface area (namely number of active sites) available for the photocatalytic reaction as the dosage of photocatalyst increased. However, when TiO₂ was overdosed, the number of active sites on the TiO₂ surface may become almost constant because of the decreased light penetration *via* shielding effect of the suspended particles (Burns *et al.*, 2002; Sobczynski *et al.*, 2004) and the loss in surface area caused by agglomeration (Chen *et al.*, 2007).

In any given application, an optimum photocatalyst concentration has to be found in order to avoid excess photocatalyst and ensure total adsorption of efficient photons (Qamar and Muneer, 2005). Furthermore, according to Kabir *et al.*, (2006) and Naeem and Feng (2009), phenol degradation decreases above the optimum TiO₂ loading. The optimal photocatalyst loading or effective optical penetration length, under given conditions, is then very important in designing a slurry reactor for efficient use of the photocatalyst and the reactor volume.

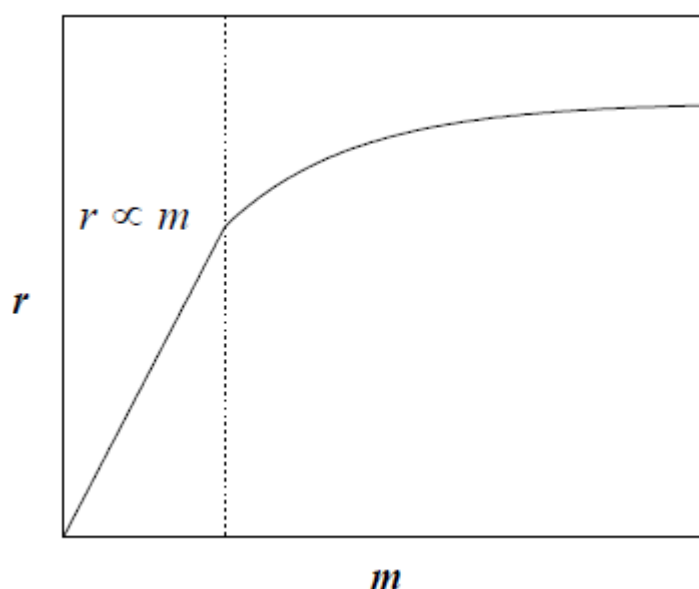
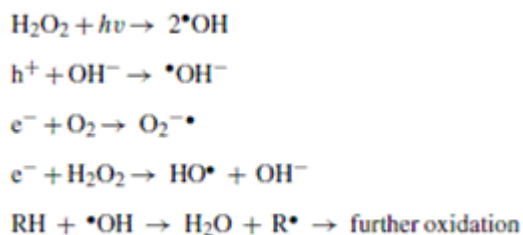


Fig.I-14. Influence of the mass of catalyst on the reaction rate, r .

f. Effect of electron acceptors

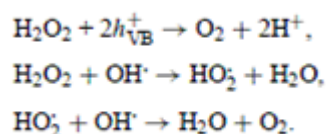
One practical problem in using TiO₂ as photocatalyst is the energy lost in the electron hole recombination which results in low degradation efficiency. Hence the prevention of electron hole recombination becomes very important. Molecular oxygen has been employed as an effective electron acceptor in most photocatalysis applications (Augugliaro *et al.*, 1991; Gupta and Tanaka, 1995). In heterogeneous photocatalytic reaction, molecular oxygen (air) has been used for this purpose as an electron acceptor for prevention of electron hole recombination. One approach used to prevent electron hole recombination is to add electron acceptors into the reaction media. The presence of H₂O₂ as electron acceptor can serve as electron scavengers to prevent the recombination and enhance photodegradation efficiency. H₂O₂ has several effects including: (a) avoid recombination of electron-hole by accepting the conduction band electron and (b) increase the concentrations of the hydroxyl radical

(Aceituno *et al.*, 2002; Burns *et al.*, 2002; Chu and Wong, 2003; Bertelli and Selli, 2006; Mahmoodi *et al.*, 2006).



Where, RH refers to phenolic compound.

Furthermore, the enhanced degradation rate observed with H_2O_2 is probably due to direct photolysis by UV light. This generates $\cdot\text{OH}$ radicals, which are likely to be dominant rate improving mechanism in the process. H_2O_2 has two hydrogen atoms bounded to oxygen atoms (H–O–O–H), thus it is more electropositive than O_2 , suggesting that H_2O_2 is a better electron acceptor than oxygen (Chen and Liu, 2007). However, when present at high concentrations, H_2O_2 also becomes a scavenger of both the valence band holes and hydroxyl radicals as follows (So *et al.*, 2002).



Electron scavenging and the consequent e^- - h^+ recombination suppression can also be achieved by the use of other inorganic oxidants such as $\text{S}_2\text{O}_8^{2-}$ and BrO_3^- (Naeem and Feng, 2009).

3.2.3. TiO_2 support

Over the past few decades, the scientific and engineering interest in the application of heterogeneous photocatalysis by using TiO_2 powder for the decomposition of organic hazardous materials in water has grown exponentially. However, there are some drawbacks of the practical use of the powder TiO_2 during the photocatalytic process (Sopyan *et al.*, 1996): (1) separation of TiO_2 powder from water is difficult; (2) the suspended TiO_2 powder tends to aggregate especially at high concentrations (Araña *et al.*, 2003b). Therefore, to solve these problems, much attention has been paid to the development of supported TiO_2 (Chun *et al.*, 2001; Hosseini *et al.*, 2007). Several studies have been published on the effect of the characteristics of the supported TiO_2 photocatalysts, such as crystal structure (Song *et al.*,

2006), crystal size (Zhang *et al.*, 2005a; Chen and Dionysiou, 2006), TiO₂ loading (Zhang *et al.*, 2006b), specific surface area (Chen and Dionysiou, 2006), and thickness of film (Jung *et al.*, 2005) on their reactivity to obtain the best photocatalyst or optimize the operation parameters of the photocatalyst preparation process. Obviously, only TiO₂ on the external surface of the support can be excited by light and induce the photocatalytic reaction, so the concentration of TiO₂ on the external surface of the support is a very important parameter of the supported TiO₂ photocatalyst (Jung *et al.*, 2005; Zhang *et al.*, 2005a,b,c).

Many supporting materials and coating methods were proposed for degradation of several organic compounds (Pozzo *et al.*, 1997). One possible way was the use of materials such as silica, alumina, zeolites or clays (Tanguay *et al.*, 1989), but no improvement of photo-efficiency was observed.

Among these particle supports, activated carbon (AC) is very promising for three reasons: (1) activated carbon is able to adsorb the pollutants and then release them onto the surface of TiO₂. Consequently, a higher concentration of pollutants around the TiO₂ than that in the bulk solution is created leading to an increase in the degradation rate of the pollutants (Tsumura *et al.*, 2002; Tryba *et al.*, 2003; Matos *et al.*, 2009); (2) the charge transference between TiO₂ and activated carbon can cause an acidification of TiO₂ surface hydroxylic groups. This will enhance the interaction between some pollutants and TiO₂ to further promote the degradation. Moreover, the ability to absorb visible light of the supported TiO₂ is also enhanced (Arana *et al.*, 2003a,b); and (3) the intermediates produced during degradation can be also adsorbed by activated carbon and then further oxidized. Other authors (Herrmann *et al.*, 1999; Matos *et al.*, 2001) have reported a synergistic effect for AC-supported TiO₂ systems, referring to remarkable effects in the kinetics of pollutant degradation, each pollutant being more rapidly photodegraded in the mixed system which contained activated carbon. This so called synergetic effect has been explained by the formation of a common contact interface between the different solid phases, in which AC acts as an efficient adsorption trap to the organic pollutant, which is then more efficiently transferred to the TiO₂ surface, where it is immediately photocatalytically degraded by a mass transfer to the photoactivated TiO₂ (Ao and Lee, 2003; Chiang and Huang 2001; Arana *et al.*, 2003; Tryba *et al.*, 2003; Colon *et al.*, 2004; Ingaki *et al.*, 2004; Tao *et al.*, 2005 & 2006; Wang *et al.*, 2007a). A mechanism for the enhanced activity of TiO₂/AC was illustrated in Fig. I-15 (Liu *et al.*, 2007; Lu *et al.*, 2010).

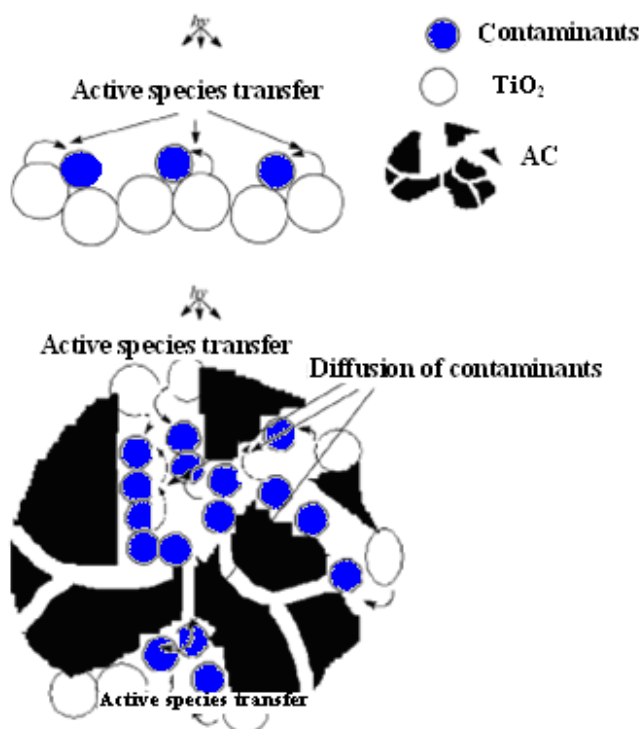


Fig.I-15. Role of AC in the enhanced activity of TiO₂ (Liu *et al.*, 2007).

Zainal *et al.* (2008) reported that the removal efficiency of Methylene Blue by using immobilised TiO₂/AC was found to be two times better than the removal by immobilised AC or immobilised TiO₂ alone. Similarly, Liu *et al.* (2006) cited that TiO₂/AC composite was much more active than P-25 for phenol degradation and exhibiting good decantability, less deactivation after several runs and less sensitivity to pH change. Moreover, Arana *et al.*, (2003b) reported that AC could perform an acidification of surface hydroxylic groups in the supported TiO₂ with the hydroxylic groups in TiO₂ supported on AC being more acidic than those in the bare-TiO₂ (P25). Since the intermediates are alkaline, they could interact strongly with TiO₂/AC to give further degradation of the intermediates. In addition, AC has a large capability of adsorbing the intermediates preventing them from dissolving into the bulk solution in the case of TiO₂/AC. Thus chain photodecomposition reactions can be preceded with the intermediates mineralized. On the contrary, the use of powder TiO₂ would allow the dissolution of some intermediates into solution and the dissolved intermediates can be decomposed further only when they collided with TiO₂ again.

Several authors argued that the development of TiO₂ photocatalysts anchored on supporting AC materials with large surface areas, by which dilute polluted substances could be adsorbed would be of great significance, not only to avoid the disadvantages of filtration

and suspension of fine photocatalyst particles, but also to lead to high photodecomposition efficiency for large numbers of pollutant (Yoneyama and Torimoto, 2000; Matos *et al.*, 2001; Colon *et al.*, 2003; Li *et al.*, 2006; Zhang and Lei, 2008; Zhu and Zou, 2009a; Ravichandran *et al.*, 2010). Consequently, TiO₂/AC is considered to be a promising photocatalyst for industrial applications.

Many techniques have been developed for immobilizing TiO₂ catalysts onto solid surface, for example in the past decade, various methods including sol-gel (Lee *et al.*, 2004), hydrothermal (Toyoda *et al.*, 2003), precipitation (Khan and Mazyck, 2003), dip coating (Sun *et al.*, 2006), and hydrolysis (El-Sheikh *et al.*, 2004). Recently, metal organic chemical vapour deposition (MOCVD), an extensively used surface coating technology, has been applied to the preparation of the TiO₂ photocatalyst (Mills *et al.*, 2002; El-Sheikh *et al.*, 2004; Zhang *et al.* 2005a). MOCVD production of supported catalysts offers the following advantages (Ding *et al.*, 2000; Aksoylu *et al.*, 2003): (1) the produced materials are mainly on the external surface of the support; (2) it has little effect on the porous structure of the support due to the use of gases as precursors; (3) many of the traditional steps in catalyst preparation, such as saturation, drying, and reduction can be eliminated; (4) The TiO₂ coating by MOCVD had a good adhesion on the surface of activated carbon; (5) the properties of the deposited material are easily controlled.

Consequently, MOCVD is a very promising method to prepare activated carbon supported TiO₂ photocatalyst. A high loading of TiO₂ is obviously needed in order to obtain a high catalytic efficiency. However, the deposition rate of supporting TiO₂ onto activated carbon by MOCVD is commonly very low, so a long deposition time is required to obtain a high loading of TiO₂ (Ding *et al.*, 2000 & 2001; Zhang *et al.*, 2004). Nevertheless, it is well known that a long deposition time will lead to several problems, such as destruction of the textural structure of AC and energy consumption.

These drawbacks limit the widespread use of MOCVD in the catalyst preparation on a large scale. There are two possible reasons for the low deposition rate (Moene *et al.*, 1996; Ding *et al.*, 2001; Serp and Kalck, 2002; Choy, 2003): (1) the rate of the mass transport of the precursor with a large molecular diameter from the gas phase to the surface of activated carbon, which is the first and crucial step during deposition and plays an important role in the deposition rate, is very small due to the low mesoporous surface area of activated carbon; (2)

the precursor cannot be efficiently adsorbed onto the surface of activated carbon because oxygen bearing groups on the support, which are the anchoring sites for the precursor during deposition, are not sufficient. On the other hand, a high loading of TiO₂ commonly results in the agglomeration of particles leading to the decrease in active surfaces for catalytic reaction. Therefore, it is necessary to enhance the deposition rate of TiO₂ by MOCVD as well as obtain smaller-sized particles well dispersed. A convenient way to enhance the mesopores surface area and the amount of oxygen bearing groups of activated carbon is performed by acid treatment such as HNO₃ oxidization (Figueiredo *et al.*, 1999; Aksoylu *et al.*, 2001). Therefore, the modification of activated carbon support by HNO₃ may lead to a significant increase in the deposition rate of MOCVD production of TiO₂.

4. Photocatalytic treatment of organic compounds

The presence of wide variety of organic compounds, which are toxic and stable to natural decomposition in water supplies and industrial effluents, is an ever increasing problem for the global concern. Nowadays, high concentrations of these compounds are introduced into the water system from various agricultural activities and industrial wastewater discharges such as coal gasification, resin manufacturing, oil refining, coking plants, chemical synthesis, dyes, plastics, textiles, pharmaceuticals, paper mill, herbicides and fungicides production (Wang *et al.*, 2009; Yang *et al.*, 2009).

Conventional water treatment technologies such as solvent extraction, activated carbon adsorption, and chemical treatment process such as oxidation by ozone (O₃) often produce hazardous by-products and generate large amounts of solid wastes, which require costly disposal or regeneration method (Venkatachalam *et al.*, 2007). Biological treatment is often not convenient for treatment of phenolic wastewater as its toxicity may cause the phytotoxic effect on the active microorganisms (Robert and Malato, 2002). Due to these reasons, considerable attention has been focused on complete oxidation of organic compounds to harmless products such as CO₂ and H₂O by the advanced oxidation process (AOP) that appears to be the most emerging technology recently (Liotta *et al.*, 2009). Photocatalytic degradation of such organic pollutants with TiO₂ semiconductor has been proved to be the most efficient and popular method because it is a stable and low-cost photosensitized material (Lathasree *et al.*, 2004; Barakat *et al.*, 2005; Colon *et al.*, 2006; Fabbri *et al.*, 2006). A list for different organic compounds being treated by the heterogeneous photocatalysis is reported in Table I-6.

Table I-6

Photocatalytic degradation of different organic compounds by heterogeneous photocatalysis (Gaya *et al.*, 2008)

Compound	Results and observation	reference
Aldehyde (Acetaldehyde)	mineralisation using film of F-TiO ₂	Kim and Choi (2007)
Carboxylic acid (phenoxyacetic acid and 2,4,5-phenoxyacetic acid)	Degussa P-25 was more efficacy than Millennium PC500	Singh <i>et al.</i> (2007)
Chloroanilines (2-Chloroaniline)	Using UV/TiO ₂ /H ₂ O ₂ system, slow degradation rate, at low pH, excess of H ₂ O ₂ decreased the degradation	Chu <i>et al.</i> (2007)
Chlorocarboxylic acid (Monochloroacetic acid)	UV/ O ₃ system, O ₃ increases the degradation by its decomposition by UV	Mas <i>et al.</i> (2005)
Phenols (Phenol)	TiO ₂ is not favourable when the concentration is more than 100 ppm	Pelizzetti and Minero (1993)
Fluorophenols (4-Fluorophenol)	The efficiency of oxides was in the following order: IO ₄ ⁻ > BrO ₃ ⁻ > S ₂ O ₈ ²⁻ > H ₂ O ₂ > ClO ₃ ⁻ and Mg ²⁺ > Fe ³⁺ > Fe ²⁺ > Cu ²⁺	Selvam <i>et al.</i> (2007)
Chlorophenols (2,4Dichlorophenol)	UV/TiO ₂ (Degussa P-25)	Bayarri <i>et al.</i> (2005)
Herbicides (Isoproturon)	UV/TiO ₂ (Degussa P-25); degradation rate increased by addition of electron acceptor	Haque and Muneer (2003)
Pharmaceutical (Tetracycline)	Solar photocatalysis; degradation rate follows the pseudo-first order.	Reyes <i>et al.</i> (2006)
Ketones (Acetone)	UV/TiO ₂ ; UltraSonic has insignificant effect on acetone photooxidation	Vorontsov <i>et al.</i> (2000)
Ethers (Methyl tert-butyl ether; MBTE)	acetone, <i>tert</i> -butyl formate and <i>tert</i> -butyl alcohol were recorded as intermediates	Bertelli and Selli (2004)

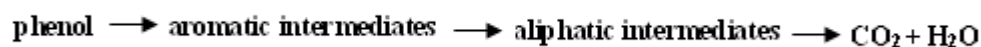
4.1. Phenols

Phenols are considered as priority pollutants since they are harmful to organisms at low concentrations and many of them have been classified as hazardous pollutants because of their potential to harm human health. It should be noted that the contamination of drinking water by phenols, at even a concentration of 0.005 mg L^{-1} could bring about significant taste and odour problems making it unfit for use. A representative of this class of compounds is phenol. Sources of phenol include the discharges of chemical process industries such as coal gasification, polymeric resin production, oil refining, coking plants, paper mill, herbicides and fungicides production (Kahru *et al.*, 1998). Human consumption of phenol-contaminated water can cause severe pains leading to damage of capillaries ultimately causing death. Phenol containing water, when chlorinated during disinfection of water also results in the formation of chlorophenols. Advanced oxidation processes (AOPs), being able to solve the problem of phenol destruction in aqueous systems were more and more checked during the last decade. Among AOPs, heterogeneous photocatalysis using TiO_2 as photocatalyst appears as the most emerging technology for phenol degradation (Grzechulska-Damszel, 2009).

4.1.1. Intermediates of phenol photodegradation

Several authors have determined the intermediates formed during this reaction and investigated their concentrations during the time (Wu *et al.*, 2001; Vione *et al.*, 2005; Andrade *et al.*, 2006; Hosseini *et al.*, 2007).

The whole process of phenol photodegradation may be simply converted into CO_2 and H_2O through three stages as follows:



To date, about twenty reaction intermediates were cited during the photocatalytic oxidation of phenol. A scheme proposed in the literature is presented in Figure (16). Seven of these intermediates were investigated: oxalic acid, formic acid, malonic acid, maleic acid (acid *cis*-but-2-ene-1,4-dioic), hydroquinone (benzene-1,4-diol), 1,4-benzoquinone, and pyrocatechol (benzene-1,2-diol). These intermediates range into two categories according to several authors in the literature: the aromatic intermediates and the aliphatic acids. Both, phenol hydroxylation products and aliphatic unsaturated acids are also reported by others as phenol destruction intermediates formed during UV irradiation in the presence of TiO_2 (Fujishima *et al.*, 2000; Ortiz-Gomez *et al.*, 2008). Sobczynski *et al.* (2004) and Ao *et al.*

(2008) reported that among these intermediates, pyrocatechol seems to be the major product. Other authors (Matos *et al.*, 2001; Zhang *et al.*, 2006a) reported that the main intermediates were experimentally identified as hydroquinone, catechol, benzoquinone and resorcinol.

In addition, significant changes in the intermediate product distributions were detected as a function of the type of AC added to TiO₂. For example, resorcinol was also quantitatively detected on TiO₂ and TiO₂-AC_{PC} (Purocarbon) but in much smaller quantities than hydroquinone or benzoquinone. Moreover, the intermediate product catechol was only detected on TiO₂-AC_M (Merk) (Matos *et al.*, 2001).

The reaction scheme (Fig. I-16) agree with the fact that the intermediates of oxidation formed by two main parallel reactions initialized by the formation of hydroquinone and pyrocatechol which will produce then 1,4-benzoquinone or 1,2-benzoquinone. Santos *et al.* (2002) reported that upon the conversion of phenol to pyrocatechol, higher rate of phenol mineralisation was obtained than through the conversion of phenol to hydroquinone or benzoquinone, because catechol oxidation yielded nothing more than oxalic acid which was further mineralized to CO₂ and water, whereas the pathways of mineralisation of hydroquinone or benzoquinone were much longer. Thus, the aromatic intermediates control the reaction pathway of phenol oxidation. Some of them, as pyrocatechol and hydroquinone, are more toxic than the phenol. However, in all cases, they are then transformed into low molecular weight carboxylic acids: maleic, fumaric, malonic, formic, oxalic and acetic acids (Guo *et al.*, 2006; Quintanilla *et al.*, 2006). As cited in the literature (Bauer and Jacques, 2001; Kanki *et al.*, 2005; Eftaxias *et al.*, 2006; Guo *et al.*, 2006; Quintanilla *et al.*, 2006), formic and oxalic acids are finally transformed into CO₂ and H₂O.

About the mechanism of the photodegradation by TiO₂, it has been reported that •OH radicals attack the phenyl ring, yielding catechol, resorcinol and hydroquinone, then the phenyl rings in these compounds break up to give malonic acid, then short-chain organic acids such as maleic, oxalic, formic, and finally CO₂ (Wang *et al.*, 1999; Wu *et al.*, 2001).

Moreover, the colour change of phenol solution during the reaction depends directly on the main reaction intermediates, the phenol oxidation resulted in coloured intermediates such as p-benzoquinone (yellow) and o-benzoquinone (red). The presence of p-benzoquinone (yellow) and hydroquinone (colorless), mixture of various reaction intermediates in the solution changed the colour to brown, revealing occasional intermolecular interactions

between quinones and dihydroxylated phenol (Mijangos *et al.*, 2006; Zhang *et al.*, 2006a; Pardeshi and Patil, 2008).

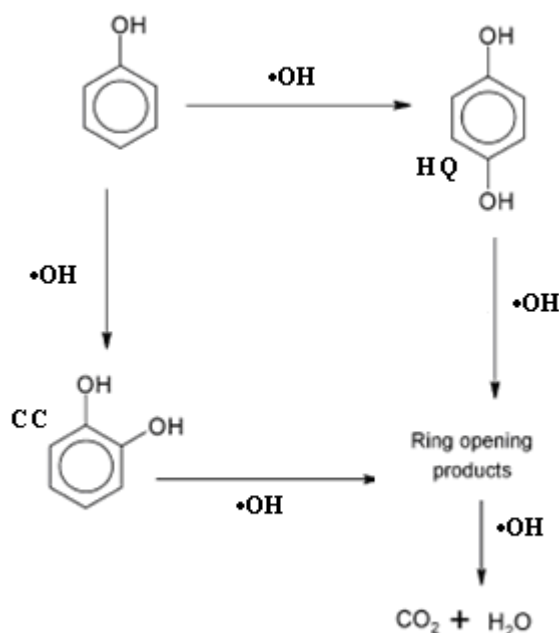


Fig.I-16. A possible reaction mechanism of phenol oxidation in the presence of illuminated TiO_2 .

By comparing other reaction pathways of phenol oxidation, the pathways of phenol wet oxidation with AC in the presence of hydrogen peroxide is represented in Figure I-17. According to this figure, phenol is hydroxylated in para position to yield hydroquinone which is oxidized in presence of H_2O_2 to p-benzoquinone. p-Benzoquinone breaks to yield CO_2 and low molecular weight acids (Eftaxias *et al.*, 2006; Quintanilla *et al.*, 2006).

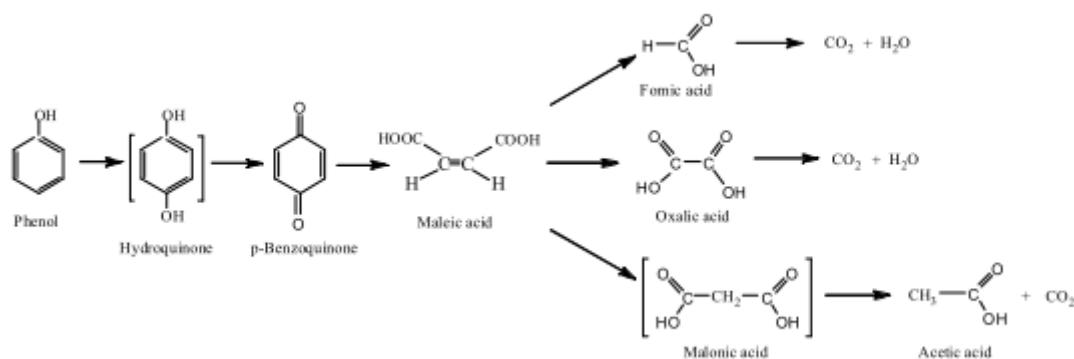


Fig. I-17. Reaction pathway for the wet oxidation of phenol with AC in presence of hydrogen peroxide.

Moreover, phenol oxidation by Fenton's reagent proceeds initially through hydroxylation of the aromatic ring to yield dihydroxybenzenes, mainly catechol and hydroquinone, which are in redox equilibrium with benzoquinones. Ring-opening of catechol gives rise to muconic acid, which is further oxidized to maleic and fumaric acids. All of the intermediates are finally oxidized to formic acid and oxalic acid, when high Fe^{2+} and H_2O_2 concentrations are used. Under these conditions, formic acid is also oxidized to CO_2 and H_2O , whereas oxalic acid shows quite refractory behaviour and remains in solution (Fig.I-18).

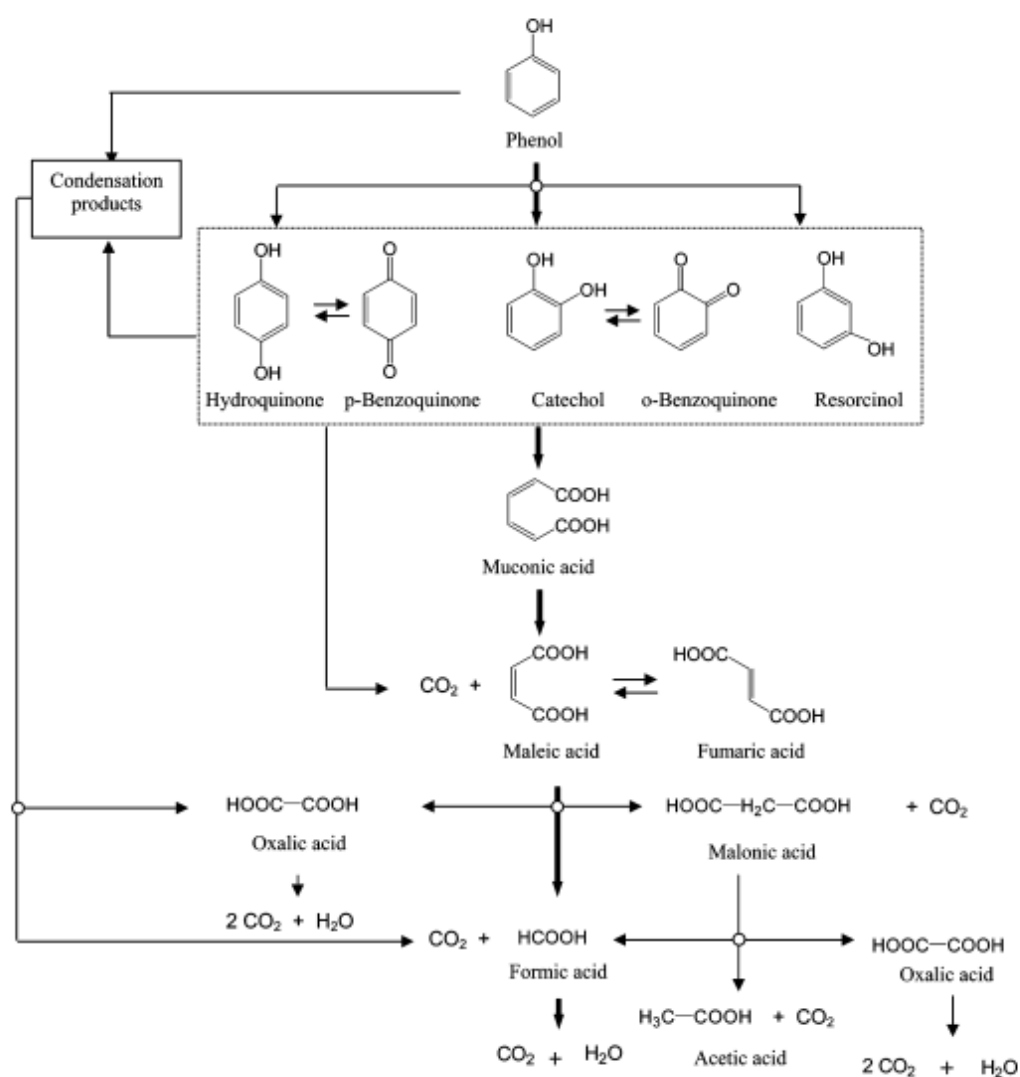


Fig. I-18. Scheme route for phenol oxidation by Fenton's reagent.

4.2. Dyes

Textile dyes and other industrial dyestuffs constitute one of the largest groups of organic compounds that represent an increasing environmental danger. About 1–20 % of the total world production of dyes is lost during the dyeing process and is released in the textile effluents (Houas *et al.*, 2001). Some dyes are toxic and even at very low concentrations may significantly affect aquatic life. Some other dyes may cause allergy, skin irritation and cancer to humans (Arami *et al.*, 2006; Yang *et al.*, 2008).

In most countries researchers are looking for appropriate treatments in order to remove pollutants, impurities and to obtain the decolourization of dye house effluents. In recent years as an alternative to conventional methods (AOPs) based on the generation of very reactive species such as hydroxyl radicals have been proposed to oxidize quickly and non selectively a broad range of organic pollutants including several dyes (Kitano *et al.*, 2007; Sano *et al.*, 2008; Khataee *et al.*, 2009a,b). Photodegradation of various classes of dyes has been often investigated (Neppolian *et al.*, 2002a,b; Ioannis *et al.*, 2004; Guettaï and Amar, 2005b; Mahmoodi *et al.*, 2006; Barka *et al.*, 2008).

Photocatalytic degradation of textile dye, Cibacron Yellow LS-R (CIY) an azo dye was carried out using semiconductor oxides by Kositzi *et al.* (2007). Similarly, Mirkhani *et al.* (2009) reported the efficiency of titanium dioxide in aqueous solution under irradiation with a 400 W high-pressure mercury lamp for photodegradation of commercial textile azo dyes (Congo red CR and Direct red DR). Several works appeared on the photocatalytic degradation properties of TiO₂ and TiO₂/AC using Methyl orange (MO) or acid fuchsine (AF) as model of dye compounds (Ruan *et al.*, 2001; Al-Qaradawi and Salman, 2002; Bing-Yu *et al.* 2007; Wang *et al.*, 2007a). Other dye, Rhodamine B (RhB), can be destroyed in aqueous suspension using TiO₂ (Asilturk *et al.*, 2006), TiO₂-coated silica (Wilhelm and Stephan, 2007), TiO₂-coated silicone (Kim and Park, 2006) and TiO₂-coated activated carbon (Li *et al.*, 2008). Moreover, Khataee *et al.* (2009a) studied complete decolorization of three commercial textile dyes (Acid Orange 10, AO10; Acid Orange 12, AO12; and Acid Orange 8, AO8) with 94% of TOC removal and claimed that the nitrogen-nitrogen double bond of the azo dyes was transformed predominantly into NH₄⁺ ions.

Tartrazine (also known as Yellow Dye No. 5) is widely used in the food industries as colouring agent. It also has a high solubility in water. Some people are extremely sensitive to tartrazine as it can cause breathing difficulties. Thus, it is crucial for tartrazine waste from the food industries to be treated with appropriate technology before being released to the environment. The degradation of tartrazine by TiO₂ was up to 80 % within two hours, which indicates that the system has the potential to be operated in a larger scale (Hashim *et al.*, 2001). Furthermore, Tanaka *et al.*, (2000) reported that Tartrazine was completely removed within 90 min whereas TOC removal was achieved within more than 200 min and its elimination rate was roughly proportional to the disappearance rate, the major intermediates being aromatic amine, phenolic compounds and several organic acids.

5. Kinetic models for photocatalysis process

Many researchers suggest that the rate of photocatalytic degradation of organic substrates can be treated empirically without consideration of detailed mechanistic steps.

5.1. Langmuir-Hinshelwood kinetic model

Langmuir-Hinshelwood kinetic model is a generally accepted expression in photocatalytic oxidation (Fox and Dulay, 1993). The model is developed based on the Langmuir adsorption isotherm under the assumptions:

- (1) The surface contains a constant number of adsorption sites,
- (2) A site can contain only one molecule,
- (3) No interaction takes place between adsorbed molecules,
- (4) Adsorption equilibrium is assumed to be established at all times.

$$r = \frac{dC}{dt} = \frac{kKC}{1 + KC} \quad (\text{I-15})$$

Where, r is the oxidation rate of the reactant (mg/L min), C the concentration of the reactant (mg/L), t the irradiation time, k is the reaction rate constant (mg/L min), and K the adsorption coefficient of the reactant (L/mg). L-H model represents a mechanism for surface catalysis in which the reaction occurs between species that are adsorbed on the surface.

Kozlova *et al.* (2004) found that the photocatalytic degradation of dimethyl phosphate, trimethyl phosphate, and triethyl phosphate can be described by Langmuir-Hinshelwood kinetic model. Similarly, this model has been used to describe the photocatalytic degradation of other compounds (Almquist and Biswas, 2001).

5.2. First-order kinetic model

When the chemical concentration C_0 is small, the equation Langmuir-Hinshelwood kinetic model can be simplified to an apparent first-order equation. Sometimes, first-order kinetic is appropriate for the entire concentration range up to few ppm.

$$\ln\left(\frac{C_0}{C}\right) = kKt = k_{app}.t \quad (\text{I-16})$$

For concentration higher than 5 mM, as KC is much larger than unity, a zero-order equation may be used.

$$\ln\left(\frac{C_0}{C}\right) = k_{app} \quad (\text{I-17})$$

Therefore, the reaction order of the simplified Langmuir-Hinshelwood kinetic model may range from 0 to 1 (Carp *et al.*, 2004).

Generally, UV/TiO₂ process is applied to degrade organic substrates with low concentrations ranging from ppb to few ppm. Therefore, the first-order kinetics can be used to simulate the degradation of organic substrates (Hung *et al.*, 2001; Rao *et al.*, 2003; Li *et al.*, 2006 & 2008; Chiou *et al.*, 2008b).

Several experimental results indicate that the destruction rates by photocatalytic oxidation of various organic contaminants over UV-irradiated TiO₂ agrees with pseudo-first-order kinetics (An *et al.*, 2002; Konstantinou and Albanis, 2003; Matos *et al.*, 2007; Tsai *et al.*, 2009). This model depends on the light intensity affected by the pollutant concentration.

Chapitre I. Revue Bibliographique

Les polluants présents dans les effluents industriels sont souvent réfractaires aux traitements biologiques qui sont pourtant économiquement les plus intéressants. Dans le but d'atteindre les performances exigées par les réglementations internationales, d'autres techniques lui sont associées comme l'adsorption ou diverses opérations d'oxydation catalytique ou non. Cette étude s'intègre dans ce contexte ; les effluents ciblés sont les effluents chargés en phénols et en colorants ; les techniques visées sont l'adsorption et l'oxydation photo-catalytique avec du TiO_2 .

Cette revue bibliographique s'est d'abord attachée à faire une synthèse des divers traitements disponibles dans le domaine de l'eau. L'accent a été mis sur les procédés d'adsorption : les mécanismes de transferts sont détaillés suivi d'un bilan succinct des caractéristiques physiques spécifiques aux adsorbants. Le charbon actif est de loin l'adsorbant le plus utilisé, ses divers modes de préparation sont présentés en commençant par la phase de carbonisation puis les différentes techniques d'activation. Cette description débute par la fabrication classique à partir de matériaux comme le bois et la noix de coco, suivi de la fabrication à partir de boues de stations d'épuration d'eaux usées. Ces traitements spécifiques ont pour objectif de conférer au charbon une structure particulière sous la forme de molécules planes de type graphène avec des fonctions de surface de nature multiples qui s'avèrent favorables ou non à l'adsorption : fonctions de type acide carboxylique, lactone, phénol, carbonyle, ether, pyrone et chromène. En fonction leur proportion relative, le charbon peut être de nature acide ou basique et sa surface peut être chargée positivement ou négativement en fonction du pH de l'effluent. Un bilan des interactions mise en jeu au cours l'adsorption des molécules phénolées a été effectué : interactions π - π dites dispersives, effet de solvant, formation de complexe donneur-accepteur, oligomérisation ou adsorption irréversible. Les performances en adsorption sont aussi liées aux différences de nature chimique et physiques des molécules ainsi qu'aux conditions opératoires. Un bilan de l'influence de ces divers paramètres a été réalisé : la solubilité, l'hydrophobicité, la nature des groupements substitués sur le noyau aromatique, la taille de la molécule, du pH, de la température, de la présence de sels. Cette étude bibliographie sur l'adsorption se termine par une présentation des modèles mathématiques en adsorption mono-constituant et multi-constituants qui seront utilisés dans la suite de ce travail : le modèle de Langmuir et le modèle de Freundlich en mono-composant ; le modèle de Langmuir généralisé et le modèle de Freundlich-Langmuir pour l'adsorption compétitive.

Dans une seconde partie, un rapide récapitulatif des différents procédés d'oxydation avancée est proposé ainsi que leurs domaines d'utilisation. Ces procédés sont particulièrement intéressants car ils produisent des radicaux hydroxyles non sélectifs qui s'attaquent à tout polluant organique. Les procédés d'oxydation avancée photochimiques sont détaillés : d'abord la photolyse homogène associée ou non à d'autres opérations comme l'ozonation ; puis la photocatalyse hétérogène en présence de divers semi-conducteurs tels que les oxydes de métaux suivants : Fe_2O_3 , TiO_2 , WO_3 et ZnO . Après avoir décrit les particularités électriques de ces matériaux sous l'action d'un rayonnement Ultra-Violet, un accent est cette fois mis sur la photocatalyse avec du dioxyde de titane TiO_2 . Ce catalyseur se présente sous deux formes cristallographiques, anatase et rutile, à l'origine de leurs différentes propriétés catalytiques. Les mécanismes mis en jeu pour produire les radicaux sont décrits suivi d'un bilan sur les facteurs pouvant affecter les performances de la photocatalyse comme le pH, la concentration, l'intensité lumineuse des Ultra-Violet, la proportion catalyseur/polluant ou la température. Ce catalyseur étant sous la forme de poudre de nanoparticules agglomérées, le principal inconvénient est qu'il s'avère difficile de le séparer du liquide après réaction. Un point a donc été fait sur les différentes formes de mise en œuvre de ce catalyseur afin de palier à ce problème de séparation. La plus grande partie des matériaux conçus sont des charbons actifs avec dépôt de TiO_2 ou imprégné de TiO_2 . Les différents modes de préparation sont brièvement indiqués. Un inventaire des performances de la photocatalyse avec TiO_2 , associée ou non à d'autres procédés d'oxydation avancée, est ensuite présenté pour un large panel de familles de molécules organiques : pesticides, médicaments ... Dans le cas des phénols, les intermédiaires formés sont essentiellement des intermédiaires aromatiques et des acides aliphaliques comme l'acide oxalique, l'acide formique, l'acide malonique et l'acide maléique. Le chemin réactionnel de dégradation du phénol par oxydation photocatalytique le plus probable est présenté et comparé à ceux proposés pour d'autres procédés d'oxydation avancée du phénol. L'étude bibliographique sur la photocatalyse se poursuit par un bilan des performances de cette technique pour les dégrader les effluents chargés en colorants. Cette revue s'achève par une description des deux modèles cinétiques les plus utilisés en spécifiant leurs conditions de validité : le modèle cinétique de Langmuir-Hinshelwood et le classique modèle cinétique du premier ordre.

CHAPTER II
MATERIALS AND METHODS

This chapter presents firstly the characteristics of the model pollutants as well as the adsorption materials and oxidizing agents. The analytical techniques for both the aqueous solutions and the solids are then detailed. Finally, the different experimental equipments are described and their operation mode are detailed:

- The device for isotherms determination
- The photocatalytic reactor of channel type operated with the Ahlstrom tissue
- The glass batch photocatalytic reactor
- The fixed bed like photocatalytic reactor

1. The model molecules, adsorption and photocatalytic materials and oxidizing agents

The study was carried out with an aromatic pollutant, phenol and a food azo-dye, tartrazine.

Several materials were used to treat these pollutants either by adsorption, photocatalysis or by a sequential process:

- The commercial activated carbons PICA F22 and S23 for adsorption,
- The sewage sludge based activated carbons for adsorption,
- The Ahlstrom tissues composed of activated carbon and TiO_2 ; AC PICA S23 with or without deposited of TiO_2 for adsorption-photocatalysis process,
- The Ahlstrom TiO_2 supported media,
- AC/ TiO_2 composite produced by CVD.

Various organic compounds were used for this work. Their characteristics are described below.

1.1. Phenol and three substituted phenols

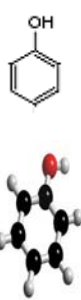
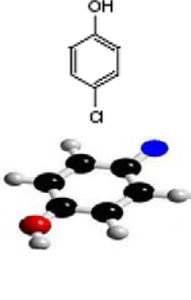
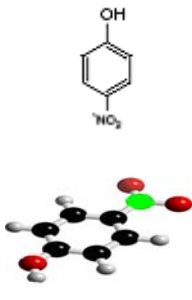
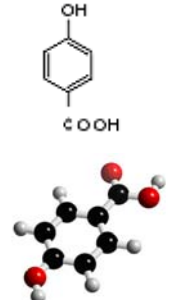
Phenol consists of an aromatic ring (aromatic hydrocarbon) and a hydroxyl function group. It is the simplest molecule of the family of phenols with a molecular weight of 94. It was supplied by Sigma Aldrich with a purity of 99 %.

The selection of this molecule as model organic pollutant results from its frequency in the residual waters coming from the diverse industries. It is also one of the most reported

aromatic pollutants in the literature and is the aromatic molecule used as model for several years in our laboratory (Suwanprasop, 2005; Creanga, 2007; Ayril, 2009).

The substituted phenols studied here are p-hydroxybenzoic acid (PHBA), p-chlorophenol (PCP) and p-nitrophenol (PNP). These molecules were selected due to their release in the residual waters from the many industries (petrochemical, pharmaceutical, paper-maker, plastic, food-processing, etc.). Furthermore, they are poorly degradable by the biological treatment and then deserve advanced oxidation processes. The present study was carried out with four organic phenols pollutants, in monocomponent and in multicomponent systems. The chemical structure and the molecular mass of four phenols pollutants studied are given in Table II-1.

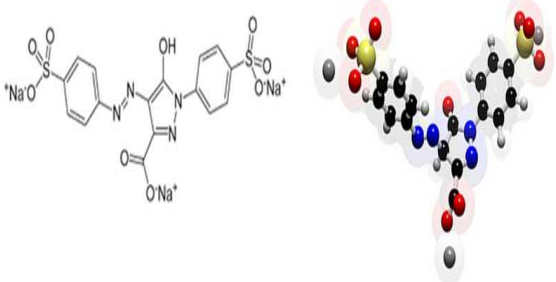
Table II-1
The physico-chemical properties of phenols studied

Properties	Phenol	p-Chlorophenol	p-Nitrophenol	p-Hydroxy benzoic acid
Symbol	P	PCP	PNP	PHBA
Molecular formula	C ₆ H ₆ O	C ₆ H ₅ OCl	C ₆ H ₅ O ₃ N	C ₇ H ₆ O ₃
Chemical structure				
pKa at 25 °C	9.89	9.37	7.15	4.58/9.23
Solubility at 25 °C (g l ⁻¹)	93	27	17	5
Log K _{ow}	1.5	2.39	1.91	1.37
Critical oxidation potential (V)	1.089 V	1.094 V	1.433 V	1.36

1.2. Tartrazine

Tartrazine is an azo-dye compound selected in this study to represent the family of dyes. It is a synthetic dye used in the food industries (E102-Yellow 5, in USA), cosmetic (CI 19140) and pharmaceutical. The physico-chemical properties of tartrazine are summarized in Table II-2.

Table II-2
The physico-chemical properties of tartrazine

Molecular formula	$C_{16}H_9N_4Na_3O_9S_2$
IUPAC name	Trinatrium-3-carboxy-5-hydroxy-1-p-sulfophenyl- 4-p-sulfophenylazo-pyrazol
Molecular mass (g.mol⁻¹)	534.36
pKa	pKa1 = 1.8 ; pKa2 = 8.3 ; pKa3 = 10.8
Fusion point (°C)	350
Boiling point (°C)	870
Solubility	Soluble in water
Chemical structure	

1.3. The activated carbons

In this work different carbons were used that can be divided in two categories: commercial AC and carbons resulting from the pyrolysis of sewage sludge (Sludge based activated carbons, SBAC).

1.3.1. Commercial activated carbon F22 and S23

These two commercial carbons were supplied by PICA and Ahlstrom. The characteristic data of these carbons are summarized in Table II-3. Some of these properties were again measured in our laboratory and all the supplementary analysis are presented in chapter III.

Table II-3

Main characteristics of commercial activated carbons studied

		F22 PICA	S23 PICA	Ahlstrom AC
Origin*		Oil	Coconut	Coconut
Specific surface*	m ² .g ⁻¹	985	1230	1065
Microporous volume*	cm ³ .g ⁻¹	0.41	0.49	0.460
Mesoporous volume*	cm ³ .g ⁻¹	0.11	0.04	0.046
Pore size diameter*	Å	20	17	-
Volume weight mean diameter : d ₄₃ (Granulometric analysis)	µm	440	447	-

*(supplier data)

1.3.2. Sewage sludge based activated carbons

The application of sludge-based carbonaceous materials has been successfully reported for adsorption (Rio *et al.*, 2005; Fan and Zhang, 2008). Through the European project REMOVALS (FP6- 018525), sewage sludge based activated carbons were synthesized by the team works of Nigel Graham and Geoff Fowler at Imperial College of London (ICL) and Laurence Le Coq and Claire Gerente in GEPEA (laboratoire de Génie des Procédés – Environnement – Agro-alimentaire , Ecole des Mines de Nantes). The fabrication of activated carbons from sewage sludge follows the same steps as the production of the commercial activated carbons : the steps of production are summarized in table II-4 and described in detail in annex 1.

Table II-4

Activated carbons resulting from the pyrolysis of municipal stations of sewage sludges

AC	Sewage sludge origin	Traitment
C_DRAW	Dewatered raw sludge (DRAW) / SA_DRAW, London	Carbonised
SA_DRAW		Steam Activated (vapor activation)
Hardened SA_DRAW		Hardened (incorporation of 5% PVA) & Steam Activated
C_DMAD	Dewatered Mesophilic Anaerobically Digested sludge (DMAD) / London	Carbonised
SA_DMAD		Steam Activated
CO ₂ A_DSBS	Dewatered Secondary Biological Sludge (DSBS) / Nantes	CO ₂ Activated

1.4. The Ahlstrom tissues

This study was carried out using three different media (tissue) provided by Ahlstrom: TiO₂ media, AC media, and AC / TiO₂ media and then compared to the original granular AC. These tissues produced by Ahlstrom Company are composed of several layers of fibres mixture of TiO₂ and SiO₂. The technique of fixation of TiO₂ on various supports was patented by Ahlström Paper Group Company (Ahlström RCC, 1998).

a. Materials used for tissue production

Titanium dioxide. The used catalyst is the titanium dioxide PC 500, supplied by Millennium. The elementary crystals, between 5 and 10 nm in diameter, of crystal anatase structure (> 99 %) with a specific surface area, S_{BET} of about 320 m².g⁻¹, are obtained after a manufacturing process called "sulphuric". The principle of this process consists of neutralization and then calcination of titanium oxysulfate solution (TiOSO₄) obtained by dissolution of concentrated titanium minerals in a bath of sulphuric acid (Petit, 2007).

The average particle diameter is $d = 1.7\mu\text{m}$, it is the average dimension of the formed agglomerates. This titanium dioxide is then used by Ahlstrom Company for producing various TiO₂ supported tissues.

Silica. The used colloidal silica has a specific surface about 700 m².g⁻¹, with particle diameter from 20 to 30 nm. It plays several roles such as inorganic binder, resistant to the effects of both ultraviolet irradiation and photocatalysis, transparent to UV and protecting to

TiO₂. Titanium dioxide forms with silica agglomerates of variable size (0.1 – 1 μm). The formation of these agglomerates decreases the risk on the human health by binding to the initial nanoparticles (Petit, 2007).

Activated carbon. AC was supplied directly by Ahlstrom Company. This granular AC made from coconut was used in all studied involving media containing carbon. It has a specific surface of 1065 m².g⁻¹, particle diameter ranging from 0.25 to 0.60 mm and is mainly microporous (0.46 cm³.g⁻¹) (Table II-3).

b. Types of media used

Media AC:

Process of fabrication: This tissue has been supplied by Ahlstrom using the proprietary Trinitex® technology. Three different mixtures of fibres have been prepared for fabricating this tissue:

- Mix.1: synthetic fibres (polyester), natural fibres (cellulose), binder (acrylic polymer) and water.
- Mix 2: natural and synthetic fibres, granular AC.
- Mix 3: natural and synthetic fibres, water and binder.

The successive layers are applied on the tissue and dried in oven. Finally, the activated carbon is trapped in the fibres between two layers of porous tissue not weaved based on synthetic and natural fibres (Fig.II-1, Table II-5).

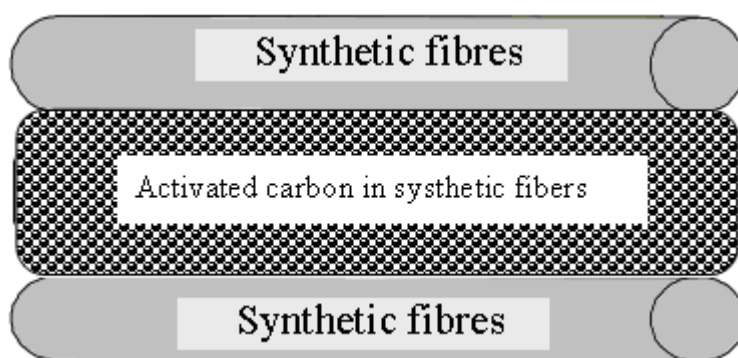


Fig.II-1. Schematic representation of media AC.

Table II-5

Composition of the activated carbon media

Material	Composition	
Media AC	Fibres: 150 g. m ⁻²	AC : 350 g. m ⁻²

Media AC / TiO₂: a mixture of TiO₂ Millenium PC 500 and SiO₂ (inorganic binder) is deposited on one side of media AC (Fig. II-2, Table II-6).

Process of fabrication: a dry mixture of TiO₂ (50%) and SiO₂ (50%) was performed and water was then added to form a paste. This paste was then applied to the AC tissue using a cylinder moving on the tissue and then dried to remove water. The diameter of silica particle is between 20 and 30 nm. The silica is called auto-bound and has the ability to form bonds during the drying leading to increased resistance of the film formed.

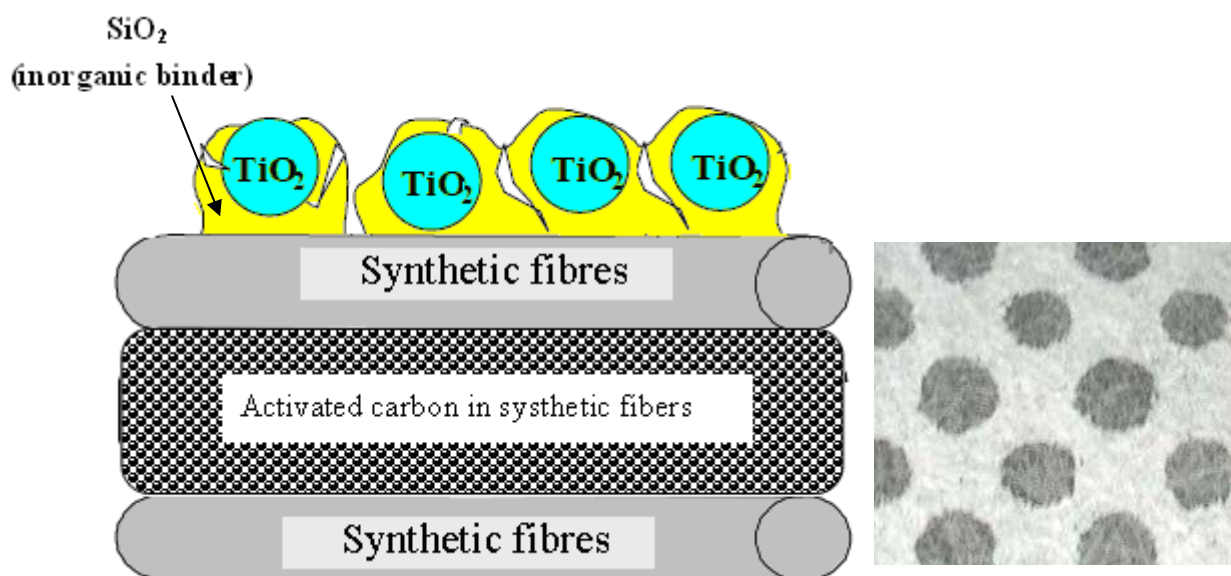
**Fig.II-2.** Schematic representation of media AC / TiO₂, composition and photo.

Table II-6
Composition of the media AC / TiO₂

Material	Composition	
Media AC / TiO ₂	Fibres: 150 g. m ⁻² SiO ₂ : 25 g. m ⁻²	AC : 350 g. m ⁻² TiO ₂ : 25 g. m ⁻²

Media TiO₂: the deposition of TiO₂ is made by the Ahlström Paper Group Company: an aqueous suspension of a mixture of TiO₂ and silica is deposited on a fibrous support. A pressure process allows the coating of fibres. The deposit is not continuous; spaces not coated in the form of circles are uniformly distributed on the surface (Fig. II-3, Table II-7).

Process of fabrication: Natural (cellulose) and synthetic (polyester) fibres are mixed with water and a small amount of binder (acrylic polymer). The mixture is then placed on the tissue and dried. A layer of TiO₂/SiO₂/water mixture is deposited on the tissue using a cylinder whose surface is composed of circular patterns, and then dried.

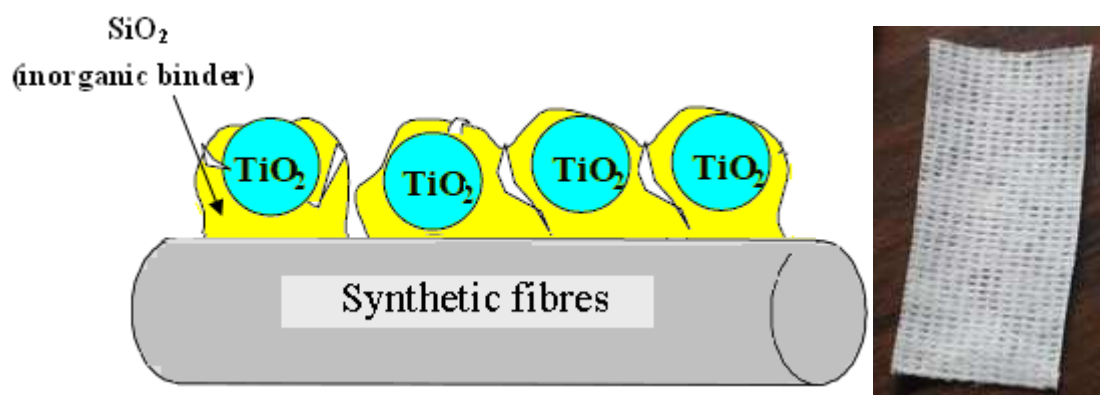


Fig.II-3. Schematic representation of media TiO₂, composition and photo.

Table II-7
Composition of the media TiO₂

Material	Composition	
Media TiO ₂	Fibres: 45 g. m ⁻² , SiO ₂ : 25.5 g. m ⁻²	TiO ₂ : 25.5 g. m ⁻²

1.5. Activated carbon coated by TiO₂

Activated carbon of type S23 has been coated with a deposit of TiO₂ obtained by a confidential process up till now made by the team work in the Laboratory of Chemical engineering of Toulouse (Cadoret *et al.*, 2010; Reuge *et al.*, 2010). TiO₂ deposition has been achieved by CVD technique; reaction implying a chemical precursor (Titanium Tetra Isopropoxide) which is decomposed to TiO₂. This material will be characterized in this study with the same techniques as the usual activated carbons reported by Duminica *et al.* (2004).

2. Analytical techniques

2.1. Analytical methods for the liquid solutions

2.1.1. High Performance Liquid Phase Chromatography or HPLC-UV

The high performance liquid chromatography (HPLC) is a technique of separation as well as qualitative and quantitative analysis of constituents (Fig.II-4).

In this technique, a fluid called mobile phase passes through a tube called column. This column can contain porous particles (filled column) or be equipped with a thin film (capillary column). The column is called stationary phase. At the initial time, the mixture to be separated is injected into the inlet of the column where it is diluted in the mobile phase which passes through the column. If the stationary phase has been well selected, the constituents of the mixture are unevenly retained during the passage through the column. From this phenomenon called retention, it results that the constituents of the injected mixture move less fast than the mobile phase. These constituents are also eluted from the column one by one and thus separated. A detector placed at the end of the column coupled with a recorder performs the chromatogram. Indeed, a constant signal on the recorder for the base line is only shown in the presence of the mobile phase; during the exit of every separated constituent, its peak time (retention time) is recorded on the detector.

In the given chromatographic conditions, the retention time characterizes qualitatively a substance. The area between a peak and the extension of the base line varies linearly with the concentration of constituents detected and isolated. The analysis of several standard solutions gives the standard curve characteristic of each constituent by plotting the peak area

versus its concentrations. From this curve, it is then possible, by measuring the area, to determine the unknown concentrations of the compounds present in the injected mixture.

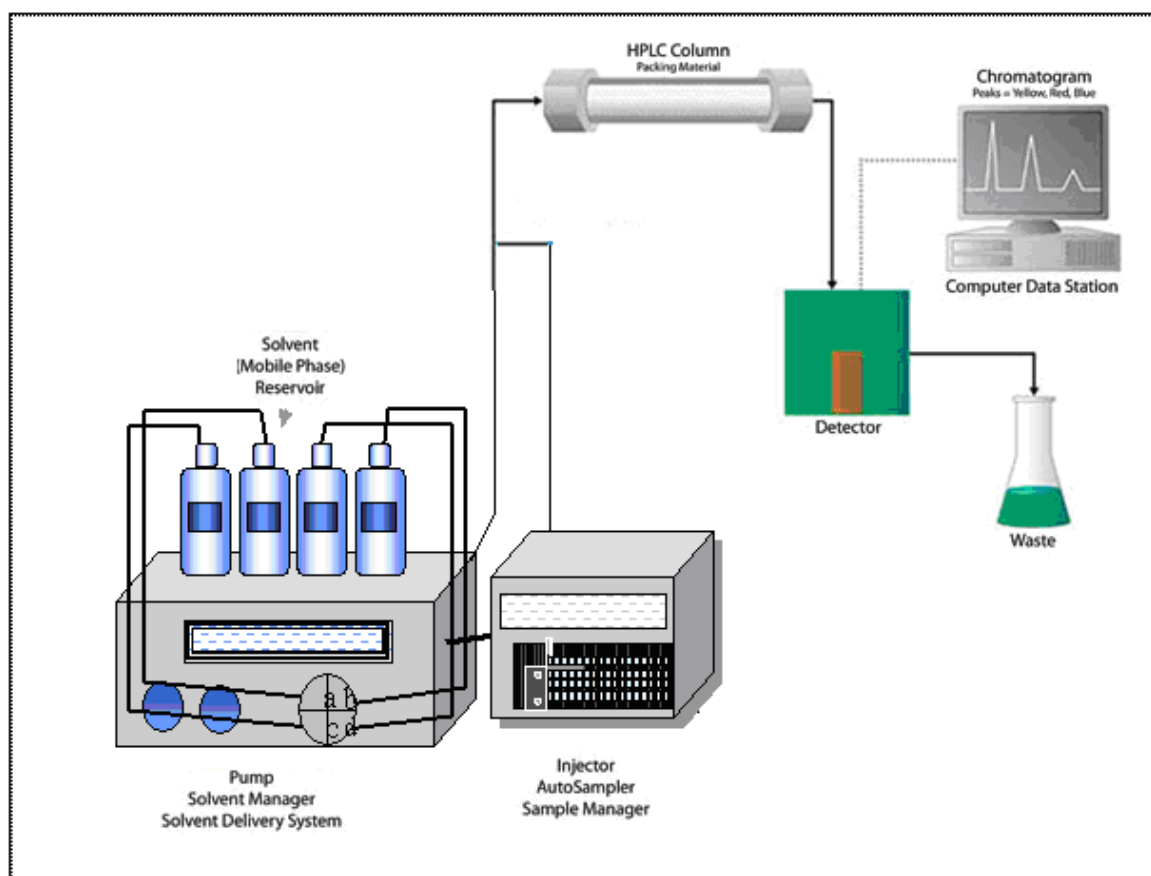


Fig.II-4. Schematic diagram of the principal technique of HPLC.

Analysis of HPLC was carried out by a chromatographic chain composed of:

- **Degazer : SpectraSystem SCM1000**
- **Injection pump: SpectraSystem P1000XR quaternary** equipped with an injection loop. It includes a gradient system for the solvent programming. It allows to perform:
 - Isocratic run, this means with an elution of constant solvent composition during all time of analysis.
 - Gradient run, this means with a variation in the concentration of the solvent mixture.

- **Chromatographic column: ProntoSIL C18, AQ of dimensions 250 x 4**, this column, thermostated at 30 °C, is composed of spherical microparticles (5 µm) of silica transplanted with alkyl chains of C18.
- **Injector: SpectraSystem AS3000**. It is an injector with sampling buckles. There are buckles of various volumes; we use a buckle of 20 µL. The selection volume of the buckle is achieved according to the size of the column and the concentration of the products to be analyzed. The system of injection loop allows a constant injected volume, this is important for the quantitative analysis.
 - **Detector: SpectraSystem UV 2000**. It measures the absorption of the light by the product at the outlet of the column. It operates at constant wavelength; this is fixed by the operator. Deuterium lamp is used at wavelengths varying from 190 to 350 nm.

The acquisition and the treatment of chromatograms are performed by the software CHROMQUEST 4.2.

Analyses were carried out using different conditions according to the treated molecule and the studied step: adsorption or oxidation. Two important types of analyses are included according to the method of analysis:

1. Analyses (fast), generally isocratic, are achieved to follow the evolution of the pollutant concentration studied during the adsorption in single solute solution.. Four aromatic pollutants (phenol, 4-hydroxybenzoic acid or PHBA, 4-nitrophenol or PNP and 4-chlorophenol or PCP) and tartrazine dye are concerned (Table II-8).
2. Gradient analyses, during the oxidation, the reaction intermediates are formed and the objective of these methods is to separate and quantify the original pollutant of the multi-component solution (Table II-9).

Table II-8

Methods of separation by HPLC for the pollutants during the adsorption process

Conditions	Adsorption process				
	PHENOLS				TARTRAZINE
	Phenol	PHBA	PCP	PNP	
Mobile phase (Aqueous/Organic)	Ultra pure water acidified by H ₃ PO ₄ (pH=2.2)/ Acetonitrile				Ultra pure water acidified by H ₂ SO ₄ (pH=1.4)/ Methanol
Method utilised : volumic composition (Aqueous/ Organic)	Isocratic : 60/40				Isocratic : 60/40
Column temperature (°C)	30 °C				
Dilution with water	Mass of analysed solution : 0.25 g / Mass after dilution: 1.5 g				
V _{injected} (µL)	10				
Flow rate (mL.min ⁻¹)	1				0.5
Wavelength (nm)	254	254	285	315	317

Table II-9

Methods of separation by HPLC for the pollutants during the oxidation process

Conditions	Oxydation Process	
	PHENOL	TARTRAZINE
Mobile phase (Aqueous/Organic)	Ultra pure water acidified by H ₃ PO ₄ (pH=2.2)/ Acetonitrile	Ultra pure water acidified by H ₂ SO ₄ (pH=1.4)/ Methanol
Method utilised : volumic composition (Aqueous/ Organic)	Gradient : 0 - 3min : 100/0 3 - 16 min : 60/40 16 - 25 min : 60/40	Gradient : 0 - 3min : 100/0 3 - 7 min : 60/40 7 - 12 min : 60/40 12 - 25 min : 100/0
Column temperature (°C)	30 °C	
Dilution with water	Mass of analysed solution : 0.25 g / Mass after dilution : 1.5 g	
V _{injected} (µL)	10	
Flow rate (mL.min ⁻¹)	1	0.5
Wavelength (nm)	254	317

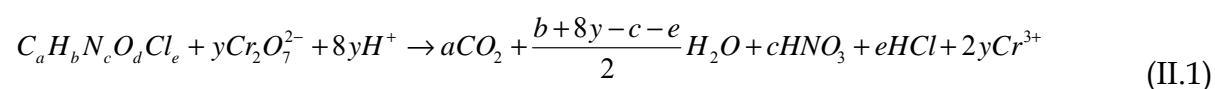
2.1.2. Global Measures of the organic pollutants

For the oxidized effluents, besides the follow-up of the concentration of the molecule analysed by HPLC, we also measured the global organic pollution rather than the formed intermediate products. We used two types of analysis: the Chemical Oxygen Demand (COD) and Total Organic Carbon (TOC).

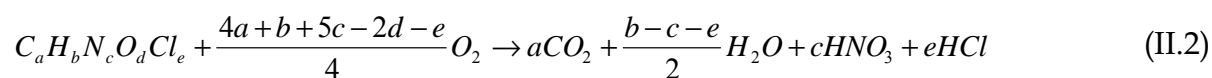
a. Chemical Oxygen Demand: COD

The Chemical Oxygen Demand (COD) represents the quantity of oxygen used for the total oxidation of organic and mineral substances by a strong chemical oxidizing agents: potassium dichromate. This method is often used in the municipal and industrial laboratories to measure the global level of organic contamination of residual waters. This quantity is expressed in mg (O₂)/L.

The COD was measured by oxidizing the organic matter by excess of potassium dichromate; the equation of the reaction is illustrated below:



To estimate the quantity of oxygen to totally oxidize a given organic pollutant, it is enough to write the total corresponding oxidation reaction.



The COD (in mg_{O₂}.L⁻¹) is then expressed by the following equation:

$$DCO_{C_aH_bN_cO_dCl_e} = \frac{4a+b+5c-2d-e}{4} \cdot M_{O_2} \cdot C'_{C_aH_bN_cO_dCl_e} \cdot 1000 \quad (II.3)$$

$C'_{C_aH_bN_cO_dCl_e}$: Mass concentration of compound $C_aH_bN_cO_dCl_e$

M_{O_2} : Molecular mass of oxygen (g.mol⁻¹)

$M_{C_aH_bN_cO_dCl_e}$: Molecular mass of compound $C_aH_bN_cO_dCl_e$ (g.mol⁻¹)

This oxidation is carried out in acid medium in presence of silver sulphate (catalyst). The oxidant is added by known and excess amounts. The reaction is performed at 150 ° C for 2 hours and give access to:

- the excess of dichromate remaining in the solution using a solution of Mohr's salt or by spectrophotometric analysis at $\lambda = 420$ nm (Hach method for COD tubes ranging from 3 to 150 $\text{mgO}_2\cdot\text{L}^{-1}$);
- or the amount of Cr^{3+} formed by spectrophotometric analysis at $\lambda = 620$ nm (Hach method for COD tubes ranging from 20 to 1500 $\text{mgO}_2\cdot\text{L}^{-1}$).

These will then determine the amount of dichromate consumed, which is equivalent to the amount of COD ($\text{mg O}_2 \text{ L}^{-1}$) of the solution.

b. Colorimetric method for the measurement of COD (Method Hach 8000)

This method (called also Method of Digestion by reactor) is particularly used for the analysis of sea water and the residual waters. The oxidation is carried out under heating, in acidic medium and in the presence of an excess of strong oxidizing agent, potassium dichromate. The oxidized organic compounds reduce the dichromate ion ($\text{Cr}_2\text{O}_7^{-2}$) to chromium ion (Cr^{3+}) of green colour (Equation II-2). Tubes of COD (Hach) contain the reagents in necessary quantity according to the used range. The COD reagent also includes salts of silver and mercury: the silver salt is used as catalyst and that of mercury is utilised to prevent the complexes and the interference of the Cl ion. The COD tubes range 0-150 $\text{mgO}_2\cdot\text{L}^{-1}$ was selected in our study.

In the colorimetric method and for the considered range, the quantity of produced Cr^{3+} is measured by using an UV spectrophotometer with a wavelength of 620 nm which shows directly the COD value (Standard Methods, 1997).

To determine the COD by this method, samples must sometimes be diluted to obtain a concentration of COD corresponding to the range of the standard tubes.

c. COD: Operating protocol

The oven Thermostat DRB 200 (Fig.II-5) is preheated at 150 °C. 2 mL of sample diluted or not, are introduced into the COD tube. The tube, once closed, is returned several times to mix its contents, then placed in the oven at 150 °C during 2 hours. Systematically, three different samples are prepared at the same time because we have two ovens including 45 (15 + 30) places, a blank of demineralised water is always prepared in the same conditions.



Fig.II-5. Thermostatic oven DRB 200 and spectrophotometer DR/2500.

After 2 hours, the tubes were left to cooling for 20 minutes in the oven at approximately 120 °C. Tubes are then removed, returned several times, left to cool at room temperature and settled down.

After adjusting the zero of the apparatus by the blank, tubes are placed in the spectrophotometer DR / 2500 one by one: the COD value corresponding to the analyzed sample is directly recorded by mg.L^{-1} . To verify the precision of the method, standard solutions of known concentrations were analyzed.

d. Standard method for the measure of TOC

The total organic carbon (TOC) is a measure of the carbon content present in an aqueous solution. To measure the TOC, it is necessary to eliminate the inorganic carbon present in the solution which is mainly under carbonate (CO_3^{2-}), monohydrogencarbonate (HCO_3^-) and dihydrogencarbonate (H_2CO_3) forms. So, some drops of concentrated phosphoric acid (84 %) are added to the sample, to produce CO_2 , degassed by a current of nitrogen.

The sample is then injected in a TOC-meter (TC Multi Analyser 2100 N/C) in which the organic molecules are totally oxidized at 850 °C in the presence of a platinum catalyst. The quantity of CO₂ released by the reaction is then measured by infra red spectrometry (IR).

This method was used to measure the global organic pollution generated by the tartrazine, as the COD generated by this pollutant, cannot be measured: a colorimetric method is not applicable for dyes, in contrast to the TOC.

2.2. Characterisation methods of the activated carbons

The analyses used to characterize new materials are represented in Figure II-6. Some of these analyses (thermogravimetric analysis and structural properties) will also be carried out for AC after several cycles of adsorption / oxidation to evaluate their modifications due to these different uses.

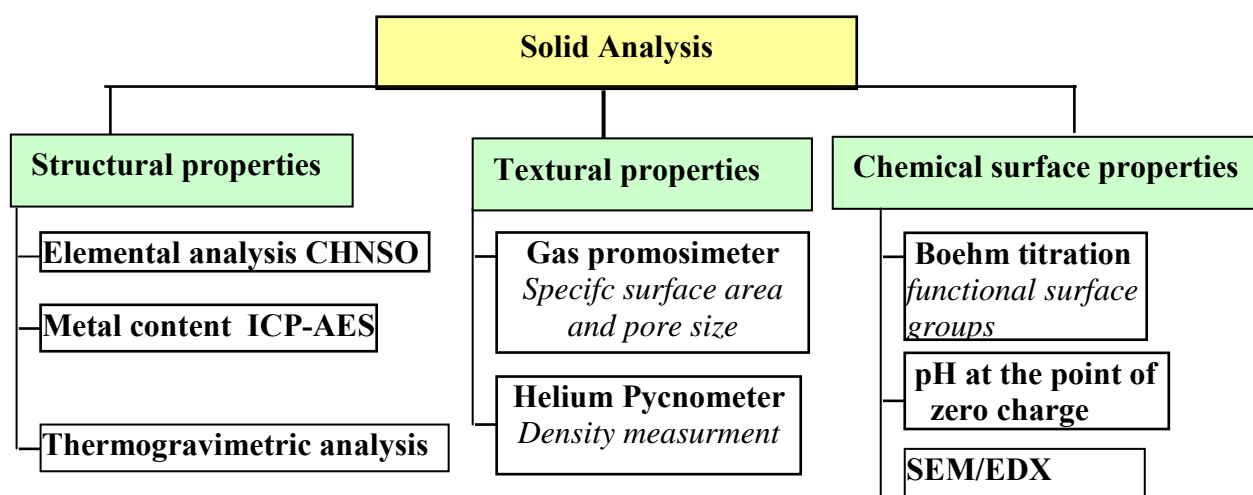


Fig. II-6. The different techniques of analysis for solid characterization.

2.2.1. Textural properties

2.2.1.1. Gas porosimeter

The measure of the specific surface area is carried out using a porosimeter multi gaz ASAP 2010 M supplied by the Micromeritics company. The measure is based on the application of the B.E.T. method (Brunauer, Emmet and Teller) (Brunauer *et al.*, 1938). This method depends on the gas physical adsorption on solid and the thermodynamic characteristics of this phenomenon, exothermic and reversibility.

The gas (nitrogen as adsorbat) is adsorbed in a cellular unit containing a solid sample of known mass (adsorbent). A degassing of the sample is carried out under vacuum at appropriate temperature; the mass of the degassed sample is then measured to calculate the final specific surface. The isotherm is determined by both the sequential introduction of known gas pressure (nitrogen) in the cellular unit and the measure of the adsorbed gas quantity according to the pressure in the system. The temperature of the system remains constant and equal to that of the liquid nitrogen.

To calculate the specific surface, it is necessary to analyse the experimental adsorption isotherm which leads to the adsorbed gas quantity on the complete monolayer, then to calculate the layer area and thus the specific surface of the solid.

The general equation for the physical adsorption of a gas on a solid is:

$$V = \frac{V_m \cdot C' \cdot \left(\frac{p}{p_0}\right)}{\left(1 - \frac{p}{p_0}\right) \cdot \left(1 + (C'-1) \cdot \frac{p}{p_0}\right)} \quad (\text{II.4})$$

Where p is the adsorption equilibrium pressure (Pa);

p_0 - the vapour pressure of adsorbat at adsorption temperature (Pa);

V - Volume of the adsorbed gas (m^3);

V_m - volume of the gas necessary to form a complete monolayer on the surface (m^3);

C' - the adsorption constant of gas used (-).

Equation B.E.T. may be given under a linear shape for relative pressure values $\left(\frac{p}{p_0}\right)$

ranged from 0.05 and 0.3:

$$\frac{p}{V \cdot (p_0 - p)} = \frac{1}{V_m \cdot C'} + \left(\frac{C'-1}{V_m \cdot C'}\right) \cdot \frac{p}{p_0} \quad (\text{II.5})$$

This equation is called transformed linear B.E.T. of the adsorption isotherm. The values of V_m and C' are obtained from the slope $\frac{p}{V \cdot (p_0 - p)} = f\left(\frac{p}{p_0}\right)$ and the intercept. If the area of a gas molecule, A_{gaz} , is known (16.2 \AA^2 for nitrogen), the specific surface of the solid (S_{BET}) is obtained according to the following relation:

$$S_{\text{B.E.T.}} = \frac{N_A \cdot A_{\text{gaz}} \cdot V_m}{V_{\text{mol}} \cdot m_{\text{solide}}} \quad (\text{II.6})$$

where N_A is Avogadro number (mol^{-1});

V_{mol} – molecular volume of gaz ($\text{m}^3 \cdot \text{mol}^{-1}$);

m_{solid} – mass of solid sample (kg).

The value of the total porous volume is based on the measurement of the nitrogen volume adsorbed until $p/p_0 = 0.98$. The model of calculation DFT or TFD (theory of the functional density) gives pore size distribution, and thus the microporous and mesoporous volumes. The mesoporous volume can be also obtained by application of the model B.J.H. (Barrett, Joyner and Halenda).

The diameter of pores is given by the following equation: $d = \frac{4 \cdot V}{S_{\text{B.E.T.}}}$

These analyses were performed at Service Analysis and Processes (SAP) of our Laboratory of “Laboratoire de Génie Chimique” of Toulouse.

2.2.1.2. The helium pycnometer

The measurement of the real density of particles is carried out using helium pycnometer ACCUPYC 1330TC. The principle of the measure is based on the determination of the volume of a solid having or not a regular surface. A simplified diagram of the used apparatus is shown in Fig. II-7.

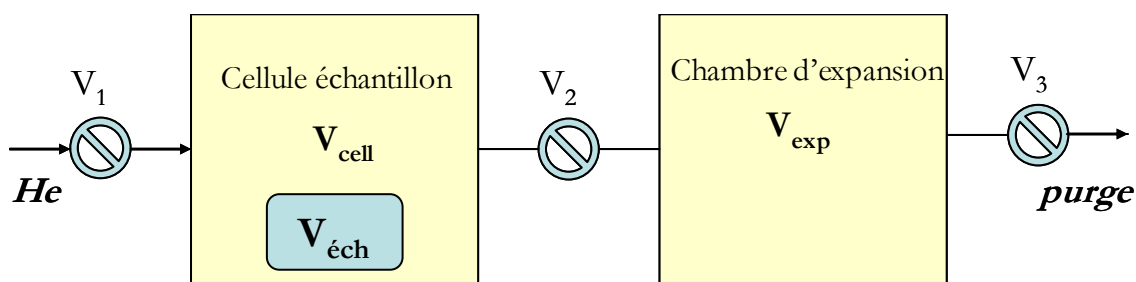


Fig.II.7. Simplified functional diagram of helium pycnometer.

Before measurement, the cellular sample and the expansion room are calibrated using standard metallic ball of known volume. A mass known of the sample is introduced into the measure room then a cycle of purge is started to eliminate the vapours. When the pressure in the room does not evolve any more (the degassing of sample is fully achieved), and series of measures (approximately 20 measures) are started. The cellular sample and the expansion room are initially at the same pressure (the ambient pressure P_A), at the same temperature T_A with the opened tap V_2 (V_1 and V_3 , closed taps). The sample is loaded with helium by opening the tap V_1 (V_2 and V_3 , closed taps). The pressure increases to stabilize at a new value P_1 . When the tap V_2 is opened (V_1 , closed), the pressure falls and reaches an intermediate value P_2 . The evolution of the pressures is recorded and the real volume of the sample is calculated from the equation:

$$V_{éch} = V_{cell} - \frac{V_{exp}}{\frac{P_1}{P_2} - 1} \quad (\text{II.7})$$

These analyses were also carried out at Service Analysis and Processes (SAP) of the Laboratoire de Génie Chimique of Toulouse.

2.2.2. Structural properties

a. Elemental analysis CHNSO

To realize these analyses, the samples must be homogeneous and dry. The contents of carbon, hydrogen, nitrogen and sulfur (CHNS) in the activated carbons were measured in GEPEA (Nantes) and the contents of oxygen (O) were determined in the Laboratory of Control at ENSIACET by Thermo Finnigan Flash EA1110. The schema of the device is presented in Fig.II-8.

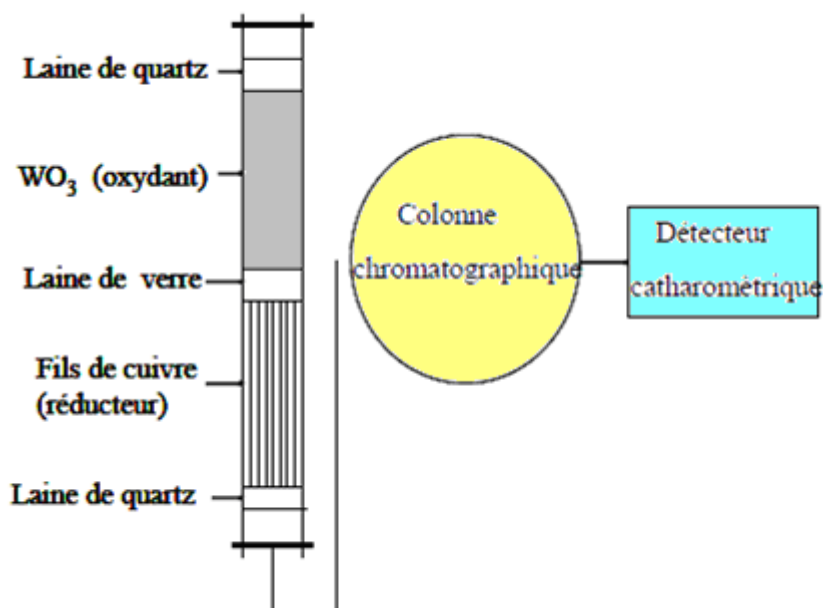
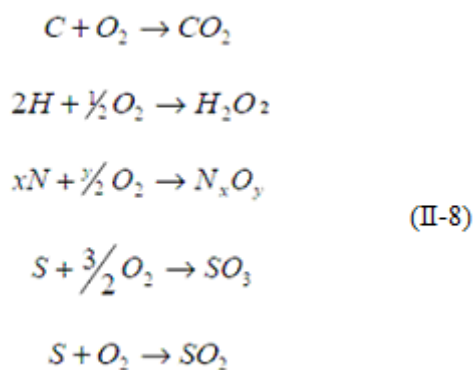


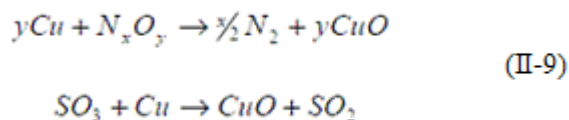
Fig.II-8. Schema of the elemental analyser for CHNS analyses.

The analysis is based on the methods of Pregi and Dumas and the determination of carbon, hydrogen, nitrogen and sulfur is carried out under CO_2 , H_2O , N_2 and SO_2 forms, respectively. The sample of AC is thus prepared in a tin paper (CHNS analyses) or silver (O analysis). The combustion of the sample at $1800\text{ }^\circ\text{C}$ (pyrolysis at $1\ 070^\circ\text{C}$ in the case of O analysis) release gases which undergo a cycle of treatment (oxidation, reduction,..) in a tube reactor.

For the analysis CHNS, the following oxidation reactions are achieved in the presence of an oxidizing agent such as Tungsten Oxide (WO_3):



Reduction reactions take then place in the presence of copper:



For the analysis of O, the pyrolysis takes place in a specific reactor and gives N₂, CO and H₂. The treated gases are then separated by a gaseous phase chromatographic method. For that purpose, a filled polar column of type PorapackR is used. The quantity of each compound is determined using a catharometric detector (TCD).

b. Ash content.

A known mass of AC (its content of humidity was previously determined) is weighed and put in a porcelain crucible and then placed in an oven. The combustion occurs at a temperature of about 650 °C until complete oxidation of organic matter into CO₂ and H₂O. The remaining inorganic compounds (metals, silica, etc...) constitute the ash contents. This analysis was carried out in ICL and GEPEA on the activated carbon arising from the pyrolysis of sewage sludge. For commercial activated carbons, the ash contents were provided by the suppliers.

c. Metal content by ICP-AES

We are interested here by certain not noble metals which represent the main ash content present in the form of oxide and their catalytic oxidation activity: Zn, Ni, Co, Mn and especially Fe and Cu.

Metals are first extracted from the activated carbons by strong acid (HCl: HNO₃ = 3:1 v/v). 0.3 g of AC powder is put in a flask filled with 10 mL of the strong acid and 10 mL of ultrapure water and shaken for 4-5 days at room temperature. The sample is then mineralized during 2 hours at 95°C in a mineralizer (DigiPREP Jr). After filtration, these lixiviate acids are diluted (50 mL) and analyzed by Inductive Coupled Plasma Atomic Emission Spectrometry (ICP-AES) allowing to identify and quantify each metallic element.

The principle of the ICP-AES is as follows: the sample is sprayed in micrometric drops with a nebuliser and introduced directly inside the argon plasma flame (6000 - 10000°C). The sample immediately collides with the electrons and the charged ions in the plasma and is itself broken down into charged ions. The various molecules break up into their

respective atoms which then lose electrons and recombine repeatedly in the plasma, giving radiation at the characteristic wavelengths of the elements involved. A quantitative analysis may then be performed to achieve a calibration condition for each element to be assayed.

d. The thermogravimetric analysis (TGA)

Thermogravimetric analyses (TGA) give the weight change under heat treatment then the amount of the volatilized species. Samples (about 20 mg) were heated from 100 to 900°C under nitrogen flow at a heating rate of 10 °C/min in a SDT Q600 (TA Instruments) Thermobalance.

2.2.3. Chemical surface properties

a. Boehm titration

The acid/base properties of ACs were determined by the classical Boehm titration method (Boehm, 1994). A mass of 1 g activated carbon sample was placed in 50 ml of 0.05N of the following solutions: sodium hydroxide, sodium carbonate, sodium bicarbonate, and hydrochloric acid. The vials were sealed and agitated for 24 hr and then filtered; 5ml of the filtrate was pipetted, and the excess base or acid was titrated with HCl (0.1 N) or NaOH (0.1 N), respectively. The number of acidic sites was determined under the assumption that NaOH neutralizes carboxylic, lactonic, and phenolic groups; and Na_2CO_3 neutralizes carboxylic and lactonic groups; and NaHCO_3 neutralizes only carboxylic groups. The number of basic sites was calculated from the amount of hydrochloric acid that reacted with the carbon. Fig.II-9. shows how to classify the surface functional groups of the activated carbon.

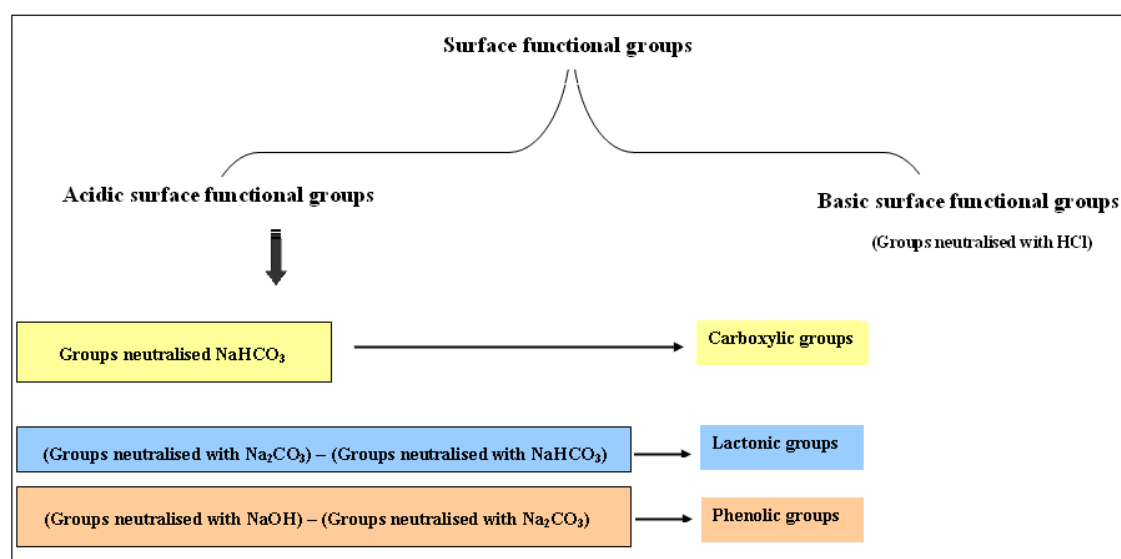


Fig.II-9. Schematic representation of the classification of Boehm titration.

These analyses could not be performed for the sewage sludge based activated carbons (SBACs) because they contain high contents of ash and then inorganic compounds which can react with the acids and bases.

b. pH at the point of zero charge

The mass titration method (adapted from Noh and Schwarz, 1989, and Menéndez *et al.*, 1996) was used to determine the pH at the point of zero charge (pH_{pzc}) of each sample.

Different solutions of NaCl (5mL, 0.1 mol/L) were prepared and their pH were adjusted between 4 to 10 (measured by using the pH-meter; Metler Toledo MP220). Then, 0.1g of AC was added in contact with 20 mL of each NaCl solution. Nitrogen was bubbled through the solutions. The suspensions were then shaken for 72 hr and the final pH was measured by using the pH-meter. The resulting pH, when constant was taken as the pH_{pzc}.

c. SEM/EDX

The Scanning Electron Microscopy (MEB or SEM) is a technique of electronic microscopy based on the electrons-material interactions, capable of producing images of the sample surface. The principle of the MEB is based on the fact that an electron beam bombards the surface of the sample to be analyzed which re-emits certain particles. These particles are analyzed by various detectors which give a three dimensions image of the surface. Due to the excited state of the atoms present in the material by interaction with the incidental electrons, photons X are emitted (de-excitation process). The emission volume of photons X, (μm^3) depends upon the energy of the incidental electrons, the atomic number of the sample and the level energy initially ionized. The chemical analysis by EDX (Energy Dispersive X-ray analysis) consists of a detection of these photons by using a solid detector Si-Li (detection by energy dispersion). The energy of these photons X is characteristic of its atoms; the possibility to realize an elemental analysis. A lines spectre (peaks) is obtained, each corresponding to the photons X of the given energy, thus has a given element. The intensity of the characteristic lines is proportional to the concentration of the element in the analytical volume, this analysis is quantitative. However, there is factors of correction depending on the experimental parameters (energy of the incidental beam, its angle...), the sample composition, and that it is difficult to calculate. Thus, only a semi-quantitative analysis is considered. The detection limit is situated at concentrations about 0.1 - 1 % (for elements having average or light atomic weight and except unfavourable superposition of characteristic peaks). The detectors allow to

detect the light elements (C, O, N) and even at limited degree the boron, but the yield is very weak because the photons of boron are absorbed by the window which protects the detector.

3. The experimental studies

3.1. Device for isotherm: the multifunction thermostatic bath

The adsorption isotherms are realized in a multifunction thermostatic bath at 25°C (Fig. II-10). Various pollutant concentrations (phenols and tartrazine) are prepared in glass bottles and mixed with the same mass of adsorbent: Alhstrom tissues, granular activated carbon, AC-TiO₂ mixture and AC/TiO₂ composite

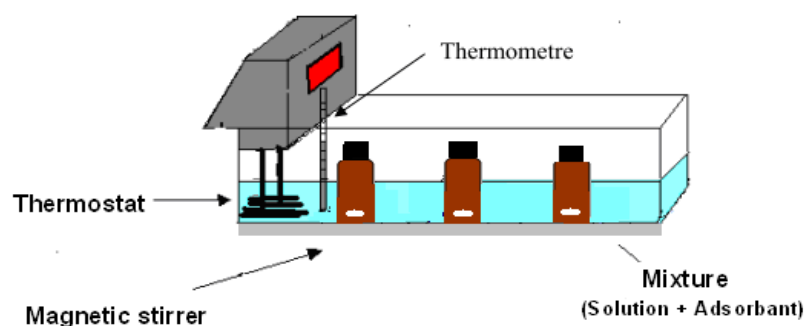


Fig.II-10. Static multifunction thermostatic bath used for the adsorption isotherm.

3.1.1. Operating protocol

- At first, 0.5 g of the activated carbon is put in a flask of 250 ml. For commercial AC, granular particles are sieved to a size between 200 and 400 μ m to reduce the equilibrium time. For sludge based activated carbon, the material is directly used without crushing and sieving because of their low mechanical resistance.
- Introduce 100 ml of solutions of phenols or tartrazine into the flasks (every flask containing a solution of different initial concentration) and a magnetic bar.

- Put the flasks in the bath and stir it using a magnetic bar to realize the adsorption for 7 days at 25 ° C.
- After adsorption, the solutions are filtered using 0.25 mm nylon membranes before analysis.
- The filtered solutions are analyzed by HPLC and their pH were also measured to quantify their variations The amount of adsorbed phenol was deduced from the initial and final concentrations in the liquid phase analyzed by HPLC as described above.

Thus, the various couples (C_e , q_e) characteristics of the studied isotherms were calculated

3.1.2. Adsorption equilibrium studies

a. Monocomponent isotherms

For single adsorbate aqueous solution, the range of initial concentrations depends on the solubility of each substituent: 0.005 - 0.05 M L⁻¹ for phenol, 0.005 - 0.025 M L⁻¹ for PNP, 0.005 – 0.05 M L⁻¹ for PCP and 0.005 – 0.025 M L⁻¹ for PHBA. The initial pH was 5.6 for phenol, 3.8 for p-hydroxy benzoic acid, 4.8 for p-nitrophenol and 5.3 for p-chlorophenol. Solutions were not buffered to avoid adsorption competition between organic and buffer. Preliminary kinetic experiments indicated that adsorption equilibrium was reached in less than 3 days for all the ACs, so a duration of 7 days was chosen to be sure that equilibrium is reached.

b. Multicomponent isotherms

The procedure for competition isotherms was the same of that of the mono-component isotherms, the initial solutions being composed of equimolar concentrations of the four phenolic compounds (0.007 – 0.025 M L⁻¹). Bottles were stirred for 7 days before sampling. The initial pH of the mixture solution was between 3.5 and 5.

3.2. Study the effects of various parameters on the adsorption

a. Influence of pH on phenols adsorption

The various pH (2.2, 7 and 10) of water solutions were used to estimate the effect of pH on phenol adsorption onto AC S23. In this study, 100 mL of various concentrations of P and PHBA were introduced into bottles and shaken with 0.5 g of AC S23. The pH of the solution was adjusted to the required value with various buffer solutions (Ammoniac, 0.1M; HCl, 0.1M; KH₂PO₄, 0.07M; Na₂HPO₄, 0.07M; NaH₂PO₄, 0.5M and citric acid, 0.5M). After equilibrium, the samples were filtered and analyzed by HPLC.

b. Influence of salt addition on phenols adsorption

The effect of the chloride concentration on the adsorption of phenols onto AC S23 was studied by adding different quantities of NaCl (0, 5, 15, 30 and 40 g. L⁻¹) to the phenols solutions.

c. Influence of temperature on phenols adsorption

All the experiments for the adsorption of phenol and PHBA onto AC S23 were carried out at the temperatures of 25, 35 and 50 °C.

3.3. The photocatalytic “channel” reactor

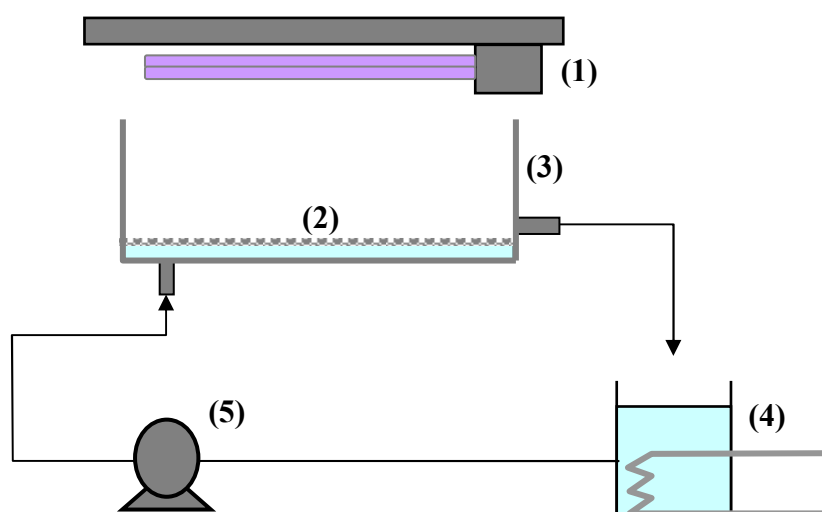
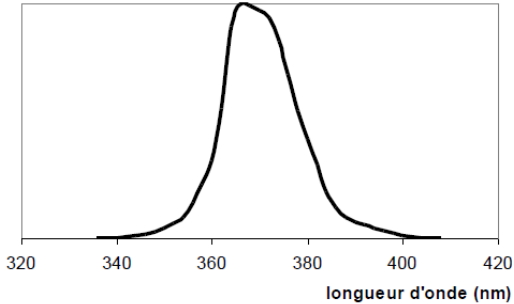


Fig. II -11. Schematic representation and photography of the channel reactor

Table II-10

Main elements of the channel reactor

Equipement	Specifications
(1) lamp UV	2 lamps : Philips PL-L 24W/10/4P Emission maximum: 365 nm  (Lhomme, 2006)
(2) catalytical materials	Alhstrom tissue or media
(3) Channel Reactor	36cm×12 cm in PVC Height : 15 mm
(4) thermostatic intermediate container	PVC Container of 2 L equipped with metallic bottom for temperature control ($T_{\text{exit}} = 30\text{ }^{\circ}\text{C}$)
(5) pump	Pump Masterflex

This reactor was designed to operate the Alhstrom tissue which is in the form of sheet. The channel reactor is presented in Fig.II-11 and the various elements are detailed in Table II-10. A volume of 2 L of solution is introduced into the device: 650 mL in the reactor and 1350 mL in the intermediate container. The flow rate of the pump is fixed at 1000 mL/min. The intermediate container was cooled by JULABO thermostatic water bath (25°C). The equipment does not include air supply: air above the tissue and in contact with the liquid in the intermediate container was considered enough to maintain dissolved oxygen in the liquid.

The operating conditions

These are summarized in Table II-11. Two concentrations of phenol were used in this study: 0.88 g/L and 0.45 g/L.

Phenol solution (2L) was placed in a PVC intermediate container with metallic bottom for temperature control. The solution was then circulated using a peristaltic pump (Master flex model) with a flow rate of 1000 ml/min. After the solution level was stabilized in the channel reactor, a sheet of tissue (media) was placed in the reactor covering approximately the whole reactor surface (36cm×12 cm) and just under the solution-air interface in order not to reduce the light emission reaching the photocatalytic layer placed in the upper position. Two successively steps was achieved; adsorption then oxidation corresponding to one cycle of the sequential process.

Adsorption step. This step is carried out in the dark (without UV irradiation). During the adsorption, the samples were taken during the day time at regular intervals. This step would terminate when the concentration of phenol in the liquid phase does not evolve any more: the adsorption equilibrium has been reached. In order not to extend too much this first step, it has been decided to limit its duration to 4 days which seems to be enough to approach AC saturation. Samples were then diluted and analysed by HPLC for determining the phenol concentration at a wavelength of 254 nm using fast analysis method described previously in table II.8.

Oxidation step. this step was started after the adsorption one by switching on two UV lamps for three days. Similarly, as in the adsorption step, during this oxidation period, samples were taken and analysed by HPLC using gradient analysis method (Table II-9) and part of the sample was also used for measuring the DCO.

After the oxidation step, the oxidized solution of phenol was removed and replaced by a new one of the same initial concentration used for the previous adsorption step (i.e. either 0.88 or 0.45 g/L) and a new cycle then begins. The temperature was controlled at 25 °C during the experiment using a thermostatic water bath

Table II-11

Operating conditions of adsorption/photocatalysis cycles with the channel reactor

Photocatalytic reactor		
	Adsorption	Oxidation Air/UV/TiO ₂
Function	Batch	Batch under 2 lamps (Philips PL-L 24W/10/4P)
Duration	4 days	3 days
Temperature	25 °C	
Pressure	Atmospheric pressure	
Flow rate	1000 ml/min	
Solution volume	1350 ml in the intermediate vessel 650 ml in the reactor	
Phenol concentrations	0.88 g/L and 0.45 g/L	
Mass of tissue	17g	
Analytical technique	HPLC	
Particular remark		
Mass of catalyst	0.44	0.86
Mass of pollutant		
Mass of AC		12
Mass of pollutant	6.15	
	<div style="display: flex; justify-content: space-around;"> <div style="text-align: center;"> <p>for 0.8 g/L phenol</p> </div> <div style="text-align: center;"> <p>for 0.45 g/L phenol</p> </div> </div>	

3.4. Glass photocatalytic reactor

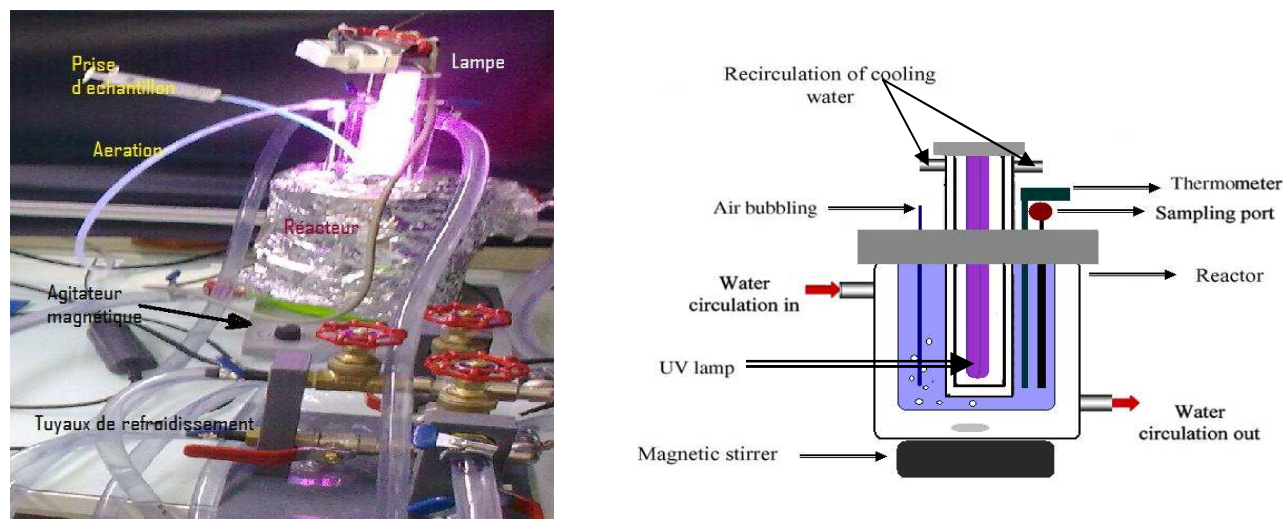


Fig.II-12. Schematic and photography of the thermostated cylindrical reactor.

The experimental device is illustrated in Fig. II-12. It is a 1,5L jacketed cylindrical reactor made of glass. On the central axis, the UV lamp (Philips PL-L 24W/10/4P) is placed in a jacketed Pyrex cylinder thermoregulated with cooling water to remove lamp heating. The reactor is closed at the top by a PVC disk maintaining the lamp. Three small orifices are used for sampling through a small tube of 2mm of diameter, for air injection, and for temperature measurement. The sampling is performed by a plastic syringe of 10 mL containing a filter of pores diameter of 0.5 μ m. The two jackets maintain the temperature at 25°C in connection with a thermostat and a pump. The external wall of the reactor jacket is covered with aluminium foil which prevents the penetration of any parasitic radiation coming from the outside environment within the reactor. The solution is stirred with a magnetic stirrer.

Operating conditions

The experimental conditions of adsorption/photocatalysis cycles into glass photocatalytic reactor are shown in Table II-12.

In this part of the work, two materials have been investigated for comparison:

- AC/TiO₂ composite: TiO₂ deposited on AC S23 by CVD.
- A mixture of the two solids :AC S23 and TiO₂ (PC 500): TiO₂ separated physically from AC.

Similarly, as described previously in the channel reactor, each cycle includes two sequential successive processes: adsorption then oxidation.

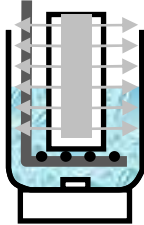
Adsorption step. 1L of 0.45 g/L Tartrazine was put in the reactor then a known mass (5g) of the used photocatalytic materials was added. The solutions were then magnetically stirred. The adsorption step is carried out without UV irradiation at 25°C. During the adsorption, several samples were taken by a plastic syringe then analysed by HPLC, table (II-8).

Oxidation step. After the adsorption step, the UV lamp was switched on and a stream of air was supplied to prevent the recombination of electron–hole pair. During the oxidation step, samples was taken regularly during day time and then analysed either by HPLC (table II-9) for determining the Tartrazine concentration or by TOC analysis as a global analysis for the formed intermediates.

Systematically, as mentioned for the reactor channel, after the oxidation step, the reactor was emptied from the oxidized solution of Tartrazine and then filled by a new one of the same initial concentration (0.45 g/L) for starting a next cycle.

Table II-12

Operating conditions of adsorption/photocatalysis cycles into glass photocatalytic reactor

Reactor	Glass batch reactor 	
Step	Adsorption	Oxydation air/UV/TiO ₂
Function	Batch	Batch under UV lamp Philips PL-L 24W/10/4P photon flux 47.5 W/m ²
Material	AC/TiO ₂	
Mass 7.91 % of TiO ₂ 92.09 % of carbon	5 g (Composite) M _{AC} =4.60 g m _{TiO₂} =0.40 g	
Stirring	Magnetic	
Temperature	25 °C	
Pressure	Atmospheric pressure	
Volume of solution	1 L	
Tartrazine concentration	0.4 g/L	
Air	Air supplier	
Duration	Cycle 1 : 7 days Cycle [2-5] : 4 days	3 days for each cycle
Analytical technique	HPLC	
Particular remark	$\frac{\text{Mass of catalyst}}{\text{Mass of pollutant}} = 1$ $\frac{\text{Mass of AC}}{\text{Mass of pollutant}} = 115$	

3.5. Fixed bed photocatalytic reactor

A continuous pseudo fixed bed photocatalytic reactor of 120 mL (tore volume) was designed to complete the study. A schematic diagram of the photocatalytic tubular reactor is shown in Fig.II-13. Instead of putting solid particles in the reactor to make a fixed bed, the AC- TiO₂ tissue was used. The sheet of tissue was cut so as to entirely cover the tore surface. The thickness of the sheet and of the tore are rather similar so that the reactor volume is nearly occupied by the photocatalytic sheet, whose TiO₂ layer is of course oriented towards the UV lamp. The experimental was consisted of a feed inlet tank with a stirrer used to ensure the complete mixing of the solution in the tank, a peristaltic pump (Master flex model) with a flow rate of 2 mL/min used to pump the reactants from the tank to the reactor, the residence time was about 60 min.

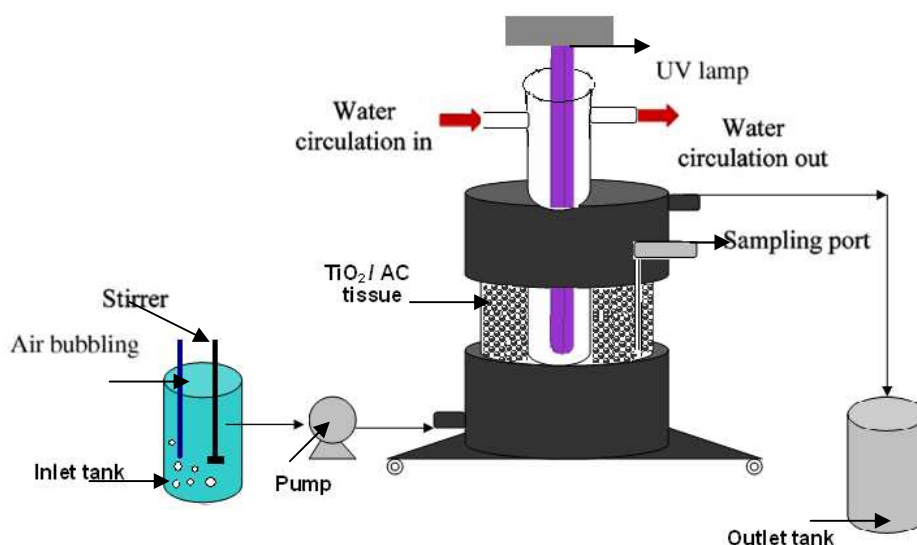
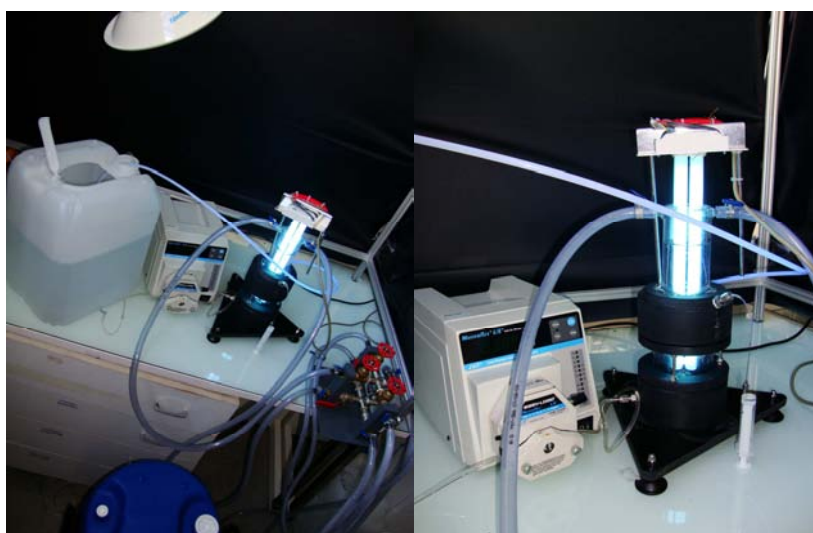
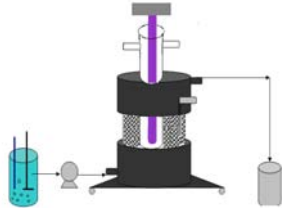


Fig.II-13. Photography of the fixed bed photocatalytic reactor.

UV lamp (Philips, $\lambda = 365$ nm) was located in the centre of the reactor to illuminate the TiO_2 photocatalyst. The lamp was surrounded with double envelope and water bath with circulation pump used to cool the UV lamp. Stream of air was used to provide air at the oxidation process.

Table II-13

The experimental conditions of adsorption / photocatalysis runs into fixed bed photocatalytic reactor

Fixed bed photocatalytic reactor		
	Adsorption	Oxidation Air/UV/ TiO_2
Function	pre-saturated in batch with a 0.2 g/L phenol solution to approach equilibrium	continuous oxidation process was then achieved using this saturated tissue in fixed bed. Irradiation: 1 lamp (Philips PL-L 24W/10/4P)
Duration	3 days	days
Temperature	25 °C	
Pressure	Atmospheric pressure	
Flow rate	2 ml/min	
Contact time	was about 60 min	
Phenol concentrations	0.017 g/L	
Mass of tissue	12.7 g	
Analytical technique	HPLC	

Operating conditions

The experimental conditions are represented in Table II-13. The TiO₂/AC tissue (12.7 g) was pre-saturated in batch for 3 days using 0.2 g/L of phenol until reached the equilibrium. The continuous oxidation process was then achieved using this loaded tissue in fixed bed reactor by successive addition of 0.017 g/L phenol (phenol concentration after the dark adsorption period). The sampling was taken each 1 hr at two different regions: one from inside the reactor by using syringe (at 6 cm) and the other from the outside of the reactor. The experiment was conducted at 25 °C. All samples were analysed by HPLC.

3.6. Radiometer

The light intensity of the lamps in the different reactors used in this study were measured by using radiometer (UVA LIGHT METER). It has a cell capture allowing to measure the light intensity at wave length range of 320-390 nm. Three measurements ranges are available: 0-1.999 uW/cm²; 0-19.99 uW/cm² and 0-199.9 uW/cm². The light intensity of the lamps was found to be: 55 W/m² (for canal reactor); 47.5 W/m² (batch reactor) and 42 W/m² (fixed bed reactor). The values obtained by radiometer represents the mean value of several points of the reactors. The quantum yield was not calculated because it needs further measurements using chemical actinometric method.

Chapitre II. Matériel et méthodes

Ce chapitre débute par la présentation des différentes molécules modèles choisies, des matériaux utilisés en adsorption et en oxydation photo-catalytique et des agents oxydants. Ensuite, sont détaillées les techniques d'analyses des solutions aqueuses et des solides. Enfin, les divers dispositifs expérimentaux sont décrits ainsi que les protocoles opératoires.

Les effluents ciblés dans cette étude sont les effluents chargés en phénols et les effluents colorés. Les molécules sélectionnées sont la tartrazine, le phénol et plusieurs aromatiques substitués dont l'acide 4-hydroxybenzoïque, le 4-chlorophénol et le 4-nitrophénol. Les principales caractéristiques physiques et chimiques de ces constituants sont rappelées. L'ensemble des charbons actifs utilisés sont ensuite exposés : deux sont des charbons actifs commerciaux et six sont fabriqués à partir de boues de station d'épuration d'eaux usées. Ces derniers ont été préparés par l'Imperial College de Londres et le laboratoire de Génie des Procédés – Environnement – Agro-alimentaire de Nantes dans le cadre d'un projet Européen REMOVALS. Dans cette partie, seules les caractéristiques des charbons commerciaux fournies par la société PICA sont reportés : origine, surface spécifique, volumes poreux, diamètre de pores et de particules. Pour les charbons de boues, les conditions de fabrication sont rappelées brièvement, toutes les analyses effectuées au laboratoire seront présentées dans le chapitre suivant. Pour la partie photocatalyse, plusieurs matériaux ont été mis en œuvre : des tissus commercialisés par la société Ahlstrom et un charbon actif avec dépôt de TiO_2 conçu au Laboratoire de Génie Chimique de Toulouse. Le principal tissu utilisé est le tissu « media AC/ TiO_2 ». Il est composé de plusieurs couches : une première de fibres synthétiques, une couche de fibres et de charbon actif, une nouvelle couche de fibres synthétiques et enfin, une imprégnation d'un mélange de TiO_2 et de SiO_2 . Les autres tissus testés correspondent à une version sans TiO_2 (media AC) et une version sans charbon actif (Media TiO_2).

Les techniques analytiques utilisées sont ensuite décrites. Les solutions aqueuses sont analysées par chromatographie liquide haute performance (HPLC en anglais) et par des techniques de mesure globales de la pollution comme la Demande Chimique en Oxygène et le Carbone Organique Total. Pour l'analyse par HPLC, après un rappel succinct du principe de mesure, les différents éléments qui constituent la chaîne sont détaillés ainsi que les deux méthodes analytiques mises en place. La méthode dite « fast » est une méthode qui permet de doser les solutions à un seul constituant. La méthode « à gradient » est adaptée pour l'analyse

des effluents composés de plusieurs substituants. Pour l'analyse des effluents oxydés constitués d'un grand nombre de molécules qui ne sont pas toujours identifiées, deux autres méthodes globales ont été choisies : la Demande Chimique en Oxygène et le Carbone Organique Total. La mesure de la DCO a été obtenue par la méthode Hach 8000 ou méthode de digestion à l'aide d'un équipement complet commercialisé par Hach (tube pré-rempli de réactifs, four et spectrophotomètre). Le COT est mesuré au laboratoire à l'aide d'un COT-mètre. Plusieurs techniques d'analyses ont ensuite été utilisées pour caractériser les différents matériaux solides. Le porosimètre à gaz a permis de déterminer les surfaces spécifiques, la distribution en taille de pores et les volumes poreux. La densité vraie des particules est obtenue à l'aide du pycnomètre à hélium. Des analyses globales ont aussi été réalisées : mesure des taux de cendres, analyse ICP-AES, analyses élémentaires CHNSO, analyses MEB/EDX et analyses thermogravimétriques (A.T.G.). Les caractérisations des surfaces sont obtenues par mesure du pH de contact, du pH au point de charge nulle et de la nature des fonctions de surface par la méthode de Boehm.

Les différents dispositifs expérimentaux ainsi que les protocoles opératoires sont détaillés. Les isothermes d'adsorption sont réalisées dans des flacons disposés dans un bain thermostaté multiposte. Les essais sont effectués en introduisant l'adsorbant et la solution dans un flacon, le mélange est assuré par un barreau aimanté. Les prises d'échantillon sont de quelques millilitres, prélevés à l'aide d'une seringue équipée d'un filtre à membrane en nylon puis analysés en HPLC. Plusieurs dispositifs photocatalytiques ont ensuite été réalisés : un réacteur de forme « canal », un réacteur cylindrique en verre et un réacteur annulaire en verre. Le réacteur « canal » est un réacteur batch conçu pour s'adapter aux tissus Ahlstrom. La circulation du liquide se fait entre le réacteur et un réservoir thermostaté tout en maintenant un niveau de quelques millimètres au dessus du tissu. La lampe est placée au dessus du dispositif. Les échantillons de phénol oxydés sont prélevés en sortie du réacteur et analysés en HPLC et DCO. Le réacteur photocatalytique cylindrique en verre est celui-ci adapté au matériau CA/TiO₂ en grains. Ce réacteur fonctionne aussi en batch et la lampe est introduite dans l'axe du réacteur à l'intérieur d'un emplacement à double enveloppe en verre thermostaté. Les échantillons de tartrazine oxydées sont prélevés régulièrement dans le réacteur et analysés en HPLC et COT. Le dernier dispositif est un réacteur annulaire en verre fonctionnant en continu testé avec du tissu Ahlstrom pour oxyder la tartrazine. Seules des analyses en HPLC ont été effectuées pour des prélèvements au cœur et en sortie du réacteur.

CHAPTER III

ADSORPTION OF PHENOLS ON

DIFFERENT ACTIVATED CARBONS

1. Introduction

In water treatments, one mean for removal of organic pollutants from aqueous solution is adsorption on activated carbon. The main drawback of adsorption processes is the necessity to regenerate the activated carbon, most often by *ex situ* high temperature processes. The highly specific high temperature regeneration plants and the large amounts of used AC to be treated require long transportation cost, high energy and moreover results in about 10-15% mass losses. This high adsorbent cost has limited adsorption applications to final water treatment. Thus, development of cheap activated carbons presents a great economical interest. In the current context of Sustainable Development, the most promising is the development of cheap adsorbent from all kind of wastes.

The objective of the present work was firstly, to compare the performance of adsorption of two commercial activated carbons (PICA S23 and F22) and six activated carbons produced from pyrolysis treatment of sewage sludge. Phenol was selected because it is widely taken as a reference model for adsorption capacity determination. Secondly, among these six sludge based activated carbons (SBACs), the one having the highest phenol adsorption capacity has been selected to study the monocomponent adsorption and competitive adsorption of different substituted phenols : *p*-Chlorophenol, PCP, *p*-Nitrophenol, PNP, and *p*-Hydroxy benzoic acid, PHBA and compared with the two commercial activated carbons.

2. The adsorbents : commercial activated carbons and sewage based activated carbons

In this study, two commercial activated carbons (F22 and S23 supplied by PICA) and sewage based activated carbons have been compared. These last carbonaceous materials were prepared from sewage sludge by Imperial College (London, England) and the laboratory GEPEA (Nantes, France) in the context of a European Project (REMOVALS, FP6- 018525). The different processes of fabrication are detailed in chapter II and annex 1. The materials produced were characterized in our Laboratoire de Génie Chimique (Toulouse, France): textural properties, elemental analysis, ash content, CHNSO analysis, different chemical analysis of the surface (pH_{PZC} and Boehm analysis) and thermogravimetric analysis.

2.1. Textural properties: Specific surface area and pore volume

The method of BET measurement using a multi-gas porosimeter is discussed in details in chapter II. The physical characteristics of the two commercial activated carbons and six

sludge based activated carbons are presented in Table III.1. These properties include the BET surface, the micro-porous volume and meso-porous volume, the pore size as well as the apparent density of these carbons. Activated carbons reveal differences in the apparent density being essentially related to their particular porosity.

Several remarks can be raised from the values in Table III.1: the carbon S23 represents the highest values of BET surface and porous volume among all carbons, moreover, F22 and S23 are almost microporous. The table III.1 shows that the BET surfaces of sludge based activated carbons vary from 90 to 265m².g⁻¹; thus 4 - 10 times lower than those of the commercial activated carbons. The carbonaceous material presenting the most important specific surface was obtained after the physical activation of dewatered, raw material (SA_DRAW).

The incorporation of 5 % of PVA (polyvinyl acetate) as a binder in SA-DRAW (to make it more hard) slightly decreased its porosity. Its surface area decreased from 265 to 201m².g⁻¹, but remains superior to that of the other sewage carbons.

Table III. 1

Comparison between the textural physical properties of two commercial and six sludge based activated carbons

Activated carbon	BET Surface (m².g⁻¹)	Microporous volume (cm³.g⁻¹)	Mesoporous volume (cm³.g⁻¹)	Pore size (A°)	Apparent density (kg.m⁻³)
PICA S23	1230	0.49	0.04	17	1013
PICA F22	985	0.41	0.11	20	993
C_DMAD	125	0.05	0.11	44	1837
C_DRAW	180	0.07	0.08	27	1710
SA_DMAD	155	0.06	0.15	45	1730
SA_DRAW	265	0.11	0.17	35	1471
Hardened SA_DRAW	201	0.08	0.16	37	1519
CO2A_DSBS	90	0.03	0.03	25	1932

2.2. Chemical analysis of the activated carbons

2.2.1. Elemental analysis and ash content

Metal composition analysis (ICP-AES) and ash content of commercial ACs and SBACs are presented in Table III.2. The conditions of these analyses are given in Chapter II.

One of the parameters influencing the adsorption properties of carbon is the ash content. The ACs are good adsorbent, when they has low ash content. In general, the ash content of the two commercial carbons is much lower than that of all sludge based activated carbons. It was noticed also from Table III.2 that F22 (produced from coal) has significantly more ash than S23. The ash content of DMAD carbons is about 10 % superior to that of the DRAW carbons. The carbon of Nantes, CO₂A_DSBS has the least ash content among all six sludge based activated carbons. Table III.2 shows higher quantities of metals, especially iron in the sludge based activated carbons than in the two commercial carbons in relation to their higher ash contents.

Table III.2

Metal composition analysis of the activated carbons estimated by ICP-AES

Activated carbon	Zn	Ni	Co	Mn	Fe	Cu	Ash content (wt %)
	(ppm)						
PICA S23	13	3	0	5	116	74	3.2*
PICA F22	13	24	0	6	578	28	12*
C_DMAD	1140	48	1	583	5.44.10 ⁴	722	79
C_DRAW	259	16	1	117	4.37.10 ⁴	576	68.5
SA_DMAD	1190	311	2	635	6.21.10 ⁴	685	78.2
SA_DRAW	613	28	1	149	4.79.10 ⁴	672	65
Hardened SA_DRAW	655	28	1	156	4.97.10 ⁴	726	-
CO ₂ A_DSBS	527	22	1	417	6590	554	59

* given by the suppliers as residual after combustion at 600 or 650 °C

2.2.2. CHNSO analysis

Table III.3 indicates the element content of ACs (carbon, hydrogen, nitrogen, sulfur and oxygen) according to the gas analyses from the combustion or pyrolysis (GEPEA, Nantes, and ENSIACET, Toulouse). The method of analysis is detailed in Chapter II.

The proportion of each element, specially the oxygen content, indeed supplies a more precise idea on the surface functions of AC. The oxygenated function groups are mainly acid groups, which give the acid character to the activated carbon (Carrott *et al.*, 2001).

The table III.3 shows that the commercial carbons, S23 and F22 have much higher carbon content than the sludge based activated carbons. This is in agreement with the ash content analysis and probably due to the lower carbon content of the sludge. Among all SBACs, DMAD has the lower carbon content. This seems to be due to the sewage sludge based carbons being firstly digested, converting the smallest carbonaceous molecules to gas (see fabrication of the sewage sludge based carbons in chapter II and annex 1).

The sewage sludge based carbons contain a relatively high proportion of oxygen with respect to the commercial carbons. The high percentage of oxygen suggests the presence of acidic surface functional groups and, at a greater extent, inorganic salts and oxides considering the large ash proportion of these materials.

Table III.3

Elemental analysis of the activated carbons

Activated carbon	%C	%H	%N	%S	%O
PICA S23	92.28	0.59	0.30	-	2.34
PICA F22	84.37	0.53	0.50	0.73	1.10
SA_DMAD	22.6	0.6	0.1	-	6.1
SA_DRAW	27.9	0.6	1.4	0.8	10.3
CO₂A_DSBS	34.2	0.6	2.7	-	10.5

2.3. Chemical analysis of the surface

2.3.1. pH

The Point of Zero Charge, pH_{PZC} is defined as the pH of the aqueous solution in which the solid presents a neutral electric potential. It allows to quantify the acidic or basic character of the carbon. The pH_{PZC} and the pH of the solution determine the charge on the surface that will be present; the carbon surface is positively charged at $\text{pH} < \text{pH}_{PZC}$ and negatively charged at $\text{pH} > \text{pH}_{PZC}$. This charge on the carbon surface is one of the parameters which explain the adsorption characteristics (Stoeckli and Hugli-Cleary, 2001; Canizares *et al.*, 2006).

The measurement of pH_{PZC} was performed for the commercial activated carbons. It is important to note that for sewage sludge carbons, the release of mineral ions in acidic and basic solutions was observed, thus only the pH of contact was measured. From Table III.4, it is clear that both pH and pH_{PZC} are mainly basic for all carbons.

Table III.4

Values of pH_{PZC} and pH of contact for the activated carbons

Commercial AC (pH_{PZC})		Sewage sludge based AC (pH of contact)				
S23	F22	C_DMAD	C_DRAW	SA_DMAD	SA_DRAW	CO ₂ A_DSBS
9.7	9.0	8.9	8.6	9.5	8.7	8.1

2.3.2. Boehm titration: surface functions

The acid/base properties of ACs were determined by the classical Boehm titration method (Boehm, 1994). The analyses were carried out for only the two commercial activated carbons, S23 and F22 (Table III.5) and not for SBACs as it is important to note that Boehm titration is not convenient for them due to the release of either carbonates in basic solutions or phosphates and ferric ions in acidic solutions.

Firstly it is confirmed from Table III.5 that the two commercial activated carbons are basic in nature. These results are in agreement with pH_{PZC} values previously measured. S23 has the greatest content of basic groups (0.98 mmol g^{-1}). The presence of basic groups

enhances the adsorption of aromatic compounds through the formation of an electron acceptor-donor complex (Haydara *et al.*, 2003). The total acidic groups content of the commercial activated carbons are 0.2 and 0.65 mmol g⁻¹ for S23 and F22, respectively. Concerning the acidic functional groups, the phenolic groups are the most important for the two commercial activated carbons.

Table III.5

Results of Boehm titration

Activated carbon	Carboxylic group (mmol g ⁻¹)	Lactonic group (mmol g ⁻¹)	Phenolic group (mmol g ⁻¹)	Total acidic sites (mmol g ⁻¹)	Total basic sites (mmol g ⁻¹)
S23	0.00	0.09	0.21	0.30	0.98
F22	0.05	0.01	0.18	0.24	0.51

2.3.3. Thermogravimetric analysis (TGA)

The thermogravimetric analysis of the ACs S23 and F22 were conducted up to 700°C under nitrogen flow at a heating rate of 10 °C/min (Fig. III.1). As the carbonaceous materials were produced at temperatures above 800 °C, their TGA were carried out up to 1100 °C in the same conditions (Figure III.2).

The thermogravimetric curve of F22 presents a first mass loss of 4.3% at temperature around 100 °C mainly due to the degree of humidity (Sricharoenchaikul *et al.*, 2008). Then the evolution of mass is negligible up to 644°C. From this temperature, the mass falls again reaching a total loss of 10.93% at the end of the experiment. For S23, a first mass loss of 3.9% for temperature up to 333°C reveals the presence of water and very small molecules. Then, a second mass loss is observed attaining 8.7% at the end of the analysis.

During the thermal decomposition of the oxygenated surface groups of the activated carbons studied, the loss of mass at temperatures ranging from 200 to 500 °C is generally attributed to the decomposition of carboxylic acid groups to CO₂ while the loss of mass observed at higher temperatures, from 500 to 700 °C, is mainly due to the decomposition of the lactonic and phenolic groups (Merle, 2009). The thermogravimetric curves obtained are in

agreement with the high amount of phenols groups of these two commercial ACs (Table III.5).

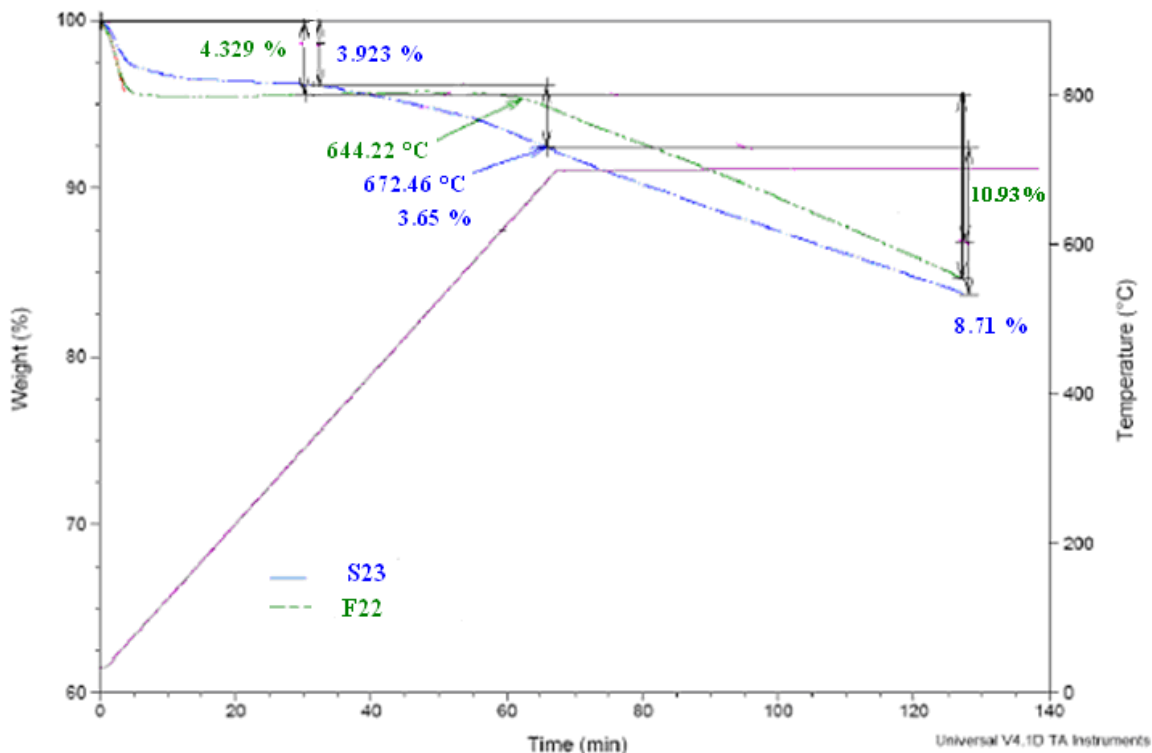


Fig. III.1. Thermogravimetric analysis of the two commercial activated carbons

For carbonaceous materials, the results do not present the same evolution. As the materials are produced at very high temperature (850 ° C), the largest mass loss occurs after 850 ° C. The total mass loss is about 20-25% with sludge DMAD and about 40% for sludge "DRAW" and "DSBs". These results are unexpected given the ash of these materials and the inert conditions of TGA analysis. This important mass loss should correspond at least partly to the decomposition of certain minerals such as carbonates.

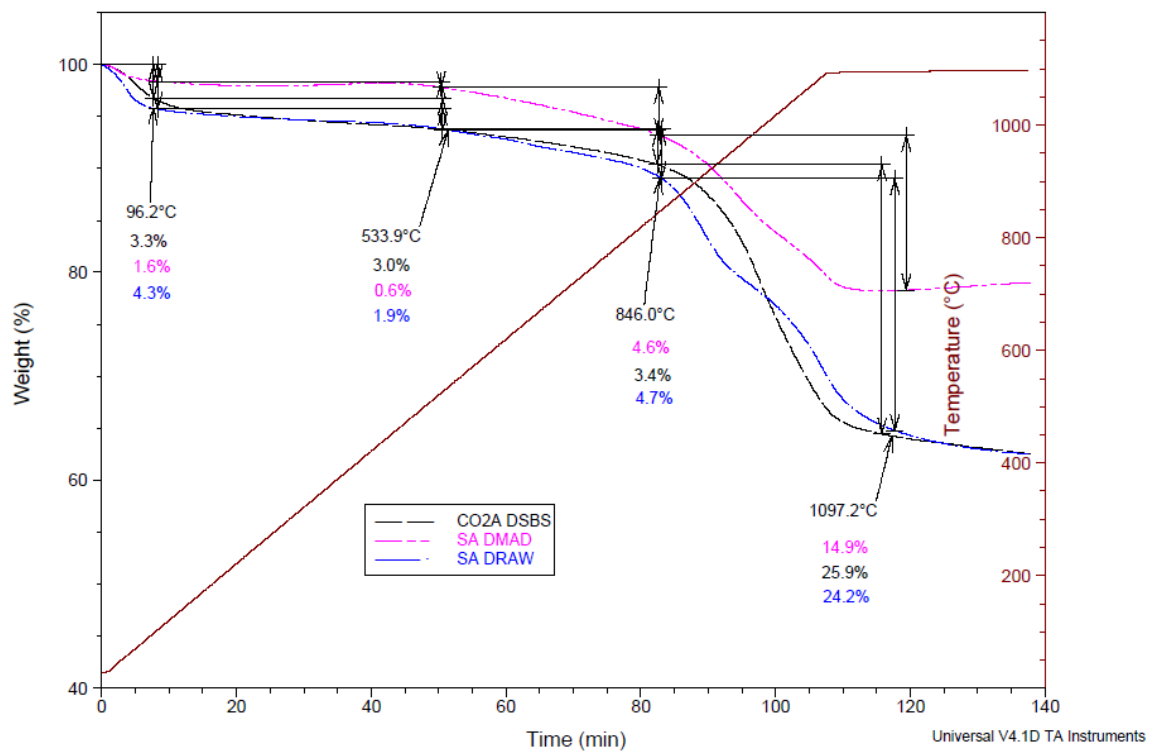
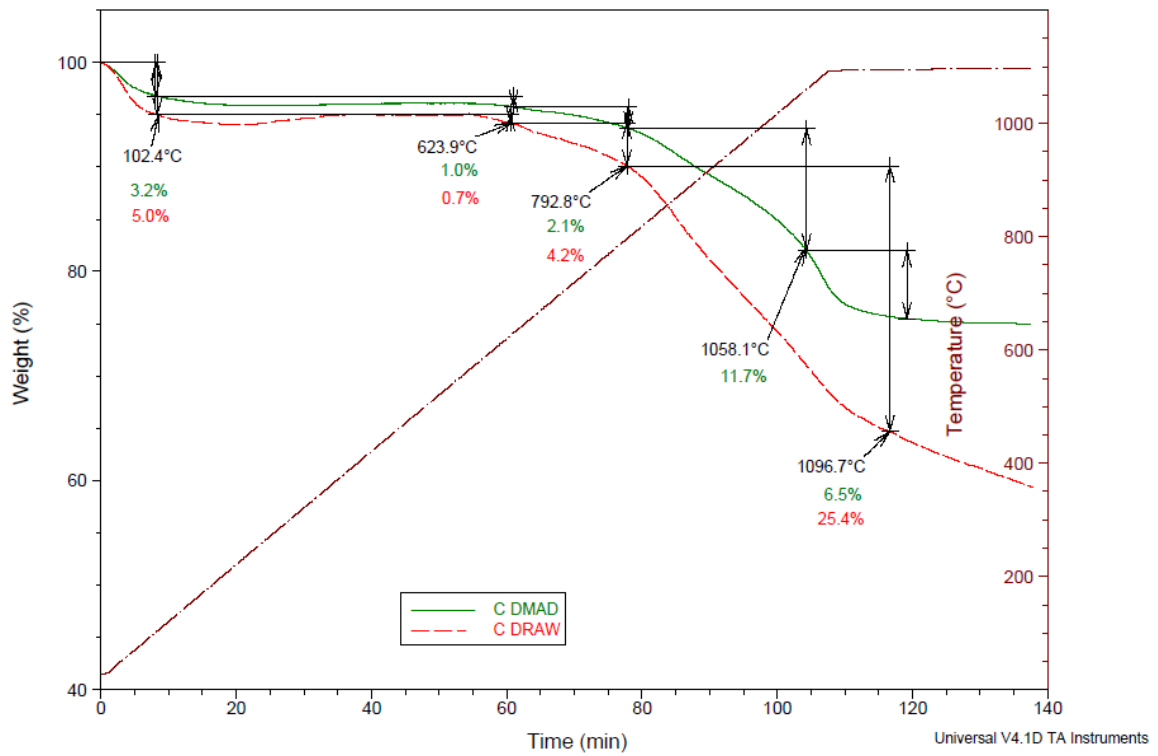


Fig. III.2. Thermogravimetric analysis of the sludge based activated carbons.

3. Preliminary study: Effect of different experimental factors on phenols adsorption onto activated carbon

This preliminary study aims to investigate the influence of some parameters on adsorption of phenols on AC: pH, presence of salt NaCl and temperature. These results allowed us to make choices in operating conditions for the next studies. Two different molecules have been tested, P and PHBA, and the activated carbon selected is AC S23.

3.1. Effect of solution pH

The pH of the solution is one of the major factors influencing the adsorption capacity of the compounds that can be ionized. In order to study the effect of the pH, several experiments were carried out with carbon S23 at a temperature of 25 °C using different initial solution pH of values (2.2, 7 and 10). The pH of the solutions are maintained by means of ionic buffer solutions composed with NH_4OH , HCl , KH_2PO_4 , Na_2HPO_4 , NaH_2PO_4 and Citric acid. The effect of pH on the isotherms AC S23 for phenol and PHBA is presented in Figures III.3.a and III.3.b. In these Figures, the adequate models for each isotherm are also represented (see calculation and parameters values in Annexe 2). The Freundlich isotherm model fits rather well except for the non-buffered solutions where Langmuir model is better. Note that the aim of this study is only to investigate the influence of pH, the difference of affinity between S23 and both molecules will be interpreted in the next part (4. Adsorption performance of the different activated carbon studied)

As can be seen in these Figures, the highest adsorbed amounts of phenol were found at neutral solution pH=7 and non-buffered solution pH=6.3. In this range of pH, AC is positively charged ($\text{pH} < \text{pH}_{\text{PZC}} = 9.7$) and phenol is in neutral form ($\text{pK}_a = 9.89$). The electrostatic interactions do not play an important role in the adsorption phenomenon. The interaction between the carbon surface and the phenols in this case can be attributed to dispersion effect between the activated carbon π -electrons of double bonds and π -electrons in aromatic ring of phenols. At pH= 7, PHBA ($\text{pK}_{a1} = 4.58$; $\text{pK}_{a2} = 9.23$) is partially ionized, a weaker adsorption capacity is observed while better adsorption was expected due to the interaction between the negative charge of PHBA ($^-\text{OO-Ph-OH}$) and AC positive charge. Nature of the aromatic group seems to have in this case a great importance. Only the electron releasing effect of the group COO^- could explain this behaviour. The electron density of the aromatic ring increases reducing the interaction between the activated carbon π -electrons and π -electrons in PHBA.

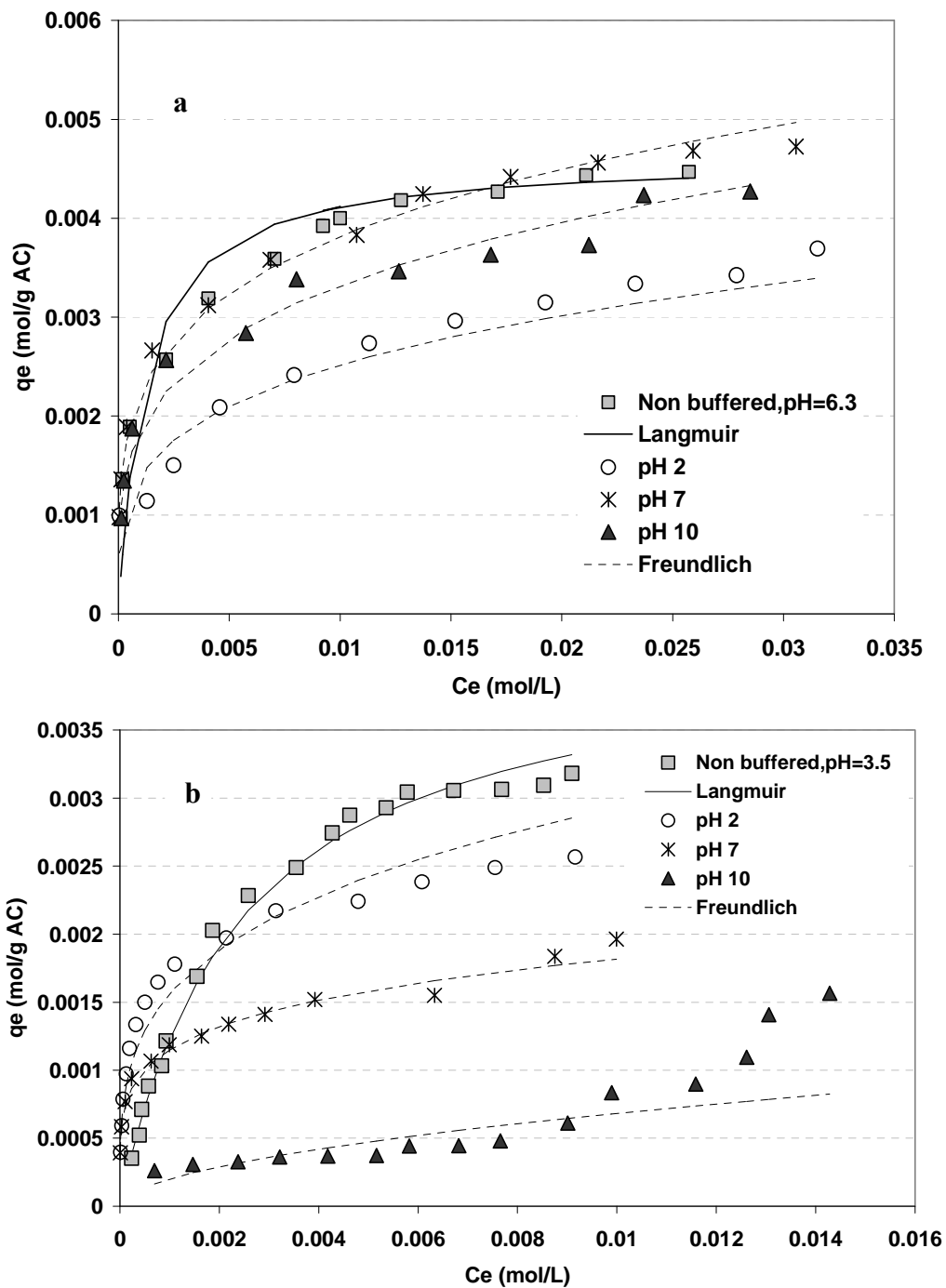


Fig. III.3. Effect of pH on the adsorption of P (a) and PHBA (b) onto AC S23 at 25°C.

At higher pH ($\text{pH} > \text{pH}_{\text{PZC}}$), both molecules are dissociated, forming Ph-O^- for the phenol and $^- \text{OO-Ph-O}^-$ for the PHBA, and AC surface is negatively charged. The electrostatic repulsion between same charges reduces the adsorption capacities.

At very low pH ($\text{pH} = 2.2$), the amount of Phenol adsorbed is lower than those obtained with other pH due to the competition with H^+ on carbonyl sites. For PHBA, low pH (2 and 3.5) seems to be more favourable: PHBA was found in the molecular form where its pH is lower than $\text{pK}_{\text{a}1}$ (4.8), so its improved adsorption capacity could be due to the presence of electron withdrawing group $-\text{COOH}$ decreasing the electron density of the aromatic ring and thus increasing adsorption of PHBA (Dabrowski *et al.*, 2005).

3.2. Effect of an inorganic salt: NaCl

In this part the effect of a selected salt, sodium chloride, very frequent in real industrial wastewater, has been investigated. The ionic strength of the solution is one of the factors that control both electrostatic and non-electrostatic interactions between the adsorbate and the adsorbent surface (Radovic *et al.*, 2001; Lorenc-Grabowska and Gryglewicz, 2007). The effect of salt concentration on adsorption of the two phenols on activated carbon S23 was studied by adding various amount of NaCl (5, 15, 30 and 40 g. L^{-1}) to the phenols solutions. The effect of salinity on the adsorption behaviour of phenol and PHBA from aqueous solution is presented in Figure III.4.a and III.4.b. This figure shows that at any concentration NaCl has only marginal effect. It seems that salt improves adsorption at low phenol concentration while no clear conclusion may be deduced at higher concentration, as difference less than 5% may be due to the experimental uncertainty.

In this study, the influence of all the others ions present in buffer solutions (phosphates, potassium...) has not been investigated but several authors report rather significant influence of some of them: favorable effect of KCl (Li *et al.*, 2008), positive impact of salts in general (Yang *et al.*, 2004). To understand the influence of the nature of AC and the adsorbed molecules on the adsorption performances, it was decided in this work to obtain the adsorption isotherms in unbuffered solutions and to measure the final pH in each run.

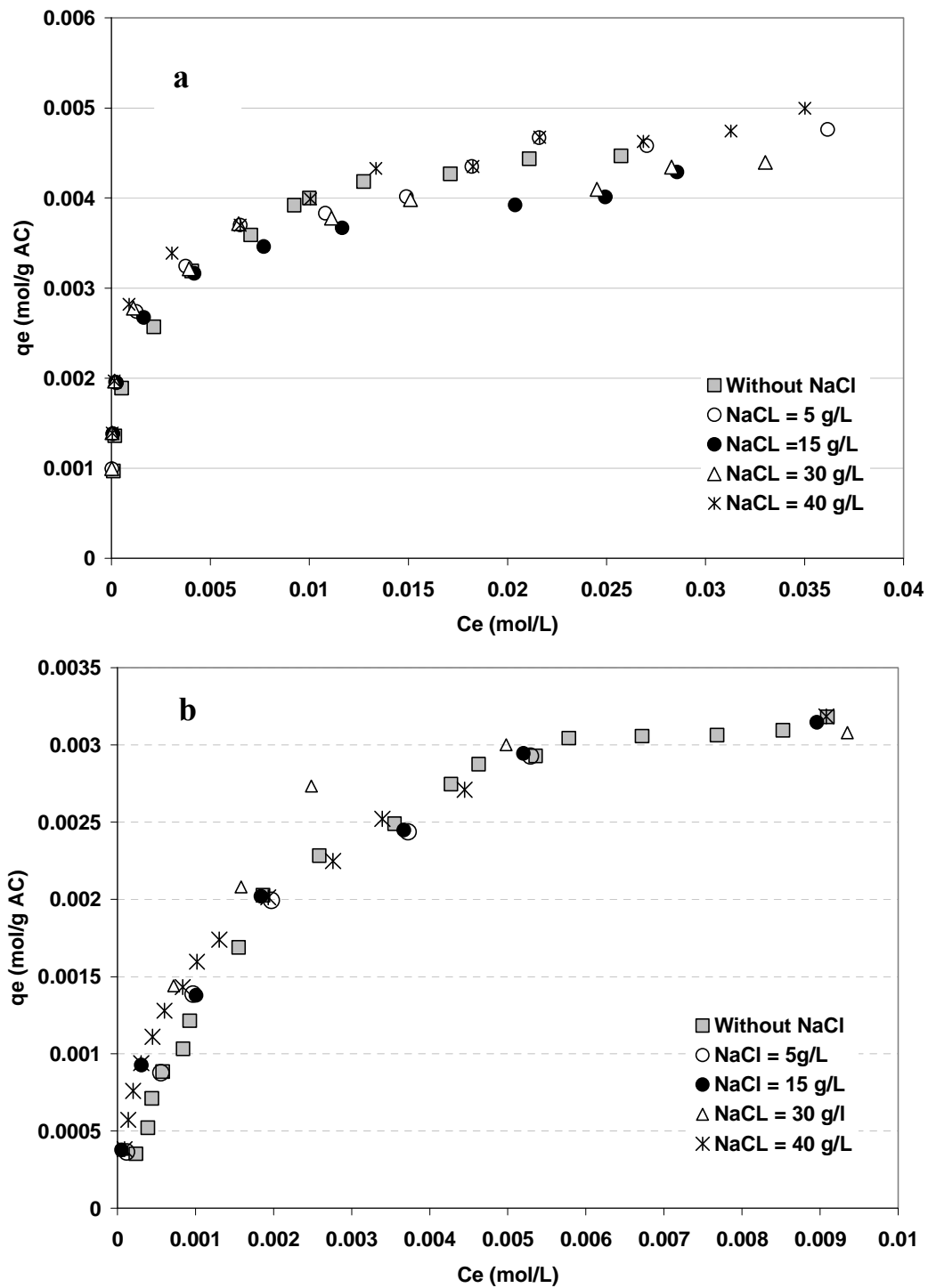


Fig.III.4. Effect of NaCl addition on the adsorption of P (a) and PHBA (b) onto AC S23 at 25°C (pH = 6.3 for P and 3.5 for PHBA).

3.3. Effect of temperature

The adsorption of phenol and PHBA from aqueous solution onto AC S23 at temperatures (25, 35 and 50 °C) is shown in Figure III.5a and III.5b. It is clear from these results that the phenols adsorption decreases with increasing temperature. This well known effect of temperature is expected for physical adsorption that is exothermic in nature in most cases (Halhouli *et al.*, 1995; Al-Asheh *et al.*, 2003; Garcia-Araya *et al.*, 2003; Li *et al.*, 2008). Due to this temperature dependence of adsorption capacity, the adsorption isotherms have been determined in a thermostatic bath at 25°C.

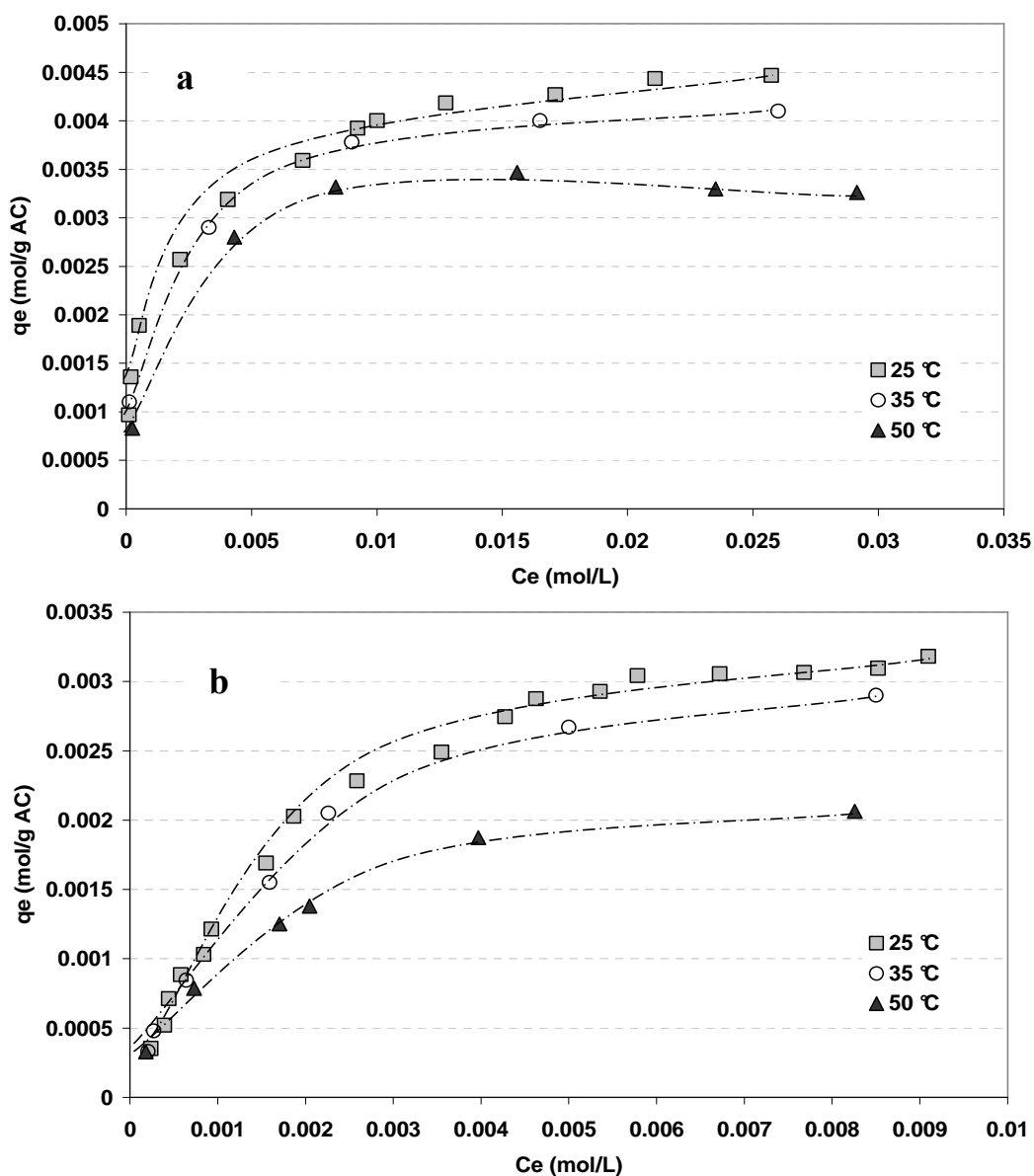


Fig. III.5. Effect of different temperatures on the adsorption of P (a) and PHBA (b) onto AC S23 (pH = 6.3 for P and 3.5 for PHBA).

4. Adsorption performance of activated carbons of various origins

4.1 Single component system

4.1.1 Screening of different activated carbons: phenol as reference model

The structural properties and the composition of six sludge based carbons being determined in previous paragraphs, their adsorption performances on phenol as a reference molecule model are investigated. The experiments were carried out by using the following conditions: 0.5 g of carbon and 100 mL of phenol solution at concentration of 0.005 mol.L^{-1} to 0.05 mol.L^{-1} .

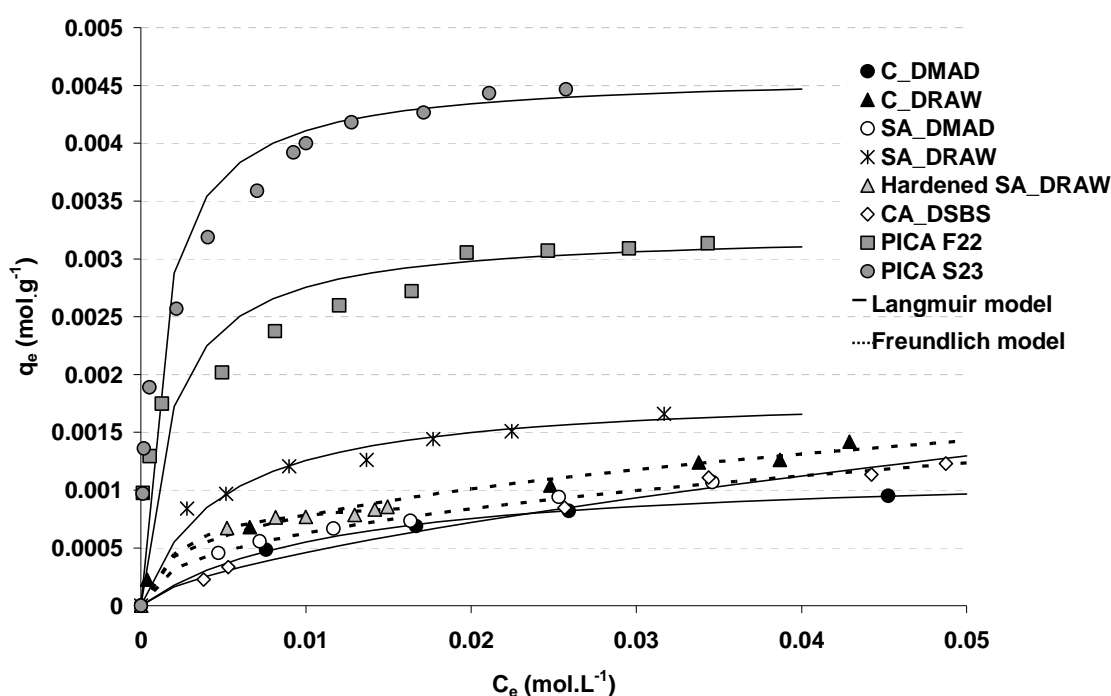


Fig. III.6. Adsorption isotherms of phenol onto different activated carbon materials at 25 °C (experimental data : symbols, Langmuir model: lines and Freundlich model: dotted lines).

Figure III.6 shows that the commercial S23 which has the highest BET surface area also lead to the highest phenol adsorption capacity in the investigated range of concentrations. The comparison of the six sludge based activated carbons reveals SA_DRAW as being sharply the best adsorbent followed by $\text{CO}_2\text{A_DSBS}$ and C_DMAD in the investigated range of concentrations. SA_DRAW presents the highest specific surface, while $\text{CO}_2\text{A_DSBS}$ has the lowest BET surface. Moreover, $\text{CO}_2\text{A_DSBS}$ contains less ash than the others SBACs which can explain its relatively good performances. It can also be noticed that the incorporation of 5 % of PVA in the SA_DRAW appears to have more effect on the phenol

uptake than expected by the change of surface area. Although, their BET surfaces are about 6 times lower than those of the commercial ACs, these carbons have rather convenient maximum adsorption capacities. The adsorption performance of SBACs for phenol is indeed higher than expected from their BET surface areas suggesting an economically attractive utilisation as adsorbents in waste water treatment.

4.1.2. Model application for phenol adsorption

The isotherms of phenol adsorption were evaluated according to the major two parameter models, Langmuir and Freundlich. The values of these parameters are reported in Table III.6.

Table III.6

Parameters of Langmuir and Freundlich models for the adsorption of phenol on the all studied activated carbons at 25 °C.

Phenols	Langmuir model (version 1)			Freundlich model		
	q_{\max} mol g ⁻¹	K_L L mol ⁻¹	R^2	n	K_F (mol g ⁻¹ (L mol ⁻¹) ^{1/n})	R^2
C_DMAD	0.0012	86.58	0.9992	0.383	0.0032	0.9864
C_DRAW	0.0015	171.11	0.9642	0.377	0.0044	0.9972
SA_DMAD	0.0014	88.15	0.9769	0.421	0.0044	0.9943
SA_DRAW	0.0019	211.47	0.9903	0.285	0.0044	0.9886
Hardened SA_DRAW	0.0018	37.76	0.9790	0.642	0.0088	0.9895
CO2A_DSBS	0.0010	431.19	0.9910	0.199	0.0019	0.9233
PICA S23	0.0046	833.17	0.9960	0.269	0.0132	0.9799
PICA F22	0.0032	567.41	0.9927	0.212	0.0066	0.9888

Firstly, from the correlation coefficient values in this Table and from Figure III.6, it is noticed that Langmuir model fitted well all the isotherms of all the ACs except the carbons C_DRAW and SA_DMAD for which Freundlich model is better than Langmuir. As expected, the two commercial activated carbons have q_{\max} (0.0046 mol g⁻¹ for S23 and 0.0032 mol g⁻¹ for F22) much higher than those of the sewage sludge activated carbons. Moreover the commercials activated carbons reveal higher K_L values indicating the strong interaction

between the phenol and the surface of these carbons. On the other hand, as expected from Figure III.6, has the highest q_{\max} and K_L values among the sewage sludge activated carbons. These data confirm the dramatic effect of adding a hardening polymer to SA_DRAW with a reduction of K_L by about 90%. CO₂A_DSBS has the lowest q_{\max} value (0.0010 mol. g⁻¹).

4.1.3. Adsorption of different substituted phenols onto S23, F22 and SA_DRAW

In the following part, the single and competitive adsorptions of four phenolic compounds (PCP; PNP; PHBA and P) onto the two commercials (S23 and F22) and SA_DRAW (the best SBAC) are investigated and compared. The experimental conditions and procedures have been explained in details in chapter II.

a- Single solute solution Isotherm

Figure III.7.a, b and c shows the single component adsorption isotherms for the four substituted phenols in aqueous solution onto SA_DRAW, S23 and F22, respectively. These results confirm that for all phenols adsorption capacity of SA_DRAW is much lower than for the two commercial activated carbons. As mentioned before, this lower performance could be due to much lower BET surface area (265 m² g⁻¹), the less developed microporous structure of SA_DRAW and its high ash content. It should also be noticed that despite S23 and F22 have nearly the same surface area, S23 exhibits the greatest adsorption capacities. This seems to be related to either the basic nature of this activated carbon and/or its lower ash content (Haydara *et al.*, 2003).

Whatever the activated carbon used, the single component isotherms revealed the strongest adsorption capacity of PCP - followed by PNP, P and PHBA. Different behaviour was observed in the case of SA_DRAW at higher concentrations, the adsorption capacities being increased strongly for PNP and PHBA, according to type II adsorption isotherm, whereas type I is convenient for all the other isotherms (Sun and Meunier, 2003). Type II isotherm indicates a multilayer adsorption consecutive to additional interactions between the molecules. The possibility of the formation of these layers generally occurs with mesoporous materials as SA_DRAW ($V_{\text{micro}} = 0.11 \text{ cm}^3 \text{ g}^{-1}$ and $V_{\text{meso}} = 0.17 \text{ cm}^3 \text{ g}^{-1}$). Even if the isotherms of PNP and PHBA seem to increase rapidly, type S isotherm, with constant value at higher concentrations, could be expected.

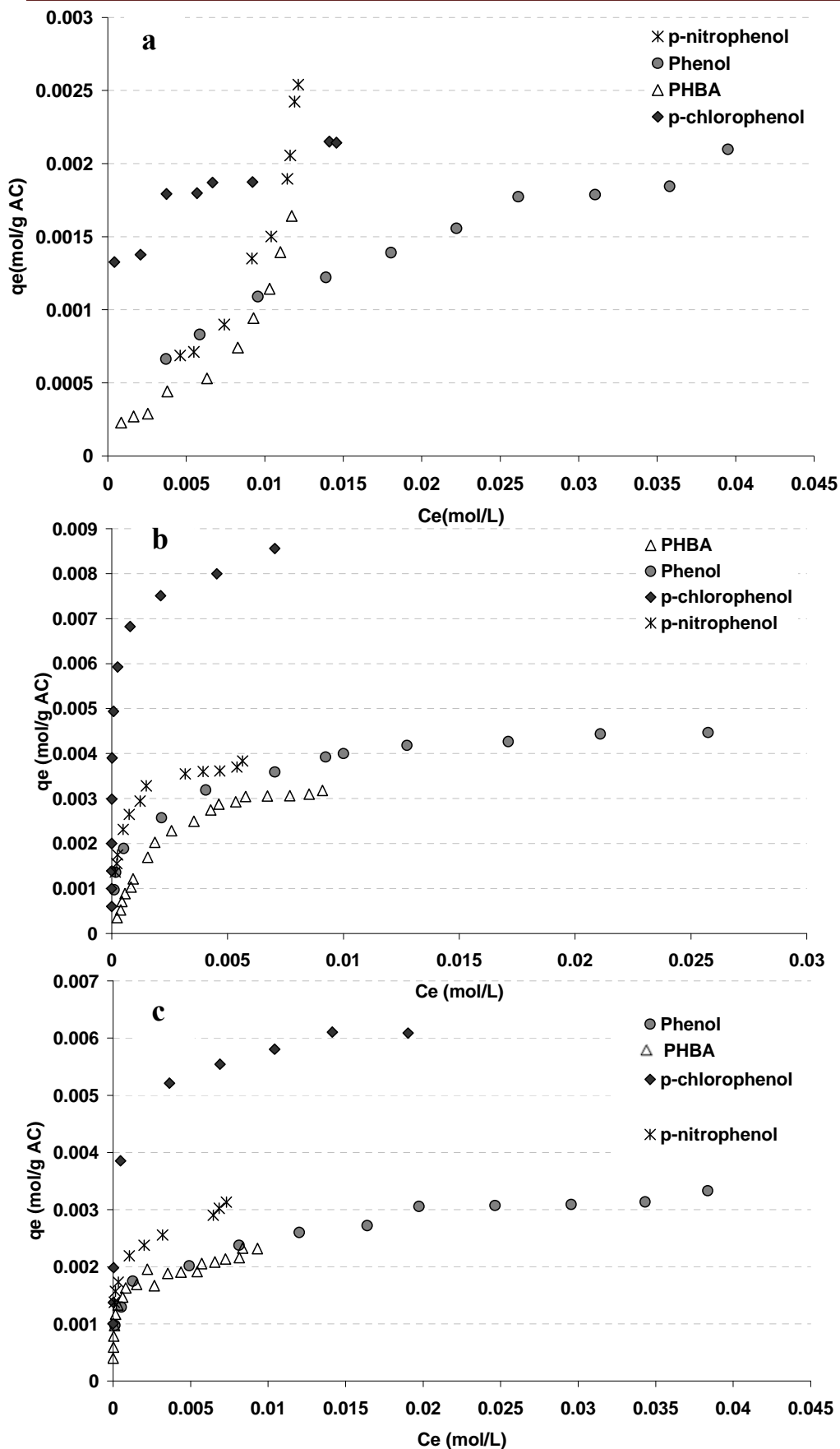


Fig.III.7. Adsorption isotherms at 25°C of single component of phenol, PHBA, *p*-nitrophenol and *p*-chlorophenol onto activated carbons (a) SA_DRAW, (b) S23 and (c) F22.

Independently of the nature of ACs, the adsorption capacities are known to depend on several characteristics of the phenols compounds in water: solubility, hydrophobicity, nature of the functional group on the aromatic molecules and ability to oligomerize (oxidative coupling). It can be noticed that comparing these characteristics leads to different trends thus it becomes complex to analyze the difference in affinities for the molecules studied as shown subsequently. These characteristics are collected in Table III.7 for the four molecules studied. The favorable or unfavorable effects are specified for each parameter and then discussed.

Table III.7

Favorable or unfavorable effects of molecules characteristics in single solute adsorption

	P	PHBA	PNP	PCP
Solubility	4	1	2	3
Hydrophobicity	3	4	2	1
Functional group	<i>unfavorable</i>	<i>unfavorable</i>	<i>favorable</i>	<i>favorable</i>
Oligomerisation	<i>Favorable</i>	<i>Unfavorable</i>	<i>Unfavorable</i>	<i>favorable</i>

Moreno-Castilla *et al.* (1995a) reported that the adsorption capacity increased with decreased water solubility of the phenolic compounds. In the present study, this parameter seems to be secondary since PHBA is the less adsorbed although it is the less soluble compound.

On the other hand, the activated carbons are mainly hydrophobic and display a strong affinity for organic molecules which have a limited solubility in water. Hydrophobic compounds tend to be pushed away towards the adsorbent surface being then more adsorbed than hydrophilic compounds (Lu and Sorial, 2007). The higher capacity of the PCP may be explained according to the hydrophobicity of the adsorbed molecules. Among these four phenols, PCP is more hydrophobic than PNP, P and PHBA, as expected from the magnitude of the logarithm of the octanol-water partition coefficient; $\log K_{ow,PCP} < \log K_{ow,PNP} < \log K_{ow,P} < \log K_{ow,PHBA}$.

Another parameter generally taken into account is the dispersive interactions between the activated carbon (electron donating) and the aromatic molecules (electron acceptor). The

nature of aromatic group could increase (electron releasing effect) or decrease (electron withdrawing effect) the electron density of the aromatic ring and influence the interactions between the surface groups and the aromatic ring. The enhanced interaction in the case of PNP and PCP is due to the electron-withdrawing effect of the -NO₂ and the -Cl substituents, as they reduce the overall electron density of the aromatic ring, increasing its ability to accept the electron of AC graphite layers (Dabrowski *et al.*, 2005).

When phenols are concerned a special adsorption mechanisms may involve oligomerization which is generally regarded as irreversible adsorption. Many researchers have been confirmed that some phenolic compounds undergo oligomerization on the surface of activated carbon when molecular oxygen is present in the test environment (Uranowski *et al.*, 1998; Lu and Sorial, 2007). As seen in chapter I, the critical oxidation potential (COP) is the most important parameter to identify the molecules which can be oligomerized: The more the value of COP, the less the molecule is able to oligomerize (Lu and Sorial, 2004). In this study, oligomerization could only occur for phenol (COP = 1.089V) and PCP (COP = 1.094V) explaining the high adsorption of PCP and rather high of phenol despite its low solubility and hydrophobicity.

The consideration of all these characteristics seems quite favorable to the adsorption of PCP and PNP in agreement with the isotherms obtained. For these single solute systems, the solubility seems to have a limited impact.

b- Langmuir and Freundlich models

For a comparison of single solute isotherm results in a quantitative manner, the isotherms were represented by Langmuir and Freundlich models and the constants obtained according to these two models are listed in Table III.8. The correlation coefficients square (R^2) for both models at 25 °C suggested that the empirical Langmuir equation was much more convenient than Freundlich equation in describing the adsorption of all the phenolic compounds onto the two commercial ACs (S23 and F22). However, for SA_DRAW no good fit could be obtained with the two models, Freundlich model being found to better represent the adsorption data for PNP and PHBA, while Langmuir model better fitted the data of PCP and P.

The Langmuir equation being convenient for the two commercial AC clearly indicates that S23 provides the highest maximum adsorption capacity (q_{max}) for the four phenols, and

the best adsorption equilibrium constant (K_L) for P and PCP. Concerning the adsorbates, the highest value for PCP proves its high affinity with this carbon surface compared to the other phenols studied in this work. For F22, the values of K_L are nearly the same for PCP, PNP and PHBA, and the higher value of q_{\max} indicates here again more affinity of PCP with the carbon surface.

Table III.8

Parameters of Langmuir and Freundlich models for the adsorption of single solute of P, PCP, PNP and PHBA on three types of activated carbons at 25 °C

ACs	Phenols	Langmuir model			Freundlich model		
		q_{\max} mol g ⁻¹	K_L L mol ⁻¹	R^2	1/n	K_F (mol g ⁻¹ (L mol ⁻¹) ^{1/n})	R^2
S23	P	0.0037	2941	0.9988	0.161	0.007	0.9296
	PCP	0.0084	15151	0.9977	0.178	0.015	0.7711
	PNP	0.0041	2777	0.9989	0.269	0.016	0.9413
	PHBA	0.0039	476	0.9886	0.443	0.031	0.9672
F22	P	0.0033	500	0.9917	0.212	0.007	0.9097
	PCP	0.0063	3333	0.9959	0.208	0.016	0.9763
	PNP	0.0031	2829	0.9934	0.639	0.191	0.7190
	PHBA	0.0021	4224	0.9935	0.444	0.041	0.6291
SA_DRAW	P	0.0026	74	0.9726	0.469	0.009	0.9926
	PCP	0.0023	909	0.9908	0.144	0.004	0.8794
	PNP	0.0025	43	0.5595	1.354	0.841	0.9253
	PHBA	0.0016	90	0.1759	0.741	0.031	0.8896

4.2. Competitive adsorption of P, PHBA, PCP and PNP

The studies of such competitive systems, especially those containing a large number of solutes, are rarely interpreted due to the complexity of the phenomena involved. Many factors influence adsorption equilibria as the structural and energetic heterogeneity of the adsorbent and the differences in physicochemical properties of adsorbates (Lu and Sorial, 2009). Thus, the same characteristics of the molecules than those used in single solute solution are involved but their effect will be entangled and then even more difficult to analyse (Table III.7).

The results of competitive adsorption of an equimolar mixture of four phenols onto SA_DRAW, S23 and F22 are shown in Figure III.8.a, b and c, respectively. The adsorption isotherms of these phenols range in the following order: PNP > PCP > PHAB or P for the three activated carbons. For these two last phenols, the order depends on the activated carbon

and the phenols concentrations and an inversion of selectivity between PHBA and P onto SA_DRAW and S23 was observed. At low liquid phase concentrations, i.e., high relative carbon loading, AC had enough sites for adsorption and thus less competition occurs. At higher concentrations, i.e., low carbon loading, two phenomena come into play. First, there were fewer sites available on AC inducing a stronger competition, and then concentrations approach the limit of the solubility of each the adsorbate: the less soluble tend to be adsorbed (Garcia Araya *et al.*, 2003). Among the four phenols investigated here, the order of decreasing solubility is PHBA < PNP < PCP < P which does not at all correspond to the order of preferential adsorption. The difference of solubility could only explain the inversion of selectivity between phenol and PHBA. This parameter would then be more influential in competitive adsorption than in single one.

The hydrophobic nature of the adsorbate could also be taken into account. In agreement with single component adsorption PNP and PCP which have hydrophobic characteristics, are preferentially adsorbed compared to P and PHBA which have hydrophilic groups. This preferential adsorption of PNP- PCP is also in agreement with the well known theory of the formation of π - π bond, where activated carbon acts as an electron donor, and the solute benzene ring has an electron withdrawing character (Chern and Chien, 2003; Bansal and Goyal, 2005). The nitro-group of PNP is electron withdrawing, thereby causing a favourable decrease in electron density of the π -electrons of the benzene ring. In the order of preferential adsorption, the PCP is the second adsorbable compound owing to the withdrawing effect of the - Cl group (Ayrançi and Duman, 2005). This is in accordance with Srivastava and Tyagi (1995) which reported that PNP is preferentially adsorbed in PNP- PCP mixture.

As mentioned before, the phenol oligomerization has to be considered as a mechanism of phenol adsorption. Among the four phenols selected in this work, only P and PCP oligomerize, thus a part on the amount of molecules adsorbed in single solute solution is due to this irreversible adsorption. When considering a mixture of several phenols on ACs, oligomerization is hampered by non oligomerisable molecules.. There are less available sites as compared to the single system and adsorbed molecules are close to each other: the presence of a molecule that does not oligomerize prevents the oligomerization of the other. (Lu and Sorial, 2009).

In this four component mixture, oligomerization of phenol and PCP should be highly reduced by the presence of PNP and PHBA. Indeed, the adsorbed amounts of phenol and PCP are rather low compared with single solute solution.

Finally, these multicomponent isotherms were modeled by the Optimized Langmuir-Freundlich model and the parameters are collected in Annex 4.

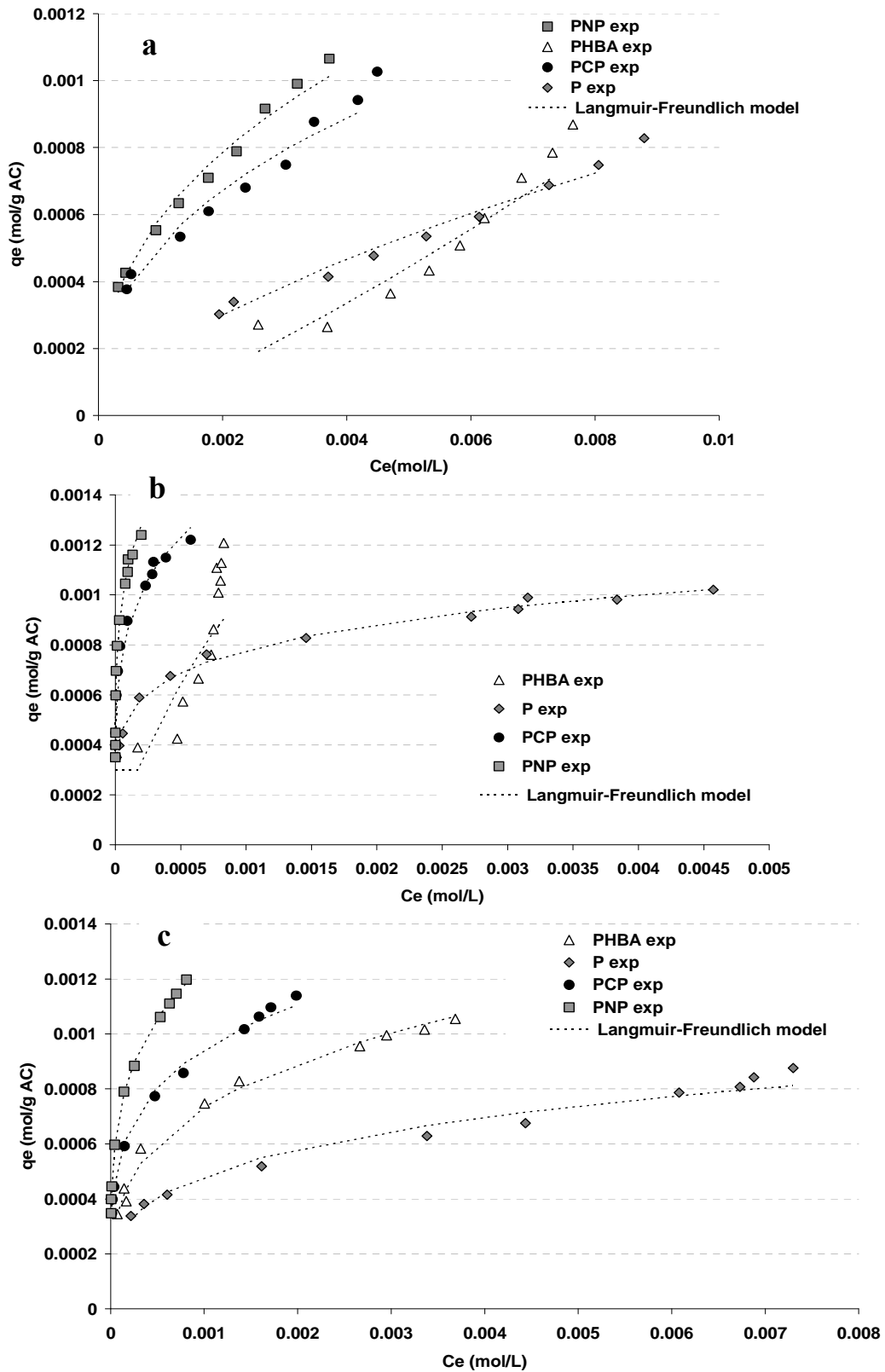


Fig. III.8. Comparison of experimental data of adsorption isotherms with the calculated data by Langmuir- Freundlich model for equimolar mixture of phenol, PHBA, p-nitrophenol and p-chlorophenol onto SA_DRAW (a), S23 (b) and F22 (c) at 25 °C.

5. Conclusions

It may be concluded that the dried activated carbons resulting from sludge treatment despite rather low surface area shows an adsorption capacity of about half the ones of high performance commercial activated carbons. As it may still be improved it should be considered as a convenient low-cost material for the removal of phenol and substituted phenols from polluted water. Production of activated carbon from sludge constitutes thus a possible way of valorisation of this abundant waste.

Concerning adsorption features of these four phenols on various activated carbons it may be concluded that for single-solute adsorption, hydrophobicity and the ability to undergo oligomerization are the main factors to explain the higher capacity of adsorption of PCP. Competitive adsorption has been performed to give insight into some of the factors affecting selective uptake of various phenols on activated carbon. Irreversible adsorption of P and PCP does not occur due to the hampering of oligomerisation. Without this irreversible adsorption, mainly solubility and hydrophobicity can explain the order of preferential adsorption : PNP > PCP > PHBA > P at high concentration.

Chapitre III. Adsorption de polluants aromatiques sur charbons actifs : des charbons actifs commerciaux et des charbons issus de la pyrolyse de boues de station d'épuration

Dans le domaine du traitement de l'eau, l'adsorption est un des moyens les plus efficaces pour éliminer les polluants organiques présents dans les effluents aqueux. Le principal inconvénient de cette technique non destructrice est qu'il faut régulièrement régénérer le charbon actif ce qui alourdit la facture globale du traitement car une grande quantité de matériau doit subir une régénération thermique onéreuse. Afin de diminuer le montant global, il apparaît aujourd'hui intéressant de développer des matériaux à faible coût. Dans le contexte actuel de développement durable, la fabrication de charbon actif à partir de déchets d'origines diverses est une voie de valorisation économiquement et écologiquement intéressante.

L'objectif de cette première étude est de comparer les performances de charbons actifs commerciaux (PICA S23 et F22) et de six charbons actifs produits à partir de la pyrolyse de boues de stations d'épuration. Ces matériaux carbonés ont été préparés par l'Imperial College (Londres, Angleterre) et le laboratoire GEPEA (Nantes, France) dans le cadre du projet Européen REMOVALS (FP6-018525). Les propriétés texturales et chimiques de ces charbons actifs ont été déterminés puis ces matériaux ont été comparés à l'aide des isothermes d'adsorption obtenues avec le phénol. Enfin, les trois adsorbants les plus performants ont été sélectionnés pour une étude plus complète sur l'adsorption de différents composés organiques seuls ou en compétition.

Les charbons actifs ont subi les analyses suivantes : analyse des propriétés texturales (surface BET et volumes poreux), teneur en métaux (Zn, Ni, Co, Mn, Fe), taux de cendres, composition élémentaire (C, H, N, S, et O), pH au point de charge nulle pH_{PZC} ou pH de contact, fonctions de surface par analyse de Boehm (uniquement pour les charbons commerciaux) et analyse thermogravimétrique. Il ressort de cette première étude que les charbons issus de la pyrolyse des boues ont une surface BET 4 à 10 fois plus faible que les charbons commerciaux. Ils affichent des proportions en métaux, en taux de cendre et en oxygène particulièrement élevés, par contre leurs compositions en carbone est plutôt faible. Les charbons synthétisés sont très différents des charbons actifs commerciaux : ils sont très fortement chargés en oxydes métalliques et en sels inorganiques.

Les performances des différents charbons ont été évaluées en comparant les isothermes d'adsorption du phénol. Les charbons de boues présentent des capacités d'adsorption plus

faibles que les charbons commerciaux. Il ressort de cette étude comparative que le charbon actif SA_DRAW est le plus performant avec des quantités adsorbées correspondant à environ la moitié de celle du F22 ($q_{\max} = 0.032 \text{ mol g}^{-1}$) et du tiers du S 23 ($q_{\max} = 0.046 \text{ mol g}^{-1}$), ce qui reste une performance très intéressante compte tenu de sa faible surface spécifique.

Le charbon de boue SA_DRAW et les charbons actifs commerciaux ont ensuite été utilisés pour adsorber différents composés phénoliques seuls et en compétition avec le phénol : *p*-Chlorophenol, PCP, *p*-Nitrophenol, PNP, and *p*-Hydroxy benzoic acid, PHBA. Globalement, les capacités d'adsorption du SA_DRAW restent plus faibles que celles des charbons commerciaux à cause de sa plus petite surface BET et de son fort taux de cendre. Pour les trois charbons utilisés, les isothermes des composés seuls montrent que l'ordre des capacités d'adsorption est le suivant : PCP > PNP > P > PHBA. Notons que la différence entre le P et le PHBA n'est pas très marquée. Pour le charbon de boue SA_DRAW, à forte concentration, les isothermes P et PCP sont de type I alors que celles du PNP et du PHBA suivent une allure de type II. Ce comportement est sûrement lié à son caractère mésoporeux mais on peut s'attendre à une évolution en S pour des concentrations plus fortes que celle testées. Pour les charbons actifs commerciaux, les isothermes sont de type I avec formation d'un plateau à forte concentration. Outre la nature du charbon actif, certaines caractéristiques des molécules aromatiques ont une influence sur l'adsorption. L'hydrophobicité et le caractère attracteur des substituant aromatiques favorisent l'adsorption alors que la solubilité lui est défavorable. L'hydrophobicité donne un ordre de capacité en accord avec les résultats, conforté par le caractère attracteur des groupements -Cl et -NO₂. Par contre, il apparaît que la solubilité soit un paramètre secondaire. Notons, que le PCP et le P sont les seules molécules qui peuvent oligomériser par couplage oxydant. Cette part d'adsorption irréversible peut expliquer les fortes quantités de PCP adsorbés. Ces quatre molécules ont ensuite été étudiées en compétition dans des mélanges équimolaires. Les isothermes obtenues pour les trois charbons montrent une adsorption préférentielle du PNP suivi du PCP, puis en fonction du domaine de concentration le P ou le PHBA. En effet, une inversion de sélectivité est observée pour le SA_DRAW et le S23 : à faible concentration, le P s'adsorbe préférentiellement, à forte concentration c'est le PHBA. Cette inversion peut s'expliquer par la solubilité du PHBA beaucoup plus faible que celle du P donc favorable à l'adsorption du PHBA dans le domaine des fortes concentrations. En compétition, le PCP et le P sont plutôt décevants, la diminution des capacités d'adsorption s'explique la diminution de leur adsorption irréversible par oligomérisation. En présence de molécules qui ne peuvent pas participer au couplage oxydant (PHBA et le PNP), le P et le PCP n'oligomérisent pas.

CHAPTER IV
PHOTOCATALYTIC OXIDATION

A- Oxidation using tissue

1. Introduction

Heterogeneous photocatalytic process using anatase TiO_2 as catalyst is one of the most promising advanced oxidation processes. This process is based on the generation of very reactive species such as hydroxyl radicals ($\cdot\text{OH}$) that can oxidize a broad range of organic pollutants quickly and non-selectively (Vohra *et al.*, 2006). Most organics can be mineralized to water, carbon dioxide and mineral acids by successive hydroxyl radical attack and fragmentation.

Titanium dioxide (TiO_2) catalyzed photocatalysis is broadly used because of its capability in removing a wide range of pollutants. The photochemical stability, low toxicity and low cost are the other advantages of TiO_2 (Arana *et al.*, 2002; Lianfeng *et al.*, 2003; Shon *et al.*, 2005; Areerachakul *et al.*, 2007). However, the application of fine TiO_2 powder is generally accompanied by complications arising from the need for separation of the powder from the treated pollutants, which hinders their wide-scale application in industry. Several efforts have been made to enhance the separation performance of TiO_2 powder, such as immobilization of TiO_2 powder onto various supports (Durgakumari *et al.*, 2002; Kang, 2002; Thevenet *et al.*, 2005; Han *et al.*, 2007). Among these supports, activated carbon (AC) is an excellent alternative because of its high adsorption capacity and high specific surface area. Furthermore, adding TiO_2 to AC could induce some beneficial effect because of the highly adsorptive characteristic of AC with respect to organic molecules and also resolve the problem of achieving optimum adsorption strength of the adsorbed molecules on the adsorbent to improve TiO_2 photocatalytic activity (Matos *et al.*, 2007). In addition, some authors have also reported a synergistic effect for AC-supported TiO_2 systems of some organic pollutants in the photocatalytic process (Lee *et al.*, 2004; Li *et al.*, 2006 & 2007; Liu *et al.*, 2007).

In the present work, supported TiO_2/AC tissue (supplied by Ahlström) photocatalyst was used. The photocatalytic activity of this media was evaluated by degradation of phenol in the channel photoreactor presented in chapter II. The studied process is composed of two sequential batch steps: every cycle alternates a step of adsorption and a step of photocatalytic oxidation in the presence of UV, at 25 °C and atmospheric pressure. During the oxidation step, the phenol is oxidized and the tissue is regenerated, and then used for a new adsorption /

oxidation cycle. The effects of several operating parameters such as the initial phenol concentration and H₂O₂ addition on the photocatalytic activity of TiO₂/AC tissue were investigated. The kinetics of phenol adsorption and degradation were studied.

2. Characterization of materials

In this part of the work, a special multilayer material produced by Ahlström Paper Group Company was used. The methods used for preparation of these materials and their characteristics were discussed in details in chapter II.

Our study was carried out using three different media; AC media, TiO₂/AC media (tissue) and TiO₂ media (Figs.II-1, 2 and 3, respectively, in Chapter II) and then compared to the original granular AC made from coconut which used in all studied media containing carbon. The compositions of these different media are summarized in chapter II.

The specific surface area of samples was determined using a Micrometrics ST-2000 automated apparatus based on the Brunauer–Emmett–Teller (BET) method at 77K with N₂ as adsorbent and H₂ as the carrier gas. The surface structure and particle size of the used media were investigated using Scanning Electron Microscopy (SEM). Additionally, the composition of AC in the tissue (AC/ TiO₂) and the original AC powder was analyzed by EDX. The thermogravimetric analysis, TGA was used to identify the thermal loss of the original AC sample. This TGA analysis will be later used to compare the thermal behaviour of the used and virgin AC samples.

2.1. Surface area and porosity

The analyzed values of specific surface areas (S_{BET}) and pore size distribution for the original granular AC and those of TiO₂ media are presented in Table IV-1.

As expected, the TiO₂ media exhibits very small S_{BET} (75 m².g⁻¹) as compared to that of AC powder (1065 m².g⁻¹). The original activated carbon has a microporous volume of 0.46 cm³.g⁻¹, and a mesoporous one of 0.046 cm³.g⁻¹. For TiO₂ media, a significant decrease in microporous volume was observed and it was mainly mesoporous.

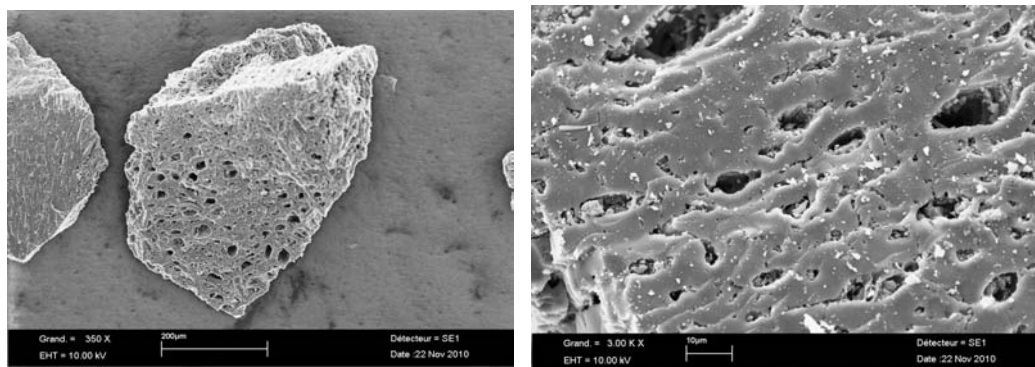
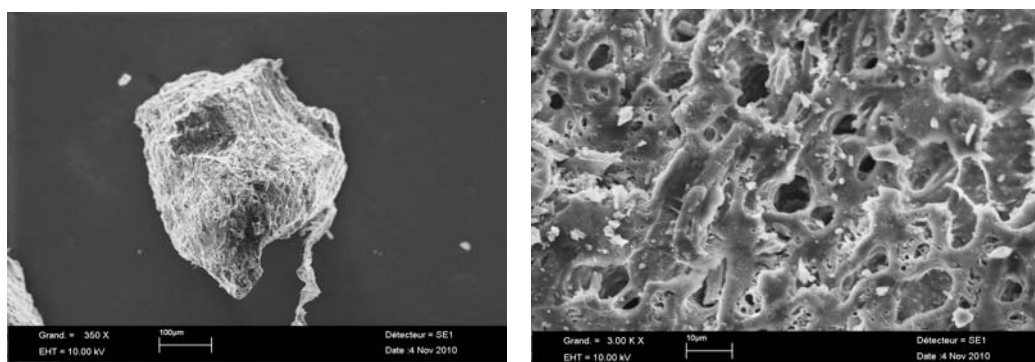
Table IV-1Apparent surface area and pore volume distribution of AC powder and TiO₂ media

Material	BET Surface (m ² .g ⁻¹)	*Microporous Volume (cm ³ .g ⁻¹)	*Mesoporous Volume (cm ³ .g ⁻¹)	Size of grains (mm)
Media TiO ₂	75	0.010	0.094	0.005 - 0.01
Granular AC	1065	0.460	0.046	0.25 - 0.60

*Microporous volume: pore size < 2nm, Mesoporous volume: 2nm < pore size < 50 nm.

2.2. Electron microscopic analysis

The SEM morphology of the granular AC, TiO₂ media and the AC in TiO₂/ AC tissue is presented in Figures IV-1, IV-2 and IV-3, respectively. Selected SEM images of these media are compared. As it is clearly shown in Figure IV-1, the pores are well developed in the granular AC. Figure IV-3 shows the binding of TiO₂ to the surface media.

**Fig. IV-1.** SEM image of the original granular AC (x350, left and x 3000, right).**Fig. IV-2.** SEM image of AC in TiO₂ / AC tissue (x350, left and x 3000, right).

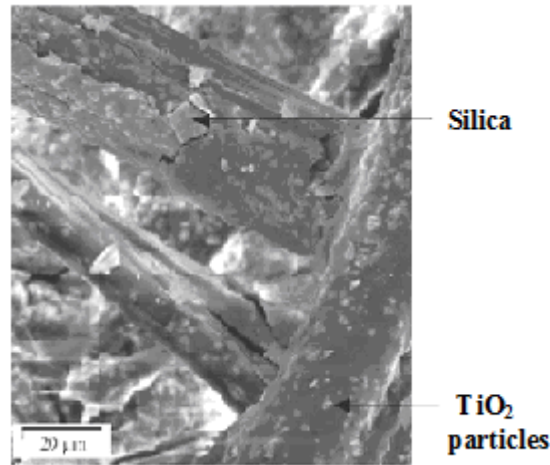


Fig. IV-3. SEM image of the surface of TiO₂ media (x 1000, right) (Thevenet *et al.*, 2005).

2.3. Energy dispersive X-ray microanalyses (EDX)

EDX analysis was used to determine qualitatively the elemental composition of the original AC powder and the AC in the TiO₂/AC tissue in the selected regions shown in Fig. IV-4a and IV-4b. Figure IV-5a shows the main peaks of carbon and oxygen in the original granular AC sample. For the AC in the TiO₂/AC tissue, two regions are analysed, showing very different results concerning the presence of significant amounts of Ti, Si and O in Region I and the absence of Ti in Region II (Fig. IV-5b). So it is considered that the sample of AC in the TiO₂/AC tissue contained these three main elements (Ti, Si, and O) beside C. The elemental composition percentages of these samples are given in Table IV-2.

Table IV-2

EDX elemental composition of the original granular AC and AC in TiO₂ /AC tissue, in two different regions as indicated in Fig. IV.4

Sample	Composition							
	C		O		Ti		Si	
	Wt %	*At%	Wt%	*At%	Wt%	*At %	Wt%	*At %
Original granular AC	95.20	96.35	4.80	3.65	-	-	-	-
AC in TiO ₂ /AC tissue (region I)	0.18	0.09	60.16	76.47	17.61	7.48	22.05	15.96
AC in TiO ₂ /AC tissue (region II)	78.98	83.55	20.39	16.19	-	-	0.37	0.17

*At: atomic percentage.

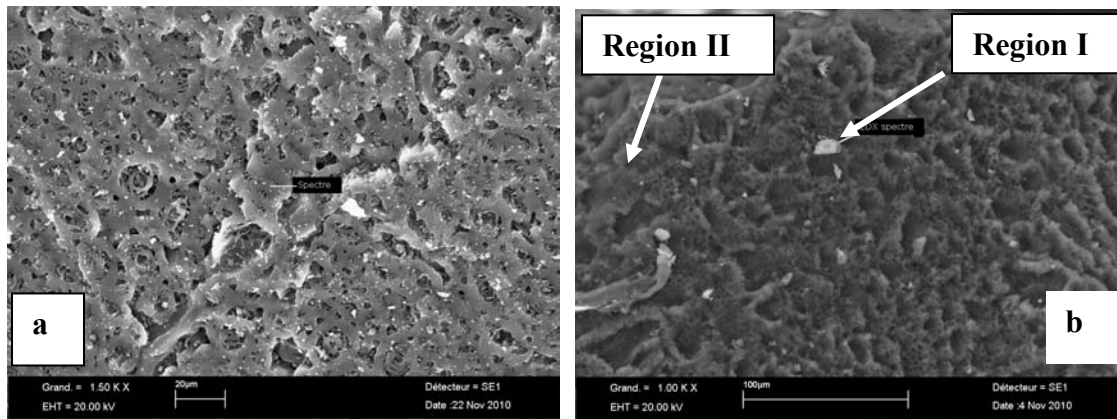


Fig IV-4. Cross sectional SEM of the original granular AC (a) and AC in the TiO₂/AC tissue (b; Region I & Region II) in which two different regions are pointed out.

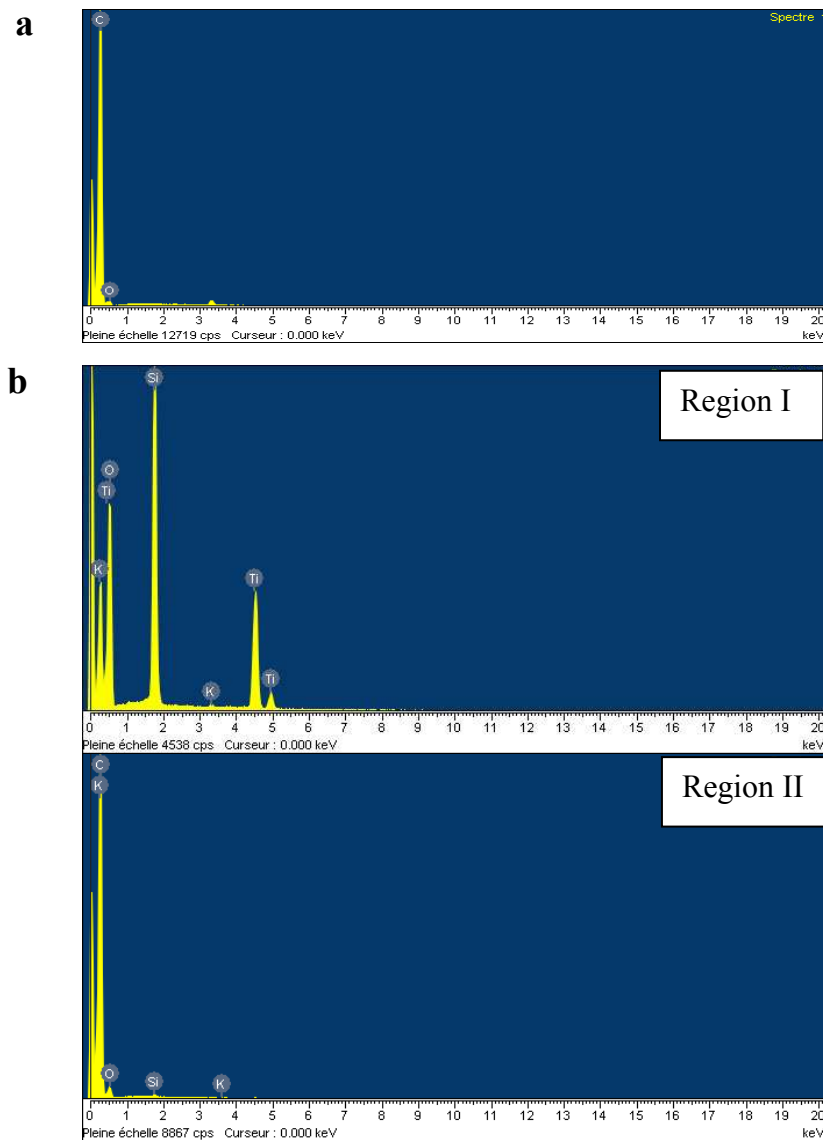


Fig. IV-5. EDX diagrams of the original granular AC (a) and AC in the TiO₂/AC tissue in two different regions (b; Region I & Region II).

It must be emphasized that the elemental percentages obtained by EDX analysis in this table give qualitatively and not quantitatively an idea about the proportion of certain elements in specific region on the sample surface and not on the whole surface.

2.4. Thermogravimetric analysis of the original activated carbon

According to the literature, the thermogravimetric analysis (TGA) allows the thermal decomposition of acidic groups on the activated carbon surface (De la Puente *et al.*, 1997; Figueiredo *et al.*, 1999). It shows also the thermal desorption of adsorbed species after adsorption and oxidation steps.

The protocol of the thermogravimetric analysis is detailed in the chapter II. These measures were made under atmosphere of nitrogen for overcoming the combustion of activated carbon.

The results of TGA of AC are represented in Figure IV-6. A first loss of weight (3.92 %) is observed at nearly 100 °C corresponding to the rate of humidity of AC. There is then a second weight loss (4.39 %) much slower and progressive until approximately 630 °C. Then, there is an inflexion point and another weight loss (12.74 %) at 700 °C corresponding to the calcination of the surface functions formed during the activation of carbon.

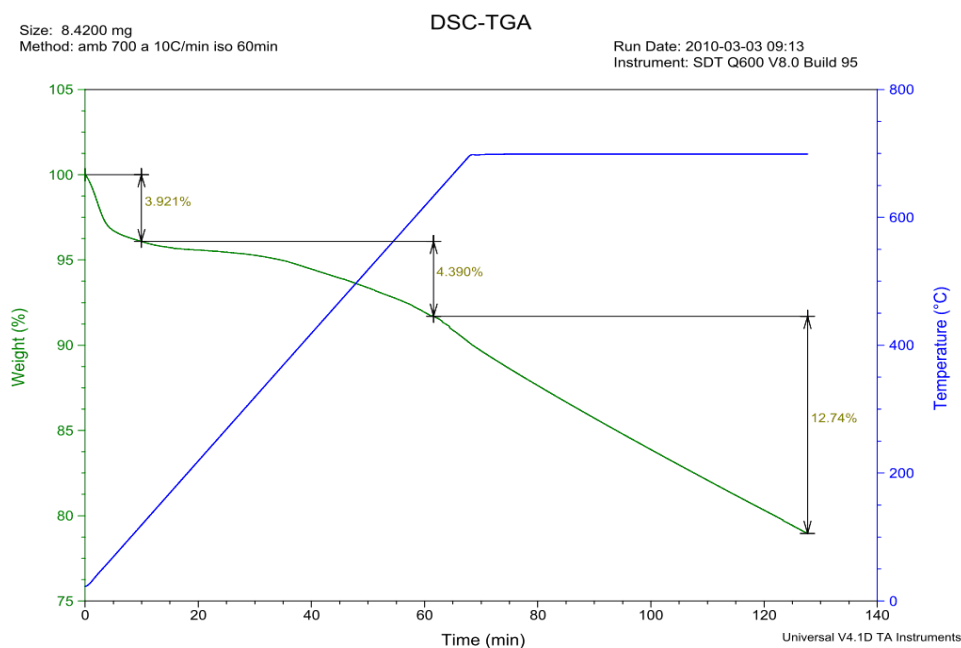


Fig. IV- 6. Thermogravimetric analysis of the original granular AC.

De la Puente *et al.* (1997) and Figueiredo *et al.* (1999) cited that the successive weight losses by increasing the temperature corresponds to the decomposition of the carboxylic groups (150-400 °C), lactones functions (350-600°C) and phenols groups (which are decomposed between 600 and 700 °C). Moreover, Stratakis and Stamatelos (2003) assumed the first decrease up to about 150°C to be mainly due to the water evaporation– desorption. A second loss observed between 200 and 420°C was attributed to desorption of organic compounds.

3. Adsorption isotherms

3.1. Comparison of the adsorption isotherms of different adsorbents

The adsorption on the surface of adsorbent is the initial step preceding the photocatalytic degradation step. It is an interaction between the molecules to be degraded and the surface of adsorbent. It is principally these molecules in the adsorbed state onto TiO₂ that would determine the initial speed of photocatalysis (Amalric *et al.*, 1996; Robert *et al.*, 2000; Guillard *et al.*, 2003).

To understand well the processes of adsorption as well as their modelling, it is necessary to carry out the isotherms of adsorption. These experiments allow to show the differences between the adsorbents.

To determine the capacities of adsorption of various adsorbents, the isotherms of adsorption at 25 °C were realized. The study was carried out using four adsorbents, TiO₂ media AC media, TiO₂/ AC tissue and the original granular AC using phenol as a pollutant reference model. The experimental conditions are discussed in the previous chapter II. As previously mentioned for the original granular AC, the mass was equal to 0.5 g and for the tissue, the total mass was 0.8 g corresponding to 0.5 g of AC. The calculation is then made by two different ways for AC media and AC / TiO₂ tissue: the classic calculation which used for the total mass of media and the other calculation by taking into account only the mass of AC. The adsorption isotherms of phenol using granular AC, AC media, TiO₂/ AC tissue and TiO₂ media are represented in Fig. IV-7.

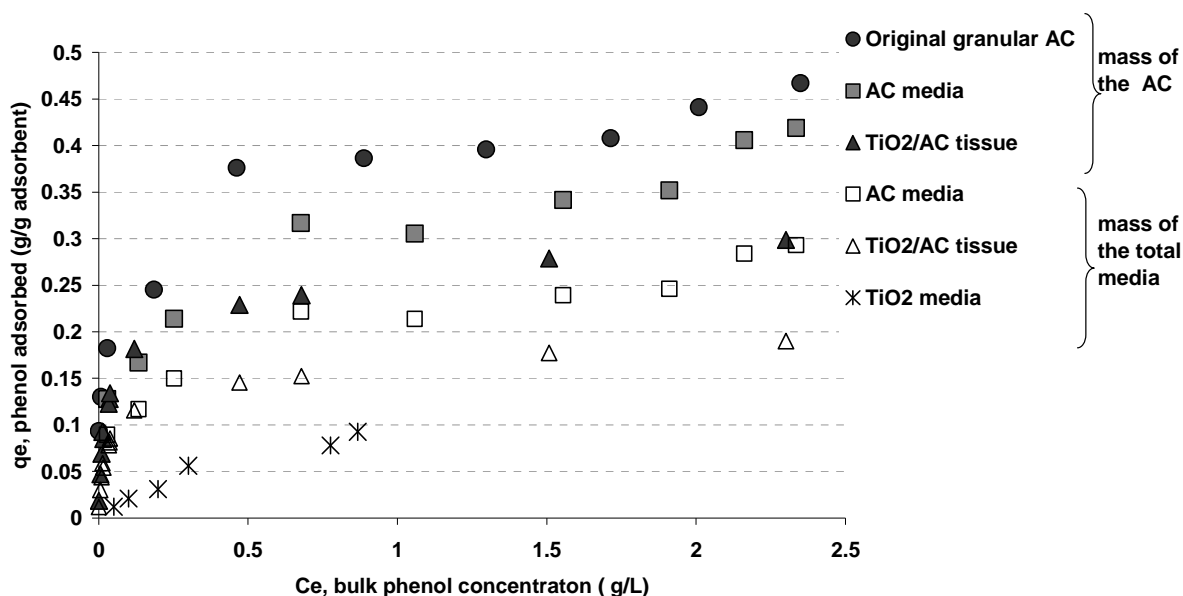


Fig. IV-7. Adsorption isotherms of phenol onto original granular AC, AC media, TiO₂/ AC tissue and TiO₂ media at 25 °C.

It was noticed that the adsorption capacity of original granular AC was about 10-20% higher than that of AC media on the plateau when comparing the same AC weights. It may be explained on the assumption that some sites of AC in the media were not in contact with the aqueous solution owing to the binding with the fibres used for fabricating it. These fibres recover partially the grains of AC and hinder some of its sites of adsorption.

A decrease of the capacity of adsorption of the TiO₂/AC tissue is observed as compared to the AC media. The same trend is even observed when the isotherms are calculated by taking into account only the mass of AC, the isotherms remains lower than that of original granular AC. This phenomenon seems to be due to the decrease of the available number of sites of adsorption due to the blocking of the access to some of them by TiO₂/ SiO₂ mixture, deposited in the form of aqueous suspension on the fibres. These results were well supported by SEM and EDX analyses discussed earlier. In these results, SEM and EDX analyses confirmed the presence of Ti and Si blocking some of the adsorption sites of the AC in the TiO₂/ AC tissue (Figs. IV-2 and IV-5).

Figure IV-7 also indicated that among all studied adsorbents, TiO₂ media has the lowest adsorption capacity. This can be partially explained on the basis of the much lower S_{BET} ($75 \text{ m}^2 \cdot \text{g}^{-1}$) of TiO₂ media support as compared to that of the original granular AC ($1065 \text{ m}^2 \cdot \text{g}^{-1}$).

3.2. Comparison of the Langmuir and Freundlich models parameters

The Langmuir and Freundlich models of adsorption are tested for comparison and used to obtain the parameters of phenol adsorption on different media. The isotherm equations were detailed in chapter I.

The Langmuir model has two linearization procedures. As seen in the preceding chapter I, the first version is more accurate at low concentrations while the second is rather applied at high concentrations. The first linearization is used with TiO₂ media, while the second is applied with all other adsorbents used

The parameters of Langmuir and Freundlich models as well as the correlation coefficients indicating the agreement between the experimental and the calculated data by these two models are summarized in Table IV-3. The adsorption constant of Langmuir (K_L) is higher for the original granular AC than for all studied adsorbents, indicating a more favourable adsorption of the phenol onto the original granular AC than onto the others adsorbents. It was noticed that TiO₂ media exhibits the lower K_L value. For all the tissues, the presence of fibres and/or TiO₂/SiO₂ induced an apparent decrease in the affinity of these materials to phenol as they are themselves adsorbents with worst affinity. Finally, for adsorbents composed with several materials like these tissues, K_L is a global value where the negative impact of the worst adsorbent has an important influence.

For TiO₂/AC tissue, the value of q_{max} calculated from Langmuir model support the hypothesis of the unfavourable role that played by the binder on the phenol adsorption. The q_{max} calculated for TiO₂/ AC tissue is lower than that of original granular AC; this means that the sites of adsorption of TiO₂/ AC tissue are partially masked by the binder.

Based on the correlation coefficients, the equilibrium data was slightly better fitted in the Langmuir adsorption isotherm than the Freundlich equation (Table IV-3).

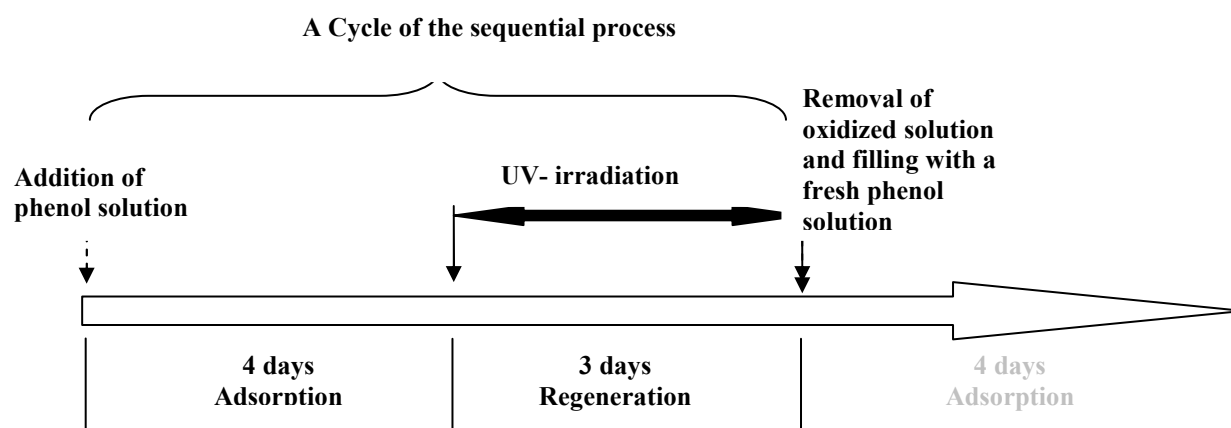
Table IV-3

Parameter constants of Langmuir and Freundlich models for phenol adsorption

Adsorbent	Parameters of Langmuir model			Parameters of Freundlich model		
	q_{\max} (g/g)	K_L (l/g)	R^2	K_F $(\text{g/g} \cdot (\text{g/l})^{1/n})$	1/n	R^2
TiO ₂ /AC tissue	0.25	4.76	0.98	0.16	0.28	0.93
AC media	0.30	4.33	0.98	0.22	0.27	0.97
Original granular AC	0.45	11.66	0.99	0.38	0.21	0.98
TiO ₂ media	0.13	2.01	0.97	0.10	0.68	0.90

4. Kinetics of adsorption and photocatalytic oxidation of phenol onto AC media

All data presented have been obtained in a batch reactor of “channel” type. This reactor may achieve successively the adsorption and photocatalytic oxidation of phenol onto different tissues, at controlled temperature (25 °C). These two successive steps, adsorption then oxidation, correspond to one cycle of the sequential process. They have been analysed separately. The adsorption step is carried out without UV irradiation. This step would terminate when the concentration of phenol in the liquid phase does not evolve any more; the adsorption equilibrium being reached. In order not to extend too much this first step it has been decided to limit its duration to 4 days which seems to be enough to approach AC saturation. Then, the UV lamps were switched on to start the second step: the photocatalytic oxidation. Sampling is carried out, to determine the concentration of pollutant during each cycle which is schematized in Figure IV-8.

**Fig. IV-8.** Schematic representation of one cycle of the sequential process.

In this figure, the duration step of phenol adsorption on the tissue was nearly 4 days to ensure that the AC was reached the equilibrium. In the second step, UV lamp switched on to start the photocatalytic oxidation process. This step of phenol oxidation and regeneration of the tissue takes three days. Finally, the oxidized solution of phenol was replaced by a new one with the same initial concentration and a new cycle then begins.

The operating conditions are summarized in the previous chapter II. Two concentrations of phenol were used in this study; the first one is enough concentrated (0.88 g/L) to approach the maximum adsorption capacity in the first cycle. The second one is 0.45 g/L selected according to the ratio between the amount of catalyst and that of pollutant recommended in the literature (Matos *et al.*, 2001).

4.1. Direct photolysis of phenol onto AC media

Some organic compounds are degraded by direct UV irradiation. Therefore, it should be examined to what extent the phenol is oxidized by photolysis if no photocatalyst was used. Blank experiment was carried out for the phenol without catalyst for this purpose.

To obtain relevant information about the photocatalytic process, it was necessary to carry out experiments in which any possible direct photolysis was excluded. Experiments were carried out using the highest phenol concentration (0.88 g/L):

- (i) without TiO₂ ; with AC and UV irradiation. (control test)
- (ii) without TiO₂ and AC ; with UV irradiation (neat photochemical regime).

4.1.1. Control test

Prior to the evaluation of photocatalytic activity of TiO₂/AC tissue, an experiment of four cycles was achieved using a tissue without TiO₂; the AC media. This control experiment was investigated with an aqueous solution of phenol (0.88 g/L). Firstly, the AC media was left in contact for 4 days in the dark. After this period, the system was exposed to UV irradiation with UV-lamp for 2 days. The oxidized solution was then substituted by a new volume of the initial phenol solution to operate another cycle.

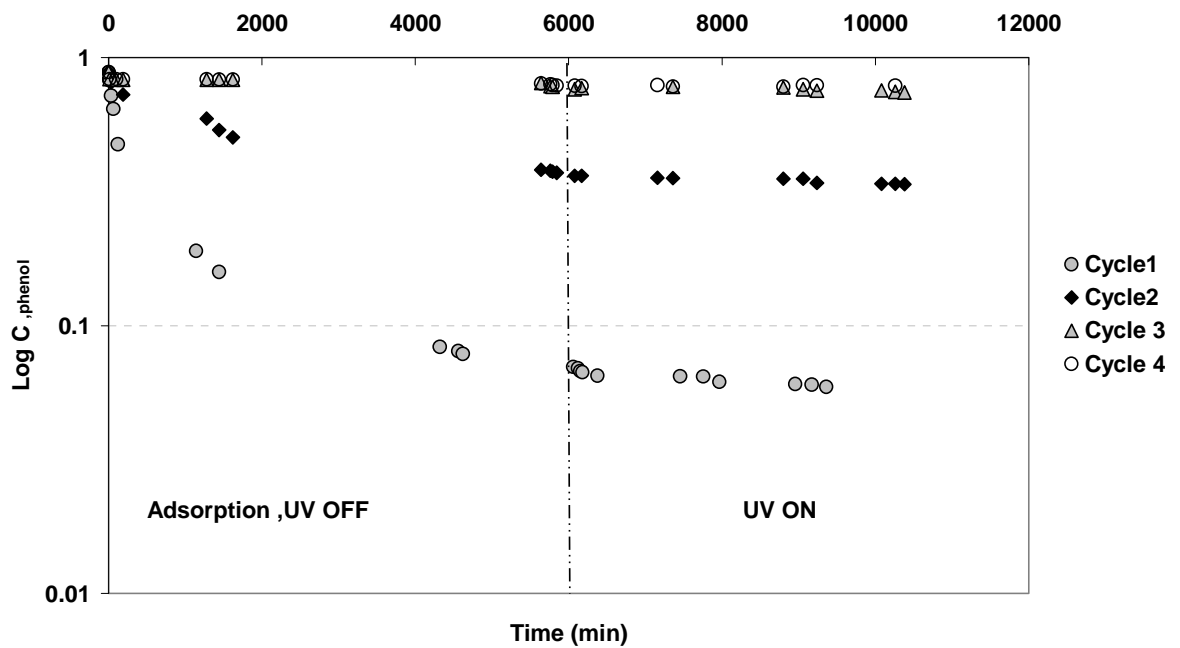


Fig. IV-9. Adsorption /UV irradiation cycles of phenol ($C_0 = 0.88$ g/L) onto activated carbon media at 25 °C.

Figure IV-9 shows the change of phenol concentration in the bulk of the solution by the adsorption/photocatalytic oxidation onto the AC media versus the time during all cycles. It was noticed from figure IV-10 that the activated carbon equilibrium was started at 4600 min. Moreover, the percentage of phenol disappearance in the first adsorption cycle was 90 % as compared to the initial concentration. The phenol concentration was then decreased to 54 % in the second cycle and to nearly 6 % in the two last cycles.

Figure IV-11 shows changes in phenol concentration under UV irradiation in the aqueous solution. The phenol disappearance in the first and second cycles was approximately less than 15 % within 3480 min and nearly negligible in cycles 3 and 4 as compared to the initial concentration of phenol. These indicate that the system is working in pure adsorption regime without any activated carbon regeneration by UV irradiation.

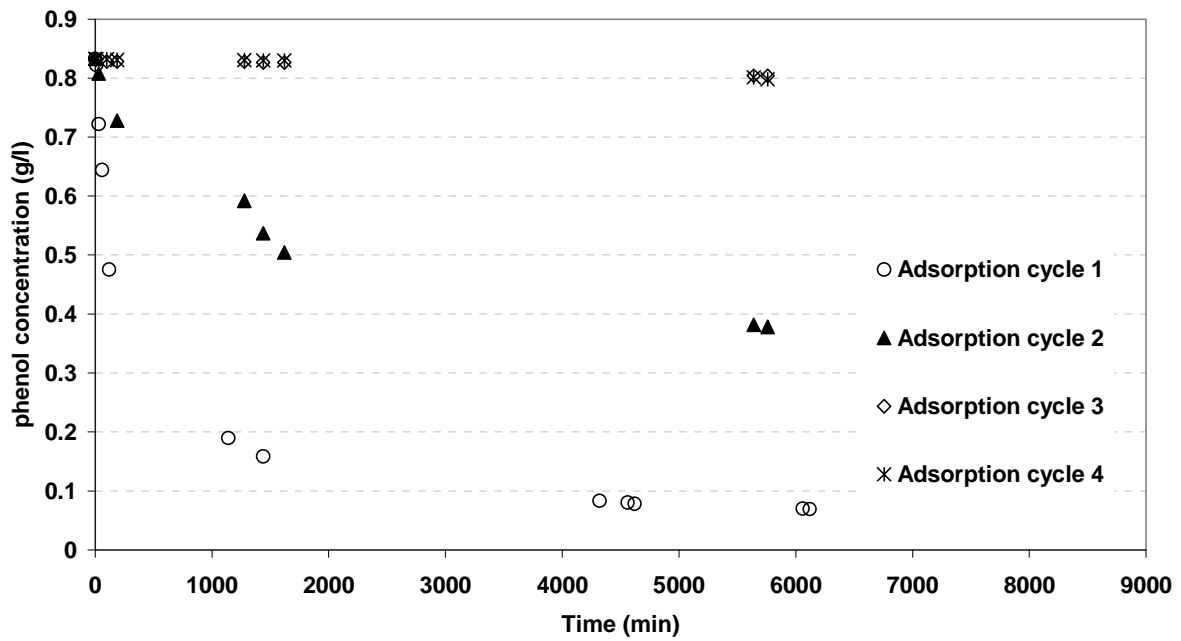


Fig. IV-10. Adsorption cycles of phenol ($C_0 = 0.88$ g/L) onto activated carbon media at 25°C.

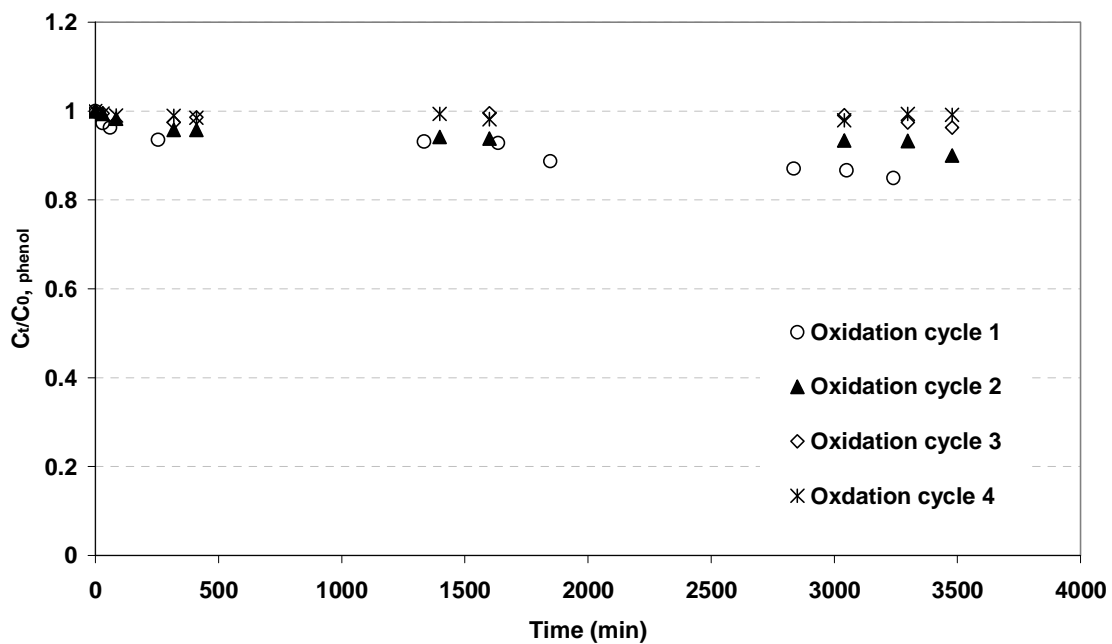


Fig. IV-11. Evolution of phenol concentration under UV irradiation during 4 cycles of photo-oxidation onto AC media at 25 °C ($C_0 = 0.88$ g/L).

The effect of direct photolysis on the decomposition of phenol was also studied using the same condition without AC (neat photochemical regime). As shown in Fig. IV-12, there is no significant effect of UV on phenol concentration: phenol is quite stable when irradiated under UV without TiO₂, suggesting that the disappearance of phenol in both precedent cycles 1 and 2 is mainly caused by the continuous adsorption and not due to the effect of UV irradiation. It can be also observed that both direct photolysis (i.e., without solids) and phenol decomposition in the presence of UV-irradiation and AC without TiO₂ are negligible, which confirms that the activated carbons are photoinactive in phenol photodegradation in agreement with the previous studies (Matos *et al.*, 2001; Trypa *et al.*, 2003; Cordero *et al.*, 2007).

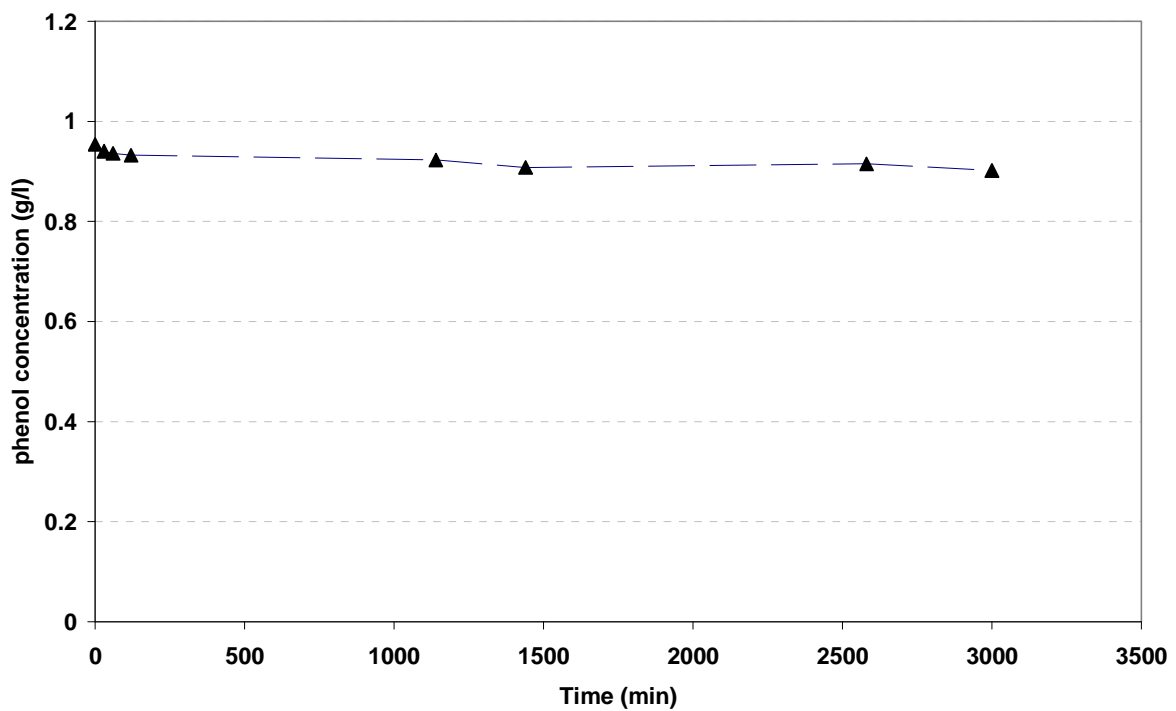


Fig. IV-12. Photolysis of phenol without activated carbon at 25 °C.

4.1.2. Quantity of adsorbed phenol during successive cycles.

The quantities adsorbed during each cycle are calculated as follows:

$$q_{i,t} = \frac{(C_0 - C_{i,t}) * V}{m_{\text{adsorbent}}} \quad (\text{IV-1})$$

Where $q_{i,t}$, the quantity adsorbed during cycle i at time t , V the total liquid volume in the reactor, $m_{\text{adsorbent}}$ the mass of adsorbent, C_0 the initial concentration of solution and $C_{i,t}$ the concentration at time t .

Figure IV-13 compares the quantities of phenol adsorbed during the adsorption phases of every cycle. This Figure shows also the quantities q_{max} of Langmuir model and q_{isotherm} (q at equilibrium for the initial concentration of the solution studied, $C_0 = 0.88 \text{ g/L}$): they are given by the isotherm. Finally, the histogram represents the total quantity of phenol adsorbed during the reutilisation of the activated carbon (from cycle 1 to cycle 4).

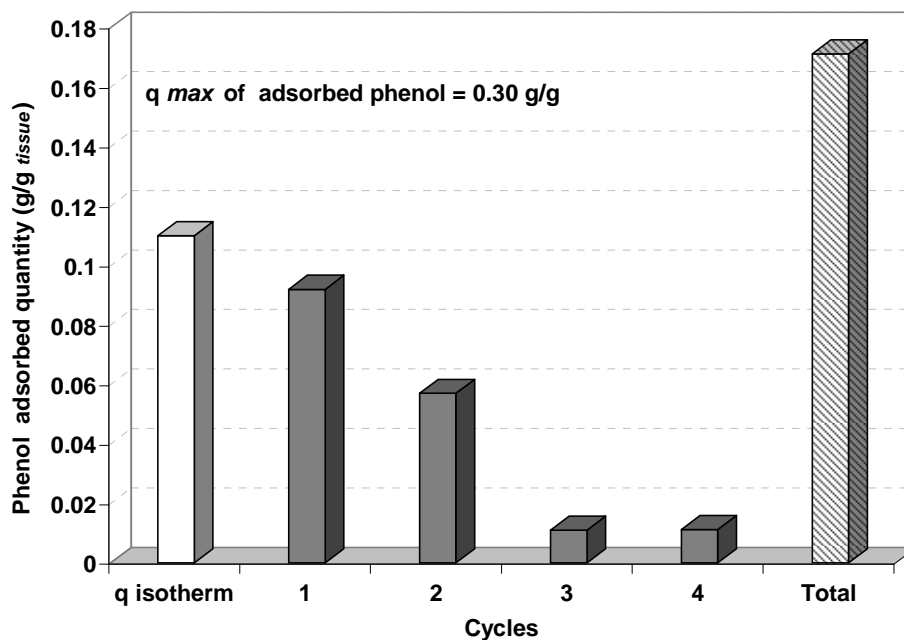


Fig. IV-13. Comparison of the quantity of adsorbed phenol during the cycles of adsorption

(■) for AC media (▨ : sum of the adsorbed quantities of phenol from cycle 1 to cycle 4,

□ : q_{isotherm}).

The comparison of the theoretical adsorbed quantity derived from isotherm (q_{isotherm}) and that of the first adsorption cycle shows that at the end of the first adsorption cycle, the activated carbon is approached to the equilibrium according to the isotherm: the quantity adsorbed during the first adsorption cycle is 84 % of q_{isotherm} . For the second cycle, it was observed that the adsorbed quantity of phenol was reduced to 60 % with respect to that of the first cycle. However, for the next cycles, the adsorption capacities were almost negligible. This indicates that the AC in the used media has nearly reached the equilibrium after the two first runs and no significant regeneration occurs on cycles 3 and 4.

The sum of total quantities of phenol adsorbed during the 4 cycles is 35 % more than the equilibrium adsorbed quantity based on the isotherm (q_{isotherm} ; 0.11 g/g adsorbent) and this value is still small as compared to the maximal adsorption capacity of AC (0.3 g/g adsorbent).

Consequently, it can be concluded that the degradation of phenol by UV irradiation without catalyst is negligible and the decrease in phenol concentration in cycles 1 and 2 is due to the continuous adsorption of phenol onto AC, not yet at equilibrium and not to any regeneration of activated carbon by UV irradiation.

4.2. Evolution of physical properties of AC media

4.2.1. BET surface area and pore size distribution

The analysis of AC media after these 4 cycles shows that its physical properties was modified (Table IV-4): the surface BET of the used activated carbon was reduced by 47.7 % ($S_{\text{BET,usage}} = 508.7 \text{ m}^2.\text{g}^{-1}$). The modification of the specific surface of the AC may be attributed to the molecules of adsorbed phenol which block the pores of AC decreasing the specific surface of activated carbon.

Table IV-4

Physical properties of AC media (before and after adsorption/UV cycles)

Activated carbon	Surface BET ($\text{m}^2.\text{g}^{-1}$)	Microporous volume ($\text{cm}^3.\text{g}^{-1}$)	Mesoporous volume ($\text{cm}^3.\text{g}^{-1}$)	Pore size Å°
AC non used	1065.40	0.46	0.046	19.02
AC used	508.71	0.22	0.042	20.26

The microporous volume was decreased by 47.8 %, the mesoporous volume was slightly reduced by 9 % as compared to the non used AC. The strong decrease in microporous volume can be attributed to the fact that phenol is mainly adsorbed in micropores. These results are in agreement with Stoeckli and Hugi-Cleary (2001) and Tryba *et al.* (2003) who reported a preferential phenol adsorption in micropores.

4.2.2. Thermogravimetric Analysis

The results of TGA of used and non used activated carbon (after 4 cycles of AD and UV irradiation) are represented in Figure IV-14.

For the used AC, we observe that at 100 °C, the loss of mass is 5.70 % as compared to 3.92 % in the non used AC. This loss of mass corresponds to the phenol desorption and the humidity content in the activated carbon. At temperatures between 100°C and 250°C, a loss of mass of 8.52 % is observed corresponding to the desorption of the phenol quantity which is still present on the carbon, this range of temperature corresponds to the physisorption of organic molecules (Merle, 2009). Both carbons then present similar behaviour corresponding to the oxidation of the acidic functions on the surface. Hence, the AC seems to have not been altered by UV.

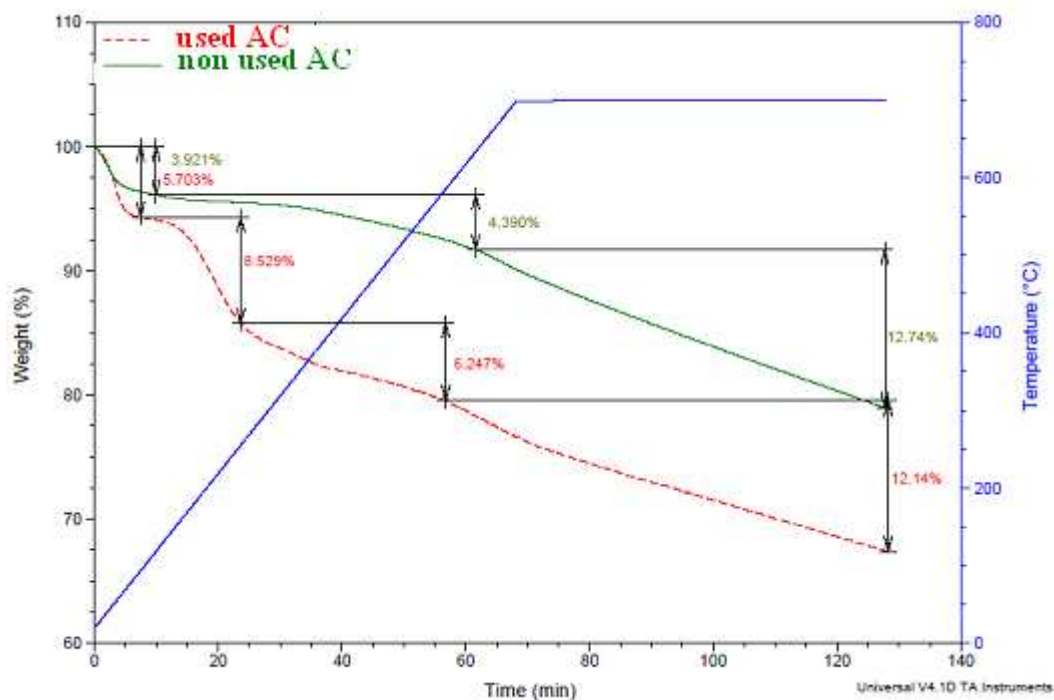


Fig. IV-14. Comparison of thermogravimetric analysis of AC media; used AC after phenol adsorption and UV irradiation and non used AC.

5. Kinetics of adsorption and photocatalytic oxidation of phenol onto AC / TiO₂ tissue

In this part, we will study the sequential process; adsorption then photocatalytic oxidation of phenol using TiO₂/ AC tissue for several cycles. The experimental conditions are the same as that previously used for the control test with AC media without TiO₂ using two different concentrations of 0.88 g/L and 0.45 g/L. Figures IV-15 and IV-16 represent the sequential process of adsorption/photocatalytic oxidation of phenol using TiO₂/ AC tissue for several cycles for the initial phenol concentrations 0.88 g/L and 0.45 g/L, respectively. Each process is focused and discussed later in a separate figure.

5.1. Adsorption step of phenol onto tissue

Experiments were carried out to evaluate the phenol adsorption onto tissue using two different concentrations of 0.45 g/L and 0.88 g/L.

5.1.1. Kinetic adsorption cycles of phenol onto tissue

The experiments were carried out in the dark conditions. 2 L of a solution of phenol at 25 °C and pH 5.6 was added in a photoreactor containing 17 g of TiO₂/AC tissue. Two concentrations 0.45 g/L and 0.88 g/L were successively used. At regular time intervals, samples were taken and filtered through a 0.25 µm filter syringe and then analysed by HPLC to determine phenol concentration.

The reduction of phenol concentration in the bulk of solution due to adsorption on the tissue versus time is presented in Figure IV-17a and b for the two concentrations of phenol, 0.88 and 0.45 g/L, respectively. It was noticed from the figure that the phenol disappearance started very fast at the beginning of the adsorption and then decreased towards equilibrium. It can be seen that the adsorptive balance of phenol could be arrived within 1600 min and 4600 min for all the adsorption cycles for phenol concentrations of 0.45 g/L and 0.88 g/L, respectively.

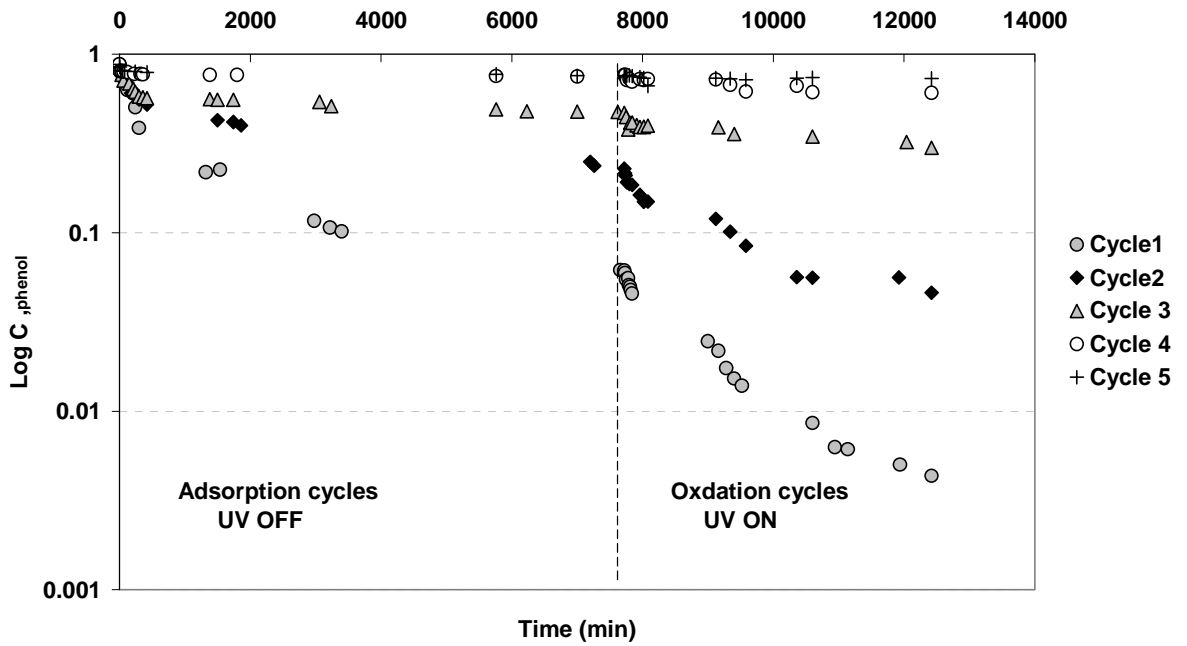


Fig. IV-15. Adsorption and photocatalytic oxidation cycles of phenol ($C_0 = 0.88$ g/L) onto TiO_2/AC tissue at 25°C .

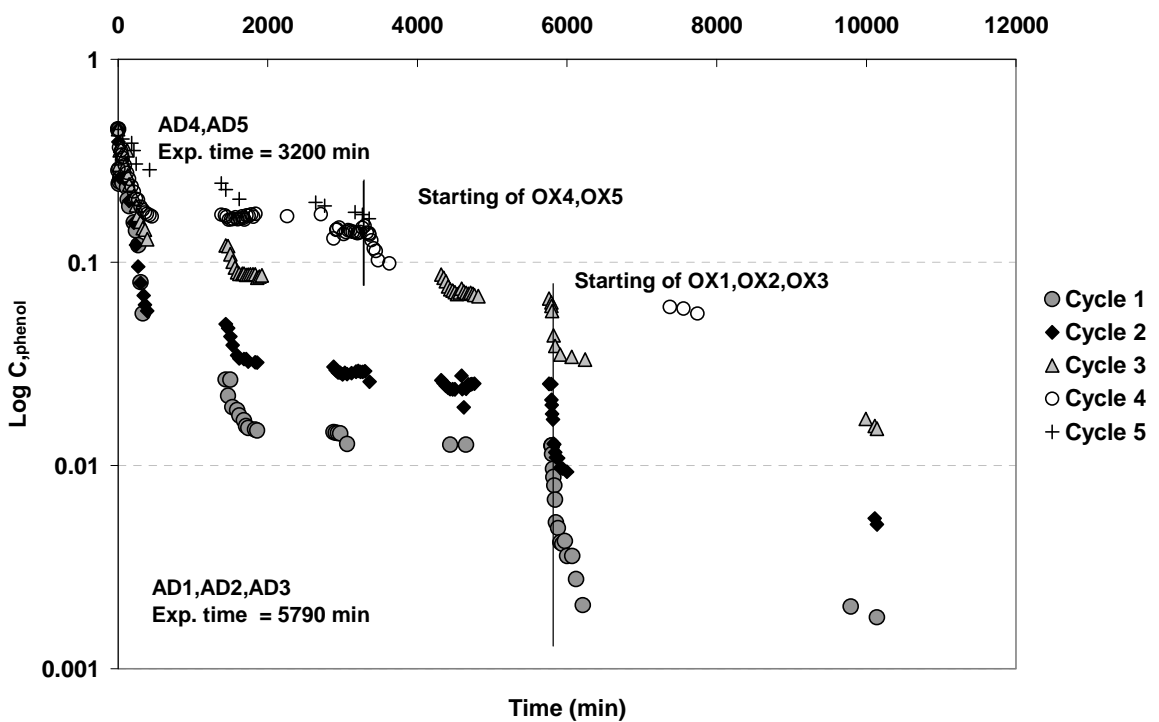


Fig. IV-16. Adsorption and photocatalytic oxidation cycles of phenol ($C_0 = 0.45$ g/L) onto TiO_2/AC tissue at 25°C .

Table IV-5 presents the percentages of phenol eliminated by adsorption during each cycle. For the two different initial concentrations, the adsorptive capacity decreased gradually by the reused of the tissue. For the lowest concentration solution, this decrease in the adsorptive capacity was less important than that observed when high concentration of phenol was used (0.88 g/L). From the 4th cycle, it can be observed a dramatically reduce of adsorption capacity in the case of the high phenol concentration (0.88 g/L). The decrease in the adsorption capacity by increasing the cycles may be due to the process of regeneration in the oxidation is not enough to degrade all the phenol, so probably an important quantity of phenol rest in the tissue as residual. Theoretically, the total phenol mass at the start of each adsorption cycle included the residual phenol after the regeneration and the initial phenol concentration, which added at the beginning of each adsorption cycle. These are in agreement with Ao *et al.* (2008) who cited that phenol remains adsorbed on the TiO₂ catalyst after 6 hours of UV irradiation although all phenol had nearly disappeared from the solution. Similarly, Lee *et al.* (2004) found that presence of residual amount of toxic microcystin LR on the TiO₂ surface after its oxidation to non toxic products.

Table IV-5

Evolution of the phenol adsorption percentages (based on the decrease in concentration) during the adsorption cycles using two phenol concentrations onto TiO₂/ AC tissue

Phenol Concentration	Phenol disappearance (%)				
	Cycle 1	Cycle 2	Cycle 3	Cycle 4	Cycle 5
0.45 g/L	97 %	94 %	86 %	69 %	64 %
0.88 g/L	> 90	74 %	47 %	13 %	13 %

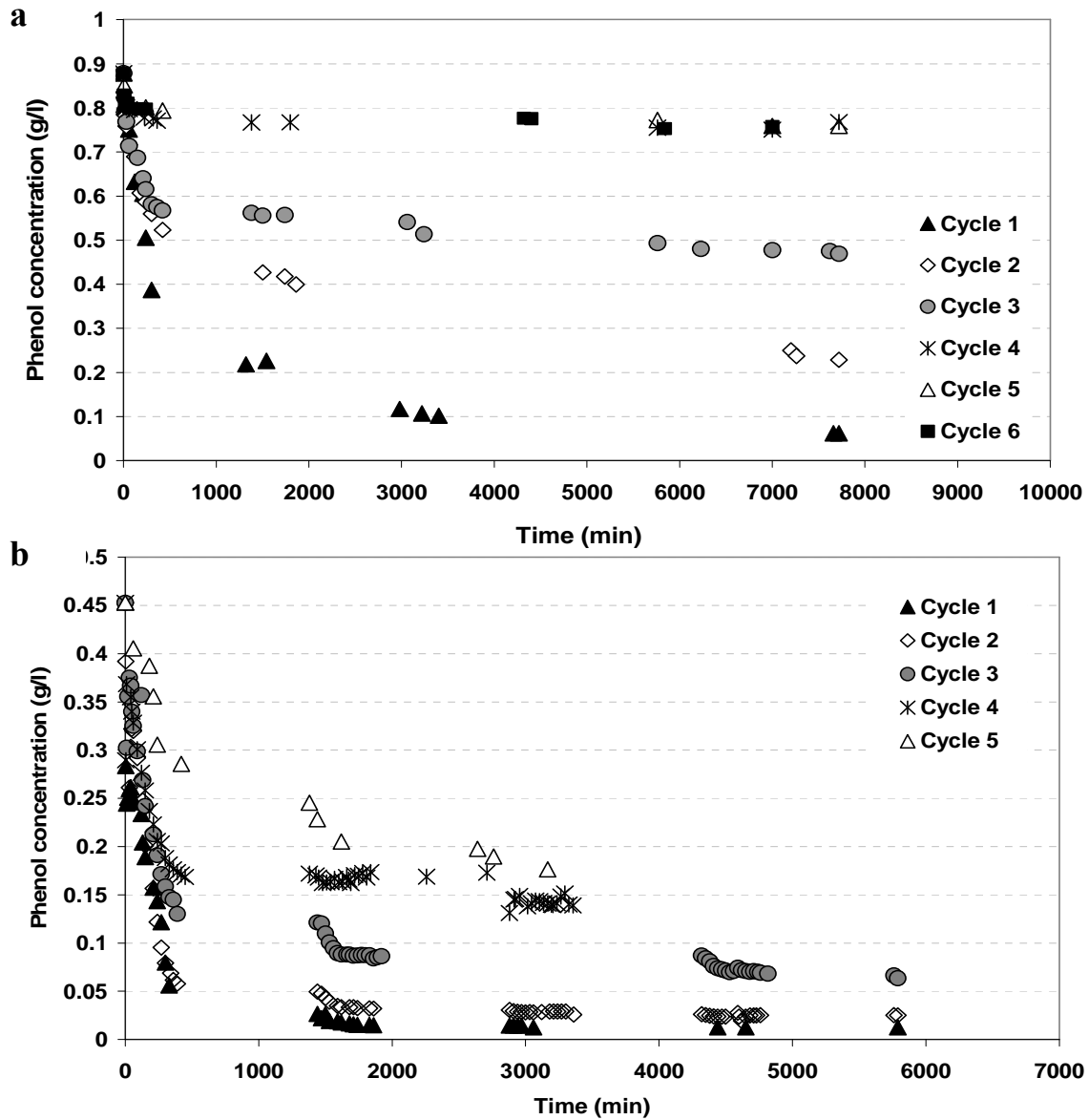


Fig.IV-17. Kinetic of the phenol adsorption cycles onto TiO_2/AC tissue after the regeneration using two different initial phenol concentrations, 0.88 g/L (a) and 0.45 g/L (b).

5.1.2. The adsorbed phenol quantity during the adsorption cycles

Figure IV-18a and b compares the quantities of phenol adsorbed during the adsorption phases of every cycle for the two different initial phenol concentrations (0.88 g/L and 0.45 g/L, respectively). This figure shows also q_{\max} of the Langmuir model parameter, q_{isotherm} ; the equilibrium quantities given by the isotherms corresponding to the two concentrations (0.45 g/L and 0.88 g/L), the total quantity of the phenol adsorbed during all cycles and finally $q_{\text{estimated}}$: the maximum quantity of phenol adsorbed assuming complete adsorption up to equilibrium but without any photocatalytic oxidation. This estimated quantity is obtained from the isotherm for a concentration of phenol calculated by taking into account the phenol mass present on the AC (from the previous adsorption) and that added in liquid phase at the beginning of the concerned adsorption cycle (annexe 5). The comparison of these calculated quantities with those experimentally obtained by the sequential process will give good information on the effectiveness of the photocatalytic regeneration.

It is important to compare the effective adsorbed phenol after the first adsorption cycle to the maximum value corresponding to equilibrium, in order to quantify the adsorption efficiency.

The comparison of the adsorbed quantity given by isotherm (q_{isotherm}) and that of the first adsorption cycle shows that at the end of the first adsorption cycle, the activated carbon has almost reached the equilibrium for the two concentrations.

For the high initial concentration, the quantity adsorbed during the first adsorption cycle is 0.0926 g/g tissue. For the second cycle, it was observed that the adsorbed quantity of phenol was reduced to 0.0737 g/g tissue. Then, this quantity reduced to about 0.0464 g/g tissue in the third cycle. Dramatically decreased of the adsorbed capacity of the regenerated tissue was then observed for the next consecutive cycles (nearly 0.0137 g/g tissue). The calculation of the total quantities of phenol adsorbed during the cycles of reutilisation shows that the total value of 6 cycles is nearly equal to that of the maximal adsorption capacity of tissue (0.25 g/g tissue) while this total value is nearly 3 times more than that of the adsorbed quantity given by isotherm (q_{isotherm} ; 0.1 g/g tissue).

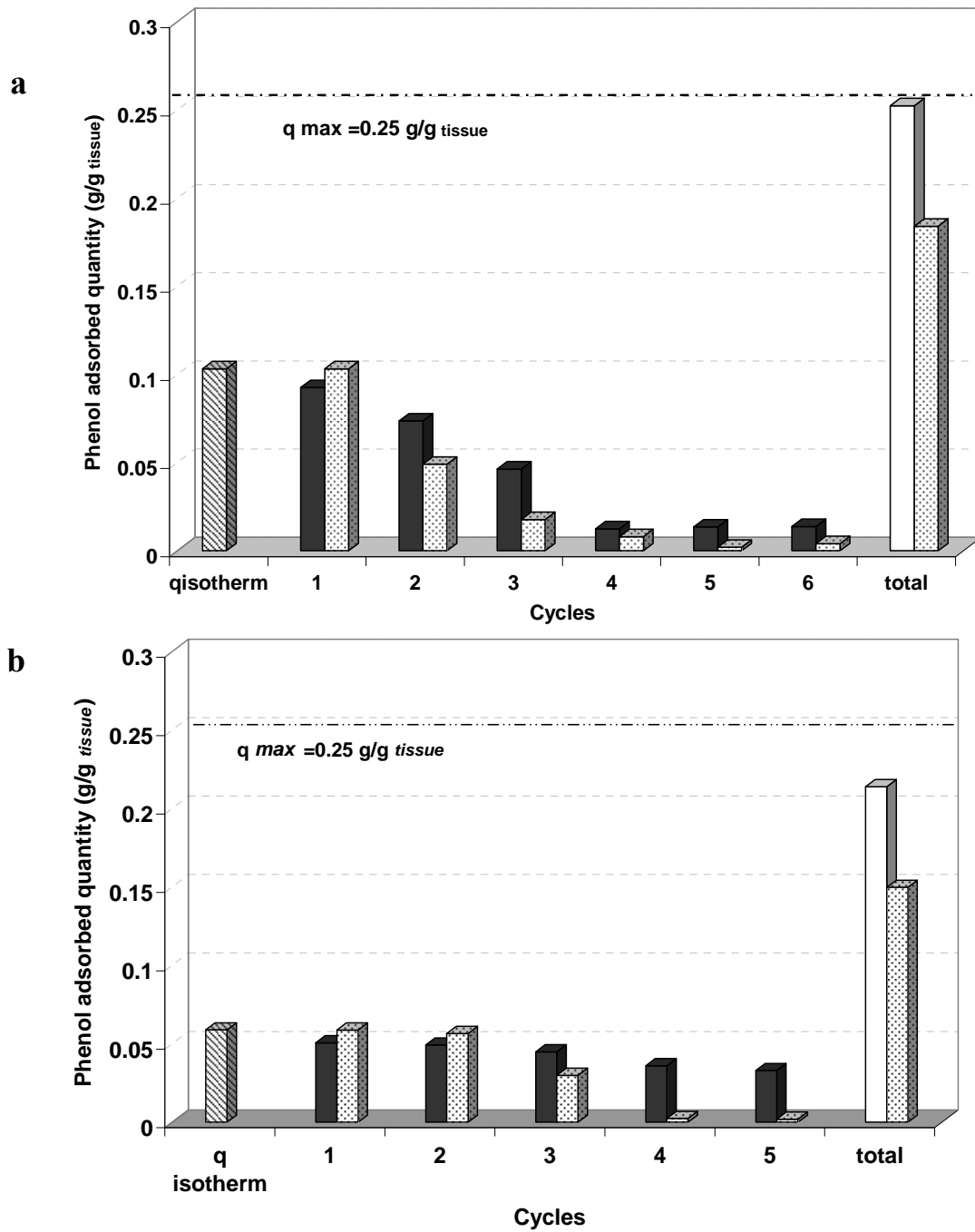


Fig.IV-18. Comparison of the quantity of adsorbed phenol during the cycles of adsorption (■) onto tissue (□: sum of the adsorbed quantities of phenol, ▨ $q_{isotherm}$, ▤ $q_{estimated}$ estimated quantity of phenol) for initial phenol concentrations of 0.88 g/L (a) and 0.45 g/L (b).

For the second initial phenol concentration (0.45 g/L), at the end of the first adsorption cycle, the activated carbon is loaded up to 88 % of the value of the isotherm ($0.051 \text{ g/g}_{\text{tissue}}$ compared to $q_{\text{isotherm}}; 0.058 \text{ g/g}_{\text{tissue}}$). At the second cycle, the adsorbed quantity of phenol was slightly reduced to $0.05 \text{ g/g}_{\text{tissue}}$. Then, this quantity gradually decreased to 0.045, 0.036 and $0.033 \text{ g/g}_{\text{tissue}}$ in the next adsorption cycles. By calculation of the total quantities of phenol adsorbed ($0.214 \text{ g/g}_{\text{tissue}}$) during the 5 cycles, it was found that 88 % of the maximal adsorption capacity of tissue ($0.25 \text{ g/g}_{\text{tissue}}$) was reached.

For the concentration 0.45 g/L, the estimated quantity ($q_{\text{estimated}}$) from the 4th cycle shows that the tissue can not adsorb any more while the experimental phenol elimination still continues (FigureIV-18a and b). This comparison indicates that the regeneration is very effective. However, for the high concentration (0.88 g/L), this phenomenon is observed from the 2nd cycle. Finally, by comparing the results obtained for the two concentrations, the total adsorption estimated quantities are lower than those of the experimental values. Totally, we eliminate approximately 30 % more. This result reflects that there is an effect of regeneration besides the adsorption. It was noticed that it is impossible to identify the part of adsorption on the sites still available (adsorbent sites not used) and the part of adsorption on the regenerated sites. According to the results previously obtained with the AC media, we can confirm that during the second cycle, an important quantity of the eliminated phenol is adsorbed on the still available sites (not regenerated).

From the results, the total quantity after all consecutive adsorption runs were nearly the same and equal to the maximum capacity of tissue with the two initial phenol concentrations used. However, at the end of adsorption cycles, it was noticed that only 15 % of the adsorption capacity was recovered with respect to that of the virgin tissue for phenol concentration of 0.88 g/L as compared to 65 % in the case of low initial concentration (0.45 g/L). This observation gives an impression that we can reuse the tissue several times after the fifth cycle without significant loss in the adsorption capacity by using low initial phenol concentration.

The regeneration is the consequence of desorption of the reversible adsorbed molecules. As a result of the decrease of the pollutant concentration by oxidation in the solution, the molecules are transferred from the inside of the pores of AC towards the solution then towards the surface of the catalyst to be degraded there. The negative effect on the

recovery of the AC adsorption capacity due to the increase in the regeneration cycles could be explained by several possibilities.

One of these explanations, the intermediates of phenol produced by photocatalytic oxidation are not completely decomposed but are adsorbed onto the AC adsorption sites. So, during the adsorption of the next cycle, the presence of these intermediaries prevents the phenol to be adsorbed.

Moreover, the active sites on the catalyst will be occupied by these intermediates to form monolayer; as a result of this, the rate of activated carbon recovery in the tissue is more significantly decreased with the high phenol concentration than with the low concentration. These coincide with Okawa *et al.* (2007) who reported that the reduced catalyst efficiency may be ascribed to the high concentration of intermediates adsorbed on the surface of the photocatalyst, which prevent the photocatalytic reactions. Chakrabarti and Dutta (2004).cited also that the decrease in efficiency of the recycled catalyst may be due to deposition of photosensitive hydroxides on the photocatalyst surface blocking its active sites also referred to as fouling of the catalyst.

Similar studies (Einaga *et al.*, 2002; Grzechulska and Morawski, 2003) proved that photocatalyst loses its activity and its colour by increasing the concentration of phenol during the oxidation runs. They found that new absorption bands in the region of 1200–1800 cm^{-1} appeared on the spectra of photocatalyst used in the reaction of phenol photo-oxidation at concentration of 300 mg/dm^3 when the sample colour changed to dark brown. These bands are due to the presence of carbon intermediates on the catalyst surface.

Furthermore, as the concentration of intermediates increases, the concentration of un-adsorbed phenol in the solution increases, leading to lesser penetration of light through the solution onto the surface of TiO_2 , thereby decreasing the concentration of $\cdot\text{OH}$ radical which is the most reactive species formed on the surface and hence, decreasing the rate of degradation. Since the relative number of the $\cdot\text{OH}$ radicals attacking the substrate decreases, the photo-efficiency of the reaction also decreases. However, the reverse effect is observed at lower substrate concentration, where the light intensity and time of irradiation is same but the

interception of the photons to the catalyst surface is decreased leading to the formation of more number of OH radicals, thereby increasing the rate of reaction (Merabet *et al.*, 2009).

As the oxidation stage is limited by the diffusion of phenol and its intermediates adsorbed into the AC pores towards the catalyst, especially the molecules present in the deepest pores. The molecules in the solution which are situated near the TiO₂ are quickly degraded, the concentration then decreases, but the major quantity of phenol is accumulated in the AC. The slowly transfer of the different molecules to the neat TiO₂ limits the efficiency of the regeneration. A high quantity of the adsorbed phenol remains on the AC and is not oxidized.

The efficiency could be also adversely affected by the possibility of deterioration, of the AC with other regeneration processes such as wet catalytic oxidation where the oligomers formed by oxidative coupling were irreversibly adsorbed and could be neither desorbed nor degraded by the oxidation (Krou, 2010).

Consequently, the residual concentration ratio was lower at the first cycle, and an obvious decrease in adsorptive capacity was observed at the second cycle. When it was used once more, the residual concentration ratio increased further, which mean that the adsorptive capacity of tissue decreased gradually. This finding is coincided with Shi *et al.* (2008) who observed that the adsorption capacity of Methyl Orange (MO) and Acid Fuchsine (AF) on TiO₂/AC_{F-600} sample was disappeared gradually during 4 cycles.

5.2. Photodegradation step of phenol onto tissue

The photocatalytic oxidation was carried out at 25 °C, with two UV lamps. This step of photocatalytic oxidation has a double effect: degradation of the adsorbed organic compounds which also will result in the regeneration of adsorption capacity of the activated carbon.

In this part, the consecutive oxidation cycles after the saturation of the AC in the tissue using two different initial phenol concentrations (0.45 g/L and 0.88 g/L) are analyzed.

5.2.1. Kinetics of photodegradation cycles of phenol onto tissue

After adsorption equilibrium was reached, the UV lamps were switched on. Figure IV-19a and b represents the variation of the phenol concentration in liquid phase during UV irradiation. It should be emphasized that this is the only information available for the analysis of photocatalytic oxidation kinetics, while in fact a complex process including simultaneously phenol desorption and oxidation is occurring. Where the reaction takes place and the quantity of phenol which is still adsorbed is not known. In this situation, only apparent kinetics of photodegradation of phenol (C/C_0) will be observed. Here again two initial phenol concentrations (0.45 g/L and 0.88 g/L) have been used. This figure shows that, when the solution was irradiated, the phenol is approximately eliminated as compared to the initial concentration used during a period of time of 4000 min for both concentrations studied. The half life time required to the initial phenol concentration to reach the half is much lower (≈ 500 min) in case of phenol concentration (0.45 g/L) than that (~ 1000 min) with phenol concentration of 0.88 g/L. These findings coincide with Wang et al. (2009) which reported that the half life time increased with increasing the initial concentration of Methyl Orange. It also shows that the decrease in phenol concentration with respect to the initial one in the 1st cycle is faster than that in the other next cycles.

The results explain that the initial concentration of every cycle of oxidation is different because the capacity of the adsorption of AC in the tissue is not the same for every cycle of adsorption as mentioned previously in the adsorption step. During the oxidation cycles, the TiO₂/AC/UV system begins with a fast degradation first stage followed by a rather slow second stage. Figure 16a and b also shows that the catalytic activity decreased during the runs. For the first oxidation cycle in both concentrations used, almost 93 % of the phenol is oxidized at the end of reaction (% calculated with respect to the final concentration of phenol of the adsorption cycle, $C_{f, ad}$ prior to this oxidation) but let us not forget that a part of the remaining phenol is always adsorbed onto AC in the tissue. For both initial concentrations, the catalytic activity of the TiO₂ in the tissue remains high because this rate of conversion based on the liquid phase was 78 %, for the second oxidation cycle. However, with 0.88 g/L of phenol concentration, a dramatically decrease in the photocatalytic activity during the three last cycles (OX3: 36 %, OX4: 21 % and OX5: 3.4 %) is observed. Indeed, in this case, the performance of the AC in the tissue during the adsorption cycles deteriorated and the total quantity oxidized by catalyst (in the liquid and carbon) also decreased during the oxidation runs.

It's obvious that at the end of the three last consecutive runs, 3, 4 and 5, although the final concentrations are different, the next adsorptions show the same small quantities of adsorbed phenol (Fig. IV-18a). At oxidation cycle 3, a diminution in the phenol concentration oxidized in the aqueous phase is observed (40%). At the same time, its intermediates are partially adsorbed by the AC. So, in the following adsorption cycles, only few quantities of phenol are adsorbed by the AC which is in competition with the intermediates.

On the other hand, for the second low initial phenol concentration (0.45 g/L), the oxidation cycles 2 and 3 are similar (79%) but a small decrease in the catalyst activity is found during the 4th cycle (60 %). It's clear that the percentages of phenol degradation during the last three runs in the case of 0.88 g/L are significantly lower than those of 0.45 g/L of phenol concentration.

During the photocatalysis stage, the phenol molecules were desorbed from the carbon and then migrated via the catalyst which found here in very small quantity as compared to the high quantity of phenol ($C_i = 0.88$ g/L): this operation is very slow and few sites are available. In present study, it was found that the ratio of mass catalyst to that of phenol was 0.44 with 0.88 g/L of phenol and increased to 0.86 in the case of low phenol concentration (0.45 g/L). Indeed, most of studies reported that there is an irreversibly relationship between TiO_2 mass and that of organic pollutant (Lhomme, 2006; Lam *et al.*, 2010). This may explain partially the low rate of carbon regeneration. Moreover, the ratio between the AC and the TiO_2 in the tissue could play an important role in the catalytic efficiency decreased of tissue (ratio of AC: TiO_2 is 10:1), which is much higher than that found in the literature (Crittenden *et al.*, 1997; Zhu and Zou, 2009b). However, the use of TiO_2 photocatalyst and AC in a suitable ratio combines the advantages of both techniques, i.e. AC works as the support of nanosized TiO_2 photocatalyst and concentrates the pollutants and intermediates around the TiO_2 ; on the other hand, the TiO_2 photocatalyst can destroy the pollutants thus regenerating the AC in situ. Thus, based on this, the regeneration decreased could be due to the presence of TiO_2 in very little quantity in the tissue as compared to those of phenol and intermediates adsorbed by the AC.

At high phenol concentration (0.88 g/L), for 3rd, 4th and 5th cycles, the catalyst has nearly no more effect; it takes a brown colour which is generally characteristic of the presence of coloured quinones. These intermediates are adsorbed on the TiO_2 and might prevent the UV to activate the catalyst leading to a dramatically decreased in the photocatalyst activity (annexe 13).

The negative effect of the increase in the initial phenol concentration on the photocatalytic activity in the first cycle is represented well in Figure IV-20. It can be concluded that the photodegradation conversion of phenol decreases with increasing the initial concentration of phenol. A possible explanation of this behaviour can be the following: as the initial concentration increases, more and more organic substances are adsorbed on the surface of TiO_2 , but the intensity of light and illumination time are constant; consequently, the $\cdot\text{OH}$ formed on the surface of TiO_2 is constant, the relative number of $\cdot\text{OH}$ attacking phenol decreases, and thus the photodegradation efficiency decreases too (Rideh *et al.*, 1997).

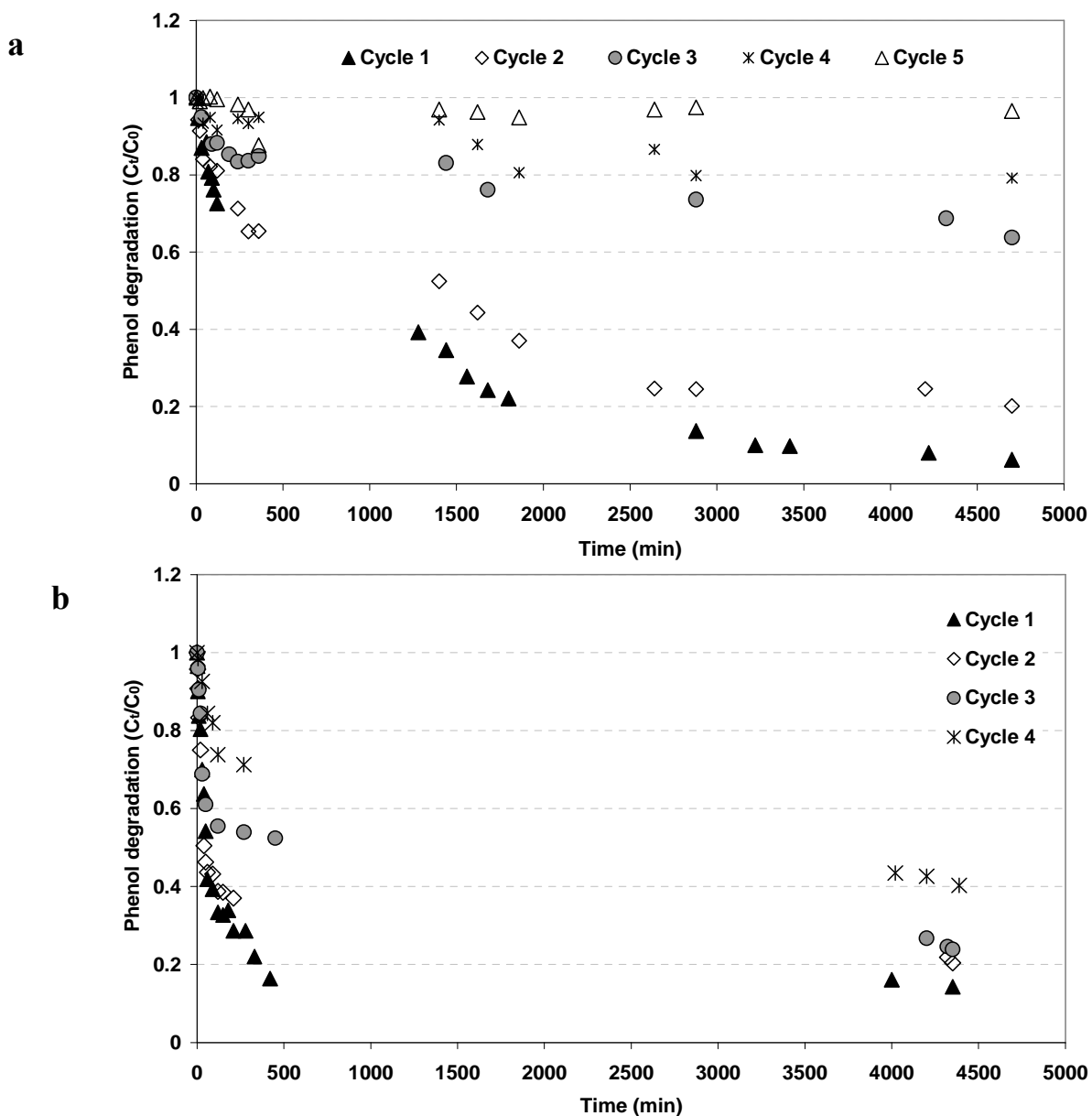


Fig.IV-19. Kinetic of the phenol oxidation cycles onto TiO_2/AC tissue using two different initial phenol concentrations; 0.88 g/L (a) and 0.45 g/L (b).

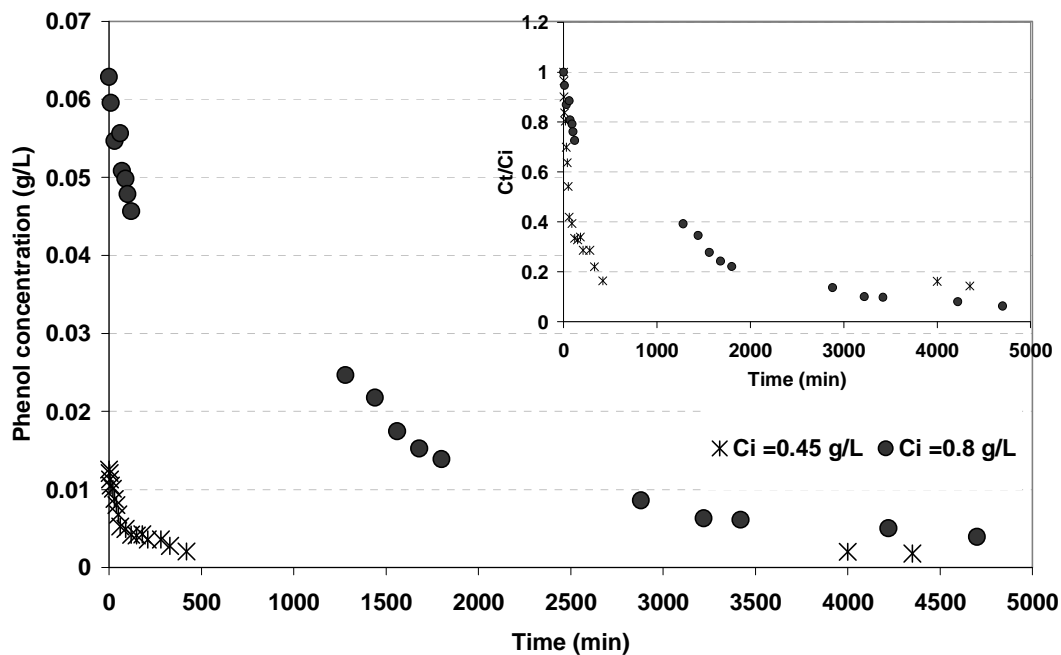


Fig.IV-20. Comparison of the phenol degradation kinetic for the two different initial phenol concentrations during the first cycle of the photocatalytic oxidation.

Moreover, the photocatalytic oxidation of TiO_2 in tissue should have occurred in the region of the surface or in the shallow pore sites, because effect of TiO_2 and UV light are not able to penetrate into the pores of AC. Therefore, the diffusion of substrate from the interior of the AC to near surface is important for regeneration. These results coincided with Minero *et al.* (1992) and Darko *et al.* (2010) who studied the role of adsorption on inert materials in TiO_2 photocatalyzed reactions for organic removal and reported that the chemicals strongly adsorbed on inert materials could not exchange with other support (TiO_2) quickly and the degradation reaction occurs within a few nanometres of the photocatalytic surface, to which the substrates migrate and ultimately degrade. Furthermore, the adsorbed pollutants on the AC should diffuse to TiO_2 site for photodegradation. A possible way to increase the regeneration capacity is to increase the desorption rate through heating or purging (Ao and Lee, 2003).

Based on this study the photocatalytic regeneration process was found to be limited by the reaction rate at the beginning of the regeneration cycle and then by desorption of adsorbates from the pores of AC.

Other hypothesis for the decreased catalytic efficiency, if the titania released into solution, in the repetitive use of the catalyst, the photocatalytic activity would be decreased sharply because the support activated carbon has no photocatalytic activity (Okawa *et al.*, 2007).

5.2.2. Regeneration efficiency

In this part, the results obtained may be well analyzed by the regeneration efficiency proposed by Narbaitz and Cen (1997). The regeneration efficiency of tissue (Eq. IV-2), was evaluated based on the following parameters: the phenol quantity (q_R) representing the phenol re-adsorbed to the regenerated tissue after each cycle of phenol adsorption (Eq. IV-3); and the pre-oxidation of phenol quantity on the virgin tissue (q_V) (Eq. IV-4). This method of estimating regeneration efficiency is based on the re-adsorbed quantity on the regenerated tissue compared to adsorption capacity of the virgin tissue

$$\text{Regeneration efficiency (\%)} = \frac{q_R}{q_V} \times 100 \quad (\text{IV-2})$$

$$q_R = \frac{([\text{phenol}]_{\text{initial}} - [\text{phenol}]_{\text{final}})_{\text{tissue, regenerated}} * V}{m_{\text{tissue, regenerated}}} \quad (\text{IV-3})$$

$$q_V = \frac{([\text{phenol}]_{\text{initial}} - [\text{phenol}]_{\text{final}})_{\text{tissue, virgin}} * V}{m_{\text{tissue, virgin}}} \quad (\text{IV-4})$$

Where $[\text{phenol}]_{\text{initial}}$ and $[\text{phenol}]_{\text{final}}$ are the initial and final phenol aqueous concentrations (g/L), V the volume of adsorbate solution applied (L), and m_{tissue} is the mass of tissue (g).

Figure IV-21 represents the effect of initial phenol concentrations on the regeneration efficiency for recovering the AC adsorption capacity compared to virgin AC (Cycle = 1) during the oxidation runs. As seen from the results for the initial phenol concentration (0.45 g/L), phenol removal efficiency of the used TiO_2/AC sample was slightly decreased in the 2nd

cycle (97 %) compared to that of the virgin. As discussed before, part of the eliminated phenol is adsorbed on the AC adsorption sites still available (not used). The regeneration efficiency slightly then decreased to (88.6 %) in the next cycle. Further decrease in the regeneration efficiency was observed by increasing the number of the reused times to 71% and 66 % respectively. These is in agreement with Park *et al.* 2010 who found that the UV-irradiation with TiO₂ catalyst was found to facilitate the recovery of AC, which was fully charged by Bisphenol A (BPA), up to about 50 %.

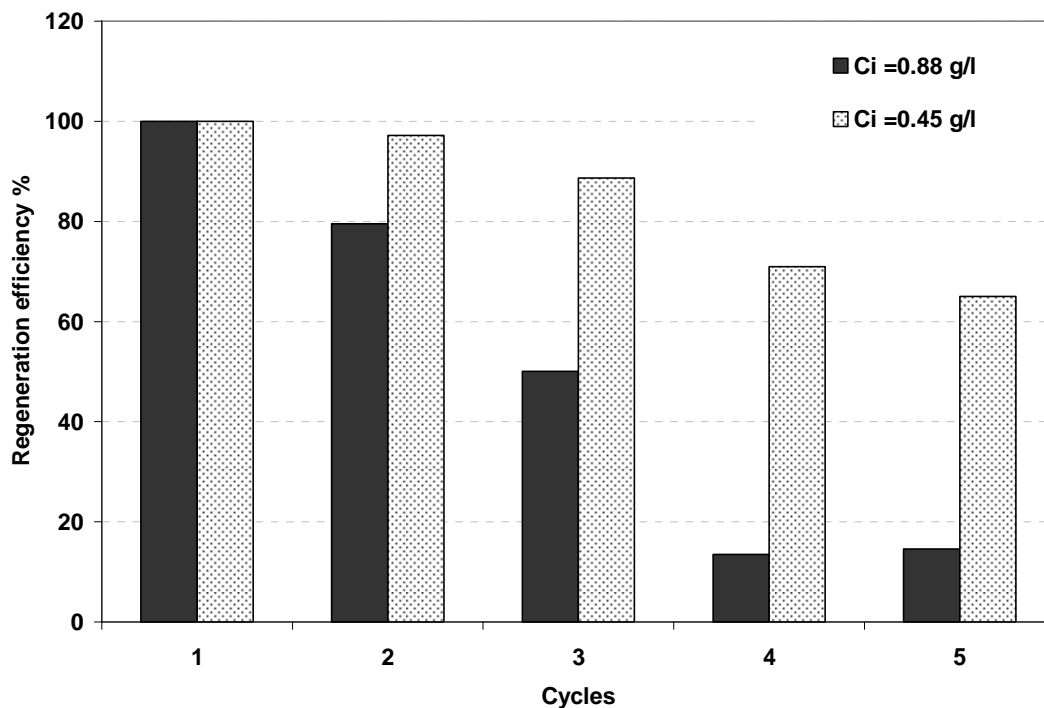


Fig. IV-21. Effect of the initial phenol concentration on the regeneration efficiency during photocatalytic degradation runs onto tissue.

However, by increasing the initial phenol concentration to 0.88 g/L, the regeneration efficiency after two full regeneration cycles was calculated to be 79 % and 50 % for the second and third cycles, respectively. For the next cycles, an almost steady state was reached (14 %). This dramatic decrease in the efficiency shows that at high concentration, the conditions of the photocatalysis do not allow to enough regenerate the tissue. In this case, as yet mentioned, the quantity of TiO₂ is not adapted to the high quantity of phenol and so the accumulation of intermediates on the catalyst surface reducing its activity. On the other hand, when the proportion of mass TiO₂ / pollutant is more important, efficiency is better maintained. In these conditions, additional cycles can be carried out.

5.2.3. Kinetic model for photodegradation of phenol

To describe the kinetics of phenol degradation, the results reported in the literature (Higarashi and Jardim, 2002; Macounova *et al.*, 2003; Farran and Ruiz, 2004) can give us important trends about the reaction rate. In the most of cases, the initial kinetics of the photodegradation of several organic molecules, are described as a pseudo first order with a rate of degradation represented as follows:

$$r = -\frac{dC}{dt} = k_{ap} C \quad (IV-5)$$

Where

r: Rate of photocatalytic degradation (g/l . min⁻¹)

k_{ap} : Apparent constant of degradation (min⁻¹)

C: Concentration of phenol (g/L)

t: Time of irradiation (min)

The integration of this equation (with: C = C₀ when t = 0) give the following equation:

$$\ln\left(\frac{C_0}{C}\right) = k_{ap} t \quad (IV-6)$$

The plot of Ln (C₀ / C) versus time (t) for different initial phenol concentrations gives straight line. The slope of linear regression equals to the apparent first-order rate constant k_{ap}.

In this study, beside the first order model, other models were used such as Langmuir-Hinshelwood and second order models (annexe 14) but all these models did not fit well the experimental data. These may be due to during photocatalytic degradation, intermediates are formed and may interfere in the determination of kinetics because of competitive adsorption and degradation. Therefore, calculations were done using first order model with a constant ΔC (15%) for all cycles at the beginning illuminated conversion. During this time interval, any changes such as intermediates effects or pH changes could be considered as negligible. The parameters of pseudo first-order apparent constants during all the oxidation cycles are regrouped in Table IV-6.

The graphical representations of the values of phenol concentration calculated from the kinetic of pseudo first order using the obtained k_{ap} values versus the time are shown in Figures IV-22 a and b for two different initial phenol concentrations; 0.45 and 0.88 g/L,

respectively. These figures demonstrate that good results are obtained when the kinetic model is done at the beginning of the reaction whereas after this period, the pseudo first order can not fit well, there the estimation errors increase by increasing the cycle and time of the reaction for all cycles (up to 44 %). Cordero *et al.* (2007) reported that most of the studies on the photocatalysis of organic products fit well the kinetic of pseudo first order; this is only valid in the preliminary stage of the reaction, when the time of photocatalysis is short. Nevertheless when the time of photocatalysis is sufficiently long, the kinetic changes and the order of the reaction can then change. These results may be explained by the competition adsorption-desorption between the phenol molecules and the intermediates produced from its degradation.

Table IV-6

Pseudo first-order apparent constants (K_{ap}) and correlation coefficients (R^2) corresponding to different initial phenol concentrations (0.45 g/L and 0.88 g/L, before dark adsorption) during the consecutive photocatalytic oxidation runs

Cycles No	Initial phenol concentration C_0 (0.88 g/L)			Initial phenol concentration C_0 (0.45 g/L)		
	* $C_{0,i}$ (g.L ⁻¹)	K_{ap} (min ⁻¹)	R^2	* $C_{0,i}$ (g.L ⁻¹)	K_{ap} (min ⁻¹)	R^2
1 st run	0.062	0.46×10^{-2}	0.99	0.013	1.85×10^{-2}	0.97
2 nd run	0.228	0.42×10^{-2}	0.99	0.025	1.87×10^{-2}	0.99
3 rd run	0.469	0.17×10^{-2}	0.99	0.064	0.86×10^{-2}	0.99
4 th run	0.768	0.17×10^{-2}	0.99	0.164	0.53×10^{-2}	0.96

* The initial phenol concentration after dark adsorption for each run, i.

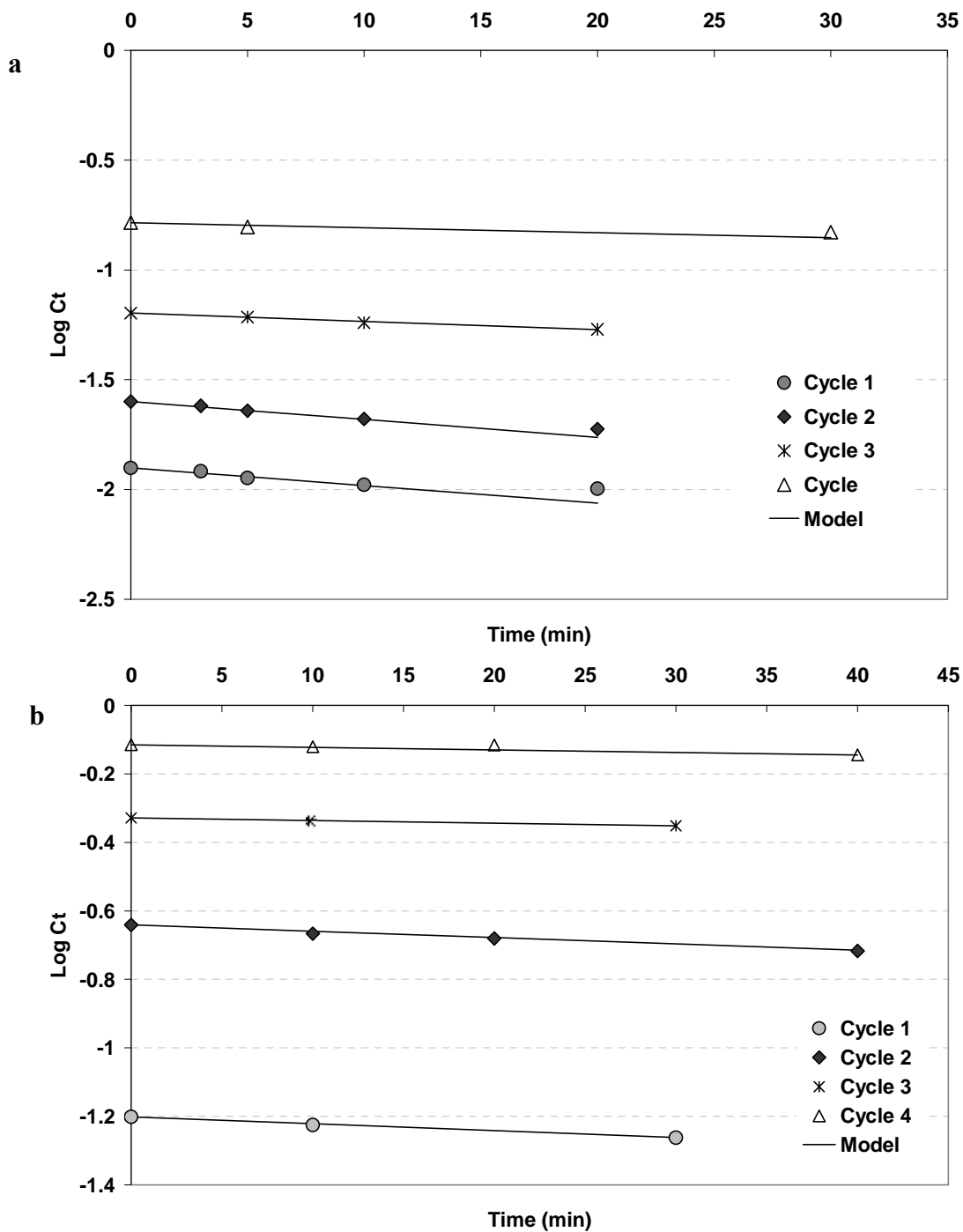


Fig.IV-22. Comparison between the experimental (symbols) and theoretical (lines) data during the photocatalytic degradation cycles of phenol onto tissue [T: 25 °C, C_0 : 0.45 g/L (a) and 0.88 g/L (b)]. The lines represent the values calculated from the kinetic model of pseudo first order.

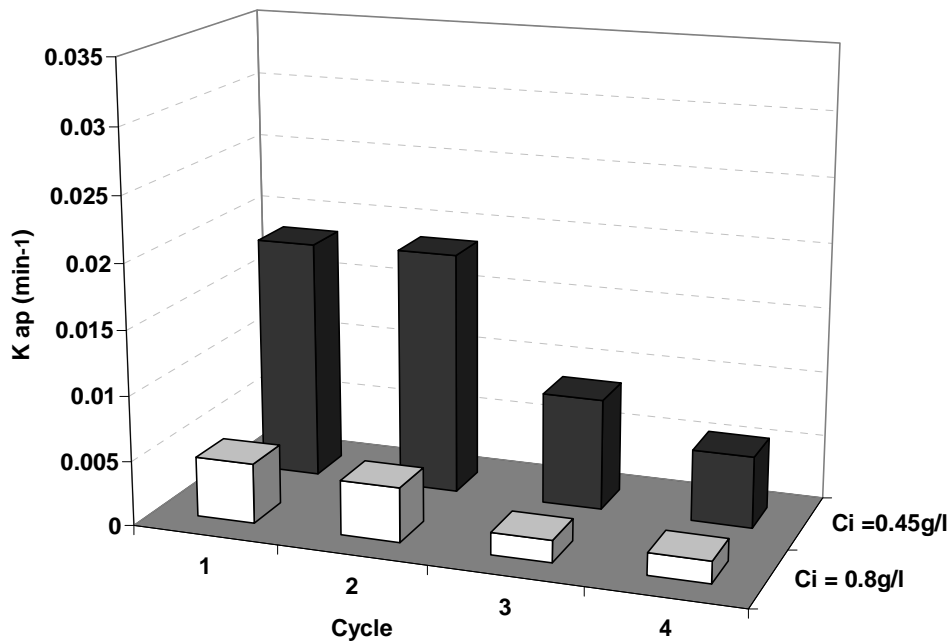


Fig.IV-23. Comparison of apparent rate constant (K_{ap}) between two different initial phenol concentrations during the photocatalytic oxidation runs onto tissue.

Table IV-6 and Figure IV-23 show the apparent constants k_{ap} decrease by increasing the cycles. Li *et al.* (2006) reported the same result in the case of degradation of the methyl orange onto TiO_2/AC . The values of k_{ap} are considerably higher with phenol concentration of 0.45 g/L than those obtained by the high concentration (0.88 g/L). In this case, the value of k_{ap} seems to be dependent on the phenol concentration and this is inconvenient with the first order law model where k_{ap} depends only on the quantity of dissolved O_2 and the light flux. The decrease in k_{ap} at higher concentration has been sometimes attributed to the fact that phenol absorbs more light than TiO_2 leading to a loss of light efficiency (Na *et al.*, 2005).

Furthermore, the equilibrium adsorption of phenol on the catalyst surface active sites increases and more molecules of phenol are adsorbed on the surface of the catalyst (Naeem and Feng, 2009). Additionally, when the competitive adsorption of phenol and OH^- groups (from H_2O) on the same site increases, the generated $\cdot\text{OH}$ radicals on the surface of catalyst decreases thus the ratio of the $\cdot\text{OH}$ radicals /phenol decreases (Lam *et al.*, 2010). For the two phenol concentrations (0.88 g/L and 0.45 g/L), the catalyst, irradiation time and intensity of light were constant.

It is also clear from table IV-6 that phenol concentration at the end of adsorption steps ($C'_{0, i}$) increases cycle after cycle. This increase leads to a decrease in the apparent rate constant k_{ap} of the process which is more significant in the high phenol concentration before the dark adsorption (0.88 g/L). The observed decrease in k_{ap} is explained by the less availability of photons as the initial concentration of the organic substrates increases (Wang *et al.*, 2007a).

For the last two cycles with high concentration ($C_0 = 0.88$ g/L), k_{ap} values are significantly low. The deactivation of catalyst by its recycle led to a dramatically decrease in the kinetic rate constant values confirming the decrease of photocatalytic reaction by augmenting the regeneration cycles. This result can be explained on the basis of the competition of adsorption / desorption between the phenol molecules and the intermediates resulting from its degradation, which could be more considerable for a high concentration in the solution.

As discussed above, deactivation of the photocatalyst was reached at the last cycles when 0.88 g/L of initial phenol concentration was used; these may be due to the formation of high concentrations of intermediates blocking the active sites of photocatalyst. Thus, further analysis like the chemical oxygen demand, COD will be investigated for this later high concentration to give us more information about this deactivation effect.

5.2.4. Chemical Oxygen Demand

The chemical oxygen demand (COD) gives a measure of degradation of phenol and generated intermediates during the irradiation and also a measure of the oxygen equivalent of the organic content in a sample at the end of each oxidation cycle. The test allows the measurement of sample solution in terms of the total quantity of oxygen required for the oxidation of organic matter to CO_2 and water. The rate of COD removal efficiency of tissue was shown in Figures IV-24 and IV-25.

The degradation of the samples was evaluated through COD analyses. The quantity of organic matter reported in the COD analysis includes the amount of phenol remaining after every evaluation interval, plus the intermediate substances generated during phenol degradation. Moreover, occurrence of phenol degradation was confirmed from the measurement of COD, which showed that by-products of phenol degradation are present in

the reaction mixture after UV irradiation. We notice the limits of the oxidation stage after the first cycle where at the end of this stage, it remains about 40 % of the initial COD value while it rests only 5 % of the initial phenol. Thus, the oxidation did not allow to completely mineralize the phenol and a high quantity of the formed intermediates is not oxidized. The difference between COD calculated for phenol concentration evaluated by HPLC and the total analysed value of COD was 85, 57, 20 and 16 % in the first, 2nd, 3rd and 4th oxidation cycles, respectively. This confirms that the intermediates represent the most percentage of the value of COD in the first run. The organic matter oxidation levels reached after total elimination of the phenol were 60 % in the first oxidation cycle, 52 % in cycle 2 and then dramatically decreased to 19 % and 5% in the next two oxidation cycles, 3 and 4, respectively. This result confirmed the deactivation of the TiO₂ in the tissue is mainly due to the increase in the intermediates concentrations by the reuse of the tissue.

Okamoto *et al.* (1985) reported that the concentration of COD, however, still retains a high value even after phenol is decomposed perfectly. This is attributed to the existence of the intermediate products like hydroquinone, catechol and hydroxyhydroquinone.

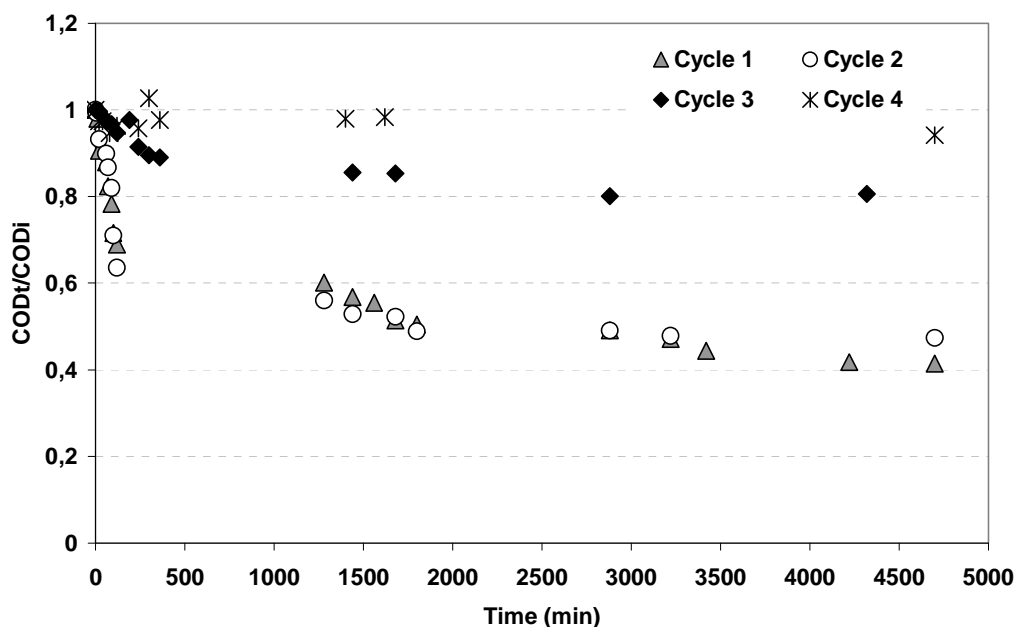


Fig. IV-24. Kinetics of the photocatalytic disappearance of COD during phenol removal ($C_0 = 0.88$ g/L).

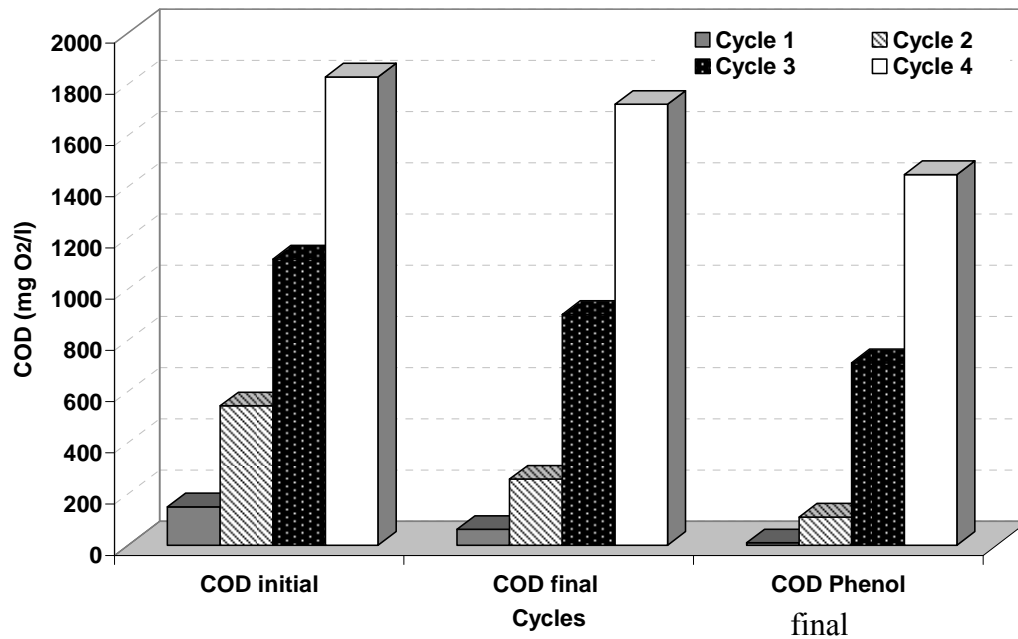


Fig. IV-25. Evolution of COD initial and final during 4 photocatalytic oxidation cycles of tissue as compared to the COD final of phenol ($C_0 = 0.88$ g/L).

The first order model was used for describing the kinetic of COD removal for only three oxidation runs where the 4th cycle was not fitted well by this model and its parameters are postulated in Table IV-7. Figure IV-26 compares the COD values calculated from the pseudo first order model and that obtained by the experimental analyses. It's clear from this figure that the kinetic model fitted well the data within 120 min whereas, the estimation errors increased by increasing the reaction time for all cycles. The same observation was previously found in our study for the kinetic evaluation of phenol degradation.

Table IV-7

Pseudo first-order apparent constants (K_{ap}) and correlation coefficients (R^2) detected in COD removal during the consecutive photocatalytic oxidation runs; $C_{i\text{ phenol}}$ (0.88 g/L)

Cycles No	K_{ap} (min^{-1})	R^2
1 st run	0.28×10^{-2}	0.99
2 nd run	0.22×10^{-2}	0.99
3 rd run	0.04×10^{-2}	0.98

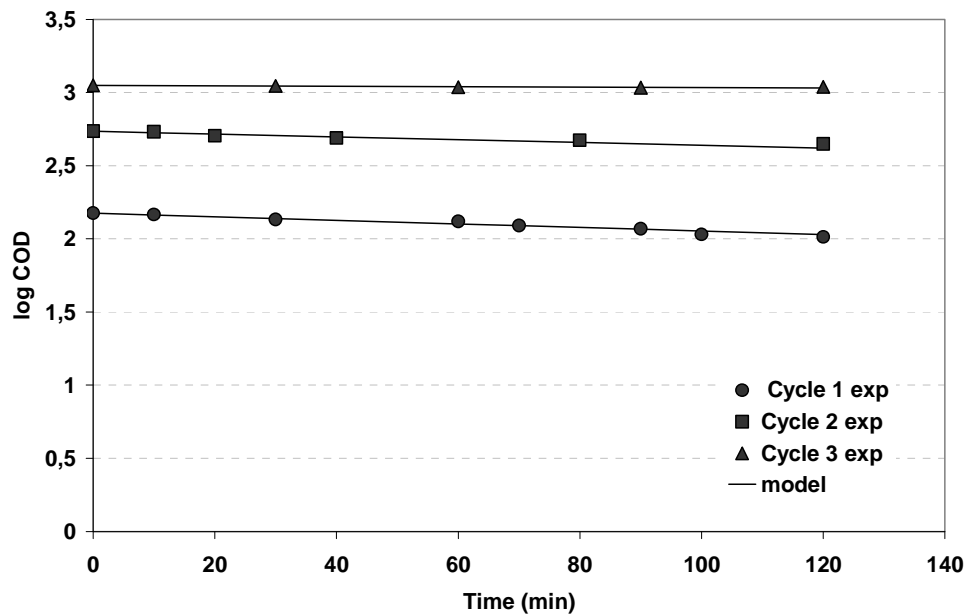


Fig.IV-26. Comparison between the COD experimental (symbols) and theoretical (lines) data during the photocatalytic degradation cycles of phenol onto tissue within 120 min (T: 25 °C, C_i; 0.88 g/L). The lines represent the values calculated from the kinetic model of pseudo first order.

5.3. Physical properties of activated carbon in the tissue

The carbon present in the tissue was analyzed to follow the evolution of its physical properties after several utilisations, the last stage before its analysis is the adsorption. This carbon was divided into two parts, the first part was analyzed without any specific treatment, the second was rinsed with a continuous stream of water. Samples were then characterized by several types of analysis (BET, porosimetry and TGA) and compared with the properties of the origin AC.

5.3.1. BET surface area and pore-size distribution

BET surface area and pore-size distribution of the untreated used AC in the tissue were found to change markedly at the end of the photocatalytic runs as compared to the non used AC (Table IV-8). The surface area of the non used carbon ($1065.40 \text{ m}^2 \cdot \text{g}^{-1}$) was reduced by 80 % as compared to the used carbon ($207.94 \text{ m}^2 \cdot \text{g}^{-1}$). These are in agreement with Tryba *et al.*, (2003) who reported that the BET surface area of AC (CWZ14-900) sample after one run of photocatalytic process decreased by about 60 % ($200 \text{ m}^2 \cdot \text{g}^{-1}$). This is attributed to the

reversible adsorption of phenol and intermediates still present on the untreated carbon and/or modifications of the carbon surface (Huling *et al.*, 2005). The modification of the carbon structure may be due to the oligomerisation of phenol; this polymerisation reaction "coupling oxidation" can be produced even at low temperature forming small-size polymers adsorbed irreversibly on the surface of the activated carbon blocking its pores (El-sheikh *et al.*, 2007; Quintanilla *et al.*, 2007).

Table IV-8

Comparison of physical properties of used (5 cycles) and virgin AC in the tissue with two initial phenol concentrations; 0.88 and 0.45 g/L

Activated carbon	Surface BET ($\text{m}^2 \cdot \text{g}^{-1}$)	Microporous volume ($\text{cm}^3 \cdot \text{g}^{-1}$)	Mesoporous volume ($\text{cm}^3 \cdot \text{g}^{-1}$)	Pore size A°
AC non used	1065.40	0.460	0.046	19.02
AC used ($C_{\text{phenol, initial}}=0.88\text{g/L}$ Without treatment)	207.94	0.075	0.071	28.25
AC used ($C_{\text{phenol, initial}}=0.88\text{g/L}$ AC rinsed with H_2O)	230.40	0.093	0.036	21.67
AC used ($C_{\text{phenol, initial}}=0.45\text{g/L}$ Without treatment)	550.00	0.199	0.062	19.00
AC used ($C_{\text{phenol, initial}}=0.45\text{g/L}$ rinsed with H_2O)	695.70	0.255	0.053	17.76

From the comparison of pore-size distribution of AC sample before and after photocatalytic process, it is seen that phenol molecules block the most microporous of this sample after adsorption. The decrease in microporous volume ($0.075 \text{ cm}^3 \cdot \text{g}^{-1}$) is observed by comparing with that for AC before phenol adsorption ($0.460 \text{ cm}^3 \cdot \text{g}^{-1}$), and as a consequence mesoporous became detectable. This decrease in volume of microporous is reasonably supposed to be due to preferential adsorption of phenol molecules into microporous. The decrease in surface area and changes in pore-size distribution were reasonably may be caused by blocking the pore entrances on the surface of activated carbon by very low molecular weight intermediates.

By cleaning the samples by rinsing with a continuous stream of water we obtained specific surface area, S_{BET} equal to 695.70 and $230.40 \text{ m}^2 \cdot \text{g}^{-1}$ and microporous volume (0.255

$\text{cm}^3.\text{g}^{-1}$ and $0.093 \text{ cm}^3.\text{g}^{-1}$) for the phenol concentrations of 0.45 g/L and 0.88 g/L, respectively. This indicates that phenol and its aromatic intermediates may be oligomerized and irreversible adsorbed into the pores of AC and can not be removed either by cleaning methods or by oxidation, thus leading to decrease in the porous volume and the specific surface area.

5.3.2. Thermogravimetric analysis

Thermogravimetric analysis (TGA) of the non used and used AC samples, after the photocatalytic oxidation runs using two initial phenol concentrations (0.88 and 0.45 g/L) was investigated (Figure IV-27 a and b respectively).

The results show a first loss of mass of 6.95 % and 5.37 % at 103 °C with 0.88 and 0.45 g/L of phenol concentrations, respectively (humidity and small adsorbed molecules). It is lower for non used carbon than for the used carbon because of the presence of short chain intermediates. Then the profiles of the used AC after oxidation reveal an important loss of mass until 700 °C which is not found for the non used AC.

Additionally, the used AC in the case of phenol concentration 0.88 g/L shows TGA profiles of three inflexion points. The first loss of mass nearly at 300 °C is due to desorption of organic molecules, here phenol, intermediates, and possibly oligomers in small quantities. The losses of mass are then 8.9, 7 and 6.5 %, at temperatures 300 - 600 °C, 600 °C and 700 °C, respectively, these losses may be due to the elimination of carboxylic groups (decomposition via 150-400 °C) and lactones functional groups (350 - 600 °C).

However, for the second concentration (0.45 g/L), four inflexion points are observed at temperatures nearly 270 °C, 450 °C, 600 °C and 700 °C corresponding losses of mass of 5, 3.6, 5.2 and 7.2 %, respectively. At temperature between 0 and 200 °C, the loss of mass is due to the elimination of water, phenol and the intermediates. Then, the behaviour is the same of the non used AC. The profiles of the used AC/TiO₂ composite after different cleaning methods reveal mainly the same profiles of the virgin AC/TiO₂ sample.

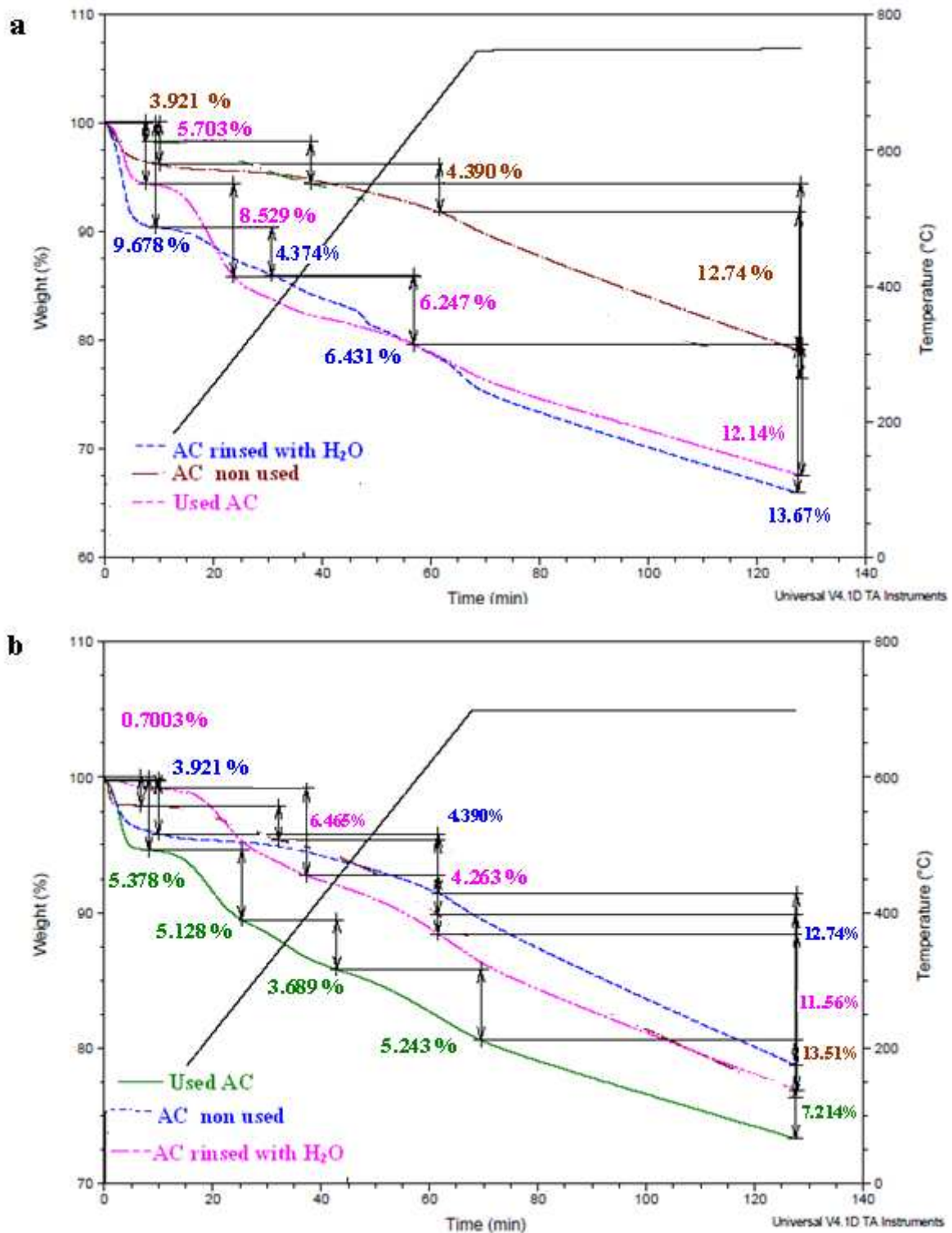


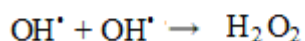
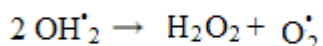
Fig.IV-27. Comparison of thermogravimetric analysis of the activated carbon in Ahlstrom tissue; used AC (at the end of consecutive oxidation runs without cleaning, rinsed with H₂O, and cleaning with acetonitrile/US) and non used AC using two initial phenol concentrations; 0.88 (a) and 0.45 g/L (b).

6. Effect of H₂O₂ addition on the photocatalytic degradation of phenol

In the previous section on photocatalytic regeneration of activated carbon by TiO₂ (in AC/TiO₂ tissue), the increase in deactivation of the TiO₂ catalyst was supposed to be due to either the presence of high quantity of pollutant as compared to that of the catalyst or hole-electron pair recombination. Furthermore, high amounts of adsorbed intermediates not degraded, at the end of the cycles, have coloured the TiO₂ surface preventing the UV to reach it and to produce the radicals for the oxidation. Moreover, a possible way to improve the reaction conditions is to minimize the hole-electron pair recombination which occurs during the oxidation reaction. Many Authors (Chen and Ray, 1998; Chu and Wong, 2003) reported that this deactivation may be due to the presence of hole-electron pair recombination. For this reason, oxidizing agent such as H₂O₂ is added to prevent this recombination. Therefore, it seems important to study the effect of H₂O₂ addition on the catalyst performance.

6.1. The operating conditions: quantity of H₂O₂

Many authors (Chu, 2001; Ghaly *et al.*, 2001; Chen and Cao, 2002; So *et al.*, 2002; Chu and Wong, 2004; Dionysiou *et al.*, 2004; Aleboyeh *et al.*, 2005; Chen and Liu, 2007) reported that the higher concentrations of hydrogen peroxide inhibited the photocatalytic reactions because of its scavenging effect on hydroxyl radical (see equations below).



Therefore, the addition of hydrogen peroxide may accelerate the photodegradation rate of phenol. However, in order to keep the efficiency of the added hydrogen peroxide, it was necessary to choose the convenient amount of hydrogen peroxide, according to the kinds and the concentrations of the pollutants.

Several authors reported in the literature (Amin *et al.*, 2008) the optimum effect of H₂O₂ addition on the photodegradation efficiency of pollutant to be obtained by varying the H₂O₂/pollutant weight ratio from 5 to 15. Above this range an excess of H₂O₂ inhibited the reaction. Thus a H₂O₂/phenol weight ratio of 10 has been selected in this work.

6.2. Control test

In order to evaluate the degradation ability of H_2O_2 , irradiation experiment was conducted without TiO_2 photocatalyst. Hydrogen peroxide 30% (50 ml, 0.22 M) was added to 2 L of phenol solution (0.88 g/L) in a batch photoreactor. The reactor was then exposed to UV irradiation source ($\lambda = 310 - 400 \text{ nm}$). This experiment was compared to that with TiO_2 media at the same condition, where the solution was kept in contact with the TiO_2 catalyst for a day in the dark. It is known that the photolysis of H_2O_2 does not occur significantly in this range of wavelength but at 200-280 nm (annexe 13). As the previous study was carried out at 365 nm, it is interesting to perform the rest study at the same conditions. It should be mentioned that Rodriguez (2003) showed that at this wavelength, the absorbance is very small but sufficient to produce OH radicals.

The variation of phenol concentration during the two experiments is shown in Figure IV-28. From these results, it was found that phenol concentration decreased continuously within the irradiation time. About 45 % of phenol is degraded within 220 min when H_2O_2 is added to phenol solution under UV irradiation. By comparison, about 30 % of phenol has disappeared within the same time of UV irradiation with TiO_2 media. These can be interpreted by the lower amount of TiO_2 catalyst to that of phenol as previously discussed.

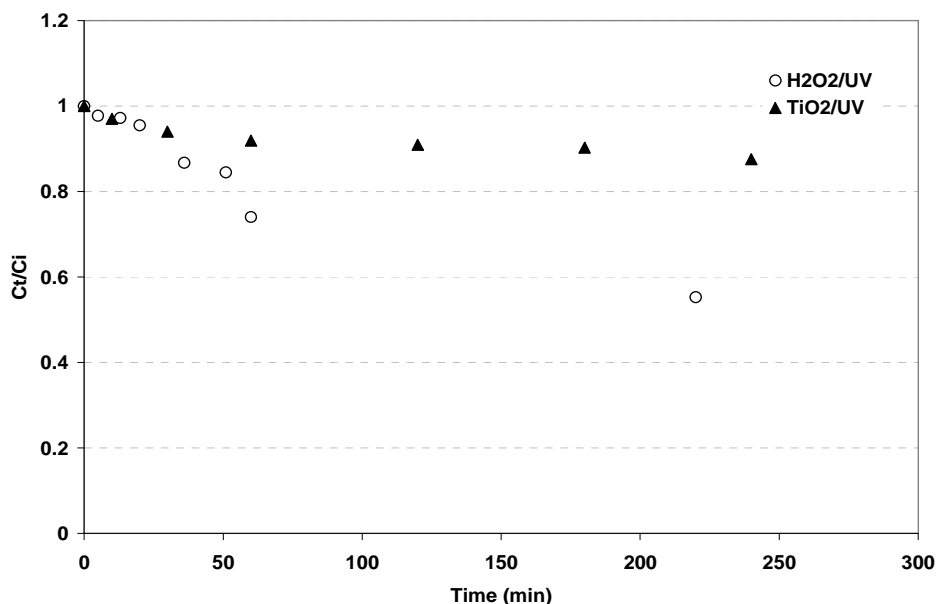


Fig.IV-28. Kinetic of phenol removal by UV/ H_2O_2 and TiO_2 media at 25 °C ($C_{i \text{ phenol}} = 0.88 \text{ g/L}$, $V_{\text{H}_2\text{O}_2} = 50 \text{ ml}$).

Chu and Wong (2004) stated that the H_2O_2 has low absorption at UV light of 365 nm, However, it can be enough to cause the H_2O_2 photolysis and in consequence the $\cdot\text{OH}$ radical production. The absorption of H_2O_2 at 365 nm was also increased with its concentration (Rodriguez, 2003). In the present study, a double stoichiometric amount of H_2O_2 was used.

6.3. Kinetics of adsorption and photocatalytic oxidation of phenol onto tissue with H_2O_2 addition.

In this section, the effect of H_2O_2 addition on the rate of phenol photocatalytic degradation by TiO_2 catalyst in tissue was investigated. All the conditions of the last experiment in the previous section, which was carried out without H_2O_2 are respected. In this experiment, tissue was firstly pre-saturated by 0.88 g/L of phenol for 4 days to ensure that AC has nearly reached the equilibrium state (cycle 1 adsorption). In the second step, 50 ml of H_2O_2 were added to the sample solution and the UV lamps were then switched on for starting the first photocatalytic oxidation run. After this run, new re-adsorption cycle was achieved by replacing the phenol solution in the reactor by another one (0.88 g/L; 2L) to examine the recovered activated carbon capacity in tissue. The above steps were repeated consequently for several runs.

6.3.1. Evolution of adsorption step

The experiments were carried out in dark with 2 L of phenol solution (0.88 g/L) and 17.6 g TiO_2/AC tissue at 25 °C.

The kinetic of phenol adsorption onto tissue is shown in Figure IV-29. In general, it was found that at the beginning, the adsorption rate of phenol was fast and then the rate was slowly declined, the equilibrium was not reached. Moreover, the adsorption rate and the phenol disappearance decreased from the first cycle with the virgin tissue to the other cycles with the reused tissue.

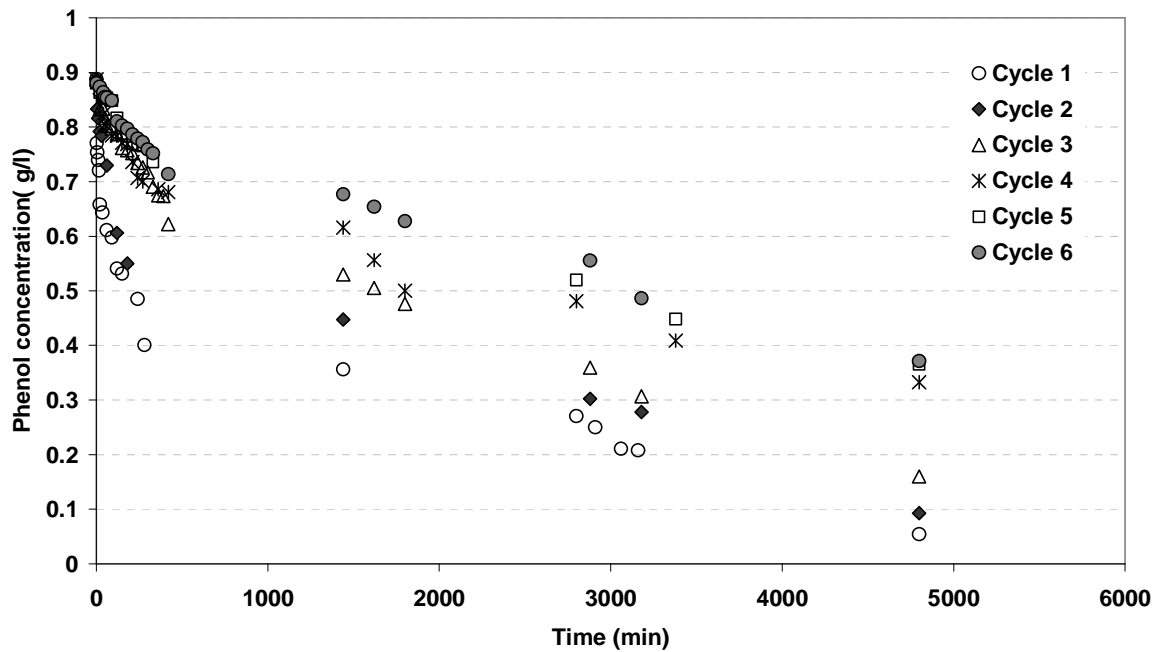


Fig.IV-29. Kinetics of phenol adsorption cycles onto tissue at 25 °C.

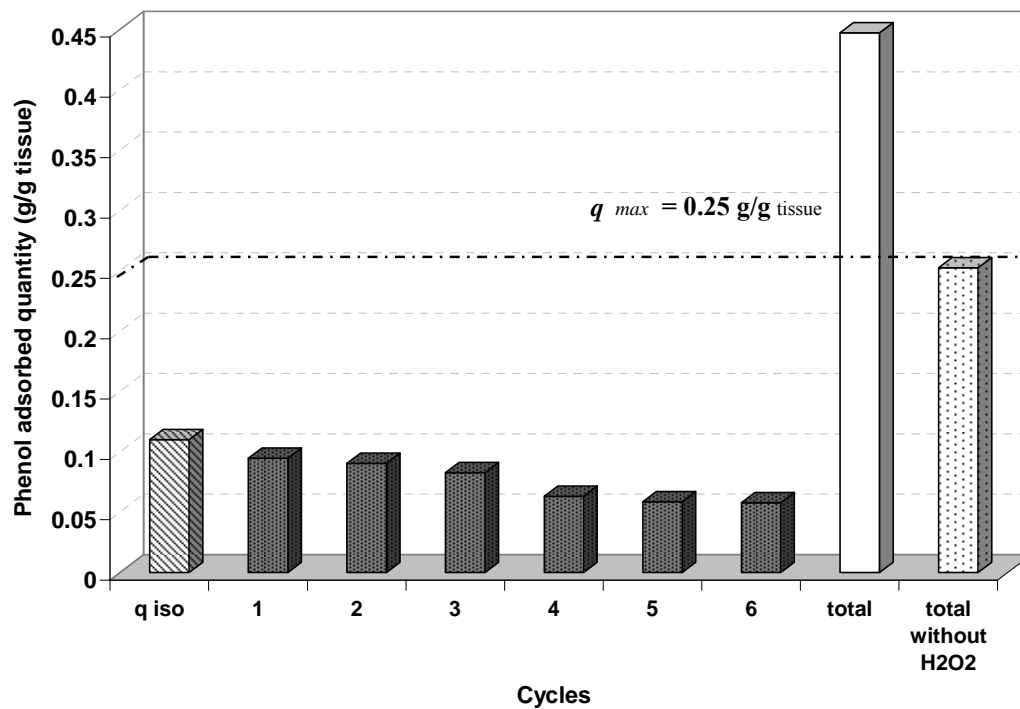


Fig.IV-30. Comparison of the quantity of adsorbed phenol (\blacksquare) during the cycles of adsorption onto tissue (\square : sum of the adsorbed quantities of phenol from cycle 1 to cycle 6, \square : sum of the adsorbed quantities of phenol without H_2O_2 , \square : q_{isotherm}).

Figure IV-30 represents the quantities of phenol adsorbed by tissue during 6 adsorption cycles. By comparison q_{isotherm} (0.11 g/g_{tissue}) with the quantity of phenol adsorbed during the first adsorption cycle (0.095 g/g_{tissue}), it can conclude that at the end of the first adsorption cycle, the activated carbon was nearly at equilibrium with the solution. For the next two cycles 2 and 3, the adsorbed quantities of phenol were slightly reduced to 0.090 g/g_{tissue} and 0.083 g/g_{tissue}, respectively. Then, this quantity was nearly the same (~ 0.06 g/g_{tissue}) in the next consecutive cycles. When summing up, the total quantity of phenol adsorbed during all cycles of reutilisation (0.487 g/g_{tissue}) was almost two times higher than the maximal adsorption capacity of virgin tissue (0.25 g/g_{tissue}) and the sum of the adsorbed quantities of phenol without H₂O₂. Therefore, from these results, the coupling of hydrogen peroxide (H₂O₂) and TiO₂ catalyst improves significantly the activated carbon regeneration. This positive effect is mainly able to treat a quantity of phenol to approximately two times more than the maximum quantity (q_{max}) of the virgin activated carbon.

6.3.2. Photodegradation step

In this part, the effect of H₂O₂ addition on 5 consecutive photo-oxidation cycles after preliminary adsorption step.

a. Kinetic of photodegradation cycles of phenol

The study of the reaction kinetics was performed according to all conditions previously used in the photocatalytic oxidation experiment, without H₂O₂. After the step of adsorption without UV, 50 mL of H₂O₂ (30 %) was added to the reaction solution in the reactor and the UV lamps were switched on. The decrease in phenol concentration with the time variation during 5 photooxidation cycles is represented in Figure IV-31. It was observed that when H₂O₂ was added and the solution was irradiated, the phenol was totally eliminated as compared to the initial concentration used during a period of time of almost 200 min in the first and second oxidation cycles. The phenol degradation then slightly decreased to 97 % in the next oxidation cycles during 360 min. It was also observed that the rate of phenol degradation in the 1st cycle is faster than that in the next cycles. This may be due to the fact that the initial concentration of phenol in the first cycle (0.05 g/L) was smaller than those in the next cycles and also probably due to the lower intermediates concentrations in the first cycle than that in the next oxidation cycles.

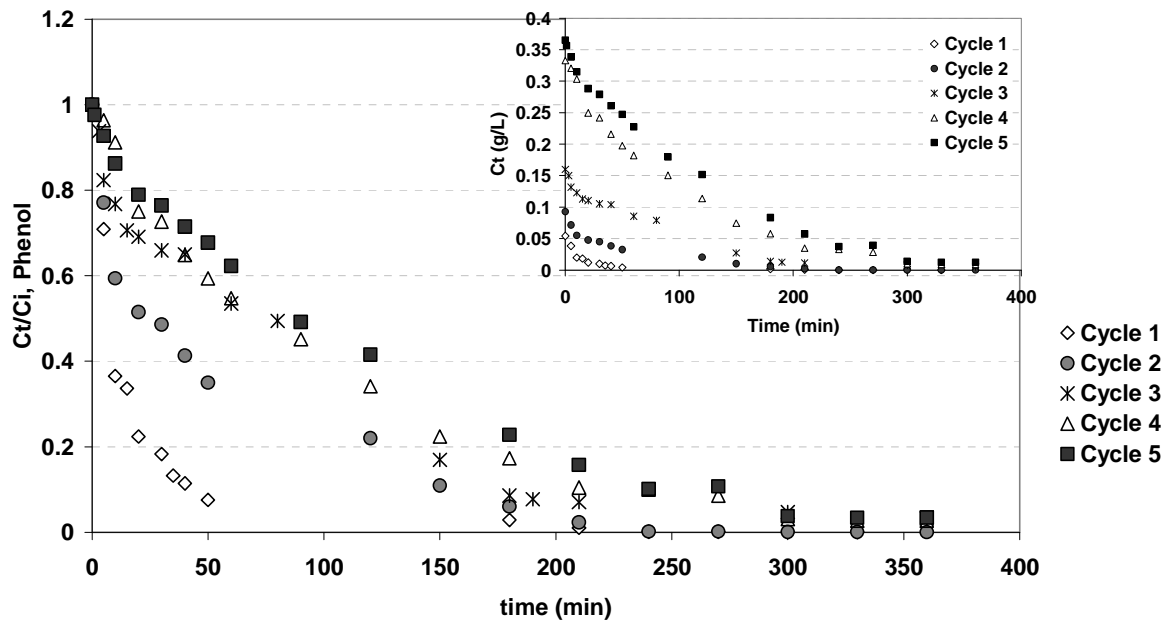


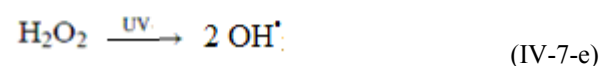
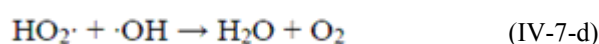
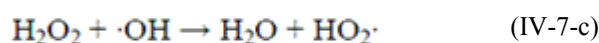
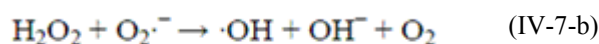
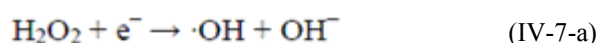
Fig. IV-31. Kinetics of phenol photocatalytic degradation cycles onto tissue in the presence of H_2O_2 at 25 °C.

When comparing with the results of photocatalytic oxidation of phenol onto tissue previously obtained without H_2O_2 , it is very clear that phenol degradation is much faster with H_2O_2 . It was found that the phenol concentration decreased to 0.0039 g/L during a period of time of 4700 min in the first run without H_2O_2 , while phenol was totally photodegraded to reach a very small concentration of 0.0001 g/L within 200 min in the presence of H_2O_2 . Therefore, the combination of the TiO_2 catalyst in tissue with H_2O_2 leads to an important increase of the photooxidation rates. Similar findings were found with Zhu and Zou (2009b) who reported that the organic compounds were similarly removed by TiO_2 coated activated carbon system in presence of H_2O_2 after 4 hrs and 16 hrs using TiO_2/AC alone. In the present work, successive cycles have also been performed with H_2O_2 showing the elimination percentage of phenol to range from 99 % in cycle 1 to 97 % in the last cycle of photocatalytic oxidation when H_2O_2 /phenol equal to 10.

As reported in the literature (Herrmann *et al.*, 1993; Poullos *et al.*, 1999; Hachim *et al.*, 2001; Sauer *et al.*, 2002, Barakat *et al.*, 2005) the increase in concentration of $\cdot OH$ radicals by the addition of hydrogen peroxide leads to the increase in the rate of degradation.

These can easily attack the adsorbed organic molecules or those located close to the surface of the catalyst, thus finally leading to their complete mineralization.

It is known that hydrogen peroxide can enhance the reaction of phenol degradation by providing additional hydroxyl radicals as shown in equations (IV-7-a) to (IV-7-e) by trapping photogenerated electrons produced by TiO₂ whatever the wavelength. This trapping would also help to suppress recombination of electron-hole pair produced at the activated TiO₂ catalyst surface, which would lead to the increased rate of phenol degradation (Dionysiou *et al.*, 2004; Yano *et al.*, 2005).



b. Model application for photodegradation of phenol in the presence of H₂O₂

As mentioned above, the photocatalytic degradation process follows a first order model. The first order kinetic constant (K_{ap}) and R^2 of all the oxidation cycles are reported in Table IV-9.

Table IV-9

Pseudo first-order apparent constants (K_{ap}) and correlation coefficients (R^2) during the consecutive phenol photocatalytic oxidation runs in the presence of H₂O₂

Cycles No	* $C_{0,i}$ (g.L ⁻¹)	K_{ap} (min ⁻¹)	R^2
1 st run	0.054	0.057	0.99
2 nd run	0.093	0.017	0.98
3 rd run	0.159	0.011	0.98
4 th run	0.332	0.010	0.99
5 th run	0.365	0.008	0.99

* The initial phenol concentration after dark adsorption for each run, i.

From the results, it was found that the first order model having R^2 values 0.99, were fitted well in terms of the photocatalysis kinetics of phenol degradation with AC/TiO₂ tissue in the presence of H₂O₂. The comparison of the experimental data with the theoretical values of phenol concentration calculated from the kinetic of pseudo first order confirmed that data are well described by this model for all cycles (Fig.IV-32). The results in table IV-10 show that even with H₂O₂, cycle 1 has a much greater K_{ap} value (0.057 min⁻¹) than the next consecutive cycles (0.01 min⁻¹). Thus the apparent “deactivation” of the sequential process adsorption- regenerative photo-degradation is still very important.

This decrease in K_{ap} may be again due to the increase in the concentration of phenol and its intermediates from one cycle to other. Here, this decrease in K_{ap} during the cycles is less than that observed in the previous case using the same TiO₂/AC tissue without H₂O₂ addition (Table IV-6).

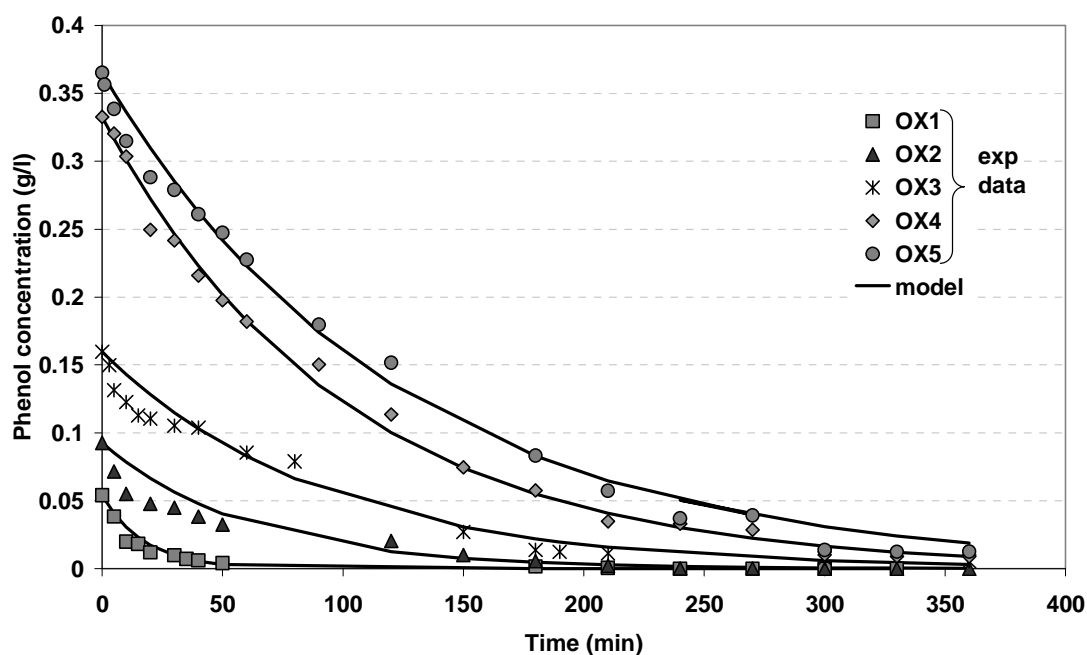


Fig.IV-32. Comparison between the experimental (symbols) and theoretical (lines) data during the photocatalytic degradation cycles of phenol onto tissue in the presence of H₂O₂ (T: 25 °C, C₀; 0.88 g/L).

In addition, our study agrees with several authors (Reeves *et al.*, 1992; Augugliaro *et al.*, 2002; Saquib and Muneer, 2003; Styliidi *et al.*, 2003) who report that the experimental

data were reasonably well fitted by first-order kinetic model for the photodegradation of several organic pollutants.

6.3.3. Synergetic effect of H₂O₂ addition to TiO₂ in the tissue.

Without H₂O₂, the photocatalytic regeneration was more effective in the first two cycles of photo-oxidation than that in the other next runs, where deactivation of the photocatalyst was reached (in previous section, Fig.IV-19a).

Therefore, the synergetic effect of H₂O₂ addition was tested using cycle 1 as indicator for this effect. First order kinetic model constant (K_{ap}) is used for this calculation (Table IV-10). Moreover, this table shows also K_{ap} for homogeneous photocataysis using H₂O₂ alone.

Table IV-10

Apparent first order rate constants detected in the photodegradation of phenol by UV irradiation of tissue (TiO₂/AC) and Synergetic factor (S) in the presence and in the absence of H₂O₂.

System	First order model		Synergetic factor : $S = \frac{K_{ap,withH_2O_2}}{K_{ap,withoutH_2O_2} + K_{ap,H_2O_2alone}}$
	$K_{ap} (min^{-1})$	R^2	
With H ₂ O ₂ alone	0.30×10^{-2}	0.98	7.5
Tissue(TiO ₂ /AC) without H ₂ O ₂	0.46×10^{-2}	0.99	
Tissue(TiO ₂ /AC) with H ₂ O ₂	5.7×10^{-2}	0.99	

As an increase in the rate constant, the photocatalytic activity increase. The results show the rate constant in presence of H₂O₂ is higher ($5.7 \times 10^{-2} min^{-1}$) than that without H₂O₂ addition ($0.46 \times 10^{-2} min^{-1}$). Therefore, the presence of H₂O₂ creates a kinetic synergetic effect (S) of the system with increase of the rate constant by a factor of 7.5 in the first photocatalytic run. This is similar to Terzian *et al.* (1991) who reported that the combination of TiO₂ catalyst with H₂O₂ leads to an increase of the photooxidation rates. Moreover, it is clear from the table that K_{ap} of homogeneous photocatalysis using H₂O₂ alone is lower than those obtained when TiO₂/AC is coupled with H₂O₂.

These results confirm that a major practical problem when using TiO₂ as photocatalyst is electron-hole recombination which, in the absence of proper electron acceptors. One

strategy for inhibiting electron-hole recombination is to add other electron acceptors to the reaction. The use of inorganic peroxides such as hydrogen peroxide, ozone and peroxydisulphate had been demonstrated to remarkably enhance the rate of degradation of different organic contaminants (Herrmann *et al.*, 1993; Chen and Liu, 2007).

6.3.4. Regeneration efficiency of tissue in presence of H₂O₂

Figure IV-33 shows the photocatalytic regeneration efficiency of the phenol adsorption capacity of tissue (TiO₂/AC) in the presence and absence of H₂O₂ during five cycles of sequential adsorption / photoregeneration as compared with the virgin tissue (cycle 0).

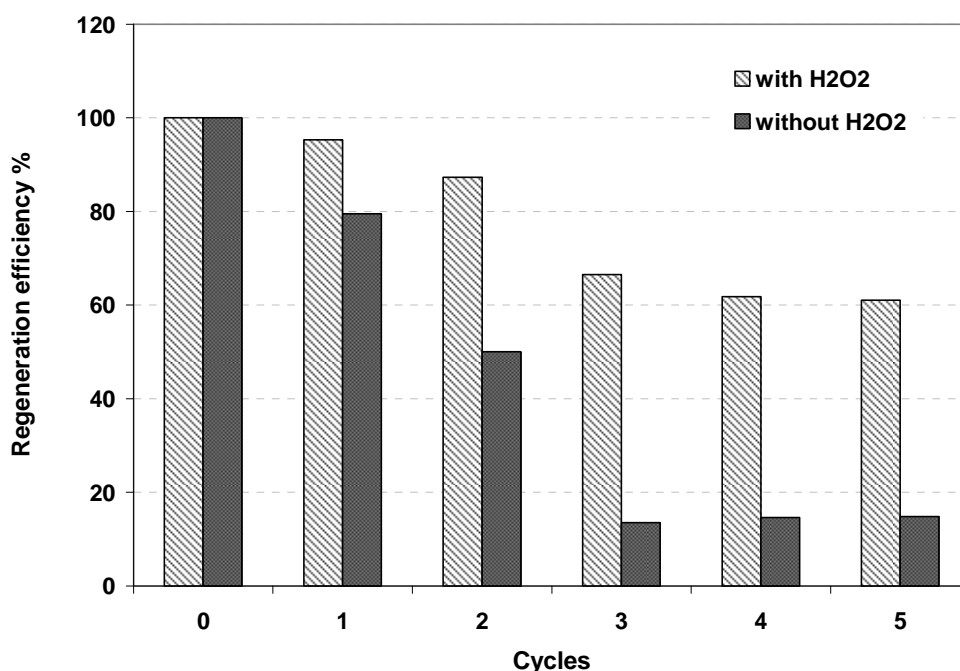


Fig. IV-33. Comparison between the regeneration efficiency of tissue (AC/TiO₂) during the photocatalytic degradation runs in the presence and absence of H₂O₂.

A clear improvement is obtained with H₂O₂ especially for the apparent final state (above 60%) four times more than without H₂O₂.

At the first cycle, with H₂O₂, the efficiency of AC regeneration based on recovering the adsorption capacity is 96 %. As increasing the recycling time, the efficiency is slightly decreased to 89 % then steady state obtained in the last 3 next cycles, above 60 % as compared to that of virgin tissue (cycle 0; 100 %). These indicate that the capacity of the used

tissue is nearly completely recovered after photocatalytic regeneration in the presence of H_2O_2 during a total time of 360 min UV irradiation in the two first runs. These results coincide with several investigators in the literature (Bertelli and Selli, 2006; Zhu and Zou, 2009a). Consequently, it can be concluded that under condition of the low catalyst/pollutant ratio, adding H_2O_2 enhances the regeneration efficiency of the activated carbon in tissue for several runs.

Kabir *et al.* (2006) reported that the addition of a small amount of the photocatalyst to hydrogen peroxide showed superior performance for phenol degradation; almost 98% of phenol was found to be degraded within 2.5 hr irradiation thus, combined effect of relatively small amounts of hydrogen peroxide and the photocatalyst was found to be the most efficient means of degrading phenol.

6.3.5. Photo-mineralization of phenol in the presence of H_2O_2

In order to assess the degree of mineralization reached during the photocatalytic treatment, the change of Total Organic Carbon (TOC) is generally determined. Mineralization of phenol by UV/ H_2O_2 / tissue (TiO_2/AC) process was then studied using a 0.88 g/L solution of phenol according to TOC loss evolution. A plot of TOC as a function of time during the photocatalytic oxidation process in the presence of H_2O_2 is presented in Figure IV-34.

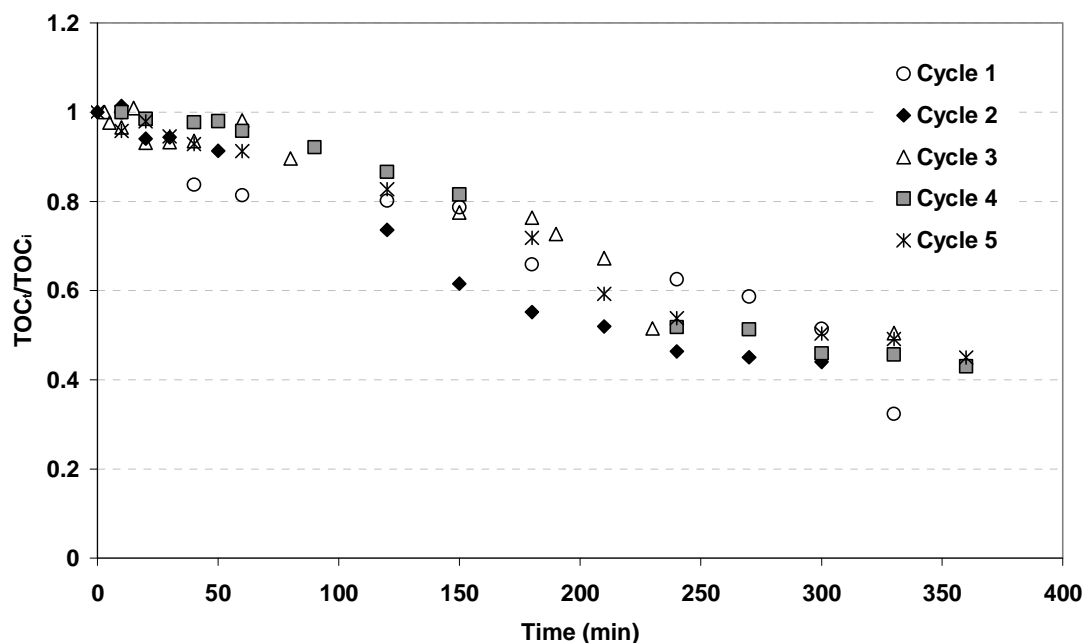


Fig.IV-34. Total Organic Carbon (TOC) removal from the solution during 5 cycles of photocatalytic degradation of phenol by tissue (TiO_2/AC) in the presence of H_2O_2 .

It can be seen that the TOC decreases slowly by increasing the time of UV irradiation. Furthermore, the S- shape of the TOC removal curve, very different to the phenol concentration evolution (Figure IV-31), denotes an important initial formation of by-products. This result is in agreement with Karkmaz *et al.* (2004) who reported that TOC exhibits an S-shape with a slower degradation rate during the photocatalysis of the coloured organic compounds.

In the present work, TOC values remain high even at the end of the oxidation run. After 360 min of UV irradiation, the extent of TOC decay was about more than 67 %, 56 %, 56 %, 49% and 55 % for the 1st, 2nd, 3rd, 4th and 5th photooxidation cycles, respectively (Fig. IV-34). This is in agreement with Zhang *et al.* (2006) who reported that the TOC was found to still remain at appreciably high value even when the aromatic intermediate products were completely degraded. This implies that the further oxidized intermediate products exist. These intermediate products are thought to be organic acid without aromatic ring: carboxylic acids as oxalic acid, formic acid, malonic acid...etc. The overall oxidation kinetics are very slow, and the carboxylic acids are very difficult to oxidize to carbon dioxide at the beginning of the reaction (Santos *et al.*, 2002).

These results of TOC removal are also consistent with Silva *et al.* (2004) who cited that the photodegradation of the organic pollutants by H₂O₂/TiO₂ after 240 min of irradiation achieved an overall TOC removal of 46 %. These experiments were carried out with an initial TOC concentration of about 1800 mg.L⁻¹, TiO₂ of 1 g.L⁻¹, H₂O₂ concentration of 0.59 M and at temperature of 35 °C.

The comparison between the analyses of TOC values at the beginning (TOC_{initial}) and end (TOC_{final}) of the reaction and those calculated from final oxalic (TOC_{f,oxalic}) and the final phenol concentration (TOC_{f,phenol}) as determined by HPLC for each cycle is presented in Fig.IV-35. After adsorption, at the beginning of reaction, the values of TOC_{initial} were 54, 345, 443, 475 and 627 mg/L for cycles 1, 2, 3, 4 and 5, respectively. At the end of the photocatalytic oxidation reaction, it decreased to 17.4, 152, 161, 177 and 240 mg/L for these cycles, respectively. In addition, TOC_{initial} is sharply increased from cycle to other, indicating a “deactivation” or a “transient” of the sequential process. This progressive increase of initial TOC shows that the balance between adsorption and regeneration is not achieved: the adsorbed TOC is progressively reduced due to either reduction of the adsorption capacity as

observed in air oxidation process or, more probably, to a reduction of the photocatalytic relative efficiency due to the increase in the adsorption of the intermediates formed during the photocatalytic oxidation of phenol, as mentioned above. When comparing the absolute efficiency, the amount of degraded TOC increases by cycles due to the much higher concentration in liquid phase which results from lower adsorption.

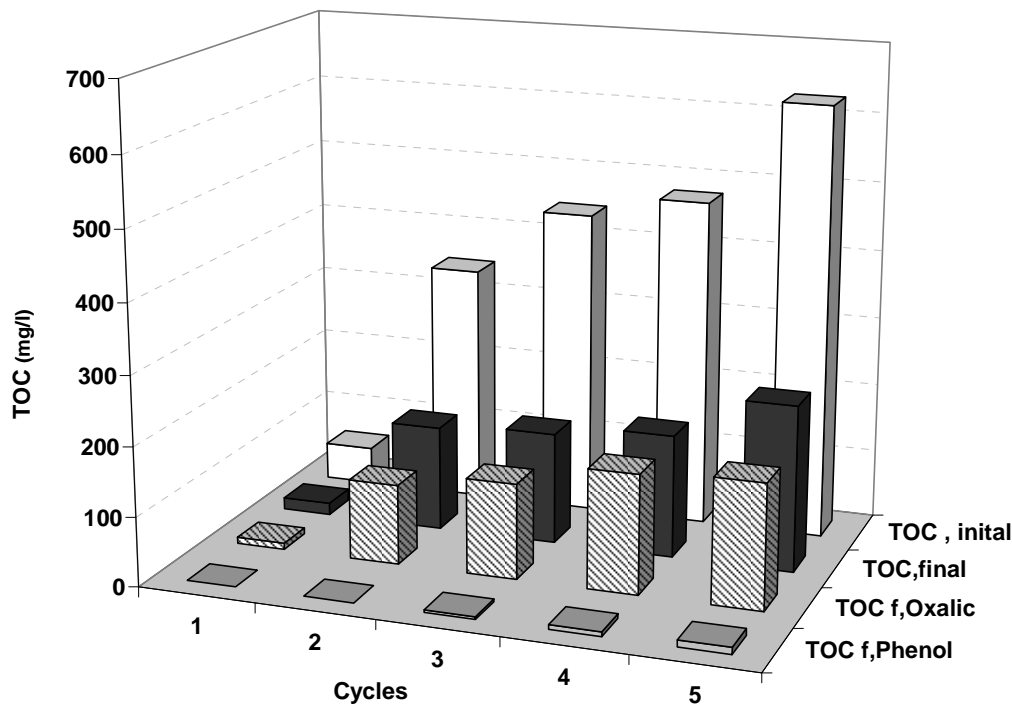


Fig. IV-35. Comparison between $TOC_{initial}$, at the beginning of oxidation ($t = 0$) and TOC_{final} , at the end of the oxidation process and the TOC calculated from oxalic ($TOC_{f,oxalic}$) and phenol concentration at the end of reaction ($TOC_{f,phenol}$) during 5 photocatalytic oxidation cycles by TiO_2 in tissue in the presence of H_2O_2 .

On the other hand, the TOC values calculated from phenol concentration at the end of oxidation are negligible as compared to overall TOC. On the contrary, the TOC calculated from final oxalic represents the predominant part of the HPLC analysed TOC values.

The study of TOC removal kinetic has again been achieved by using the first-order model. Figure IV-36 shows this model fitted rather well the experimental data, despite the S-shaped curves, with correlation coefficient values (R^2) greater than 0.97 for all cycles. Roughly, and contrary to the data based on phenol concentration, the apparent constant (K_{ap}) is slightly increased with the number of cycles and their values ranged from 0.22×10^{-2} to $0.39 \times 10^{-2} \text{ min}^{-1}$ (Table IV-11). These K_{ap} values are much lower than those of phenol degradation (Table IV-9). These mean that the phenol degradation rate is much faster than the

TOC removal rate: the opening of aromatic ring is easy compared to the carboxylic mineralization. The low mineralization rate is due to the fact that CO_2 molecules are mainly formed from the small acid intermediates generated during the oxidation whose reaction kinetic is very slow.

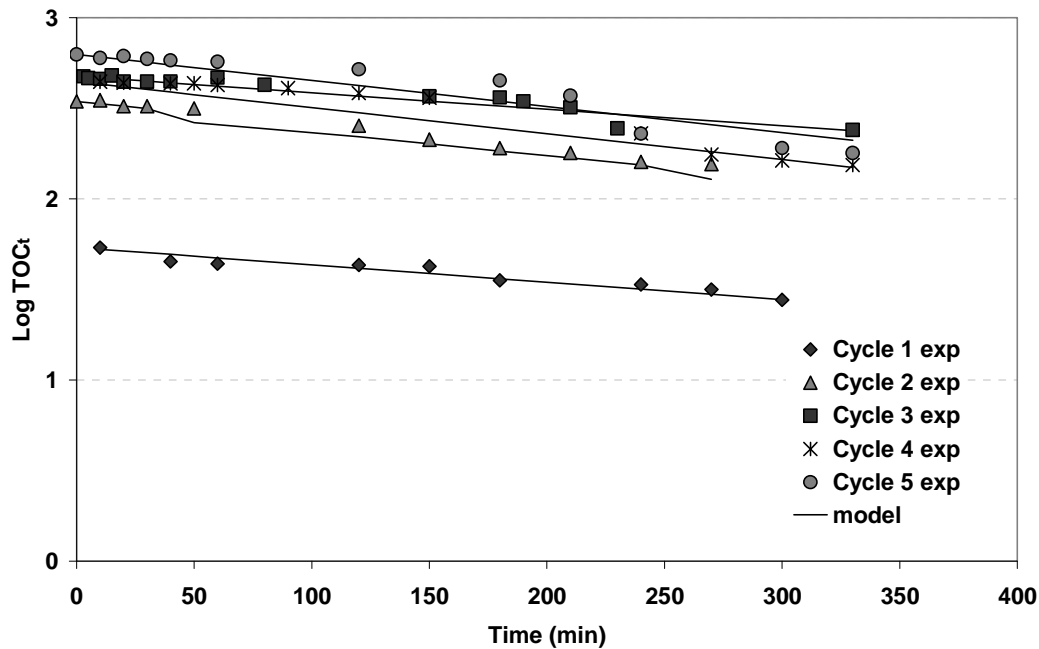


Fig.IV-36. Comparison between TOC values of the experimental (symbols) and theoretical (lines) data during the photocatalytic degradation cycles of phenol onto tissue within 360 min in the presence of H_2O_2 (T: 25 °C, C_0 ; 0.88 g/L).

Table IV-11

Pseudo first-order apparent constants (K_{ap}) and correlation coefficients (R^2) for TOC removal during the consecutive phenol photocatalytic oxidation runs in the presence of H_2O_2

Cycles No	$\text{TOC}_{\text{initial}}$ (mg.l^{-1})	K_{ap} (min^{-1})	R^2
1 st run	54	0.22×10^{-2}	0.97
2 nd run	345	0.30×10^{-2}	0.98
3 rd run	475	0.21×10^{-2}	0.98
4 th run	443	0.33×10^{-2}	0.98
5 th run	627	0.39×10^{-2}	0.99

6.4. Evolution of physical properties of activated carbon in the tissue

6.4.1. BET surface area and pore-size

The change in BET surface area and pore-size distribution of the used AC with and without H₂O₂ in the tissue and non used AC is summarized in Table IV-12. In our study, the surface area of the virgin activated carbon (1065m²/g) was reduced by nearly 52 % as compared to the used carbon (562 m²/g). As mentioned previously, this decrease may be due to the accumulation of phenol intermediates by cycles on the AC.

Although, the microporous volume decreased to 0.113 cm³.g⁻¹ in the used AC, it is noticed that its mesoporous volume increased to 0.147 cm³.g⁻¹. This decrease in microporous volume is due to preferential adsorption of phenol molecules into microporous forming monolayer. This slight increase in mesoporous volume may hardly be explained; only modifications of surface function groups might occur.

Table IV-12

Comparison of physical properties of used AC in the tissue after the 5 adsorption-regeneration cycles with and without H₂O₂ addition and virgin AC.

Activated carbon	Surface BET (m ² .g ⁻¹)	Microporous volume (cm ³ .g ⁻¹)	Mesoporous volume (cm ³ .g ⁻¹)	Pore size A°
Virgin AC	1065	0.46	0.046	19.0
Used AC -with H ₂ O ₂	562	0.113	0.147	18.5
Used AC -Without H ₂ O ₂	208	0.075	0.071	28.2

6.4.2. Thermogravimetric analysis

Thermogravimetric analysis (TGA) of both the virgin AC and used AC in the tissue, after 5 cycles of adsorption and photocatalytic oxidation of phenol in the presence of H₂O₂ is represented in Figure IV-37.

For used AC in tissue a first loss of mass of 9.953 % appears at 132 °C which mainly represents the degree of humidity. It is not surprising to found less humidity in the virgin AC. As found previously in the TGA of the used AC (oxidation without H₂O₂, Fig.IV-26a), the

profile of the used AC after oxidation with H_2O_2 reveals also a loss of mass until almost $300^\circ C$ corresponding to aromatics and intermediates. Then, the AC used presents the same behaviour of virgin AC and its structure is not modified.

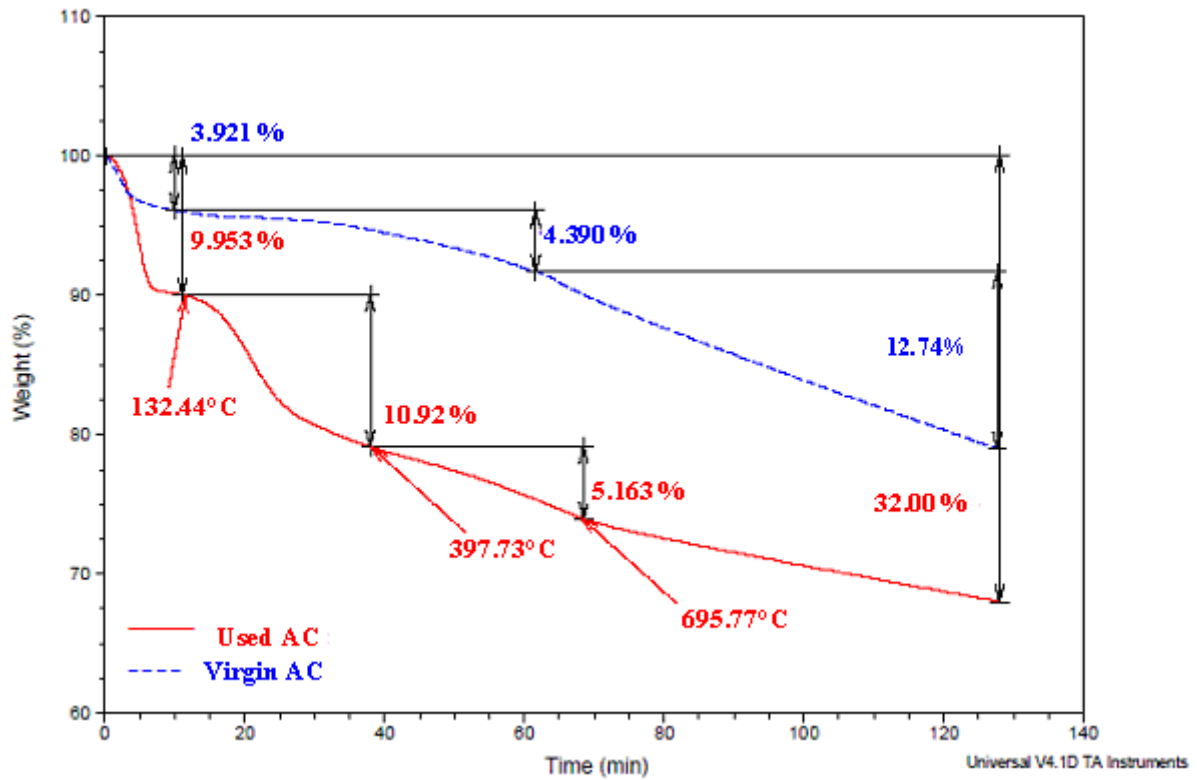


Fig. IV-37. Comparison of thermogravimetric analysis of the activated carbon in tissue; used AC (at the end of 5 consecutive cycles in the presence of H_2O_2) and virgin AC.

7. Photocatalytic oxidation of phenol using fixed bed continuous reactor

After having previously investigated the tissue system for phenol removal in batch, it was interesting to investigate the performance of this system in continuous conditions using a kind of fixed bed photocatalytic reactor.

A tubular continuous fixed bed photocatalytic reactor of 120 mL was used for the study. A schematic diagram of the photocatalytic tubular reactor system is shown in Fig.II-13, chapter II. The tissue is placed in the toroidal reactor, with TiO₂ film facing the central lamp; the volumes of the toroidal reactor and the TiO₂/ AC tissue are approximately equal. The experimental device consists of a feed inlet tank with a stirrer used to ensure the complete mixing of the solution in the tank, a peristaltic pump (Master flex model) with a flow rate of 2 ml/min used to pump the reactants from the tank to the reactor, the apparent residence time (excluding the volume of the tissue) was about 60 min. The UV lamp (Philips, $\lambda = 365$ nm) was located in the centre of the reactor to illuminate the TiO₂ photocatalyst. The lamp was surrounded with double envelope and water bath with circulation pump used to cool the UV lamp. Stream of air was used to provide air, which worked as an electron scavenger to prevent the recombination of electron-hole pairs. The experiment was conducted at 25 °C. The TiO₂/AC tissue (12.7 g) was pre-adsorbed in 5L batch reactor for 3 days using 0.2 g/L of phenol to approximately reach the equilibrium. The continuous oxidation process was then achieved using this loaded tissue in fixed bed reactor by continuous addition of 0.017 g/l phenol (phenol concentration after the dark adsorption period). The sampling was taken each 1 hr at two different regions: one from inside the reactor by using a syringe (at 6 cm) and the other from the outside of the reactor.

Figure IV-38 shows the evaluation of phenol concentration during the adsorption process in the dark at 25°C. The rate of phenol adsorption started fast and reached approximately the equilibrium after 4000 min. By comparing the couple C_e 0.0179 g/L and q_e 0.07505 g/L at the end of the selected adsorption step (4200 mn) and the isotherm of tissue previously evaluated in this study, it can be concluded that the activated carbon in tissue was very close to equilibrium.

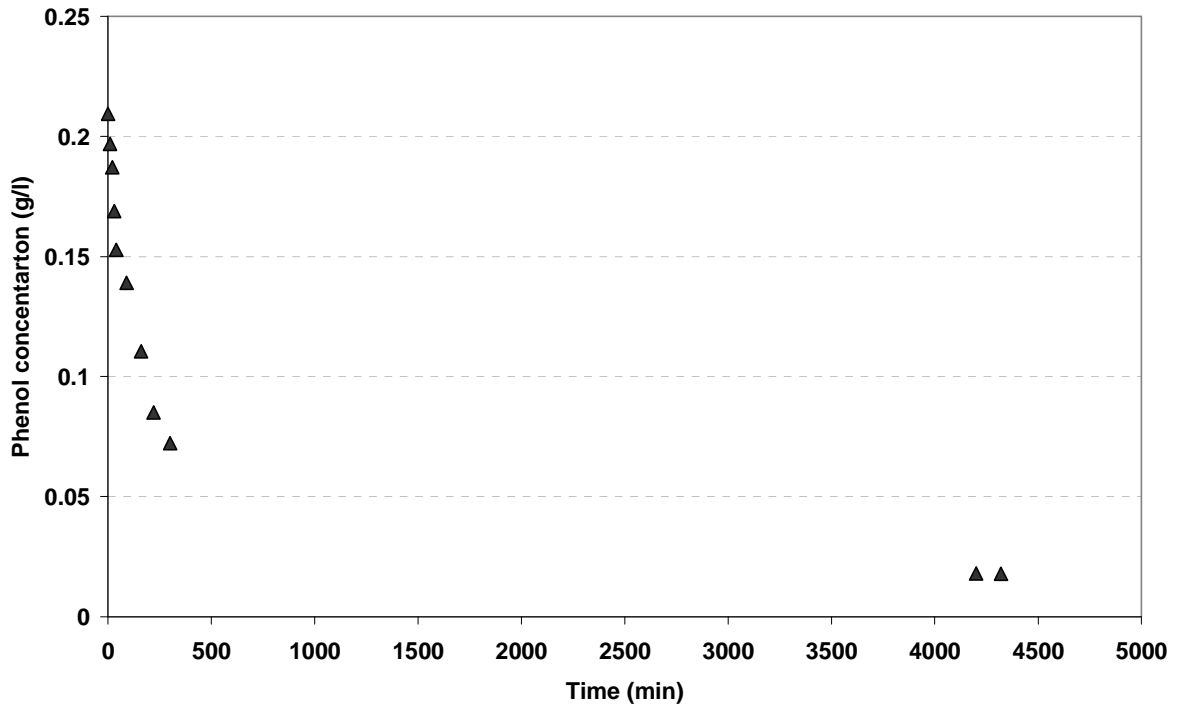


Fig.IV-38. Kinetic adsorption of phenol ($C_i = 0.2$ g/l) onto TiO_2/AC tissue (12.7 g) at 25 °C.

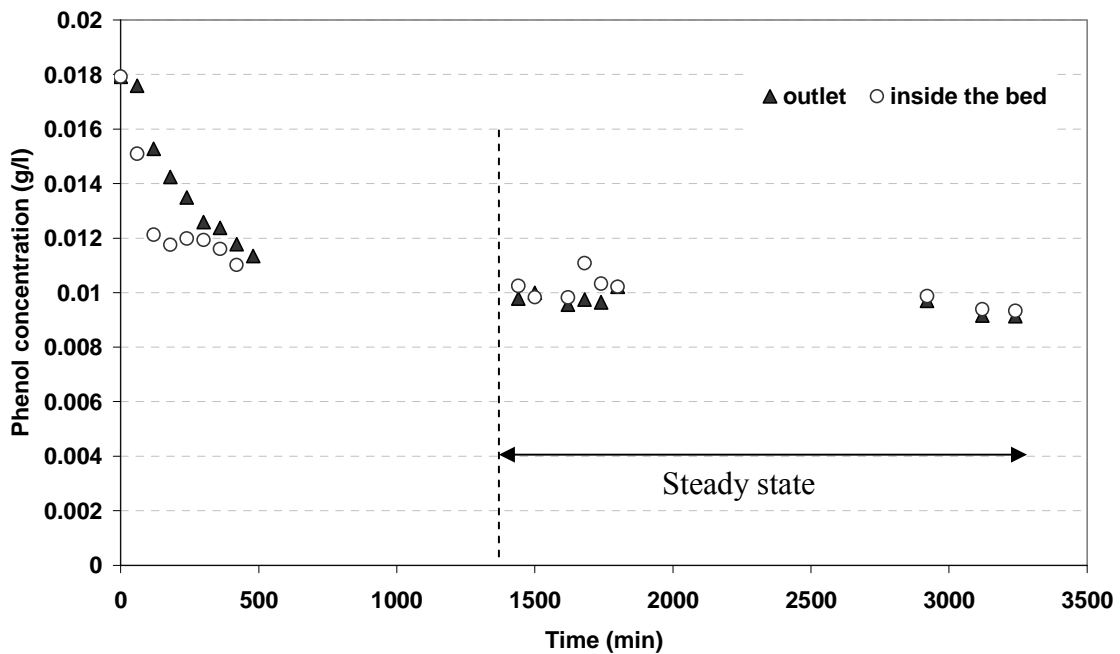


Fig.IV-39. Continuous photocatalytic oxidation of phenol in fixed bed type reactor (TiO_2/AC tissue) at 25°C ($C_i = 0.0179$ g/L, flow rate = 2 ml/min) mass of tissue = 12.7 g).

The experimental results of photocatalytic degradation of phenol using tubular fixed bed reactor are presented in Fig.IV-39. The location of sampling inside the reactor at a distance of 6 cm from inlet allows to take a sample of the solution near the TiO₂ catalyst surface where the reaction takes place. The other sampling was at the outlet of the reactor: the sample taken includes not only the solution being in direct contact with UV but also that passing through the AC zone and the thin external layer between the tissue and the jacket wall. Concerning the overall performance of this set up the outlet measurement mixing all fluid passing through the reactor, even possible by-pass in the external layer, is much more significant and should be selected.

At first, the decrease in the phenol concentration is due to the photocatalysis consuming phenol in liquid phase then changing the adsorption equilibrium. Then a new equilibrium state AC and the solution is reached and steady state is obtained, thus there is not any more of desorption. At steady state the concentration difference gives the true reaction rate. It is important to note that only this run gives access to this reaction rate (here $r = 1.25 \times 10^{-6} \text{ min}^{-1}$) calculated as the following equation:

$$r = \frac{Q \times ([\text{phenol}]_{\text{inlet}} - [\text{phenol}]_{\text{outlet}})}{m_{\text{tissue}}} \quad (\text{IV-8})$$

Where $[\text{phenol}]_{\text{inlet}}$ and $[\text{phenol}]_{\text{outlet}}$ are the inlet and outlet phenol aqueous concentrations (g/L), Q the flow rate (mL /min), and m_{tissue} is the mass of tissue (g).

With a residence time of 60 min in a single pass, about 50 % photocatalytic degradation of phenol was observed when a quasi steady state was reached (after approximately 1500 min, and up to the end of the run, 3300 min). These findings showed an encouraging continuous photocatalytic reactor performance for the treatment of organic compounds present in water which can be applied for water purification with much higher contact time. Similar findings were observed by Chin *et al.* (2004) who reported that photocatalytic degradation of 40 μM methylene blue dye (MB) using semicontinuous tubular reactor and thin film of TiO₂ photocatalyst was successfully synthesized and immobilized on glass reactor operated at re-circulation process mode with residence time $s = 2.2 \text{ min}$ in a

single pass. It was observed 50% photocatalytic degradation of MB under circulation mode after 5 passes.

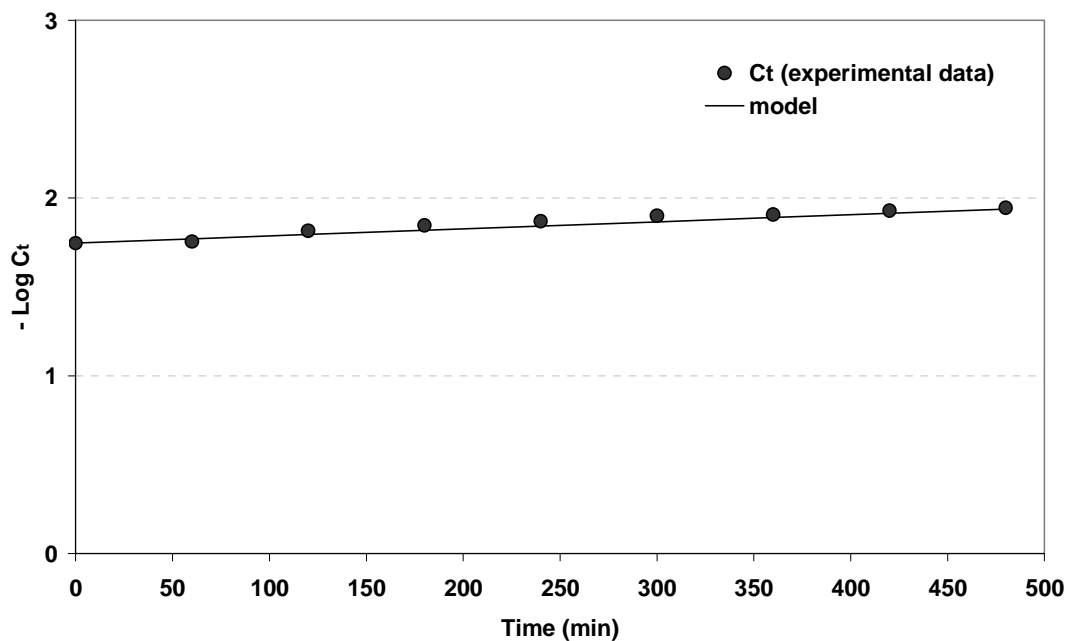


Fig.IV-40. Comparison between the experimental (symbols) and theoretical (lines) data of phenol photodegradation using TiO_2/AC tissue in fixed bed reactor (T: 25 °C, C_i ; 0.0179 g/L).

It was found that the photocatalytic degradation of phenol using fixed bed reactor obeyed pseudo-first-order kinetics. The apparent rate constants, k_{ap} (min^{-1}) were calculated from the slopes of the lines and R^2 values are shown in Table IV-13. From the results, it was found that the first order model having R^2 values 0.98, were fitted well in terms of the photocatalysis kinetics of phenol degradation by tissue (AC/TiO_2) in the fixed bed reactor. Moreover, by plotting the $\log C$ experimental and calculated against the reaction time using the first order model (Fig.IV-40), the validity of the model can be confirmed at only the first 480 min of the reaction time where the linearization is incorrect after this time; the estimation error percentage increased to about 69%.

Table IV-13

The values of the apparent rate constant (k_{ap}) and correlation coefficient (R^2) of the first order model for phenol photocatalytic oxidation onto tissue in fixed bed reactor

Sampling	K_{ap} (min^{-1})	R^2
Outside the bed reactor	0.09×10^{-2}	0.98
Inside the bed reactor	0.11×10^{-2}	0.92

In conclusion, this device is not interesting if we work with a constant inlet pollutant concentration because an equilibrium state is rapidly reached, then the AC plays no more role. On the other hand, if the inlet concentration is variable, the AC adsorbs a part of the pollutant and the photocatalyst degrades the remaining part of the pollutant in the solution.

B. Photocatalytic degradation of Tartrazine using immobilized TiO₂ on activated carbon S23

Dyes are an abundant class of coloured organic compounds that represent increasing environmental hazards. During dye production and textile manufacturing processes, a large amount of wastewater containing dyestuffs with intensive colour and toxicity can be introduced into aquatic systems. In most countries researchers are looking for appropriate treatments in order to remove pollutants, impurities and to obtain the decolourization of dye effluents. Various chemical and physical processes, such as chemical precipitation and separation of pollutants, electrocoagulation (Alinsafi *et al.*, 2007) elimination by adsorption on activated carbon (Daneshvar *et al.*, 2007) etc., are currently used. One drawback of these methods is that they are not destructive but only transfer the contamination from one phase to another. Therefore, a new and different kind of pollution is faced and further treatments are necessary (Tunay *et al.*, 1996; Slokar and Marechal, 1998). Similarly conventional biological methods have not proven to be particularly effective for coloured effluents. In most cases, dyes are absorbed onto biomass without being really degraded (Hai *et al.*, 2007; Sano *et al.*, 2008). In recent years as an alternative to conventional methods “advanced oxidation processes” (AOPs), based on the generation of very reactive species such as hydroxyl radicals that have been proposed to oxidize quickly and non-selectively a broad range of organic pollutants (Kitano *et al.*, 2007; Sano *et al.*, 2008; Khataee *et al.*, 2009).

As mentioned before, due to the difficult of TiO₂ powder separation, many studies recommended the development of supported TiO₂ (Hosseini *et al.*, 2007). Therefore, we previously used AC/TiO₂ supported tissue supplied by Ahlström for the removal of phenol. This support proved to be very effective not only to solve the problem of TiO₂ separation and filtration but also to enhance the photocatalytic performance. However, it must be pointed here that the adsorption sites of AC and the active sites of TiO₂ catalyst are far away from each other. For this reason, it seemed useful to examine the performance of other AC/TiO₂ composite prepared by CVD technique in which the sites of AC and TiO₂ are close to each other. As part of the project region CTP (Communauté de Travail des Pyrénées with URV Tarragona) concerned with removing of dyes from industrial water, we selected Tartrazine as an example of azo dye to study the efficiency of this AC/TiO₂ composite for its removal.

1. Photocatalysis using TiO₂ deposited on activated carbon: AC/TiO₂

In this part, the same principal idea used in the previous part with AC/TiO₂ tissue is here investigated but applied on other material (granular AC/TiO₂) prepared by CVD technique. In this study of photocatalysis as in previous ones in this work, a sequential method of treatment is carried out involving adsorption then photocatalytic regeneration and pollutant degradation. The material chosen is an innovative material: the catalyst, TiO₂, is deposited on the porous surface of a commercial activated carbon, S23. The first stage is the adsorption where the pollutants are concentrated inside the pores. The second stage is the photocatalysis under UV irradiation: TiO₂ situated in this zone of high pollutant concentration allows to catalyse the reaction. The stage of regeneration can then be carried out in the fluid. In the present work, two materials for the adsorption/photocatalysis process have been investigated for comparison:

- A new AC/TiO₂ material: TiO₂ deposited on AC S23 by CVD.
- A simple mixture of AC S23 and TiO₂: TiO₂ separated physically from AC.

In this study, we investigate the efficiency of these materials during several cycles of adsorption / photocatalytic oxidation in photocatalytic cylindrical reactor batch as detailed before (Fig IV-8).

1.1. Materials

The material consists of AC S23 on which TiO₂ is deposited (AC/TiO₂) obtained by a confidential process made by the CVD, team of LGC (Toulouse). The deposition of TiO₂ is achieved by CVD technique at high temperature in a reaction implying a chemical precursor (Titanium Tetra Isopropoxyde) which decomposed to give TiO₂ (Duminica *et al.*, 2004).

1.2. Characterization of AC / TiO₂ sample

The surface structure and particle size of the used AC / TiO₂ samples were first studied using Scanning Electron Microscopy (SEM). Moreover, the AC/TiO₂ composition was analyzed by EDX. The specific surface area of samples was measured using a Micrometrics ST-2000 automated apparatus based on the Brunauer–Emmett–Teller (BET) method at 77K with N₂ as adsorbent and H₂ as the carrier gas. In addition, TGA was used to determine the degree of sample thermal stability. All these analyses were performed at LGC and explained in details in chapter II.

1.2.1. Electron microscopic analysis

Figure IV-41 shows the SEM morphology of the activated carbon and AC/TiO₂ composite. Selected SEM images of the AC (Fig. IV-41a) and AC/TiO₂ (Fig. . IV-41b) used in this study are compared. Comparison of these figures shows that a number of TiO₂ aggregated particles are embedded at the entrance of larger macropores and on the external surface of AC support.

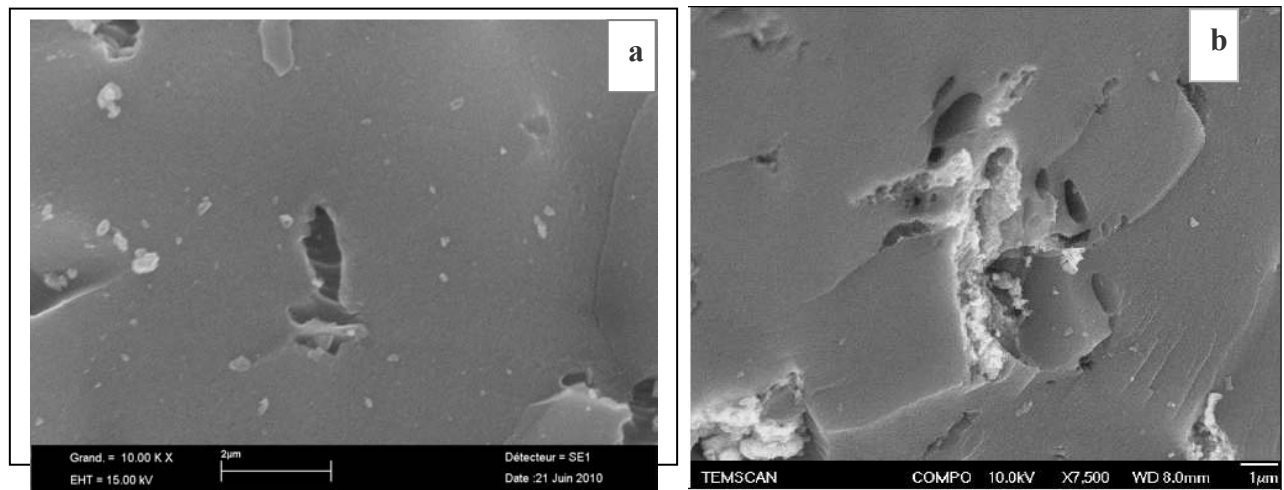


Fig. IV-41. SEM image of AC (a) and AC/TiO₂ (b).

1.2.2. Energy dispersive X-ray microanalyses (EDX)

To confirm the presence of TiO₂ on the sample, EDX analysis was carried out. EDX analysis was performed on both the AC (Fig. IV-42a) and the AC/ TiO₂ composite in two different regions: I and II (Fig.IV-42 b). EDX analysis was used to qualitatively characterize the elemental composition of the TiO₂ /AC sample. The elemental composition of the surface of the AC/TiO₂ sample was found to be about 24.89 % Ti, 39.07 % C, and 36.04 % O where the presence of Ti on the sample was confirmed (Fig.IV-43, Table IV-14). It's observed that the larger amount of Ti and O is placed on the external surface, but when the EDX probe is going deep into the AC particle the percentages of Ti and O slightly decrease, for example in the case of Ti 24.89 wt % at the wall (region I) and fall to 17.5 wt % in the region II. Of course for the powder AC samples no Ti was detected (Fig.IV-43a, Table IV-14). This indicates that the catalyst is not uniformly distributed on the AC substrate; this fact can also be seen in the SEM micrography (Fig.IV-41).

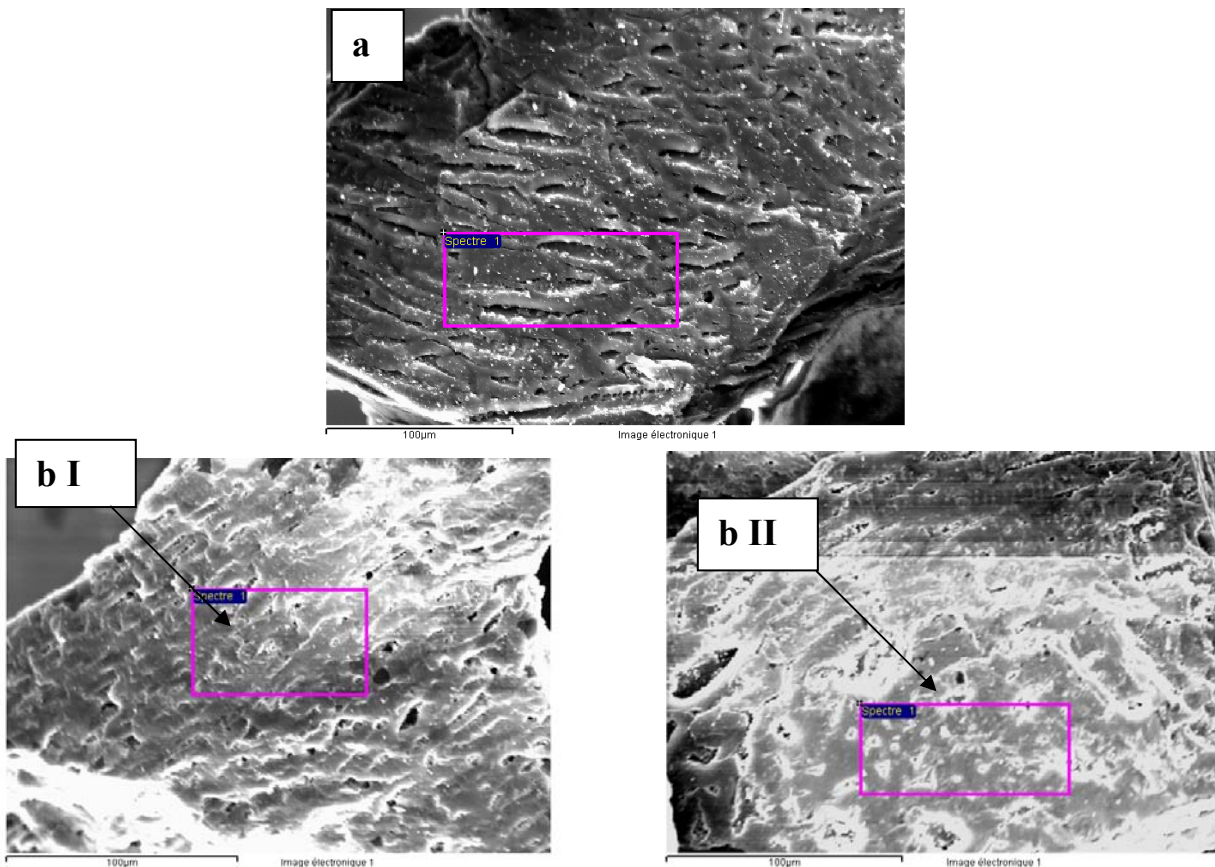


Fig.IV-42. Cross sectional SEM of AC (a) and AC/TiO₂ (b I & b II) sample in which two different regions are pointed out.

Table IV-14

EDX elemental composition of AC and TiO₂ /AC composite, in two different regions as indicated in Fig .IV-42.

Sample	Composition					
	C (Wt %)	*At%	O (Wt%)	*At%	Ti (Wt%)	*At%
AC alone	94.53	95.84	5.47	4.16	-	-
AC/TiO ₂ (region I)	39.07	53.99	36.04	37.39	24.89	8.62
AC/TiO ₂ (region II)	49.36	62.81	33.06	31.58	17.58	5.60

*At: automatic percentage.

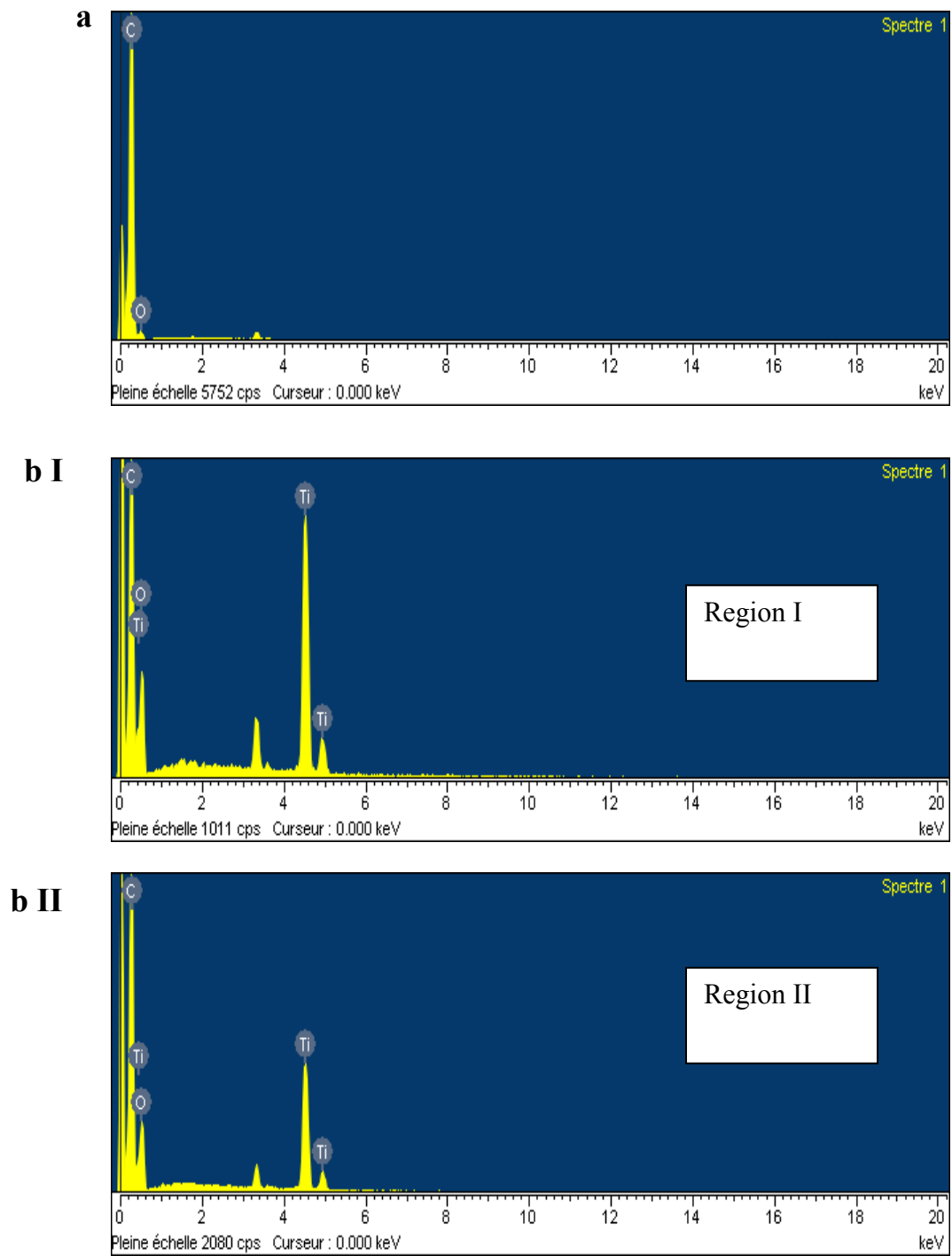


Fig.IV-43. EDX diagrams of AC (a) and AC/TiO₂ composite (b I & b II), obtained in two different regions: region I (b I) and region II (b II).

1.2.3. Physical properties

Specific surface areas were calculated for AC and AC/TiO₂ samples. Differences between AC/TiO₂ composite and the AC powder are shown in Table IV-15. As expected, the AC/TiO₂ composite exhibits a slightly smaller superficial area than AC samples.

It is clear from these data that the surface area of AC/TiO₂ composite and AC are very similar, the decrease in BET being nearly 10 %, suggesting that a small fraction of pores located on the external AC surface is partially blocked by a very thin layer of TiO₂ (Zhang and Lei, 2008; Zhu and Zou, 2009). This shows that when TiO₂ is deposited into AC by CVD method, the surface area is not significantly altered although the original AC was microporous. The original activated carbon has microporous volume of 0.375 cm³.g⁻¹, and mesoporous of 0.099 cm³.g⁻¹ being detected. For AC/TiO₂ sample, small decreases in both microporous (0.33 cm³.g⁻¹) and mesoporous (0.087 cm³.g⁻¹) were observed. These slight changes in pore-size are qualitatively consistent with the slight change in BET surface area. Moreover, it was founded that the particles size of the original activated carbon and that of the composite was approximately the same (annex 7). The Sauter diameter for S23 AC samples used in the suspension mixture and that used for TiO₂ deposition were 403 μm and 277 μm, respectively.

Table IV-15
Main characteristics of studied samples

Material	BET Surface (m ² .g ⁻¹)	Microporous Volume (cm ³ .g ⁻¹)	Mesoporous Volume (cm ³ .g ⁻¹)	Pore size (Å)	Sauter diameter d ₃₂ (μm)	Volume weight mean diameter d ₄₃ (μm)	Wt. % TiO ₂	Layer thickness TiO ₂ (nm)
AC (S23) Used in mixture	1090	0.376	0.099	17.7	403	447	-	-
AC (S23) Used for TiO ₂ deposition					277	427	-	-
AC/TiO ₂	928	0.328	0.087	18.4	257	287	7.91	410

1.2.4. Thermal gravimetric analysis

Thermal behaviour provided by TGA for AC S23 and the AC/ TiO₂ composite has been investigated (Fig.IV-44). An early start of weight loss, 2.8 % and 9.8 % respectively, at nearly 100 °C is observed which attributed to the humidity. The total weight loss is less for the AC/ TiO₂ sample (17.52 %), than that for raw AC S23 (22.26 %). This difference in the total weight loss between the two samples is mainly due to the first loss at low temperature corresponding to different wetness.

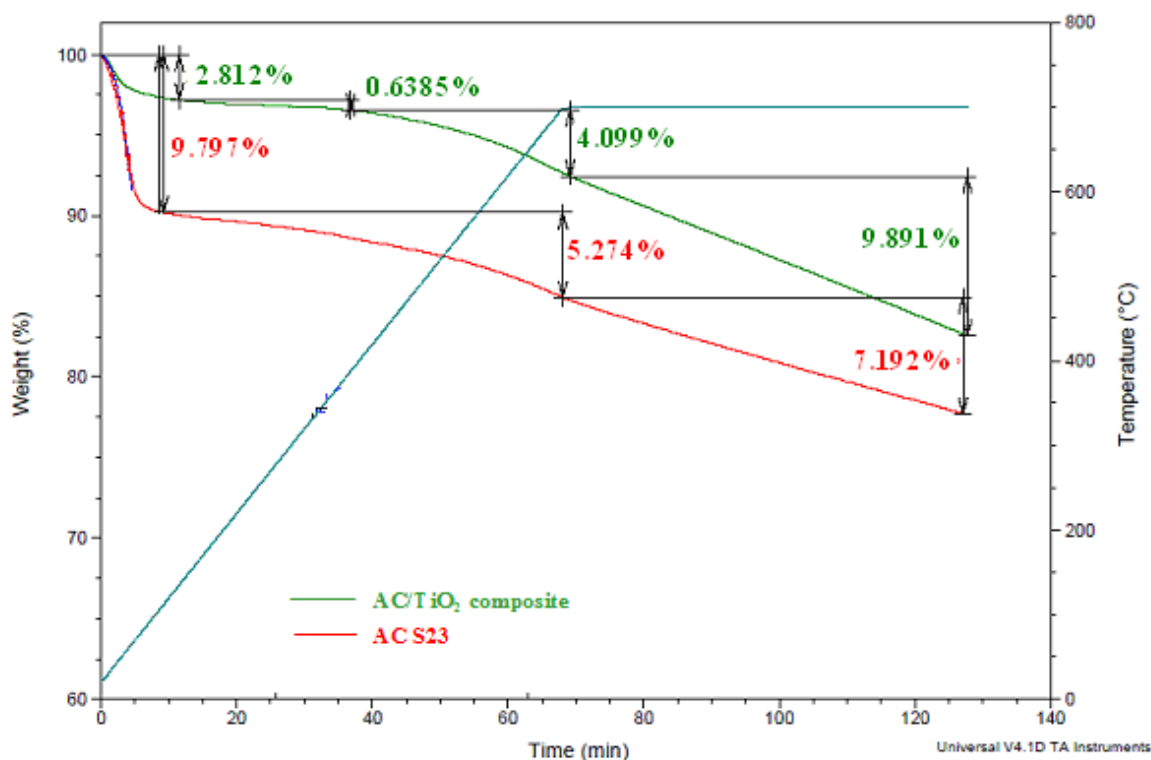


Fig.IV-44. Thermal gravimetric analysis of the original AC S23 and AC/ TiO₂ composite.

1.3. Adsorption isotherms

The experimental conditions are summarized in Table IV-16.

Figure IV-45 compares the isotherms of these two materials at 25 °C. It is clear from the figure that the two isotherms are of type I according to UICPA classification. It can be seen from figure that the adsorption capacity on AC/TiO₂ is slightly smaller than on virgin AC. The amount adsorbed on AC/TiO₂ and AC gets very close to each other. The slight decrease of surface area, according to BET may explain the small difference.

Table IV-16
Experimental conditions of Tartrazine adsorption

Reactor	in batch (Brown flasks)	
Adsorbent	AC S23 and TiO ₂ (in mixture)	AC S23/TiO ₂
Temperature	thermostatic Bath - 25 °C	
Volume of solution	100 mL	
Material mass 92.09 % of carbon and 7.91 % of TiO ₂	m _{AC} = 0.5 g m _{TiO₂} = 0.039 g	M _{material} = 0.5 g
Analytical technique	HPLC	
Duration	8 days (equilibrium point reached)	

Langmuir and Freundlich isotherm models were used to describe the isotherms. The different parameters of the two models and the correlation coefficients values are given in Table IV-17. It can be seen from this table that Langmuir model is more convenient to describe the two isotherms as the correlation coefficients of Langmuir are higher than that of Freundlich. The poor fit with Freundlich model indicates that there is no formation of adsorbed tartrazine multilayers.

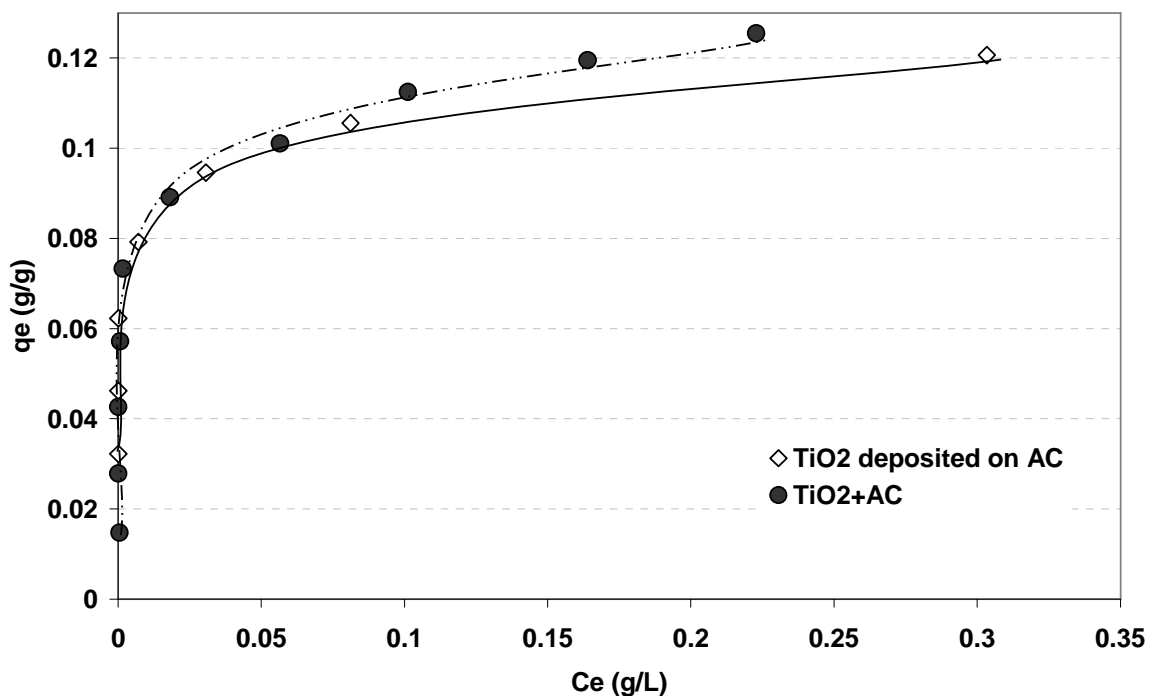


Fig.IV-45. Isotherms of Tartrazine adsorption onto suspension mixture of AC - TiO₂ and onto TiO₂ deposited onto AC at 25 °C.

Table IV-17

Parameter constants of Langmuir and Freundlich models for Tartrazine

Adsorbent	Parameters of Langmuir model			Parameters of Freundlich model		
	q_{\max} (g/g)	K_L (l/g)	R^2	K_F (g/g.(g/l)) ^{1/n}	1/n	R^2
TiO ₂ + AC	0.124	262	0.996	0.1653	0.1764	0.6822
TiO ₂ deposited onto AC	0.121	259	0.997	0.1343	0.1195	0.8565

As expected from Figure IV-45 the value of q_{\max} of AC /TiO₂ composite (0.121 g/g) is slightly smaller than that of the activated carbon S23 (0.124 g/g). Moreover, K_L values representing the interaction strength are very similar for the two samples. This decrease of adsorption performances is very low compared to the results obtained by Ao *et al.* (2007) who reported a decrease in the amount of phenol adsorbed around 30% using TiO₂ coated activated carbon by a rotatory evaporator under vacuum technique. Here the deposition of TiO₂ onto AC support using CVD technique had almost no negative impact on the adsorption performances of the tested AC/TiO₂ samples.

1.4. Photolysis and photocatalysis of Tartrazine

As some organic dyes are degraded by direct UV irradiation an experiment was designed in order to measure the percentage of photolysis by UV irradiation without catalyst prior to the evaluation of photocatalytic activity of TiO₂. Figure IV-46 shows that Tartrazine degradation under UV irradiation without catalyst (photolysis) was about 10% only after 2000 min in agreement with its absorption spectrum (annexe 13). These results are to be compared with Hashim *et al.* (2001) who reported a 20 % degradation of Tartrazine at very low initial concentrations (0.025 g/L).

In addition, the degradation of Tartrazine by using TiO₂ catalyst without AC but under UV irradiation was also carried out. For this control experiment, 1L of aqueous solution of Tartrazine (0.35 g/L) and TiO₂ (0.03 g, equal to the amount present in AC/TiO₂ composite) were left in contact for one day in the dark for preliminary adsorption. After this period, the system was exposed to UV irradiation with 24W UV-lamp for 4 days (Fig.IV-48).

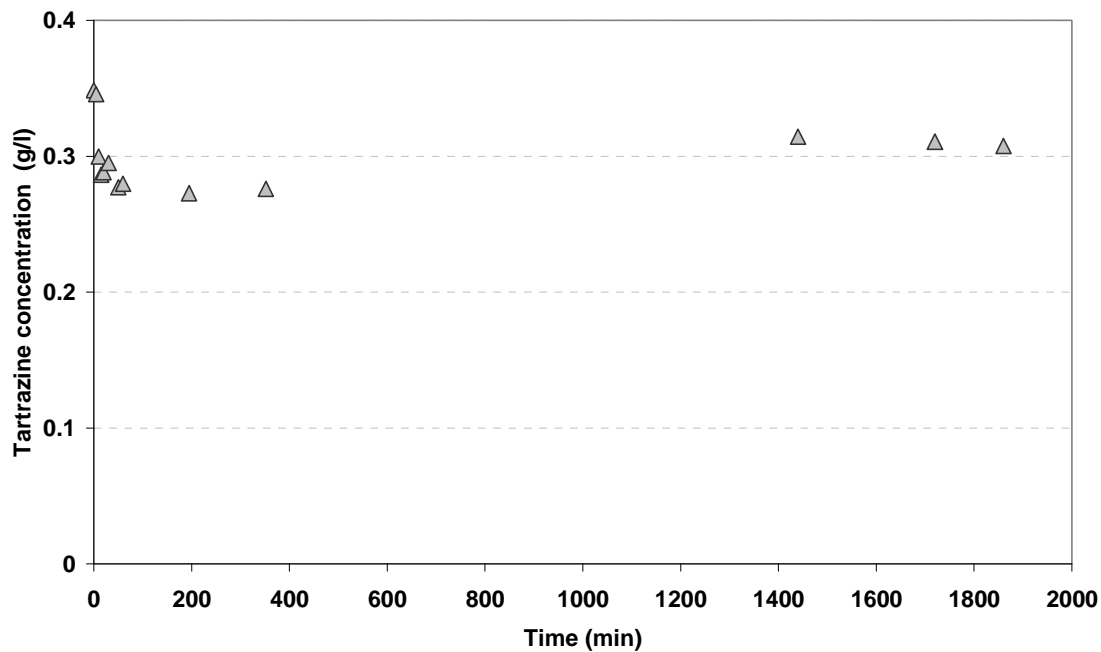


Fig.IV-46. Direct photolysis of Tartrazine using UV irradiation at 25 °C (light intensity; 47.5 W/m², Treated volume = 1L).

In the presence of catalyst, Figure IV-47 shows that 19 % of the tartrazine is removed by adsorption onto TiO₂ catalyst while about 70% of the remaining fraction is photocatalytically degraded (Figure IV-48). It is important to note that the main part of Tartrazine removal proceeds in the first hour of UV irradiation. After 420 min of irradiation, Tartrazine removal is very slow: at the end of the experiment (6000 min) only 30 % additionally increase in the removal is observed; these may be related to the high Tartrazine /TiO₂ weight ratio. As mentioned before, when the quantity of catalyst is lower than that of pollutant, several layers of adsorbed pollutants are formed on the catalyst surface leading to block the active sites. Furthermore, these lead to decrease the amount of photon reached the catalyst surface thus reducing the degradation rate.

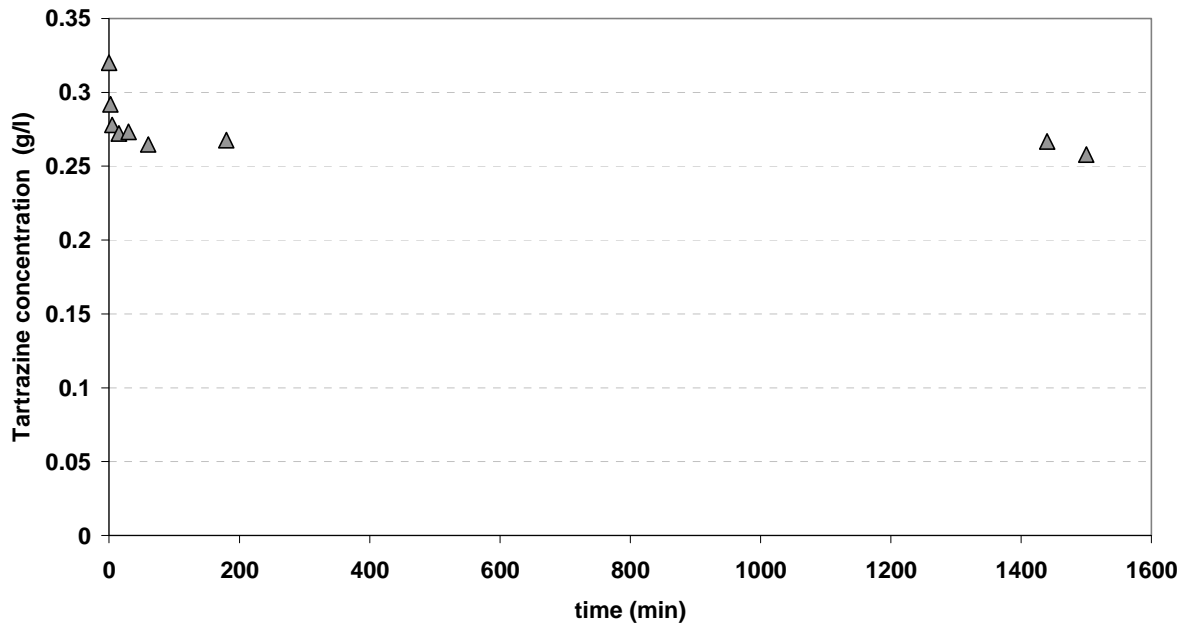


Fig.IV-47. Kinetics of Tartrazine adsorption in the dark onto TiO₂ catalyst at 25 °C.

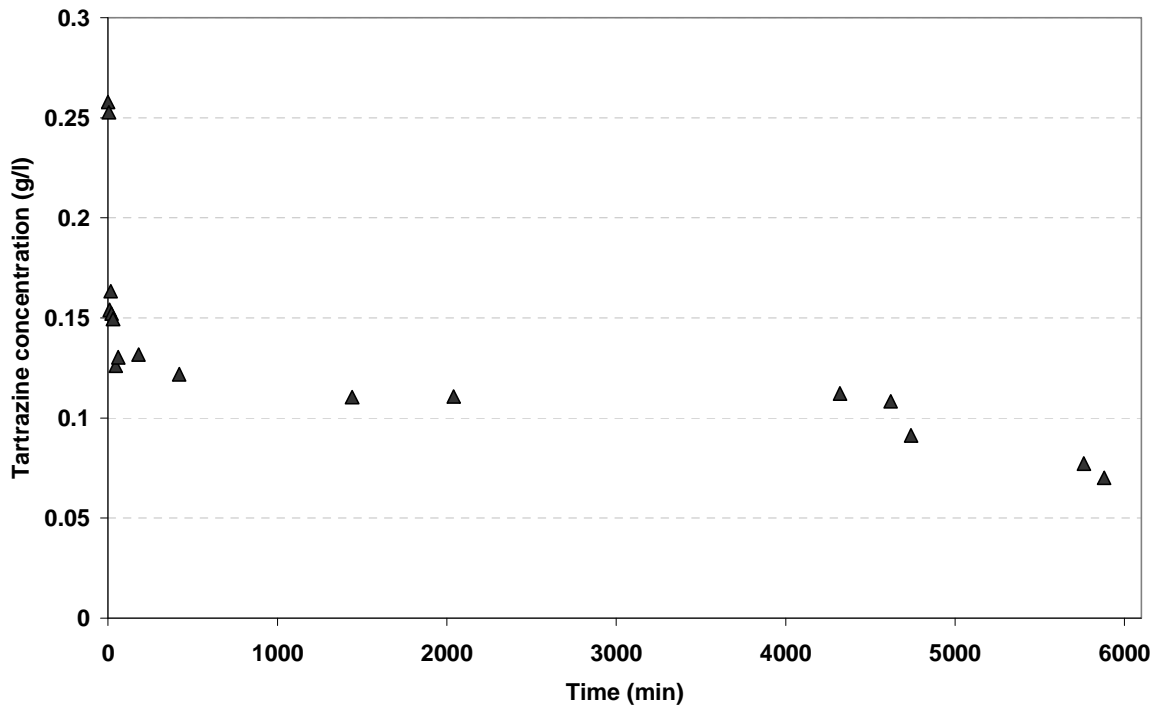


Fig.IV-48. Kinetic of Tartrazine photodegradation by TiO₂ catalyst under UV irradiation at 25 °C (light intensity; 47.5 W/m²).

1.4.1. Adsorption/ photocatalytic oxydation cycles

The operating conditions are summarized in Table II-12 (Chapter II). In this study, the molecule selected is Tartrazine and the concentration solution is chosen to be high enough to nearly reach the maximum adsorption capacity. As mentioned above, two studies will be presented in parallel: one with the new AC/TiO₂ material and the other one with a mixture of the same AC S23 and TiO₂ with the same amounts of AC and TiO₂. The adsorption kinetics in both conditions are represented in Figures IV-49, with a mixture of AC S23 and TiO₂ and IV-50, with AC/TiO₂ composite. Here again 5 consecutive adsorption/ photocatalytic oxidation runs have been carried out and analysed.

Firstly, the comparison of these two figures shows that for the first adsorption, the equilibrium is more quickly reached with the mixture than with the AC/ TiO₂ composite. This large difference of the first adsorption cycle in both conditions is separately presented in Figure IV- 51. At the end of the first adsorption cycle with AC/TiO₂, the equilibrium is not reached as only 90 % of the pollutant has left the liquid phase against nearly 100 % for the solid mixture. This result is not as expected according to the well known effect of particle size on diffusion in pores: AC particle size of the two samples being: 257 μm for AC/ TiO₂ and 403 μm for AC of the solid mixture. As it was shown that there is only marginal pore size modification during TiO₂ coating the explanation of this surprising result could be the modification of the nature of the AC surface by TiO₂ deposition which would influence the surface diffusion.

Secondly, Figures IV-49 and IV-50 show that for the other next kinetics cycles, adsorption is significantly reduced in both systems but in case of AC and TiO₂ mixture, this reduction is clearly more important: the difference between Cycle 1 and 2 is much lower with the AC /TiO₂ composite suggesting that the photocatalytic regeneration was better achieved.

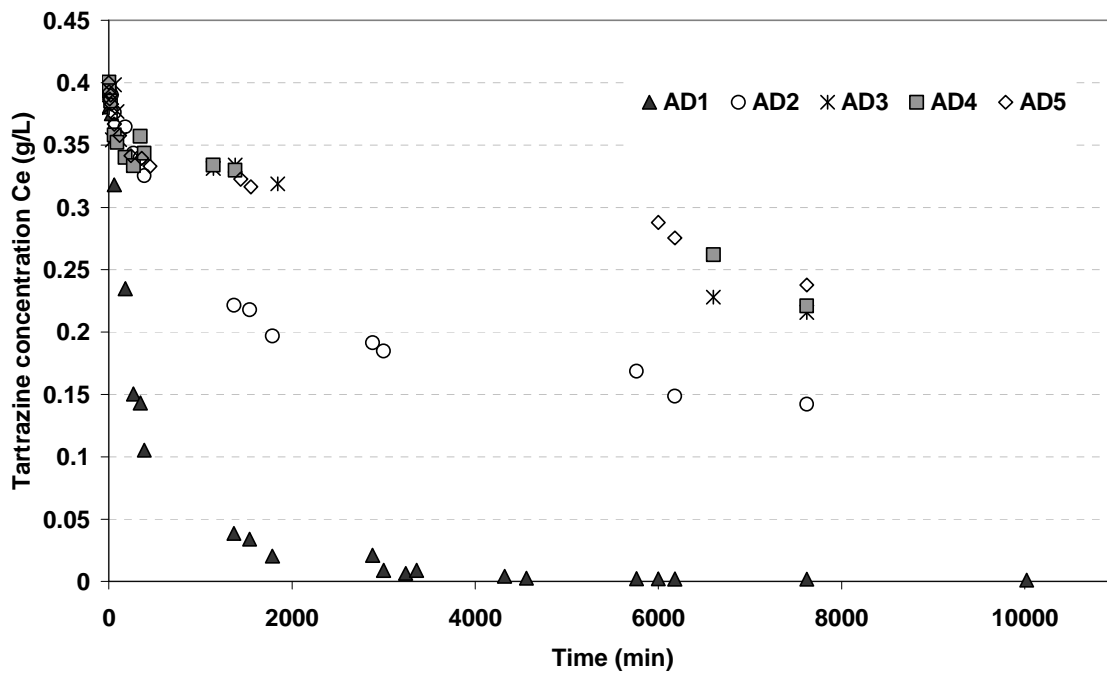


Fig.IV-49. Kinetic of Tartrazine adsorption cycles onto AC-S23 + TiO₂ mixture at 25 °C.

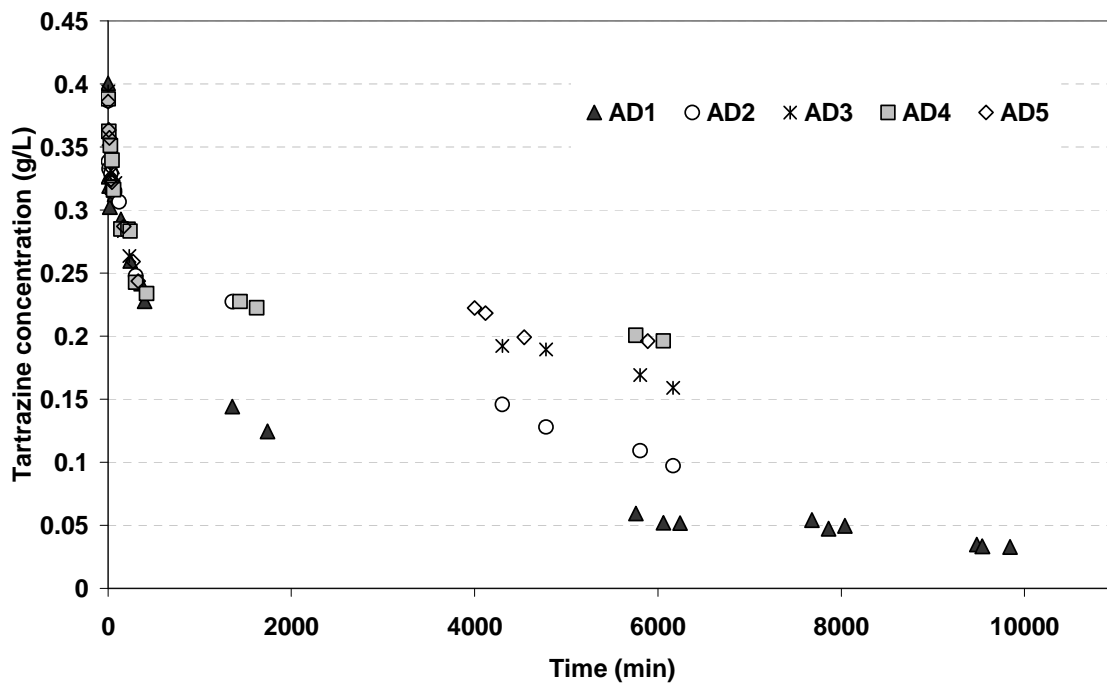


Fig.IV-50. Kinetic of Tartrazine adsorption cycles onto AC /TiO₂ composite at 25 °C.

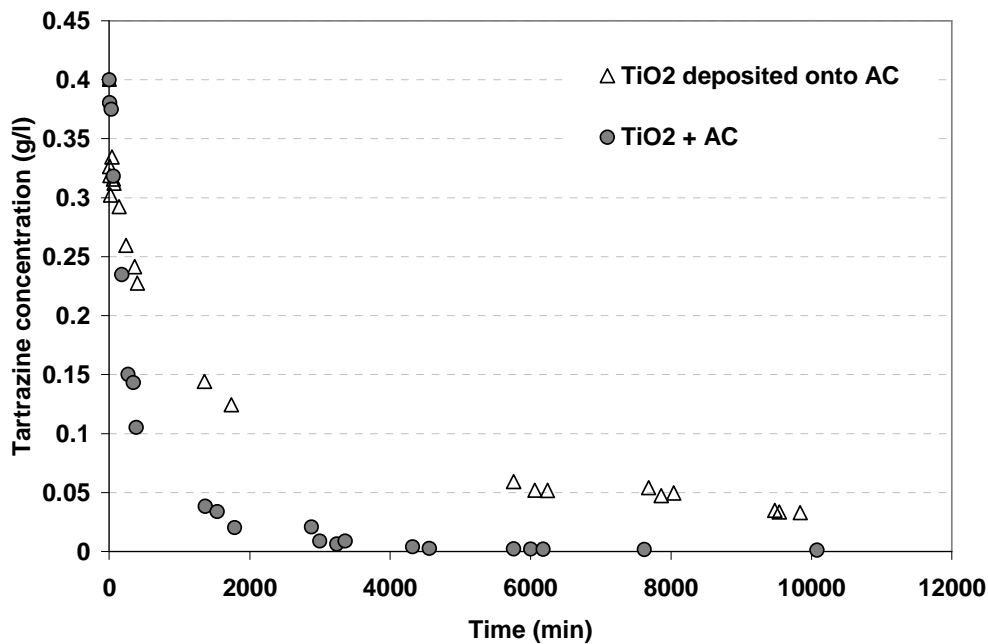


Fig.IV-51. Comparison of the kinetics of the first adsorption cycle of Tartrazine. Comparison of a mixture AC-S23 +TiO₂ and AC/TiO₂ composite (CVD).

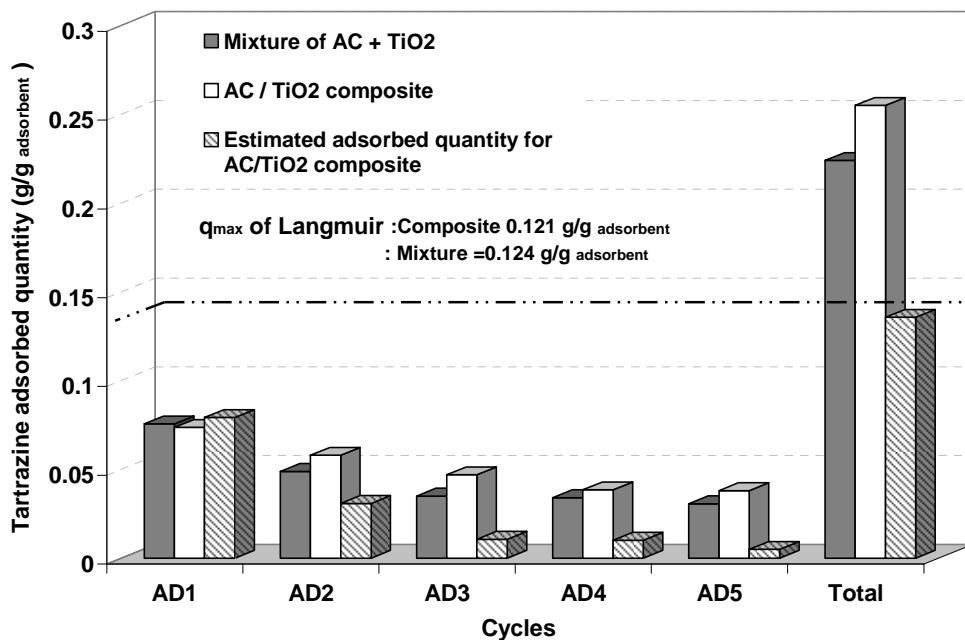


Fig.IV-52. Comparison of the quantity of adsorbed Tartrazine during the cycles of adsorption for AC / TiO₂ composite (□), a mixture of AC +TiO₂ (■) and the estimated adsorbed quantity for AC/TiO₂ composite; assuming that only the adsorption process occurs (▨) at 25°C.

Figure IV-52 and Table IV-18 compares the amount adsorbed during each cycle. The regeneration allows to recover a large fraction of the initial adsorption capacity: more than 79% and 65% for composite and the suspension mixture, respectively. This figure and table clearly confirms the better results obtained with AC/TiO₂ composite despite the slower first adsorption: the total quantity of the adsorbed Tartrazine on AC/TiO₂ composite was about 14 % higher than on the solid mixture. This may reflect the efficiency of the composite which may be due to the presence of TiO₂ inside the AC leading to facility the transfer of the pollutant from the AC to the surface of catalyst. For both systems, the accumulated amounts adsorbed during 5 cycles correspond to about 4 times of the amount adsorbed in the first cycle and nearly twice the maximum adsorption capacity, q_{max} of Langmuir. Regeneration is then much more effective than in phenol experiments with AC/TiO₂ tissue (nearly equal to the maximum adsorption capacity, q_{max} of Langmuir for $C_i = 0.88$ g/L of phenol).

Table IV-18

Comparison of the of Tartrazine adsorbed quantity during the cycles of adsorption for AC / TiO₂ composite, a mixture of AC +TiO₂ and the estimated adsorbed quantity for AC/TiO₂ composite

System	Tartrazine adsorbed quantity (g/ g _{adsorbant})					Total quantities assumes of AD1 :AD5
	AD1	AD2	AD3	AD4	AD5	
AC / TiO ₂ composite	0.074	0.058	0.047	0.038	0.038	0.255
mixture of AC +TiO ₂	0.076	0.049	0.035	0.034	0.031	0.226
estimated adsorbed quantity (AC/TiO ₂ composite)	0.079	0.031	0.011	0.010	0.005	0.136

The theoretical quantities of adsorbable Tartrazine onto AC/TiO₂ composite without regeneration are also reported in Fig IV-52 and Table IV-18. This calculation assumes that only adsorption operates: the amount of adsorbable tartrazine is estimated from isotherm considering the initial concentration C_0 at a given step and the tartrazine adsorbed at the previous adsorption step. Indeed, this value must achieve, for an infinite number of adsorption, the adsorbed amount obtained from the isotherm for the equilibrium concentration equal to 0.35 g L⁻¹ which is very close to q_{max} . The comparison of these very low quantities with the much larger ones achieved after photocatalytic regeneration clearly reflects the effectiveness of this regeneration.

2. Photocatalytic oxidation of Tartrazine

As explained previously, after each adsorption cycle a photo-oxidation cycle was started by switching on the UV lamp in the presence of air stream. The temperature was adjusted at 25 °C using a thermostatic bath. In this paragraph, oxidation kinetic cycles are reported and analyzed.

2.1. Kinetic of Tartrazine photodegradation cycles

The time variation of the concentration of Tartrazine during photocatalysis is illustrated in Figures IV-53 and IV-54 for both systems: a mixture of AC - TiO₂ and AC/TiO₂ composite, respectively. In figure IV-54, the kinetic of oxidation for the third cycle do not present a convenient shape due to several break down of electric power during this cycle.

The removal rate for Tartrazine by the two systems (solid mixture and AC /TiO₂ composite) reaches approximately the same value (99 %) during the first oxidation cycle, but contrary to the adsorption step, the tartrazine concentration decrease evolution is faster with the AC /TiO₂ composite. When looking after repeated cycles with each system, the oxidation kinetics is again clearly faster with AC/TiO₂. Figure IV-54 shows that this AC/TiO₂ composite reveals more than 80 % of degradation tartrazine in liquid phase at every cycle. On the other hand, Figure IV-53 exhibits a continuous decrease of the rate of Tartrazine degradation with the solid mixture, until reaching only 50 % in the 5th cycle.

The main result is then the better efficiency of the photocatalyst when it is deposited on the carbon. The location of the sites of adsorption and that of photocatalysis closed to each other improves the conditions of oxidation. After desorption from AC, tartrazine will easily reach TiO₂ adsorption sites to be photo-degraded. This result, though apparently logical, is contradictory to the slower adsorption step which was attributed to lower diffusion due to lower porosity and/or lower surface diffusion in pores. This means that the improvement of photocatalysis is even greater than globally observed.

Similarly, Wang *et al.* (2009) compared the reactivity of composite (AC/ TiO₂) which were prepared by dip-hydrothermal method at 180 °C and mixture of pure commercial TiO₂

with AC. It was found that composite (AC/ TiO₂) had higher photocatalysis activity than the mixture. This result is also in agreement with those obtained by Subramani *et al.* (2007) who found a more important photocatalytic activity when TiO₂ impregnated on the activated carbon by hydrothermal method. Similarly, Xue *et al.* (2011) cited that there were synergy between surface adsorption and photocatalysis during degradation of humic acid on TiO₂/activated carbon composites prepared by a sol–gel process where the adsorbed molecules migrate to the surface to react more easily with TiO₂ situated near the surface.

It should be noticed that some authors explained that a part of the deteriorated performance of the TiO₂ and AC mixture after several cycles may be attributed to the loss of TiO₂ by cycle. Indeed, the treated solution was filtered because TiO₂ was more difficult to isolate from the solution than with AC/TiO₂ composite. Similarly, Zhang *et al.* (2005a) compare between AC supported TiO₂ by CVD (TiO₂; 12 wt %) and P25 with AC for methyl orange (MO; 100 mg/L) degradation, after 10 cycles, the catalytic efficiency of AC/TiO₂ decreased slightly whereas that for the TiO₂ P25 and AC mixture showed a dramatic decrease. The stable performance of AC supported TiO₂ reveals that the TiO₂ particles are strongly adhered to the AC surface. The deteriorated performance of P25 and AC mixture after 10 cycles should be attributed to the loss of P25 at each run.

The first order model is used for the description of kinetics of photocatalytic oxidation reaction. However, the calculation showed that the data are not well described by this model for all cycles (annex 12).

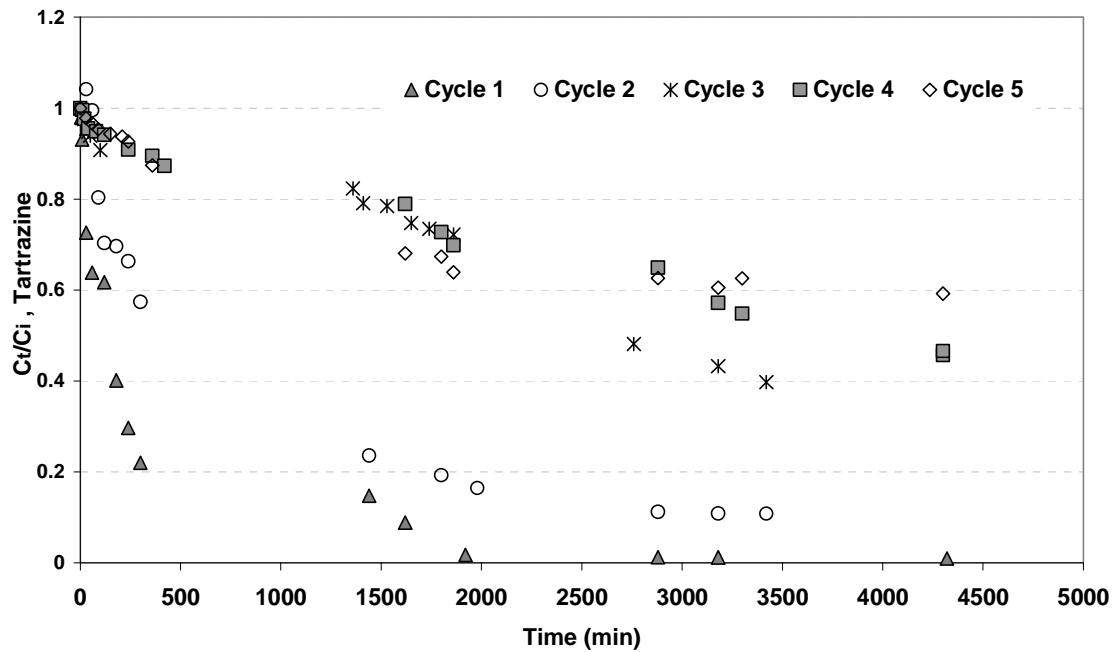


Fig. IV-53. Kinetics of Tartrazine photocatalytic degradation cycles using solid mixture of AC and TiO₂ (photon flux: 47.5 W/m²).

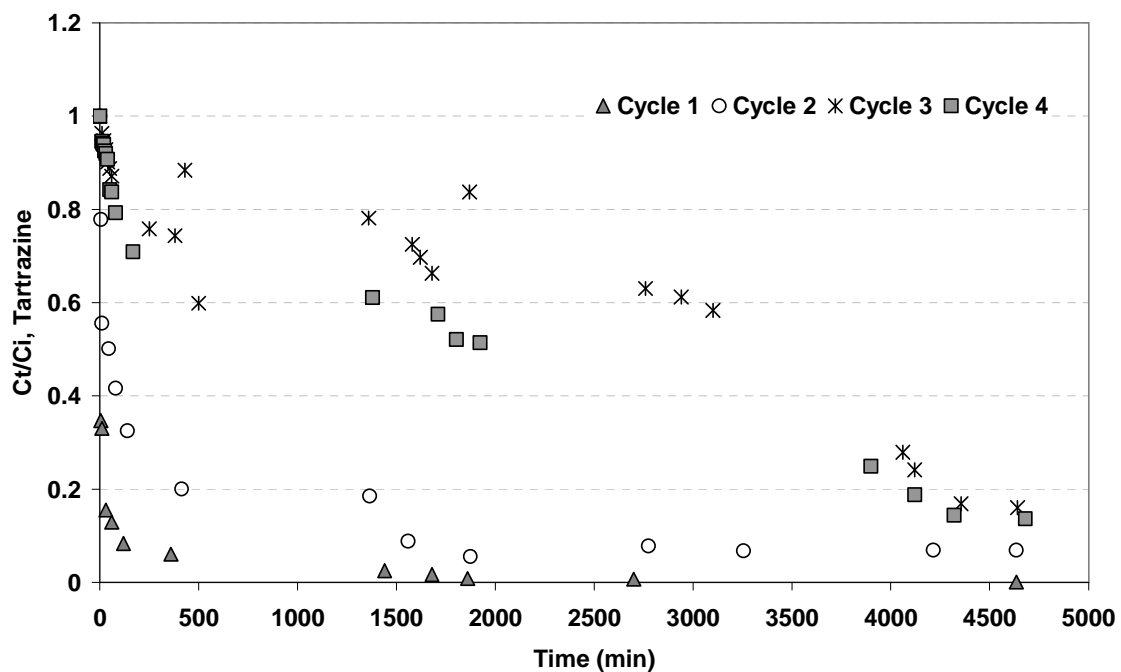


Fig. IV-54. Kinetics of Tartrazine photocatalytic degradation cycles using AC/TiO₂ composite (photon flux: 47.5 W/m²).

2.2. Regeneration efficiency

Fig. IV-55 represents the rate of the regeneration efficiency of the AC during 4 runs as compared with the cycle 1. As seen from the results, the regeneration efficiency of the AC/TiO₂ composite is higher than that of the powder TiO₂ catalyst in the suspension mixture with the AC. In the second cycle about 78 % of the activated carbon capacity was recovered by the photocatalytic regeneration in the AC/TiO₂ composite. The regeneration efficiency then gradually decreased to 63 %, 52 % and 51 % in the third, fourth and fifth cycles, respectively which calculated with respect to the value of cycle 1. For the powder catalyst in the suspension mixture, the recovering of the activated carbon adsorption capacity is lower than that with the AC/TiO₂ composite for all the cycles. It's observed that the regeneration efficiency in the second cycle is 64 % then an almost steady state was reached in the next cycles (40 %). which was fully charged by Tartrazine, up to about 50 %.

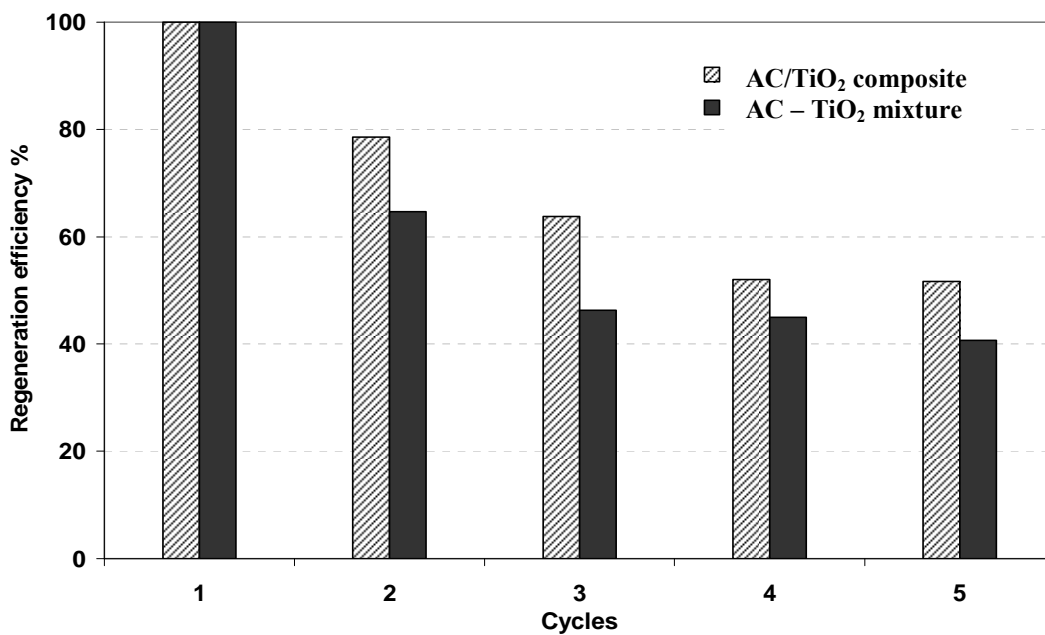


Fig. IV-55. Comparison of the regeneration efficiency of suspension mixture of AC - TiO₂ and AC/TiO₂ composite.

2.3. Photocatalytic mineralization of Tartrazine

The change of Total Organic Carbon (TOC) is generally used to study the degree of mineralization during any oxidation. The difference between Tartrazine removal measured by HPLC and TOC removed is a measure of organic intermediates resulting from the Tartrazine degradation.

Results from TOC measurement versus the irradiation time are presented in Figures IV-56 and IV-57 for TiO_2 - AC powder mixture and for TiO_2 deposited on AC system, respectively. The fast initial decrease in TOC at the first run, indicates that organic carbon is rapidly removed during the first cycles in both studied systems. By comparing the Tartrazine removal (Fig. IV-54) and the TOC removal (Fig. IV-57) using AC/ TiO_2 composite during the first cycle, it was found that the TOC removal is less important than the Tartrazine degradation. This difference is even more significant with the solid mixture of AC and TiO_2 (Figs. IV-53 and IV-56) confirming the best photooxidation on the composite system.

As for Tartrazine consumption, the initial TOC removal is less and less efficient cycle after cycle. Nevertheless it should be pointed out that at the end of the oxidative step (4280 min) the differences between cycles is much less visible, especially for the best system (AC/ as shown in Figures IV-57 and IV-58.

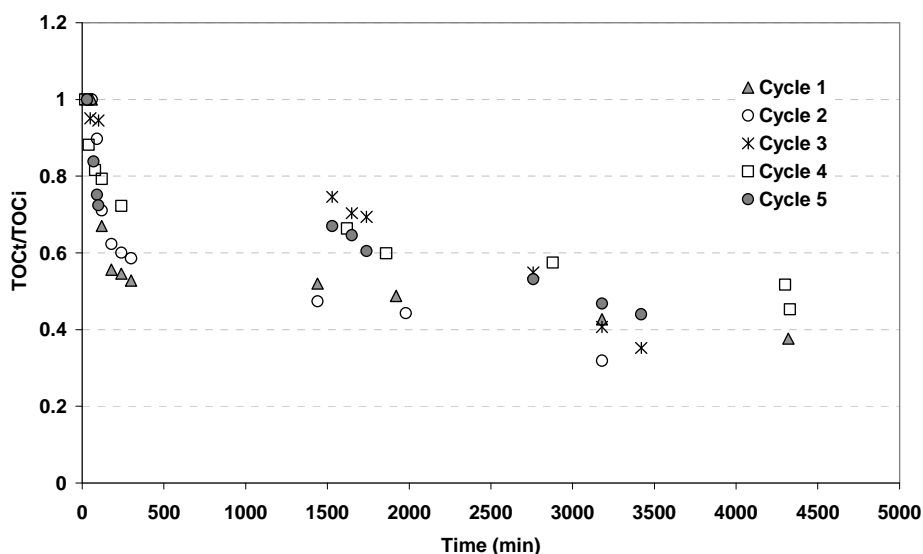


Fig.IV-56. Total Organic Carbon (TOC) remaining in the solution during 5 cycles of photocatalytic degradation of Tartrazine by the suspension mixture of TiO_2 and AC.

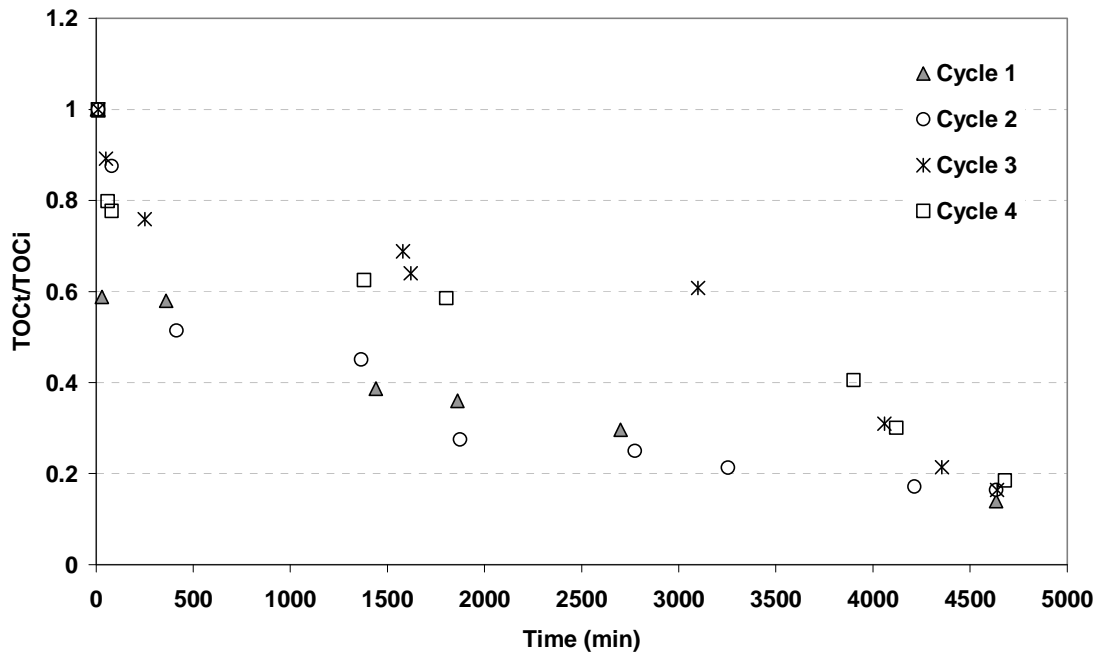


Fig.IV-57. Total Organic Carbon (TOC) remaining in the solution during 4 cycles of photocatalytic degradation of Tartrazine by AC/ TiO₂ composite.

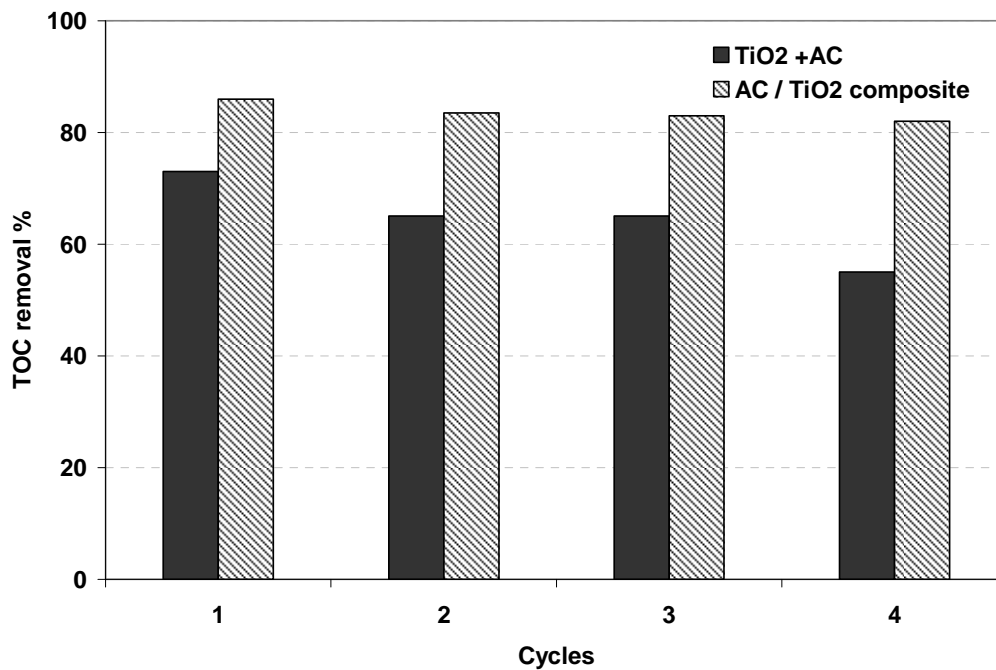


Fig. IV-58. Comparison between final TOC removal by the suspension mixture of AC - TiO₂ and that by the AC/ TiO₂ composite during 4 photocatalytic oxidation cycles of Tartrazine.

Comparison the percentage of the reduction in TOC values for each cycle for both studied systems is represented in Fig.IV-58. The results show that the TOC removal (86 %) using AC/TiO₂ is higher than that by the powder TiO₂ in the suspension mixture (73 %) in the first cycle. We also noticed that the percentage of TOC removal decreases only slightly during the cycles in the case of AC/TiO₂ composite. On the contrary, by the repetitive use of the powder catalyst in the mixture system, the TOC removal decreased to 56 %.

2.4. Physical properties of activated carbon after the oxidation cycles of Tartrazine

2.4.1. BET surface area and pore-size distribution

BET surface area and pore-size distribution of the used AC in the two used systems after the regeneration runs as compared to the non used samples are reported in Table IV-19. It must be notified here that the last cycle performed before BET analysis was the oxidation cycle for the AC sample in solid mixture while it was the adsorption cycle for AC/ TiO₂ composite.

Table IV-19

Physical properties of AC in both studied systems; AC/ TiO₂ composite and suspension mixture of TiO₂ and AC as compared to the virgin

Activated carbon	Surface BET (m ² .g ⁻¹)	Microporous volume (cm ³ .g ⁻¹)	Mesoporous volume (cm ³ .g ⁻¹)	Pore size A°
AC S23 virgin	1089.6	0.376	0.099	17.7
TiO ₂ +AC suspension (used; last cycle: oxydation)	691.6	0.305	0.044	19.0
AC S23/TiO ₂ composite; virgin	927.9	0.328	0.087	18.4
AC/ TiO ₂ composite (used; last cycle: adsorption)	717	0.320	0.022	19.4
AC/ TiO ₂ composite (used; desorbed by water)	779.2	0.293	0.039	17

BET surface area was reduced by about 37 % for AC in the solid mixture and by only 22 % for AC/TiO₂ composite. This result is not surprising as after oxidation less organic compounds are covering the AC surface and clogging its pores. A small change of the pore structure of samples is shown in Table IV-19. The decrease in microporous volume is only 2 % in the AC/TiO₂ system however it was about 18 % in the solid mixture system, as compared with the virgin samples. An important decreased in the mesoporous volume was reported in the both samples more than 50 %. The decrease in surface area and changes in pore-size distribution were reasonably may be caused by blocking the pore entrances on the surface of activated carbon by Tartrazine and its intermediates. On the other hand, after cleaning one week under water flow BET surface remained lower than that of virgin AC/TiO₂ composite; the microporous volume was mainly recovered but not the mesoporous one (Table IV-19): this would suggest an irreversible adsorption by oligomerisation of Tartrazine intermediates in the presence of dissolved oxygen (Lu and Sorial, 2009).

2.4.2. Thermogravimetric analysis

Thermogravimetric analysis (TGA) of the virgin AC, virgin AC/TiO₂ composite and used AC/TiO₂ composite (after 4 runs of photocatalytic oxidation of Tartrazine) is represented in Figure IV-59a.

Used sample of AC/TiO₂ composite exhibits a first loss of mass of 20.07 % at 132 °C which mainly represents the degree of humidity and small adsorbed molecules. The profiles of the used AC/TiO₂ composite after used for several times and after different cleaning methods reveal mainly the same profiles of the virgin AC/TiO₂ sample except in the range 100-400 °C, where a small mass loss is observed (3%) even after washing characteristic of decomposition of irreversible adsorbed oligomers (oxidative coupling) and decomposition of carboxylic acid function group. This may be indicated that the photocatalytic oxidation of Tartrazine using TiO₂ deposited on AC does not damage a lot the AC and TiO₂ in the sample.

Figure IV-59b shows TGA of the used AC S23 after regeneration by powder TiO₂ in the solid mixture. A first loss of mass of 14.8 % was at nearly 100 °C (humidity and small adsorbed molecules). It is higher than that of non used carbon because of the presence of Tartrazine and intermediates in the used one. Then, the profiles of the used AC after oxidation reveal another small loss of mass 2.33% at 328.8 °C attributed to the decomposition of

oligomers and the carboxylic acid function group. After 700 °C in the case of used AC, the variations of mass are higher than those for the non used AC.

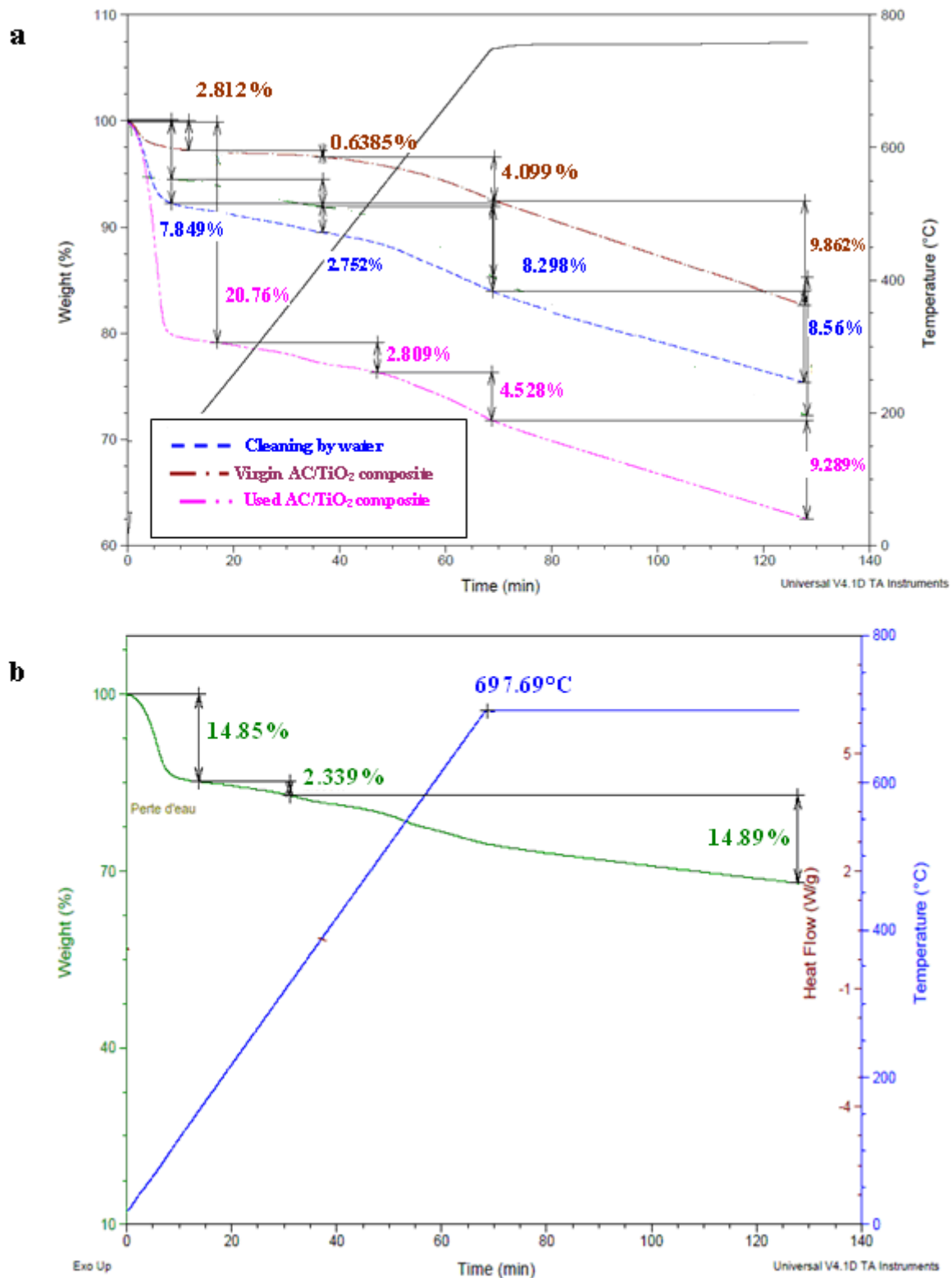


Fig.IV-59. Comparison between TGA of virgin AC/TiO₂ and used AC/TiO₂ samples (a) and used AC S23-TiO₂ mixture (b).

3. Conclusions

Nanocrystalline TiO₂ anatase deposited on activated carbon with a CVD method shows good adherence and preserves most of AC adsorption capacity. Such composite of AC/TiO₂ materials exhibited high photocatalytic activity for the degradation of Tartrazine with the rate constant four-fold faster than by TiO₂ powder in the suspension mixture with AC. By cyclic use of the catalyst deposited on activated carbon up to 80 % of Tartrazine degradation was observed in liquid phase until the 4th cycle while only 50 % with powder TiO₂ mixed with granular AC. The best performances with TiO₂ deposited on AC can be explained by the vicinity of photocatalyst and AC adsorption sites. After 5 utilisations of the AC/ TiO₂ composite, only 15 % of its adsorption capacity was lost. This process is thus very promising compared to the other techniques as, for example, the ADOX process where the activated carbon is highly damaged by CWAO (Krou, 2010).

Chapitre IV. Dégradation de polluants par photocatalyse

Pour éliminer les polluants réfractaires aux traitements biologiques, l'adsorption est le procédé économiquement le plus intéressant. Le principal inconvénient de cette technique est que les polluants sont déplacés d'une phase liquide vers une phase solide sans être détruits. L'élimination complète de ces polluants ne peut être obtenue qu'en utilisant une technique destructrice d'oxydation qui s'avère généralement beaucoup plus coûteuse. Une combinaison de ces deux types de techniques a alors été envisagée sous la forme d'un procédé séquentiel. Ce procédé enchaîne des cycles constitués d'une première étape d'adsorption et une seconde étape d'oxydation photocatalytique. La photocatalyse sur TiO_2 a été choisie car elle produit des radicaux hydroxyle OH° non sélectifs qui s'attaquent à tous types de polluants organiques. De plus, le catalyseur étant activé par les UV, il est possible d'imaginer un développement de ce procédé en utilisant le rayonnement solaire.

Dans cette étude deux matériaux catalytiques ont été utilisés : un tissu contenant du charbon et imprégné de TiO_2 commercialisé par la société Ahlstrom, et un charbon actif avec dépôt de TiO_2 en surface. Le choix des molécules a été défini en fonction du type d'effluent ciblé : le phénol pour représenter un effluent phénolés et la tartrazine pour un effluent coloré. Le tissu a été testé avec le phénol dans un réacteur batch conçu de façon à s'adapter à la forme du matériau et en continu dans un réacteur annulaire. Le charbon avec dépôt de TiO_2 a été utilisé pour éliminer la tartrazine dans un réacteur photocatalytique en verre opérant en batch.

Partie A : Elimination du phénol en utilisant un tissu Ahlstrom TiO_2/AC

Pour cette étude, un réacteur de type « canal » a été conçu de manière à pouvoir placer le tissu TiO_2/AC en surface de la solution aqueuse en maintenant une épaisseur de liquide de quelques millimètres. La face imprégnée de TiO_2 en surface est illuminée par une lampe UV placée au plus près du tissu. Un bac intermédiaire thermostaté fonctionnant en batch permet de refroidir le liquide et de le faire circuler. Les matériaux présents dans le tissu ont été analysés : analyse granulométrique et analyses texturales (surface B.E.T. et volumes poreux) du charbon actif et du TiO_2 , photos MEB, analyses EDX et thermogravimétrie. Une étude préliminaire a été conduite pour évaluer les capacités d'adsorption de ce tissu et le comparer au charbon seul, à un tissu sans charbon actif (TiO_2 media) et à un tissu sans TiO_2 (AC media). Les capacités d'adsorption du tissu TiO_2/AC sont globalement deux à trois fois plus faibles que celles du charbon actif original. Le charbon piégé dans les fibres semble avoir été très partiellement recouvert au cours du procédé d'imprégnation. Le tissu TiO_2/AC a ensuite été utilisé en mode séquentiel en alternant plusieurs cycles composés d'une étape d'adsorption

dans le noir pendant 4 jours et d'une étape d'oxydation photocatalytique sous UV pendant 3 jours. Des essais « blancs » ont été conduits dans 2 conditions : sous UV seuls, puis avec le tissu AC media sans TiO₂ et sous UV. Les résultats ont montré l'inefficacité du procédé dans ces conditions. Ensuite, le procédé a été mis en œuvre avec le tissu TiO₂/AC, pour des concentrations égales de 0.45 g/L et 0.88 g/L, et en présence ou non de H₂O₂. Ces concentrations initiales élevées ont volontairement été choisies, l'objectif étant de dépasser les performances obtenues par une adsorption seule et ainsi mettre en évidence l'efficacité catalytique du tissu. En 5 cycles, le tissu permet d'éliminer 1.5 fois plus de phénol que le tissu utilisé seul en adsorption. Pour une concentration de 0.45 g/L, les réutilisations successives altèrent les performances du procédé mais l'efficacité de la régénération reste élevée (>60% au dernier cycle). Par contre, pour une eau fortement chargée en phénol (0.88 g/L), les performances du procédé séquentiel chutent rapidement. La dernière oxydation dégrade moins de 5% de phénol et moins de 10% de la DCO. Le catalyseur se couvre d'intermédiaires réactionnels qui l'isolent des rayons UV, il change de couleur et ne produit plus de radicaux. L'utilisation conjointe de H₂O₂ permet d'enrayer ce phénomène et d'atteindre des taux de dégradation plus intéressants. En 6 cycles, le tissu élimine 75% de phénol en plus, la dégradation du phénol est quasi-complète (97% au dernier cycle) mais la DCO reste élevée à la fin de chaque cycle (45% au dernier cycle). Enfin, un essai a été conduit en continu dans un réacteur annulaire dans des conditions non optimisées. Après une première phase d'adsorption, la photocatalyse a atteint un régime permanent avec un taux de dégradation intéressant de l'ordre de 50%.

Partie B : Elimination de la tartrazine en utilisant un charbon actif avec dépôt de TiO₂

Cette étude a été conduite dans un réacteur cylindrique en verre, la lampe est placée au centre dans une enveloppe double paroi en verre Pirex où circule un fluide thermique à 25°C. Il est reconnu que l'inconvénient majeur de la photocatalyse avec du TiO₂ est que ce catalyseur est sous la forme de petits agglomérats de particules nanométriques difficilement séparables du milieu dans lequel ils se trouvent. Afin de palier à ce problème, un matériau a été synthétisé directement le TiO₂ sur le charbon actif S23 par C.V.D par le L.G.C. (département GIMD). Ce charbon actif (CA/TiO₂) a d'abord été caractérisé : analyse granulométrique, analyse texturales (surface B.E.T. et volumes poreux), photos MEB, analyses EDX et thermogravimétrie. Puis ces performances ont été comparées à celle d'un mélange de CA et de TiO₂ (Millenium P-500) dans les mêmes proportions massiques. Les isothermes d'adsorption de la tartrazine ont montré que la présence du TiO₂ en dépôt avait pour effet de diminuer très légèrement les capacités du charbon. Le charbon TiO₂ et le

mélange ont ensuite été testés en procédé séquentiel en enchainant cinq cycles composés chacun d'une étape d'adsorption dans le noir (quatre jours) et d'une étape d'oxydation photocatalytique sous UV (trois jours). Cette étude a permis de montrer l'activité catalytique du matériau CA/TiO₂. En cinq cycles, ce charbon actif permet d'éliminer deux fois plus de polluants que le maximum qu'il peut adsorber. Notons que le mélange de charbon et de dioxyde de titane affiche des performances intéressantes mais la quantité éliminée est environ 14% inférieure. Au cours des oxydations successives, il apparait nettement que la minéralisation des polluants adsorbés est plus complète pour le charbon CA/TiO₂ : à la fin de la dernière oxydation, il reste 20% du COT contre 50 % pour le mélange. La conclusion principale de cette étude est que la meilleure efficacité du matériau CA/TiO₂ s'explique par la proximité des sites d'adsorption et ceux de réaction photocatalytique. Les analyses texturales et thermogravimétriques des charbons après ces différentes utilisations montrent que les oxydations successives n'ont pas altérées la surface des deux matériaux.

GENERAL CONCLUSIONS AND FUTURE WORK

This work aimed to study a new hybrid water treatment process based on adsorption with activated carbon and photocatalytic oxidation using TiO_2 . Both processes having several drawbacks in application scale it appeared interesting to study the performance of the combination of adsorption and photocatalytic oxidation in a sequential process. Therefore, our contribution work includes two principal parts: a preliminary one to describe in details the adsorption process using activated carbon. Secondly, the investigation of the sequential processes (ADOX) coupling adsorption then regenerative photocatalysis.

The main conclusions derived from this investigation are summarized as follows:

Adsorption process onto activated carbons

1. The first part of this study consisted of fully characterisation of activated carbons supplied by project PHARE: two commercial Picahydro activated carbons (S23 and F22) and six carbonaceous materials prepared from sewage sludges (Sludge based Activated carbons, SBACs) according to different procedures (with and without physical activation). The physico-chemical properties of the resulting carbonaceous materials (e.g. hardness, BET surface area, ash and elemental content, surface chemistry) were evaluated and compared with a commercial reference activated carbons (PICA F22 and S23). Screening of the adsorption capacity of these SBACs using phenol was investigated and compared with a commercial reference activated carbons (PICA F22 and S23).

It was found that their adsorption capacity for phenol was higher than that expected from their low BET surface area suggesting an economically attractive utilisation of sludge-based materials as adsorbents in waste water treatment. Dewatered raw sludge (SA_DRAW) had the greatest adsorption capacity of the SBCMs.

2. The second part focuses on the performance of the best SBAC (SA_DRAW) as compared with two commercial activated carbons (S23 and F22) in the case of multicomponent adsorption. Four phenolic compounds (*p*-nitrophenol (PNP); *p*-chlorophenol (PCP); *p*-hydroxy benzoic acid (PHBA); and phenol (P) were used either in single or multicomponent aqueous solutions. Concerning adsorption features of four phenols on various activated carbons, it may be concluded that despite moderate micropore and mesopore surface areas, SBAC had remarkable adsorption capacity for phenols although less than PICA carbons. Uptake of the phenolic compounds was found to be dependent on both the porosity and surface chemistry of the carbons. Furthermore, the electronegativity and the

hydrophobicity of the adsorbate have significant influence on the adsorption capacity. The preferential adsorption of PNP followed by PCP could be explained by the electron-withdrawing effect of the -NO₂ group and -Cl group. The Langmuir and Freundlich models were used for the representation of the single-solute adsorption isotherms. Despite the rather low surface area, it may be concluded that the dried activated carbon resulting from sludge treatment (SBAC) shows an adsorption capacity of about half those of the commercial activated carbons. As it may still be improved, it should be considered as a convenient low-cost material for the removal of phenol and substituted phenols from polluted water. Production of SBAC from sludge thus constitutes a possible way of valorisation of this abundant waste.

3. After studying the adsorption competition, the effect of various parameters like temperature, pH, and the presence of inorganic salt NaCl on the adsorption of these phenols were investigated. A decrease in the pH of solutions led to a significant increase in the adsorption capacity of activated carbon. The removal of phenol and PHBA at acidic and neutral pH is high as compared to alkaline pH. The decrease of phenol and PHBA adsorptions by increasing temperature was quantified. The adsorption capacity of phenol and PHBA was slightly enhanced by an increase of salinity. This influence is particularly important for the application of the adsorption process to saline industry wastewater treatment systems.

Coupling of the TiO₂ photocatalytic oxidation and activated carbon adsorption

The objective of this part of the study was to evaluate the performance of adsorption/photodegradation combination for organic pollutants removal from water and to investigate the efficiency of photocatalytic process on the *in situ* regeneration of activated carbon.

1. Performance of TiO₂/AC tissue supplied by Ahlström towards the phenol removal by two different and successive steps: adsorption then oxidation was quantified. Several cycles of adsorption and oxidation were carried out by using “channel” type photoreactors. Two different phenol concentrations were used. The result showed that the regeneration efficiency was 97 % compared to the non used tissues in the second cycle in the case of low initial phenol concentration. Further decrease in the regeneration efficiency was observed by increasing the number of the reused times until 66 % in the last cycle. However, at higher initial phenol concentration, the regeneration efficiency dramatically decreased until 14 % in

the last cycle. This result was mainly related to the accumulation of coloured intermediates on the catalyst surface.

2. Addition of H_2O_2 as electron acceptor ($\text{H}_2\text{O}_2/\text{phenol} = 10$) showed that the elimination percentage of phenol ranged from 99 % in first cycle to 97 % in the last cycle for phenol removal by adsorption-oxidation on TiO_2/AC tissue.

3. After these previous results with the tissue system for phenol removal in batch, interesting the investigation of its performance in continuous conditions using a fixed bed type photocatalytic reactor proved such combination of AC and TiO_2 to be attractive.

4. A new confidential TiO_2/AC composite prepared at LGC by CVD was tested for the removal of tartrazine (project region CTP) in a quartz batch photoreactor. The new TiO_2/AC composite was characterized by SEM, EDX and nitrogen porosimetry. It was shown that the presence of TiO_2 , catalyst is not uniformly distributed on the AC and the surface area of the activated carbon is not significantly altered. A simple solid mixture of TiO_2 and S23 powders was investigated in order to compare its performance with that of the TiO_2/AC composite. Composite of TiO_2/AC materials clearly showed a higher photocatalytic activity for tartrazine degradation than the solid TiO_2 -AC powder mixture. Moreover, the repetitive use of the TiO_2/AC composite also gave better results. The higher performance of TiO_2/AC composite may be explained in two ways: (1) AC concentrated tartrazine around the loaded TiO_2 by adsorption, and improved the rate of photooxidation, allowing faster regeneration of the activated carbon (2) AC could prevent TiO_2 agglomerating, and provide adequate contact between TiO_2 and solution.

Compared to previous attempts concerning AD-OX process as wet air oxidation, Fenton and photo Fenton this work shows very promising results at room temperature avoiding severe corrosion by chloride ions, and convenient regeneration efficiency at low cost. These positive results open the way to future works at LGC to improve the design of such hybrid sequential process, especially concerning the coupling of fixed bed adsorption to photocatalysis at large scale. Nevertheless the major improvement is expected from material laboratories which should develop new photocatalyst able to be efficiently used under solar irradiation.

Conclusion Générale

Dans le domaine du traitement des eaux industrielles, on constate un besoin croissant en procédés économiques qui puissent s'adapter aux nouvelles exigences des réglementations internationales. En effet, les valeurs limites de rejets des substances dites prioritaires atteignent des valeurs tellement faibles qu'il devient primordial de proposer de nouvelles solutions. Ce challenge n'est pas aisé car les effluents industriels sont constitués de molécules de natures très diverses, plus ou moins réfractaires aux traitements proposés. Il semble donc aujourd'hui nécessaire de combiner plusieurs opérations pour atteindre de hauts rendements d'épuration. Ce travail s'intègre dans ce cadre, il a pour objectif de proposer des procédés innovants dans le domaine du traitement de l'eau à partir de techniques classiques telles que l'adsorption et la photocatalyse en présence de TiO_2 . Le caractère novateur de l'adsorption se situe dans l'utilisation de charbons actifs fabriqués à partir de boues de stations d'épuration d'eau usée alors que pour la photocatalyse il réside dans la mise en œuvre du catalyseur.

Dans le contexte actuel de développement durable, la bibliographie abonde de matériaux adsorbants fabriqués à partir de déchets dont les performances peuvent être variables. Dans le cadre d'un projet européen commun avec Imperial College et le laboratoire de Génie des Procédés – Environnement – Agro-alimentaire de Nantes, des charbons actifs conçus par ces laboratoires à partir de boue ont été comparés à des charbons commerciaux PICA. L'ensemble des charbons utilisés ont subi un grand nombre d'analyses : analyses texturales (surface spécifique, volumes meso- et microporeux), mesures de la composition chimiques (taux de cendres, analyse élémentaire), analyses chimiques de la surface (pH_{PZC} ou $\text{pH}_{\text{contact}}$, analyse de Boehm, thermogravimétrie). Cette première étude a permis de mettre en évidence d'importantes différences entre les charbons de boues et les charbons commerciaux. Les charbons de boues présentent des surfaces spécifiques de 4 à 10 fois plus faibles avec un fort taux de cendre et une composition en élément Oxygène élevée. Ces deux dernières caractéristiques traduisent une forte proportion en oxydes métalliques et en sels inorganiques. Ces charbons ont été ensuite comparés sur la base des isothermes obtenues avec le phénol. Il ressort que certains charbons de boues présentent des performances intéressantes malgré leurs faibles surfaces BET. La fabrication de charbon à partir de boue de station d'épuration apparaît comme une voie de valorisation économiquement viable.

Parmi ces charbons, le SA_DRAW a été sélectionné pour être comparé aux charbons commerciaux en adsorption compétitive avec des phénols : *p*-nitrophenol (PNP); *p*-chlorophenol (PCP); *p*-hydroxy benzoic acid (PHBA); et phenol (P). De nombreux paramètres entrent en jeu dans le phénomène d'adsorption, certains liés au charbon d'autres aux molécules adsorbées. En adsorption mono-constituant, l'hydrophobicité des molécules permet de justifier l'ordre des capacités d'adsorption obtenu : PCP > PNP > P > PHBA ; ordre conforté par le caractère attracteur des substituants -NO₂ et -Cl. Les fortes quantités de PCP et P adsorbées s'expliquent par leur faculté à réagir avec l'oxygène dissous par couplage oxydant pour former des oligomères qui s'adsorbent irréversiblement à la surface des charbons. En compétitif, il ressort de cette étude que le charbon de boue présente des performances toujours aussi notables. Les ordres d'adsorption préférentielle sont sensiblement les mêmes qu'avec les charbons commerciaux : PNP > PCP > P ou PHBA selon le domaine de concentration. Entre le P et le PHBA, une inversion de sélectivité est observée liée à leur forte différence de solubilité favorable au PHBA à forte concentration. Enfin, la diminution du phénomène d'oligomérisation en compétitif joue un rôle non négligeable car le PCP et le P ne s'adsorbent plus autant qu'en adsorption mono-constituant. En perspective de ce travail, il serait donc intéressant de tenter de quantifier cette part d'adsorption irréversible qui semble impacter fortement les performances d'adsorption compétitive en effectuant des isothermes dans des conditions anoxiques.

La bibliographie regorge d'études sur la photocatalyse avec du dioxyde de titane appliquée au traitement des effluents phénolés ou colorés. Ce catalyseur, sous sa forme classique nano-particulaire, se trouve difficilement séparable de l'effluent après traitement. Des études récentes proposent de nouvelles mises en œuvre de ce catalyseur par dépôt direct sur d'autres matériaux. Dans cette partie, l'idée est d'abord de répondre à cette attente en proposant un procédé utilisant un des matériaux plus faciles à séparer mais aussi de combiner cette oxydation à l'adsorption afin d'augmenter les performances du traitement. Deux formes de catalyseur très différentes ont été testées dans cette étude : un tissu commercialisé par la société Ahlstrom et un charbon actif avec dépôt de TiO₂ fabriqué au laboratoire de Génie Chimique. Le tissu est un tissu constitué de fibres synthétiques et de charbon en grains sur lequel une couche de dioxyde de titane et silice est déposée par imprégnation. Le charbon avec dépôt de TiO₂ est un charbon commercial S23 PICA sur lequel le catalyseur a été synthétisé directement par CVD. Les performances de ces matériaux ont été déterminées en

mode séquentiel en enchainant plusieurs cycles constitués d'une étape d'adsorption dans le noir et d'une étape de photo-oxydation sous UV.

Le tissu a été mis en œuvre dans un réacteur « canal » et dans un réacteur annulaire pour dégrader des solutions de phénol. Les principales conclusions de cette étude sont que cinq cycles de réutilisation du tissu permettent de dépasser les performances de l'adsorption seule. L'étape d'adsorption concentre les polluants à proximité du catalyseur augmentant ainsi les performances de l'oxydation photocatalytique. Cette étude montre aussi que la proportion quantité de polluant/quantité de catalyseur est un facteur important dans l'optique d'une réutilisation multiple du catalyseur. Les oxydations successives génèrent des intermédiaires qui engorgent le catalyseur altérant inexorablement son efficacité. L'ajout de peroxyde d'hydrogène permet d'entraver ce phénomène et d'obtenir des taux de dégradation du phénol très élevée même après plusieurs réutilisations du tissu (> 97%) mais la minéralisation reste incomplète avec 45% de diminution de la DCO traduisant une durée de traitement trop court. L'essai conduit en continu dans un réacteur annulaire montre que la photocatalyse est bien effective. En régime permanent, le taux de dégradation est de l'ordre de 50% dans des conditions qui restent à optimiser.

Le charbon actif avec dépôt de TiO_2 a été testé dans un réacteur batch cylindrique en verre pour traiter une solution de tartrazine. Comparé au charbon actif d'origine, le dépôt n'a pas modifié sa granulométrie par contre la surface spécifique et les volumes poreux ont légèrement diminués. Ce matériau catalytique a lui aussi été utilisé en procédé séquentiel. Après cinq cycles d'utilisation, le charbon élimine deux fois plus que ce qu'il traite en adsorption seule. La conclusion principale de cette étude est que la meilleure efficacité du matériau s'explique par la proximité des sites d'adsorption et ceux de réaction photocatalytique.

Les perspectives de ce travail sont multiples car l'objectif principal étant de mettre en évidence des propriétés catalytiques des matériaux, les conditions opératoires n'ont pas été optimisées et finalement les molécules testées ne sont pas représentatives de l'ensemble des effluents au cœur de la problématique du traitement de l'eau. Il serait donc dans un premier temps intéressant de tester un plus grand nombre de cycles en optimisant les durées des étapes d'adsorption et d'oxydation pour obtenir une régénération du matériau plus complète. Ce procédé séquentiel a essentiellement été expérimenté en batch mais la mise en œuvre de ce procédé en continu présente aussi un vif intérêt. Il serait donc particulièrement intéressant d'envisager des essais avec le charbon avec dépôt de TiO_2 sous la forme d'un lit fixe placé dans le réacteur annulaire. Enfin, ce procédé devrait aussi être testé avec d'autres molécules

comme par exemple certaines substances pharmaceutiques car ce type de traitement peut s'avérer efficace pour traiter les effluents hospitaliers avant leur acheminement vers les stations d'épuration classique pas assez performantes. Un traitement semi-batch pourrait être imaginé avec une première étape d'adsorption en continu et une étape d'oxydation photocatalytique en batch une fois le charbon actif saturé.

REFERENCES

A

Aboul-Kassim TAT (1998). Dissertation, Department of Civil, Construction and Environmental Engineering, College of Engineering, Oregon State University, Corvallis, Oregon, USA. **Ph.D**

Aceituno M., Stalikas C.D., Lunar L., Rubio S., Perez-Bendito D. (2002). H₂O₂/TiO₂ photocatalytic oxidation of metol: identification of intermediates and reaction pathways. *Water Res.* **36**: 3582–3592.

Adinata D., W.M.A.Wan Daud, Aroua M.K. (2007). Preparation and characterization of activated carbon from palm shell by chemical activation with K₂CO₃, *Bioresour. Technol.* **98**: 145–149.

Ahmed S., Rasul M.G., Martens W.N., Brown R., Hashib M.A. (2010). Heterogeneous photocatalytic degradation of phenols in wastewater: a review on current status and developments, *Desalination* **261**: 3–18.

Ahmed S., Rasul M.G., Brown R., Hashib M.A. (2011). Influence of parameters on the heterogeneous photocatalytic degradation of pesticides and phenolic contaminants in wastewater: A short review. *Journal of Environmental Management* **92**: 311-330.

Ahlstrom RCC (1998). Composition photocatalytique. France, EP 1069950B1.

Akbal F., Onar A. N. (2003). Photocatalytic degradation of phenol. *Environmental Monitoring and Assessment*, **83**: 295–302.

Aksoylu AE, Madalena M, Freitas MMA, Fernando M, Pereira MFR, Figueiredo JL. (2001). The effects of different activated carbon supports and support modifications on the properties of Pt/AC catalysts. *Carbon* **39**:175–85.

Aksoylu AE, Faria JL, Pereira MFR, Figueiredo JL, Serp P, Hierso JC, et al. (2003). Highly dispersed activated carbon supported platinum catalysts prepared by OMCVD: a comparison with wet impregnated catalysts. *Appl.Catal. A* **243**: 357–65.

Al-Asheh S., Banat F., Masad A. (2003). Physical and chemical activation of pyrolyzed oil shale residue for the adsorption of phenol from aqueous solutions. *Environmental Geology* **44**:333–342.

Al-Degs Y.S., El-Barghouthi M.I., El-Sheikh A.H., Walker G.M. (2008). Effect of solution pH, ionic strength, and temperature on adsorption behaviour of reactive dyes on activated carbon. *Dyes Pigments* **77**: 16–23.

Aleboye A., Moussa Y., Aleboye H. (2005). Kinetics of oxidative decolourisation of Acid Orange 7 in water by ultraviolet radiation in the presence of hydrogen peroxide. *Separation and Purification Technology* **43** (2):143-148.

Alinsafi A., Evenou F., Abdulkarim E.M., Pons M.N., Zahraa O., Benhammou A., Yaacoubi A., Nejmeddine A. (2007). Treatment of textile industry wastewater by supported photocatalysis, *Dyes Pigments* **74**: 439–445

Allen N. S., Edge M., Verran J., Stratton J., Maltby J., Bygott C. (2008). Photocatalytic titania based surfaces: environmental benefits. *Polymer Degradation and Stability*, **93** (9): 1632–1646.

Allen S.J., Koumanova B. (2005). Decolourisation of water/wastewater using adsorption (Review). *Journal of the University of Chemical Technology and Metallurgy* **40** (3): 175-192.

Almquist, C.B., Biswas P. (2001). A mechanistic approach to modeling the effect of dissolved oxygen in photo-oxidation reactions on titanium dioxide in aqueous systems. *Chem. Eng. Sci.*, **56**(11): 3421-3430

Al-Qaradawi S., Salman S. R.(2002). *J. Photochem. Photobiol. A: Chem.* **148**: 161.

Amalric L., Guillard C., Blanc-Brude E., Pichat P. (1996). Correlation between the photocatalytic degradability over TiO₂ in water of meta and para substituted methoxybenzenes and their electron density, hydrophobicity and polarizability properties. *Water Res.* **30**: 1137-1142.

Amin N. K. (2009). Removal of direct blue-106 dye from aqueous solution using new activated carbons developed from pomegranate peel: Adsorption equilibrium and kinetics. *Journal of Hazardous Materials* **165**: 52–62.

Amin H., Amer A., El Fecky A., Ibrahim I. (2008). Przeróbka wody odpadowej za pomocą sytemu H₂O₂ /UV , *Physicochemical Problems of Mineral Processing*, **42**: 17-28.

An T.C., Zhu X.H., Xiong Y. (2002). Feasibility study of photoelectrochemical degradation of methylene blue with three-dimensional electrodephotocatalytic reactor, *Chemosphere* **46**: 897–903.

Andrade L.S., Laurindo E.A., de Oliveria R.V., Rocha-Filho R.C., Cass Q.B. (2006). *J. Braz.Chem. Soc.* **17**

Andreozzi *et al.* (1999). Advanced oxidation processes (AOP) for water purification and recovery. *Catalysis Today* **53**: 51-59.

Ao C.H., Lee S.C. (2003). Enhancement effect of TiO₂ immobilized on activated carbon fiber for the photodegradation of pollutants at typical indoor air level. *Applied Catalysis B: Environmental* **44**: 191–205.

Ao Y., Xu J., Fu D., Shen X., Yuan C. (2008). Low temperature preparation of anatase TiO₂-coated activated carbon. *Colloids and surfaces. A, Physicochemical and engineering aspects.* **312** (2-3):125-130.

Augugliaro V., Baiocchi C., Bianco-Prevot A., Garcia-Lopez E., Loddo V., Malato S., Marci G., Palmisano L., Pazzi M., Pramauro E. (2002). *Chemosphere* **49**: 1223.

- Augugliaro, V., Palmisano L., Schiavello M., Sclafani A. (1991).** Photocatalytic degradation of nitrophenols in aqueous titanium dioxide dispersion. *Appl. Catal.*, **69** (1): 323-340.
- Arafat H. A., Franz M., Pinto N. G.. (1999).** Effect of Salt on the Mechanism of Adsorption of Aromatics on Activated Carbon. *Langmuir* **15**: 5997-6003.
- Arami M., Limaee N.Y., Mahmoodi N.M., Tabrizi N.S. (2006).** Equilibrium and kinetics studies for the adsorption of direct and acid dyes from aqueous solution by soy meal hull. *J. Hazard. Mater.* **135**: 171–179.
- Arana J. , Melian J.A.H., Rodriguez J.M.D., Diaz O.G., Viera A., Pena J.P., Sosa P.M.M., Jimenez V.E. (2002).** TiO₂-photocatalysis as a tertiary treatment of naturally treated wastewater. *Catal. Today* **76** (2–4): 279– 289.
- Aran˜a J, Don˜a-Rodríguez JM, Tello Rendo˜n E, Garriga i Cabo C, Gonza˜lez-Dı´az O, Herrera-Melia˜n JA, et al. (2003a).** TiO₂ activation by using activated carbon as a support Part I. Surface characterisation and decantability study. *Appl Catal B* **44**: 161–72.
- Aran˜a J, Don˜a-Rodríguez JM, Tello Rendo˜n E, Garriga i Cabo C, Gonza˜lez-Dı´az O, Herrera-Melia˜n JA, et al. (2003b).** TiO₂ activation by using activated carbon as a support. Part II. Photoreactivity and FTIR study. *Appl Catal B* **44**:153–60.
- Areerachakul N., Vigneswaran S., Ngo H.H., Kandasamy J. (2007).** Granular activated carbon (GAC) adsorption–photocatalysis hybrid system in the removal of herbicide from water. *Sep. Purif. Technol.*, **55**(2): 206–211.
- Asilturk M., Sayilkan F., Erdemoglu S., Akarsu M., Sayilkan H., Erdemoglu M., Arpac E. (2006).** *J. Hazard. Mater.* **B129**: 164–170.
- Attia A. A, Girgis B. S, Khedr S. A. (2003).** Capacity of activated carbon derived from pistachio shells by H₃PO₄ in the removal of dyes and phenolics. *J. Chem. Technol. Biotechnol.*, **78**:611–619.

Ayral C. (2009). Elimination de polluants aromatiques par oxydation catalytique sur charbon actif. Thèse de l'INP Toulouse (France)..

Ayranci E., Duman O. (2005). Adsorption behaviors of some phenolic compounds onto high specific area activated carbon cloth. *J. Hazard. Mater.* **124**: 125–132.

B

Bakardjieva S., Stengl V., Szatmary L., Subrt J., Lukac J., Murafa N., Niznansky D., K. Cizek, J. Jirkovsky, N. Petrova. (2006). *J. Mater. Chem.*, **16**: 1709–1716.

Banat F.A., Al-Bashir B., Al- Asheh, Hayajneh O. (2000). Adsorption of phenol by bentonit. *Environ. Pollut.*, **107**: 391-398.

Bansal R.C., Donnet JB, Stoeckli F. (1988). *Active carbon*. New York: Marcel Decker.

Bansal R.C., Goyal M. (2005). *Activated Carbon Adsorption*, CRC Press, New York, pp. 168–178.

Bansal R., Donne J., Stoeckli H. (1998). *Active Carbon*, Mercel Dekker, New York.

Bauer C., Jacques P. (2001). Kalt, Photooxidation of an azo dye induced by visible light incident on the surface of TiO₂, *J. Photochem. Photobiol. A: Chem.* **140**: 87–92.

Barakat M.A., Schaeffer H., Hayes G., Ismat-Shah S. (2005). Photocatalytic degradation of 2-chlorophenol by Co-doped TiO₂ nanoparticles. *Appl. Catal. B: Environ.* **57**: 23–30.

Barka N., Qourzal S., Assabbane A., Nounahb A., Ait-Ichou Y. (2008). Factors influencing the photocatalytic degradation of Rhodamine B by TiO₂-coated non-woven paper. *Journal of Photochemistry and Photobiology A: Chemistry* **195**: 346–351.

Bayarri B., Gimenez J., Curcoi D., Esplugas S. (2005). *Catal. Today* **101**: 227-232.

- Beker U., Ganbold B., Dertli H., Duranog D., Gulbayir I. (2010).** Adsorption of phenol by activated carbon: Influence of activation methods and solution pH. *Energy Conversion and Management* **51**: 235–240.
- Bertelli M., Selli E. (2006).** Reaction paths and efficiency of photocatalysis onTiO₂ and of H₂O₂ photolysis in the degradation of 2-chlorophenol. *J. Hazard. Mater. B* **138**: 46–52.
- Bertelli M., Selli E. (2004).** *Appl. Catal. B: Environ.* **52**: 205-212.
- Bessa E, Sant’Anna Jr G L, Dezotti M. (2001).** Photocatalytic/H₂O₂ treatment of oil field produced waters. *Applied Catalysis B: Environmental*, **29**: 125–134.
- Bing-Yu J., Li-Yan D., Chuan-Li MA, Chun-Ming W. (2007).** Characterization of TiO₂ Loaded on Activated Carbon Fibers and Its Photocatalytic Reactivity. *Chinese Journal of Chemistry* **25**: 553-557.
- Blanco J.G., Malato R. S. (2001).** Handbook of ‘Solar Detoxification’, Natural Sciences, Energy, including world solar programme 1996–2005, UNESCO.
- Boehm HP. (1994).** Some aspects of the surface chemistry of carbon blacks and other carbons. *Carbon* **32**: 759–764.
- Buffle J., Stumm W. (1994).** In: Buffle J, Devitre RR (eds) *Chemical and biological regulation of aquatic systems*. CRC Press, Boca Raton, FL, p 42.
- Burns A., Li W., Baker C., Shah S.I. (2002).** Sol–gel synthesis and characterization of neodymium-ion doped nanostructured titania thin film. *Mater. Res. Soc. Symp. Proc.*, **703**: 193–198.
- Butler JAV, Ockrent C. (1930).** *J. Phys. Chem.*, **34**: 2841.

Brunauer S., Emmett P. H., Teller E. (1938). Adsorption of gases in multi molecular layers. *J. Am. Chem. Soc.*, **60**: 309-319.

Byrappa K., Subramani A. K, Ananda A, Rai K M L, Dinesh R, Yoshimura M (2006). Photocatalytic degradation of Rhodamine B dye using hydrothermally synthesized ZnO. *Bulletin of Material Science*, **29**: 433–438.

C

Cadoret L, Rossignol C, Dexpert-Ghys J, et al. (2010). Chemical vapor deposition of silicon nanodots on TiO₂ submicronic powders in vibrated fluidized bed. *Materials Science and Engineering B- Advanced Functional Solid- State Materials*, **170** (1-3): 41-50.

Calvo L.F., Otero M., Mor'an A., Garc'ia A.I. (2001). Upgrading sewage sludges for adsorbent preparation by different treatments. *Bioresour. Technol.* **80**: 143–148.

Canizares P, Carmona M, Baraza O, Delgado A, Rodrigo MA. (2006). Adsorption equilibrium of phenol onto chemically modified activated carbon F400. *Journal of Hazardous Materials* **131**: 243-248.

Carrott PJM, Nabais JMV, Carrott MMLR, Menendez JA (2001). Thermal treatments of activated carbon fibres using a microwave furnace. *Microporous and Mesoporous Materials*. **47**: 243-252.

Carp, O., Huisman C.L., Reller A. (2004). Photoinduced reactivity of titanium dioxide. *Prog. Solid State Ch.*, **32**(1): 331-177.

Catena G.C., Bright F.V. (1989). Thermodynamic study on the effects of β -cyclodextrin inclusion with anilinonaphthalenesulfonates. *Analytical chemistry* **61** (8): 905-909.

Chakrabarti, S., Dutta B.K. (2004). Photocatalytic degradation of model textile dyes in wastewater using ZnO as semiconductor catalyst. *J. Haz. Mat. B*, **112**: 269-278.

Chattopadhyaya, B., Di Cristo, G., Wu, C.Z., Kuhlman, S.J., Palmiter, R.D., and Huang, Z.J. (2006). GAD67-mediated GABA synthesis and signaling regulate inhibitory synaptic innervation in adolescent visual cortex. CSHL GABA Workshop, p. 7.

Chen, D., Ray A.K. (1998). Photodegradation kinetics of 4-nitrophenol in TiO₂ suspension. *Wat. Res.*, **32** (11): 3223 -3234.

Chen C C, Lu C S, Chung Y C, Jan J L (2007). UV light induced photodegradation of malachite green on TiO₂ nanoparticles. *J. Hazard. Mater.*, **141** (3): 520-528.

Chen S F, Liu Y Z (2007). Study on the photocatalytic degradation of glyphosate by TiO₂ photocatalyst. *Chemosphere*, **67** (5): 1010–1017.

Chen S., Cao G. (2002). Photocatalytic oxidation of nitrite by sunlight using TiO₂ supported on hollow glass microbeads. *Solar Energy* **73** (1): 15-21.

Chen Y., Dionysiou D. (2006). TiO₂ photocatalytic films on stainless steel: The role of degussa P 25 in modified sol-gel methods. *Appl. Catal. B Environ.* **63**(1): 255 -264.

Chern J, Chien Y. (2003). Competitive adsorption of benzoic acid and p-nitrophenol onto activated carbon: isotherm and breakthrough curves. *Water Research* **37**: 2347–2356.

Chiang Y.C., Huang C.P. (2001). *Carbon* **39**: 523.

Chin, P., Yang, L. P., Ollis, D. F. (2006). Formaldehyde Removal from Air via a Rotating Adsorbent Combined with a Photocatalyst Reactor: Kinetic Modeling. *Journal of Catalysis* **237**: 29-37.

Chin M. L., Abdul Rahman M., Subhash B (2004). Performance of photocatalytic reactors using immobilized TiO₂ film for the degradation of phenol and methylene blue dye present in water stream. *Chemosphere* **57**: 547–554.

Chiou C., Wu C., Juang R. (2008a). Influence of operating parameters on photocatalytic degradation of phenol in UV/TiO₂ process. *Chemical Engineering Journal* **139** (2): 322-329.

Chiou C-H., C-Y. Wu, R-S. Juang. (2008b). Photocatalytic degradation of phenol and *m*-nitrophenol using irradiated TiO₂ in aqueous solutions. *Separation and Purification Technology* **62**: 559–564.

Choy K.L. (2003). Chemical vapor deposition of coatings. *Prog. Mater. Sci.*, **48**: 57–170.

Chu W. (2001). Modeling the quantum yields of herbicide 2,4-D decay in UV/H₂O₂ process. *Chemosphere* **44** (5): 935-941.

Chu W., Wong C.C. (2003). The photocatalytic degradation of dicamba in TiO₂ suspension with the help of hydrogen peroxide by different near irradiation. *Water Res.* **38**: 1037–1043.

Chu W., Wong C. C. (2004). The photocatalytic degradation of dicamba in TiO₂ suspensions with the help of hydrogen peroxide by different near UV irradiations. *Water Research* **38** (4): 1037-1043.

Chu W., Choy W. K., So T.Y. (2007). *J. Hazard. Mater.* **141**: 86-91.

Chun H., Yizong W., Hongxiao T. (2001). Preparation and characterization of surface bond-conjugated TiO₂/SiO₂ and photocatalysis for azo dyes. *J. Appl. Catal. B: Environ.*, **30**: 277-285.

Coleman, H.M., Abdullah M.I., Eggins B.R., Palmer F.L. (2005). Photocatalytic degradation of 17- β -oestradiol, oestriol and 17- α -withynyloestradiol in water monitored using fluorescence spectroscopy. *Appl. Catal. B Environ.*, **55** (1): 23-30.

Colon G., Belver C., Ferna'ndez-Garci'a M. (2007). In: M. Ferna'ndez-Garci'a, J.A. Rodri'guez (Eds.), *Synthesis, Properties and Application of Oxide Nanoparticles*, Wiley, USA.

Colon G., Hidalgo M.C., Macías M., Navío J.A., Doña J.M. (2003). Appl. Catal. B: Environ. **43**: 163.

Colon G.M., Hidalgo C., Macias M. (2004). Appl. Catal. A: Gen. **259**: 235.

Colon G., Sanchez-Espana J.M., Hidalgo M.C., Navio J.A. (2006). Effect of TiO₂ acidic pretreatment on the photocatalytic properties for phenol degradation. J. Photochem. Photobiol. A: Chem. **179**: 20–27.

Contescu, A., Vass, M., Contescu, C., Putyera, K., and Schwarz, J.A. (1998). Acid buffering capacity of basic carbons revealed by their continuous p*K* distribution. Carbon **36**: 247–258.

Cooney D. O., Xi Z. (1994). Activated carbon catalyzes reactions of phenol during liquid-phase adsorption. J AICHE, **40** (2): 361-364.

Coughlin R. W., Ezra F. S. (1968). Role of surface acidity in the adsorption of organic pollutants on the surface of carbon. Environ. Sci. Technol., **2**: 291-298.

Cordero T., Duchamp C., Chovelon J-M., Ferronato C., Matos J. (2007). Influence of L-type activated carbons on photocatalytic activity of TiO₂ in 4-chlorophenol photodegradation. Journal of Photochemistry and Photobiology A: Chemistry **191**: 122–131.

Creanga C. (2007). Procédé AD-OX d'élimination de polluants organiques non biodégradables (par adsorption puis oxydation catalytique). Thèse de l'INP Toulouse (France).

Crittenden J. C., Suri R.P. S., Perram D. L., Hand D. W. (1997). Decontamination of water using adsorption and photocatalysis. Water Research **31** (3): 411-418.

D

- Dabrowski A., Podkoscielny P., Hubicki Z., Barczak M. (2005).** Adsorption of phenolic compounds by activated carbon - a critical review. *Chemosphere* **58**: 1049 - 1070.
- Daneshvar N., Khataee A.R., A.R. Amani Ghadim, Rasoulifard M.H. (2007).** Decolorization of C.I. Acid Yellow23 solution by electrocoagulation process: investigation of operational parameters and evaluation of specific electrical energy consumption (SEEC). *J. Hazard. Mater.*, **148**: 566–572.
- Darko S. A., Maxwell E., Park S. (2010).** Photocatalytic activity of TiO₂ nanofilms deposited onto polyvinyl chloride and glass substrates. *Thin Solid Films* **519**(1) : 174-177.
- de Lasa, H., Serrano, B., and Salaices, M. (2005).** Photocatalytic reaction engineering. New York, USA: Springer Science+Business Media Inc.
- De la Puente G, Pis J, Menéndez J, Grange P. (1997).** Thermal stability of oxygenated functions in activated carbons. *Journal of Analytical and Applied Pyrolysis*. **43**: 125-138.
- Deryło-Marczewska A., Swiatkowski A., Biniak S., Walczyk M. (2008).** Effect of properties of chemically modified activated carbon and aromatic adsorbate molecule on adsorption from liquid phase. *Colloids and Surfaces A: Physicochem. Eng. Aspects* **327**: 1–8.
- Deryło-Marczewska A., Goworek J., Swiaztkowski A., Buczek B. (2004).** Influence of differences in porous structure within granules of activated carbon on adsorption of aromatics from aqueous solutions. *Carbon* **42**: 301–306.
- Detlef B. (2004).** Photocatalytic water treatment: solar energy applications. *Solar energy* **77**: 445-459.

Diaz-Flores P.E., Leyva-Ramos R., Guerrero-Coronado R.M., Mendoza-Barron J. (2006). Adsorption of pentachlorophenol from aqueous solution onto activated carbon fiber. *Ind. Eng. Chem. Res.* **45**: 330–336.

Diebold, U. (2003). The surface science of titanium dioxide. *Surf. Sci. Rep.*, **48(5-8)**: 53-229.

Dionysiou D. D., Suidan M. T., Baudin I., Laine J-M. (2004). Effect of hydrogen peroxide on the destruction of organic contaminants-synergism and inhibition in a continuous-mode photocatalytic reactor. *Applied Catalysis B: Environmental* **50** (4): 259-269.

Ding Z, Hu XJ, Yue PL, Lu GQ, Greenfield PF. (2000). Novel silica gel supported TiO₂ photocatalyst synthesized by CVD method. *Langmuir* **16**: 6216–22.

Ding Z., Hu XJ, Yue PL, Lu GQ. (2001). Greenfield PF. Synthesis of anatase TiO₂ supported on porous solids by chemical vapour deposition. *Catal Today* **68**:173–82.

Doll T.E., Frimmel F.H. (2004). Kinetic study of photocatalytic degradation of carbamazepine, clofibric acid, iomeprol and iopromide assisted by different TiO₂ materials—determination of intermediates and reaction path. *Water Res.* **38**: 955–964.

Duminica F.D., Maury F., Senocq F. (2004). Atmospheric pressure MOCVD of TiO₂ thin films using various reactive gas mixtures. *Surface and Coatings Technology* **188-189**: 255-259.

Durgakumari V., Subrahmanyam M., Subba Rao K. V., Ratna-mala A., Noorjahan M., Tanaka K. (2002). An easy and efficient use of TiO₂ supported HZSM-5 and TiO₂+ HZSM-5 zeolite combine in the photodegradation of aqueous phenol and p-chlorophenol. *Appl. Catal. A: Gen.*, **234**: 155-165.

E

Eftaxias A., Font, J., Fortuny A., Fabregat, A. and Stuber, F., (2006). *App. Catal. B: Environ.* **67**: 112-23.

El-Sayed Y, Badosz TJ. (2004). Adsorption of valeric acid from aqueous solution onto activated carbons: role of surface basic Sites. *J. Colloid Interf. Sci.*, **273**: 64-72.

El-Sheikh A.H., Newman A.P., Al-Daffae H., Phull S., Cresswell N., York S. (2004). Deposition of anatase on the surface of activated carbon. *Surf. Coat. Technol.* **187**: 284–292.

El-Sheikh A.H., Al-Degs Y.S., Newman A.P., Lynch D. E. (2007). Oxidized activated carbon as support for titanium dioxide in UV-assisted degradation of 3-chlorophenol. *Separation and Purification Technology* **54**: 117–123.

Epling G.A., Lin C. (2002). Photoassisted bleaching of dyes utilizing TiO₂ and visible light. *Chemosphere* **46**: 561–570.

F

Fan, X., Zhang, X. (2008). Adsorption properties of activated carbon from sewage sludge to alkaline-black. *Mater. Lett.* **62**: (10-11), 1704-1706.

Fabrizi D., Prevot A.B., Pramauro E. (2006). Effect of surfactant microstructures on photocatalytic degradation of phenol and chlorophenols. *Appl. Catal. B: Environ.* **62**: 21–27.

Farran A., Ruiz S. (2004). *J. Chromatog. A.* **1024**: 267-274.

Fenton H.J.H. (1894). Oxidation of tartaric acid in presence of iron. *J. Chem. Soc. Trans.* **65**: 899-910.

Fierro V., V. Torné-Fernández, Celzard A. (2006). Highly microporous carbons prepared by activation of kraft lignin with KOH, *Stud. Surf. Sci. Catal.* **160**: 607–614.

Fierro V., Torne'-Ferna'ndez V., Montane D., Celzard A. (2008). Microporous and Mesoporous Materials **111**: 276–284.

Figueiredo J.L., Pereira M.F.R., Frbitas M.M.A, Órfao J.J.M. (1999). Modification of the surface chemistry of activated carbons. *Carbon* **37**: 1379–89.

Einaga H., Futamura S., Ibusuki T. (2002). Heterogeneous photocatalytic oxidation of benzene, toluene, cyclohexene and cyclohexane in humidified air: comparison of decomposition behavior on photoirradiated TiO₂ catalyst. *Applied Catalysis B: Environmental* **38** (3): 215-225.

Fox, M.A., Dulay M.T. (1993). Heterogeneous photocatalysis. *Chem. Rev.*, **93**(1): 341-357.

Fujishima A., Zhang X., Tryk D. A. (2007). Heterogeneous photocatalysis: from water photolysis to applications in environmental cleanup. *International Journal of Hydrogen Energy*, **32** (14): 2664–2672.

Fujishima A., Honda K. (1972). Electrochemical Photolysis of Water at a Semiconductor Electrode. *Nature*, **238**: 37.

Fujishima A., Rao T. N., Tryk D. A. (2000). Titanium Dioxide Photocatalysis. *Journal of Photochemistry and Photobiology C: Photochemistry Reviews*, **1**: 1–21.

Franz M., Arafat H.A., Pinto N.G. (2000). Effect of chemical surface heterogeneity on the adsorption mechanism of dissolved aromatics on activated carbon. *Carbon* **38**: 1807 – 1819.

Frazer L. (2001). Titanium Dioxide: Environmental White Knight. *Environmental Health Perspectives*, **109**: A174.

Freundlich H. (1926). *Colloid and capillary chemistry.* Methuen, London.

G

Garcia, J.C., Takashima K.(2003). Photocatalytic degradation of imazaquin in an aqueous suspension of titanium dioxide. *J. Photochem. Photobiol. A Chem.*, **155**(1-3): 215-222.

Garcia-Araya J.F., Beltra F.J., Lvarez P. A, Masa F.J. (2003). Activated Carbon Adsorption of Some Phenolic Compounds Present in Agroindustrial Wastewater. *Adsorption* **9**: 107–115.

Gaya U. I., Abdullah A. H. (2008). Heterogeneous photocatalytic degradation of organic contaminants over titanium dioxide: a review of fundamentals, progress and problems. *Journal of Photochemistry and Photobiology C*, **9** (1): 1–12.

Ghaly M. Y., Härtel G., Mayer R., Haseneder R. (2001). Photochemical oxidation of *p*-chlorophenol by UV/H₂O₂ and photo-Fenton process. A comparative study. *Waste Management* **21**(1):41-47.

Glaze, W.H., Kwang, J.W., Chapin, D.H. (1987). Chemistry of water treatment processes involving ozone, hydrogen peroxide and ultraviolet radiation. *Ozone Science and Engineering* **9**: 335-352.

Gogate P.R., Pandit A.B. (2004). *AIChE J.* **50**: 1051.

Gokturk S., Kaluc S. (2008). Removal of selected organic compounds in aqueous solutions by activated carbon. *J. Environ. Sci. Technol.*, **1**: 111-123.

Grant, T. M., King, J. (1990). Mechanism of irreversible adsorption of phenolic compounds by activated carbons. *Ind. Eng. Chem. Res.*, **29**(2): 264-271.

Grzechulska-Damszel J.(2009). Removal of Organic Impurities from Water Using a Reactor with Photoactive Refill. *International Journal of Photoenergy* Volume **2009**, Article ID 304712, 6 pages.

Grzechulska J., Morawski A. W. (2003). Photocatalytic labyrinth flow reactor with immobilized P25 TiO₂ bed for removal of phenol from water. *Applied Catalysis B: Environmental* **46** (2):415-419.

Guettaï N., Amar H. A. (2005a). Photocatalytic oxidation of methyl orange in presence of titanium dioxide in aqueous suspension. Part I: Parametric study. *Desalination* **185**: 427–437.

Guettaï N., Amar H. A. (2005b). Photocatalytic oxidation of methyl orange in presence of titanium dioxide in aqueous suspension. Part II: kinetics study. *Desalination* **185**: 439–448.

Guillard C., Lachheb H., Houas A., Ksibi M., Elaloui E., Hermann J.M. (2003). Influence of chemical structure of dyes, of pH and of inorganic salts on their photocatalytic degradation by TiO₂ comparison of the efficiency of powder and supported TiO₂. *J. Photochem. Photobiol. A. Chem.*, **158**: 27-36.

Guo J., Lua A.C. (2000). Preparation of activated carbons from oil-palm-stone chars by microwave-induced carbon dioxide activation. *Carbon* **38**: 1985–1993.

Guo Z., Ma R., Li G. (2006). Degradation of phenol by nanomaterial TiO₂ in wastewater. *Chemical Engineering Journal* **119**: 55–59.

Gupta, H., Tanaka S. (1995). Photocatalytic mineralisation of perchloroethylene using titanium dioxide. *Wat. Sci. Tech.*, **31**(9): 47-54.

Gutiérrez-Segura E.; A. Colín-Cruz; C. Fall; M. Solache-Ríos; P. Balderas-Hernández, (2009). Comparison of Cd–Pb adsorption on commercial activated carbon and carbonaceous material from pyrolysed sewage sludge in column system, *Environ. Technol.*, **30**: 455–461.

H

Hai F.I., Yamamoto K., Fukoshi K. (2007). Hybrid treatment systems for dyewastewater. *Crit. Rev. Environ. Sci. Technol.* **37**: 315–377.

Haimour N.M., Emeish S. (2006). Utilization of date stones for production of activated carbon using phosphoric acid. *Waste Manage*, **26**: 651– 660.

Halhouli K. A., Darwish N. A., Al-Jahmany Y. Y. (1997). Effects of Temperature and Inorganic Salts on the Adsorption of Phenol from Multicomponent Systems onto a Decolorizing Carbon. *Separation Science and Technology*, **32** (18): 3027-3036.

Halhouli K.A., Darwish N.A., Al-Dhoon N.M. (1995). *Sep. Sci. Technol.* **30** : 3313- 3324.

Hameed B.H., A.T. Mohd Din, A.L. Ahmad (2007). Adsorption of methylene blue onto bamboo-based activated Carbon: kinetics and equilibrium studies, *J. Hazard. Mater.* **141**: 819–825.

Hameed B.H., Rahman, A.A. (2008). Removal of phenol from aqueous solutions by adsorption onto activated carbon prepared from biomass material. *Journal of Hazardous Materials* **160**: 576–581.

Han W. Y., Zhu W. P., Zhang P. Y., Zhang Y., Li L. S. (2004). Photocatalytic degradation of phenol in aqueous solution under irradiation of 254 and 185 nm UV light. *Catalysis Today*, **90**: 319–324.

Han J. K., Choi S. M., Lee G. H. (2007). Synthesis and photocatalytic activity of nanocrystalline TiO₂-SrO composite powders under visible light irradiation. *Mater. Lett.*, **61** (18): 3798- 3801.

Haque M.M., Muneer M. (2003). *J. Environ. Manage.* **69**: 169-176.

Hashim H. A. A., Mohamed A. R., Teong L. K. (2001). Solar photocatalytic degradation of tartrazine using titanium dioxide. *Jurnal Teknologi*, **35**: 31–40.

Haydara S., Ferro-Garciab M.A., Rivera-Utrillab J., Jolya J.P. (2003). Adsorption of p nitrophenol on an activated carbon with different oxidations, *Carbon* **41**: 387–395.

Herrmann J.-M. (1999). Heterogeneous photocatalysis: fundamentals and applications to the removal of various types of aqueous pollutants. *Catalysis Today*, **53** (1): 115-129.

Herrmann J.M., Matos J., Disdier J., Guillard C., Laine J., Malato S., Blanco J. (1999). Catal. Today **54**: 255.

Herrmann J.-M., Duchamp C., Karkmaz M., et al. (2007). Environmental green chemistry as defined by photocatalysis. Journal of Hazardous Materials, **146** (3): 624–629.

Herrmann J. -M., Guillard C., Pichat P. (1993). Heterogeneous photocatalysis : an emerging technology for water treatment. Catalysis Today **17** (1-2): 7-20.

Higarashi M.M., Jardim W.F. (2002). Catal. Today **76**: 201-207.

Hoffmann, M.R., S.T. Martin, W. Choi, D.W. Bahnemann (1995). Environmental applications of semiconductor photocatalysis. Chem. Rev., **95**(1): 69 -96.

Houas, A., Lachheb, H., Ksibi, M., Elaloui, E., Guillard, C., Hermann, J.M., (2001). Photocatalytic degradation pathway of methylene blue in water. Appl. Catal. B: Environ. **31**: 145–157.

Hosseini S.N., Borghei S.M., Vossoughi M., Taghavinia N. (2007). Immobilization of TiO₂ on perlite granules for photocatalytic degradation of phenol. Applied Catalysis B: Environmental **74**: 53–62.

Hu Z.H., Srinivasan M.P., Ni Y.M. (2001). Novel activation process for preparing highly microporous and mesoporous activated carbons. Carbon **39**: 877–886.

Huang C-C., Li H-S., Chen C-H. (2008). Effect of surface acidic oxides of activated carbon on adsorption of ammonia. J. Hazard. Mater., **159** (2-3):523-7.

Huang E.,Weber W.J. Jr. (1997). Environ Sci Technol **31**: 2562.

Huang W., Young T.M., Schlautman M.A., Yu H.,Weber W.J. Jr. (1997). Environ. Sci. Technol. **31**:1703.

Huchon R. (2002). Activité photocatalytique de catalyseurs déposés sur différents supports « Médias » Application à la conception d'un photoréacteur pilote. UNIVERSITE CLAUDE BERNARD - LYON 1, Ph.D. Thesis.

Hung, C.-H., P.-C. Chiang, C. Yuan, and C.-Y. Chou (2001). Photocatalytic degradation of azo dye in TiO₂ suspended solution. *Wat. Sci. Tech.*, **43**(2): 313-320.

Huling S.G., Jonesa P.K., Elab W. P., Arnold R. G (2005). Fenton-driven chemical regeneration of MTBE-spent GAC. *Water Res.*, **39**(10): 2145-53.

I

Iliev V., Mihaylova A., Bilyarska L. (2002). Photooxidation of phenols in aqueous solution. *Mol. Catalysis A. Chemical.*, **184** (1-2): 121-30.

Ingaki M., Hirose Y., Matsunaga T. (2004). *Carbon* **41**: 2619.

Ioannis K. Konstantinou, Triantafyllos A. Albanis, (2004). *Applied Catalysis B: Environmental*, **49**: 1–14.

J

Jung S., Kim S., Imaishi N. et al. (2005). Effect of TiO₂ thin film thickness and specific surface area by low-pressure metal-organic chemical vapour deposition on photocatalytic activities. *Applied Catalysis B: Environmental* **55**: 253–257.

Jung M.W., Ahn K.H., Lee Y., Kim K.P., Rhee J.S., Park J.T., Paeng K.J. (2001). Adsorption characteristics of phenol and chlorophenols on granular activated carbons (GAC), *Microchem. J.* **70**: 123–131.

K

Kabir M. F., Vaisman E., Langford C. H., Kantzas A. (2006). Effects of hydrogen peroxide in a fluidized bed photocatalytic reactor for wastewater purification. *Chemical Engineering Journal* **118**: 207–212.

Kahru, A., Põllumaa, L., Blinova, R., Reiman, R., Rätsep, A.(1998). Chemical versus toxicological analysis in characterization of phenolic pollution: a test battery approach. *Toxicology Letters* **95** (1): 236.

Kamble S. P., Mangrulkar P.A., Bansiwai A. K., Rayalu S. S. (2008). Adsorption of phenol and *o*-chlorophenol on surface altered fly ash based molecular sieves. *Chemical Engineering Journal* **138**: 73–83.

Kang M. (2002). Preparation of TiO₂ photocatalyst film and its catalytic performance for 1,1'-dimethyl-4, 4'- bipyridium dichloride decomposition. *Appl. Catal. B: Environ.*, **37**: 187-196.

Kanki T., Hamasaki S., Sano N., Toyoda A., Hirano K. (2005). Water purification in a fluidized bed photocatalytic reactor using TiO₂-coated ceramic particles. *Chemical Engineering Journal* **108**: 155–160.

Karkmaz M., Puzenat E., Guillard C., Herrmann J.M. (2004). Photocatalytic degradation of the alimentary azo dye amaranth Mineralization of the azo group to nitrogen. *Applied Catalysis B: Environmental* **51**: 183–194.

Kawahara T., Konishi Y., Tada H., Tohge N., Nishii J., Ito S. (2002). *Angew. Chem. Int. Ed.* **114**: 2935–2937.

Khalil, L.B., Girgis B.S., Tawfik T.A.M. (2001). Decomposition of H₂O₂ on activated carbon obtained from olive stones. *J. Chem. Technol. Biotechnol.* **76**(11): 1132-1140.

Khalid, N., Ahmad, S., Toheed, A., Ahmad, J. (2000). Potential of rice husks for antimony removal. *Applied Radiation and Isotopes* **52**: 30-38.

Khan A.Y., Mazyck D.W. (2003). A new route for preparation of TiO₂-mounted activated carbon. *Appl. Catal. B: Environ.* **46**: 203–208.

Khataee A.R., Vantanpour V., Amani A.R. (2009a). Decolorization of C.I. Acid Blue 9 solution by UV/Nano-TiO₂, Fenton, Fenton-like, electro-Fenton and electrocoagulation processes: a comparative study. *J. Hazard. Mater.*, **161**: 1225–1233.

Khataee A.R., Pons M.N., Zahraa O. (2009b). Photocatalytic degradation of three azo dyes using immobilized TiO₂ nanoparticles on glass plates activated by UV light irradiation: Influence of dye molecular structure. *J. Hazard. Mater.*, **168**: 451–457.

Kim H., Choi W. (2007). *Appl. Catal. B: Environ.* **69**: 127-132.

Kim D.S., Park Y.S. (2006). *Chem. Eng. J.* **116**: 133–137.

Kim B.J., Park S.J. (2007). Effects of carbonyl group formation on ammonia adsorption of porous carbon surfaces. *J. Colloid Interface Sci.*, **311**: 311–314.

Kitano M., Matsuoka M., Ueshima M., Anpo M. (2007). Recent developments in titanium oxide-based photocatalysts. *Appl. Catal. A-Gen.* **325**: 1–14.

Konstantinou I.K., Albanis T.A. (2004). *Applied Catalysis B Environmental* **49**: 1–14.

Konstantinou I.K., Albanis T.A. (2003). Photocatalytic transformation of pesticides in aqueous titanium dioxide suspensions using artificial and solar light: intermediates and degradation pathways. *Appl. Catal. B* **42**: 319–335.

Kositzi M., Poullos I., Samara K., Tsatsaroni E., Darakas E. (2007). Photocatalytic oxidation of Cibacron Yellow LS-R. *Journal of Hazardous Materials* **146**: 680–685.

Kozlova, E.A., Smirniotis P.G., Vorontsov A.V. (2004). Comparative study on photocatalytic oxidation of four organophosphorus simulants of chemical warfare agents in aqueous suspension of titanium dioxide. *J. Photochem. Photobiol. A Chem.*, **162** (2-3): 503-511.

Krou N. (2010). Etude expérimentale et modélisation d'un procédé sequential AD-OX d'élimination de polluants organiques, Thèse de l'INP Toulouse (France).

Kumar B.G. P., Shivakamy K., Miranda L.M., Velan M. (2006). Preparation of steam activated carbon from rubberwood sawdust (*Hevea brasiliensis*) and its adsorption kinetics, *J. Hazard. Mater.* **136**: 922–929.

Kumar A., Kumar S., Kumar S., Gupta D. V. (2007). Adsorption of phenol and 4-nitrophenol on granular activated carbon in basal salt medium: Equilibrium and kinetics. *Journal of Hazardous Materials* **147**: 155–166.

L

Lachheb H., Puzeat E., A. Houas, M. Ksibi, E. Elaloui, C. Guillard and J.M. Herrmann. (2002). Photocatalytic degradation of various types of dyes (Alizarin S, Crocein Orange G, Methyl Red, Congo Red, Methylene Blue) in water by UV-irradiated titania. *Applied Catalysis B. Environmental* **39**: 75 –90.

Lam S-M., Sin J-C., Mohamed A-R. (2010). Parameter effect on photocatalytic degradation of phenol using TiO₂-P25/activated carbon (AC). *Korean J. Chem. Eng.*, **27**(4): 1109-1116.

Langmuir I. (1918). *J. Am. Chem. Soc.* **40**: 1362.

Laszlo K., Tomb'acz E., Nov'ak C. (2007). pH-dependent adsorption and desorption of phenol and aniline on basic activated carbon. *Colloids and Surfaces A: Physicochem. Eng. Aspects* **306**: 95–101.

- Lathasree S., Rao A.N., SivaSankar B., Sadasivam V., Rengaraj K. (2004).** Heterogeneous photocatalytic mineralization of phenols in aqueous solutions. *J. Mol. Catal. A: Chem.* **223**: 101–105.
- Lee D., S. Kim, I. Cho, S. Kim (2004).** Photocatalytic oxidation of microcystin-LR in a fluidized bed reactor having TiO₂-coated activated carbon. *Sep. Purif. Technol.* **34**: 59–66.
- Leuch L.M., Bandosz T.J. (2007).** The role of water and surface acidity on the reactive adsorption of ammonia on modified activated carbons. *Carbon* **45**: 568–578.
- Lhomme L. (2006).** Dégradation de produits phytosanitaires par photocatalyse sur support: application aux effluents agricoles, thèse Ecole Nationale Supérieure de Chimie de Rennes (france)
- Li Y., Li X., Li J., Yin J. (2006).** Photocatalytic degradation of methyl orange by TiO₂-coated activated carbon and kinetic study. *Water Research* **40**: 1119 – 1126.
- Li Y. J., Zhang S. Y., Yu Q. M., Yin W. B. (2007).** The effects of activated carbon supports on the structure and properties of TiO₂ nanoparticles prepared by a sol-gel method. *Appl. Surf. Sci.*, **253**: 9254- 9258.
- Li Y., Sun S., Ma M., Ouyang Y., Yan W. (2008).** Kinetic study and model of the photocatalytic degradation of rhodamine B (RhB) by a TiO₂-coated activated carbon catalyst: Effects of initial RhB content, light intensity and TiO₂ content in the catalyst. *Chemical Engineering Journal* **142**: 147–155.
- Li J.M., Meng X.G., Hu C.W., Du J. (2009).** Adsorption of phenol, p-chlorophenol and p-nitrophenol onto functional chitosan. *Bioresource Technology* **100** (3): 1168-1173.
- Li Q., Snoeyink V. L., Mariñas B. J., Campos C. (2003).** Elucidating Competitive Adsorption Mechanisms of Atrazine and NOM Using Model Compounds. *Water Res.* **37**: 773–784.

- Lianfeng Z., Tatsuo K., Noriaki S., Atsushi T. (2003).** Development of TiO₂ photocatalyst reaction for water purification. *Sep. Purif. Technol.* **31** (1): 105–110.
- Liding, V. S noeyink, B . M arinas, Z hongrenyue, J.Economy (2008).** Effects of Powdered Activated Carbon Pore Size Distribution on the Competitive Adsorption of Aqueous Atrazine and Natural Organic Matter. *Environ. Sci. Technol.* **42**: 1227–1231.
- Lifongo, L.L., D.J. Bowden, P. Brimblecombe. (2004).** Photodegradation of haloacetic acids in water. *Chemosphere*, **55**(3): 467-476.
- Ling C. M., Mohamed A., Bhatia S. (2004).** Performance of photocatalytic reactors using immobilized TiO₂ film for the degradation of phenol and methylene blue dye present in water stream. *Chemosphere* **57**: 547–554.
- Liotta L.F., Gruttadauria M., Carlo G.D., Perrini G., Librando V.(2009).** Heterogeneous catalytic degradation of phenolic substrates: catalysts activity. *J. Hazard. Mater.***162**: 588–606.
- Liu S. X., Chen X. Y., Chen X., Sun C. L. (2006).** A Novel High Active TiO₂/AC Composite Photocatalyst Prepared by Acid Catalyzed Hydrothermal Method. *Chinese Chemical Letters* **17** (4): 529-532.
- Liu Y., Yang S., Hong J., Sun C. (2007).** Low-temperature preparation and microwave photocatalytic activity study of TiO₂-mounted activated carbon. *Journal of Hazardous Materials* **142**: 208–215.
- Liu C., Z. Tang, Y. Chen, S. Su, W. Jiang (2010).** Characterization of mesoporous activated carbons prepared by pyrolysis of sewage sludge with pyrolusite. *Bioresour. Technol.* **101**: 1097–1101.
- Liu Q-S., Zheng T., Wang P., Jiang J-P., Li N. (2010).** Adsorption isotherm, kinetic and mechanism studies of some substituted phenols on activated carbon fibers. *Chemical Engineering Journal* **157** (2-3) 348-356.
- Lorenc-Grabowska E., Gryglewicz G. (2007).** Adsorption characteristics of Congo Red on coal-based mesoporous activated carbon. *Dyes and Pigments* **74**: 34-40.

Lu Y., Wang D., Ma C., Yang H. (2010). The effect of activated carbon adsorption on the photocatalytic removal of formaldehyde. *Building and Environment* **45**: 615–621.

Lu Q., Sorial G. A. (2007). The effect of functional groups on oligomerization of phenolics on activated carbon. *J. Hazard. Mater.* **148**: 436–445.

Lu Q., Sorial G. A. (2004). The role of adsorbent pore size distribution in multicomponent adsorption on activated carbon. *Carbon* **42**: 3133–3142.

Lu Q., Sorial G. A. (2009). A comparative study of multicomponent adsorption of phenolic compounds on GAC and ACFs. *Journal of Hazardous Materials* **167**: 89–96.

Luck F. (1999). Wet air oxidation: past, present and future. *Catalysis Today* **53**: 81-91.

M

Macounova K., Krysova H., Ludvik J., Jirkovsky J. (2003). *J. Photochem. Photobiol. A: Chem.* **156**: 273-282.

Mahalakshmi M., Priya S. V., Arabindoo B., Palanichamy M., Murugesan V. (2009). Photocatalytic degradation of aqueous propoxur solution using TiO₂ and H₂O₂/Zeolite-supported TiO₂. *Journal of Hazardous Materials* **161**: 336 –343.

Mahmoodi N.M., Arami M., Limaee N. Y., Tabrizi N. S. (2006). Kinetics of heterogeneous photocatalytic degradation of reactive dyes in an immobilized TiO₂ photocatalytic reactor. *Journal of Colloid and Interface Science* **295**: 159–164.

Malato S., Blanco J., Vidal A., Richter C. (2002). Photocatalysis with solar energy: at a pilot-plant scale: an overview. *Applied Catalysis B: Environmental*, **37** (1): 1-15.

Maldonado M. I., Passarinho P. C., I. Oller, et al. (2007). “Photocatalytic degradation of EU priority substances: a comparison between TiO₂ and fenton plus photo-fenton in a solar pilot plant. *Journal of Photochemistry and Photobiology A*, **185** (2-3): 354–363.

Malik, P.K. (2003). Use of activated carbons prepared from sawdust and rice-husk for adsorption of acid dyes: a case study of acid yellow 36. *Dyes. Pigments* **56**: 239- 249.

Mantzavinos D., Lauer E., Hellenbrand R., Livingston A. G., Metcalfe I. S.. (1997). Wet oxidation as a pretreatment method for wastewaters contaminated by bioresistant organics. *Water Science and Technology* **36** (2-3): 109–116.

Marci G., Augugliaro V., Prevot A. B., Baiocchi C., Garcia-Lopez E., Loddo V., L. Palmisano, E. Pramauro, M. (2003). Schiavello. *Annali di Chimica by Societa Chimica Italiana*, **93**: 639–645.

Martin M.J., Artola A., Balaguer M.D., Rigola M. (2003). Activated carbons developed from surplus sewage sludge for the removal of dyes from dilute aqueous solutions. *Chem. Eng. J.* **94**: 231–239.

Mas D., Pichat P., Guillard C., Luck F. (2005). Ozone: *Sci. Eng.* **27**: 311-316.

Matos J, Laine J, Herrmann JM. (2001). Effect of the type of activated carbons on the photocatalytic degradation of aqueous organic pollutants by UV-irradiated titania. *J. Catal.* **200**: 10–20.

Matos J., Garcia A., Cordero T., Chovelon J-M., Ferronato C. (2009). Eco-friendly TiO₂–AC photocatalyst for the selective photooxidation of 4-chlorophenol. *Catal Lett.***130**: 568–574.

Matos J., Laine J., Herrmann J-M., Uzcategui, J.L. Brito. (2007). Influence of activated carbon upon titania on aqueous photocatalytic consecutive runs of phenol photodegradation. *Applied Catalysis B: Environmental* **70**: 461–469.

Mattson J.S., Mark H.B. Jr., Malbin M.D., Weber W.J. Jr., Crittenden J.C. (1969). Surface chemistry of active carbon: specific adsorption of phenols. *J. Colloid Interface Sci.* **31**: 116–130.

Mehrotra K., Yablonsky G.S., Ray A.K. (2003). Kinetic studies of photocatalytic degradation in a TiO₂ slurry system: Distinguishing working regimes and determining rate dependences. *Ind. Eng. Chem. Res.* **42**: 2273 –2281.

Menendez J, Phillips J, Xia B, Radovic L. (1996). On the modification and characterization of chemical surface properties of activated carbon: In the search of carbons with stable basic properties. *Langmuir* **12**: 4404-4410.

Merabet S., Bouzaza A., Wolbert D. (2009). Photocatalytic degradation of indole in a circulating upflow reactor by UV/TiO₂ process—Influence of some operating parameters. *J. Hazard.Mater.,166(2-3):1244-1249.*

Merle T. (2009). Thèse du LISBP à l'INSA de Toulouse (France).

Merle T., Pic J.-S., Manero M-H., Debellefontaine H. (2010). Comparison of Activated Carbon and Hydrophobic Zeolite Efficiencies in 2,4-Dichlorophenol Advanced Ozonation, *Ozone: Science & Engineering: The Journal of the International Ozone Association* **32** (6): 391 - 398.

Mijangos F, Varona F, Villota N. (2006). Changes in solution color during phenol oxidation by Fenton reagent. *Environ Sci Technol.* **40** (17): 5538-43.

Mills A., McFarlane M. (2007). Current and possible future methods of assessing the activities of photocatalyst films. *Catalysis Today*, **129**(1-2): 22–28.

Mills A, Elliott N, Parkin IP, O'Neill SA, Clark RJ. (2002). Novel TiO₂ CVD films for semiconductor photocatalysis. *J. Photochem Photobiol A* **15**:171–9.

Minero C., Catozzo F., Ezio P. (1992). Role of adsorption in photocatalyzed reactions of organic molecules in aqueous TiO₂ suspension. *Langmuir* **8**: 481–486.

Mirkhani V., Tangestaninejad S., Moghadam M., Habibi M.H., Rostami-Vartooni A. (2009). Photocatalytic Degradation of Azo Dyes Catalyzed by Ag Doped TiO₂ Photocatalyst. *J. Iran. Chem. Soc.*, **6** (3): 578-587.

Moene R, Boon HT, Schoonman J, Makkee M, Moulijn JA. (1996). Coating of activated carbon with silicon carbide by chemical vapor deposition. *Carbon* **34**: 567–79.

Moreno-Castilla C. (2004). Adsorption of organic molecules from aqueous solutions on carbon materials. *Carbon* **42**: 83–94.

Moreno-Castilla C, Rivera-Utrilla J, Joly JP, López- Ramon LV, Ferro-García MA, Carrasco-Marín F (1995a). Thermal regeneration of an activated carbon exhausted with different substituted phenols. *Carbon* **33**(10):1417–23.

Moreno-Castilla C., Rivera-Utrilla J., López-Ramón M.V., Carrasco-Marin F. (1995b). Adsorption of some substituted phenols on activated carbons from a bituminous coal. *Carbon* **33**: 845-851.

Moser, J., S. Punchihewa, P.P. Infelta, M. Grätzel. (1991). Surface complexation of colloidal semiconductors strongly enhanced interfacial electron-transfer rates. *Langmuir*, **7**(12): 3012-3018.

Muranaka C.T., C. Julcour- Lebigue, A.M. Wilhelm, H. Delmas, and C.A.O. Nascimento (2010). Regeneration of activated carbon by (photo)Fenton oxidation for the treatment of phenol wastewater, *Ind. Eng. Chem. Res.* **49**: 989–995.

N

Na Y.S., Song S.K., Park Y.S. (2005). *Korean J. Chem. Eng.*, **22**: 196.

Naeem K., Feng O. (2009). Parameters effect on heterogeneous photocatalysed degradation of phenol in aqueous dispersion of TiO₂. *Journal of Environmental Sciences* **21**: 527–533.

Nakhla G., Abuzaid N., Farooq S. (1994). Activated carbon adsorption of phenolics in oxic systems: Effect of pH and temperature variations. *Water Environ. Res.*, **66**(6): 842-850.

Namasivayam C., Sangeetha D. (2005). Kinetic studies of adsorption of thiocyanate onto ZnCl₂ activated carbon from coir pith, an agricultural solidwaste, *Chemosphere* **60**: 1616–1623.

Narbaitz R. M., Cen J. (1997). Alternative methods for determining the percentage regeneration of activated carbon. *Water Research* **31** (10): 2532-2542.

Neppolian B., Choi H.C., Sakthivel S., Arabindoo B., Murugesan B.V. (2002a). *Chemosphere*, **46**: 1173.

Neppolian B., Choi H.C., Sakthivel S., Arabindoo B., Murugesan V. (2002b). Solar/UV induced photocatalytic degradation of three commercial textile dyes, *J. Hazard. Mater.* **89**: 303–317.

Noh J. S., Schwarz J. A. (1989). *J. Colloid Interface Sci.* **130**: 157.

O

Okada K., Yamamoto N., Kameshima Y., Yasumori A. (2003). Porous properties of activated carbons from waste newspaper prepared by chemical and physical activation, *J. Colloid Interface Sci.* **262**: 179–193.

Okamoto K., Yamamoto Y., Tanaka H., Tanaka M., Itaya A. (1985). Heterogeneous photocatalytic decomposition of phenol over TiO₂ powder, *Bull. Chem. Soc. Jpn.* **58**: 2015-2022.

Okawa, K., Suzuki, K., Takeshita, T., Nakano, K. (2007). Regeneration of Granular Activated Carbon with Adsorbed Trichloroethylene Using Wet Peroxide Oxidation. *Water Res.*, **41**: 1045-1051.

Ortiz-Gomez A., Serrano-Rosales B., de Lasa H. (2008). *Chem. Eng. Sci.* **63**: 520–558.

Otero M., Rozada F., Calvo L.F., Garc'ia A.I., Mor'an A. (2003a). Kinetic and equilibrium modelling of the methylene blue removal from solution by adsorbent materials produced from sewage sludges, *Biochem. Eng. J.* **15**: 59–68.

Otero M., Rozada F., Calvo L.F., Garc'ia A.I., Mor'an A. (2003b). Elimination of organic water pollutants using adsorbents obtained from sewage sludge. *Dyes and Pigments* **57**: 55–65.

Ozacar M., Sangil I.A. (2003). Adsorption of reactive dyes on calcined alunite from aqueous solutions. *J. Hazard. Materials B***98**: 211- 224.

P

Palmer, F.L., Eggins B.R., Coleman H.M. (2002). The effect of operational parameters on the photocatalytic degradation of humic acid. *J. Photochem. Photobiol. A Chem.*, **148** (1-3): 137-143.

Pan B., Pan Bi, Zhang W., Zhang Q., Zhang Q., Zheng S. (2008). Adsorptive removal of phenol from aqueous phase by using a porous acrylic ester polymer. *Journal of Hazardous Materials* **157** (2-3): 293-299.

Pardeshi S.K., Patil A.B. (2008). A simple route for photocatalytic degradation of phenol in aqueous zinc oxide suspension using solar energy. *Solar Energy* **82**: 700–705.

Park S-j, Chin S.S., Jia Y., Fane A.G. (2010). Regeneration of PAC saturated by bisphenol A in PAC/TiO₂ combined photocatalysis system. *Desalination* **250**: 908–914.

Pecchi, G., Reyes, P., Sanhueza, P., Villasenor, J. (2001). Photocatalytic degradation of pentachlorophenol on TiO₂ sol-gel catalysts. *Chemosphere* **43**: 141–146.

Pelekani C., Snoeyink V.L. (2000). Competitive adsorption between atrazine and methylene blue on activated carbon: the importance of pore size distribution. *Carbon* **38**: 1423–1436.

Pelizzetti E., Minero C. (1993). *Electrochimica acta* **38**: 47-55..

Pera-Titus M., Garćia-Molina V., B̃anos M., Gim´enez J., Esplugas S. (2004). *Appl. Catal. B* **47**: 219.

Piscopo A., Robert D., Weber J.V. (2001). Influence of pH and chloride on the photocatalytic degradation of organic compounds. I. Effect on the benzamide and *para*-hydroxybenzoic acid in TiO₂ aqueous solution. *Appl.Catal. B: Environ.*, **35**: 117–124.

Petit N. (2007). Couplage des procédés d’asorption sur charbon actif et de photocatalyse TiO₂/UV pour l’élimination de composés organiques volatiles. Thèse de l’Université de Rennes1 (France).

Poulios I., Makri D., Prohaska X. (1999). Photocatalytic treatment of olive milling waste water: oxidation of protocatechuic acid. *Global Nest: the Int. J.*, **1** (1): 55-62.

Pozzo R.L., Baltan M.A., Cassano A.E. (1997). *Catal. Today* **39**: 219.

Prakash D. Vaidya, Vijaykumar V. Mahajani. (2002). Insight into heterogeneous catalytic wet oxidation of phenol over a Ru/TiO₂ catalyst. *Chemical Engineering Journal* **87**: 403–416.

Q

Qamar M., Muneer M., Bahnemann D. (2006). Heterogeneous photocatalysed degradation of two selected pesticide derivatives, triclopyr and daminozid in aqueous suspensions of titanium dioxide. *Journal of Environmental Management*, **80**: 99–106.

Qamar, M., Saquib M., Muneer M.(2005a). Semiconductor-mediated photocatalytic degradation of an azo dye, chrysoidine Y in aqueous suspensions. *Desalination*, **171**(2): 185-193.

Qamar, M., Muneer M. (2005). Comparative photocatalytic study of two selected pesticide derivatives, indole-3-acetic acid and indole-3-butyric acid in aqueous suspensions of titanium dioxide. *J. Hazard. Mater.*, **120** (1-3): 219-227.

Quintanilla A., Casas J.A., Zazo J.A., Mohedano A.F. and Rodriguez J.J., (2006). *Appl. Catal. B: Environ.*, **62**: 115–120.

Quintanilla A., Casas J.A., Rodríguez J.J. (2007). Catalytic wet air oxidation of phenol with modified activated carbons and Fe/activated carbon catalysts. *Applied Catalysis B: Environ.*, **76**(1-2) :135-145.

R

Rabindranathan S., Suja D.P., Yesodharan S. (2003). Photocatalytic degradation of phosphamidon on semiconductor oxides. *J. Hazard. Mater.*, B **102**: 217– 229.

Radovic, L.R. (1999). Surface chemistry of activated carbon materials: state of the art and implications for adsorption, in: J.A. Schwarz, C.I. Contescu (Eds.), *Surfaces of Nanoparticles and Porous Materials*, Marcel Dekker, NewYork, pp. 529–565.

Radovic L. R., Moreno-Castilla C., Rivera-Utrilla J. (2001). Carbon materials as adsorbents in aqueous solutions. In *Chemistry and Physics of Carbon, Vol. 27*; Radovic, L. R., Ed.; Marcel Dekker: New York, pp 227-405.

Radovic, L. R. (2001). *Chemistry and Physics of Carbon*. 1st Edition ed., Marcel Dekker, New York, NY, USA.

- Rahmani AR., Samadi MT, Enayati M. A. (2008).** Investigation of Photocatalytic Degradation of Phenol by UV/TiO₂ Process in Aquatic Solutions. *J. Res. Health Sci.*, **8** (2): 55-60.
- Rao J.R., Viraraghavan T. (2002).** Biosorption of phenol from an aqueous solution by *Aspergillus niger* biomass. *Bioresour. Technol.* **85**: 165–171.
- Rao N.N., Dubey A.K., Mohanty S., Khare P., Jain R., Kaul S.N. (2003).** Photocatalytic degradation of 2-chlorophenol: a study of kinetics, intermediates and biodegradability, *J. Hazard. Mater.* **B101**: 301–314.
- Rao M.M., Ramesh A., G.P. Rao, K. Sessaiah (2006).** Removal of copper and cadmium from the aqueous solutions by activated carbon derived from *Ceiba pentandra* hulls. *J. Hazard. Mater.* **129**: 123–129.
- Ravichandran L., Selvam K., Swaminathan M. (2010).** Highly efficient activated carbon loaded TiO₂ for photo defluoridation of pentafluorobenzoic acid. *Journal of Molecular Catalysis A: Chemical* **317**: 89–96.
- Reddy S.S., Kotaiah B. (2006).** Comparative avaluation of commercial and sewage sludge based activated carbons for the removal of textile dyes from aqueous solutions. *Iran J. Environ. Health Sci. Eng.* **3** (4): 239- 246.
- Reeves P., Ohlhausen R., Sloan D., Pamplin K., Scoggins T., Clark C., Hutchinson B., Green D. (1992).** Photocatalytic destruction of organic dyes in aqueous TiO₂ suspensions using concentrated simulated and natural solar energy. *Solar Energy* **48** (6): 413-420.
- Reuge N, Dexpert-Ghys J, Caussat B. (2010).** Fluidized-Bed MOCVD of Bi₂O₃ Thin Films from Bismuth Triphenyl under Atmospheric Pressure. *Chemical Vapor Deposition*, **16** (4-6): 123.
- Reyes C., Fern J. ´andez, Freer J., Mondaca M.A., Zaror C., Malato S., Mansilla H.D. (2006).** *J. Photochem. Photobiol. A: Chem.* **184**: 141-146.

- Rideh L, Wehrer A., Ronze D., Zoulalian A. (1997).** Photocatalytic Degradation of 2-Chlorophenol in TiO₂ Aqueous Suspension: Modeling of Reaction Rate. *Ind. Eng. Chem. Res.*, **36**: 4712-4718
- Rio S., C. Faur, L. Le Coq, P. Le Cloirec (2005a).** Structure characterization and adsorption properties of pyrolyzed sewage sludge. *Environ Sci. Technol.* **39**: 4249-4257.
- Rio S., C. Faur, L. Le Coq, P. Courcoux, P. Le Cloirec (2005b).** Experimental design methodology for the preparation of carbonaceous sorbents from sewage sludge by chemical activation: application to air and water treatments. *Chemosphere* **58**: 423-437.
- Rio S., L. Le Coq, C. Faur, P. Le Cloirec (2006).** Production of porous carbonaceous adsorbent from physical activation of sewage sludge: application to wastewater treatment. *Water Sci Technol.*, **53**: 237-44.
- Rivera-Utrilla J., Bautista-Toledo I., Ferro-Garcia M.A., Moreno-Castilla C. (2001).** *J. Chem. Technol. Biotechnol.*, **76**: 1209–1215.
- Rivera-Utrilla J., Sanchez-Polo, M. (2002).** The role of dispersive and electrostatic interactions in the aqueous phase adsorption of naphthalenesulphonic acids on ozone-treated activated carbons. *Carbon*, **40**: 2685-2691.
- Robert D., Malato S. (2002).** Solar photocatalysis: a clean process for water detoxification. *Sci. Total Environ.* **291**: 85–97.
- Robert D., Parra S., Pulgarin C., Krzton A., Weber J.V. (2000).** Chemisorption of phenols and acids on TiO₂ surface. *Appl. Surf. Sci.*, **167**: 51-58.
- Rodriguez-Reinoso F., A Linares-Solano. (1989).** Chemistry and physics of carbon: a series of advances (P.A.Thrower, Ed.), Marcel Dekker, Inc., New York.

Rodríguez M. (2003). Fenton and UV-vis based advanced oxidation processes in wastewater treatment: Degradation, mineralization and biodegradability enhancement. University of Barcelona, Spain.

Rozada F., Otero M., A. Mor'an, A.I. Garc'ia. (2005). Activated carbons from sewage sludge and discarded tyres: Production and optimization. *Journal of Hazardous Materials B124*: 181–191.

Rozada F., Calvo L.F., A.I. Garc'ia, J. Mart'ın-Villacorta, M. Otero (2003). Dye adsorption by sewage sludge-based activated carbons in batch and fixed-bed systems. *Bioresour. Technol.* **87**: 221–230.

Ruan S., Wu F., Zhang T., Gao W., Xu B., Zhao M. (2001). *Mater. Chem. Phys.* **69**: 7.

S

Safarzadeh-Amiri, A. (2001). O₃/H₂O₂ treatment of methyl-*tert*-butyl ether (MTBE) in contaminated waters. *Wat. Res.*, **35** (15): 3706 -3714.

Salem I. (2003). Recent studies on the catalytic activity of titanium, zirconium, and hafnium oxides. *Catalysis Reviews*, **45**: 205–296.

Sano T., Puzenat E., Guillard C., Geantet C., Matsuzawa S. (2008). Degradation of C₂H₂ with modified-TiO₂ photocatalysts under visible light irradiation. *J. Mol. Catal. A-Chem.* **284**: 127–133.

Santos A., Yustos P., Quintanilla A., Rodr'iguez S., Garc'ia-Ochoa F. (2002). *Appl. Catal. B: Environ.* **39**: 97–113.

Saquib M., Muneer M. (2003). Titanium dioxide mediated photocatalyzed degradation of a textile dye derivative, acid orange 8, in aqueous suspensions. *Desalination* **155** (3): 255-263.

Sauer, T.G., C. Neto, H.J. José, R.F.P.M. Moreira. (2002). Kinetics of photocatalytic degradation of reactive dyes in a TiO₂ slurry reactor. *J. Photochem. Photobiol. A Chem.*, **149** (1-3): 147-154.

Selvam K., Muruganandham M., Muthuvel I., Swaminathan M. (2007). *Chem. Eng. J.* **128**: 51-57.

Serp P., Kalck P. (2002). Chemical vapor deposition methods for the controlled preparation of supported catalytic materials. *Chem. Rev.*, **102**: 3085–128.

Serpone, N. (1995). Brief introductory remarks on heterogeneous photocatalysis. *Sol. Energy Mat. Sol. Cell.*, **38**(1-4): 369-379.

Shankar M.V., Anandan S., Venkatachalam N., Arabindoo B., Murugesan V. (2004a). Novel thin-film reactor for photocatalytic degradation of pesticides in aqueous solutions. *J. Chem. Technol. Biotechnol.*, **79**: 1279–1285.

Shankar M.V., Cheralathan K.K., Arabindoo B., Palanichamy M., Murugesan V. (2004b). Enhanced photocatalytic activity for the destruction of monocrotophos pesticide by TiO₂/H₂O₂. *J. Mol. Catal.* **223**: 195–200.

Shen W., Li Z., Liu Y. (2008). Surface Chemical Functional Groups Modification of Porous Carbon. *Recent Patents on Chemical Engineering* **1**: 27-40.

Shi J., Zheng J., Wua P., Ji X.. (2008). Immobilization of TiO₂ films on activated carbon fiber and their photocatalytic degradation properties for dye compounds with different molecular size. *Catalysis Communications* **9**: 1846–1850.

Shon H.K., Vigneswaran S., Ngo H.H., Kim J.H. (2005). Chemical coupling of photocatalysis with flocculation and adsorption in the removal of organic matter. *Water Res.* **39**: 2549 –2558.

Silva C. A., Madeira L. M., Boaventura R. A., Costa C. A. (2004). Photo-oxidation of cork manufacturing wastewater. *Chemosphere* **55**: 19–26.

Silva C. G., Faria J. L. (2009). Effect of key operational parameters on the photocatalytic oxidation of phenol by nanocrystalline sol–gel TiO₂ under UV irradiation. *Journal of Molecular Catalysis A: Chemical* **305**: 147–154.

Silva A.M.T., Nouli E., Xekoukoulotakis N. P., Mantzavinos D. (2007). Effect of key operating parameters on phenols degradation during H₂O₂-assisted TiO₂ photocatalytic treatment of simulated and actual olive mill wastewaters. *Applied Catalysis B: Environmental* **73**: 11–22.

Singh H.K., Saquib M., Haque M.M., Muneer M., Bahnemann D.W. (2007). *J. Mol. Catal. A: Chem.* **264**: 66 -72.

Singh K. P., Malik A., Sinha S., Ojha P. (2008). Liquid-phase adsorption of phenols using activated carbons derived from agricultural waste material. *J. Hazard.Mater.*, **150**: 626–641.

So C.M., Cheng M.Y., Yu J.C., Wong P.K. (2002). Degradation of azo dye Procion Red MX-5B by photocatalytic oxidation. *Chemosphere* **46**: 905–912.

Sobczynski A., Duczmal L., Zmudzinski W. (2004). Phenol destruction by photocatalysis on TiO₂: an attempt to solve the reaction mechanism. *J. Mol. Catal. A: Chem.* **213**: 225–230.

Song P., Irie Y., Shigesato Y. (2006). Crystallinity and photocatalytic activity of TiO₂ films deposited by reactive sputtering with radio frequency substrate bias. *Thin Solid Films*, **496** (1): 121-125.

Sopyan I, Watanabe M, Murasawa S. et al. (1996). An efficient TiO₂ thin-film photocatalyst: Photocatalytic properties in gas-phase acetaldehyde degradation. *J Photochem Photobiol A*, **98** (1-2): 79- 86.

Slokar Y.M., Marechal A.M.L. (1998). Methods of decoloration of textile wastewaters. *Dyes Pigments* **37**: 335–356.

Sricharoenchaikul V., Pechyen C., Aht-ong D., Atong D. (2008). Preparation and Characterization of Activated Carbon from the Pyrolysis of Physic Nut (*Jatropha curcas* L.) Waste. American Chemical Society.

Srivastava S. K., Tyagi R. (1995). Competitive adsorption of substituted phenols by activated carbon developed from the fertilizer waste slurry. *Water. Res.* **29**: 483–488.

Stoeckli F., Hugi-Cleary D. (2001). On the mechanisms of phenol adsorption by carbons. *Russ. Chem. B* **50**: 2060–2063.

Stratakis G.A., Stamatelos A.M. (2003). Thermogravimetric analysis of soot emitted by a modern diesel engine run on catalyst-doped fuel. *Combustion and Flame* **132**: 157–169.

Stumm, W. (1992). *Chemistry of the Solid-Water Interface*, John Wiley & Sons, New York, USA.

Stumm W., Morgan J.J. (1981). *Aquatic chemistry*, 2nd edn. Wiley, New York, p 463.

Stylidi M., Kondarides D.I., Verykios X. E. (2003). Pathways of solar light-induced photocatalytic degradation of azo dyes in aqueous TiO₂ suspensions. *Applied Catalysis B: Environmental* **40** (4): 271-286.

Subramani A.K., Byrappa K., Kumaraswamy G.N., Ravikumar H.B., Ranganathaiah C., Rai K.M. L., Ananda S., Yoshimura M. (2007). Hydrothermal preparation and characterization of TiO₂:AC composites. *Materials Letters* **61**: 4828–4831.

Suhas P.J.M., M.M.L. R. Carrot. (2007). Lignin-from natural adsorbent to activated carbon: a review. *Bioresour. Technol.*, **98**: 2301–2312.

Sun J., Wang X., Sun J., Sun R., Sun S., Qiao L. (2006). Photocatalytic degradation and kinetics of Orange G using nano-sized Sn(IV)/TiO₂/AC photocatalyst, *J. Mol. Catal. A: Chem.* **260**: 241–246.

Sun L.M., Meunier F. (2003). Adsorption. Aspects théoriques, Tech. Ing. Génie Procédés, **J2** : J2730.1–J2730.16.

Sunder M., Hempel D.-C. (1997). Oxidation of tri- and perchloroethene in aqueous solution with ozone and hydrogen peroxide in a tube reactor. *Wat. Res.* **31**(1): 33-40.

Suwanprasop S (2005). I-Aromatisation de n-hexane et d'essence sur zéolithe ZSM-5. II-Oxydation catalytique en voie humide du phenol sur charbon actif. Thèse de l'INP Toulouse (France).

T

Tanaka K., Padermpole K., Hisanaga T. (2000). Photocatalytic degradation of commercial of azo dyes. *Wat. Res.* **34** (1): 327-333.

Tang D., Zheng Z., Lin K., Luan J., Zhang J.. (2007). Adsorption of *p*-nitrophenol from aqueous solutions onto activated carbon fiber. *Journal of Hazardous Materials* **143**: 49–56.

Tanguay J.F., Suib S.L., Coughlin R.W. (1989). *J. Catal.* **117**: 335.

Tao Y., Schwartz S., Wu C.Y., Mazyck D.W. (2005). *Ind. Eng. Chem. Res.* **44**: 7366.

Tao Y., Wu C-Y., Mazyck D. W. (2006). Removal of methanol from pulp and paper mills using combined activated carbon adsorption and photocatalytic regeneration. *Chemosphere* **65**: 35–42.

Tay J.H., Chen X.G., Jeyaseelan S., Graham N. (2001). A comparative study of anaerobically digested and undigested sewage sludges in preparation of activated carbons. *Chemosphere* **44**: 53–57.

Tchobanoglous, G., Burton, F. L., Stenset, H. D. (2003). *Wastewater Eng, Treatment and Reuse.* 4th Edition ed. McGraw-Hill Edition, New York, NY, USA.

- Terzian R., Serpone N., Minero C., Pelizzetti E. (1991).** Photocatalyzed mineralization of cresols in aqueous media with irradiated titania. *Journal of Catalysis* **128** (2): 352-365.
- Terzyk A.P. (2004).** Molecular properties and intermolecular forces—factors balancing the effect of carbon surface chemistry in adsorption of organics from dilute aqueous solutions. *J. Colloid Interface Sci.* **275**: 9–29.
- Tessmer, C. H., Vidic, R. D., Uranowski, L. J. (1997).** Impact of oxygen-containing surface functional groups on activated carbon adsorption of phenols. *Environ. Sci. Technol.*, **31**(7): 1872-1878.
- Thevenet F., Guaitella O., Herrmann J. M., Rousseau A., Guillard C. (2005).** Photocatalytic degradation of acetylene over various titanium dioxide-based photocatalysts. *Appl. Catal. B: Environ.*, **61**(1-2) : 58-68.
- Thibaud-Erkey C., Guo Y., Erkey C., Akgerman A. (1996).** *Environ. Sci. Technol.* **30**: 2127.
- Tompkins, D. T., Lawnicki, B. J., Zeltner, W. A., and Anderson, M. A. (2005).** Evaluation of photocatalysis for gas-phase air cleaning part 1: Process, technical and sizing considerations. *ASHRAE Transactions*, **111**(2): 60-84.
- Toyoda M., Nanbu Y., Kito T., Hiranob M., Inagaki M. (2003).** Preparation and performance of anatase-loaded porous carbons for water purification. *Desalination* **159**: 273–282.
- Tunay O., Kabdasli I., Eremektar G., Orhon D. (1996).** Color removal from textile wastewaters. *Water Sci. Technol.* **34**: 9–16.
- Turchi, C. S., Ollis, D. F. (1990).** Photocatalytic Degradation of Organic-Water Contaminants Mechanisms Involving Hydroxyl Radical Attack. *Journal of Catalysis* **122**: 178-192.

Turmuzi M., Daud W.R.M., Tasirin S.M., Takriff M.S., Iyuke S.E. (2004). Production of activated carbon from candlenut shell by CO₂ activation. *Carbon* **42**: 423–460.

Trillas, M., Peral J., Domènech X. (1995). Redox photodegradation of 2,4-dichlorophenoxyacetic acid over TiO₂. *Appl. Catal. B Environ.*, **5** (4): 377-387.

Tryba B., Morawski A.W., Inagaki M. (2003). Application of TiO₂-mounted activated carbon to the removal of phenol from water. *Appl. Catal. B* **41**: 427–33.

Tryk D. A., Fujishima A., Honda K. (2000). Recent Topics in Photoelectrochemistry: Achievements and Future Prospects. *Electrochimica Acta*, **45**: 2363.

Tsai W-T., Leeb M-K., Suc T-Y., Changa Y-M. (2009). Photodegradation of bisphenol-A in a batch TiO₂ suspension reactor. *Journal of Hazardous Materials* **168**: 269–275.

Tsumura T., Kojitani N., Umemura H., Toyoda M., Inagaki M. (2002). Composites between photoactive anatase-type TiO₂ and adsorptive carbon. *Appl. Surf. Sci.*, **196**: 429–36.

U

Uranowski L.J., Tessmer C.H., Vidic R.D. (1998). The effect of surface metal oxides on activated carbon adsorption of phenolics. *Water Res.* **32**: 1841–1851.

V

Vasiljevic T., Spasojevic J., Bacic M., Onjia A., Lausevic M. (2006). Adsorption of phenol and 2,4-dinitrophenol on activated carbon cloth: the influence of sorbent surface acidity and pH. *Sep. Sci. Technol.* **41**: 1061–1075.

Vázquez G., González-Álvarez J., García A.I., Freire M.S., Antorrena G. (2007). Adsorption of phenol on formaldehyde-pretreated *Pinus pinaster* bark: equilibrium and kinetics. *Bioresour. Technol.*, **98**: 1535–1540.

Venkatachalam N., Palanichamy M., Murugesan V. (2007). Sol-gel preparation and characterization of alkaline earth metal doped nano TiO₂: efficient photocatalytic degradation of 4- chlorophenol. *J. Mol. Catal. A: Chem.* **273**: 177–185.

Verhoeven J. W. (1996). Glossary of Terms Used in Photochemistry. *Pure and Applied Chemistry*, **68**: 2223.

Vidic, R. D., Tessmer, C. H. & Uranowski, L. J. (1997). Impact of surface properties of activated carbons on oxidative coupling of phenolic compounds. *Carbon* **35**(9): 1349-1359.

Vidic, R. D., Suidan, M. T., Brenner, R. C. (1993). Oxidative coupling of phenols on activated carbon: Impact on adsorption equilibrium. *Environ. Sci. Technol.*, **27**(10): 2079-2085.

Villarreal, T.L., P. Bogdanoff, P. Salvador, and N. Alonso-Vante. (2004). Photocatalytic oxidation on nanostructured chalcogenide modified titanium dioxide. *Sol. Energy Mat. Sol. Cells*, **83**(4): 347-362.

Vione D., Minero C., Maurino V., Carlotti M.E., Picattonitto T., Pelizzetti E. (2005). *Appl. Catal. B* **58**: 79.

Vohra A., Goswami D.Y., Deshpande D.A., Block S. (2006). Enhanced photocatalytic disinfection of indoor air. *Appl. Catal. B: Environ.*, **25**: 57-65

Vora, J.J., Chauhan, S.K., Parmar, K.C., Vasava, S.B., Sharma, S., Bhutadiya, L.S. (2009). Kinetic study of application of ZnO as a photocatalyst in heterogeneous medium. *E- Journal of Chemistry* **6** (2): 531-536.

Vorontsov A.V., Savinov E.N., Smirniotis P.G. (2000). *Chem. Eng. Sci.*, **55**: 5089-5098.

W

Wang J.P., Chen Y.Z., Feng H.M., Zhang S.J., Yu H.Q. (2007a). Removal of 2,4-dichlorophenol from aqueous solution by static-air-activated carbon fibers. *J. Colloid Interface Sci.* **313**: 80–85.

Wang J.P., Feng H.M., Yu H.Q. (2007b). Analysis of adsorption characteristics of 2,4-dichlorophenol from aqueous solutions by activated carbon fiber. *J. Hazard. Mater.* **144**: 200–207.

Wang Y.Q., Gu B., Xu W.L. (2009). Electro-catalytic degradation of phenol on several metal-oxide anodes. *J. Hazard. Mater.* **162**: 1159–1164.

Wang X., Hu Z., Chen Y., Zhao G., Liu Y., Wen Z. (2009). A novel approach towards high performance composite photocatalyst of TiO₂ deposited on activated carbon. *Applied Surface Science*, **255**: 3953–3958.

Wang X., Zhu N., Yin B. (2008). Preparation of sludge-based activated carbon and its application in dye wastewater treatment. *Journal of Hazardous Materials* **153**: 22–27.

Wang K-H., Y.-H. Hsieh, M.-Y. Chou, C.-Y. Chang, (1999). Photocatalytic degradation of 2-chloro and 2-nitrophenol by titanium dioxide suspensions in aqueous solution, *Appl. Catal. B: Environ.* **21**: 1–8.

Wilhelm P., Stephan D. (2007). *J. Photochem. Photobiol. A* **185**: 19–25.

Wu C., Lu X., Wei D., Fan J., Wang L. (2001). Photosonochemical degradation of phenol in water *Wat. Res.*, **35**: 3927–3933.

X

Xue G., Liu H., Chen Q., Hills C., Tyrer M., Innocent F. (2011). Synergy between surface adsorption and photocatalysis during degradation of humic acid on TiO₂/activated carbon composites. *J. Hazard. Mater.*, **186**: 765–772.

Y

Yang Y., Chun Y., Sheng G., Huang M. (2004). pH-dependence of pesticide adsorption by wheat-residue-derived black carbon. *Langmuir* **20**: 6736-6741.

Yang J.K., Lee S.M. (2006). Removal of Cr (VI) and humic acid by using TiO₂ photocatalysis. *Chemosphere*; **63**(10): 1677-84.

Yang X., Zou R., Huo F., Cai D., Xiao D. (2009). Preparation and characterization of Ti/SnO₂-Sb₂O₃-Nb₂O₅/PbO₂ thin film as electrode material for the degradation of phenol. *J. Hazard. Mater.* **164**: 367–373.

Yang W., Wu D., Fu R. (2008). Effect of surface chemistry on the adsorption of basic dyes on carbon aerogels. *Colloid Surf. A: Physicochem. Eng. Aspects* **312**: 118–124.

Yang R.T. (2003). *Adsorbents: Fundamentals and Applications*, John Wiley & Sons Inc., New York

Yano J., Matsuura J., Ohura H., Yamasaki S. (2005). Complete mineralization of propyzamide in aqueous solution containing TiO₂ particles and H₂O₂ by the simultaneous irradiation of light and ultrasonic waves. *Ultrasonics Sonochemistry* **12** (3): 197-203.

Yoneyama H, Torimoto T. (2000). Titanium dioxide/adsorbent hybrid photocatalysts for photodestruction of organic substances of dilute concentrations. *Catal Today* **58**: 133 – 40.

Z

Zainal Z., Keng C. S., Abdullah A. (2008). Removal of dye by immobilised photocatalyst loaded activated carbon. *The Malaysian Journal of Analytical Sciences* **12** (1): 111.

- Zang, Y., Farnood R. (2005).** Photocatalytic decomposition of methyl *tert*-butyl ether in aqueous slurry of titanium dioxide. *Appl. Catal. B Environ.*, **57**(4): 275-282.
- Zhang XW, Zhou MH, Lei LC. (2004).** Synthesis of TiO₂ supported on activated carbon by MOCVD: operation parameters study. *J. Zhejiang Univ. Sci.*, **5**: 1548–53.
- Zhang X., Zhou M., Lei L. (2005a).** Preparation of photocatalytic TiO₂ coatings of nanosized particles on activated carbon by AP-MOCVD. *Carbon*, **43** (8): 1700 - 1708.
- Zhang X, Zhou M, Lei L. (2005b).** Enhancing the concentration of TiO₂ photocatalyst on the external surface of activated carbon by MOCVD. *Mater Res. Bull.*, **40** (11): 1899-1904.
- Zhang X, Zhou M, Lei L. (2005c).** Preparation of anatase TiO₂ supported on alumina by different metal organic chemical vapor deposition methods. *Appl. Catal. A Gen.*, **282**(1-2): 285-293.
- Zhang X., Zhou M., Lei L. (2006b).** TiO₂ photocatalyst deposition by MOCVD on activated carbon. *Carbon*, **44** (2): 325- 333.
- Zhang X., Li A.M., Jiang Z.M., Zhang Q.X. (2006a).** Adsorption of dyes and phenol from water on resin adsorbents: effect of adsorbate size and pore size distribution, *J. Hazard. Mater. B137*: 1115–1122.
- Zhang X., Lei L. (2008).** Effect of preparation methods on the structure and catalytic performance of TiO₂/AC photocatalysts. *Journal of Hazardous Materials* **153**: 827–833.
- Zhang W., Zou L., Wang L. (2009).** Photocatalytic TiO₂/adsorbent nanocomposite prepared via wet chemical impregnation for wastewater treatment: a review, *Appl. Catal. A: Gen.* **71**: 1–9.
- Zhanga W., Zoua L., Wang L. (2011).** A novel charge-driven self-assembly method to prepare visible-light sensitive TiO₂/activated carbon composites for dissolved organic compound removal. *Chemical Engineering Journal* **168**: 485–492.

Zhang L., Kanki T., Sano N., Toyoda A. (2006). Pathways and kinetics on photocatalytic destruction of aqueous phenol. *Environmental Monitoring and Assessment* **115**: 395–403.

Zheng Z., Liu H., Ye J., Zhao J., Waclawik E. R., Zhu H. (2010). Structure and contribution to photocatalytic activity of the interfaces in nanofibers with mixed anatase and TiO₂ (B) phases. *Journal of Molecular Catalysis A: Chemical* **316**: 75 –82.

Zheng Y.H., Zheng L.R., Zhan Y.Y., Lin X.Y., Zheng Q., Wei K.M. (2007). Ag/ZnO heterostructure nanocrystals: synthesis, characterization and photocatalysis. *Inorg. Chem.*, **46** (17): 6980- 6986.

Zhu C., Wang L., Kong L., Yang X., Zheng S., Chen F., Maizhi F., Zong H. (2000). Photocatalytic degradation of azo dyes by supported TiO₂/UV in aqueous solution. *Chemosphere* **41**: 303–309.

Zhu B., Zou L. (2009a). Removal of color compounds from recycled water using combined activated carbon adsorption and AOP decomposition. *J. Adv. Oxid. Technol.* **12**: 47–54.

Zhu B., Zou L. (2009b). Trapping and decomposing of color compounds from recycled water by TiO₂ coated activated carbon. *J. Environ. Manage.* **90**: 3217–3225.

ANNEXES

Annexe 1: Preparation of sewage sludge activated carbons

The used sewage sludge were coming from municipal stations of water treatment: sewages DRAW and DMAD were collected from England (Little Marlow and Ashford, respectively) and the sewage DSBS from Nantes. Every batch treats approximately 250 g of the dried sewage. Firstly, the pyrolysis allows to eliminate the volatile materials to leave only the fixed carbon. The used raw sludge consists of 65.9 % volatile contents, 41 % C and 20.4 % Ash (Pullket *et al.*, 2009). Prior to carbonization, the sludges were sterilized in steam at 122 °C for 15 minutes in an autoclave, then dried to constant mass at 105-110 °C and finally ground below 10 mm in size. Subsequently, *ca.* 210 g of sample were loaded into a quartz reactor, which was then installed within a Carbolite rotary furnace (model HTR11/150). They were heated at 5 or 10 °C/min under a flowing (500 mL.min⁻¹) nitrogen atmosphere. After the desired temperature (from 250 to 1000 °C) was reached, the furnace was automatically cooled down to produce carbonized samples. This carbonization is possibly completed by the activation step to develop the porous structure. The activation may be physical (carbonization in the presence of CO₂), activation by vapour steam of water, or chemical (by addition of reagents such as K₂CO₃, KOH or KH₂PO₄).

The carbons C_DMAD and C-DRAW were synthesized by simple pyrolysis at 900 °C from dried sewages (flow of 0.5 L.min⁻¹ of N₂).

The carbons SA_DMAD and SA_DRAW were obtained after activation in the vapour at 838°C (73 and 80 min of activation, respectively, under a flow of 0.7 g.min⁻¹ of vapour steam of water mixed with the nitrogen flow and after a rise in temperature of 10 °C.min⁻¹).

Finally, the carbon CO₂ A_DSBS was produced by carbonization during one hour under 2 L.min⁻¹ of N₂ at 600 °C, followed by one hour of activation under 1.5 L.min⁻¹ of CO₂ at 875°C.

These activated carbons fabricated from three different sewages are: **C_DMAD** “Carbonised Dewatered Mesophilic Anaerobically Digested sludge” (ICL); **C_DRAW** “Carbonised Dewatered Raw sludge” (ICL); **SA_DMAD** “Steam Activated Dewatered Mesophilic Anaerobically Digested sludge” (ICL); **SA_DRAW** “Steam Activated Dewatered Raw sludge” (ICL); **CO₂ A_DSBS** “CO₂ Activated Dewatered Secondary Biological Sludge” (GEPEA) and **Hardened SA_DRAW**, obtained from material **SA_DRAW** by incorporating 5% (mass) of a binder PVA (polyvinyl acetate) to increase its hardness.

Annexe 2 – Influence of pH and presence of salt - Calculation of the Freundlich and Langmuir parameters for single solute adsorption of P and PHBA onto AC S23

The Freundlich and Langmuir were used to analyze the adsorption equilibrium. The selection of the most adequate model was performed using the Fisher's test. The model selected was that exhibited the highest value F_{calc} of Fisher parameter and having lower average of absolute relative errors (AARE).

Effect of solution pH on Fisher parameter F_{calc} and the average of absolute relative errors (AARE %) for Phenol and PHBA using Langmuir-Freundlich model

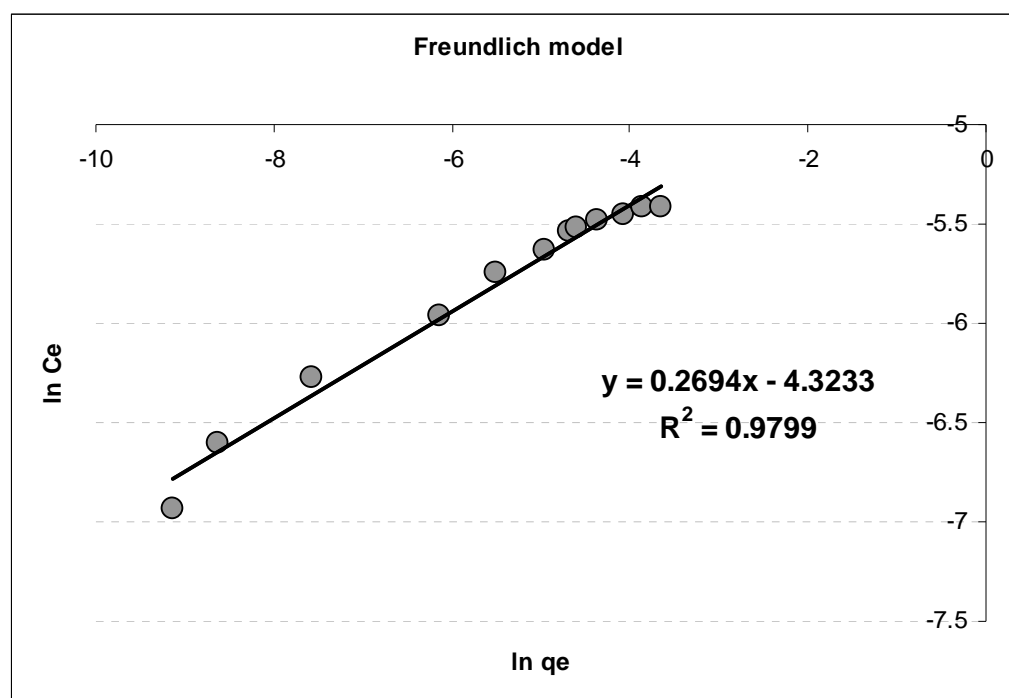
Pollutant	pH	Langmuir model				Freundlich model			
		q_{max} $mol\ g^{-1}$	K_L $L\ mol^{-1}$	F_{calc}	AARE %	$1/n$	K_F $(mol\ g^{-1} (L\ mol^{-1})^{1/n})$	F_{calc}	AARE %
Phenol	Non buffer (pH 6.3)	0.0043	8822	31	6.2	0.27	0.0056	9	15.9
	pH 2	0.0036	3480	7	13.4	0.26	0.004	15	10
	PH 7	0.0040	4126	11	27	0.24	0.007	111	0.94
	pH 10	0.0035	2413	11	32	0.25	0.005	31	6.2
PHBA	Non buffer (pH 3.5)	0.0041	301	128	4.88	0.58	0.008	11	15
	pH 2	0.0028	741	6	14	0.27	0.056	17	9
	PH 7	0.0016	3092	8	18	0.20	0.059	79	3.2
	pH 10	0.0040	17.77	3	26	0.53	0.002	5	22

2. Effect of NaCl addition on Fisher parameter F_{calc} and the average of absolute relative errors (AARE %) for Phenol and PHBA using Langmuir-Freundlich model

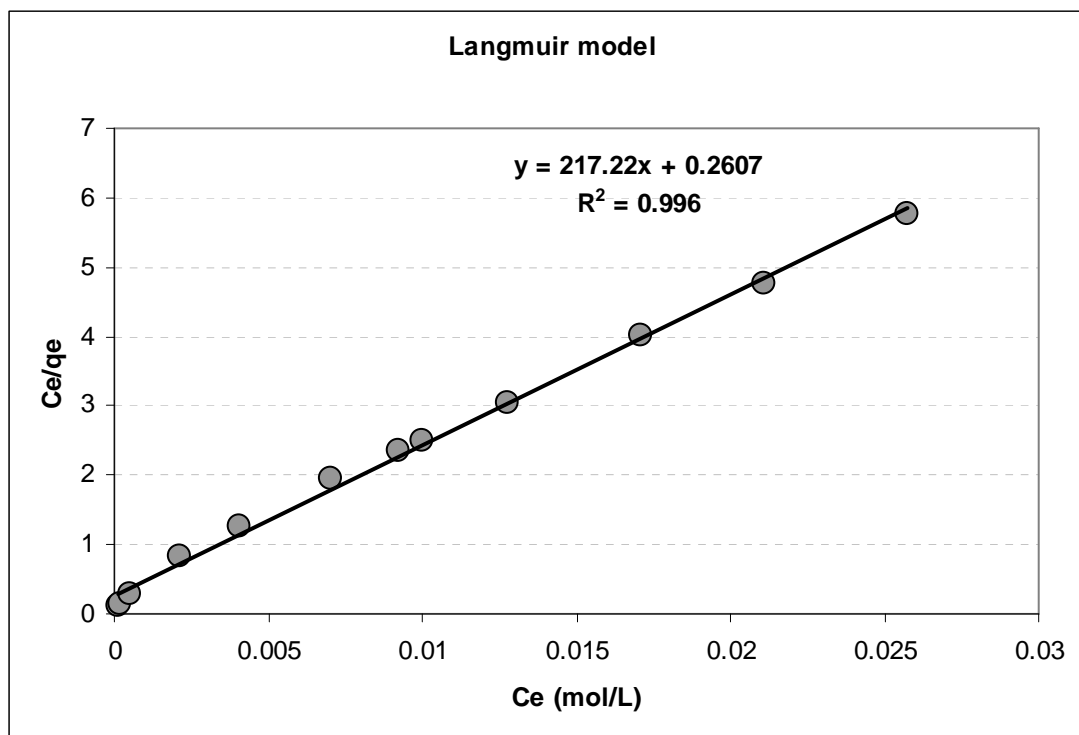
Pollutant	NaCl Conc. (g/L)	Langmuir model				Freundlich model			
		q_{max} mol g ⁻¹	K_L L mol ⁻¹	F_{calc}	AARE %	1/n	K_F (mol g ⁻¹ (L mol ⁻¹) ^{1/n})	F_{calc}	AARE %
Phenol	Without NaCl	0.0043	8822	31	6	0.27	0.0056	9	15.9
	5	0.0036	3480	7	13	0.26	0.004	15	10
	15	0.0040	4126	11	27	0.24	0.0071	111	0.94
	30	0.0035	2413	11	32	0.25	0.0055	31	6.2
	40								
PHBA	Without NaCl	0.0041	301	128	4	0.58	0.0082	11	15
	5	0.0044	610	32	8	0.55	0.011	35	6
	15	0.0049	535	28	16	0.42	0.024	26	6
	30	0.0043	1115	29	10	0.43	0.023	7	15
	40	0.0040	1119	8	7	0.44	0.022	7	9

Annexe 3: Adsorption isotherms of phenol onto AC S23 at 25°C representing by Langmuir and Freundlich models

Experimental data		Langmuir model		Freundlich model		
C_e (mol/L)	q_e (mol/g)	C_e/q_e	q_e Langmuir	$\ln q_e$	$\ln C_e$	q_e Freundlich
0.00011	0.00097	0.111340	0.000380	-9.133379	-6.938214	0.001131
0.00018	0.00136	0.132206	0.000599	-8.623665	-6.600270	0.001298
0.00052	0.00189	0.273439	0.001385	-7.567854	-6.271178	0.001725
0.00215	0.00257	0.836575	0.002954	-6.142287	-5.963849	0.002533
0.00410	0.00318	1.2735257	0.003553	-5.506572	-5.748361	0.003006
0.00704	0.00359	1.961002	0.003933	-4.956147	-5.629603	0.003487
0.00923	0.00392	2.354054	0.004073	-4.685014	-5.541153	0.003751
0.01000	0.00400	2.500000	0.004110	-4.605170	-5.521460	0.003833
0.01274	0.00418	3.047543	0.004207	-4.362773	-5.477109	0.004091
0.01712	0.00426	4.010965	0.004301	-4.067624	-5.456656	0.004430
0.02109	0.00443	4.756675	0.004355	-3.858814	-5.418362	0.004686
0.02574	0.00446	5.761103	0.004398	-3.659864	-5.410993	0.004944



Linearization of Freundlich model for phenol adsorption onto AC S23.



Linearization of Langmuir model for phenol adsorption onto AC S23.

Annexe 4 – Langmuir-Freundlich model in competitive adsorption

The Langmuir-Freundlich model was initialized with the parameters obtained from Langmuir and Freundlich models of single solute isotherms. The values of the Optimized Extend Langmuir-Freundlich model parameters were then calculated minimizing the residual sum of squares (RSS). Statistical analysis of the multi-component isotherms data obtained at 25 °C shows that the equilibrium data for all the pollutants fitted well to Langmuir - Freundlich model (Table below). For the three activated carbons, the higher values of correlation coefficient (R^2) and the lower values of residual sum of squares (RSS), the objective function values (F_{OBJ}) and the relative average deviation (RAD) obtained with this model confirm the good agreement between the experimental and calculated data for the four-component system.

Correlation coefficient (R^2) residual sum of squares (RSS) objective function values (F_{OBJ}) and the relative average deviation (RAD) for multicomponent system using Langmuir-Freundlich model

ACs	Phenols	R^2	RSS	F_{OBJ}	RAD%
S23	P	0.9945	2.88E-07	0.7765	6.4708
	PCP	0.9623			
	PNP	0.9923			
	PHBA	0.7897			
F22	P	0.9730	2.39E-08	0.0676	0.6756
	PCP	0.9949			
	PNP	0.9981			
	PHBA	0.9902			
SA_DRAW	P	0.9782	6.92E-08	0.2340	2.6002
	PCP	0.9606			
	PNP	0.9846			
	PHBA	0.9335			

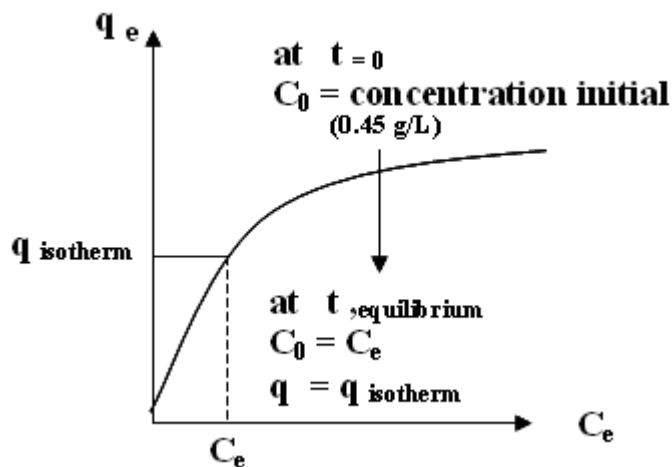
Annexe 5. Calculation of the estimated adsorbed quantities of phenol using AC/TiO₂ tissue (Ahlstrom).

The theoretical quantities of adsorbed phenol onto AC/TiO₂ tissue ($C_0 = 0.45$ g/L) without any regeneration are estimated from the isotherm and assuming that the initial concentration C_i at a given step was equal to the sum of the prepared C_0 and the phenol adsorbed at the previous adsorption step. The calculation of these quantities was as follows:

For Cycle 1:

$C_{i,1} = 0.45$ g/L (the concentration of the prepared solution C_0) at the equilibrium, the quantity of phenol adsorbed for this concentration was determined from the isotherm as represented in the following figure and it was found to be equal to 0.0588 g/g tissue.

Explication q_{isotherm}



The quantity of phenol adsorbed for the concentration of 0.45 g/L.

For Cycle 2:

$$C_{i,2} = C_0 + \left(\frac{(q_{\text{isotherm}}, \text{ at the previous cycle}) * V_t}{\text{mass of tissue}} \right)$$

Where:

q_{isotherm} : quantity of phenol adsorbed onto the tissue at the previous cycle obtained from the isotherm

V_t : total volume of the solution (2L)

C_0 : prepared concentration of initial phenol (0.45 g/L)

$$C_{i,2} = 0.45 + \left(\frac{0.0588 \times 17.5}{2} \right)$$

From the isotherm, the $q_{e,1,2}$ for this concentration (0.960 g/L) at equilibrium was 0.116 g/g adsorbant representing the quantity adsorbed at cycle 2 + the quantity adsorbed at cycle 1. So, the quantity estimated for cycle 2 = $q_{e,1,2} - q_{\text{isotherm}}$ for cycle 1.

Hence, $q_{\text{isotherm},2} = 0.116 - 0.0588 = 0.0566$ g/g adsorbant.

For cycles 3:

$$C_{i,3} = C_0 + \left(\frac{\sum (q_{\text{isotherm}}, \text{ at the previous cycles}) * V_t}{\text{mass of tissue}} \right)$$

$C_{i,3} = 1.452$ g/L, from the isotherm the quantity adsorbed at the equilibrium for this concentration = 0.145 g/g adsorbant.

So, $q_{\text{isotherm},3} = 0.145 - 0.116 = 0.03$ g/g adsorbant

The same principal was used for calculation the estimated adsorbed quantity of phenol for cycles 4 and 5.

Annexe 6. Calcul d'erreur pour Tartrazine photolyses expérimentales.

Incertitudes sur la méthode d'analyse du Tartrazine.

L'incertitude de préparation d'un échantillon est quantifiée à partir de la formule de calcul de la concentration (établie en énumérant des différentes étapes effectuées).

Pour la préparation d'une concentration initiale C_0 , il a tout d'abord été nécessaire de peser une masse (mg) de produit pur (à 99% environ) et de le diluer dans un volume déterminé d'eau distillée (V_f).

L'incertitude absolue sur la concentration initial C_0 : ΔC_0

Elle peut être calculée en suivant la même procédure que précédemment en partant de l'expression d'origine:

$$C_0 = \frac{m_p}{M_p V_f}$$

où V_f est le volume de la fiole (m^3);
 m_p - la masse du produit pesé (kg);
 M_p - la masse molaire du produit pesé ($kg \cdot mol^{-1}$).

On obtient finalement :
$$\Delta C_0 = C_0 \left(\frac{\Delta V_f}{V_f} + \frac{\Delta m_p}{m_p} \right)$$

Les incertitudes absolues associées sont :

- $\Delta m_p = 10^{-6}$ kg (balance analytique de précision)
- $\Delta V_f = 10^{-6} m^3$ pour une fiole de 0,5 L ($5 \cdot 10^{-4} m^3$); $2 \cdot 10^{-6} m^3$ pour une fiole de 1L ($10^{-3} m^3$)
- $\Delta M_p = 0$

L'incertitude relative sur la concentration à temps :

$$C_t: \frac{\Delta C_t}{C_t}$$

Elle est aussi calculée en partant de l'expression d'origine qui prend en compte une éventuelle dilution de l'échantillon avant analyse par CLHP:

$$C_t = \frac{m_2}{m_1} C_{t,CLHP}$$

On obtient :

$$\frac{\Delta C_t}{C_t} = \frac{\Delta m_2}{m_2} + \frac{\Delta m_1}{m_1} + \frac{\Delta C_{t,CLHP}}{C_{t,CLHP}}$$

où $C_{t,CLHP}$ est la concentration obtenue analytiquement par CLHP (mol.m^{-3}) ;

m_1 - la masse d'échantillon prélevée avant dilution (kg) ;

m_2 - la masse après dilution (kg).

Les incertitudes absolues associées sont :

- $\Delta m_1 = \Delta m_2 = 10^{-6}$ kg (balance)

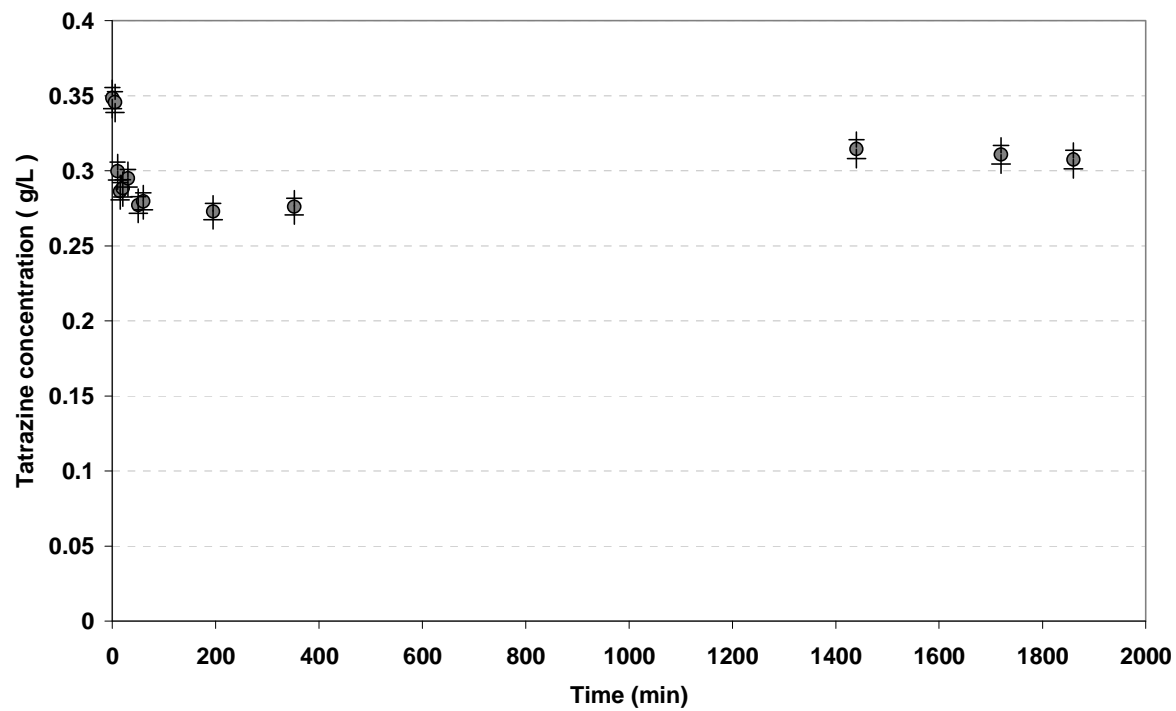
- $\frac{\Delta C_{t,CLHP}}{C_{t,CLHP}} = 0,02$

Incertitude relative sur la valeur de la concentration obtenue analytiquement par CLHP sans tenir compte de l'erreur par dilution. Elle a été estimée à 2%.

Le tableau ci-dessous indique les différentes concentrations des solutions de tartrazine diluées et analysées.

Incertitudes de la méthode analytique pour le dosage du Tatrazine.

Time	C_t (g/L)	C_t min	C_t max	ΔC_t	$\Delta C_t / C_t$
0	0.348	0.341	0.355	0.0069	2.005
5	0.345	0.338	0.352	0.0069	2.003
10	0.299	0.294	0.305	0.0060	2.003
15	0.286	0.280	0.292	0.0057	2.004
20	0.288	0.282	0.294	0.0057	2.004
30	0.295	0.289	0.300	0.0059	2.003
50	0.277	0.271	0.282	0.0055	2.003
60	0.279	0.274	0.285	0.0056	2.003
195	0.273	0.267	0.278	0.0054	2.004
352	0.2761	0.270	0.281	0.0055	2.003
1440	0.314	0.308	0.320	0.0063	2.004
1720	0.310	0.304	0.316	0.0062	2.0029
1860	0.307	0.301	0.313	0.0061	2.0038



Incertitude de calculs de la concentration de Tartrazine pour chaque point de la cinétique de Tartrazine photolyses.

Annexe 7: Distribution of particles size of the original activated carbon before TiO₂ deposition (1) and after TiO₂ by CVD method (2).

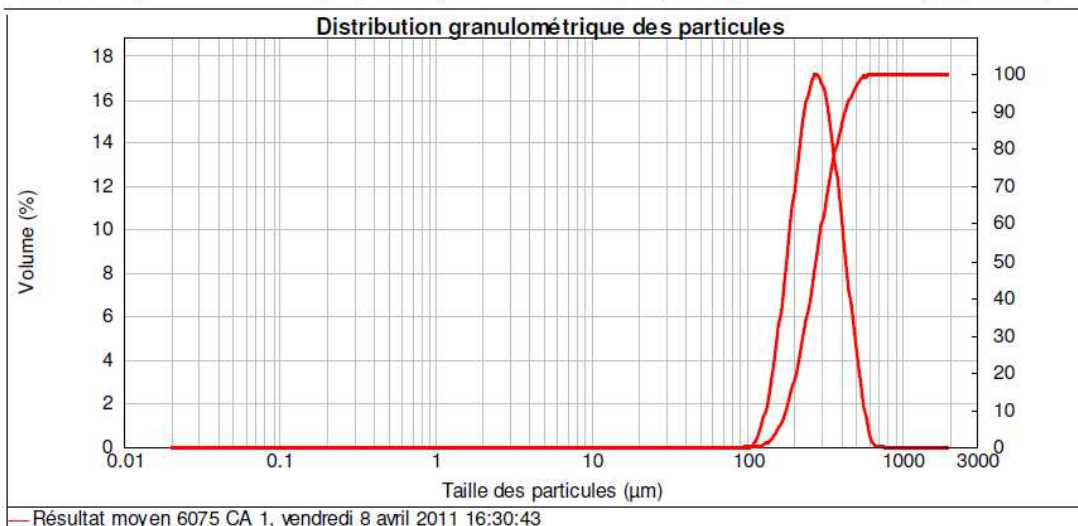

MASTERSIZER 2000

Rapport d'analyse

Echantillon: Résultat moyen 6075 CA 1	SOP: Hydro2000s Charbon elham	Mesuré : vendredi 8 avril 2011 16:30:43
	Mesuré par: Christine Rey-Rouch	Analysé : vendredi 8 avril 2011 16:30:44
Sample bulk lot ref:	Source Resultat: Moyenne établie	Vitesse : 17... Tr/min
		US : 0 %

Nom Particule: Charbon 2.42; 0.1	Accessoire: Hydro 2000S (A)	Modèle d'analyse: Analyse standard	Sensitivity: Normal
RI Particule: 2.420	Absorption: 0.1	Gamme de Mesure: 0.020 to 2000.000 um	Obscuration: 6.99 %
Dispersant: Eau	RI Dispersant: 1.330	Résiduel Pondéré: 1.108 %	Modif. de Résultat: Désactivé

Concentration: 0.2692 %Vol	Span : 0.897	Uniformité: 0.28	Type de Distribution: Volume
Surface Spécifique: 0.0229 m ² /g	Surface Weighted Mean D[3,2] ou Diamètre de Sauter : 261.549 um	Vol. Weighted Mean D[4,3] ou Diam Moyen pondéré (dm) : 291.789 um	
D(0.10) : 178.29 um	D(0.50) : 277.30 um	D(0.90) : 427.06 um	D(1.00) : 2000.00 um



Taille (µm)	Passant en %	Taille (µm)	Passant en %	Taille (µm)	Passant en %	Taille (µm)	Passant en %	Taille (µm)	Passant en %	Taille (µm)	Passant en %
0.020	0.00	0.142	0.00	1.002	0.00	7.096	0.00	50.238	0.00	356.656	76.25
0.022	0.00	0.159	0.00	1.125	0.00	7.962	0.00	56.368	0.00	399.052	85.64
0.025	0.00	0.178	0.00	1.262	0.00	8.934	0.00	63.246	0.00	447.744	92.50
0.028	0.00	0.200	0.00	1.416	0.00	10.024	0.00	70.963	0.00	502.377	96.92
0.032	0.00	0.224	0.00	1.589	0.00	11.247	0.00	79.621	0.00	563.677	99.39
0.036	0.00	0.252	0.00	1.783	0.00	12.619	0.00	89.337	0.00	632.456	99.95
0.040	0.00	0.283	0.00	2.000	0.00	14.159	0.00	100.237	0.00	709.627	100.00
0.045	0.00	0.317	0.00	2.244	0.00	15.887	0.00	112.468	0.03	796.214	100.00
0.050	0.00	0.356	0.00	2.518	0.00	17.825	0.00	126.191	0.49	893.367	100.00
0.056	0.00	0.399	0.00	2.825	0.00	20.000	0.00	141.589	1.92	1002.374	100.00
0.063	0.00	0.448	0.00	3.170	0.00	22.440	0.00	158.866	4.90	1124.683	100.00
0.071	0.00	0.502	0.00	3.557	0.00	25.179	0.00	178.250	9.99	1261.915	100.00
0.080	0.00	0.564	0.00	3.991	0.00	28.251	0.00	200.000	17.52	1415.892	100.00
0.089	0.00	0.632	0.00	4.477	0.00	31.698	0.00	224.404	27.45	1588.656	100.00
0.100	0.00	0.710	0.00	5.024	0.00	35.566	0.00	251.785	39.27	1782.502	100.00
0.112	0.00	0.796	0.00	5.637	0.00	39.905	0.00	282.508	52.10	2000.000	100.00
0.126	0.00	0.893	0.00	6.325	0.00	44.774	0.00	316.979	64.80		

Operator notes: Moyenne de 6 mesures de char - 08 avril 2011



Laboratoire de Génie Chimique
UMR 5503 CNRS-UPS-INP/ENSIACET
Campus Labège
4 allée Emile Momo - BP 84234
31030 Toulouse cedex 4
Tél : +33 (0) 534 323 600
Fax : +33 (0) 534 323 700
http://lge.inp-toulouse.fr



MASTERSIZER 2000

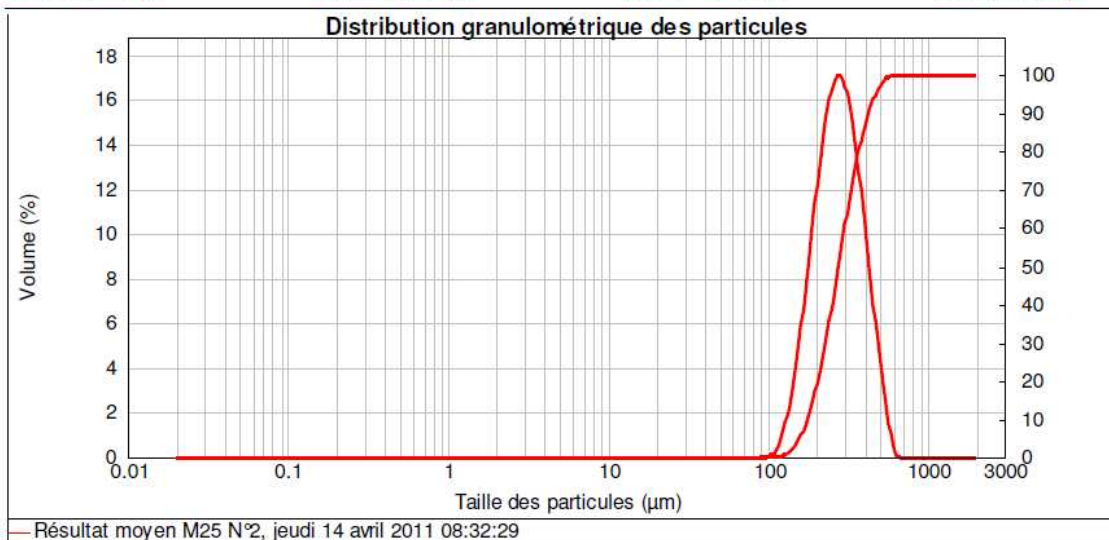
Rapport d'analyse

Echantillon: Résultat moyen M25 N°2	SOP:	Mesuré : jeudi 14 avril 2011 08:32:29
	Mesuré par: Christine Rey-Rouch	Analysé : jeudi 14 avril 2011 08:32:30
Sample bulk lot ref:	Source Resultat: Moyenne établie	Vitesse : 17... Tr/min
		US : 0 %

Nom Particule: Carbon	Accessoire: Hydro 2000S (A)	Modèle d'analyse: Analyse standard	Sensitivity: Normal
RI Particule: 2.420	Absorption: 1	Gamme de Mesure: 0.020 to 2000.000	Obscuracion: um 7.96 %
Dispersant: Water	RI Dispersant: 1.330	Résiduel Pondéré: 1.135 %	Modif. de Résultat: Désactivé

Concentration: 0.3033 %Vol	Span : 0.896	Uniformité: 0.279	Type de Distribution: Volume
Surface Spécifique: 0.0233 m ² /g	Surface Weighted Mean D[3,2] ou Diamètre de Sauter : 257.363 µm	Vol. Weighted Mean D[4,3] ou Diam Moyen pondéré (dm) : 287.123 µm	

D(0.10) : 175.30 µm D(0.50) : 273.19 µm D(0.90) : 420.10 µm D(1.00) : 610.99 µm



Taille (µm)	Passant en %	Taille (µm)	Passant en %	Taille (µm)	Passant en %	Taille (µm)	Passant en %	Taille (µm)	Passant en %	Taille (µm)	Passant en %
0.020	0.00	0.142	0.00	1.002	0.00	7.096	0.00	50.238	0.00	356.656	77.63
0.022	0.00	0.159	0.00	1.125	0.00	7.962	0.00	56.368	0.00	399.052	86.74
0.025	0.00	0.178	0.00	1.262	0.00	8.934	0.00	63.246	0.00	447.744	93.31
0.028	0.00	0.200	0.00	1.416	0.00	10.024	0.00	70.963	0.00	502.377	97.45
0.032	0.00	0.224	0.00	1.589	0.00	11.247	0.00	79.621	0.00	563.677	99.63
0.036	0.00	0.252	0.00	1.783	0.00	12.619	0.00	89.337	0.00	632.456	100.00
0.040	0.00	0.283	0.00	2.000	0.00	14.159	0.00	100.237	0.01	709.627	100.00
0.045	0.00	0.317	0.00	2.244	0.00	15.887	0.00	112.468	0.08	796.214	100.00
0.050	0.00	0.356	0.00	2.518	0.00	17.825	0.00	126.191	0.66	893.367	100.00
0.056	0.00	0.399	0.00	2.825	0.00	20.000	0.00	141.589	2.29	1002.374	100.00
0.063	0.00	0.448	0.00	3.170	0.00	22.440	0.00	158.866	5.54	1124.683	100.00
0.071	0.00	0.502	0.00	3.557	0.00	25.179	0.00	178.250	10.92	1261.915	100.00
0.080	0.00	0.564	0.00	3.991	0.00	28.251	0.00	200.000	18.76	1415.892	100.00
0.089	0.00	0.632	0.00	4.477	0.00	31.698	0.00	224.404	28.93	1588.656	100.00
0.100	0.00	0.710	0.00	5.024	0.00	35.566	0.00	251.785	40.91	1782.502	100.00
0.112	0.00	0.796	0.00	5.637	0.00	39.905	0.00	282.508	53.77	2000.000	100.00
0.126	0.00	0.893	0.00	6.325	0.00	44.774	0.00	316.979	66.38		

Operator notes: Moyenne de 6 mesures de char - 08 avril 2011

Annexe 8: Fiches internationales de sécurité chimique pour phénol**PHENOL****ICSC: 0070**

PHENOL
Acide carbolique
Acide phénique
 C_6H_6O/C_6H_5OH

Monohydroxybenzène ;Masse moléculaire : 94.1

N° CAS : 108-95-2

N° RTECS : SJ3325000

N° ICSC : 0070

N° ONU : 1671 (phénol, solide); voir Notes

N° CE : 604-001-00-2

TYPES DE RISQUES/ EXPOSITIONS	RISQUES/ SYMPTOMES AIGUS	PREVENTION	PREMIER SECOURS/ AGENTS D'EXTINCTION
INCENDIE	Combustible.	PAS de flammes nues. PAS de contact avec les agents oxydants forts.	Mousse résistant aux alcools, poudre, eau pulvérisée, mousse, dioxyde de carbone.
EXPLOSION	Au-dessus de 79°C, des mélanges air/vapeur explosifs peuvent se former.	Au-dessus de 79°C, système en vase clos, ventilation.	En cas d'incendie: maintenir les fûts, etc., à basse température en les arrosant d'eau.
CONTACT PHYSIQUE		EVITER LA FORMATION DE BROUILLARDS! OBSERVER UNE HYGIENE STRICTE!	DANS TOUS LES CAS, CONSULTER UN MEDECIN!
• INHALATION	Sensation de brûlure. Toux. Vertiges. Maux de tête. Nausées. Essoufflement. Perte de conscience. Vomissements. Symptômes d'effets retardés (voir Notes).	Eviter l'inhalation de fines poussières ou de brouillard. Ventilation, aspiration locale ou protection respiratoire.	Air frais, repos. Position semi-assise. Respiration artificielle si nécessaire. Consulter un médecin.
• PEAU	PEUT ETRE ABSORBEE ! Sérieuses brûlures cutanées. Choc. Collapsus. Coma. Convulsions. Effet anesthésique local. Mort (Suite, voir Inhalation).	Gants de protection. Vêtements de protection.	Retirer les vêtements contaminés. Rincer la peau abondamment à l'eau ou prendre une douche. Consulter un médecin. Porter des gants de protection pour administrer les premiers secours. Pour éliminer ou neutraliser la substance, utiliser du

			polyéthylèneglycol 300 ou de l'huile végétale.
• YEUX	Perte permanente de la vue. Brûlures profondes graves.	Ecran facial, ou protection oculaire associée à une protection respiratoire.	Rincer d'abord abondamment à l'eau pendant plusieurs minutes (retirer si possible les lentilles de contact), puis consulter un médecin.
• INGESTION	Corrosive. Douleurs abdominales. Convulsions. Diarrhée. Choc ou collapsus. Mal de gorge. Urines gris vert foncé.	Ne pas manger, ne pas boire ni fumer pendant le travail. Se laver les mains avant de manger.	Rincer la bouche. Donner abondamment à boire. Repos. Consulter un médecin. Faire boire de l'huile végétale en grande quantité, ne PAS donner d'alcool!


DEVERSEMENTS & FUITES	STOCKAGE	CONDITIONNEMENT & ETIQUETAGE
NE PAS rejeter à l'égout. Balayer et récupérer la substance répandue dans des récipients hermétiques; si approprié, humidifier d'abord afin d'éviter la formation de poussière. Recueillir soigneusement les résidus, puis emporter en lieu sûr. (protection individuelle spéciale: tenue de protection complète comprenant un appareil de protection respiratoire autonome).	Prévoir un dispositif pour contenir l'écoulement des résidus lors de l'extinction. Séparer des oxydants forts, des aliments et des produits alimentaires. Conserver au froid. Conserver au sec. Bien fermer. Conserver dans un local bien ventilé.	Ne pas transporter avec des aliments ni des produits alimentaires. Symbole T R: 24/25-34 S: (1/2-)28-45 Classe de danger ONU: 6.1 Classe d'emballage ONU: II
VOIR IMPORTANTES INFORMATIONS AU DOS		
ICSC: 0070	Préparé dans le cadre de la coopération entre le Programme International sur la Sécurité Chimique et la Commission Européenne (C) 1993	

D O N N E E S I M P O R T A N T E S	ASPECT PHYSIQUE; APPARENCE: CRISTAUX INCOLORES A JAUNES OU ROSE CLAIR , D'ODEUR CARACTERISTIQUE.	VOIES D'EXPOSITION: La substance peut être absorbée par l'organisme rapidement par inhalation de ses vapeurs, à travers la peau et par ingestion.
	DANGERS PHYSIQUES: La vapeur est plus lourde que l'air.	RISQUE D'INHALATION: Une contamination dangereuse de l'air est lentement atteinte lors de l'évaporation de cette substance à 20°C.
	DANGERS CHIMIQUES: Des fumées toxiques se forment sous l'effet de la chaleur. La solution dans l'eau est un acide faible. Réagit avec les oxydants en provoquant des risques d'incendie et d'explosion.	EFFETS DES EXPOSITIONS DE COURTE DUREE: La substance et la vapeur sont corrosives pour les yeux, la peau et les voies respiratoires. L'inhalation de la vapeur peut causer un oedème pulmonaire (voir Notes). La substance peut avoir des effets sur le système nerveux central, le coeur et les reins , entraînant des convulsions, le coma, des troubles
	LIMITES D'EXPOSITION PROFESSIONNELLE (LEP): TLV: 5 ppm; 19 mg/m ³ (TWA) (peau) (ACGIH 1997) MAK: 5 ppm; 19 mg/m ³ ; peau (MAK 1993).	

	<p>cardiaques, une défaillance respiratoire, un collapsus. L'exposition peut entraîner la mort. Les effets peuvent être retardés. L'observation médicale est conseillée.</p> <p>EFFETS DES EXPOSITIONS PROLONGEES OU REPETEES: Un contact répété ou prolongé avec la peau peut causer une dermatite. La substance peut avoir des effets sur le foie et les reins.</p>
PROPRIETES PHYSIQUES	<p>Point d'ébullition : 182°C Point de fusion : 43°C Densité relative (eau = 1) : 1.06 Solubilité dans l'eau : 7 g/100 ml (modérée) Tension de vapeur à 20°C : 47 Pa Densité de vapeur relative (air = 1) : 3.2</p> <p>Densité relative du mélange air/vapeur à 20°C (air = 1) : 1.00 Point d'éclair : 79°C c.f. Température d'auto-inflammation : 715°C Limites d'explosivité en volume % dans l'air : 1.36-10 Coefficient de partage octanol/eau tel que log Poe : 1.46</p>
DONNEES ENVIRONNEMENTALES	La substance est toxique pour les organismes aquatiques.
NOTES	
<p>Autres numérotations ONU: 2312 (fondu); 2821 (en solution). La consommation de boissons alcooliques aggrave les effets nocifs. Suivant le niveau de l'exposition, une surveillance médicale périodique est recommandée. Les symptômes de l'oedème pulmonaire ne se manifestent souvent qu'après quelques heures et sont aggravés par l'effort physique. Le repos et la surveillance médicale sont par conséquent essentiels. L'administration immédiate d'une thérapie inhalatoire appropriée (par ex., aérosol) devrait être envisagée par un médecin ou par une personne habilitée par lui. NE PAS utiliser à proximité d'un feu, d'une surface chaude ou pendant les opérations de soudage.</p> <p style="text-align: right;">Carte de données d'urgence pour le transport: TREMCARD (R)-8A Code NFPA: H 3; F 2; R 0.</p>	
AUTRES INFORMATIONS	
ICSC: 0070	PHENOL
© PISSC, CEC, 1993	
NOTICE LEGALE IMPORTANTE:	<p>La CE de même que le PISSC ou toute presonne agissant au nom de la CE ou du PISSC ne sauraient être tenues pour responsables de l'utilisation qui pourrait être faite de ces informations. Cette fiche exprime l'avis du comité de révision du PISSC et peut ne pas toujours refléter les recommandations de la législation nationale en la matière. L'utilisateur est donc invité à vérifier la conformité des fiches avec les prescriptions en usage dans son pays.</p> <p>Traduction autorisée de l'International Chemical Safety Card (ICSC), publié par l'UNEP/ILO/WHO dans le cadre de la coopération entre le PISSC et la CE. Programme International sur la Sécurité des Substances Chimiques - Commission Européenne, 1993.</p>

Annexe 9: Fiches internationales de sécurité chimique pour p-Chlorophénol**p-CHLOROPHENOL**

ICSC: 0850



p-CHLOROPHENOL
4-Chlorophénol
C₆H₅ClO/C₆H₄ClOH
Masse moléculaire : 128.6

N° CAS : 106-48-9
N° RTECS : SK2800000
N° ICSC : 0850
N° ONU : 2020
N° CE : 604-008-00-0

TYPES DE RISQUES/ EXPOSITIONS	RISQUES/ SYMPTOMES AIGUS	PREVENTION	PREMIER SECOURS/ AGENTS D'EXTINCTION
INCENDIE	Combustible. Emission de fumées (ou de gaz) irritantes ou toxiques lors d'incendie.	PAS de flammes nues.	Poudre, eau pulvérisée, mousse, dioxyde de carbone.
EXPLOSION			En cas d'incendie: maintenir les fûts, etc., à basse température en les arrosant d'eau.
CONTACT PHYSIQUE		EVITER LA DISPERSION DE POUSSIERE!	
• INHALATION	Toux. Vertiges. Maux de tête. Respiration difficile. Mal de gorge.	Ventilation (sauf en présence de poudre), aspiration locale ou protection respiratoire.	Air frais, repos. Respiration artificielle si nécessaire. Consulter un médecin.
• PEAU	PEUT ETRE ABSORBEE ! Rougeur.	Gants de protection. Vêtements de protection.	Retirer les vêtements contaminés. Rincer et laver la peau abondamment à l'eau et au savon. Consulter un médecin.
• YEUX	Rougeur.	Lunettes à coques, ou protection oculaire associée à une protection respiratoire.	Rincer d'abord abondamment à l'eau pendant plusieurs minutes (retirer si possible les lentilles de contact), puis

• INGESTION	Douleurs abdominales.	Ne pas manger, ne pas boire ni fumer pendant le travail.	Rincer la bouche. Consulter un médecin.
DEVERSEMENTS & FUITES	STOCKAGE	CONDITIONNEMENT & ETIQUETAGE	
Balayer et récupérer la substance répandue dans des récipients; si approprié, humidifier d'abord afin d'éviter la formation de poussière. Recueillir soigneusement les résidus, puis emporter en lieu sûr. (protection individuelle spéciale: tenue de protection complète comprenant un appareil de protection respiratoire autonome).	Séparer des oxydants forts, des aliments et des produits alimentaires. Fermer de façon étanche. Conserver au froid.	Ne pas transporter avec des aliments ni des produits alimentaires. Symbole Xn R: 20/21/22 S: 2-28 Note: C Classe de danger ONU: 6.1 Classe d'emballage ONU: III	
VOIR IMPORTANTES INFORMATIONS AU DOS			

D O N N E E S I M P O R T A N T E S	ASPECT PHYSIQUE; APPARENCE: CRISTAUX INCOLORES , D'ODEUR CARACTERISTIQUE.	VOIES D'EXPOSITION: La substance peut être absorbée par l'organisme par inhalation de ses aérosols et à travers la peau.
	DANGERS PHYSIQUES: La vapeur est plus lourde que l'air.	RISQUE D'INHALATION: Aucune indication ne peut être donnée sur la vitesse à laquelle une concentration dangereuse dans l'air est atteinte lors de l'évaporation de cette substance à 20°C.
	DANGERS CHIMIQUES: La substance se décompose en chauffant fortement , produisant des fumées toxiques et corrosives (acide chlorhydrique, chlore). Réagit avec les oxydants.	EFFETS DES EXPOSITIONS DE COURTE DUREE: La substance est irritante pour les yeux, la peau et les voies respiratoires. La substance peut avoir des effets sur le système nerveux central and la vessie.
	LIMITES D'EXPOSITION PROFESSIONNELLE (LEP): Pas de TLV établie.	EFFETS DES EXPOSITIONS PROLONGEES OU REPETEES: La substance peut avoir des effets sur le foie, les poumons, les reins, le sang, le coeur.
PROPRIETES PHYSIQUES	Point d'ébullition : 220°C Point de fusion : 43°C Densité relative (eau = 1) : 1.2 Solubilité dans l'eau : modérée (2.7 g/100 ml à 20°C)	Tension de vapeur à 20°C : 13 Pa Densité de vapeur relative (air = 1) : 4.44 Point d'éclair : 121°C (c.c.)°C Coefficient de partage octanol/eau tel que log Poe : 2.39
DONNEES ENVIRONNEMENTALES	La substance peut être dangereuse pour l'environnement; une attention particulière doit être accordée à l'eau.	
NOTES		
NE PAS emporter de vêtements de travail chez soi.		

Carte de données d'urgence pour le transport: TREMCARD (R)-804.
Code NFPA: H 3; F 1; R 0.

AUTRES INFORMATIONS

ICSC: 0850

p-CHLOROPHENOL

© PISSC, CEC, 1993

**NOTICE LEGALE
IMPORTANTE:**

La CE de même que le PISSC ou toute personne agissant au nom de la CE ou du PISSC ne sauraient être tenues pour responsables de l'utilisation qui pourrait être faite de ces informations. Cette fiche exprime l'avis du comité de révision du PISSC et peut ne pas toujours refléter les recommandations de la législation nationale en la matière. L'utilisateur est donc invité à vérifier la conformité des fiches avec les prescriptions en usage dans son pays.

Traduction autorisée de l'International Chemical Safety Card (ICSC), publié par l'UNEP/ILO/WHO dans le cadre de la coopération entre le PISSC et la CE. Programme International sur la Sécurité des Substances Chimiques - Commission Européenne, 1993.

**D
O
N
N
E
E
S

I
M
P
O
R
T
A
N
T
E
S**

**ASPECT PHYSIQUE;
APPARENCE:**
CRISTAUX INCOLORES ,
D'ODEUR CARACTERISTIQUE.

DANGERS PHYSIQUES:
La vapeur est plus lourde que l'air.

DANGERS CHIMIQUES:
La substance se décompose en chauffant fortement , produisant des fumées toxiques et corrosives (acide chlorhydrique, chlore). Réagit avec les oxydants.

**LIMITES D'EXPOSITION
PROFESSIONNELLE (LEP):**
Pas de TLV établie.

VOIES D'EXPOSITION:
La substance peut être absorbée par l'organisme par inhalation de ses aérosols et à travers la peau.

RISQUE D'INHALATION:
Aucune indication ne peut être donnée sur la vitesse à laquelle une concentration dangereuse dans l'air est atteinte lors de l'évaporation de cette substance à 20°C.

**EFFETS DES EXPOSITIONS DE
COURTE DUREE:**
La substance est irritante pour les yeux, la peau et les voies respiratoires. La substance peut avoir des effets sur le système nerveux central and la vessie.


**EFFETS DES EXPOSITIONS
PROLONGEES OU REPETEES:**
La substance peut avoir des effets sur le foie, les poumons, les reins, le sang, le coeur.

DONNEES ENVIRONNEMENTALES	La substance peut être dangereuse pour l'environnement; une attention particulière doit être accordée à l'eau.
NOTES	
NE PAS emporter de vêtements de travail chez soi. Carte de données d'urgence pour le transport: TREMCARD (R)-804. Code NFPA: H 3; F 1; R 0.	
AUTRES INFORMATIONS	
ICSC: 0850	p-CHLOROPHENOL

NOTICE LEGALE IMPORTANTE:	<p>La CE de même que le PISSC ou toute personne agissant au nom de la CE ou du PISSC ne sauraient être tenues pour responsables de l'utilisation qui pourrait être faite de ces informations. Cette fiche exprime l'avis du comité de révision du PISSC et peut ne pas toujours refléter les recommandations de la législation nationale en la matière. L'utilisateur est donc invité à vérifier la conformité des fiches avec les prescriptions en usage dans son pays.</p> <p>Traduction autorisée de l'International Chemical Safety Card (ICSC), publié par l'UNEP/ILO/WHO dans le cadre de la coopération entre le PISSC et la CE. Programme International sur la Sécurité des Substances Chimiques - Commission Européenne, 1993.</p>
----------------------------------	---

Annexe 10 : Fiches internationales de sécurité chimique pour p-Nitrophénol**p-NITROPHENOL**

ICSC: 0066



p-NITROPHENOL
4-Nitrophénol
4-Hydroxynitrobenzène
 $C_6H_5NO_3$
Masse moléculaire : 139.1

N° CAS : 100-02-7
N° RTECS : SM2275000
N° ICSC : 0066
N° ONU : 1663
N° CE : 609-015-00-2

TYPES DE RISQUES/ EXPOSITIONS	RISQUES/ SYMPTOMES AIGUS	PREVENTION	PREMIER SECOURS/ AGENTS D'EXTINCTION
INCENDIE	Combustible. Emission de fumées (ou de gaz) irritantes ou toxiques lors d'incendie.	PAS de flammes nues.	Poudre, eau pulvérisée, mousse, dioxyde de carbone.
EXPLOSION	Les particules finement dispersées forment des mélanges explosifs dans l'air.	Eviter le dépôt de poussières; système en vase clos, équipement électrique et éclairage protégés contre les explosions.	En cas d'incendie: maintenir les fûts, etc., à basse température en les arrosant d'eau.
CONTACT PHYSIQUE		EVITER LA DISPERSION DE POUSSIERE! OBSERVER UNE HYGIENE STRICTE!	
• INHALATION	Toux. Sensation de brûlure. Vertiges. Faiblesse.	Aspiration locale ou protection respiratoire. Ventilation, aspiration locale ou protection respiratoire. Système en vase clos et ventilation.	Air frais, repos. Consulter un médecin.
• PEAU	PEUT ETRE ABSORBEE ! (Suite, voir Inhalation).	Gants de protection. Vêtements de protection.	Retirer les vêtements contaminés. Rincer et laver la peau abondamment à l'eau et au savon. Consulter un médecin.

• YEUX	Rougeur. Douleur.	Ecran facial, ou protection oculaire associée à une protection respiratoire.	Rincer d'abord abondamment à l'eau pendant plusieurs minutes (retirer si possible les lentilles de contact), puis consulter un médecin.
• INGESTION			

DEVERSEMENTS & FUITES	STOCKAGE	CONDITIONNEMENT & ETIQUETAGE
Balayer et récupérer la substance répandue dans des récipients hermétiques; si approprié, humidifier d'abord afin d'éviter la formation de poussière. Recueillir soigneusement les résidus, puis emporter en lieu sûr. NE PAS laisser ce produit contaminer l'environnement. (protection individuelle spéciale: appareil de protection respiratoire à filtre P2 pour particules nocives).	Séparer des substances combustibles et des réducteurs, des aliments et des produits alimentaires.	Ne pas transporter avec des aliments ni des produits alimentaires. Symbole Xn R: 20/21/22-33 S: (2-)28 Classe de danger ONU: 6.1 Classe d'emballage ONU: III

VOIR IMPORTANTES INFORMATIONS AU DOS

ICSC: 0066

Préparé dans le cadre de la coopération entre le Programme International sur la Sécurité Chimique et la Commission Européenne (C) 1993

D O N N E S I M P O R T A N T E S	<p>ASPECT PHYSIQUE; APPARENCE: CRISTAUX INCOLORES A JAUNE PALE , D'ODEUR CARACTERISTIQUE.</p> <p>DANGERS PHYSIQUES: Possibilité d'explosion de poussière si sous forme de poudre ou de granulés mélangés à l'air.</p> <p>DANGERS CHIMIQUES: Peut exploser après échauffement. La substance se décompose en chauffant fortement ou en brûlant produisant des fumées toxiques comprenant des oxydes d'azote , en provoquant des risques d'incendie et d'explosion. La substance est un oxydant fort qui réagit violemment avec les matières combustibles et les réducteurs. Les mélanges avec l'hydroxyde de potassium sont explosifs.</p> <p>LIMITES D'EXPOSITION PROFESSIONNELLE (LEP): Pas de TLV établie.</p>	<p>VOIES D'EXPOSITION: La substance peut être absorbée par l'organisme par inhalation et à travers la peau.</p> <p>RISQUE D'INHALATION: Une contamination dangereuse de l'air n'est pas ou est seulement très lentement atteinte lors de l'évaporation de cette substance à 20°C; beaucoup plus rapidement par dispersion de la poussière.</p> <p>EFFETS DES EXPOSITIONS DE COURTE DUREE: L'inhalation de concentrations élevées peut causer un accroissement du métabolisme.</p> <p>EFFETS DES EXPOSITIONS PROLONGEES OU REPETEES:</p>
---	--	---

PROPRIETES PHYSIQUES	Point d'ébullition (décomposition) : 279°C Point de fusion : 113°C Densité relative (eau = 1) : 1.48 Solubilité dans l'eau à 25°C : 1.6 g/100 ml	Tension de vapeur à 20°C : 0.0032 Pa Point d'éclair : 169°C Coefficient de partage octanol/eau tel que log Poe : 1.91
DONNEES ENVIRONNEMENTALES	La substance peut être dangereuse pour l'environnement; une attention particulière doit être accordée aux poissons.	
NOTES		
Suivant le niveau de l'exposition, une surveillance médicale périodique est recommandée. Carte de données d'urgence pour le transport: TREMCARD (R)-61G12c Code NFPA: H 3; F 1; R 0.		
AUTRES INFORMATIONS		
ICSC: 0066		p-NITROPHENOL
© PISSC, CEC, 1993		

NOTICE LEGALE IMPORTANTE:	<p>La CE de même que le PISSC ou toute personne agissant au nom de la CE ou du PISSC ne sauraient être tenues pour responsables de l'utilisation qui pourrait être faite de ces informations. Cette fiche exprime l'avis du comité de révision du PISSC et peut ne pas toujours refléter les recommandations de la législation nationale en la matière. L'utilisateur est donc invité à vérifier la conformité des fiches avec les prescriptions en usage dans son pays.</p> <p>Traduction autorisée de l'International Chemical Safety Card (ICSC), publié par l'UNEP/ILO/WHO dans le cadre de la coopération entre le PISSC et la CE. Programme International sur la Sécurité des Substances Chimiques - Commission Européenne, 1993.</p>
--------------------------------------	---

Annexe 11: Fiches internationales de sécurité chimique pour acide 4-hydroxybenzoïque

SIGMA ALDRICH

1. Identification du produit et de la société

Nom du produit	Acide 4-hydroxybenzoïque
Code produit	54630
Société	Sigma Aldrich Chimie S.A.R.L. L'Isle D'Abeau Chesnes F-38297 St. Quentin Fallavier
Numéro de téléphone	
Technique	08 00 31 24 67
Fax	08 00 03 10 52
Numéro d'appel d'urgence	05 56 91 99 19

2. Informations sur les composants

Nom du produit	Numéro CAS	N° CEE	Numéro d'index
<i>acide 4-hydroxybenzoïque</i>	99-96-7	202-804-9	None
Formule	C ₇ H ₆ O ₃		
Poids moléculaire	138,12 AMU		
Synonymes	Acido p-idrossibenzoico (Italian) * benzoic acid, 4 – hydroxy – (9CI) * 4 – carboxyphénol * p – hydroxybenzoic acid * 4 – hydroxybenzoic acid * kyselina 4 – hydroxybenzoova (Czech) * p – oxybenzoésaure (German) * p – salicylic acid		

3. Identification des dangers

Indication spécifique des risques pour les hommes et l'environnement
Irritant pour les yeux

4. Mesures de premiers secours

Après inhalation

En cas d'inhalation, renouveler l'air. En cas d'arrêt respiratoire, utiliser une respiration artificielle. En cas de respiration difficile, donner de l'oxygène.

Après contact avec la peau

En cas de contact, laver immédiatement la peau avec du savon et à grande eau.

Après contact avec l'œil

En cas de contact, laver immédiatement les yeux à grande eau pendant 15 minutes au minimum.

Après ingestion

En cas d'ingestion, rincer la bouche avec de l'eau à condition que la personne soit consciente.
Appeler au médecin.

5. Mesures de lutte contre l'incendie

Moyen d'extinction

Adapté : atomiseur d'eau. Anhydride carbonique, poudre chimique sèche ou mousse appropriée.

Risques spéciaux

Danger(s) spécifique(s) : émet des fumées toxiques durant un incendie

Équipement de protection spéciale pour combattre l'incendie

Porter un équipement respiratoire autonome et des vêtements de protection pour empêcher tout contact avec la peau et les yeux

6. Mesures à prendre en cas de dispersion accidentelle

Procédure(s) de(s) précaution(s) individuelle(s)

Porter un appareil respiratoire, des bottes en caoutchouc et de gros gants en caoutchouc.

Méthodes de nettoyages

Balayer, placer dans un sac et évacuer avec les déchets. Eviter de soulever la poussière. Ventiler la zone et laver le lieu de déversement après avoir complètement absorbé le produit.

7. Manipulation et stockage**Manipulation**

Instruction pour une manipulation en toute sécurité : ne pas respirer les poussières. Eviter tout contact avec les yeux, la peau et les vêtements. Eviter toute exposition prolongée ou répétée.

Stockage

Conditions de stockage : conserver le récipient bien fermé

8. Contrôles d'exposition / Equipement de protection Individuelle**Contrôles par engineering**

Douche de sécurité et bain d'œil, mécanisme d'évacuation nécessaire

Mesures générales d'hygiène

Bien se laver après manipulation

Equipement de protection individuelle

Protection respiratoire : appareil de protection respiratoire homologué par NIOSH / MHSA

Protection manuelle : gants adaptés, résistant aux produits chimiques

Protection oculaire : lunette de sécurité

9. Propriétés physiques et chimiques

Aspect	Etat physique:	solide
	Couleur :	très légèrement beige
Propriété	Valeur	A température ou pression
pH	3,3	Concentration : 1 g/L
Point d'ébullition / variation du point d'ébullition	N / A	
Point de fusion / variation du point de fusion	214°C	
Point éclair	N / A	
Inflammabilité	N / A	
Température d'auto-allumage	N / A	
Propriétés oxydantes	N / A	
Propriétés explosives	N / A	
Limites d'explosion	N / A	
Pression de vapeur	N / A	
Gravité spécifique / densité	N / A	
Viscosité	N / A	
Densité de vapeur	N / A	
Conc. de vapeur saturé	N / A	
Taux d'évaporation	N / A	
Masse volumique apparente	600 kg/L	
Température de décomposition	N / A	
Pouvoir de solvatation	N / A	
Teneur en eau	N / A	
Tension de surface	N / A	
Conductivité	N / A	
Données diverses	N / A	
Solubilité	Hydro solubilité : 5 mg/mL H ₂ O	

10. Stabilité et réactivité**Stabilité**

Stable : stable

Produit à éviter : agents oxydants fort

Produits de décomposition dangereux

Produits de décomposition dangereux : monoxyde de carbone, dioxyde de carbone, phénol

Polymérisation dangereuse

Polymérisation dangereuse : ne se produira pas

11. Informations toxicologiques

Numéro de RTECS DH1925000

Toxicité aiguë

DL50

Oral

Rat

> 10000 mg/kg

Remarque : effet comportemental : faiblesse musculaire poumons, thorax ou respiration : dyspnée

DL50

Intra péritonéal

Rat

340 mg/kg

Remarque : effet comportemental : faiblesse musculaire

DL50

Oral

Souris

2200 mg/kg

DL50

Intra péritonéal

Souris

210 mg/kg

Remarque : sensibilité et nerf périphérique : paralysie flasque sans anesthésie (habituellement blocage neuromusculaire). Effet comportemental : somnolence (activité générale diminuée), ataxie

DL50

Sous-cutané

Souris

1050 mg/kg

Données sur l'irritation RTECS

Yeux

Lapin

Remarque : conséquence d'une irritation modérée

Peau

Lapin

24h

Remarque : conséquence d'une irritation modérée

Signes et symptômes d'une exposition

Autant que nous sachions, les propriétés chimiques, physiques et toxicologiques doivent être examinées minutieusement.

Voie d'exposition

Contact avec la peau : peut irriter la peau

Absorption cutanée : peut être nocif par contact avec la peau

Contact avec les yeux : irritant pour les yeux

Inhalation : peut être nocif par inhalation. Le produit est un irritant des muqueuses et des voies respiratoires supérieures.

Ingestion : peut être nocif en cas d'ingestion.

12. Informations ecotoxicologiques

Élimination

Élimination : > 90%

Conséquences ecotoxicologiques

Type de test : LCO poisson

Espèce : *Leuciscus idus*

Temps : 48h

Valeur : 200 mg/L

13. Informations sur les possibilités d'élimination des déchets**Élimination de substance**

Se mettre en rapport avec une entreprise spécialisée dans l'élimination de déchets pour procéder à l'élimination de ce produit. Dissoudre ou mélanger le produit avec un solvant combustible et brûler dans un incinérateur chimique équipé d'un système de postcombustion et d'épuration. Se conformer aux réglementations fédérales de l'état et locales sur l'environnement.

14. Informations relatives au transport**RID / ADR**

Non-dangereux pour le transport routier

IMDG

Non-hazardous for sea transport

IATA

Non-hazardous for air transport

15. Informations réglementaires**Classification et étiquetage selon les directives de l'UE**

Indication du danger : Xi

Irritant

Prases – R : 36

Irritant pour les yeux

Phrases S : 26

En cas de contact avec les yeux, laver immédiatement et abondamment avec de l'eau et consulter un spécialiste

Information spécifique au pays

Allemagne

WGK : 1

Suisse

Classe des poisons suisses : 4

16. Autres informations**Garantie**

Les informations ci-dessus ont été préparées sur la base des renseignements disponibles les plus sûrs. Elles ne prétendent pas être exhaustives et devront être considérées comme un guide. Le groupe Sigma-Aldrich Inc. Ne pourra être tenu responsable des dommages résultant de l'utilisation ou de tout contact avec le produit susmentionné. Voir verso de la facture ou du bulletin de livraison pour nos termes et conditions de vente. Copyright 2005 Sigma Aldrich Co. Copies en papier autorisées pour usage interne uniquement.

Limite de responsabilité

A utilisation exclusive pour la recherche et le développement ; ne pas utiliser à des fins pharmaceutiques.

*** Conformément OECD SIDS :

Propriétés physiques et chimiques	
Point d'ébullition :	Décomposé
Pression de vapeur :	$3,9 \cdot 10^{-3}$ Pa à 100°C
Coefficient de partage (Log Pow) :	1,37
Propriétés environnementales	

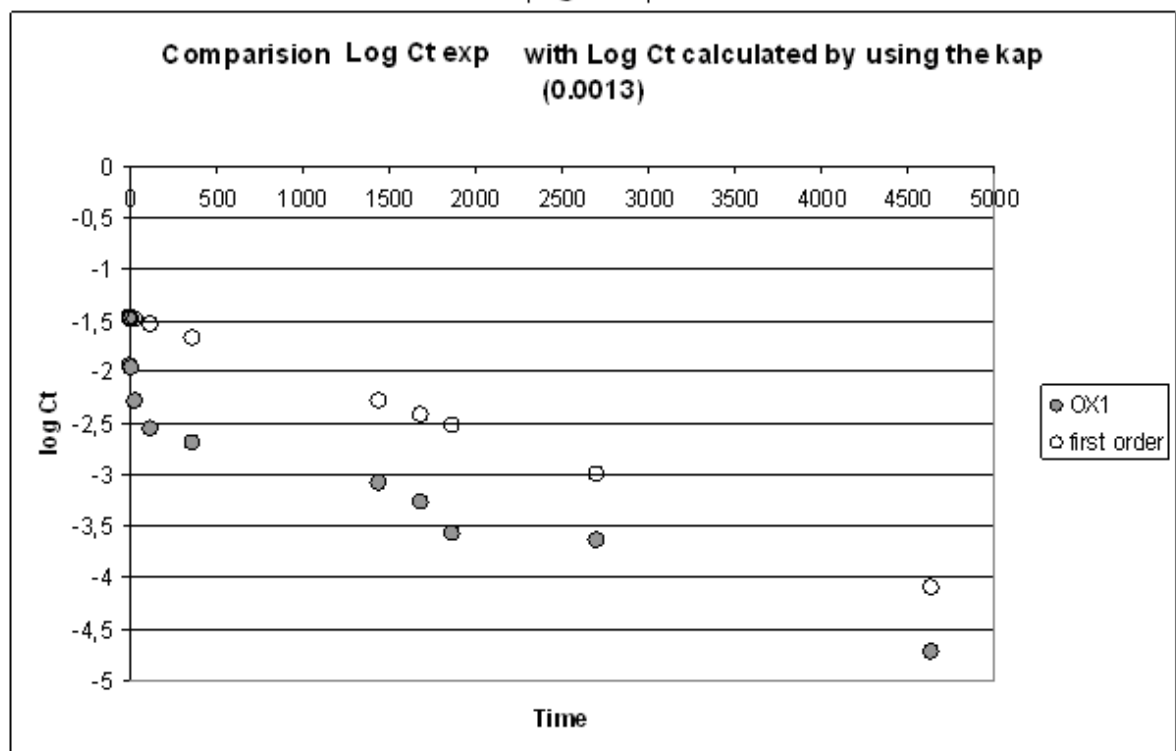
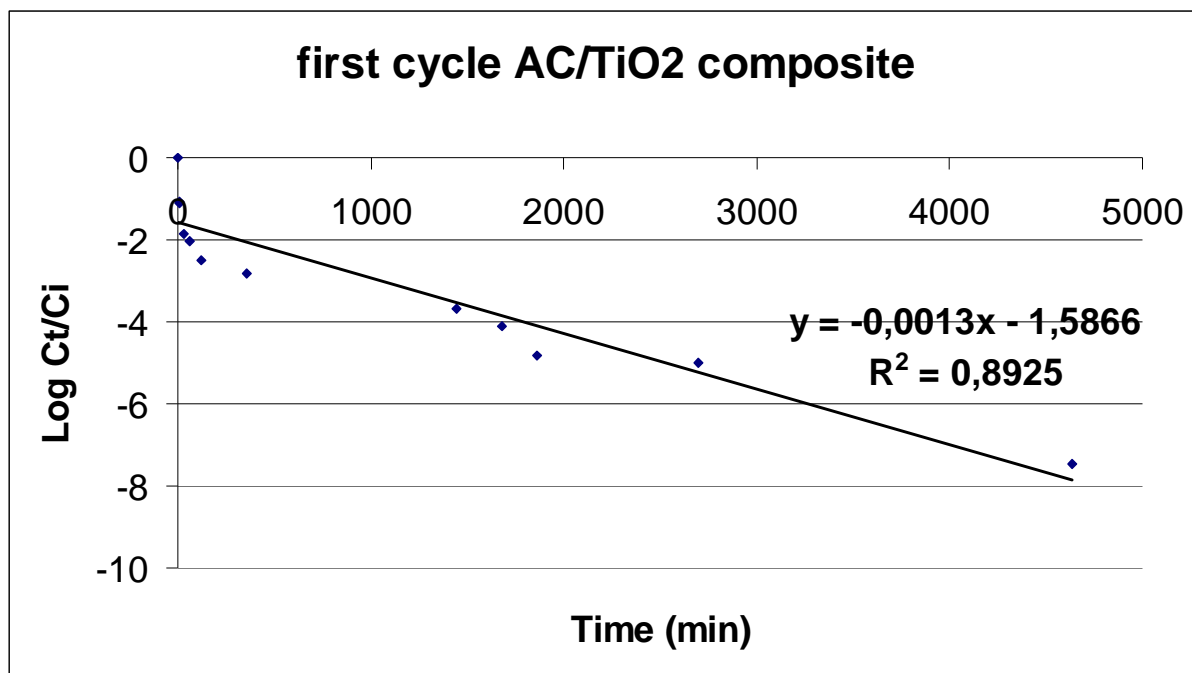
Stabilité dans l'eau :	Stable à pH = 4,7 et 9
	pK ₁ = 4,582 pK ₂ = 9,23
Biodégradabilité :	Facilement biodégradable 100% dans 28 jours

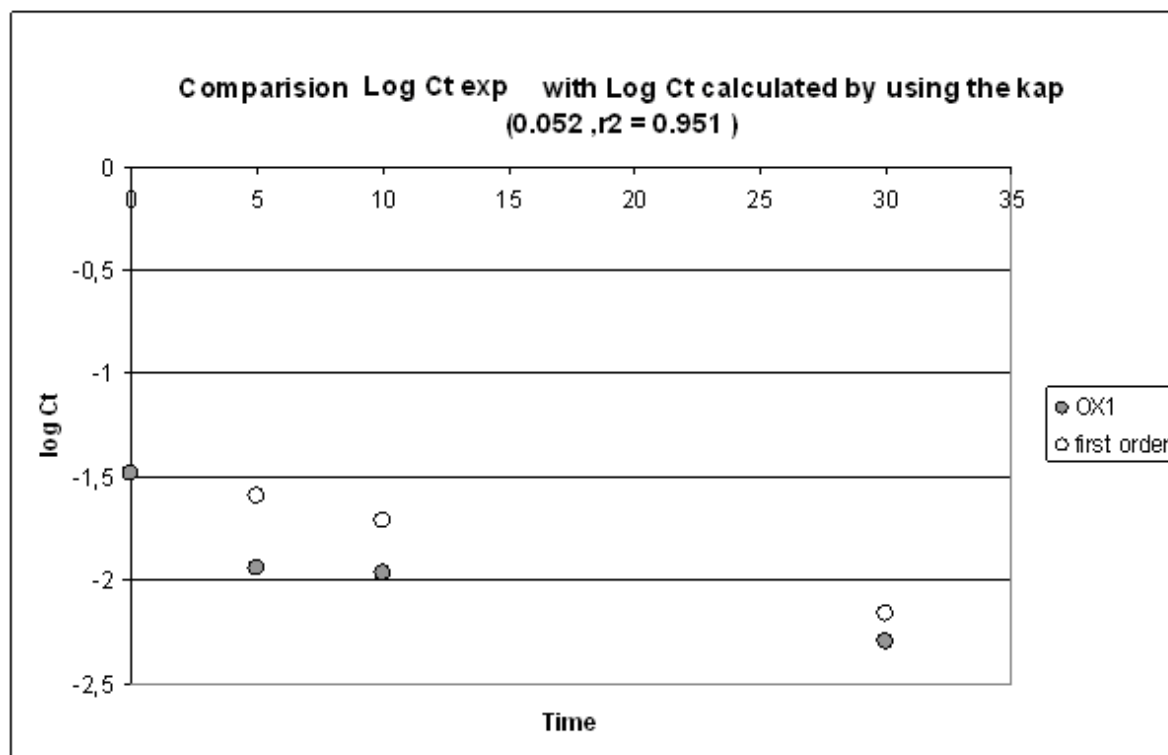
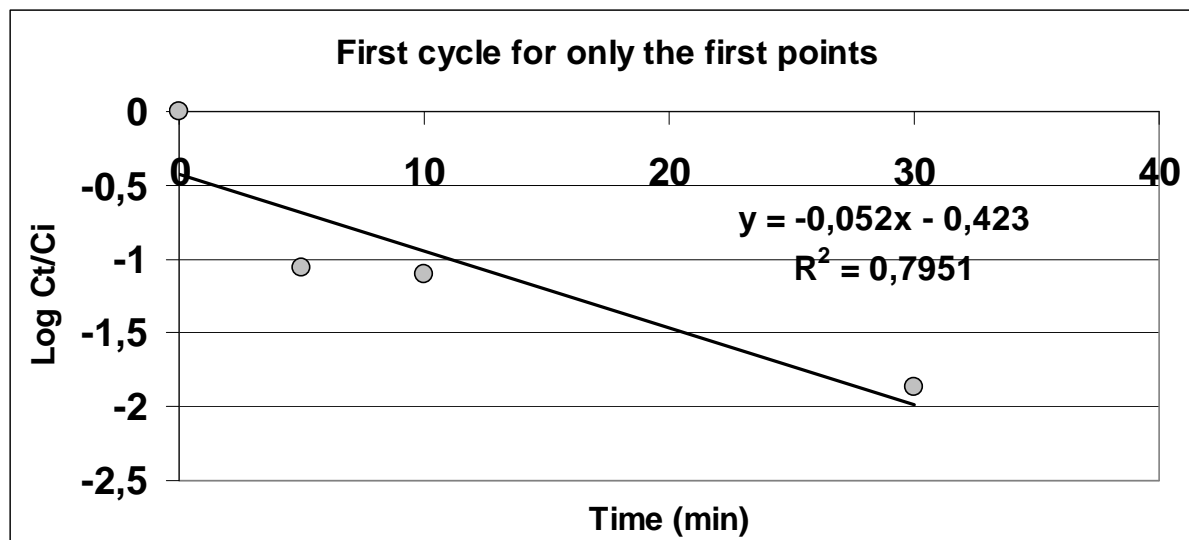
Annexe 12: First order model of Tartrazine degradation by AC/TiO₂ Composite and AC-TiO₂ mixture

1- AC/TiO₂ Composite

1.1 FIRST CYCLE

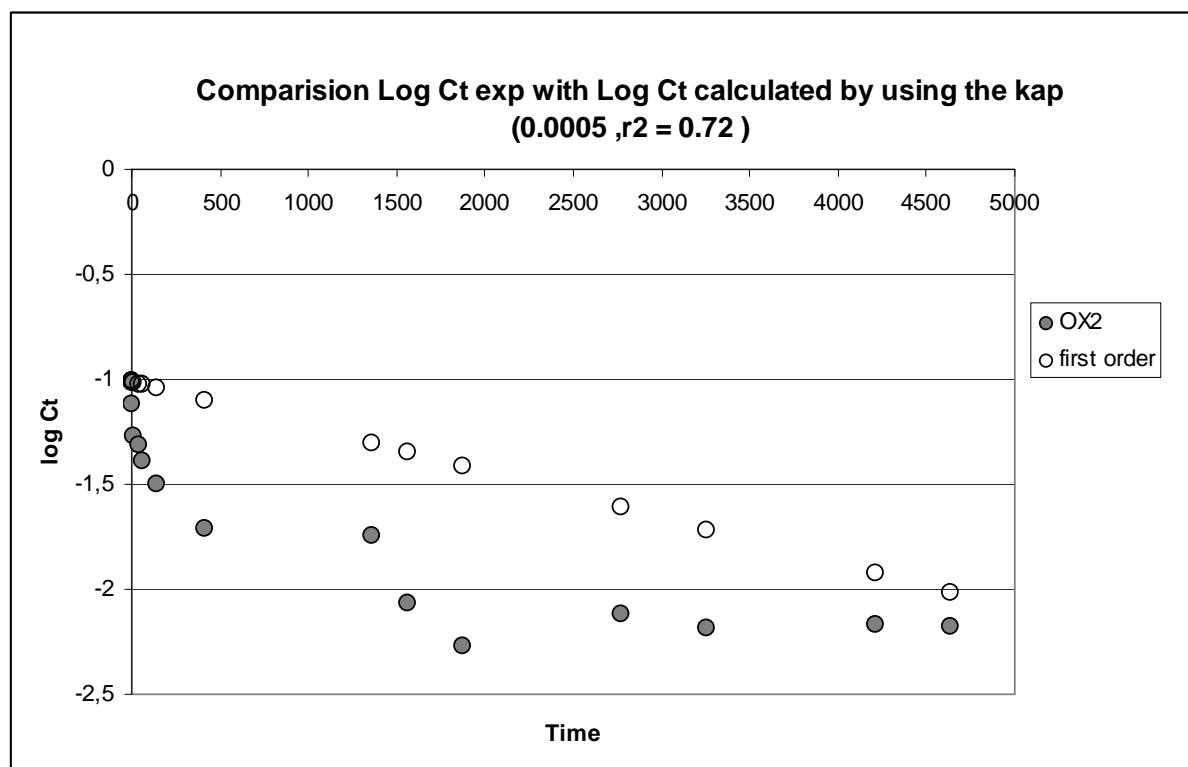
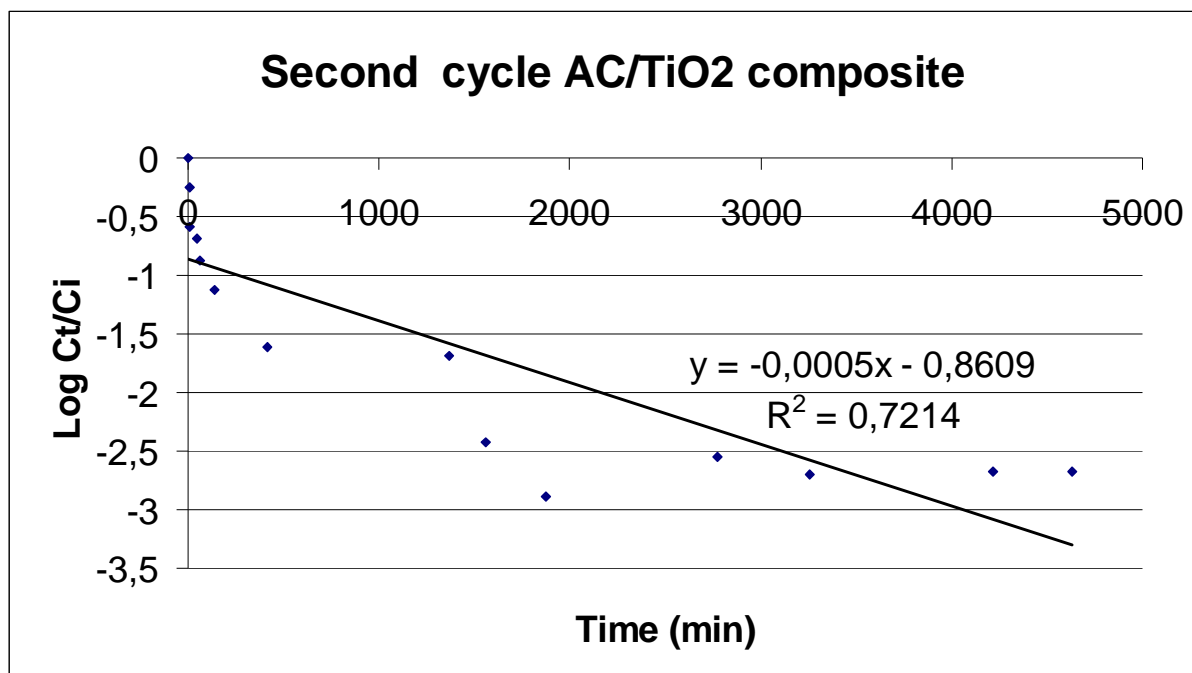
a-Kapp of all oxidation time at first cycle

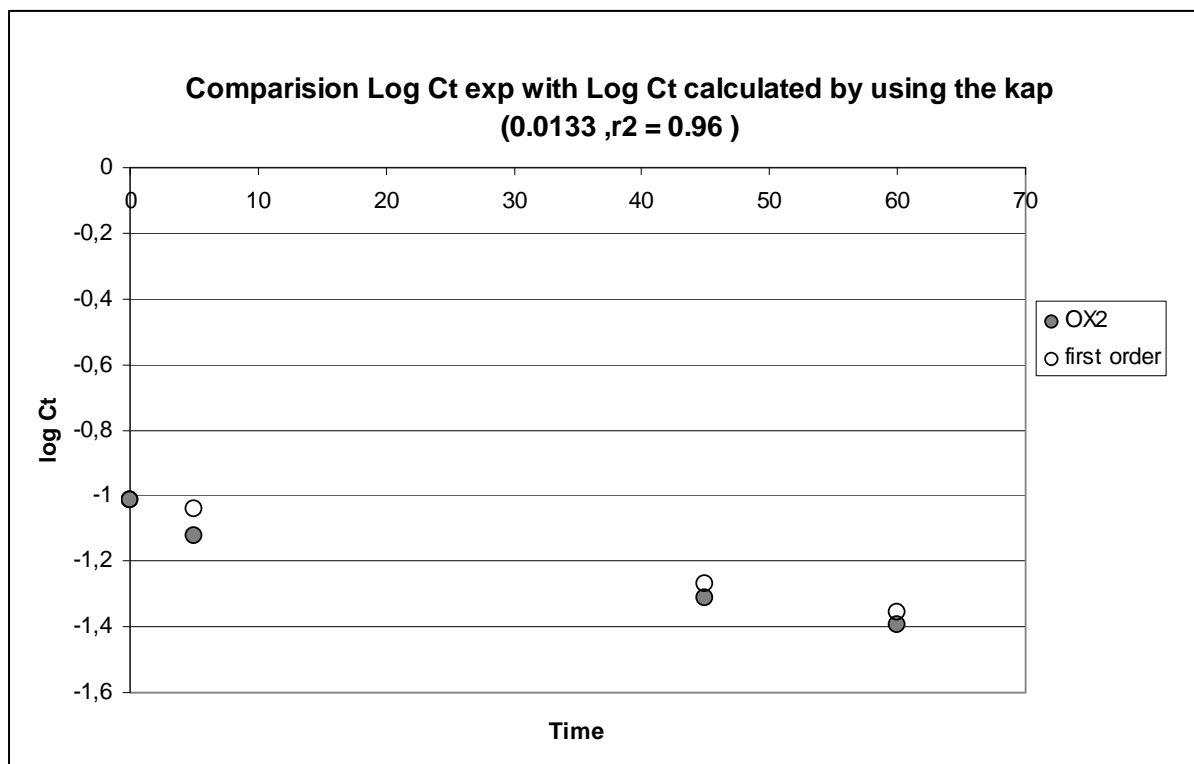
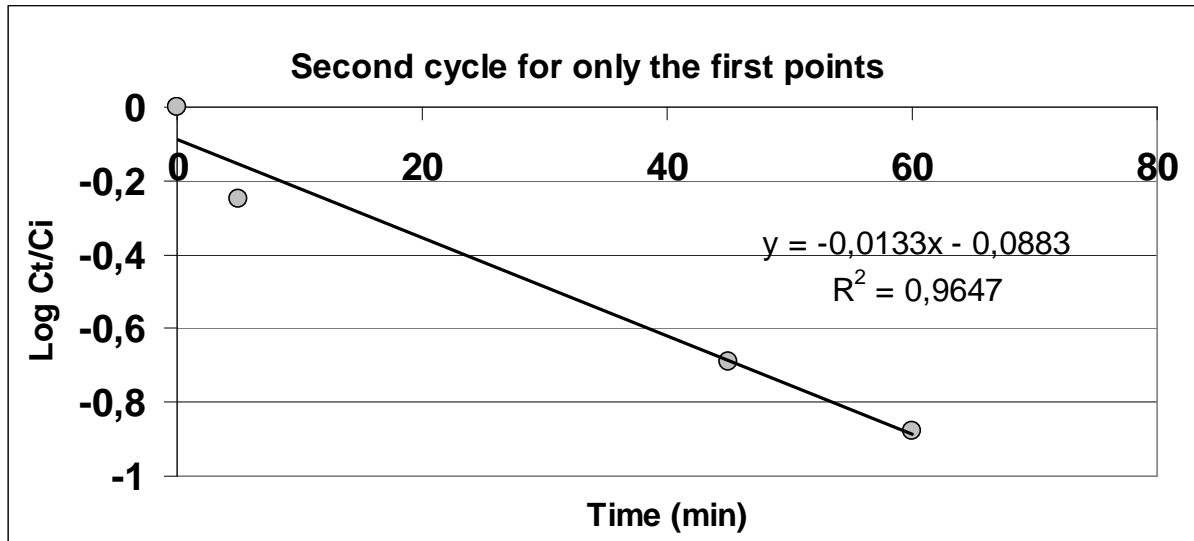


b-Kapp for the only first linear points of oxidation time at first cycle

1.2.Second CYCLE

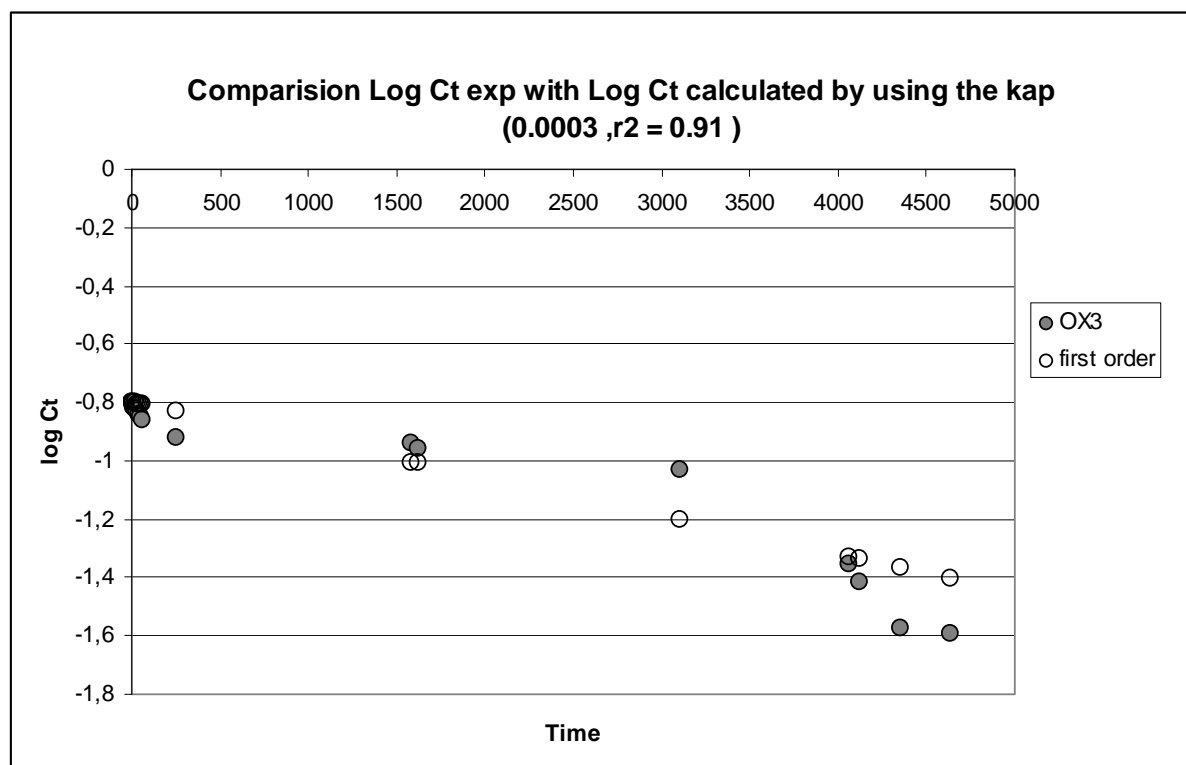
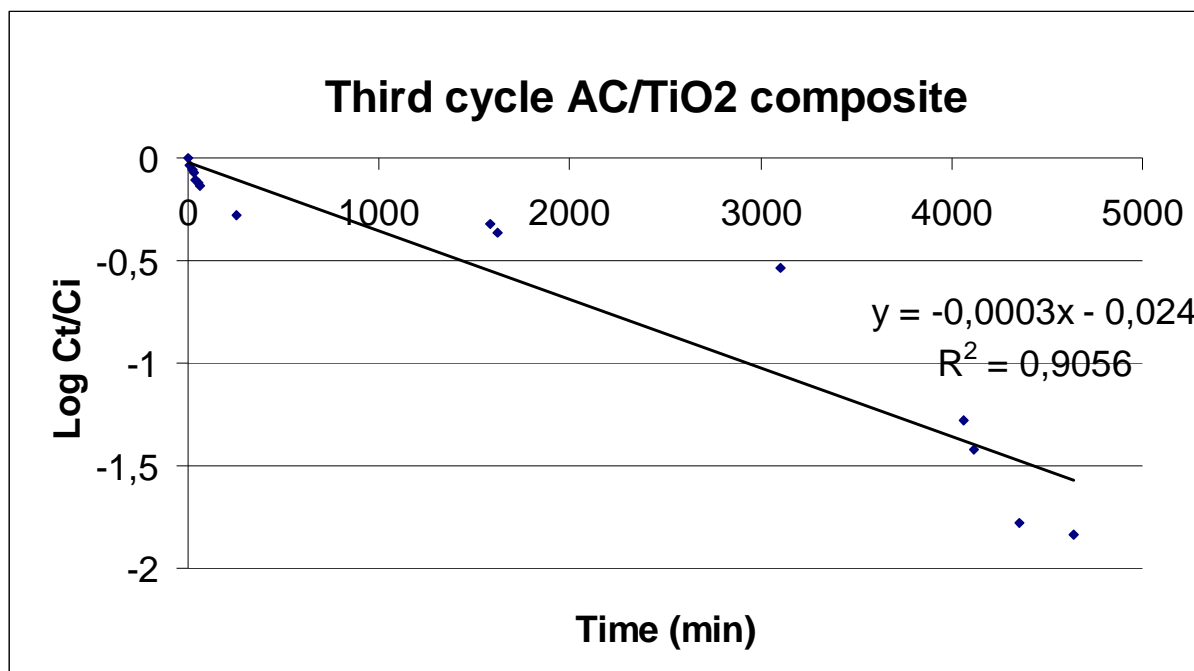
a-Kapp of all oxidation time at second cycle

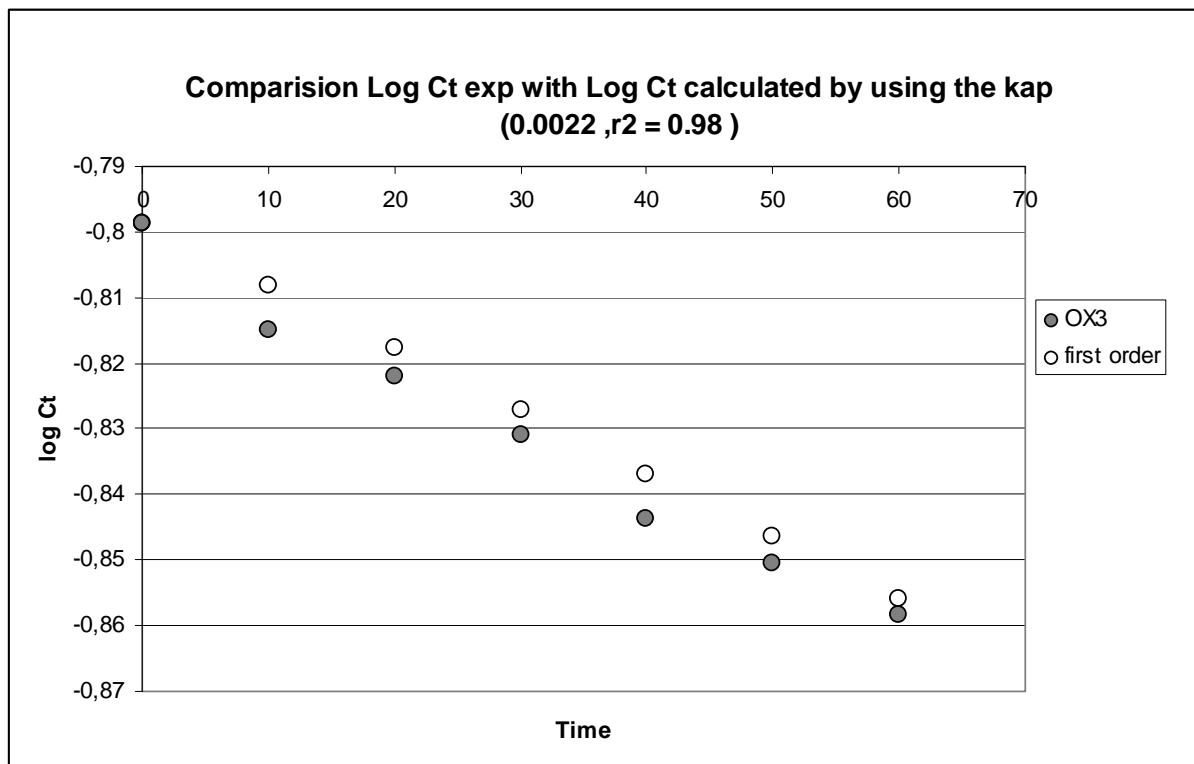
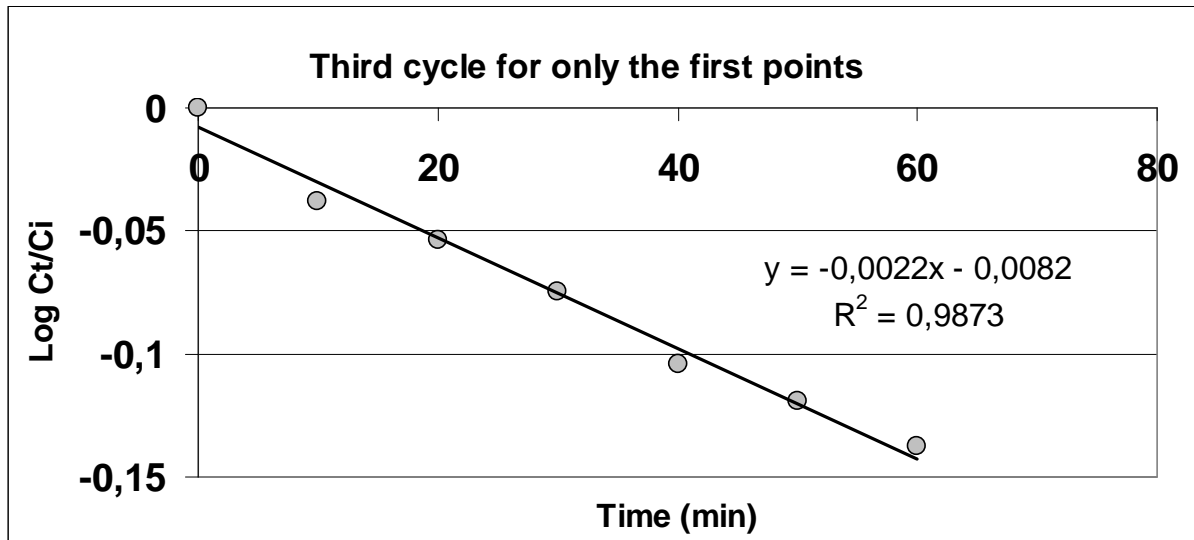


b-Kapp for the only first linear points of oxidation time at second cycle

1.3. Third CYCLE

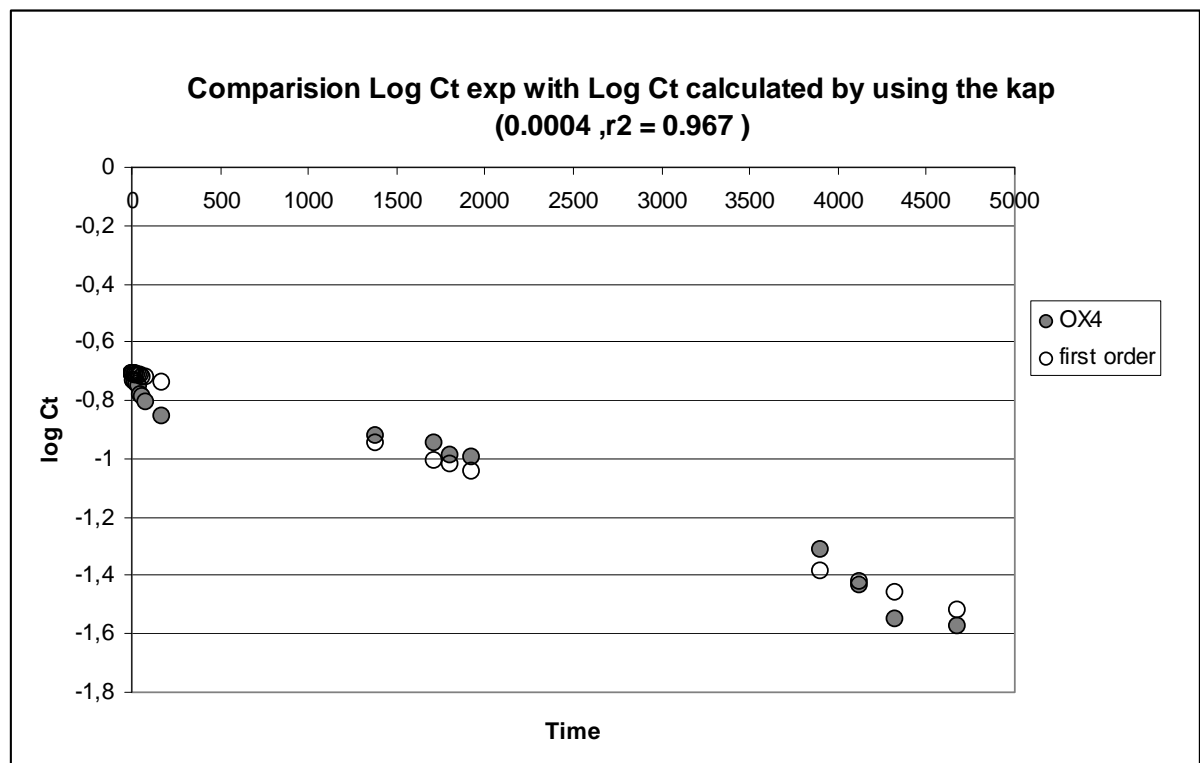
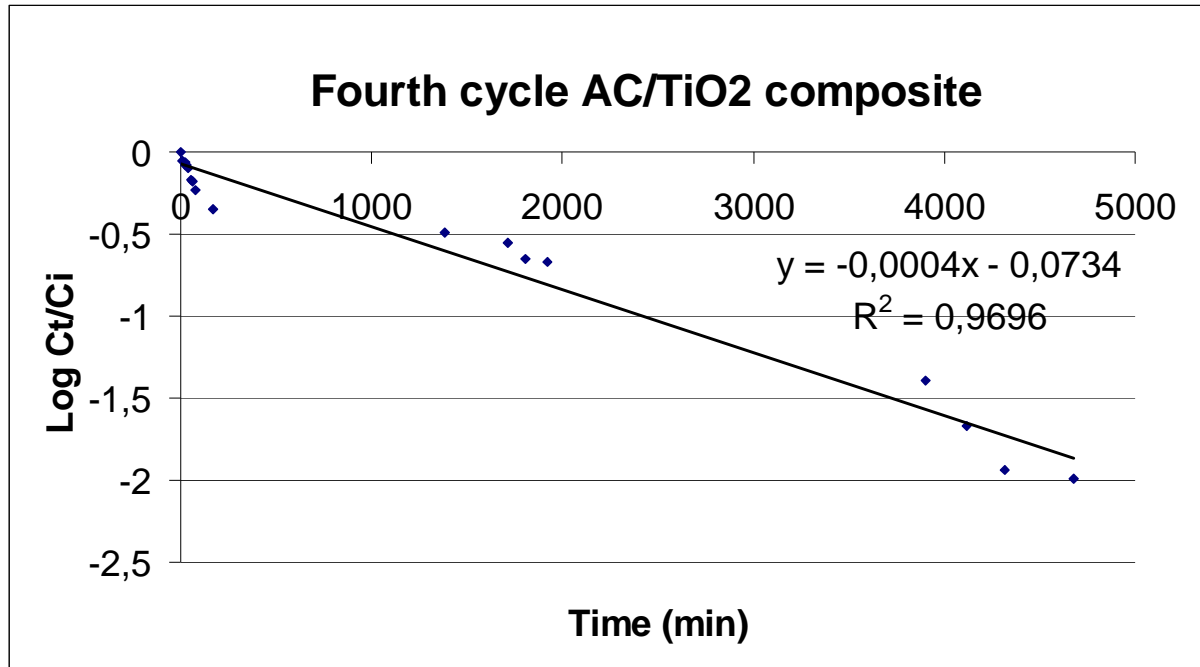
a-Kapp of all oxidation time at Third cycle

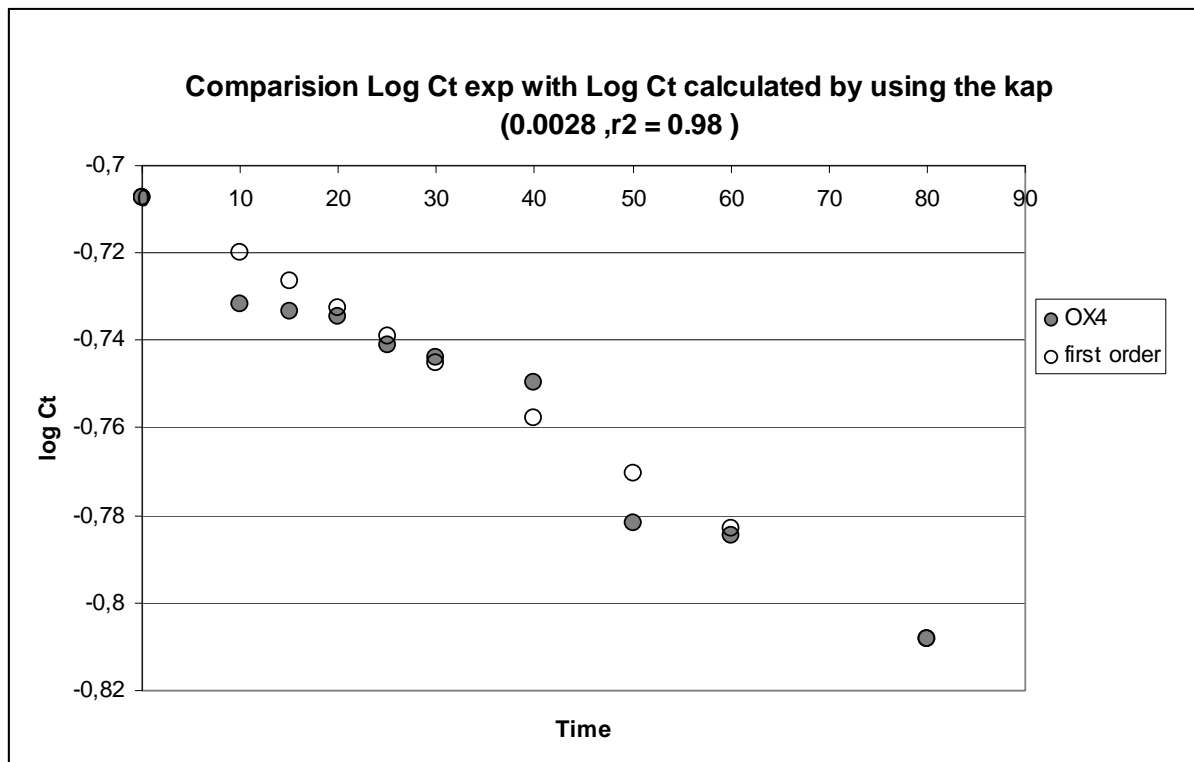
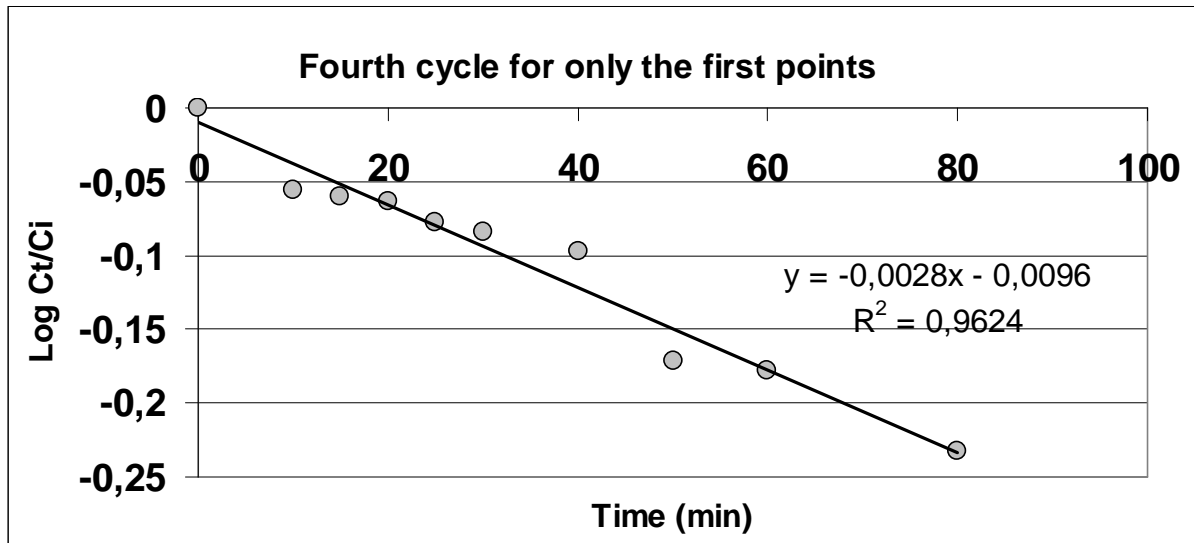


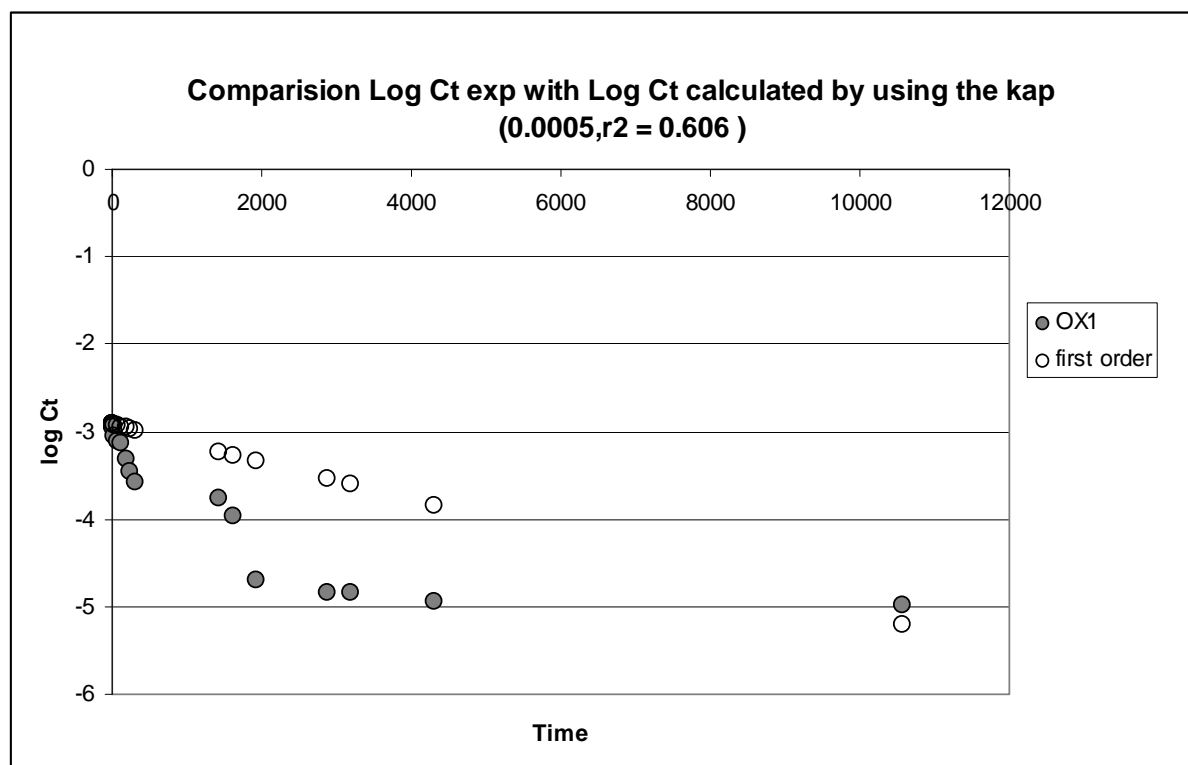
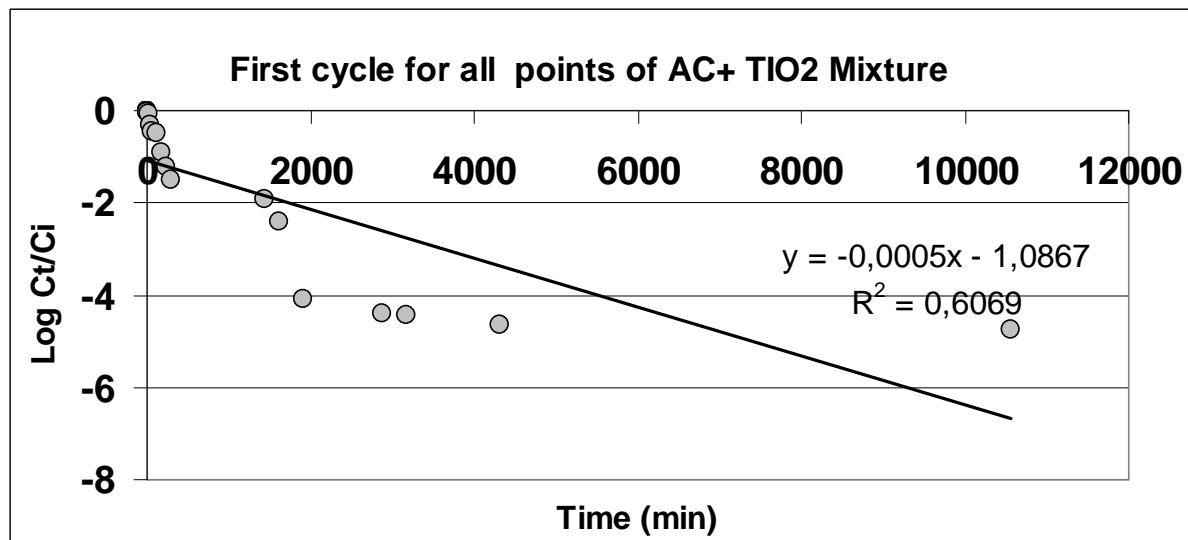
b-Kapp for the only first linear points of oxidation time at Third cycle

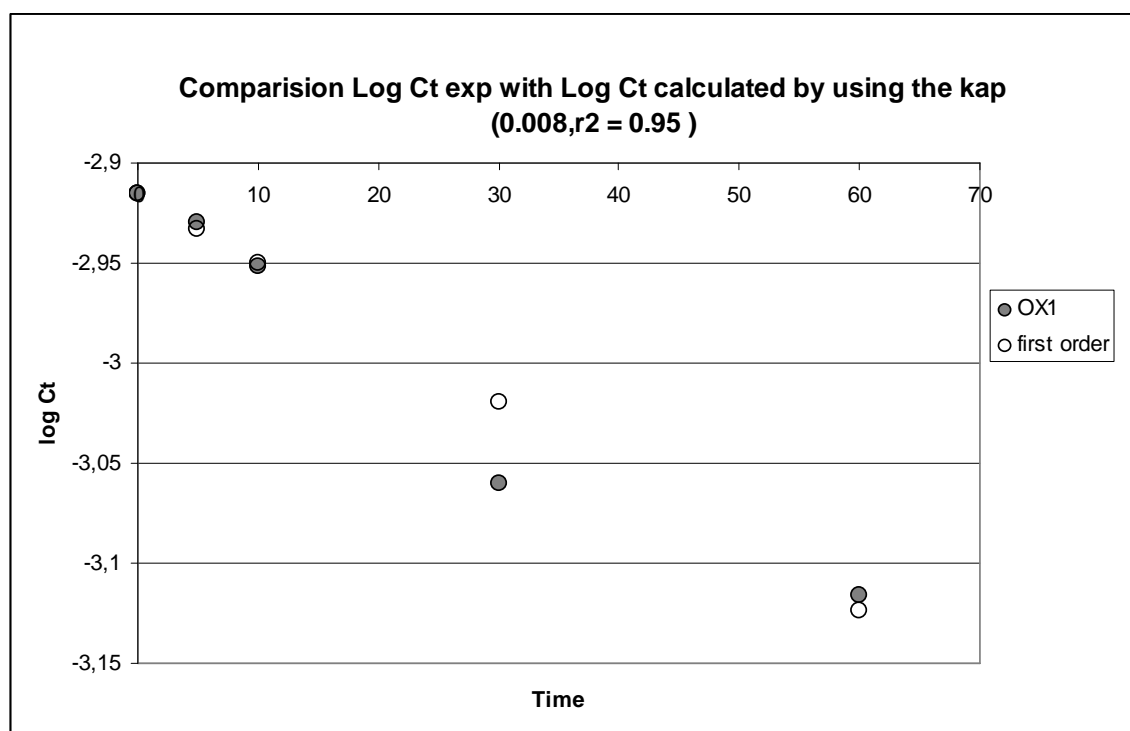
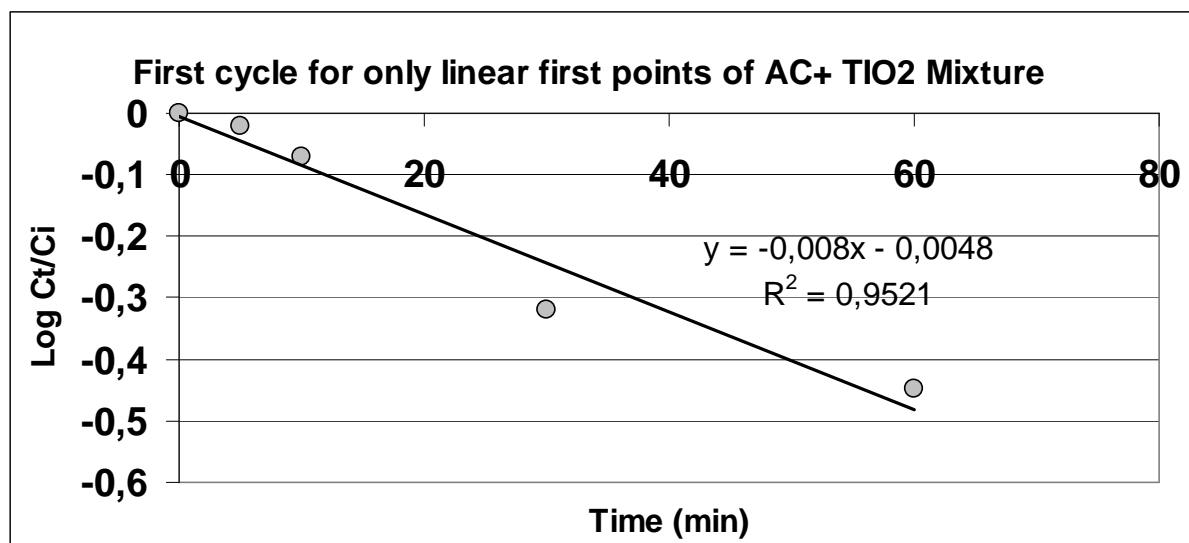
1.4. Fourth CYCLE

a-Kapp of all oxidation time at fourth cycle



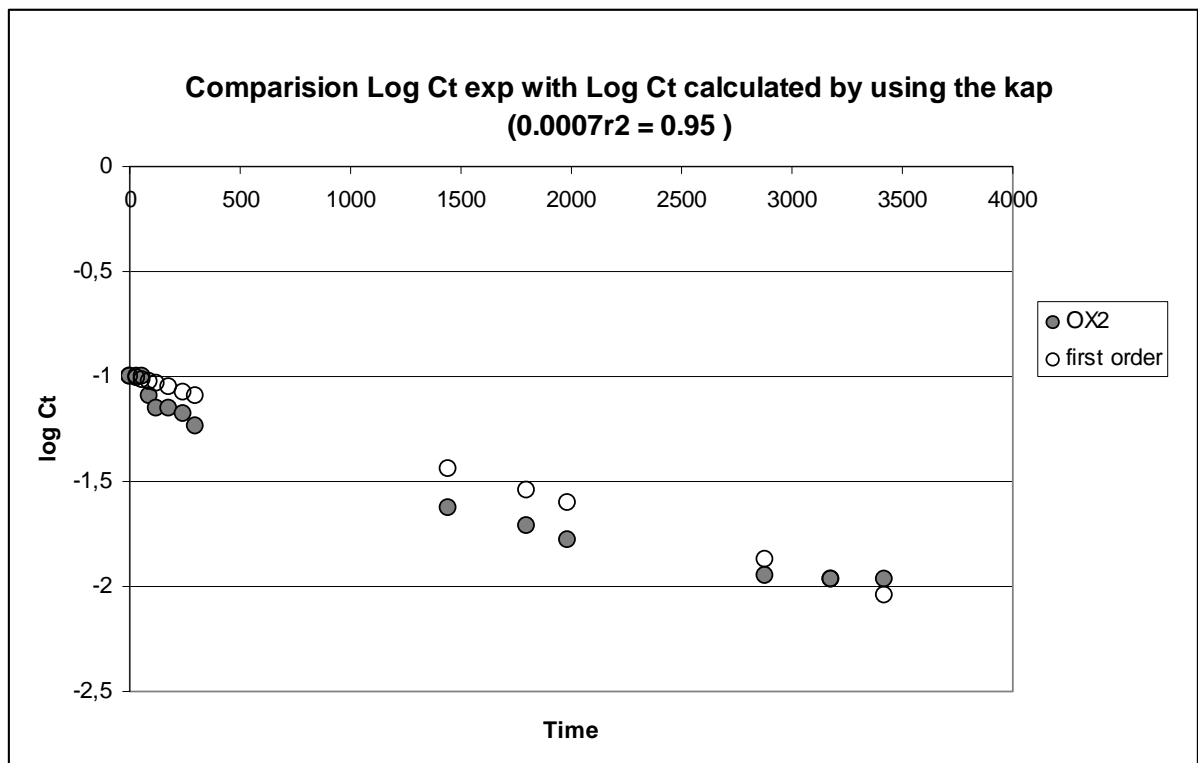
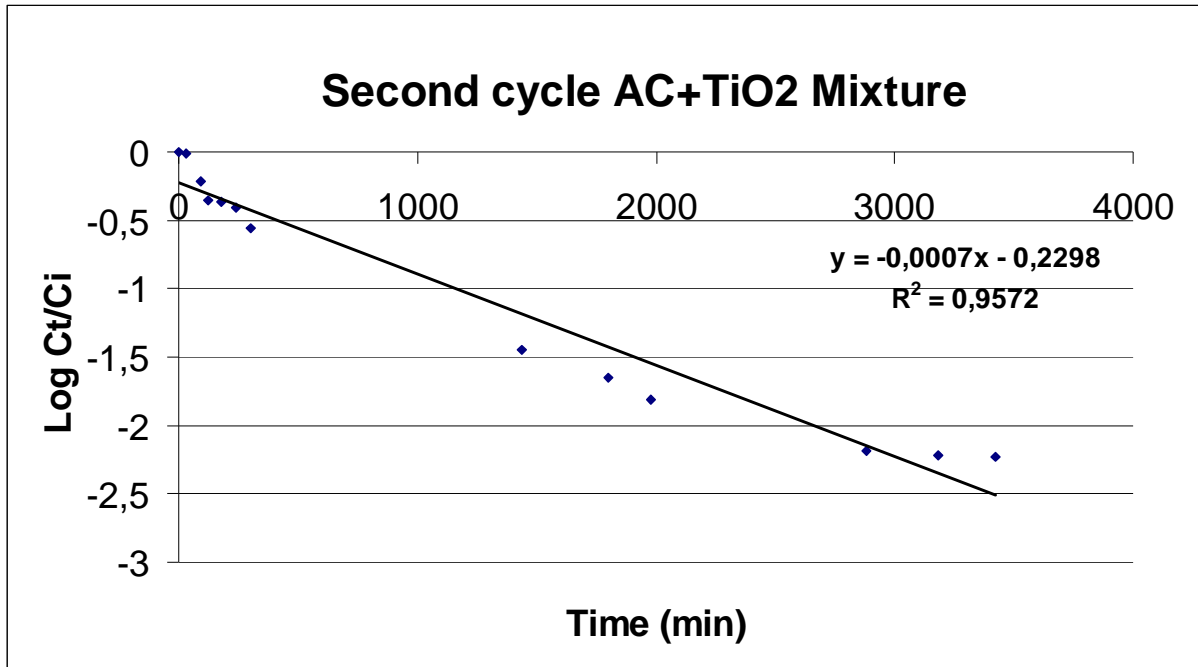
b-Kapp for the only first linear points of oxidation time at Fourth cycle

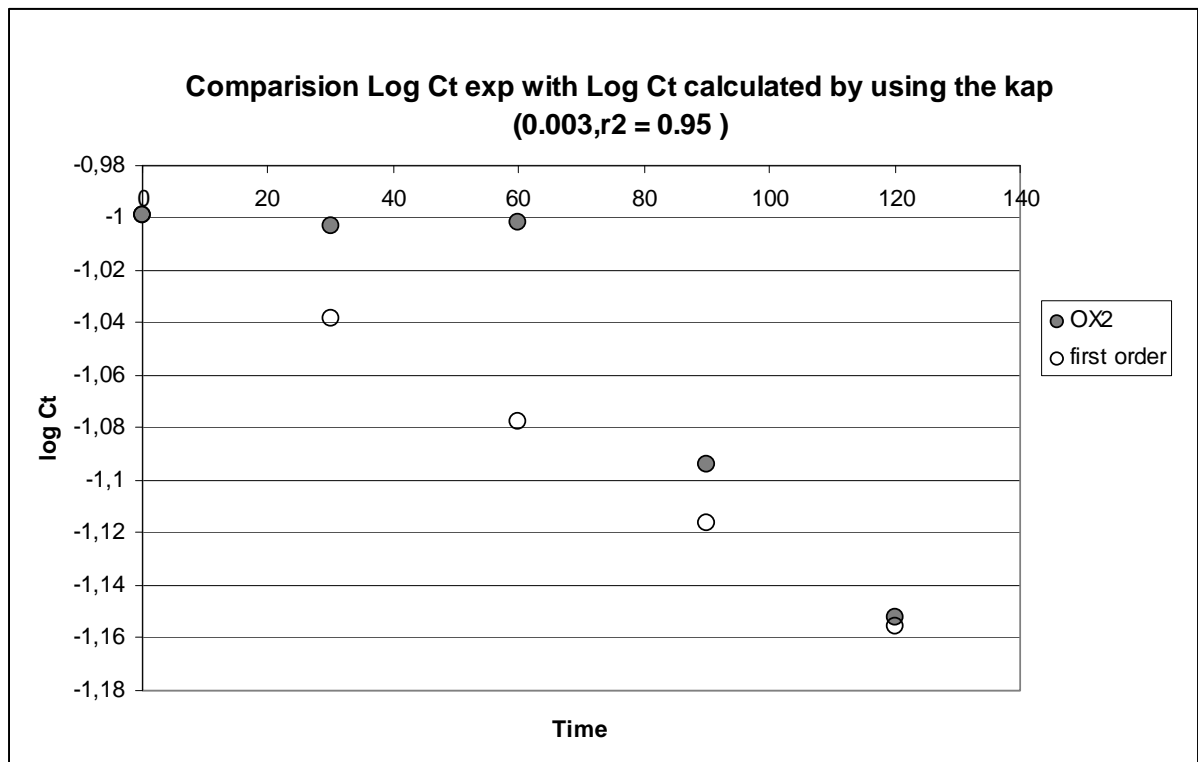
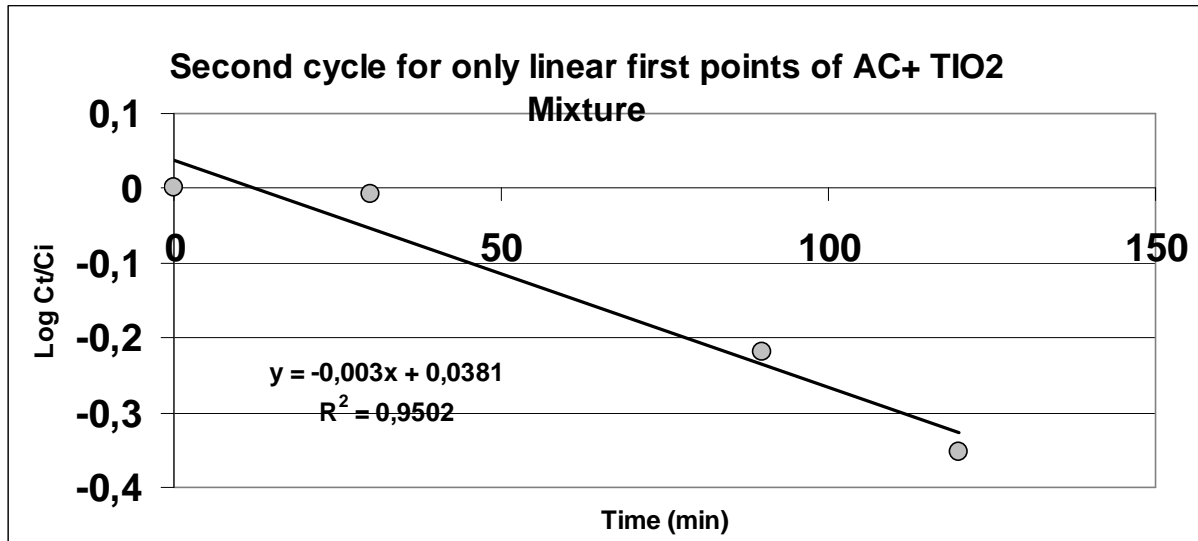
2- AC+TiO₂ suspension mixture2.1 FIRST CYCLEa-Kapp of all oxidation time at first cycle

b-K_{app} for the only first linear points of oxidation time at first cycle

2.2.Second CYCLE

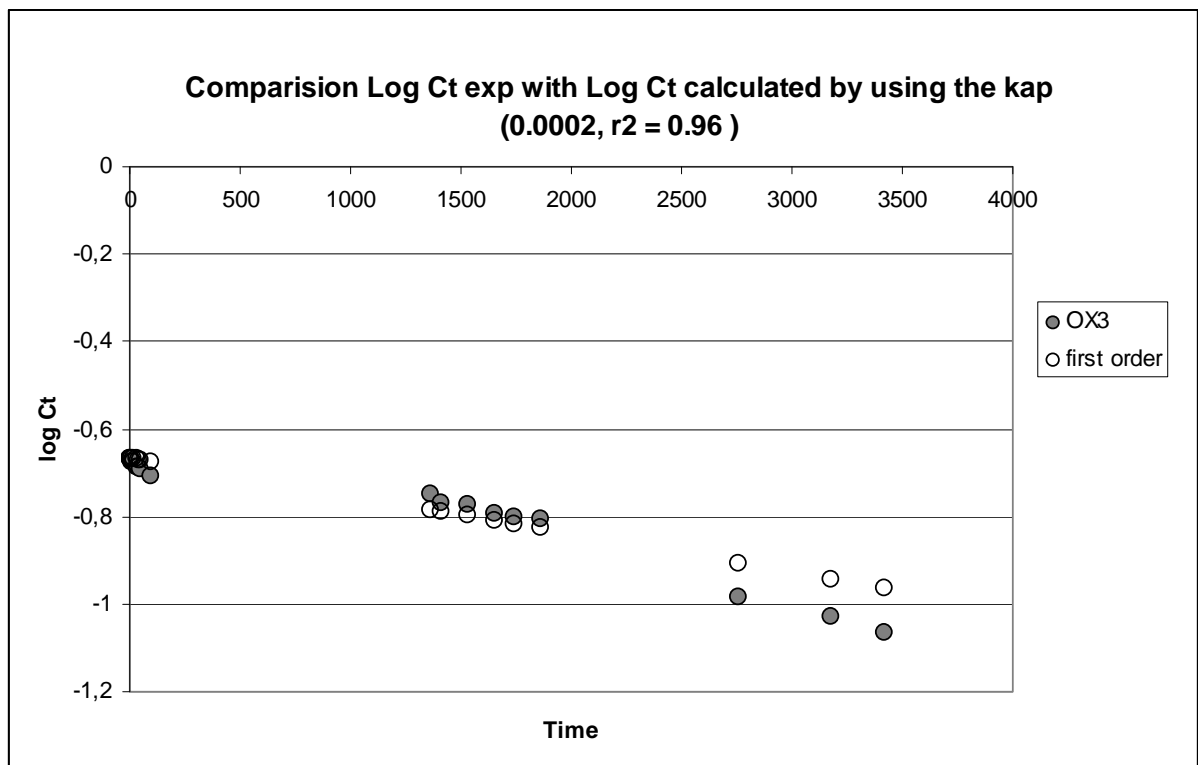
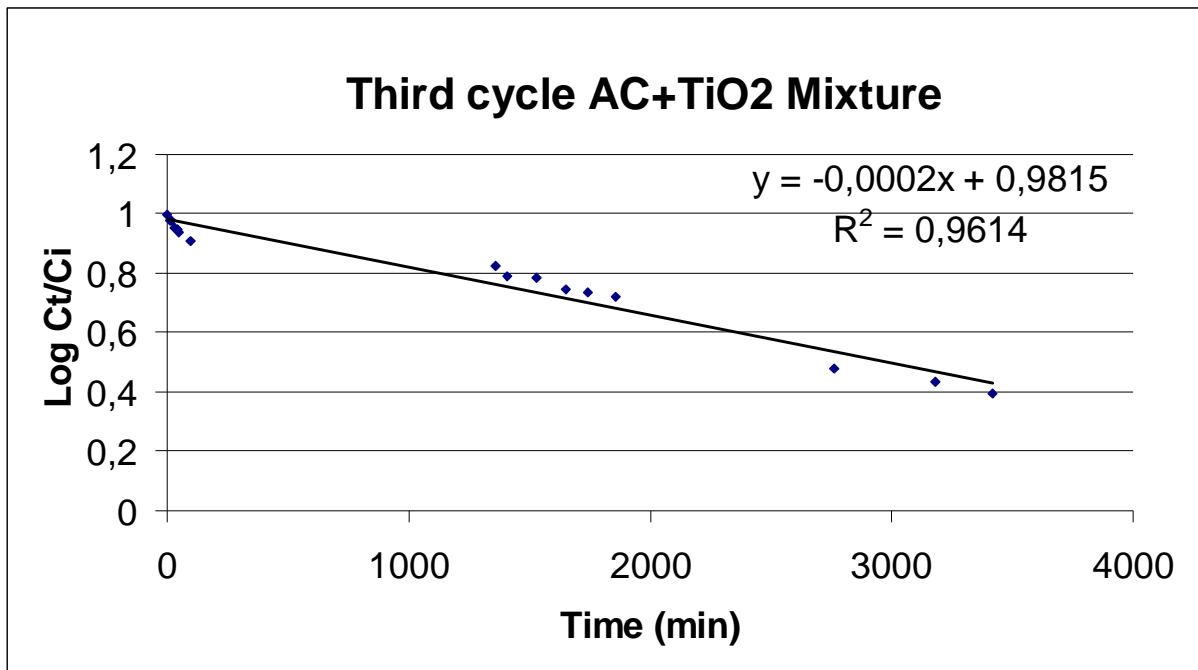
a-Kapp of all oxidation time at second cycle

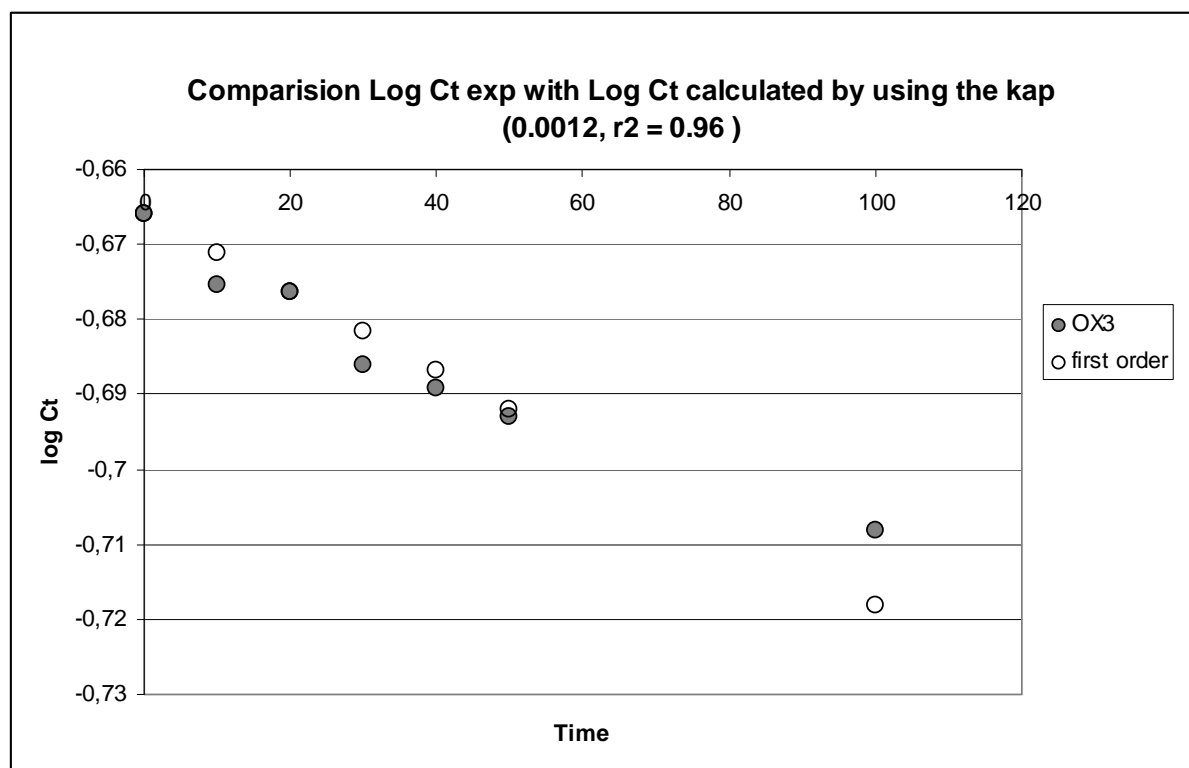
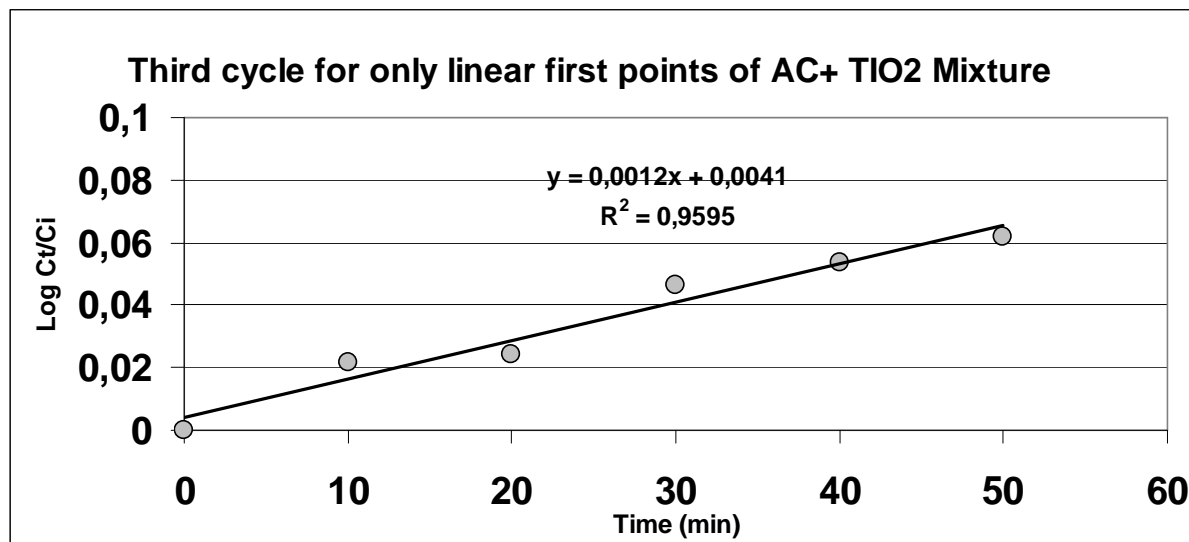


b-K_{app} for the only first linear points of oxidation time at second cycle

2.3. Third CYCLE

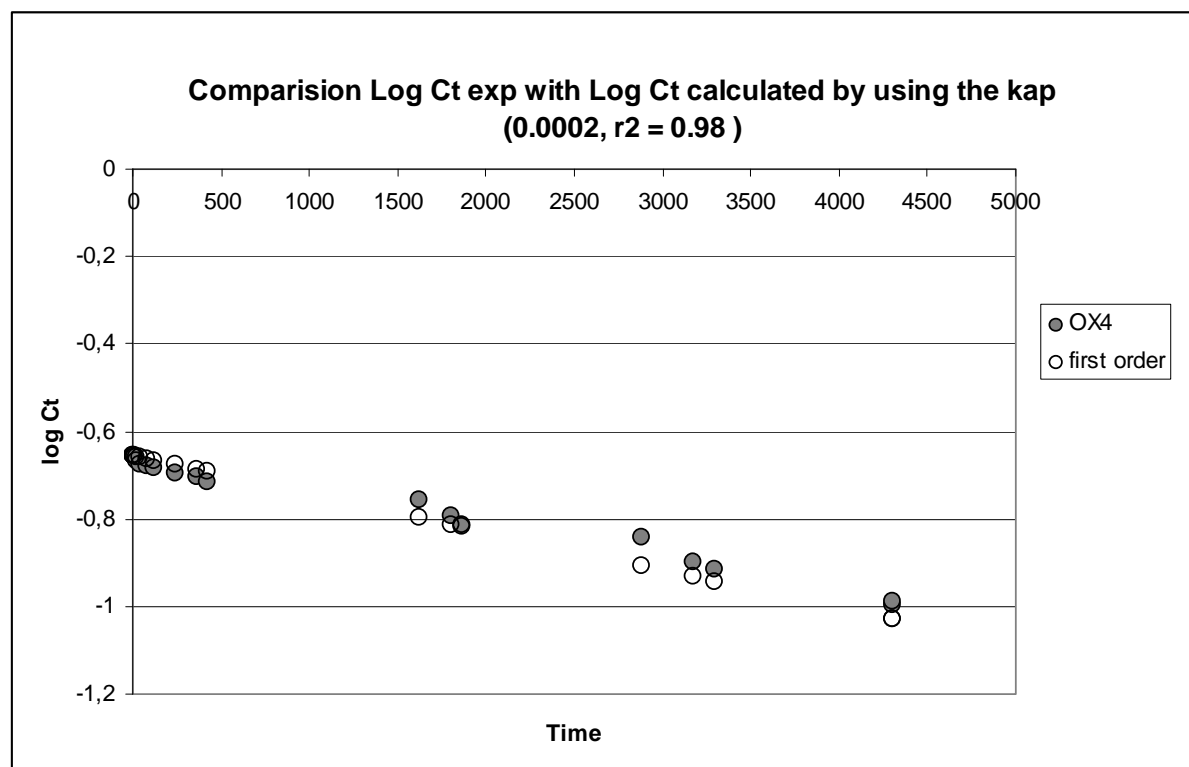
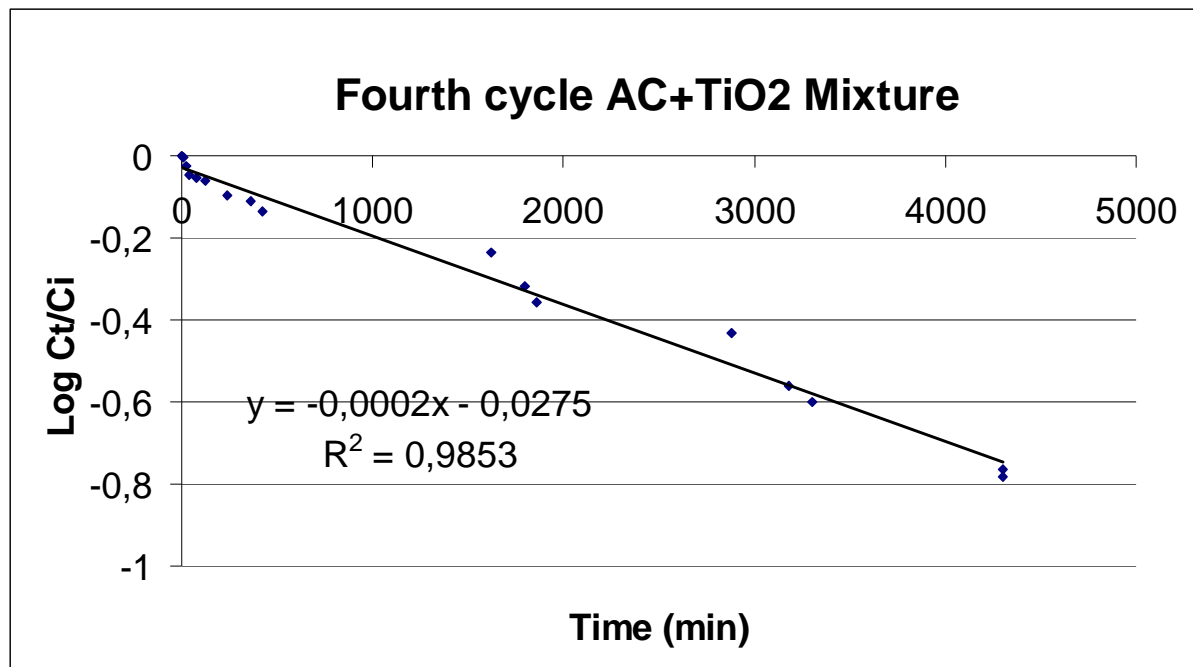
a-Kapp of all oxidation time at Third cycle

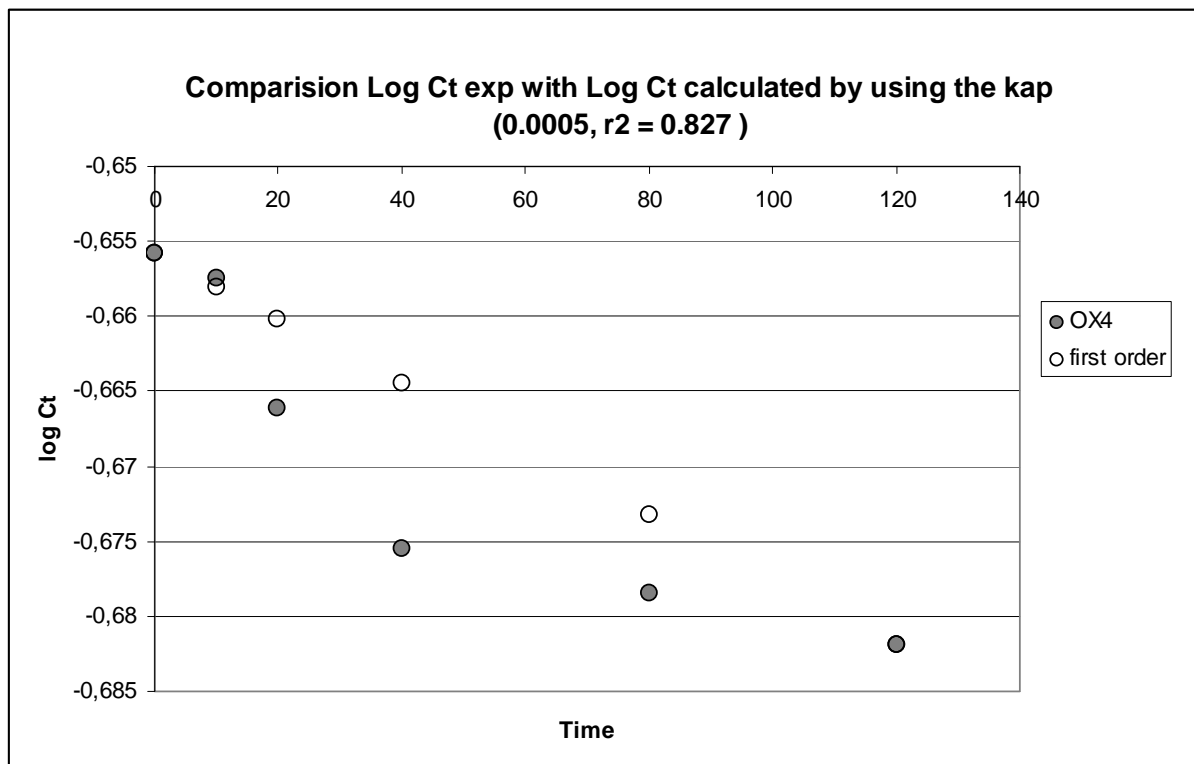
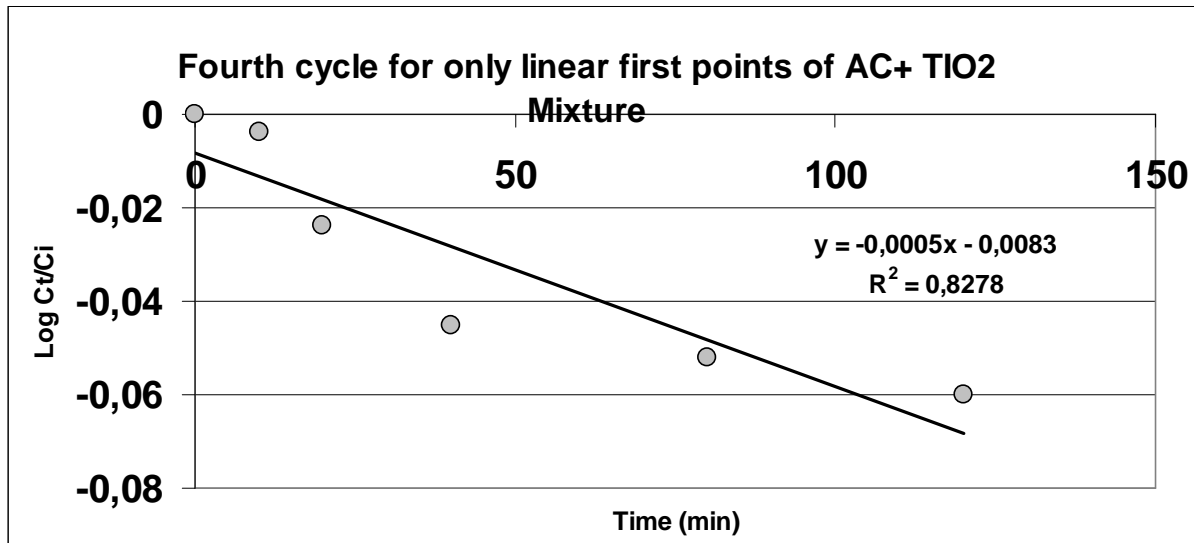


b-Kapp for the only first linear points of oxidation time at Third cycle

2.4. Fourth CYCLE

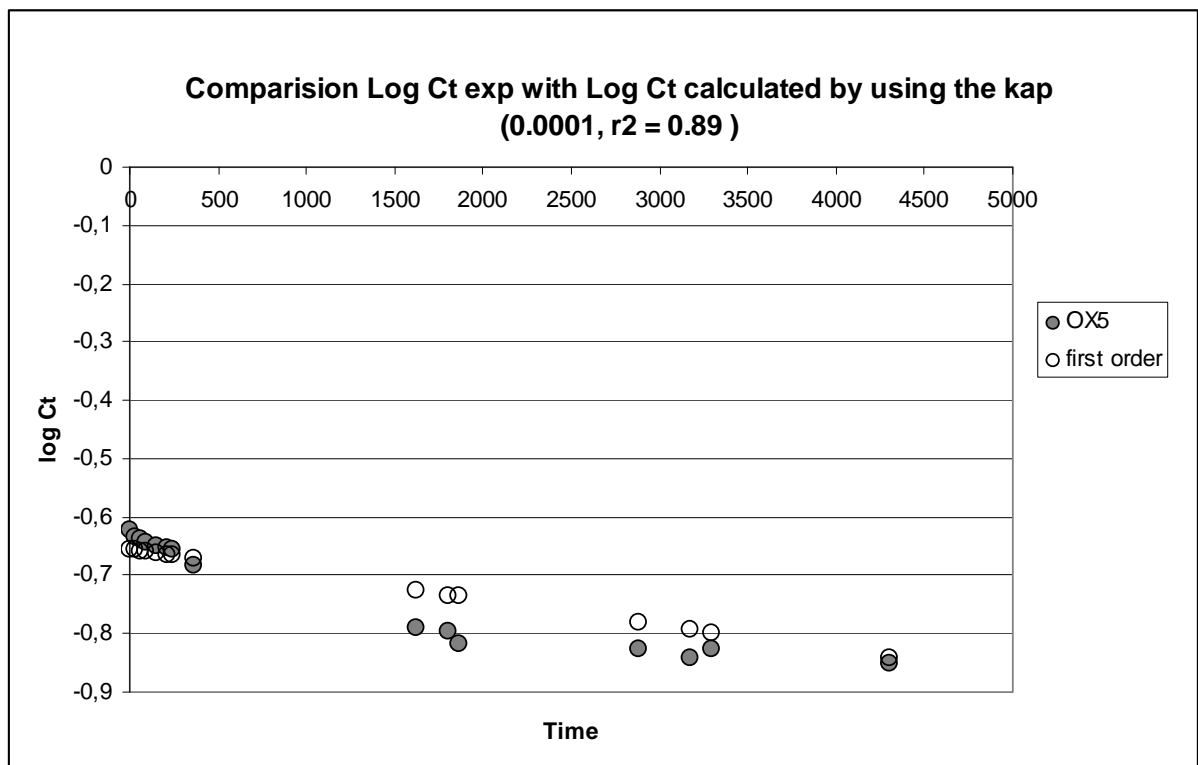
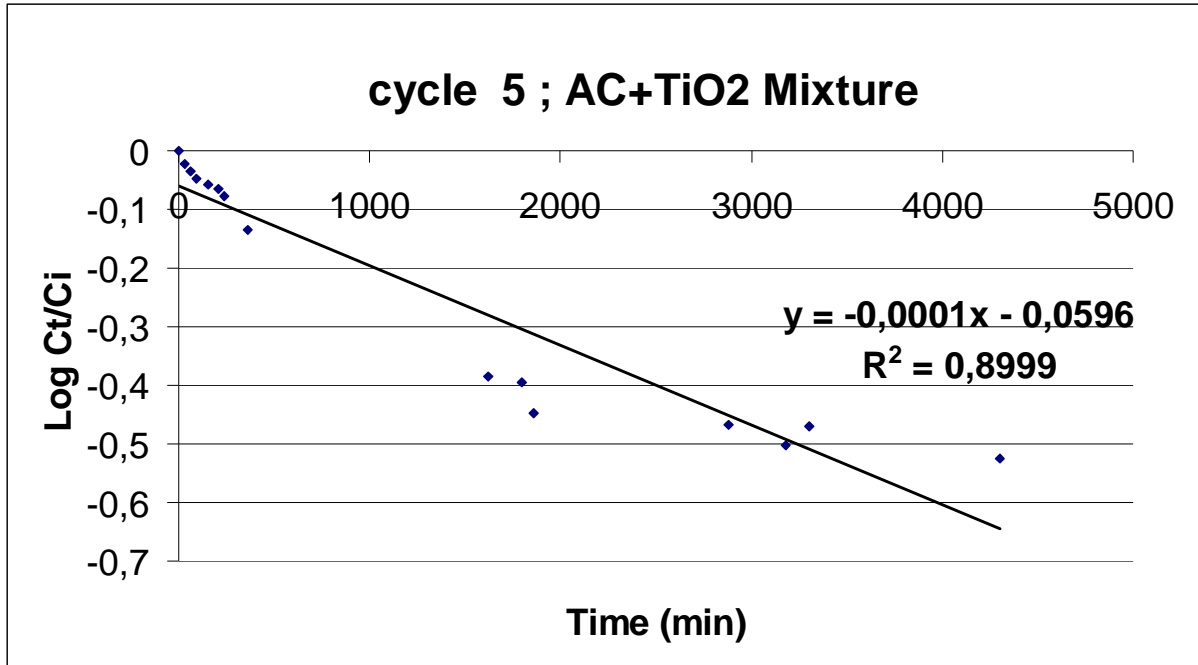
a-Kapp of all oxidation time at fourth cycle

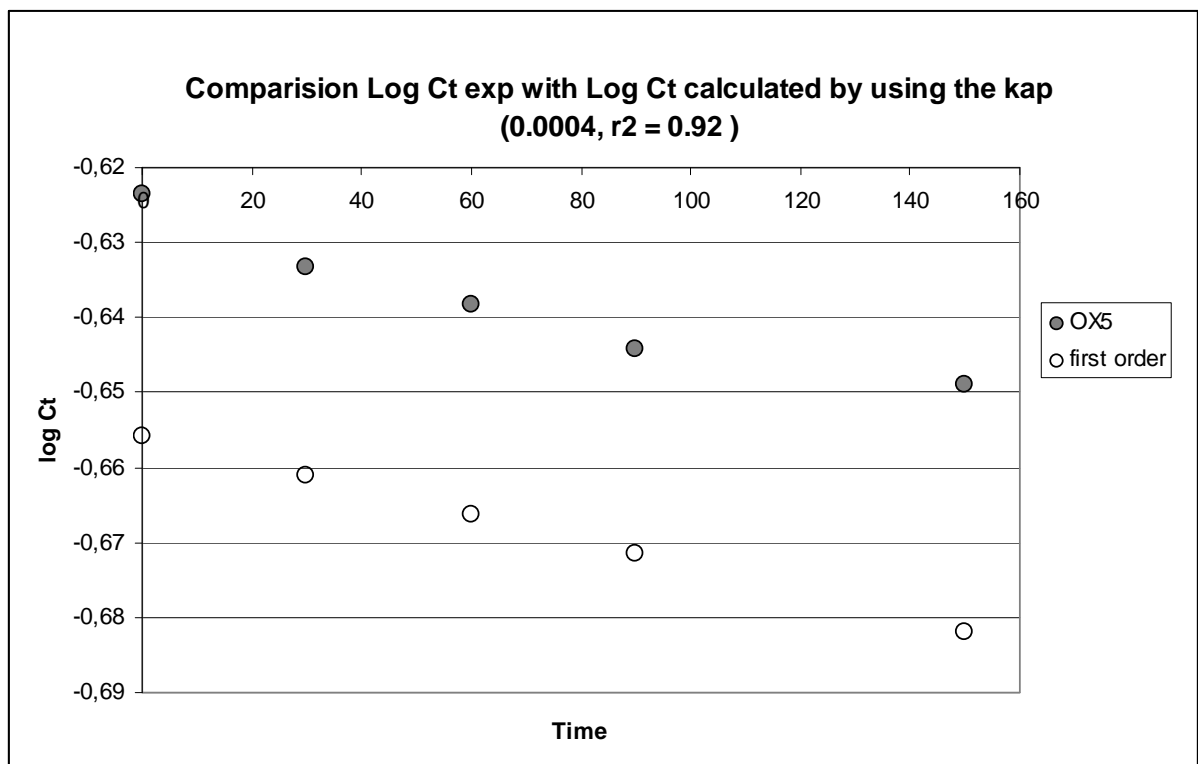
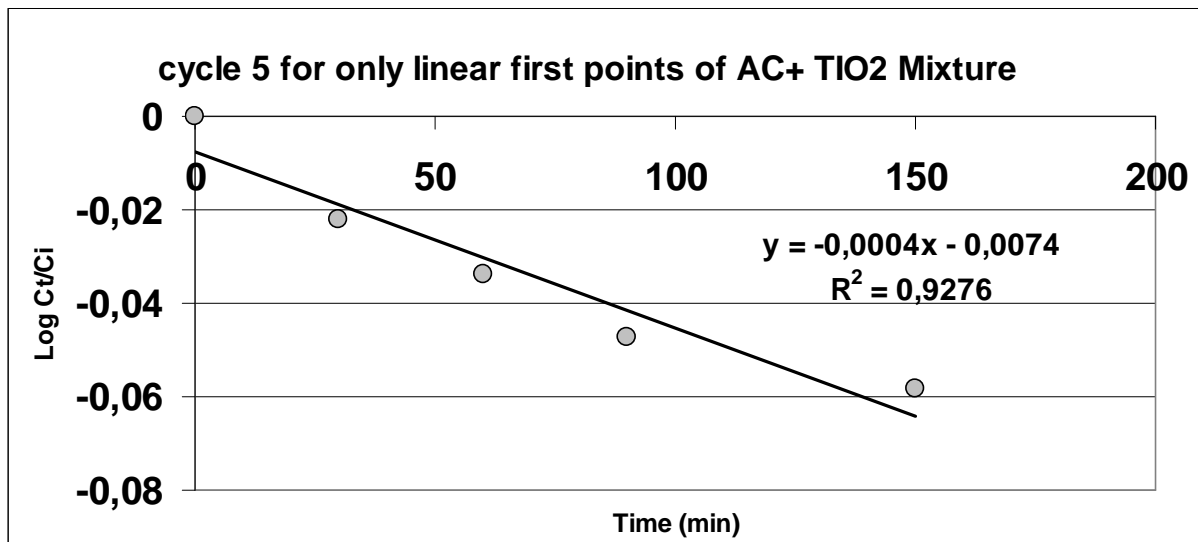


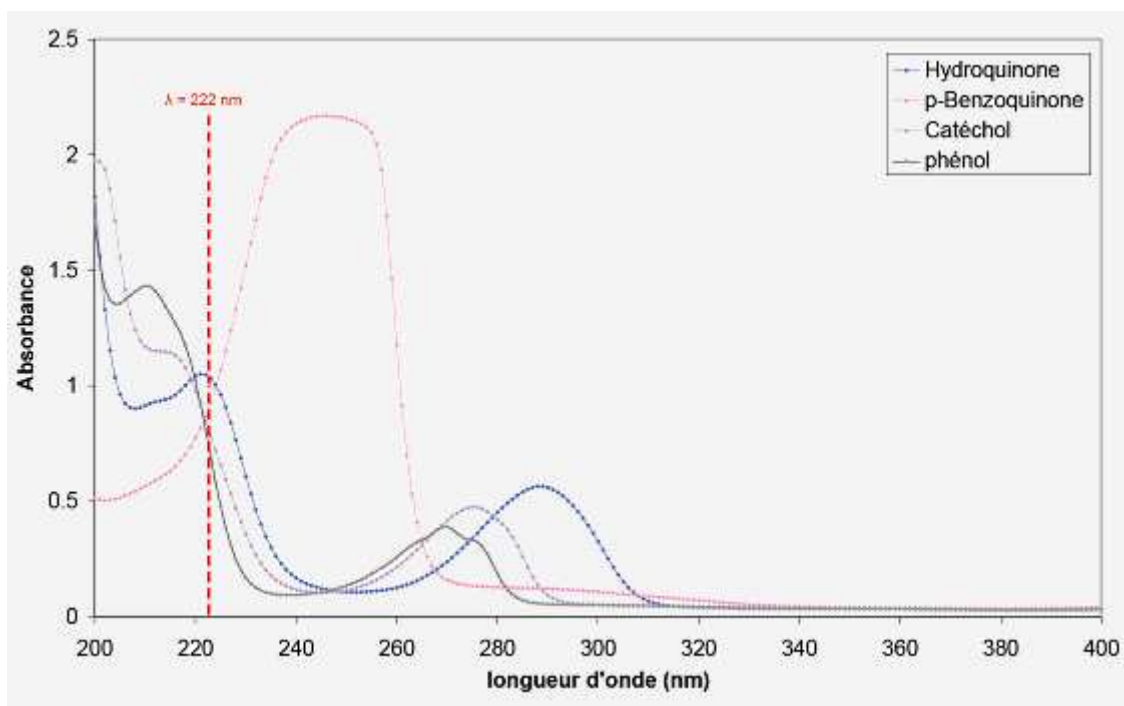
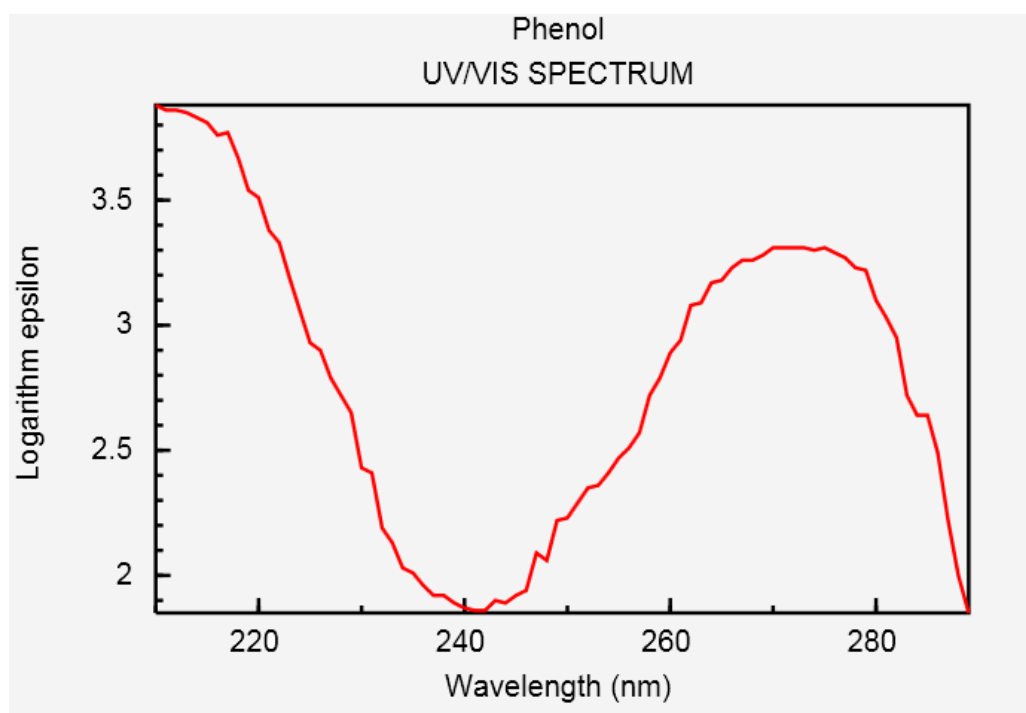
b-Kapp for the only first linear points of oxidation time at fourth cycle

2.5. Fifth CYCLE

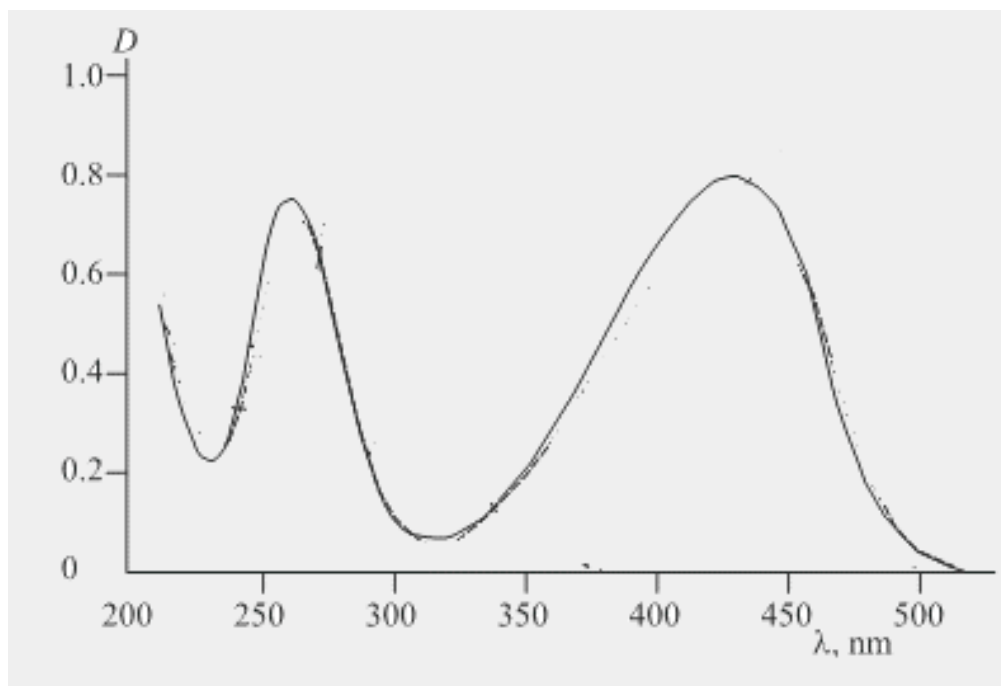
a-Kapp of all oxidation time at cycle 5



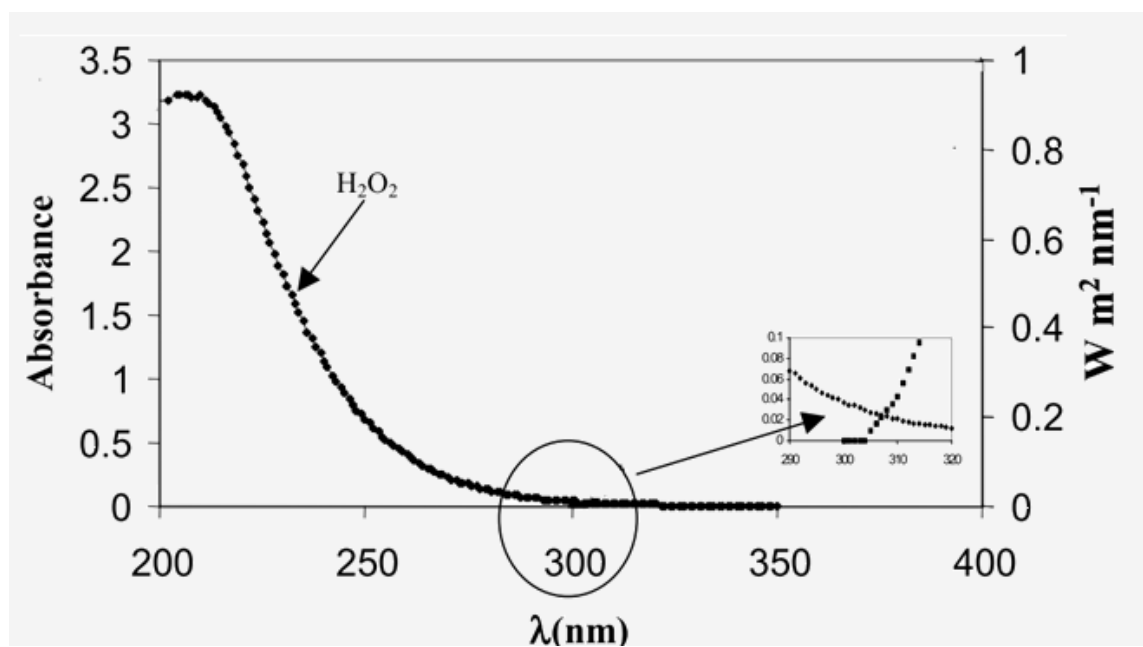
b-Kapp for the only first linear points of oxidation time at cycle 5

Annexe 13: Absorption spectra of the used compounds

Absorption spectra of phenol and its intermediates.

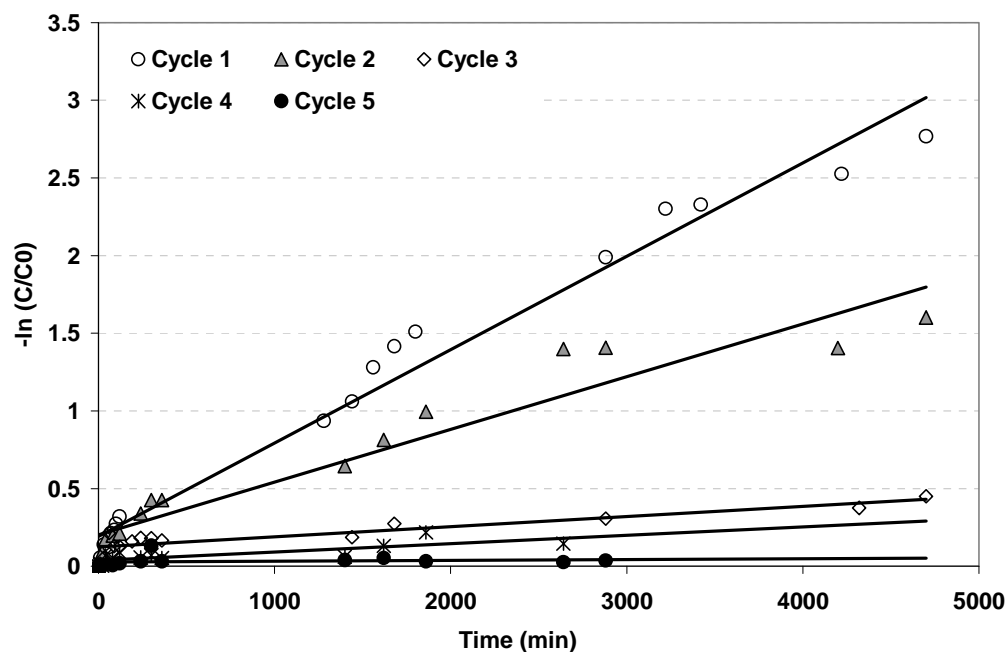


Absorption spectrum of tartrazine.

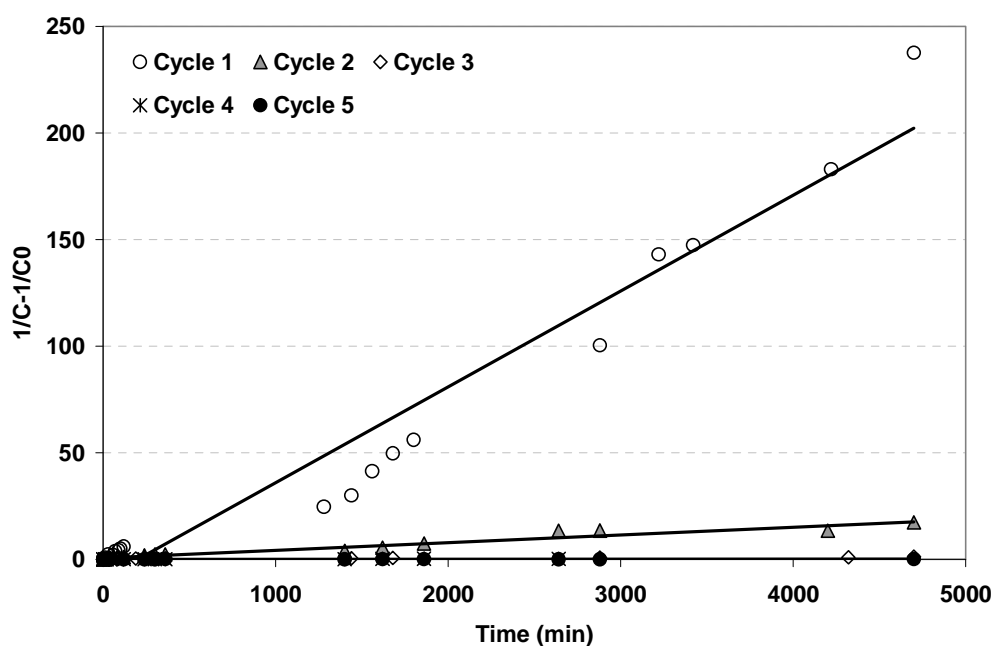
UV-vis absorption spectrum for H_2O_2 .

Annexe 14: Different models used for description of the experimental data of phenol photodegradation using tissue Ahlstrom

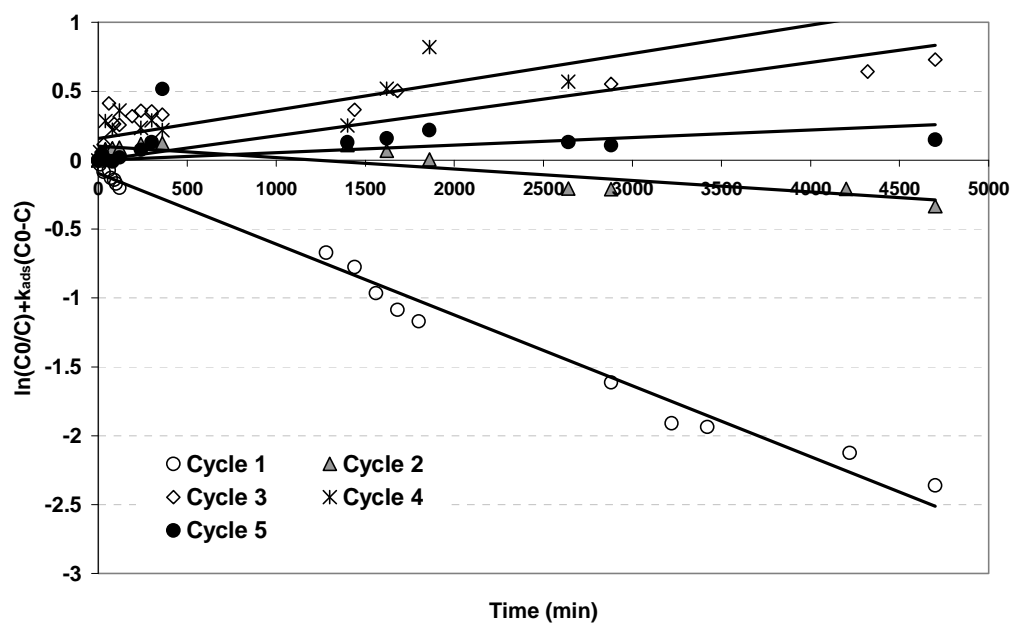
For phenol concentration 0.88 g/L without H₂O₂



First order kinetic model for the photodegradation of phenol on tissue during photo-oxidation cycles.



Second order kinetic model for the removal of phenol from tissue during photo-oxidation cycles.

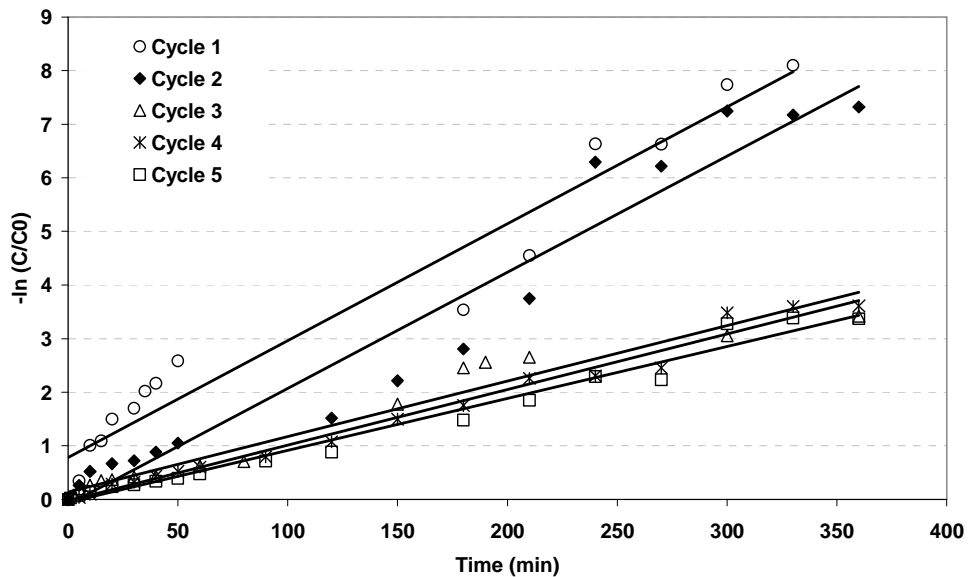


Langmuir–Hinshelwood (L-H) kinetic model for the removal of phenol from tissue during photo-oxidation cycles.

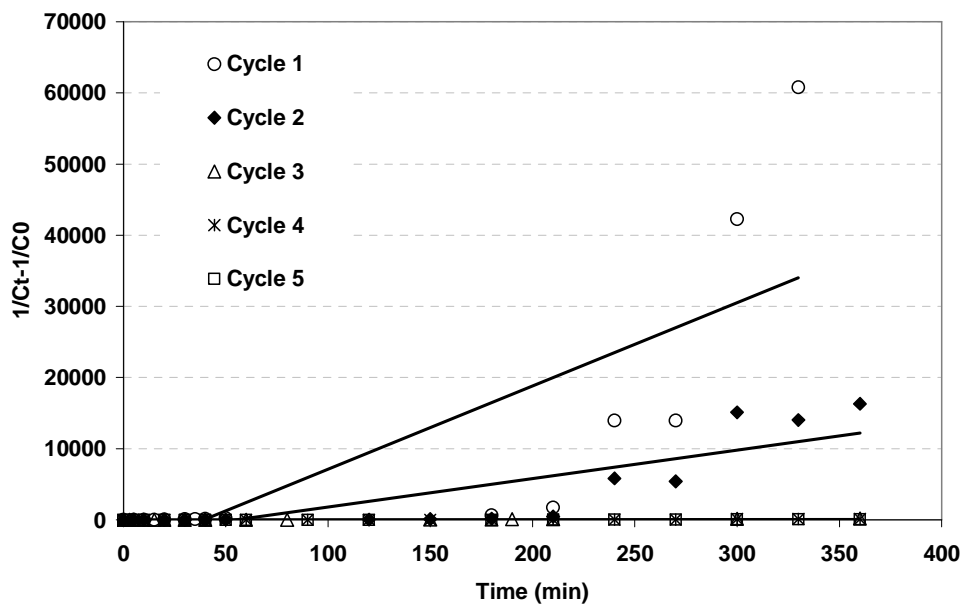
Photocatalysis kinetic parameters of phenol on tissue in term of repetitive oxidation cycles

Oxidation cycles	First order model		Second order model		L-H model	
	K1	R ²	K2	R ²	K _{L-H}	R ²
Cycle 1	0.000600	0.98	0.044900	0.95	0.00007	0.97
Cycle 2	0.000300	0.92	0.003600	0.95	0.00001	0.78
Cycle 3	0.000070	0.81	0.000200	0.84	0.00001	0.73
Cycle 4	0.000050	0.62	0.000080	0.63	0.00002	0.62
Cycle 5	0.000004	0.04	0.000004	0.01	0.00002	0.04

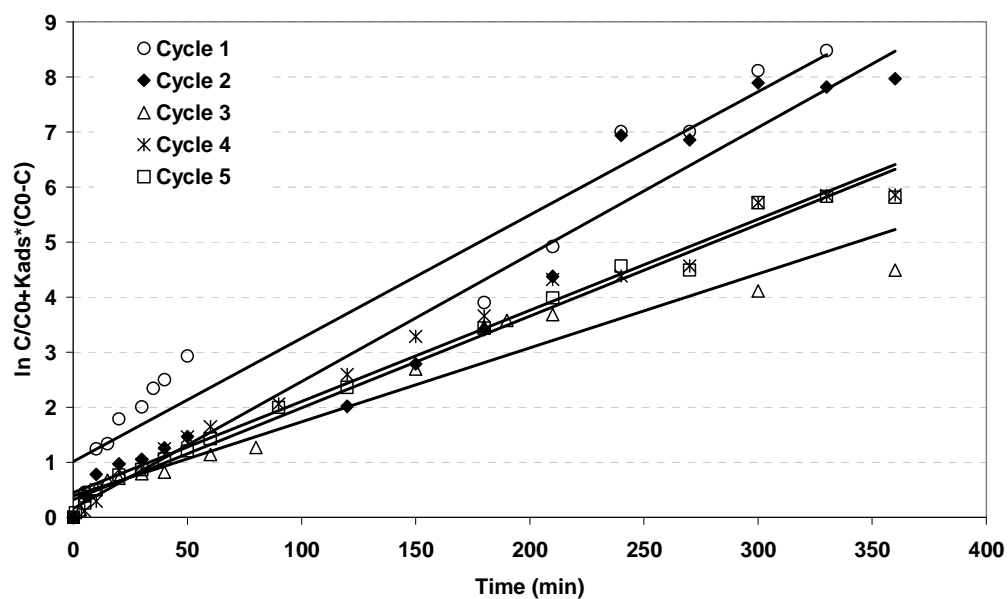
For phenol concentration 0.88 g/L with H₂O₂



First order kinetic model for the photodegradation of phenol on tissue during photo-oxidation cycles.



Second order kinetic model for the removal of phenol from tissue during photo-oxidation cycles.

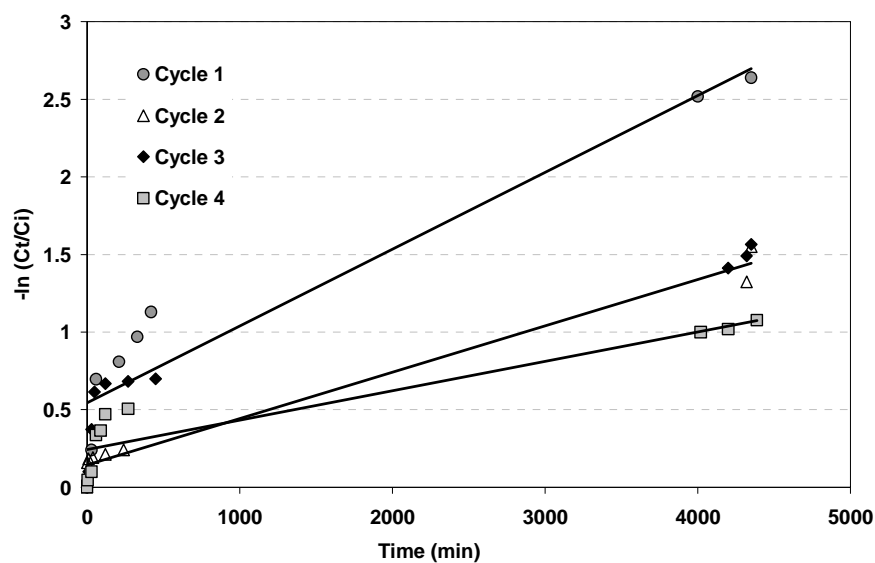


Langmuir–Hinshelwood (L-H) kinetic model for the removal of phenol from tissue during photo-oxidation cycles.

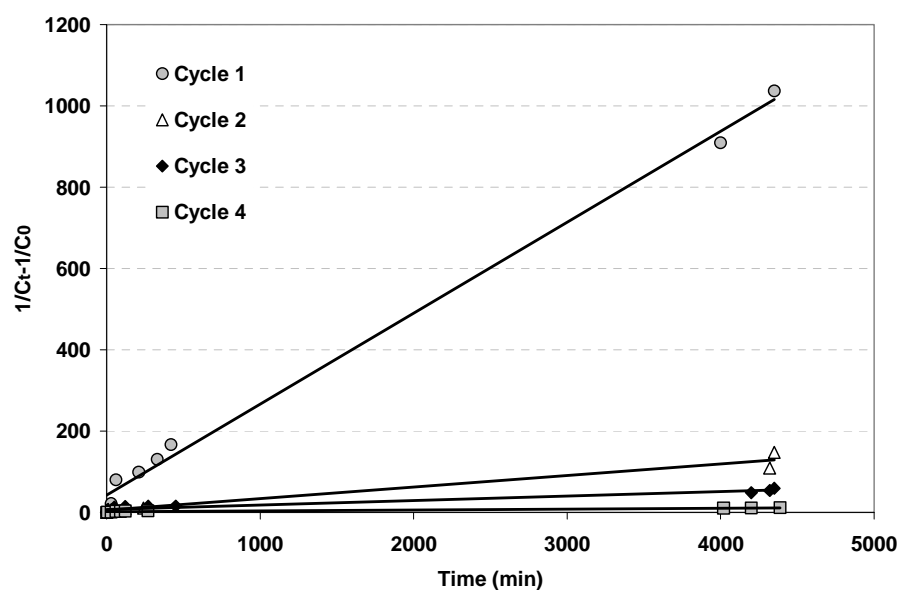
Photocatalysis kinetic parameters of phenol on tissue in term of repetitive oxidation cycles

Oxidation cycles	Frst order model		Second order model		L-H model	
	K1	R ²	K2	R ²	K _{L-H}	R ²
Cycle 1	0.0218	0.956	117.000	0.622	0.003	0.951
Cycle 2	0.0217	0.948	39.000	0.709	0.003	0.957
Cycle 3	0.0103	0.959	0.468	0.942	0.002	0.944
Cycle 4	0.0104	0.985	0.273	0.774	0.002	0.979
Cycle 5	0.0100	0.980	0.194	0.783	0.002	0.988

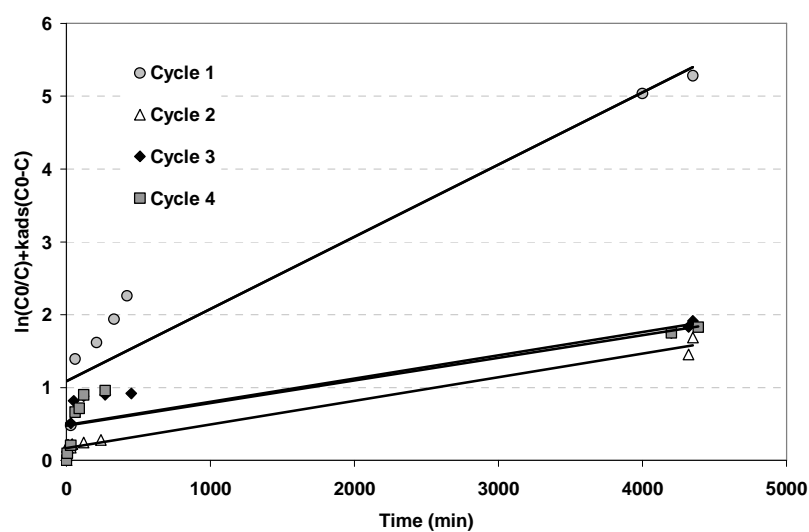
For phenol concentration 0.45 g/L



First order kinetic model for the photodegradation of phenol on tissue during photo-oxidation cycles.



Second order kinetic model for the removal of phenol from tissue during photo-oxidation cycles.



Langmuir–Hinshelwood (L-H) kinetic model for the removal of phenol from tissue during photo-oxidation cycles.

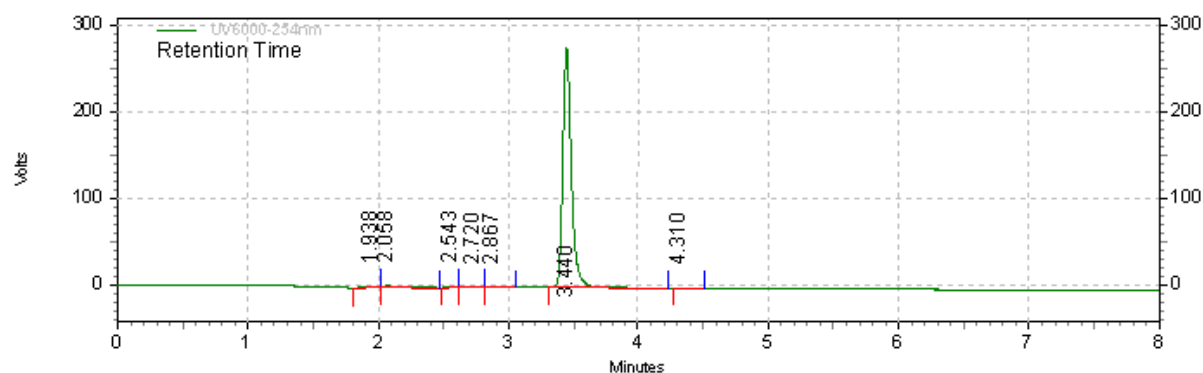
Photocatalysis kinetic parameters of phenol on tissue in term of repetitive oxidation cycles

Oxidation cycles	Frst order model		Second order model		L-H model	
	K1	R ²	K2	R ²	K _{L-H}	R ²
Cycle 1	0.00050	0.9009	0.2236	0.9954	0.0014	0.90009
Cycle 2	0.00030	0.8251	0.0264	0.9006	0.00044	0.824
Cycle 3	0.00030	0.8321	0.011	0.943	0.00044	0.8079
Cycle 4	0.00020	0.8511	0.0022	0.9306	0.00044	0.7633

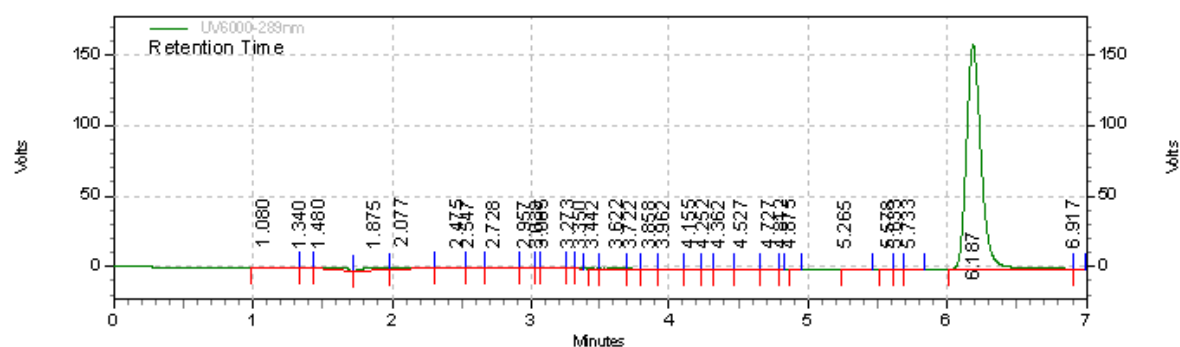
Annexe 15: Chromatograms for different used compounds

a-Fast analysis

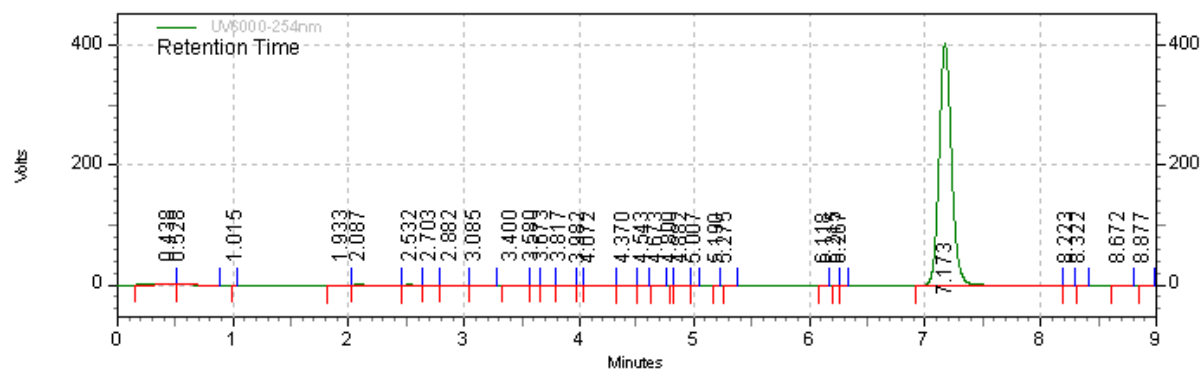
p-Hydroxy Benzoic Acid



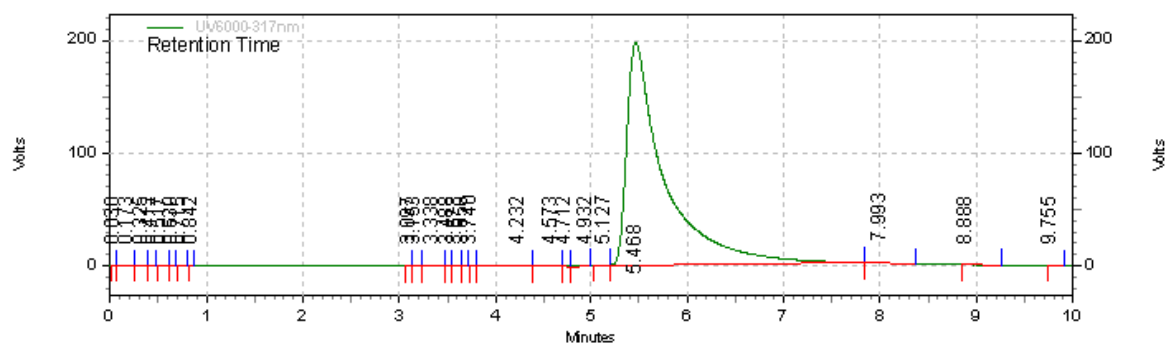
p-Nitrophenol



Phenol



Tartrazine



b- Gradient analysis

Phenol

